Tesis Doctoral

Compuestos organometálicos en reacciones de acoplamiento deshidrogenante, transformación del dióxido de carbono y otros procesos catalíticos

Pablo Ríos Moreno

Sevilla, 2019

Fdo. Salvador Conejero Iglesias

Científico Titular

Instituto de Investigaciones Químicas

Fdo. Amor Rodríguez Iglesias

Científico Titular

Instituto de Investigaciones Químicas

"Nothing is so dangerous to the progress of the human mind than to assume that our views of science are ultimate, that there are no mysteries in nature, that our triumphs are complete and that there are no new worlds to conquer."

Sir Humphry Davy

"Don't waste your time, or time will waste you."

Muse

A mis padres

Agradecimientos

Bueno, pues me temo que esta etapa está llegando a su fin, y es hora de ir cerrando el chiringuito. A su vez, es bueno hacer balance de todo lo vivido durante estos 4 años y sacar conclusiones que nos hagan mejorar un poco más en lo que queda más adelante. Aunque he aprendido infinidad de cosas en el ámbito profesional, las personas que han compartido este periodo de tiempo conmigo son por supuesto lo más importante, y es algo injusto que solo tengan unas pocas páginas en todo este trabajo, ya que sin ellas habría sido impensable llevar esto a cabo. Sin embargo, el realizar la tesis me ha enseñado a ser optimista sobre todo, así que vamos a aprovechar el poquito espacio del que disponemos, ¿no?

No puedo empezar de otra forma que agradeciendo a mis dos directores de tesis, Amor y Salva, la oportunidad que me brindaron al poder realizar la tesis doctoral con ellos. Confiaron en mí desde el principio, y desde entonces no han dejado de apoyarme, aconsejarme y animarme durante todo este tiempo. Ha sido todo un placer poder trabajar con vosotros, montar vuestro propio laboratorio desde 0, y haber aportado mi granito de arena para que vuestro proyecto salga hacia delante, porque no conozco a nadie que lo merezca más. Repetiría la experiencia una y mil veces. Si mi predecesor Orestes se alegraba de ser el primero de muchos *Conejeros*, yo me alegro enormemente de ser el primero de muchos *Rodríguez-Conejero*. Gracias por compartir toda vuestra experiencia conmigo, y por contagiarme vuestro entusiasmo por la química organometálica. Ojalá todo vaya bien, y podamos volver a trabajar codo con codo dentro de no mucho tiempo (¡crucemos los dedos!).

Sé que sois un tándem perfecto, pero es injusto que os considere como tal yo también, y más cuando he tenido la oportunidad de conoceros mejor a cada uno por separado, así que allá voy.

Amor, ¿qué voy a decir que en realidad no sepas? Sabes de sobra que detrás de todas esas bromas y chistes hay muchísimo afecto, respeto y admiración. Gracias por ser una tía tan clara, tanto para lo bueno como para lo malo, y tan buena persona. En estos tiempos donde por fin las mujeres están adquiriendo el mismo protagonismo que los hombres, tú eres un claro ejemplo de profesional en la que fijarse. Sigue así, tanto dentro como fuera del laboratorio.

Salva, gracias por aportarme tantísimo también, tanto a nivel profesional como personal. Es difícil olvidar las incontables charlas sobre química en el despacho, y cómo nos veníamos arriba con un folio en blanco y un boli, sugiriendo ideas. En esos momentos intentaba encender el modo esponja y absorber toda la

información posible. Aunque me alegro de no haber aprendido solo eso, ya que la ética y la moral también se pegan. Agradezco la bondad y amabilidad con la que la puerta siempre ha estado abierta para cualquier cosa, fuese de química o no. No cambies tú tampoco, porque gente tan buena como tú escasea.

Los siguientes en la lista son los que desgraciadamente me han tenido que aguantar durante la tesis. Los que me sufrieron en el Laboratorio 9 al principio, y en el Laboratorio 203 en la segunda mitad, son mis compañeros de fatigas Leonardo y Jose. Leonardo es el brasileño *más grande que hay*, al igual que los chicharrones (según él). No conozco un tío que sea más "cacho de pan" que tú. Echando la vista atrás, creo que no ha habido ni un solo día en estos 4 años en el que no te haya visto con una sonrisa trabajando. Espero que ese detalle no cambie nunca, y que la suerte te siga en tu vuelta a Brasil. En cuanto a Jose, sabes de sobra que se te echa en falta muchísimo, tanto fuera como dentro del lab. Eres una máquina trabajando (bien lo saben los jefes), y eres otra persona buenísima de las que merece la pena conocer. Gracias por haber estado ahí día sí día también echándome un cable, o animándome el día con algún gesto o comentario positivo. Por supuesto no puedo olvidarme tampoco de Hugo, o *el nota*. En tan solo unos meses de estancia el tío se hizo querer muchísimo en todo el grupo y en el instituto (lo cual es muy comprensible). Además, su ayuda fue crucial en el proyecto de platino, ya que gracias a él pudimos darle un empujón bueno cuando nos faltaban manos para sacar adelante todo lo que nos estábamos proponiendo. Me alegro de no haber perdido el contacto, y de seguir visitándonos de vez en cuando. Espero que siga así!

La siguiente parada obligada es el laboratorio 1-2. En primer lugar, me gustaría agradecerle a Juanjo (o *GuajitoDFT*, o *Juanj*) todos los buenos momentos disfrutados dentro y fuera de cartuja. Tal y como te he descrito alguna vez, has sido uno de los grandes descubrimientos de la tesis (y reitero la palabra *grande*, casi como tus tapers de comida). Sabes que he aprendido mucho de ti, tanto de química como de tu forma de ser. Tío más noble no hay, y además es el responsable de que gran parte de mi dieta en la última etapa de la tesis esté basada en pad thai de pollo al 3 (qué sudores más ricos). Te mereces que te vaya de maravilla (a ti y a Andrea, ¡que bastante te aguanta también!), y espero que así sea. Moviéndome por el laboratorio llego hasta el mítico puesto de mando del señor Carlos, el terror de las galaxias del Ogame. A ti te tengo que agradecer enormemente que le des vida a la parte inorgánica del IIQ, y la hagas un poco más "orgánica" en el sentido social. La cantidad de risas y buenos momentos echados allí han hecho las innumerables horas bastante más amenas, así que muchísimas gracias. Por otro lado, agradecer también a los otros habitantes de este lab: Mario, Juanín, Sonia, Marina, Nere (los más *senior*), y a la nueva generación que

ha llegado ahora, como Macarena, Lola o María. No se me olvidan antiguos huéspedes de este lab como Juanje o Macarena, o antiguas doctorandas como Ángela, Laura, María y Natalia, a las cuales les agradezco todo lo que me enseñaron durante mi primer año de tesis y los buenos ratos que pasamos en diferentes comidas y escapadas. Dicho laboratorio sería un completo caos si no fuese por la presencia de Riccardo o de Jesús (antiguo compañero de lesiones futbolísticas).

En el lab 3-4 se encuentra Tomás, un tío currante donde los haya y bueno a más no poder también. Espero que no pierdas ese entusiasmo que te caracteriza, y que la última recta de la tesis sea lo más suave y exitosa posible. Este lab se encontraba frecuentado anteriormente por buena gente como John, Carmen o Astrid. Destacar también los numerosos buenos momentos compartidos con Elena. Espero que esa bondad que te caracteriza siga acompañándote allá por Cambridge. Por último, agradecer también a Juan, Pilar y Antonio Rodríguez lo atentos y dispuestos que han sido siempre conmigo.

Para terminar con la parte organometálica, tengo que mencionar a los residentes del Lab 10-11/207, Félix y Práxedes. A ellos, y a los asturianos Pedro y Eire (breves visitantes), tengo que agradecerles que hicieran más amenas algunas salidas y comidas de navidad.

No me puedo olvidar tampoco de la parte orgánica del instituto, que con la que si bien he tenido menos contacto durante este tiempo, lo poco que he podido coincidir con ellos ha sido muy bueno: Javi Ramos, Ainhoa, Abel, Valentín, Rute, Noelia, José Alberto, Tania, Pedro Domínguez, Antonio Romero, Antonio Di Maio, José Juan, Vero, Pedro Ramírez…¡Muchas gracias a todos!

Por otra parte, merece mención especial Joaquín, por su enorme paciencia y disponibilidad a la hora de enseñarme a defenderme en el mundo de los cálculos DFT, y por su paciencia corrigiendo cada espacio accidental que introducía frecuentemente en el input, haciendo que el cálculo se fuese al garete. Y merecen mención especial "las niñas", Laura, Nuria y Patri, por estar ahí con una sonrisa siempre que he necesitado hablar con ellas, y por guiarme con nociones básicas de docencia cuando me ha tocado trabajar con estudiantes, y no con líneas de vacío ni cámaras secas. Muchas gracias a los 4 por vuestro tiempo y amabilidad.

Este trabajo no sería posible si no estuviese en el Instituto de Investigaciones Químicas. Por tanto, debo agradecer que éste se sostiene en dos pilares fundamentales: Fran y Marga. Mientras que el primero es un todoterreno en cuestiones técnicas, la segunda es una máquina en cuanto a burocracia se refiere. Sin ellos, todos los que trabajamos aquí estaríamos perdidos, y tardaríamos una

eternidad en conseguir lo que ellos realizan en un periquete. Así que gracias, por facilitarnos muchísimo nuestro trabajo, y por hacerlo con la mejor de las sonrisas.

Me gustaría agradecer también a José Manuel la eficacia y rapidez a la hora de analizar las muestras de análisis elemental, y a Agustín Cota (CITIUS) su inagotable paciencia para medir mis cristales, y probar uno tras otro tras otro y hacer lo imposible por conseguir buenos datos de rayos X que pudiéramos utilizar, ya que ha sido de gran ayuda. Muchas gracias por hacer que los ratos de incertidumbre fueran más llevaderos. Asimismo, agradezco a la Dra. Josefina Díez la resolución de numerosas estructuras de rayos X plasmadas en esta tesis, y al Dr. Javier Borge el esfuerzo y dedicación con una de las últimas estructuras de esta tesis (bastante complicada, por cierto). Por otro lado, debo darle las gracias nuevamente a Natalia en este aspecto, debido a que ha buscado tiempo cuando no lo había para dedicarle algún rato a la resolución de estructuras, algunas de las cuales eran duras de pelar.

Quisiera mencionar también a Miguel Anaya, junto con el cual me comí numerosas reuniones que acabaron culminando en las PhD Talks, las cuales van ya por la tercera edición. Espero que dicho proyecto siga adelante durante mucho más tiempo.

Por otra parte, el marco de la tesis doctoral ha facilitado la realización de estancias en diferentes universidades, en la cual he conocido a gente estupenda y de la cual he podido aprender muchísimo. En primer lugar, me gustaría agradecer al Prof. Agustí Lledós que me acogiera durante un mes en su grupo en la UAB. De la misma forma, agradezco a Sergi, Gantulga y Giuseppe toda la ayuda prestada durante mi estancia. No me puedo dejar fuera a Pablo y a Anna, los cuales se hicieron querer en poquísimo tiempo. ¡Os espero por aquí abajo! En segundo lugar, agradezco al Prof. Kit Cummins el poder trabajar durante 4 meses en sus laboratorios. Fue una experiencia fantástica, y me llevo muy buenos recuerdos de allí. Asimismo, sus estudiantes Wes, Mike, Scott, Martin, Yingying, Kevin, Wendy, Liz, June y Paul crearon un ambiente de trabajo genial.

Sin embargo, me veo obligado a separar de esta última estancia a un grupo de personas que hicieron de mi período en Boston una etapa inolvidable, ya que hicieron que me sintiese en familia desde el minuto 1. Steve, Isabel, Leslie, Emily y Brendan, muchísimas gracias por todo lo vivido juntos. Y por supuesto, gracias a Tim, por ser como un hermano para mí. Te veo próximamente.

Volviendo a tierras sevillanas, me gustaría mencionar a Angelita, Ana, Pedro y Víctor del IBVF, por todas las cervecitas y las risas que nos hemos echado (¡y por las que quedan!).

Me gustaría agradecer a mis amigos toda la comprensión que han tenido conmigo cuando no he podido reunirme con ellos debido al trabajo, y por los buenos ratos y los ánimos que me han dado cuando sí ha sido posible verlos: Porras, Pedro, Rubén, Rulo, Bastos, Guille, Davile, Fran, Antonio, Luisa, y en especial a Germán y Ángela, los cuales me siguen aguantando después de todo este tiempo. Sois tela de grandes, y yo muy afortunado por teneros.

Para ir terminando, me gustaría darles las gracias a ciertos miembros de mi familia que me han apoyado especialmente durante este período de tiempo, y los cuales también van sobrados de paciencia. Entre ellos se encuentran mis titos Rosa y Manolo, mis titos Charo y Juanmi (y por supuesto mis primas Irene y Esther) y mi tía Ani. Quiero mencionar también a mi familia morilense: Manuela, Manolo, Olga, Manuel, Salud, Charo...¡Muchas gracias por acogerme tan bien, y por entenderme cuando he faltado por allí!

Por último, quiero agradecerle a mi hermano Javi y a mi cuñada Rebeca el haber estado siempre ahí, animándome y entendiéndome sin dudarlo un segundo, y disfrutando conmigo todos los buenos momentos que nos hayamos podido ir encontrando. Tengo muchísima suerte de que estéis ahí. Y por supuestísimo, me siento muy orgulloso de tener los mejores padres del mundo, Carmen y Juan, por todo el cariño con el que me han tratado siempre y por comprenderme, aunque en realidad no entendieran qué eran esas "colmenitas" que dibujaba día tras día y que me robaban semanas, meses, años... Sois un ejemplo a seguir, en absolutamente todo. De mayor quiero ser como vosotros, tanto dentro como fuera del curro. Gracias por enseñarme el valor del trabajo, y a disfrutar de la vida al mismo tiempo. Os quiero mucho.

Y antes de dar comienzo al contenido de esta tesis, quiero darle las gracias a Valle. A ti, que *llegaste por casualidad*, quiero darte mil gracias por compartir tu vida conmigo, por ser tan buena y tan dulce, por animarme los días con solo verte, y por entusiasmarte conmigo ante todo lo bueno que nos espera. Sé que aunque el futuro que se nos plantea es algo incierto, sabremos cómo superar todo lo que nos propongamos, juntos, caminando de la mano. Te quiero. *And our dreams will break the boundaries of our fears...*

TABLE OF CONTENTS

Chapter 3 – Cationic Pt(II) σ-SiH complexes as reactive intermediates

Chapter 4 – Catalytic processes assisted by cationic Pt(II) σ-SiH complexes

Table of Contents

General considerations

This Doctoral Thesis has been carried out in the group *Design of organometallics molecules and applications* in the Institute of Chemical Research of Seville (mixed center between the University of Seville and the Spanish Research Council), under the supervision of Dr. Salvador Conejero and Dr. Amor Rodríguez (both of them Tenured Scientists of the Spanish Research Council). The content of this thesis is included in the field of inorganic chemistry, and more specifically in organometallic chemistry and homogeneous catalysis. The results discussed herein deal with the synthesis and characterization of nickel and platinum complexes stabilized by di(phosphino)boryl (PBP) and *N*-heterocyclic carbene ligands, respectively. The reactivity shown by some of these complexes led to their utilization as catalysts in carbon dioxide reduction, C−H activation and dehydrogenative coupling processes, being the mechanism interrogated in most of the cases. In turn, several reactive intermediates have been detected and isolated.

The characterization of the synthesized compounds has been accomplished through spectroscopic and X-Ray diffraction techniques. In this latter aspect, data processing and crystal structure solving were carried out by Dr. Natalia Curado, Dr. Javier Borge (Chapters 1 and 2) and Dr. Josefina Díez (Chapter 3).

Regarding the reactivity of the complexes, experimental studies were performed as well as DFT calculations in order to obtain evidences so as we can propose plausible mechanistic pathways in which these species are involved. In this regard, it is necessary to mention that part of the calculations were developed by Dr. Joaquín López-Serrano or Prof. Agustí Lledós.

This thesis begins with a **General Introduction** followed by 4 chapters which are divided into **Introduction**, **Results and discussion**, and **References**. Last, the **Experimental Part** is located at the end of this dissertation. In order to ease

[1]

the lecture, the bibliography can be found either as footnotes or at the end of each chapter. In addition, attached to this thesis there is a CD with spectroscopic data, crystal structures and results derived from computational work, in case their query is needed. While numbering of schemes and figures is independent for each chapter, numbering of compounds is common for the whole dissertation (a laminated sheet containing all the numbered complexes can be found for a more comfortable reading).

With the purpose of obtaining the International Distinction in the PhD degree (RD 99/2011; BOE 20-02-2011, Article 15), most of the thesis is written in English, except for the **General Considerations** and **Conclusions** sections, which are available both in English and Spanish. Besides, the PhD student spent 4 months in the laboratories of Prof. Christopher C. Cummins at the Massachusetts Institute of Technology (MIT), in Cambridge (United States). The results derived from that research, which are not included in this work, consist of the utilization of sulphur oxoanions as starting material for the formation of C−S bonds.

The content of this thesis is summarized as follows: in **Chapter 1**, the synthesis and characterization of nickel complexes stabilized by a PBP ligand are described, as well as their influence in CO_2 activation and its subsequent transformation into bis(silyl)acetal derivatives. Additionally, experimental and theoretical studies are discussed, which lead to the proposal of a mechanism for the catalytic hydrosilation of CO_2.

Chapter 2 describes the synthesis and characterization of nickel boryl complexes, stabilized by the same molecular platform as in Chapter 1. Also, the structure of one of them is discussed, and the role of such species in catalytic processes of dehydrogenative borylation of styrene species is demonstrated.

[2]

In **Chapter 3**, the detection and characterization of cationic σ-silane platinum complexes stabilized by NHC ligands is accomplished. In turn, such ligands are modified so as to optimize the complex-silane interaction and to isolate several species of this kind. Moreover, the role of these compounds as reactive intermediates in C–Si and/or Pt–Si bond formation reactions is demonstrated, both by experimental and theoretical methods.

In **Chapter 4**, catalytic processes on CO_2 hydrosilation to the formic acid level and catalytic dehydrogenative coupling reactions of silanes and amines to give mono- and disilazanes are performed, utilizing some of the platinum complexes described in Chapter 3. Again, experimental and theoretical studies lead to the proposal of a mechanism for the catalytic Si–N bond formation.

Part of the results discussed herein are still unpublished, albeit there are several other fragments already published in diverse scientific journals. These publications are detailed below, along with some other papers not related to this work, but they were published during the realization of this Doctoral Thesis:

Publications

Papers related to this Doctoral Thesis

P. Ríos, N. Curado, J. López-Serrano, A. Rodríguez. Selective reduction of carbon dioxide to bis(silyl)acetal catalyzed by a PBP-supported nickel complex. *Chem. Commun.,* **2016**, *52*, 2114-2117. DOI: 10.1039/C5CC09650B

P. Ríos, A. Rodríguez, J. López-Serrano. Mechanistic Studies on the Selective Reduction of CO2 to the Aldehyde Level by a Bis(phosphino)boryl (PBP)-Supported Nickel Complex. *ACS Catal*., **2016**, *6*, 5715-5723. DOI: 10.1021/acscatal.6b01715

General Considerations

P. Ríos, J. Díez, J. López-Serrano, A. Rodríguez, S. Conejero. Cationic Platinum(II) σ-SiH Complexes in Carbon Dioxide Hydrosilation. *Chem. Eur. J.,* **2016**, *22*, 16791-16795. DOI:10.1002/chem.201603524

P. Ríos, M. Roselló-Merino, O. Rivada-Wheelaghan, J. Borge, J. López-Serrano, S. Conejero. Selective catalytic synthesis of amino-silanes at part-per million catalyst loadings. *Chem. Commun.*, **2018**, *54*, 619-622. DOI: 10.1039/C7CC08530C

P. Ríos, H. Fouilloux, P. Vidossich, J. Díez, A. Lledós, S. Conejero. Isolation of a Cationic Platinum(II) σ-Silane complex. *Angew. Chem. Int. Ed.,* **2018**, *57*, 3217-3221. DOI: 10.1002/anie.201712791

P. Ríos, H. Fouilloux, J. Díez, P. Vidossich, A. Lledós, S. Conejero. Manuscript in preparation. σ-Silane Platinum(II) Complexes as Intermediates in C–Si Bond Coupling Processes. *Manuscript in preparation*.

Papers not related to the content of this Doctoral Thesis

P. Rios, T. S. Carter, T. J. Mooibroek, M. P. Crump, M. Lisbjerg, M. Pittelkow, N. T. Supekar, G.-J. Boons, A. P. Davis. Synthetic Receptors for the High-Affinity Recognition of O-GlcNAc Derivatives. *Angew. Chem. Int. Ed.*, **2016**, *55*, 3387-3392. DOI: 10.1002/anie.201510611

P. Ríos, T. J. Mooibroek, T. S. Carter, C. Williams, M. P. Crump, A. P. Davis. Enantioselective Carbohydrate Recognition by Synthetic Lectins in Water. *Chem. Sci.*, **2017**, *8*, 4056-4061. DOI: 10.1039/C6SC05399H

M. B. Geeson, P. Ríos, W. J. Transue, C. C. Cummins. Oxoanions of Phosphorus and Sulfur as Entryways to Carbon–Element Bond Formation. *Manuscript in preparation*.

Patents not related to the content of this Doctoral Thesis

M. B. Geeson, P. Ríos, W. J. Transue, C. C. Cummins. Method for producing trichlorosilylsulfide anion and its use in the preparation of organosulfur compounds. Application number: 62/697,037.

[5]

Consideraciones generales

La presente Tesis Doctoral se ha llevado a cabo en el grupo *Diseño de moléculas organometálicas y aplicaciones* del Instituto de Investigaciones Químicas de Sevilla (centro mixto entre la Universidad de Sevilla y el CSIC), bajo la dirección de los doctores Salvador Conejero y Amor Rodríguez (ambos Científicos Titulares del CSIC). El contenido de esta tesis se encuentra incluido en el ámbito de la química inorgánica, y más concretamente en la química organometálica y la catálisis homogénea. Los resultados que aquí se discuten tratan sobre la síntesis y caracterización de complejos de níquel y platino estabilizados por ligandos del tipo di(fosfino)borilo (PBP) y carbeno *N*-heterocíclico (NHC), respectivamente. La reactividad de varios de estos complejos condujo a su empleo como catalizadores en procesos de reducción del dióxido de carbono, activación C−H, y acoplamiento deshidrogenante, estudiándose el mecanismo en la mayoría de los casos. A su vez, se ha llevado a cabo la detección y el aislamiento de diversos intermedios de reacción.

La caracterización de los complejos obtenidos se ha realizado a través de técnicas espectroscópicas y de difracción de rayos X. En este último aspecto, el tratamiento de datos y la resolución de estructuras cristalinas fueron realizados por la Dra. Natalia Curado, el Dr. Javier Borge (capítulos 1 y 2) y la Dra. Josefina Díez (capítulo 3).

Con respecto a la reactividad de los complejos, se hicieron pruebas experimentales y estudios teóricos por medio de cálculos DFT con el fin de obtener evidencias que permitiesen proponer rutas mecanísticas plausibles en la que estas especies estuviesen involucradas. En este punto, es necesario mencionar que una parte de los cálculos DFT fueron llevados a cabo por el Dr. Joaquín López-Serrano o el Prof. Agustí Lledós.

La Tesis comienza con una **Introducción General**, seguida por 4 capítulos que se subdividen en **Introducción**, **Resultados y Discusión**, y **Referencias**. Por último, la **Parte Experimental** se encuentra al final de este trabajo. Con el objetivo de facilitar la lectura de este trabajo, la bibliografía empleada se encuentra referenciada a pie de página y al final de cada capítulo. Además, con esta Tesis se encuentra adjunto un CD con datos espectroscópicos, estructuras cristalinas y resultados derivados de los estudios computacionales, en caso de que fuese necesaria su consulta. Mientras que la numeración de esquemas y figuras es independiente para cada capítulo, la numeración de los compuestos es común para toda la Tesis (se adjunta hoja plastificada suelta con todos los complejos numerados para una lectura más cómoda).

Con objeto de obtener la Mención Internacional en el título de Doctor (RD 99/2011; BOE 20-02-2011, Artículo 15), la mayoría de la Tesis está redactada en inglés, exceptuando las **Consideraciones Generales** y las **Conclusiones**, las cuales se encuentran disponibles tanto en inglés como en español. Además, se realizó una estancia de 4 meses en los laboratorios del profesor Christopher C. Cummins en el Instituto Tecnológico de Massachusetts (MIT), en Cambridge (Estados Unidos). Dichos resultados, los cuales no se incluyen en esta memoria, consisten en el empleo de oxoaniones de azufre como materiales de partida para la formación de enlaces C–S.

El contenido de la tesis se resume de la siguiente forma: en el **Capítulo 1**, se describe la síntesis y caracterización de complejos de níquel estabilizados por un ligando PBP, su influencia en la activación del CO_2 y su posterior transformación en derivados de bis(silil)acetal. Adicionalmente, se discuten estudios experimentales y teóricos que conllevan a la propuesta de un mecanismo para la hidrosililación catalítica del CO_2.

Consideraciones Generales

En el **Capítulo 2**, se lleva a cabo la síntesis y caracterización de borilos de níquel, utilizando para ello la misma plataforma molecular que en el Capítulo 1. Asimismo, se discute la estructura de uno de ellos, y se demuestra el empleo de estas especies en procesos catalíticos de borilación deshidrogenante de estirenos.

En el **Capítulo 3**, se efectúa la detección y caracterización de complejos σ-silano de platino catiónicos estabilizados por ligandos NHC. A su vez, se modulan dichos ligandos para optimizar la interacción complejo-silano, y así, poder aislar varias especies de esta clase. De manera adicional, se demuestra su papel como intermedios reactivos en la formación de enlaces C–Si y/o Pt–Si tanto de manera experimental como por medios computacionales.

En el **Capítulo 4**, se llevan a cabo experimentos catalíticos de hidrosililación de dióxido de carbono al nivel de ácido fórmico y de acoplamiento deshidrogenante de silanos y aminas para dar mono- y disilazanos, utilizando para ello algunos complejos de platino estudiados en el Capítulo 3. Nuevamente, se llevan a cabo estudios experimentales y teóricos que permitan proponer un mecanismo en la formación de los enlaces Si–N.

Parte de los resultados comentados en este trabajo se encuentra aún sin publicar, aunque hay otros fragmentos que están publicados y pueden consultarse en diversas revistas científicas. A continuación se detallan sus datos, a la vez que se indica la información pertinente a otras publicaciones no relacionadas con este trabajo, pero que se publicaron durante la realización de esta Tesis Doctoral.

Publicaciones

Artículos relacionados con esta Tesis Doctoral

P. Ríos, N. Curado, J. López-Serrano, A. Rodríguez. Selective reduction of carbon dioxide to bis(silyl)acetal catalyzed by a PBP-supported nickel complex. *Chem. Commun.,* **2016**, *52*, 2114-2117. DOI: 10.1039/C5CC09650B

P. Ríos, A. Rodríguez, J. López-Serrano. Mechanistic Studies on the Selective Reduction of CO2 to the Aldehyde Level by a Bis(phosphino)boryl (PBP)-Supported Nickel Complex. *ACS Catal*., **2016**, *6*, 5715-5723. DOI: 10.1021/acscatal.6b01715

P. Ríos, J. Díez, J. López-Serrano, A. Rodríguez, S. Conejero. Cationic Platinum(II) σ-SiH Complexes in Carbon Dioxide Hydrosilation. *Chem. Eur. J.,* **2016**, *22*, 16791-16795. DOI:10.1002/chem.201603524

P. Ríos, M. Roselló-Merino, O. Rivada-Wheelaghan, J. Borge, J. López-Serrano, S. Conejero. Selective catalytic synthesis of amino-silanes at part-per million catalyst loadings. *Chem. Commun*., **2018**, *54*, 619-622. DOI: 10.1039/C7CC08530C

P. Ríos, H. Fouilloux, P. Vidossich, J. Díez, A. Lledós, S. Conejero. Isolation of a Cationic Platinum(II) σ-Silane complex. *Angew. Chem. Int. Ed.,* **2018**, *57*, 3217-3221. DOI: 10.1002/anie.201712791

P. Ríos, H. Fouilloux, J. Díez, P. Vidossich, A. Lledós, S. Conejero. Manuscript in preparation. σ-Silane Platinum(II) Complexes as Intermediates in C−Si Bond Coupling Processes. *Manuscript in preparation*.

Artículos no relacionados con el contenido de esta Tesis Doctoral

P. Rios, T. S. Carter, T. J. Mooibroek, M. P. Crump, M. Lisbjerg, M. Pittelkow, N. T. Supekar, G.-J. Boons, A. P. Davis. Synthetic Receptors for the High-Affinity

Recognition of O-GlcNAc Derivatives. *Angew. Chem. Int. Ed.*, **2016**, *55*, 3387-3392. DOI: 10.1002/anie.201510611

P. Ríos, T. J. Mooibroek, T. S. Carter, C. Williams, M. P. Crump, A. P. Davis. Enantioselective Carbohydrate Recognition by Synthetic Lectins in Water. *Chem. Sci.*, **2017**, *8*, 4056-4061. DOI: 10.1039/C6SC05399H

M. B. Geeson, P. Ríos, W. J. Transue, C. C. Cummins. Oxoanions of Phosphorus and Sulfur as Entryways to Carbon–Element Bond Formation. *Manuscript in preparation*.

Patentes no relacionadas con el contenido de esta Tesis Doctoral

M. B. Geeson, P. Ríos, W. J. Transue, C. C. Cummins. Method for producing trichlorosilylsulfide anion and its use in the preparation of organosulfur compounds. Application number: 62/697,037.

Abbreviations

η	Hapticity
κ	Denticity
9-BBN	9-borabicyclo[3.3.1]nonane
APCI	Atmospheric Pressure Chemical Ionization
BAr_4^F	Tetrakis(3,5-bis(trifluoromethyl)phenyl)borate
BCF	Tris(pentafluorophenyl)borane
BCP	Bond Critical Point
BDE	Bond dissociation energy
BICAAC	Bicyclic Alkyl Amino Carbene
Bu	Butyl
CAAC	Cyclic Alkyl Amino Carbene
Cat	Catechol
CBC	Covalent Bond Classification
COD	1,5-Cyclooctadiene
Cp	Cyclopentadienyl
Cp*	Pentamethylcyclopentadienyl
Cy	Cyclohexyl
DCM	Dichloromethane
DFT	Density Functional Theory
DHB	Dehydrogenative borylation
Dme	1,2-dimethoxyethane
DMF	*N,N*-dimethylformamide
ESI	Electrospray Ionization
Et	Ethyl

[11]

Abbreviations

FAB	Fast Atom Bombardment
FLP	Frustrated Lewis Pair
GC	Gas Chromatography
HMDS	Hexamethyldisilazide
HOMO	Highest Occupied Molecular Orbital
HPLC	High Performance Liquid Chromatography
HRMS	High Resolution Mass Spectrometry
IMes	1,3-Bis(2,4,6-trimethylphenyl)imidazol-2-ylidene
IMes*	4,5-Dimethyl-1,3-bis-(2,4,6-trimethylphenyl)-imidazol-2-ylidene
I^{i}Pr	1,3-diisopropyl-4,5-dimethylimidazol-2-ylidene
IPr	1,3-bis-(2,6-diisopropylphenyl)-imidazol-2-ylidene
IR	Infra-red
IRC	Intrinsic Reaction Coordinate
I^{t}Bu	1,3-di-*tert*-butylimidazol-2-ylidene
KIE	Kinetic Isotope Effect
LA	Lewis Acid
LMO	Localized Molecular Orbitals
LUMO	Lowest Unoccupied Molecular Orbital
Me	Methyl
Mes	Mesityl
NBE	2-norbornene
NBO	Natural Bond Orbital
NHC	*N*-Heterocyclic Carbene
ORTEP	Oak Ridge Thermal Ellipsoid Plot
PBP	Bis(posphino)boryl

[12]

PES	Potential Energy Surface
Ph	Phenyl
Pin	Pinacol
Pr	Propyl
QTAIM	Quantum Theory of Atoms In Molecules
RCP	Ring Critical Point
r.t.	Room temperature
S_N2	Bimolecular nucleophilic substitution
TEP	Tolman Electronic Parameter
THF	Tetrahydrofuran
TM	Transition metal
TOF	Turnover frequency
TON	Turnover number
TS	Transition state
$\%V_{bur}$	Percent Buried Volume
VBE	Vinyl Boronate Ester
VSEPR	Valence Shell Electron Pair Repulsion
WBI	Wiberg Bond Index
ZPE	Zero-point energy

NMR abbreviations
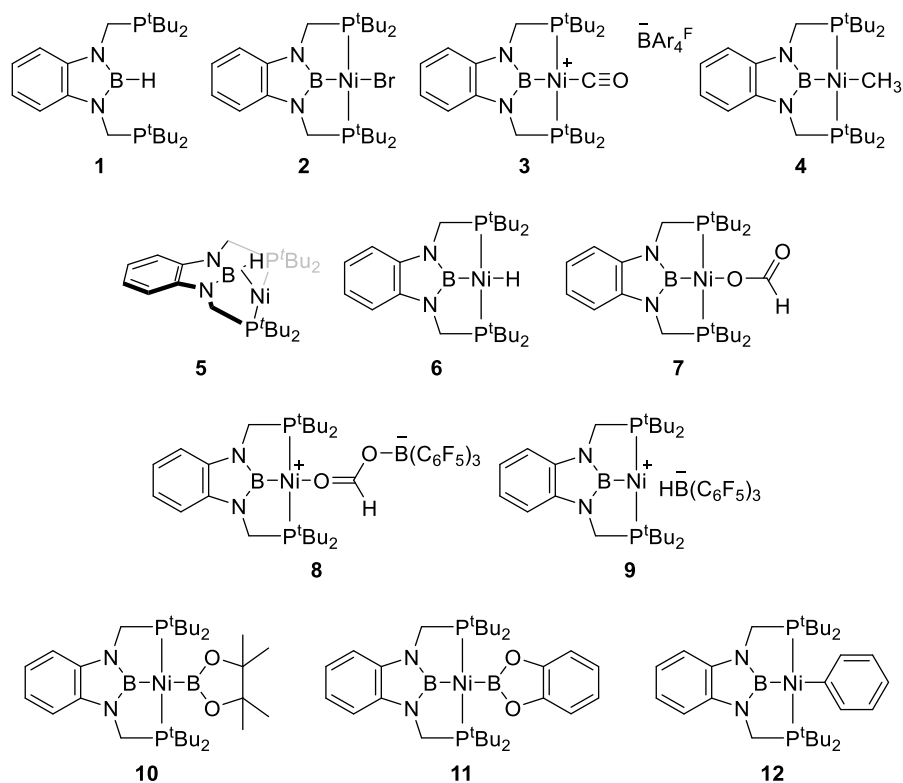
δ	Chemical Shift
COSY	Correlation Spectroscopy
HMBC	Heteronuclear Multiple Bond Correlation
HMQC	Heteronuclear Multiple-Quantum Correlation

[13]

Abbreviations
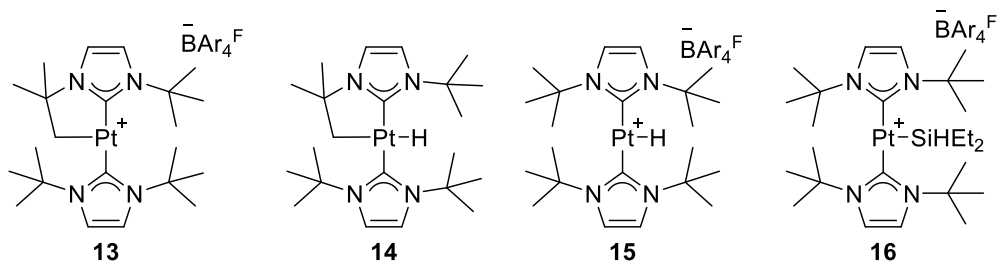

HSQC   Heteronuclear Single Quantum Coherence Spectroscopy

J   Coupling constant

NMR   Nuclear Magnetic Resonance

NOESY   Nuclear Overhauser Effect Spectroscopy

ppm   parts per million

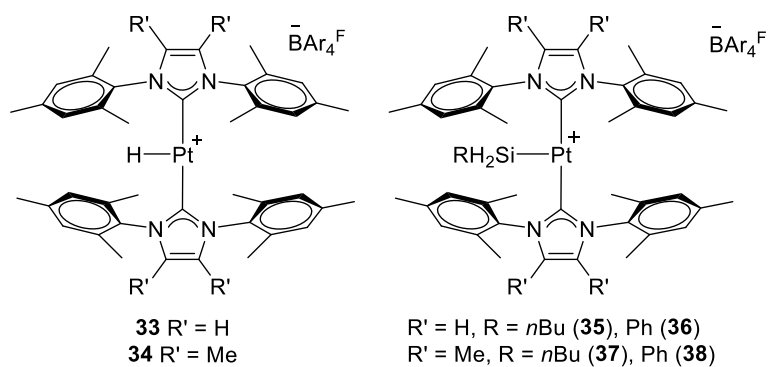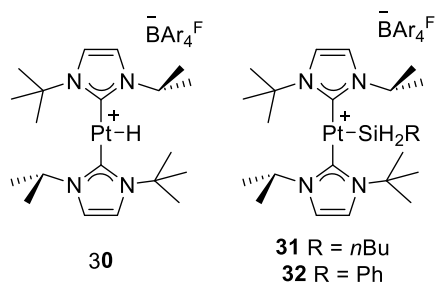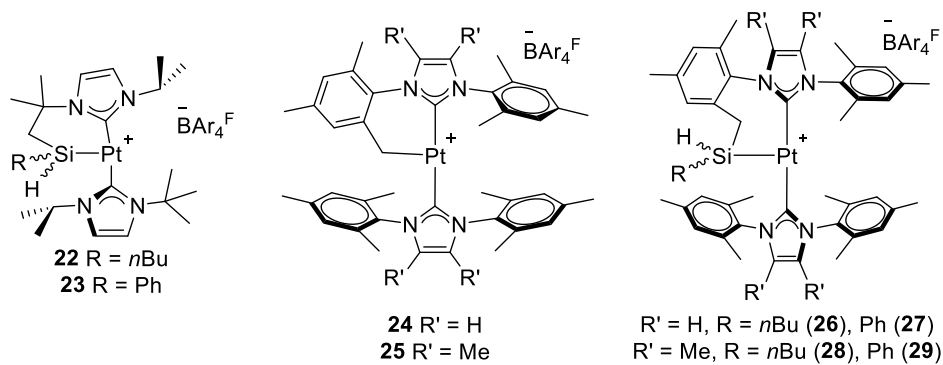## Summary of the complexes described throughout this thesis

Chapters 1 and 2

1 **2** **3** **4**

5 **6** **7**

8 **9**

10 **11** **12**

Chapters 3 and 4

13 **14** **15** **16**

Summary of compounds

17

18

19

R = Et, **20**
R = Ph, **21**

22 R = *n*Bu
23 R = Ph

24 R' = H
25 R' = Me

R' = H, R = *n*Bu (**26**), Ph (**27**)
R' = Me, R = *n*Bu (**28**), Ph (**29**)

30

31 R = *n*Bu
32 R = Ph

33 R' = H
34 R' = Me

R' = H, R = *n*Bu (**35**), Ph (**36**)
R' = Me, R = *n*Bu (**37**), Ph (**38**)

[16]

Sigma-silane complexes

$R_3Si = Et_2SiH$, **13·Et$_2$SiH$_2$**
$R_3Si = {}^nBuSiH_2$, **13·BuSiH$_3$**

R = Et, **19·Et$_3$SiH**
R = Ph, **19·Ph$_3$SiH**

25·BuSiH$_3$

34·BuSiH$_3$
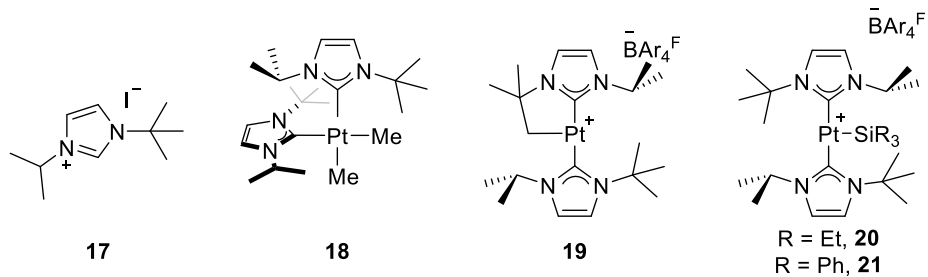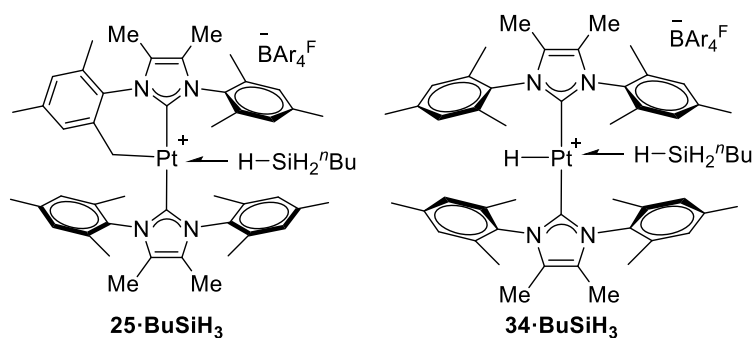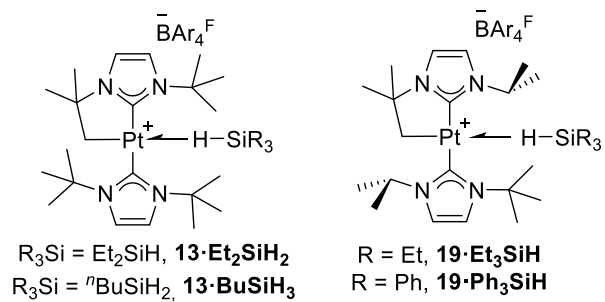
Deuterated species

15-D

39-D

40-D

41

[17]
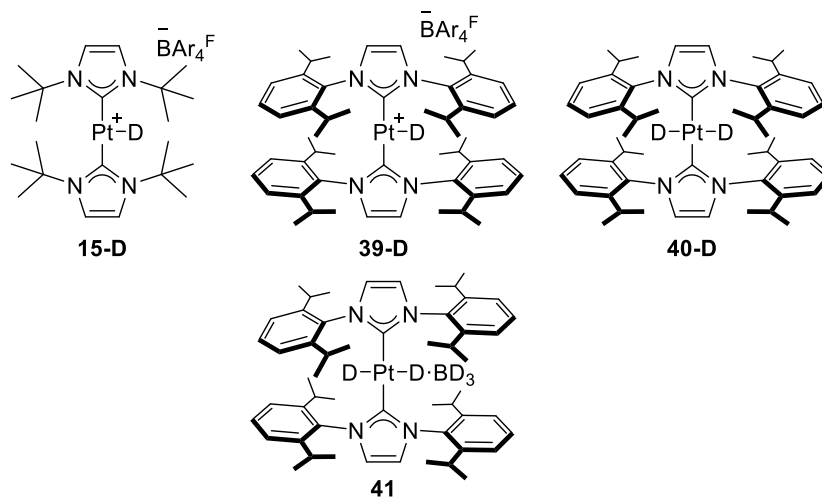
General Introduction

General Introduction

Brief description of metal-ligand interactions

Transition metals can be surrounded by some atoms, ions or molecular entities in order to form coordination compounds, or complexes. The groups bound to the metal centre are termed ligands.[1,2] In the coordination event, the nature of the bonding will depend on the type of ligand, among other aspects. A common method to classify these interactions is the Covalent Bond Classification (CBC) developed by Parkin and Green (Figure 1a).[3] According to this system, L-type ligands may be regarded as Lewis bases, since they donate 2 electrons to the metal atom (dative bond) and they do not change its oxidation state. X-type ligands can be described as radicals, and the M−X formation involves the participation of 1 electron from each fragment (covalent bond) and an increase of the oxidation state of the metal by 1. There exists a third type of ligand, named Z, composed of Lewis acids. Z-type ligands are σ-acceptor groups that interact with the metal atom by establishing a dative bond in which the metal provides the 2 electrons. However, the determination of oxidation states has given rise to some controversy,[4] given that 2 contrary points of view arised regarding the definition of the bonding in M−Z interactions: whereas Hill claimed that there is no change in the oxidation state upon the formation of a M−Z bond,[5] Parkin stated that the metal atom increases its oxidation state in 2 units (Figure 1b).[6] These cases are the limiting situations of a wide range of different types of metal−Z ligand interactions, and a M−Z bond of a certain complex will fall within

[1] F. A. Cotton, G. Wilkinson, *Advanced Inorganic Chemistry*, 3rd Edition (**1972**). Wiley-Interscience.

[2] R. H. Crabtree, *The Organometallic Chemistry of the Transition Metals,* 4th Edition (**2005**). Wiley-Interscience.

[3] M. L. H. Green, G. Parkin, *J. Chem. Educ.,* **2014**, *91*, 807-816.

[4] A. Amgoune, D. Bourissou, *Chem. Commun.,* **2011**, *47*, 859-871.

[5] A. F. Hill, *Organometallics*, **2006**, *25*, 4741-4743.

[6] G. Parkin, *Organometallics*, **2006**, *25*, 4744-4747.

these two opposite scenarios. Fortunately, numerous pieces of information are available at our disposal for describing this kind of bonds, derived from experimental (NMR spectroscopy, X-Ray crystallography) and theoretical data (Topological analysis, NBO and/or molecular orbital studies).[7]
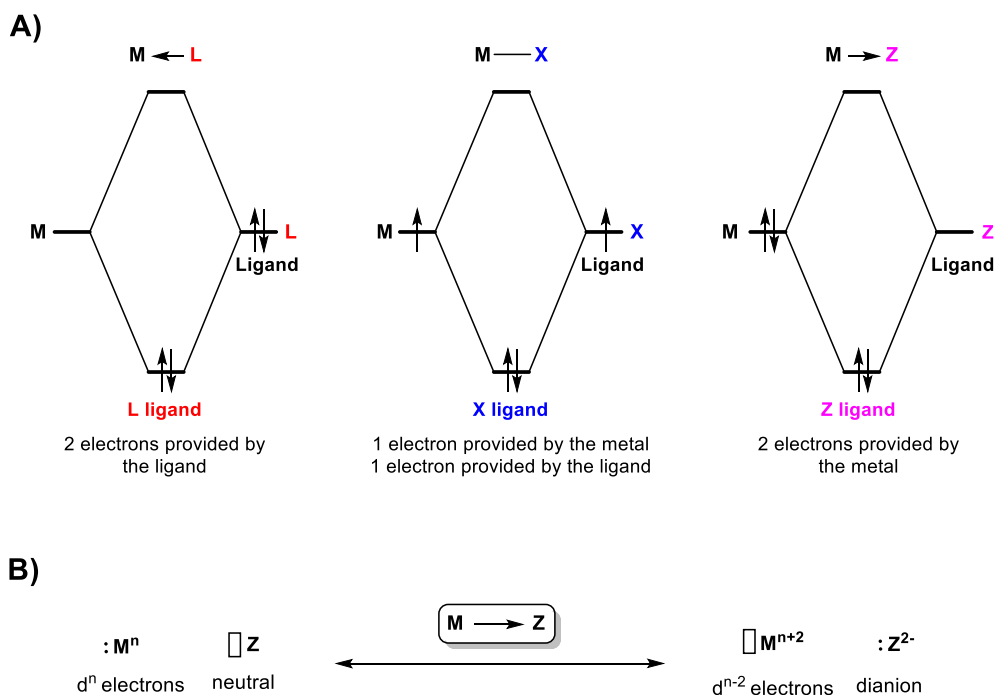

Figure 1. a) Molecular orbital diagrams displaying the different metal–ligand bonding situations according to the Covalent Bond Classification (adapted from reference 3). b) Limiting bonding scenarios for a M–Z bond (adapted from references 4 and 7).

Figure 1a exemplifies a scenario where a single pair of electrons is shared between the metal and the ligand. However, ligands can interact with a metal atom through a combination of the 3 situations described above (*e.g.* a benzene ring and a cyclopentadienyl anion can behave as L_3 and a L_2X ligands, respectively, Figure 2A). Additionally, in some cases the metal–ligand bond can

[7] G. Bouhadir, D. Bourissou in *The Chemical Bond III. Structure and Bonding* (**2006**), vol. 171. Springer, Cham. *Chapter 5: Coordination of Lewis Acids to Transition Metals: Z-Type Ligands*.

be strengthened because of electron density donation from the metal through its filled *d* orbitals (if they are high enough in energy), provided the already bound ligands possess energetically accessible π* orbitals of the right symmetry. This phenomenon is termed back-bonding, and it gives multiple bond character to the metal–ligand fragment (Figure 2B).[8] This should not be mistaken with the M–Z bonding situation, where a σ-bond is formed. In back-bonding, the orbitals involved possess π character.
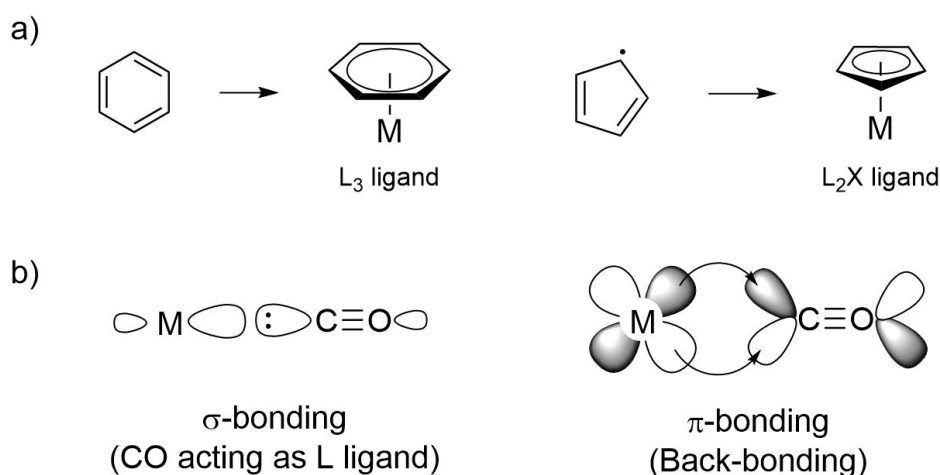

Figure 2. a) Different coordination modes depending on the nature of the ligand. b) Orbital description of the back-bonding phenomenon in a CO ligand (adapted from references 2 and 8).

Ligand Design

The reactivity and stability of the transition metal complexes is greatly influenced by the nature of the ligands surrounding the metal atom. In fact, there is a wide variety of parameters of the ligands (involving steric and/or electronic properties, in most of the cases) that can be modified and modulated so the resulting complexes possess certain properties. In this way, as it will be seen

---

[8] R. J. Lundgren, M. Stradiotto in *Ligand Design in Metal Chemistry: Reactivity and Catalysis.* 1st Edition (**2016**). John Wiley & Sons, Ltd. *Chapter 1: Key Concepts in Ligand Design: An Introduction*.

throughout this thesis, ligand design can be used to produce complexes capable of achieving the activation of *a priori* inert molecules (Chapter 1), catalytically obtaining a specific product in a selective manner (Chapters 1 and 4), or detecting and isolating intermediates whose nature is elusive and highly reactive (Chapters 2 and 3).

The following sections will describe the ligands employed during this thesis. At the same time, such description will be leveraged to explain some of the ligand properties (highlighted in bold) that are fundamental in the design process and that were taken into account when synthesizing the corresponding transition metal complexes.

Bis(phosphino)boryl (PBP) ligand

General features

The ligand utilized in the first 2 chapters of this thesis is the bis(phosphino)boryl (PBP) ligand, which is shown in Figure 3 in its hydroborane form ($C_6H_4\{N(CH_2PR_2)\}_2BH$).
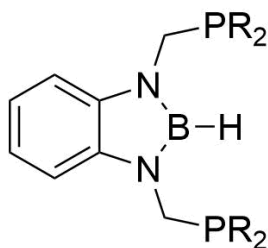

**Figure 3.** General structure of the bis(phosphino)boryl (PBP) ligand in its hydroborane form.

Originally developed by Yamashita and Nozaki in 2009,[9] the first appreciable feature that comes to mind at first glance is the presence of various donor atoms such as the phosphine groups. This makes this molecule a

---

[9] Y. Segawa, M. Yamashita, K. Nozaki, *J. Am. Chem. Soc.,* **2009**, *131*, 9201-9203.

polydentate ligand. Thus, its coordination to a metal group will take advantage of the **chelate effect**, which consists of the increased stability of polydentate ligands in comparison to monodentate ones when they are coordinated to a metal atom. This can be easily illustrated with the example of the displacement of ammonia (monodentate) ligands by the coordination of ethylenediamine (polydentate, chelating ligand), as shown in Scheme 1. It can be clearly seen that this displacement changes the number of free molecules from 4 to 7. This great increase in entropy makes the process thermodynamically favourable.[2]
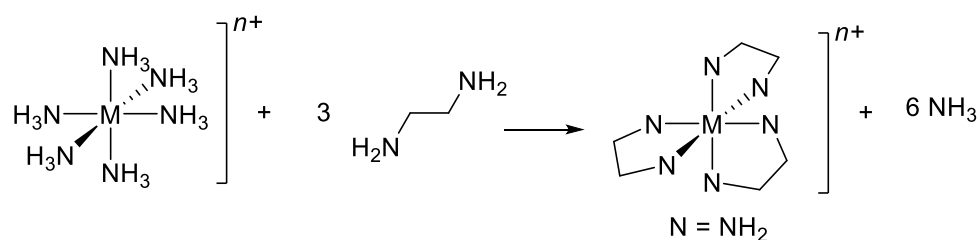

Scheme 1. Substitution of ammonia by ethylenediamine, illustrating the chelate effect (adapted from reference 2).

The designers of the PBP ligand observed activation of the B−H bond upon coordination to the transition metal center.[9] This reaction converts this molecule into an anionic tridentate ligand with adjacent donor atoms (Scheme 2).[10] For this reason, the PBP fragment is a **pincer ligand**. This type of ligands has been appearing in the literature for around 40 years and they are widely used in homogeneous catalysis, given that pincer-based transition metal complexes are capable of efficiently catalyse transformations such as cross-coupling, dehydrogenation or polymerization reactions as well as transforming challenging small molecules like CO_2, H_2 or O_2.[11]

---

[10] The authors conclude that they observe the boryl hydride arrangement displayed in Scheme 2, given that NMR, DFT and X-Ray studies rule out a σ-BH coordination mode.
[11] a) M. E. van der Boom, D. Milstein, *Chem. Rev.,* **2003**, *103*, 1759-1792; b) G. van Koten, D. Milstein, *Organometallic Pincer Chemistry*, **2012**, Springer, Heidelberg.
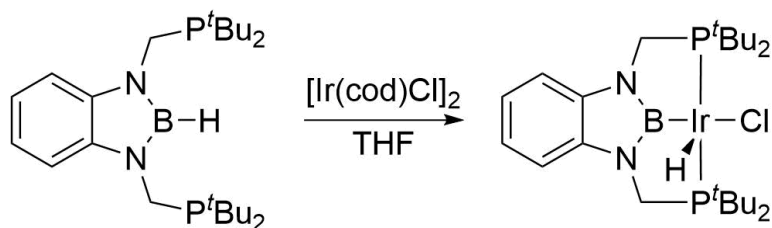
Scheme 2. Coordination of the PBP molecule to give the first transition metal complex possessing a tridentate boryl ligand (adapted from reference 9).

The majority of the pincer ligands described to date contain carbon or nitrogen as the central atom that establishes a σ-bond with the metal. Whereas the presence of boryl ligands in the coordination sphere of transition metal complexes was limited to 1,2-dioxo derivatives such as catechol (Bcat) or pinacol (Bpin), the utilization of trivalent nitrogen to form B−N bonds has opened the door to the possibility of obtaining branched boryl groups, giving rise to pincer ligands like the one used in this thesis.[9,12] However, alternative strategies have been developed to obtain pincer ligands with boryl functionalities in the central position. Some of them include the utilization of the ambiphilic (containing L and Z type ligands) diphosphanyl borane developed by Bourissou *et al.* in 2006[13] (Scheme 3a), which undergoes C−B oxidative addition in the presence of the iridium dimer [(COE)$_2$IrCl]$_2$ to give complex (PBP)Ir(Ph)(Cl), as demonstrated by the group of Ozerov.[14] In some cases, 2nd row metals like rhodium yield mixtures of PBP compounds (featuring metal−borane and metal−boryl interactions), given the lower tendency of 4d metals to undergo oxidative addition reactions against 5d ones.[14,15] Other procedures take advantage of the rigidity of a

[12] H. Braunschweig, M. Colling, *Coord. Chem. Rev.,* **2001**, *223*, 1-51.

[13] S. Bontemps, H. Gornitzka, G. Bouhadir, K. Miqueu, D. Bourissou, *Angew. Chem. Int. Ed.,* **2006**, *45*, 1611-1614.

[14] W-C. Shih, W. Gu, M. C. MacInnis, S. D. Timpa, N. Bhuvanesh, J. Zhou, O. V. Ozerov, *J. Am. Chem. Soc.,* **2016**, *138*, 2086-2089.

[15] W-C. Shih, W. Gu, M. C. MacInnis, D. E. Herbert, O. V. Ozerov, *Organometallics*, **2017**, *36*, 1718-1726.

carborane unit, like the ones shown in Scheme 3b, where the incorporation of the "arms" produces the corresponding tridentate scaffolds.[16]

a)

Bourissou
2016

[(COE)$_2$IrCl]$_2$
-COE

Ozerov
2016

b)

● = BH   E = S, Se

Mirkin
2009

● = BH   M = Ni, Rh, Pd

Nakamura
2011

● = BH   R = ^{i}Pr

Popov
Peryshkov
2016
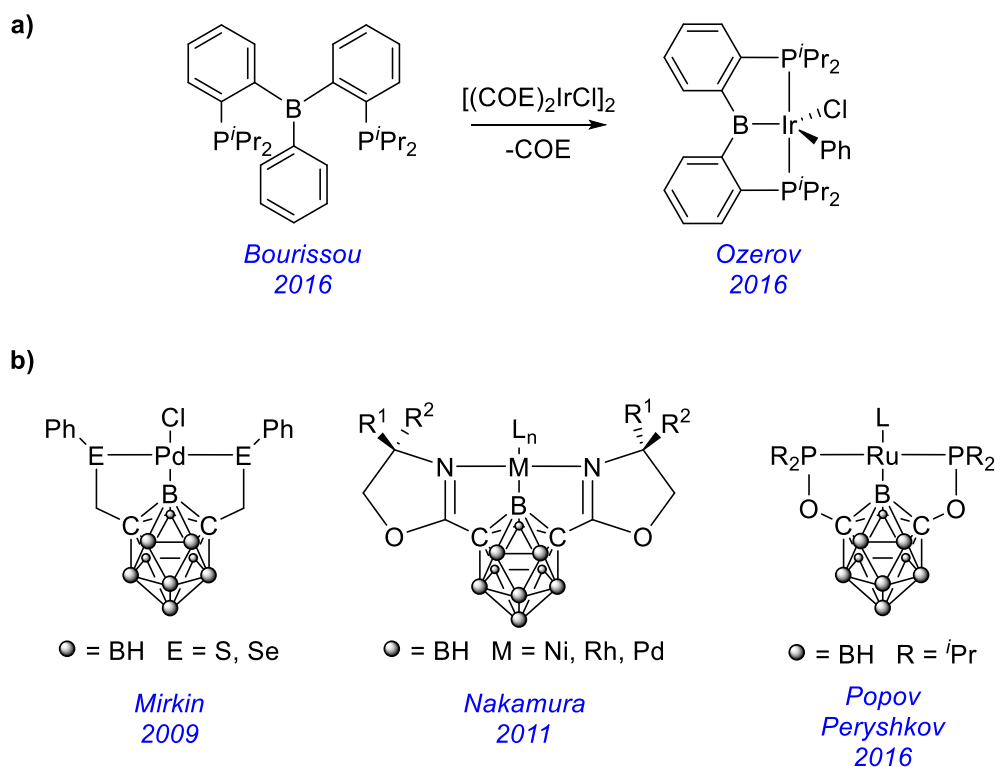
Scheme 3. Alternative methods to obtain transition metal complexes stabilized by boryl-based pincer ligands (adapted from references 13 and 14).

The many reasons that explain the success of pincer ligands are related to the high level of steric and electronic modulability that these ligands can impart on the metal complexes, leading to numerous opportunities in the field of catalysis.[17] They are summarized in Figure 4, and some of them will be described

[16] a) A. M. Spokoyny, M. G. Reuter, C. L. Stern, M. A. Ratner, T. Seiderman, C. A. Mirkin, *J. Am. Chem. Soc.,* **2009**, *131*, 9482-9483; b) M. E. El-Zaria, H. Arii, H. Nakamura, *Inorg. Chem.,* **2011**, *50*, 4149-4161; c) B. J. Eleazer, M. D. Smith, A. A. Popov, D. V. Peryshkov, *J. Am. Chem. Soc.,* **2016**, *138*, 10531-10538.

[17] E. Peris, R. H. Crabtree, *Chem. Soc. Rev.,* **2018**, *47*, 1959-1968.

in detail in this section, given their implications in the results of this work. One of the most important features of these frameworks is the stabilization they confer to the metal complexes, preventing metal leaching during the catalytic processes, which sometimes require harsh temperature and pressure conditions.[18]
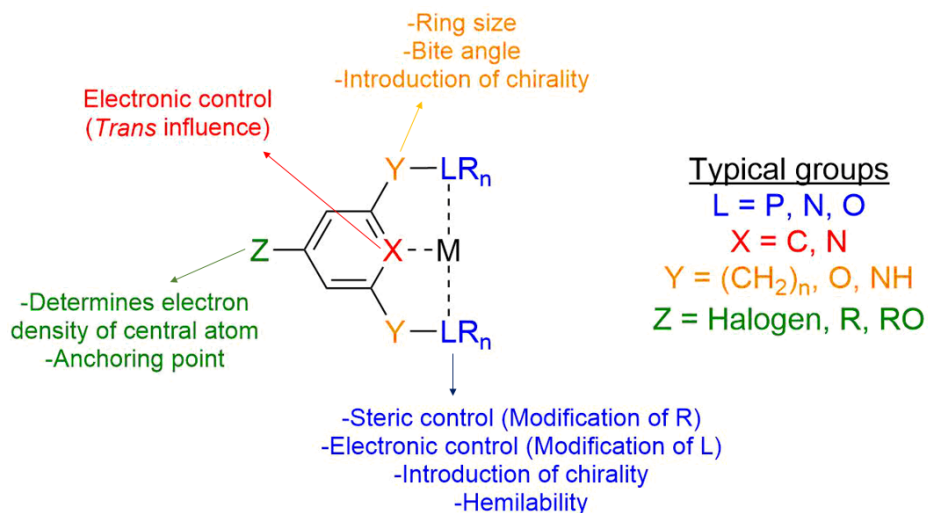

Figure 4. General structure of a pincer ligand bound to a metal atom and description of the parameters that can be modified upon modification of its structure (adapted from reference 17).

Boryl groups: electronic properties

Boryl ligands possess the general formula –BR_2, and their main feature is the presence of an anionic, sp^2-hybridized boron atom. These compounds will behave as X ligands upon coordination to a transition metal center. As the majority of the ligands, this will take place through a σ-bond (as depicted in Figure 5a), yet the presence of an *a priori* empty p orbital in the boron atom makes the boryl group a π-acceptor ligand, and may lead to back-bonding phenomena (Figure 5b). However, this will depend on the R substituents on the

---

[18] M. A. W. Lawrence, K-A. Green, P. N. Nelson, S. C. Lorraine, *Polyhedron*, **2018**, *143*, 11-27.

boron atom, since π-donor groups like oxygen or nitrogen can also donate electron density to the boron p orbital (Figure 5c), increasing the energy of the boryl acceptor π* orbital and diminishing the degree of back-bonding from the metal.[19] For this reason, the contribution of back-bonding to the overall M–B bond density is small (even in $B(C_6F_5)_2$ compounds, Table 1),[20] with values of around 15-20% at the most.[21] Although this might be seen as a competition between both parts for the p orbital of boron, the truth is that there is a synergy between them, because the lack of electron density on B must be compensated from the substituents (if the metal is not able to undergo back-bonding) or vice versa. Thus, both fragments will play a role in the stability of the boryl ligand, which will in turn have a great influence on the reactivity of the complex.[22]
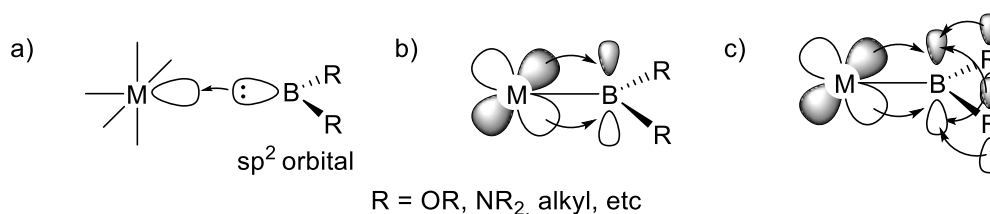

Figure 5. Orbital interactions during the metal–boryl coordination. a) σ-bonding. b) π back-bonding. c) Competitive π interactions between the metal and the R groups (adapted from reference 19).

[19] D. L. Kays, S. Aldridge in *Contemporary Metal Boron Chemistry I*, **2008**. Springer-Berlag Berlin Heidelberg. *Chapter 2: Transition metal boryl complexes.* Pages 29-122.

[20] A. Al-Fawaz, S. Aldridge, D. L. Coombs, A. A. Dickinson, D. J. Willock, L-L. Ooi, M. E. Light, S. J. Coles, M. B. Hursthouse, *Dalton Trans.,* **2004**, 4030-4037.

[21] A. A. Dickinson, D. J. Willock, R. J. Calder, S. Aldridge, *Organometallics*, **2002**, *21*, 1146-1157.

[22] G. J. Irvine, M. J. G. Lesley, T. B. Marder, N. C. Norman, C. R. Rice, E. G. Robins, W. R. Roper, G. R. Whittell, L. J. Wright, *Chem. Rev.,* **1998**, *98*, 2685- 2722.

Complex $(\eta^5\text{-}C_5H_5)Fe(CO)_2BR_2$

R	Calculated d(Fe–B)/Å[a]	Orbital contribution to Fe–B bond (%)	
		σ	π
C_6F_5	2.006 (1.965)	81.9	18.0
C_6H_5	2.107 (2.034)	90.4	9.5
H	1.988	84.1	15.8
F	2.010	94.0	6.0
Cl	2.008 (1.942)	82.1	17.8

Table 1. Influence of the boron substituents on the Fe–B bond in complex $(\eta^5\text{-}C_5H_5)Fe(CO)_2BR_2$.

[a] Crystallographically determined distances in parentheses (adapted from reference 20).

Another feature of the boron atom that must be taken into account when designing complexes bearing boryl functionalities is related to its electropositivity (χ = 2.0)[23] and its strong σ-donation ability. Because boryl groups are powerful σ-donors, they also are among the strongest ***trans influence*** ligands. This means that a ligand with a strong *trans* influence will weaken the metal–ligand bond of a ligand located *trans* to it because both ligands are sharing the same metal orbital for establishing their corresponding bonds. In other words, strong *trans* influence ligands "monopolize" the metal orbital due to their σ-donation ability, labilizing the metal–ligand bond *trans* to it.[24,25] This is a thermodynamic property, and the consequences of this labilization can be observed by elongation of bond lengths through X-Ray crystallography, by a decrease in certain coupling constants through NMR spectroscopy or the reduction of some stretching frequencies through IR spectroscopy. DFT methods

[23] N. N. Greenwood, A. Earnshaw, *Chemistry of the Elements*, 2nd ed. Butterworth-Heinemann: Woburn, MA, 1997.

[24] K. M. Anderson, A. G. Orpen, *Chem. Commun.,* **2001**, 2682-2683.

[25] This is a qualitative description of the concept of *trans* influence. For quantitative parameters that contribute to this property, see: J. K. Burdett, T. A. Albright, *Inorg. Chem.,* **1979**, *18*, 2112-2120.

are accurate enough to reproduce these structural changes and to correlate them to the *trans* influence of the ligands involved. In fact, Marder *et al.* ordered a large amount of ligands according to their *trans* influence, concluding that boryl groups were on top of this scale, way above hydride and alkyl ligands for example.[26]

For the reasons mentioned above, complexes bearing boryl functionalities will likely be highly reactive, which opens the door to the possibility of activating inert and thermodynamically stable species.

Steric properties of pincer ligands

Steric effects can be determinant when designing a pincer complex due to the fact that they can either protect the metal so much that the compound becomes unreactive or expose it to an extent that the molecule turns out unstable and very reactive. Thus, an intermediate situation would be ideal to achieve an appropriate robustness/activity proportion. Modification of the ancillary ligands (Figure 4, highlighted in blue) is a straightforward method to do this.

Phosphine groups are extensively used in transition metal chemistry, and their employment as ancillary ligands in pincer chemistry is extremely common.[11b] This is due to their wide availability and their easy modification, which allows the introduction of phosphine groups of many different sizes into the pincer scaffold. As a matter of fact, there are parameters which classify such species according to their steric volume, so the resulting cavity in the transition metal complexes can be predicted and designed to some extent. A good example of these parameters is the ***Tolman cone angle*** (θ), which is the apex angle of a cylindrical cone centered at the metal of a $M(PR_3)$ fragment that touches the van

---

[26] J. Zhu, Z. Lin, T. B. Marder, *Inorg. Chem.,* **2005**, *44*, 9384-9390.

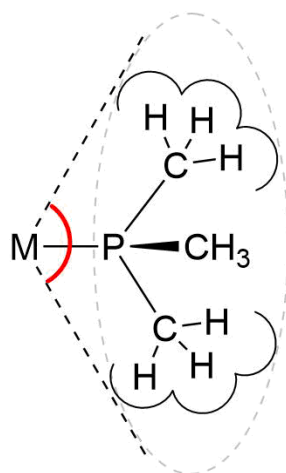der Waals radii of the substituents on P after folding them back as much as possible (Figure 6).[2,27]

Figure 6. Representation of the Tolman cone angle (highlighted in red) for the example phosphine PMe₃ (adapted from reference 2).

The importance of selecting the appropriate phosphine groups has been exemplified in the literature numerous times. For instance, Zargarian *et al.*, demonstrated that the introduction of alkyl groups (-CH$_3$ or –CH$_2$CH$_3$) into the coordination sphere of (POCOP)Ni complexes (POCOP = κ^P, κ^C, κ^P -2,6-{R$_2$PO}$_2$C$_6$H$_3$) was possible only if the substituents R on the phosphine were *iso*-propyl groups.[28] On the contrary, using diphenylphosphine as ancillary ligands rendered the compounds unstable to hydrolysis or substitution by halides (Scheme 4).[29] As a comparison, the P^{i}Pr$_2$ derivatives could be washed with water during the work-up process with no appreciable decomposition.

[27] C. A. Tolman, *Chem. Rev.,* **1977**, *77*, 313-348.

[28] V. Pandarus, D. Zargarian, *Organometallics*, **2007**, *26*, 4321-4334.

[29] A. B. Salah, D. Zargarian, *Dalton Trans.,* **2011**, *40*, 8977-8985.
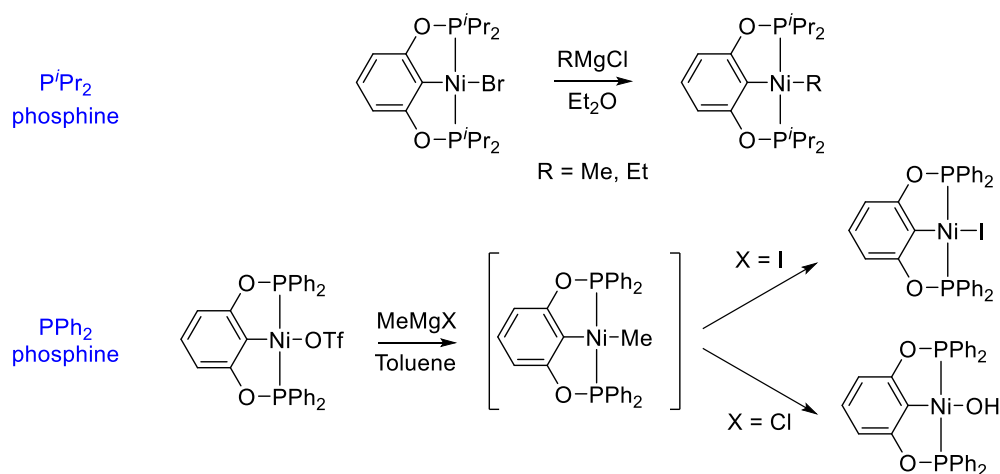
Scheme 4. Differences in reactivity depending on the phosphine groups in (POCOP)Ni complexes, as described by Zargarian *et al.*

Examples of divergent reactivity due to the steric bulk provided by the phosphine groups have also been described for PBP pincer complexes similar to those used in this thesis. Yamashita and co-workers observed a dramatic change in reactivity in (PBP)Ir complexes when these were used as catalysts for the transfer dehydrogenation reaction of cyclooctane (Scheme 5). In this case, *iso*-propyl chains were the least hindered groups, allowing the complex to perform its catalytic activity.[30] By contrast, cyclohexyl[31] and *tert*-butyl[9] groups were too bulky to allow the iridium center to interact with the substrates, leading to no catalysis. As an evidence, they compared the degree of exposure of the metal center in the three crystal structures (Figure 7), confirming their hypothesis.

---

[30] K. Tanoue, M. Yamashita, *Organometallics*, **2015**, *34*, 4011-4017.
[31] Y. Segawa, M. Yamashita, K. Nozaki, *Organometallics*, **2009**, *28*, 6234-6242.
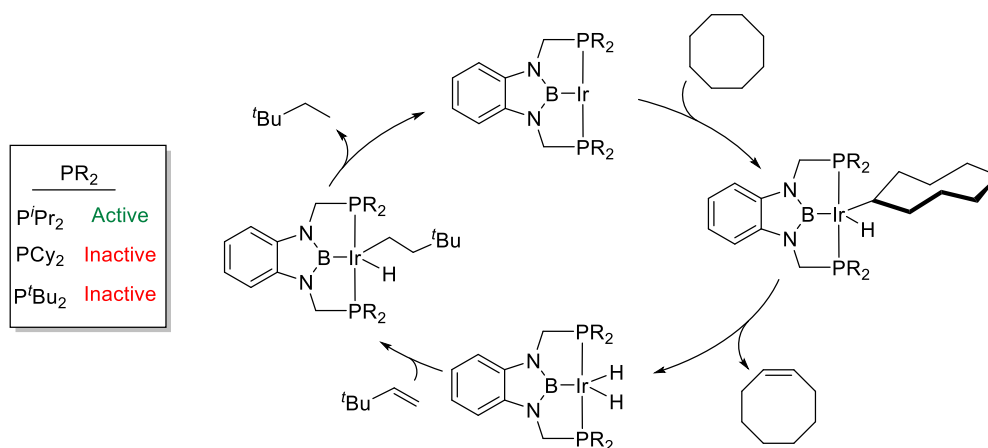
Scheme 5. Proposed cycle by Yamashita and co-workers for the catalytic dehydrogenation of cyclooctane, and comparison of the different catalysts according to their ancillary phosphine ligands (adapted from reference 30).
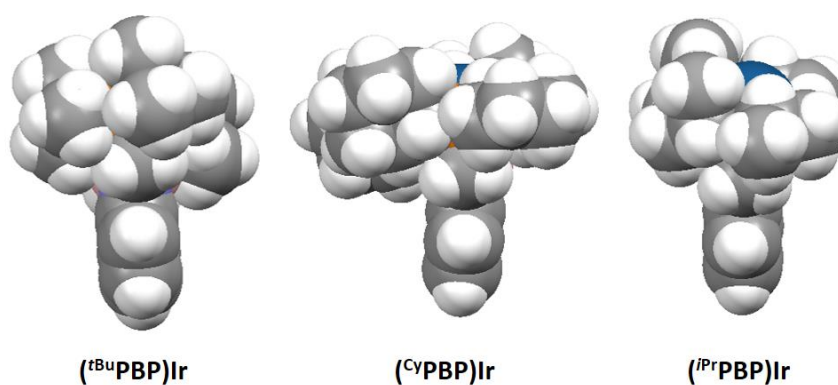

Figure 7. Comparison of the degree of exposure of the iridium center in the $(PBP)Ir(C_2H_4)$ complexes reported by Yamashita *et al.* The ethylene fragment was removed in all cases for clarity. Crystal structures obtained from references 9, 30 and 31 (adapted from reference 30).

[32]

Cooperativity in pincer ligands

Whereas initial works employed pincer ligands as mere rigid and spectator scaffolds, recent developments have shown that they can take part in chemical reactions, playing in some cases a crucial role during catalytic processes.[17,32] This **ligand cooperativity** is revealed through different mechanisms, given the great variety of tunable points of the pincer structure (Figure 4). Some diverse examples include the dearomatization of the aromatic ring that confers the rigidity to the ligand framework, like the thermal and light-driven water splitting reaction performed by Milstein *et al.* catalysed by (PNN)Ru(II) complexes (Scheme 6a), where the consecutive dearomatization/rearomatization of the pyridine moiety makes the transformation possible.[33]

Hemilability of the side arms can also be leveraged to carry out catalytic reactions. In this way, the group of Hu exploited the flexibility of the aliphatic arm in the NNN ligand shown in Scheme 6b to perform Ni-catalyzed Sonogashira couplings between primary alkyl halides and terminal alkynes at room temperature.[34] The authors emphasize the importance of the hemilability of this ligand, given that its aromatic, rigid counterpart is able to perform the same reaction albeit at much higher temperatures (100 – 140 °C), difficulting mechanistic studies and the utilization of sensitive functional groups.[35]

A different type of assistance from the ligand also includes outer-sphere interactions with the substrate. Hazari and co-workers described the establishment between a N−H bond of their (PNP)Ir(III) system and one of the oxygen atoms of carbon dioxide. This contact polarizes the CO_2 molecule, so it

[32] J. R. Khusnutdinova, D. Milstein, *Angew. Chem. Int. Ed.,* **2015**, *54*, 12236-12273.

[33] S. W. Kohl, L. Weiner, L. Schwartsburd, L. Konstantinovski, L. J. W. Shimon, Y. Ben-David, M. A. Iron, D. Milstein, *Science*, **2009**, *324*, 74-77.

[34] P. M. P. García, P. Ren, R. Scopelliti, X. Hu, *ACS Catal.,* **2015**, *5*, 1164-1171.

[35] O. Vechorkin, D. Barmaz, V. Proust, X. Hu, *J. Am. Chem. Soc.,* **2009**, *131*, 12078-12079.

can be activated upon nucleophilic attack from an adjacent hydride. This type of activation was employed in the hydrogenation of CO_2 in water to yield formate derivatives with high activity (Scheme 6c).[36]
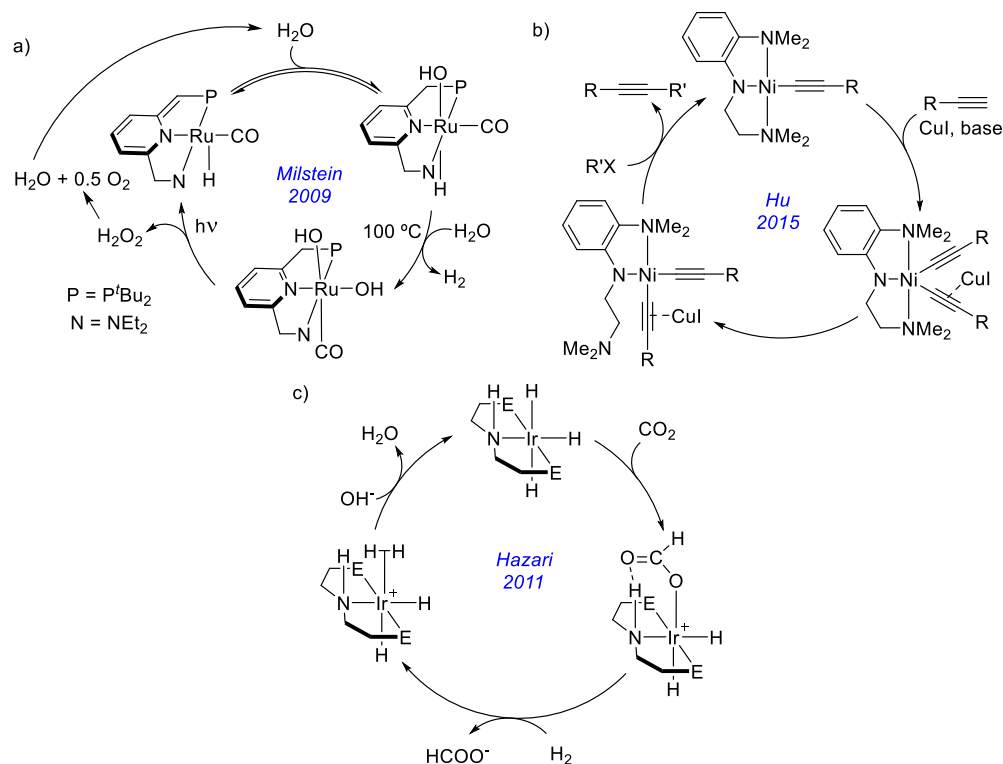
Scheme 6. Examples of assistance of pincer ligands in catalysis through a) dearomatization-rearomatization of the aromatic backbone, b) hemilability of one of the side arms or c) outer-sphere interactions (adapted from references 33, 34 and 36).

Ligand cooperativity mediated by PBP ligands has also been reported in the literature. A milestone in ligand cooperation was achieved by Peters and co-workers in 2012, where they achieved heterolytic hydrogen splitting and alkene hydrogenation by using Ni complexes stabilized by Bourissou's ambiphilic

[36] T. J. Schmeier, G. E. Dobereiner, R. H. Crabtree, N. Hazari, *J. Am. Chem. Soc.,* **2011**, *133*, 9274-9277.
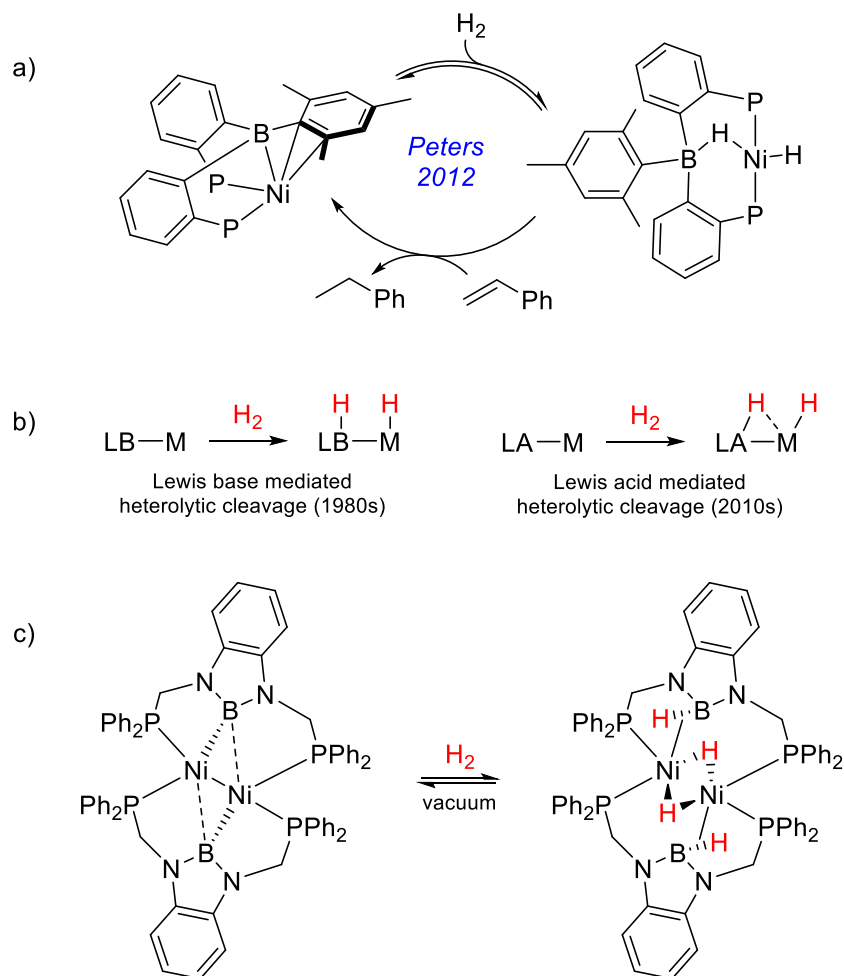
diphosphanyl boranes (Scheme 7a) similar to that described in Scheme 3.[37] This became a new way of utilizing metal–borane interactions in catalysis, given that the usual methods involved the use of Lewis bases rather than Lewis acids for the activation of substrates across a metal–ligand bond (Scheme 7b).[38] This phenomenon is not only limited to this ligand. In fact, Nozaki's bis(phosphino)boryl ligands also assist transition metal in activating small molecules like H_2. In fact, a few years ago, the Peters group demonstrated the reversible activation of dihydrogen by using a bimetallic Ni(I)Ni(I) system, as shown in Scheme 7c.[39] Additionally, as it will be seen in Chapter 1 of this thesis, our group demonstrated the crucial role of the bis(phosphino)boryl PBP ligand in the hydrogenolysis of a Ni–Me bond.

---

[37] a) W. H. Harman, J. C. Peters, *J. Am. Chem. Soc.,* **2012**, *134*, 5080-5082; b) M. Devillard, G. Bouhadir, D. Bourissou, *Angew. Chem. Int. Ed.,* **2015**, *54*, 730-732.
[38] G. R. Owen, *Chem. Commun.,* **2016**, *52*, 10712-10726.
[39] T-P. Lin, J. C. Peters, *J. Am. Chem. Soc.,* **2014**, *136*, 13672-13683.

a)

Peters
2012

b)

Lewis base mediated
heterolytic cleavage (1980s)

Lewis acid mediated
heterolytic cleavage (2010s)

c)

Scheme 7. a) and c) Examples of ligand cooperativity exhibited by PBP pincer ligands. b) General scheme of ligand-mediated heterolytic activation of small molecules (adapted from references 37a, 38 and 39).

In the first half of this thesis, the outstanding ability of nickel to activate inert substrates[40] in combination with the great reactivity of boryl ligands will be tamed by making use of some of the concepts of ligand design described above

---

[40] a) S. Z. Tasker, E. A. Standley, T. F. Jamison, *Nature*, **2014**, *509*, 299-309; b) V. P. Ananikov, *ACS Catal.,* **2015**, *5*, 1964-1971.

so as to produce stable complexes or intermediates that are able to effectively perform diverse catalytic reactions.

N-heterocyclic carbenes (NHCs)

Initial studies

Some pioneer works in the chemistry of stable carbenes started to develop around the 1960s with the work of Wanzlick, who claimed that imidazol-2-ylidenes were intermediates in the formation of tetraaminofulvenes and that there was an equilibrium between such species (Wanzlick equilibrium, Scheme 8a).[41] However, one of the first experimental evidences was provided in 1988 by the group of Bertrand, who isolated the first (phosphino)(silyl)carbene shown in Scheme 8b.[42] A few years later, Arduengo and co-workers synthesized the first isolable *N*-heterocyclic carbene thanks to the steric stabilization of adamantyl groups (Scheme 8c).[43] The stability of this molecule (whose integrity remained untouched after 7 years at room temperature dissolved in THF under a CO atmosphere)[44] demonstrated that these species could indeed be very stable depending on the surroundings around the carbene moiety. These breakthroughs were the beginning of a period, which spans until today, in which the chemistry of NHCs has advanced tremendously, transforming these compounds from mere laboratory curiosities to useful tools that are applied as

---

[41] H. W. Wanzlick, *Angew. Chem. Int. Ed.,* **1962**, *1*, 75-80. This equilibrium remained controversial for some years (see D. M. Lemal, R. A. Lovald, K. I. Kawano, *J. Am. Chem. Soc.,* **1964**, *86*, 2518-2519), but subsequent experiments proved Wanzlick right in his statement (a) Y. Liu, P. E. Lindner, D. M. Lemal, *J. Am. Chem. Soc.,* **1999**, *121*, 10626-10627; b) V. P. W. Böhm, W. A. Herrmann, *Angew. Chem. Int. Ed.,* **2000**, *39*, 4036-4038).
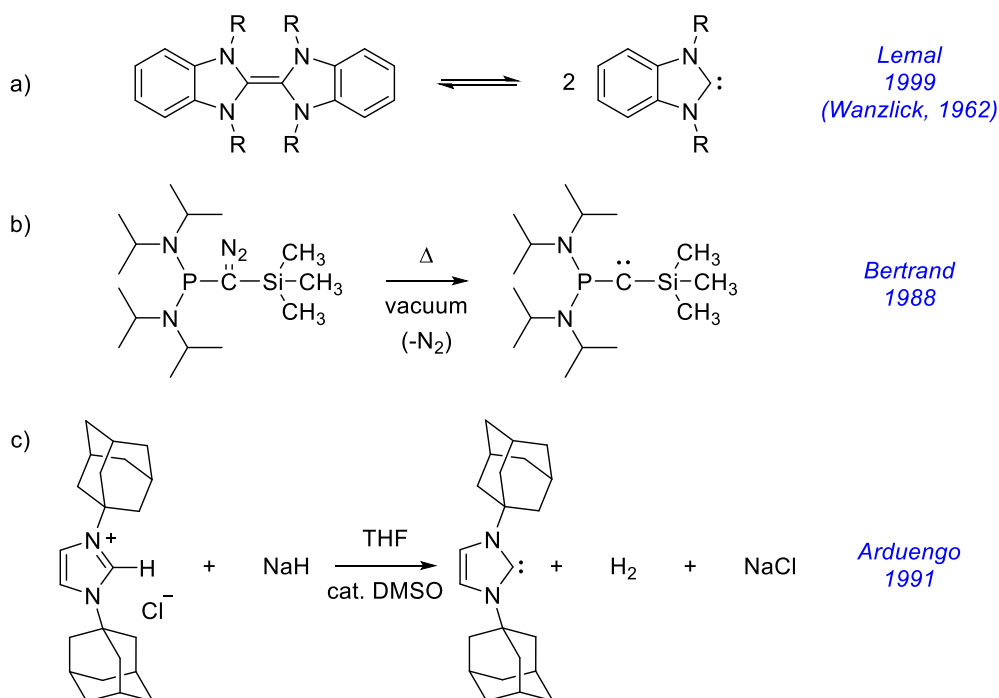
[42] A. Igau, H. Grutzmacher, A. Baceiredo, G. Bertrand, *J. Am. Chem. Soc.,* **1988**, *110*, 6463-6466.

[43] A. J. Arduengo, R. L. Harlow, M. Kline, *J. Am. Chem. Soc.,* **1991**, *113*, 361-363.

[44] A. J. Arduengo, *Acc. Chem. Res.,* **1999**, *32*, 913-921.

catalysts, in the chemical industry or in the stabilization of unusual species or materials.[45]

Scheme 8. Initial studies on carbene chemistry (adapted from references 41-43).

General features

As their own name indicate, NHCs are composed of a heterocycle ring containing a carbene unit adjacent to at least one nitrogen atom. Among these, imidazole-based carbenes (imidazol-2-ylidenes) are the most commonly used and studied.[45] The carbene moiety is a neutral fragment with 6 electrons in its valence shell. In a NHC, the lone pair of electrons on the carbon atom is usually located in a sp^2 orbital (HOMO), whereas the remaining empty p orbital

---

[45] a) W. A. Herrmann, C. Köcher, *Angew. Chem. Int. Ed.,* **1997**, *36,* 2162-2187; b) P. de Frémont, N. Marion, S. P. Nolan, *Coord. Chem. Rev.,* **2009**, *253,* 862-892; c) M. N. Hopkinson, C. Richter, M. Schedler, F. Glorius, *Nature,* **2014**, *510,* 485-496.

constitutes the LUMO. The energy difference between them (HOMO-LUMO gap, or E_{S-T}) is influenced by several factors that depend on geometrical and electronic parameters. As a consequence, the reactivity of the resulting carbene will also depend on these aspects. For instance, Figure 8 shows that linear arrangements give rise to a carbon atom with a sp hybrid orbital and 2 degenerate p orbitals.[46] Bending the carbene will favour a sp^2 hybridization on carbon, as illustrated in the figure. The magnitude of E_{S-T} (the difference between the σ and p_π orbitals) will therefore determine whether the carbene is in a singlet or triplet ground state.[47]
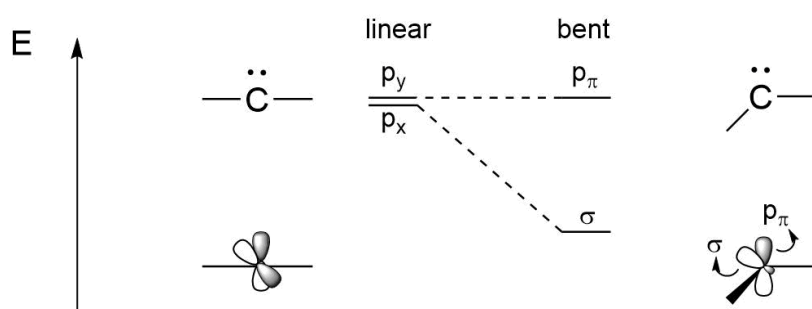

Figure 8. Distribution on the frontier orbitals depending on the geometry of the carbene (adapted from reference 46).

Apart from geometry, electronic factors also affect the HOMO-LUMO gap. In the specific case of NHCs (imidazol-2-ylidenes as a model species, since these are the carbenes employed throughout this thesis), the presence of two electronegative nitrogen atoms adjacent to the carbene fragment will stabilize the σ orbital by increasing its *s* character (inductive effects). At the same time, both N atoms possess filled π orbitals with the right symmetry to overlap with the empty p_π orbital of the carbene. Figure 9 shows how this overlap increases even more the value of E_{S-T} (mesomeric effects). For these reasons, NHCs are

---

[46] D. Bourissou, O. Guerret, F. P. Gabbai, G. Bertrand, *Chem. Rev.,* **2000**, *100*, 39-91.

[47] R. Gleiter, R. Hoffmann, *J. Am. Chem. Soc.,* **1968**, *90*, 5457-5460.

usually singlet species, and they possess a filled σ non-bonding orbital and an empty p_π orbital.[46] This makes NHCs very good σ donors and poor π-acceptors. Nonetheless, this latter aspect is not negligible given that in some cases the metal−carbene π back-bonding interaction contributes up to 30% of the overall bonding energy.[48] In a different case, π-acidic NHC ligands have proven crucial for the selectivity of gold catalysed cycloaddition reactions due to their ability to remove electron density of some intermediates, favouring one mechanistic pathway.[49]
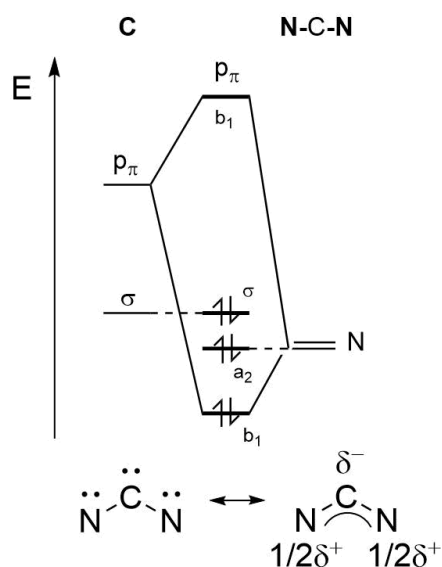

Figure 9. Molecular orbitals diagram illustrating mesomeric effects in NHCs (adapted from reference 46).

Similarly to pincer ligands, there are several parameters that can be modulated on an *N*-heterocyclic carbene. In the same way, Figure 10 shows every part of its structure that can be tuned in order to achieve certain stereoelectronic

[48] a) X. Hu, Y. Tang, P. Gantzel, K. Meyer, *Organometallics*, **2003**, *22*, 612-614; b) X. Hu, I. Castro-Rodriguez, K. Olsen, K. Meyer, *Organometallics*, **2004**, *23*, 755-764.
[49] M. Alcarazo, T. Stork, A. Anoop, W. Thiel, A. Furstner, *Angew. Chem. Int. Ed.,* **2010**, *49*, 2542-2546.

properties.[45c] As it was done in the previous section, some of these parameters will be key in the design of the complexes synthesized in this thesis and so, they will be described in detail.
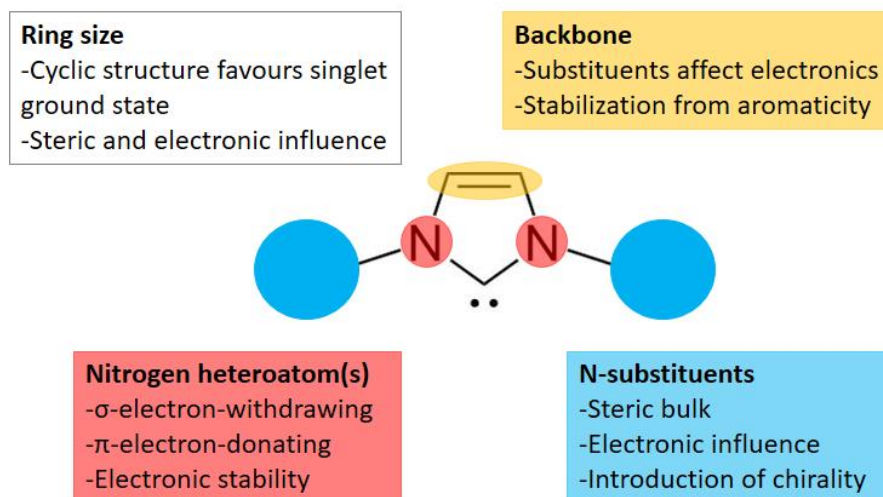

Figure 10. General structural parameters of imidazol-2-ylidenes (NHC models) (adapted from reference 45c).

Electronic properties of NHCs

N-heterocyclic carbenes are among the strongest neutral bases and nucleophiles, and they surpass strong bases like DBU or DABCO. As illustrated above, these properties can be easily adjusted by simple modification of the substituents on the nitrogen atoms, which is very convenient for organocatalytic reactions, for example.[50] As stated above, the σ-donor and π-acceptor properties of a NHC depend on their relative energy of their frontier orbitals. However, it is not straightforward to quantify these capabilities separately, as they are not

---

[50] A. Levens, F. An, M. Breugst, H. Mayr, D. W. Lupton, *Org. Lett.,* **2016**, *18*, 3566-3569.

completely independent. Nonetheless, numerous experimental methods have been developed so as to determine their overall donor-acceptor abilities.[51]

One of these methods is the **Tolman electronic parameter** (TEP), which gives the donor-acceptor capability of a ligand according to the A_1 CO stretching of a $[Ni(CO)_3(NHC)]$ complex. Electron-rich carbenes will donate electron density to the nickel atom, which will in turn undergo π back-bonding with the empty π* orbitals of the CO ligands, strengthening the M−C bonds and weakening the C−O ones. This will have an impact on the CO stretching frequency (the more electron donating carbene, the smaller CO wavenumber in the IR spectrum), which can be correlated to the donor-acceptor properties of the ligand.[52] Figure 11 shows the CO stretch for Ni complexes containing some of the NHCs used in this thesis. It is important to note that this parameter has several disadvantages such as the solvent dependence or the small range of wavenumbers ($\sim$40 cm^{-1})[53] in which the values of the CO vibrations for $[Ni(CO)_3(NHC)]$ fall. Besides, the toxicity of $[Ni(CO)_4]$ led to the utilization of different complexes so as to establish a TEP scale, like *cis*-$[IrCl(CO)_2(NHC)]$ or *cis*-$[RhCl(CO)_2(NHC)]$.[51,54]

[51] H. V. Huynh, *Chem. Rev.,* **2018**, *118*, 9457-9492.
[52] C. A. Tolman, *J. Am. Chem. Soc.,* **1970**, *92*, 2953-2956.
[53] D. Munz, *Organometallics*, **2018**, *37*, 275-289.
[54] D. J. Nelson, S. P. Nolan, *Chem. Soc. Rev.,* **2013**, *42*, 6723-6753.

$[Ni(CO)_2(I^tBu)]$ = 2009.7 cm^{-1} (in hexane)
$[Ni(CO)_3(IMes)]$ = 2050.7 cm^{-1} (in CH_2Cl_2)
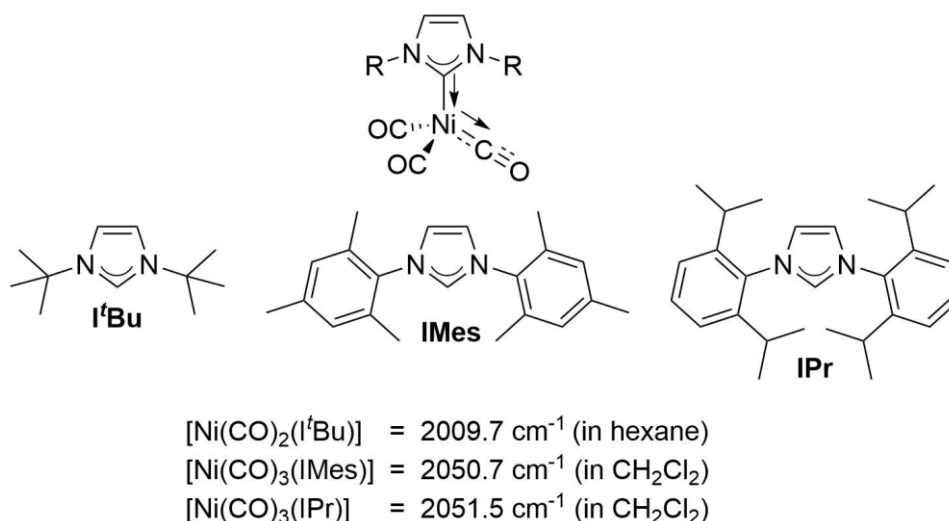$[Ni(CO)_3(IPr)]$ = 2051.5 cm^{-1} (in CH_2Cl_2)

Figure 11. Top: general scheme of the influence of the electron density of a NHC ligand on the CO stretching frequency. Bottom: Tolman electronic parameters of some NHC ligands employed in this thesis. Values obtained from reference 54.

Some other authors have been able to quantify the π acidity of the NHC ligands by means of NMR techniques, so both σ and π contributions can be known by comparison with other scales. Whereas Bertrand *et al*. developed a scale based on ^{31}P NMR chemical shifts of carbene-phosphinidene adducts,[55] the group of Ganter established a different one based on the ^{77}Se NMR chemical shift of selenium carbene compounds.[56] The idea of these scales lies on the deshielding that the ^{31}P or [77]Se undergo upon π back-bonding to the carbene moiety: the higher degree of backbonding, the lower chemical field in the NMR spectrum (Scheme 9). Apart from the deconvolution contribution, another advantage of these methods is the width of the different scales in comparison to that obtained for the TEP values, since the ^{31}P and the [77]Se scales cover a range of around 150 and 850 ppm, respectively.

---

[55] O. Back, M. Henry-Ellinger, C. D. Martin, D. Martin, G. Bertrand, *Angew. Chem. Int. Ed.,* **2013**, *52,* 2939-2943.

[56] A. Liske, K. Verlinden, H. Buhl, K. Schaper, C. Ganter, *Organometallics*, **2013**, *32*, 5269-5272.

The aforementioned experimental methods are the most common ones to study the electronic properties of carbene molecules. However, there exist several others such as pKa values, redox potentials or the Huynh's electronic parameter (HEP), among others.[51]
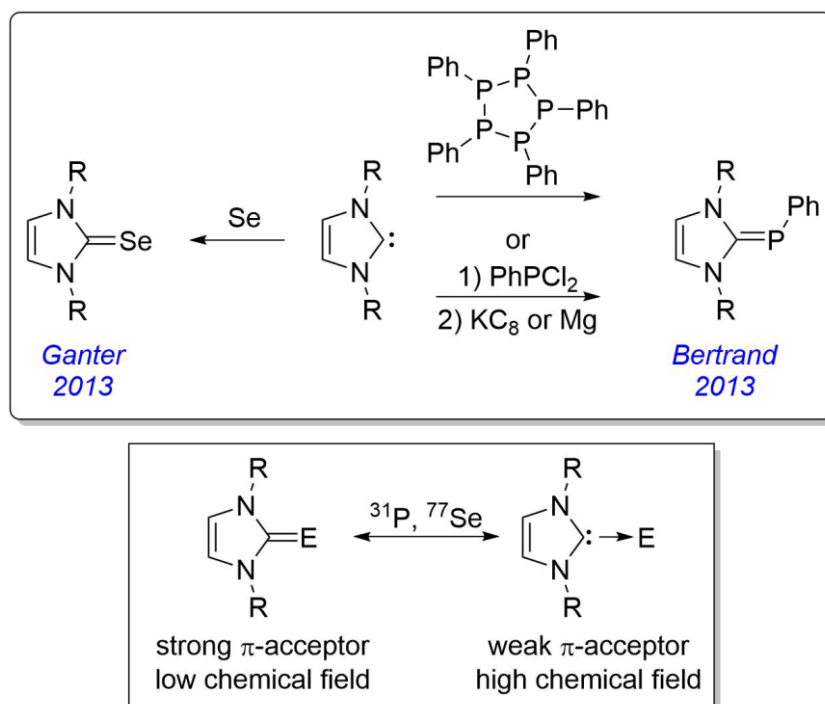
Scheme 9. Summary of the NMR scales developed by Bertrand and Ganter for the determination of the π acidity of carbene ligands (adapted from reference 53).

Steric properties of NHCs

The kinetic stability of the NHCs is greatly influenced by the nature of the substituents on the nitrogen atoms, which has a crucial role in their reactivity patterns or coordination modes in a transition metal complex. However, choosing the right carbene for a specific purpose is not straightforward. The sometimes asymmetric character of NHCs in combination with their conformational flexibility makes difficult to quantify with a single number their

[44]

steric properties in the same way as many phosphines are defined by their Tolman cone angle. This is also due to the fact that phosphine substituents point away from the metal, as illustrated in Figure 6, whereas *N*-heterocyclic carbenes form a cavity between the metal atom and the substituent on nitrogen (Figure 12, space between the green cones and the grey circle).[57] Thus, Nolan, Cavallo *et al.* defined the ***percent buried volume*** (%V_{bur}) as the percentage of volume occupied by the NHC ligand in a sphere centered at the metal atom. This parameter is usually calculated by fixing a M−$C_{carbene}$ distance of 2 Å and a sphere radius of 3 or 3.5 Å.[58]
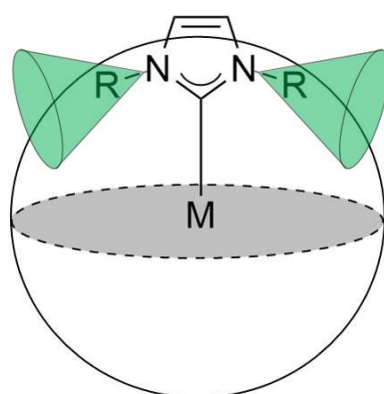
Figure 12. Representation of the steric impact of a NHC ligand.

The easiest way to calculate the percent buried volume is to utilize the *SambVca* software, which is a free online tool developed by the group of Cavallo that performs the calculation of %V_{bur} on CIF or XYZ files. This algorithm can also be employed for calculating the steric impact of other groups, such as phosphines or cyclopentadienyl-based ligands.[59] Although this gives an idea of how bulky a

[57] A. Gómez-Suárez, D. J. Nelson, S. P. Nolan, *Chem. Commun.,* **2017**, *53*, 2650-2660.

[58] A. C. Hillier, W. J. Sommer, B. S. Yong, J. L. Petersen, L. Cavallo, S. P. Nolan, *Organometallics*, **2003**, *22*, 4322-4326.

[59] A. Poater, B. Cosenza, A. Correa, S. Giudice, F. Ragone, V. Scarano, L. Cavallo, *Eur. J. Inorg. Chem.,* **2009**, 1759-1766.

NHC ligand is, it is only a numerical value and it does not illustrate the steric arrangement of the ligand in a transition metal complex, for example, which might be useful in fields like asymmetric catalysis. For this reason, the same group developed a way of displaying the **steric map** created by the ligands in a complex[60] and implemented it in a new version of the *SambVca* software (*SambVca* 2.0).[61] This resulted very useful, since the output of the calculation also gives steric information in the different quadrants of the ligand and/or complex, so the most accessible regions for a potential substrate can be easily located. This has a massive impact on the design and outcome of regioselective or enantioselective catalytic reactions, as exemplified by recent examples in the literature.[62] As an example, Figure 13 shows the typical output of *SambVca* 2.0 for the NHC ligand I*t*Bu (1,3-di-*tert*-butylimidazol-2-ylidene).

---

[60] A. Poater, F. Ragone, R. Mariz, R. Dorta, L. Cavallo, *Chem. Eur. J.,* **2010**, *16*, 14348-14353.

[61] L. Falivene, R. Credentino, A. Poater, A. Petta, L. Serra, R. Oliva, V. Scarano, L. Cavallo, *Organometallics*, **2016**, *35*, 2286-2293 (also see https://www.molnac.unisa.it/OMtools/sambvca2.0).

[62] Some recent examples include: a) A. Al-Harbi, B. Kriegel, S. Gulati, M. J. Hammond, G. Parkin, *Inorg. Chem.,* **2017**, *56*, 15271-15284; b) Y. Shikata, R. Yasue, K. Yoshida, *Chem. Eur. J.,* **2017**, *23*, 16806-16812; c) D. Hueber, M. Teci, E. Brenner, D. Matt, J-M. Weibel, P. Pale, A. Blanc, *Adv. Synth. Catal.,* **2018**, *360*, 2453-2459.
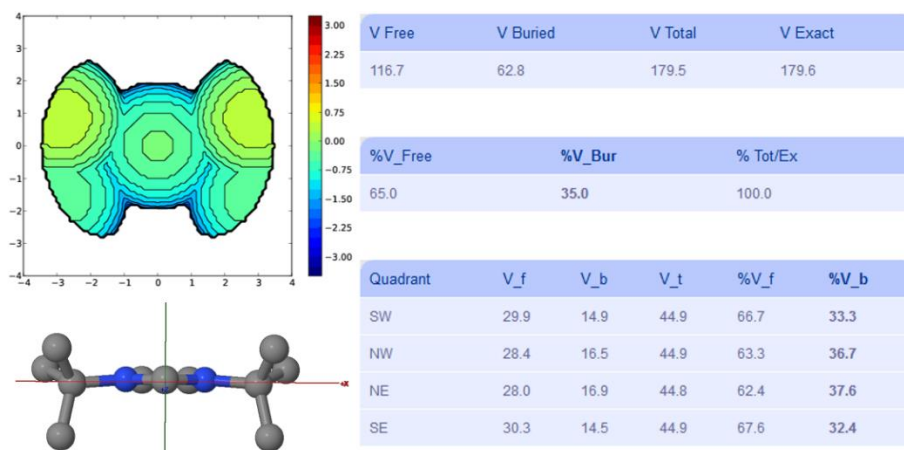
Figure 13. Steric properties of the I*t*Bu ligand provided by the *SambVca* 2.0 tool. Top left: steric map (the scale goes from less bulky (dark blue) to more bulky (dark red)). Right: distribution of percent buried volume per quadrant. These data have been obtained from the software available in reference 61.

These parameters are the most widely employed for quantifying the steric properties of NHC ligands, although there are some others like the ligand knowledge base for carbenes (LKB-C) developed by Fey and Orpen,[63] or the repulsiveness scale established by Gusev.[64]

Some applications of NHCs

The knowledge of the steric and electronic properties of *N*-heterocyclic carbenes is key when designing the resulting properties of a transition metal complex containing this kind of ligands. In fact, the behaviour of NHCs as monomers was evaluated by the group of Cavallo, analysing the Wanzlick equilibrium between the carbene and the tetraaminofulvene forms, including the

[63] N. Fey, M. F. Haddow, J. N. Harvey, C. L. McMullin, A. G. Orpen, *Dalton Trans.,* **2009**, 8183-8196.

[64] D. G. Gusev, *Organometallics*, **2009**, *28*, 6458-6461.

$\%V_{bur}$ and the E_{S-T} in the determination of the dimerization energy.[65] The studies on the properties of carbenes and their comparison with other ligands led to the conclusion that NHCs are better σ donors than phosphines and they form stronger and more robust bonds with transition metals. As a consequence, a metal bound to a NHC ligand will be richer in electron density than in the case of a phosphine.[66] This has dramatic implications in their catalytic performance. For example, the replacement of a phosphine by a NHC ligand in the 1st generation Grubbs catalyst for olefin metathesis (Grubbs I, scheme 10) was carried out simultaneously by the groups of Nolan,[67] Grubbs[68] and Fürstner.[69] They all observed an increased stability and a greater activity from the newly synthesized catalysts, along with a wider tolerance to functional groups, which eventually led to the synthesis of the 2nd generation Grubbs catalyst (Grubbs II), where one PCy_3 group has been replaced by a SIMes carbene.[70,71] The affinity of the alkene (substrate) is four orders of magnitude higher than the coordination of the phosphine in Grubbs II (Scheme 10), which translates into greater catalytic activity.[45c]

[65] A. Poater, F. Ragone, S. Giudice, C. Costabile, R. Dorta, S. P. Nolan, L. Cavallo, *Organometallics*, **2008**, *27*, 2679-2681.

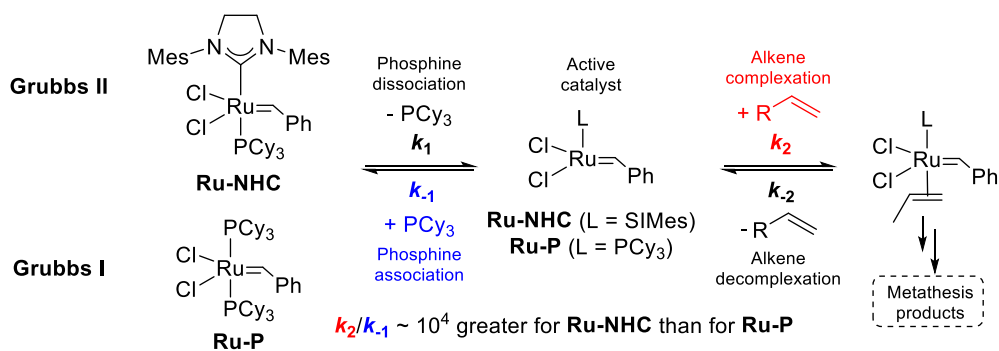[66] D. J. D. Wilson, S. A. Couchman, J. L. Dutton, *Inorg. Chem.,* **2012**, *51*, 7657-7668.

[67] J. Huang, E. D. Stevens, S. P. Nolan, J. L. Petersen, *J. Am. Chem. Soc.,* **1999**, *121*, 2674-2678.

[68] M. Scholl, T. M. Trnka, J. P. Morgan, R. H. Grubbs, *Tetrahedron Lett.,* **1999**, *40*, 2247-2250.

[69] L. Ackermann, A. Fürstner, T. Weskamp, F. J. Kohl, W. A. Herrmann, *Tetrahedron Lett.,* **1999**, *40*, 4787-4790.

[70] M. Scholl, S. Ding, C. W. Lee, R. H. Grubbs, *Org. Lett.,* **1999**, *1*, 953-956.

[71] SIMes stands for 1,3-bis(2,4,6-trimethylphenyl)-4,5-dihydroimidazol-2-ylidene.

Scheme 10. Structural and catalytic differences between olefin metathesis catalysts Grubbs I and II (adapted from reference 45c).

The remarkable features of *N*-heterocyclic carbenes have also been leveraged in Pd-catalyzed cross-coupling reactions for numerous reasons. Apart from providing robust catalysts less prone to formation of palladium black, the electronic and steric properties of these ligands are helpful in the majority of the elementary steps in the mechanism of this process (Scheme 11).[72]

---

[72] G. C. Fortman, S. P. Nolan, *Chem. Soc. Rev.,* **2011**, *40*, 5151-5169.
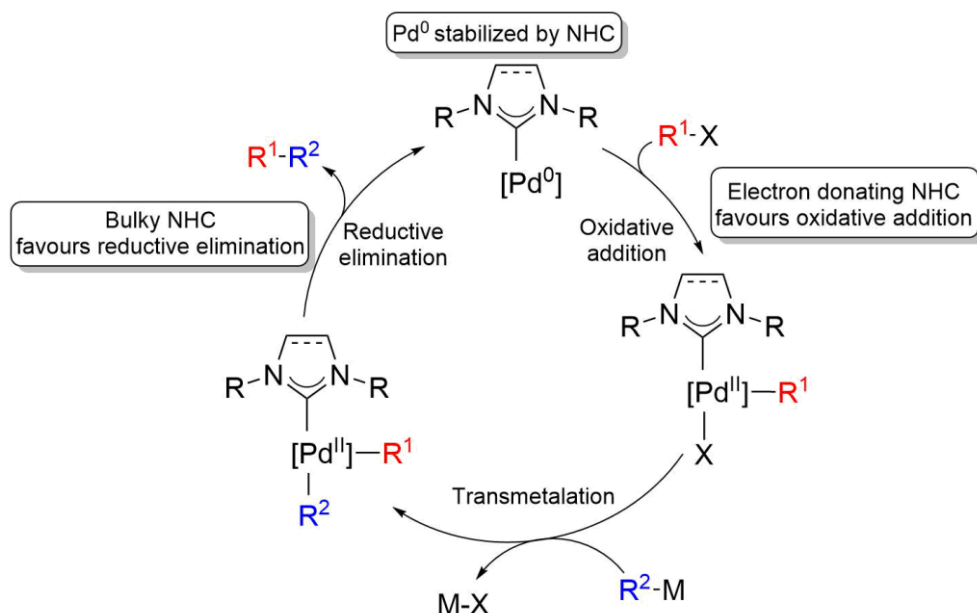
Scheme 11. Some advantages of using NHC as ligands in Pd-catalyzed cross-coupling reactions (adapted from reference 45c).

Although the main field where NHCs have proven useful is homogeneous catalysis, there are some other areas where these carbenes are frequently employed, like organocatalysis,[73] main-group chemistry (*e.g.* stabilization of diatomic molecules)[74] or the stabilization of metal nanoparticles.[75]

---

[73] a) D. Enders, O. Niemeier, A. Henseler, *Chem. Rev.,* **2007**, *107*, 5606-5655; b) D. M. Flanigan, F. Romanov-Michailidis, N. A. White, T. Rovis, *Chem. Rev.,* **2015**, *115*, 9307-9387.

[74] a) Y. Wang, G. H. Robinson, *Inorg. Chem.,* **2014**, *53*, 11815-11832; b) S. Würtemberger-Pietsch, U. Radius, T. B. Marder, *Dalton Trans.,* **2016**, *45*, 5880-5895; c) V. Nesterov, D. Reiter, P. Bag, P. Frisch, R. Holzner, A. Porzelt, S. Inoue, *Chem. Rev.,* **2018**, *118*, 9678-9842.

[75] a) J. Vignolle, T. D. Tilley, *Chem. Commun.,* **2009**, 7230-7232; b) C. M. Crudden, J. H. Horton, I. J. Ebralidze, O. V. Zenkina, A. B. McLean, B. Drevniok, Z. She, H-B. Kraatz, N. J. Mosey, T. Seki, E. C. Keske, J. D. Leake, A. Rousina-Webb, G. Wu, *Nat. Chem.,* **2014**, *6*, 409-414; c) A. V. Zhukhovitskiy, M. J. MacLeod, J. A. Johnson, *Chem. Rev.,* **2015**, *115*, 11503-11532; d) G. Wang, A. Rühling, S. Amirjalayer, M. Knor, J. B. Ernst, C. Richter, H-J. Gao, A. Timmer, H-Y. Gao, N. L. Doltsinis, F. Glorius, H. Fuchs, *Nat. Chem.,* **2017**, *9*, 152-156.

Finally, it is worth mentioning that after decades of extensive work from a large number of research groups around the world, this chemistry is still very active nowadays. Carbene chemistry is yet giving rise to new types of architectures with different properties to those exhibited by NHCs, which translates into new types of reactivity. Some of these species include the mesoionic carbenes (MICs, also known as abnormal NHCs or remote NHCs), which consist of heterocyclic frameworks containing carbene units with minor stabilization by heteroatoms, producing stronger σ-donors than NHCs.[76] A commonly used scaffold of MICs is the triazolylidene fragment, as shown in Figure 14 (left). The group of Bertrand also developed cyclic (alkyl)(amino) carbenes or CAACs, which turned out to be more ambiphilic than NHCs, since the replacement of one of the π-donating nitrogen atoms by a σ-donating alkyl fragment increases the energy of the HOMO and decreases the energy of the LUMO.[77] Therefore, the E_{S-T} value is smaller. This effect has been augmented even more with the discovery of byciclic (alkyl)(amino) carbenes, or BICAACs. The formation of a bicyclic structure leads to more nucleophilic and electrophilic carbenes (Figure 14, right), capable of displacing CAAC ligands from metal centers or even main-group elements.[78]

[76] A. Vivancos, C. Segarra, M. Albrecht, *Chem. Rev.,* **2018**, *118*, 9493-9586.

[77] M. Melaimi, R. Jazzar, M. Soleilhavoup, G. Bertrand, *Angew. Chem. Int. Ed.,* **2017**, *56*, 10046-10068.

[78] E. Tomás-Mendivil, M. M. Hansmann, C. M. Weinstein, R. Jazzar, M. Melaimi, G. Bertrand, *J. Am. Chem. Soc.,* **2017**, *139*, 7753-7756.
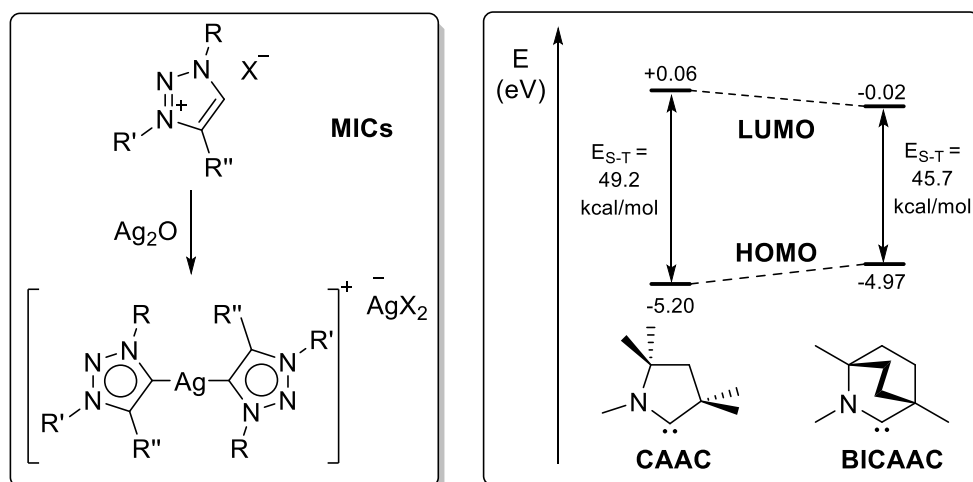
Figure 14. Examples of several families of carbenes different to NHCs (adapted from references 76 and 78).

NHC-stabilized Pt(II) complexes

Previously in our group, the tunable character of NHCs was leveraged so several Pt(II) complexes were synthesized and able to fulfil some specific needs, taking into account many of the concepts detailed in this introduction. In this way, carbenes bearing mesityl groups made possible intermolecular stoichiometric C−H activation reactions of benzene, toluene and fluoroarene derivatives (Scheme 12). Experimental and computational studies led to the conclusion that careful design of the steric and electronic properties of the complexes were crucial for this process to take place, since bulkier carbenes like I*t*Bu did not give any C−H activation product. In addition, subtle electronic effects were also important for the success of this reaction, given that only IMes* ligand afforded some Pt−aryl compounds, unlike less basic IMes ligand (traces were observed in this case).[79]

---

[79] O. Rivada-Wheelaghan, M. A. Ortuño, J. Díez, A. Lledós, S. Conejero, *Angew. Chem. Int. Ed.,* **2012**, *51*, 3936-3939.
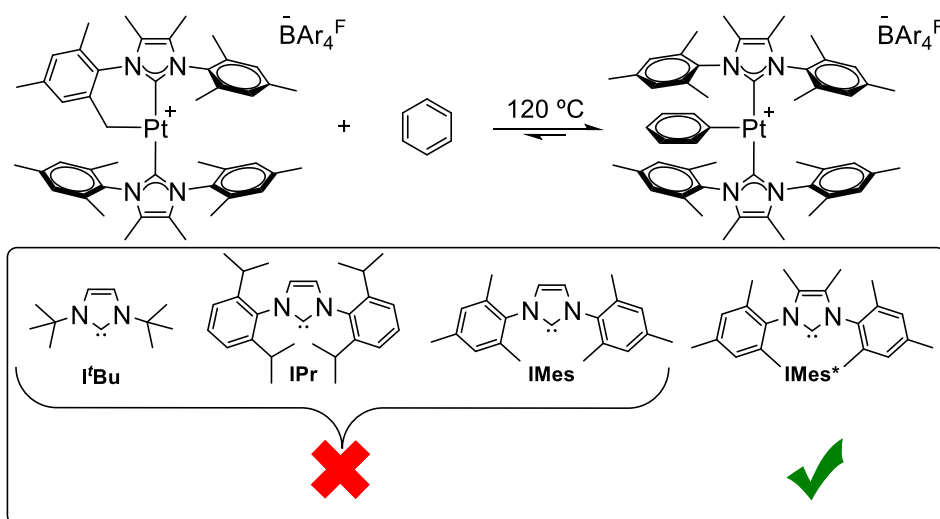
Scheme 12. C−H activation reactions of NHC-stabilized Pt(II) complexes previously explored in our group (adapted from reference 79).

On the other hand, these type of complexes made possible the stabilization and isolation of a rare and elusive cationic mononuclear Pt(III) alkyl species by making use of IPr ligands. Addition of 0.5 equivalents of Br_2 to a dichloromethane solution of the cationic cyclometalated IPr complex gave rise to the Pt(III) derivative (Scheme 13), which could be characterized by X-Ray diffraction studies. Interestingly, the uncommon seesaw structure found around the platinum center was due to electronic reasons, and not steric hindrance. In fact, computational studies shed light about this phenomenon, and concluded that the *trans* influence of the ligand trans to the bromide ligand was responsible for the observed geometry.[80]

---

[80] O. Rivada-Wheelaghan, M. A. Ortuño, J. Díez, S. E. García-Garrido, C. Maya, A. Lledós, S. Conejero, *J. Am. Chem. Soc.,* **2012**, *134*, 15261-15264.
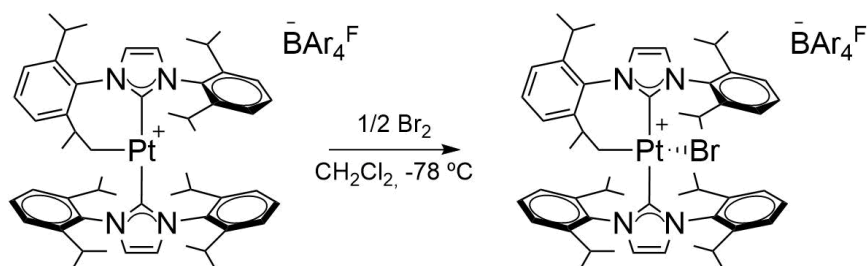
Scheme 13. Synthesis of a NHC-stabilized Pt(III) complex (adapted from reference 80).

All the examples mentioned above in this introduction reflect the importance of ligand design in transition metal complexes, as their chemical behaviour is greatly influenced by the properties conferred by these species. In the second half of this thesis, different NHCs will be used in the synthesis of Pt(II) complexes for the isolation of elusive intermediates and the development of catalytically active and selective species.

[54]

References

[1] F. A. Cotton, G. Wilkinson, *Advanced Inorganic Chemistry*, 3rd Edition (**1972**). Wiley-Interscience.

[2] R. H. Crabtree, *The Organometallic Chemistry of the Transition Metals,* 4th Edition (**2005**). Wiley-Interscience.

[3] M. L. H. Green, G. Parkin, *J. Chem. Educ.,* **2014**, *91*, 807-816.

[4] A. Amgoune, D. Bourissou, *Chem. Commun.,* **2011**, *47*, 859-871.

[5] A. F. Hill, *Organometallics*, **2006**, *25*, 4741-4743.

[6] G. Parkin, *Organometallics*, **2006**, *25*, 4744-4747.

[7] G. Bouhadir, D. Bourissou in *The Chemical Bond III. Structure and Bonding* (**2006**), vol. 171. Springer, Cham. *Chapter 5: Coordination of Lewis Acids to Transition Metals: Z-Type Ligands*.

[8] R. J. Lundgren, M. Stradiotto in *Ligand Design in Metal Chemistry: Reactivity and Catalysis.* 1st Edition (**2016**). John Wiley & Sons, Ltd. *Chapter 1: Key Concepts in Ligand Design: An Introduction*.

[9] Y. Segawa, M. Yamashita, K. Nozaki, *J. Am. Chem. Soc.,* **2009**, *131*, 9201-9203.

[10] The authors conclude that they observe the boryl hydride arrangement displayed in Scheme 2, given that NMR, DFT and X-Ray studies rule out a σ-BH coordination mode.

[11] a) M. E. van der Boom, D. Milstein, *Chem. Rev.,* **2003**, *103*, 1759-1792; b) G. van Koten, D. Milstein, *Organometallic Pincer Chemistry*, **2012**, Springer, Heidelberg.

[12] H. Braunschweig, M. Colling, *Coord. Chem. Rev.,* **2001**, *223*, 1-51.

[13] S. Bontemps, H. Gornitzka, G. Bouhadir, K. Miqueu, D. Bourissou, *Angew. Chem. Int. Ed.,* **2006**, *45*, 1611-1614.

[14] W-C. Shih, W. Gu, M. C. MacInnis, S. D. Timpa, N. Bhuvanesh, J. Zhou, O. V. Ozerov, *J. Am. Chem. Soc.,* **2016**, *138*, 2086-2089.

[15] W-C. Shih, W. Gu, M. C. MacInnis, D. E. Herbert, O. V. Ozerov, *Organometallics*, **2017**, *36*, 1718-1726.

[55]

[16] a) A. M. Spokoyny, M. G. Reuter, C. L. Stern, M. A. Ratner, T. Seiderman, C. A. Mirkin, *J. Am. Chem. Soc.,* **2009**, *131*, 9482-9483; b) M. E. El-Zaria, H. Arii, H. Nakamura, *Inorg. Chem.,* **2011**, *50*, 4149-4161; c) B. J. Eleazer, M. D. Smith, A. A. Popov, D. V. Peryshkov, *J. Am. Chem. Soc.,* **2016**, *138*, 10531-10538.

[17] E. Peris, R. H. Crabtree, *Chem. Soc. Rev.,* **2018**, *47*, 1959-1968.

[18] M. A. W. Lawrence, K-A. Green, P. N. Nelson, S. C. Lorraine, *Polyhedron*, **2018**, *143*, 11-27.

[19] D. L. Kays, S. Aldridge in *Contemporary Metal Boron Chemistry I*, **2008**. Springer-Berlag Berlin Heidelberg. *Chapter 2: Transition metal boryl complexes.* Pages 29-122.

[20] A. Al-Fawaz, S. Aldridge, D. L. Coombs, A. A. Dickinson, D. J. Willock, L-L. Ooi, M. E. Light, S. J. Coles, M. B. Hursthouse, *Dalton Trans.,* **2004**, 4030-4037.

[21] A. A. Dickinson, D. J. Willock, R. J. Calder, S. Aldridge, *Organometallics*, **2002**, *21*, 1146-1157.

[22] G. J. Irvine, M. J. G. Lesley, T. B. Marder, N. C. Norman, C. R. Rice, E. G. Robins, W. R. Roper, G. R. Whittell, L. J. Wright, *Chem. Rev.,* **1998**, *98*, 2685- 2722.

[23] N. N. Greenwood, A. Earnshaw, *Chemistry of the Elements*, 2nd ed. Butterworth-Heinemann: Woburn, MA, 1997.

[24] K. M. Anderson, A. G. Orpen, *Chem. Commun.,* **2001**, 2682-2683.

[25] This is a qualitative description of the concept of *trans* influence. For quantitative parameters that contribute to this property, see: J. K. Burdett, T. A. Albright, *Inorg. Chem.,* **1979**, *18*, 2112-2120.

[26] J. Zhu, Z. Lin, T. B. Marder, *Inorg. Chem.,* **2005**, *44*, 9384-9390.

[27] C. A. Tolman, *Chem. Rev.,* **1977**, *77*, 313-348.

[28] V. Pandarus, D. Zargarian, *Organometallics*, **2007**, *26*, 4321-4334.

[29] A. B. Salah, D. Zargarian, *Dalton Trans.,* **2011**, *40*, 8977-8985.

[30] K. Tanoue, M. Yamashita, *Organometallics*, **2015**, *34*, 4011-4017.

[31] Y. Segawa, M. Yamashita, K. Nozaki, *Organometallics*, **2009**, *28*, 6234-6242.

[32] J. R. Khusnutdinova, D. Milstein, *Angew. Chem. Int. Ed.,* **2015**, *54*, 12236-12273.

[56]

[33] S. W. Kohl, L. Weiner, L. Schwartsburd, L. Konstantinovski, L. J. W. Shimon, Y. Ben-David, M. A. Iron, D. Milstein, *Science*, **2009**, *324*, 74-77.

[34] P. M. P. García, P. Ren, R. Scopelliti, X. Hu, *ACS Catal.,* **2015**, *5*, 1164-1171.

[35] O. Vechorkin, D. Barmaz, V. Proust, X. Hu, *J. Am. Chem. Soc.,* **2009**, *131*, 12078-12079.

[36] T. J. Schmeier, G. E. Dobereiner, R. H. Crabtree, N. Hazari, *J. Am. Chem. Soc.,* **2011**, *133*, 9274-9277.

[37] a) W. H. Harman, J. C. Peters, *J. Am. Chem. Soc.,* **2012**, *134*, 5080-5082; b) M. Devillard, G. Bouhadir, D. Bourissou, *Angew. Chem. Int. Ed.,* **2015**, *54*, 730-732.

[38] G. R. Owen, *Chem. Commun.,* **2016**, *52*, 10712-10726.

[39] T-P. Lin, J. C. Peters, *J. Am. Chem. Soc.,* **2014**, *136*, 13672-13683.

[40] a) S. Z. Tasker, E. A. Standley, T. F. Jamison, *Nature*, **2014**, *509*, 299-309; b) V. P. Ananikov, *ACS Catal.,* **2015**, *5*, 1964-1971.

[41] H. W. Wanzlick, *Angew. Chem. Int. Ed.,* **1962**, *1*, 75-80. This equilibrium remained controversial for some years (see D. M. Lemal, R. A. Lovald, K. I. Kawano, *J. Am. Chem. Soc.,* **1964**, *86*, 2518-2519), but subsequent experiments proved Wanzlick right in his statement (a) Y. Liu, P. E. Lindner, D. M. Lemal, *J. Am. Chem. Soc.,* **1999**, *121*, 10626-10627; b) V. P. W. Böhm, W. A. Herrmann, *Angew. Chem. Int. Ed.,* **2000**, *39*, 4036-4038).

[42] A. Igau, H. Grutzmacher, A. Baceiredo, G. Bertrand, *J. Am. Chem. Soc.,* **1988**, *110*, 6463-6466.

[43] A. J. Arduengo, R. L. Harlow, M. Kline, *J. Am. Chem. Soc.,* **1991**, *113*, 361-363.

[44] A. J. Arduengo, *Acc. Chem. Res.,* **1999**, *32*, 913-921.

[45] a) W. A. Herrmann, C. Köcher, *Angew. Chem. Int. Ed.,* **1997**, *36*, 2162-2187; b) P. de Frémont, N. Marion, S. P. Nolan, *Coord. Chem. Rev.,* **2009**, *253*, 862-892; c) M. N. Hopkinson, C. Richter, M. Schedler, F. Glorius, *Nature*, **2014**, *510*, 485-496.

[46] D. Bourissou, O. Guerret, F. P. Gabbai, G. Bertrand, *Chem. Rev.,* **2000**, *100*, 39-91.

[47] R. Gleiter, R. Hoffmann, *J. Am. Chem. Soc.,* **1968**, *90*, 5457-5460.

[48] a) X. Hu, Y. Tang, P. Gantzel, K. Meyer, *Organometallics*, **2003**, *22*, 612-614; b) X. Hu, I. Castro-Rodriguez, K. Olsen, K. Meyer, *Organometallics*, **2004**, *23*, 755-764.

[49] M. Alcarazo, T. Stork, A. Anoop, W. Thiel, A. Furstner, *Angew. Chem. Int. Ed.,* **2010**, *49*, 2542-2546.

[50] A. Levens, F. An, M. Breugst, H. Mayr, D. W. Lupton, *Org. Lett.,* **2016**, *18*, 3566-3569.

[51] H. V. Huynh, *Chem. Rev.,* **2018**, *118*, 9457-9492.

[52] C. A. Tolman, *J. Am. Chem. Soc.,* **1970**, *92*, 2953-2956.

[53] D. Munz, *Organometallics*, **2018**, *37*, 275-289.

[54] D. J. Nelson, S. P. Nolan, *Chem. Soc. Rev.,* **2013**, *42*, 6723-6753.

[55] O. Back, M. Henry-Ellinger, C. D. Martin, D. Martin, G. Bertrand, *Angew. Chem. Int. Ed.,* **2013**, *52,* 2939-2943.

[56] A. Liske, K. Verlinden, H. Buhl, K. Schaper, C. Ganter, *Organometallics*, **2013**, *32*, 5269-5272.

[57] A. Gómez-Suárez, D. J. Nelson, S. P. Nolan, *Chem. Commun.,* **2017**, *53*, 2650-2660.

[58] A. C. Hillier, W. J. Sommer, B. S. Yong, J. L. Petersen, L. Cavallo, S. P. Nolan, *Organometallics*, **2003**, *22*, 4322-4326.

[59] A. Poater, B. Cosenza, A. Correa, S. Giudice, F. Ragone, V. Scarano, L. Cavallo, *Eur. J. Inorg. Chem.,* **2009**, 1759-1766.

[60] A. Poater, F. Ragone, R. Mariz, R. Dorta, L. Cavallo, *Chem. Eur. J.,* **2010**, *16*, 14348-14353.

[61] L. Falivene, R. Credentino, A. Poater, A. Petta, L. Serra, R. Oliva, V. Scarano, L. Cavallo, *Organometallics*, **2016**, *35*, 2286-2293 (also see https://www.molnac.unisa.it/OMtools/sambvca2.0).

[62] Some recent examples include: a) A. Al-Harbi, B. Kriegel, S. Gulati, M. J. Hammond, G. Parkin, *Inorg. Chem.,* **2017**, *56*, 15271-15284; b) Y. Shikata, R. Yasue, K. Yoshida, *Chem. Eur. J.,* **2017**, *23*, 16806-16812; c) D. Hueber, M. Teci, E.

Brenner, D. Matt, J-M. Weibel, P. Pale, A. Blanc, *Adv. Synth. Catal.,* **2018**, *360*, 2453-2459.

[63] N. Fey, M. F. Haddow, J. N. Harvey, C. L. McMullin, A. G. Orpen, *Dalton Trans.,* **2009**, 8183-8196.

[64] D. G. Gusev, *Organometallics*, **2009**, *28*, 6458-6461.

[65] A. Poater, F. Ragone, S. Giudice, C. Costabile, R. Dorta, S. P. Nolan, L. Cavallo, *Organometallics*, **2008**, *27*, 2679-2681.

[66] D. J. D. Wilson, S. A. Couchman, J. L. Dutton, *Inorg. Chem.,* **2012**, *51*, 7657-7668.

[67] J. Huang, E. D. Stevens, S. P. Nolan, J. L. Petersen, *J. Am. Chem. Soc.,* **1999**, *121*, 2674-2678.

[68] M. Scholl, T. M. Trnka, J. P. Morgan, R. H. Grubbs, *Tetrahedron Lett.,* **1999**, *40*, 2247-2250.

[69] L. Ackermann, A. Fürstner, T. Weskamp, F. J. Kohl, W. A. Herrmann, *Tetrahedron Lett.,* **1999**, *40*, 4787-4790.

[70] M. Scholl, S. Ding, C. W. Lee, R. H. Grubbs, *Org. Lett.,* **1999**, *1*, 953-956.

[71] SIMes stands for 1,3-bis(2,4,6-trimethylphenyl)-4,5-dihydroimidazol-2-ylidene.

[72] G. C. Fortman, S. P. Nolan, *Chem. Soc. Rev.,* **2011**, *40*, 5151-5169.

[73] a) D. Enders, O. Niemeier, A. Henseler, *Chem. Rev.,* **2007**, *107*, 5606-5655; b) D. M. Flanigan, F. Romanov-Michailidis, N. A. White, T. Rovis, *Chem. Rev.,* **2015**, *115*, 9307-9387.

[74] a) Y. Wang, G. H. Robinson, *Inorg. Chem.,* **2014**, *53*, 11815-11832; b) S. Würtemberger-Pietsch, U. Radius, T. B. Marder, *Dalton Trans.,* **2016**, *45*, 5880-5895; c) V. Nesterov, D. Reiter, P. Bag, P. Frisch, R. Holzner, A. Porzelt, S. Inoue, *Chem. Rev.,* **2018**, *118*, 9678-9842.

[75] a) J. Vignolle, T. D. Tilley, *Chem. Commun.,* **2009**, 7230-7232; b) C. M. Crudden, J. H. Horton, I. J. Ebralidze, O. V. Zenkina, A. B. McLean, B. Drevniok, Z. She, H-B. Kraatz, N. J. Mosey, T. Seki, E. C. Keske, J. D. Leake, A. Rousina-Webb, G. Wu, *Nat. Chem.,* **2014**, *6*, 409-414; c) A. V. Zhukhovitskiy, M. J. MacLeod, J. A. Johnson,

Chem. Rev., **2015**, *115*, 11503-11532; d) G. Wang, A. Rühling, S. Amirjalayer, M. Knor, J. B. Ernst, C. Richter, H-J. Gao, A. Timmer, H-Y. Gao, N. L. Doltsinis, F. Glorius, H. Fuchs, *Nat. Chem.,* **2017**, *9*, 152-156.

[76] A. Vivancos, C. Segarra, M. Albrecht, *Chem. Rev.,* **2018**, *118*, 9493-9586.

[77] M. Melaimi, R. Jazzar, M. Soleilhavoup, G. Bertrand, *Angew. Chem. Int. Ed.,* **2017**, *56*, 10046-10068.

[78] E. Tomás-Mendivil, M. M. Hansmann, C. M. Weinstein, R. Jazzar, M. Melaimi, G. Bertrand, *J. Am. Chem. Soc.,* **2017**, *139*, 7753-7756.

[79] O. Rivada-Wheelaghan, M. A. Ortuño, J. Díez, A. Lledós, S. Conejero, *Angew. Chem. Int. Ed.,* **2012**, *51*, 3936-3939.

[80] O. Rivada-Wheelaghan, M. A. Ortuño, J. Díez, S. E. García-Garrido, C. Maya, A. Lledós, S. Conejero, *J. Am. Chem. Soc.,* **2012**, *134*, 15261-15264.

Chapter 1

Nickel(II) catalysed Carbon Dioxide Hydrosilation

1. Introduction

1.1. Why carbon dioxide, and why is it so difficult to transform?

Since the time when early humans started to make fire, combustion of fuels has been our main source of energy. It still is nowadays (Figure 1), and the development of a constantly increasing world population gives rise to a higher energy demand, and therefore a greater accumulation of CO_2 in our atmosphere. This has a deep environmental effect and it is one of the main contributors to the 'Greenhouse Effect'.[1] The growth in the temperature on the surface of the planet is not the only measurable magnitude, as the seawater acidification can also be quantifiable.[2]

---

[1] a) International Energy Agency, Electricity Information 2017, http://www.iea.org/publications/freepublications/publication/ElectricityInformation2017Overview.pdf; b) A. Goeppert, M. Czaun, G.K.S. Prakash, G. A. Olah, *Energy Environ. Sci.*, **2012**, *5*, 7833-7853.

[2] a) J.C. Orr, V. J. Fabry, O. Aumont, L. Bopp, S. C. Doney, R. A. Feely, A. Gnanadesikan, N. Gruber, A. Ishida, F. Joos, R. M. Key, K. Lindsay, E. Maier-Reimer, R. Matear, P. Monfray, A. Mouchet, R. G. Najjar, G-K. Plattner, K. B. Rodgers, C. L. Sabine, J. L. Sarmiento, R. Schlitzer, R. D. Slater, I. J. Totterdell, M-F. Weirig, Y. Yamanaka, A. Yool, *Nature*, **2005**, *437*, 681-686; b) S. C. Doney, V. J. Fabry, R. A. Feely, J. A. Kleypas, *Annu. Rev. Mar. Sci.,* **2009**, *1*, 169-192.

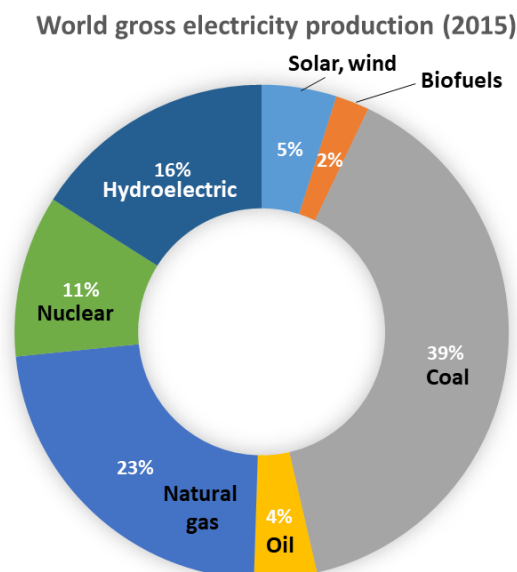**World gross electricity production (2015)**

Figure 1. Classification of the energy sources and their contribution to the world electricity production in 2015 (adapted from reference 1a)

From a more optimistic point of view, the current situation can be regarded as an opportunity to obtain a material which can be used as a C-1 feedstock. The withdrawal of CO_2 from the atmosphere by using it as a chemical reagent would not provide the solution to the problem, given that the amount of this gas employed in chemical synthesis is rather small compared to the anthropogenic emissions (as a matter of fact, some authors insist on the distinction between 'CO_2 mitigation' and 'CO_2 utilization').[3] Nonetheless, it can be the source of new chemical fuels that can replace the ones we currently use. In addition, there are important advantages in using carbon dioxide as a chemical reagent: it is very cheap, non-toxic and non-flammable. In terms of health, it is also a safer alternative to other carbon sources such as phosgene, carbon monoxide or isocyanates. It is renewable (as opposed to fossil fuels) and it can

---

[3] J. Artz, T. E. Müller, K. Thenert, J. Kleinekorte, R. Meys, A. Sternberg, A. Bardow, W. Leitner, *Chem. Rev.,* **2018**, *118*, 434-504.

be converted to many value-added products which are nowadays synthesized in industry by means of more expensive and less efficient and convenient processes. Finally, when used under supercritical conditions, it can be a valuable solvent and/or a green reaction medium.[3,4] However, if CO_2 is so versatile, why is it not a common reagent in industry or research laboratories?

The main issue resides in its lack of reactivity. Being the final carbon-containing product of the combustion process, it is the most oxidized form of the neutral carbon species and also the most thermodynamically stable one. In addition, it is a kinetically inert entity, and many processes involving this gas require an energy input in order to take place. This is why the most common resulting products derived from CO_2 come from harsh reaction conditions such as high pressures and/or temperatures (*e.g.* urea, salicylic acid)[5,6] or highly reactive compounds, like polycarbonates (using epoxides) or polycarbamates (using aziridines).[7] The majority of these reactions belong to what is known as 'horizontal utilization' of carbon dioxide, in which there is no change in the oxidation state of carbon and no energy is stored within the resulting product (Figure 2).[8] However, the recycling of CO_2 is gaining interest nowadays, and the quest for new methods of obtaining chemical commodities and/or alternative fuels like the 'Methanol economy' proposed by George A. Olah are the driving

[4] H. Arakawa, M. Aresta, J. N. Armor, M. A. Barteau, E. J. Beckman, A. T. Bell, J. E. Bercaw, C. Creutz, E. Dinjus, D. A. Dixon, K. Domen, D. L. DuBois, J. Eckert, E. Fujita, D. H. Gibson, W. A. Goddard, D. W. Goodman, J. Keller, G. J. Kubas, H. H. Kung, J. E. Lyons, L. E. Manzer, T. J. Marks, K. Morokuma, K. M. Nicholas, R. Periana, L. Que, J. Rostrup-Nielson, W. M. H. Sachtler, L. D. Schmidt, A. Sen, G. A. Somorjai, P. C. Stair, B. Ray. Stults, W. Tumas, *Chem. Rev.,* **2001**, *101*, 953-996.

[5] J. Meessen, *Chem. Ing. Tech.,* **2014**, *86*, 2180-2189.

[6] Q. Zhang, H-Y. Yuan, N. Fukaya, J-C. Choi, *ACS Sustainable Chem. Eng.,* **2018**, *6*, 6675-6681.

[7] Q. Liu, L. Wi, R. Jackstell, M. Beller, *Nat. Commun.,* **2015**, *6*, 5933.

[8] C. D. N. Gomes, O. Jacquet, C. Villiers, P. Thuéry, M. Ephritikhine, T. Cantat, *Angew. Chem. Int. Ed.,* **2012**, *51*, 187-190.

forces of the increasing effort that is being put nowadays in transforming CO_2 in an economical and efficient manner.[9]
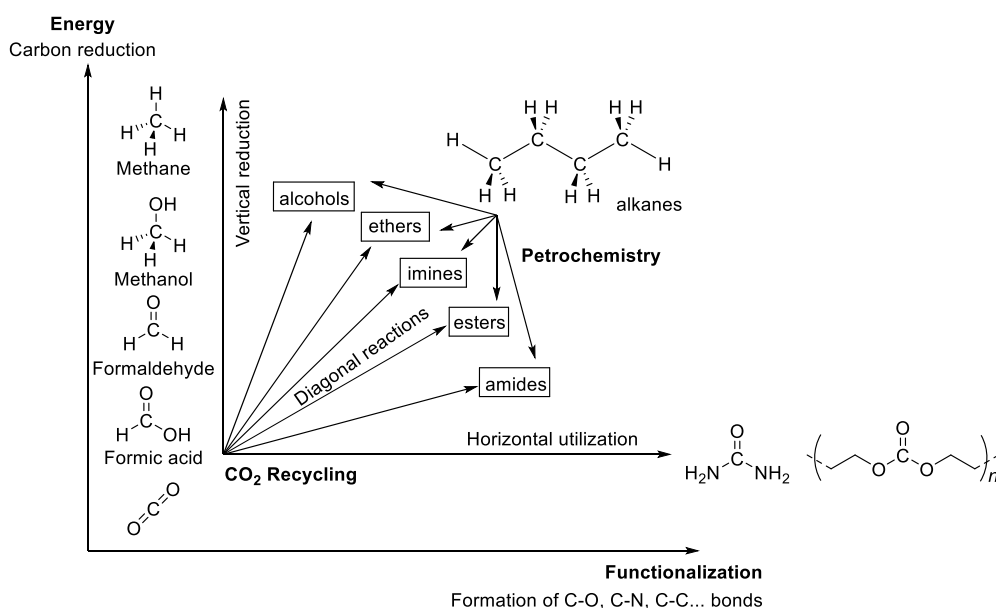

Figure 2. Versatility of carbon dioxide as a carbon source for fine chemicals and/or fuels in comparison to petrochemistry (adapted from reference 8).

1.2. The organometallic approach

The slight electrophilic character of carbon dioxide makes possible its functionalization by Lewis bases or metal-based nucleophiles such as organolithium, organotin, organozinc or Grignard reagents. Nevertheless, their applicability is limited to the formation of C−C bonds, and there are some other obvious drawbacks of its use: their high reactivity precludes chemoselective reactions in many occasions, and it can give rise to undesired side-reactions.[10]

---

[9] G. A. Olah, *Angew. Chem. Int. Ed*. **2005**, *44*, 2636-2639. For a recent review on the Methanol Economy, see W-C. Liu, J. Baek, G. A. Somorjai, *Topics in Catalysis,* **2018**, *61*, 530-541.
[10] K. Huang, C-L. Sun, Z-J. Shi, *Chem. Soc. Rev.*, **2011**, *40*, 2435-2452.

Chapter 1. Introduction

For these reasons, some alternatives have been emerging in homogeneous catalysis during the last few decades that proved useful in activating small molecules under mild conditions, such as Frustrated Lewis Pairs,[11] organocatalysis[12] or catalysis assisted by organometallic complexes.[13] Among these options, the latter is an attractive choice due to the wide variety of transition metals available. Also, the possibility of easily modulating the electronic and steric properties of the catalysts by modifying the metal (or its oxidation state) and the ligands makes this field one of the most active areas in chemistry. In fact, the role of these complexes in the chemistry of carbon dioxide has undergone an exponential growth in the last few years (Figure 3).
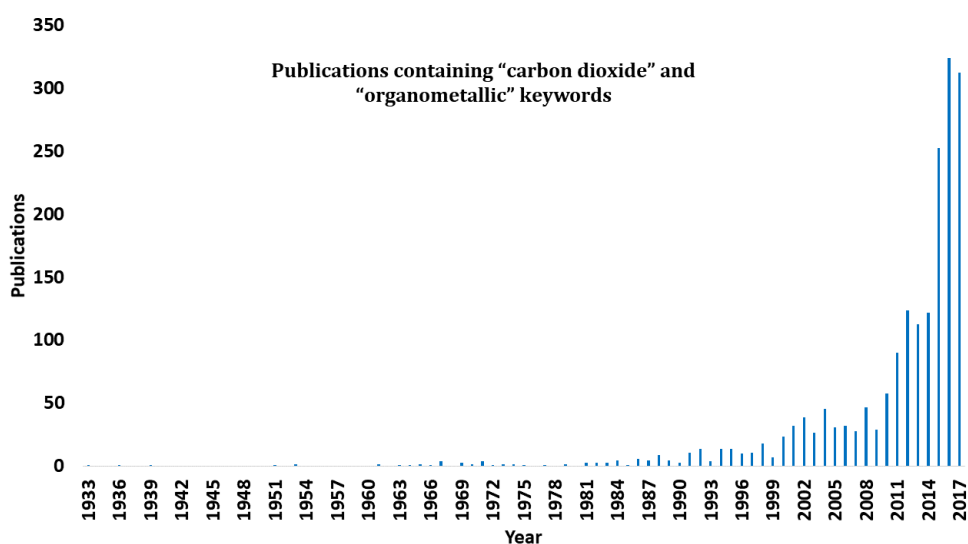

Figure 3. Illustration of the application of organometallic complexes in carbon dioxide chemistry (obtained from Scopus database).

[11] D. W. Stephan, *Org. Biomol. Chem.,* **2008**, *6*, 1535-1539.

[12] B. R. Buckley, M. C. Kimber, N. H. Slater, *Annu. Rep. Prog. Chem. Sect. B: Org. Chem.,* **2012**, *108*, 98-109.

[13] J. F. Hartwig, *Organotransition Metal Chemistry: From Bonding to Catalysis*, University Science Books, Sausalito, CA, **2009**.

In the specific case of CO_2, there are some other advantages of using transition metals for its transformation: the obtainment of carbon dioxide complexes can serve as models of intermediates that can originate on the surface of a metal during catalytic events in heterogeneous catalysis. Besides, the several coordination modes that CO_2 can adopt upon coordination to a transition metal (up to 5 when considering a 1:1 ratio) give rise to different types of functionalizing this molecule (Figure 4).[14] In this fashion, once the molecule has approached the metal atom, numerous reactive processes can occur, such as oxidative cycloaddition of carbon dioxide, transmetalation reactions or insertion of allenes, alkenes, alkynes or hydride ligands, to name a few.[10]
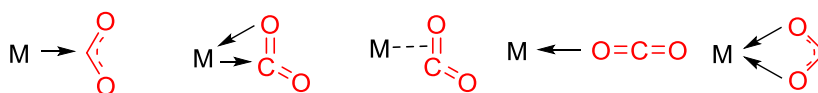

Figure 4. Different coordination modes of CO_2 upon coordination to a transition metal.

1.3. Antecedents of transition metal-catalyzed homogeneous CO_2 reduction

Even when using transition metals in the process, CO_2 reduction is not a simple task. The question of how to obtain C−H bonds from stable σ and π C−O bonds has been tackled by following different strategies depending on the reductant. Therefore, we can find examples in the literature on electrocatalysis and/or photocatalysis[15] or catalytic reduction assisted by hydride sources.[16]

The latter started its development in 1948, where Brown *et al.* observed that main-group element based hydrides such as LiAlH$_4$[17] or LiBH$_4$[18] were able to transform CO_2 by themselves, affording different types of products depending

[14] D. H. Gibson, *Chem. Rev.,* **1993**, *96*, 2063-2095.

[15] H. Takeda, C. Cometto, O. Ishitani, M. Robert, *ACS Catal.,* **2017**, *7*, 70-88.

[16] C. Chauvier, T. Cantat, *ACS Catal.,* **2017**, *7*, 2107-2115.

[17] R.F. Nystrom, W.H. Yanko, W. Brown, *J. Am. Chem. Soc.,* **1948**, *70,* 441.

[18] J. G. Burr Jr., W. Brown, H. E. Heller, *J. Am. Chem. Soc.,* **1950**, *72*, 2560-2562.

on the reaction conditions. Since then, organometallic complexes have been employed in combination with various hydride sources like hydrogen, boranes or silanes so as to overcome the kinetic barriers of this transformation (Scheme 1). Additionally, selective synthesis of any of the intermediates of this synthetic pathway can be obtained in a few cases by careful design of the catalyst, thus precluding the presence of mixtures of compounds which need to be purified afterwards.
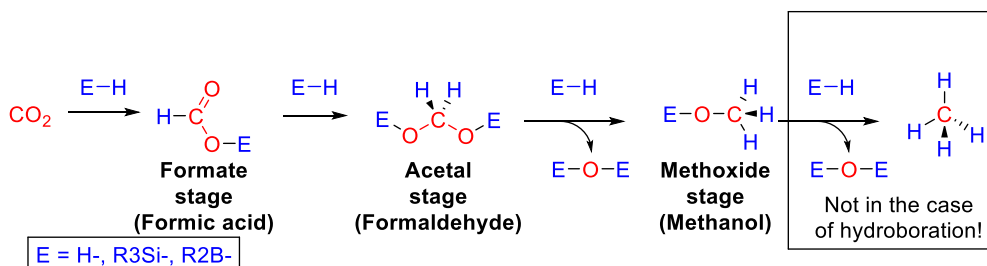
Scheme 1. Overview of the sequential steps in CO_2 reduction assisted by hydride sources (vertical reduction in Figure 2). Conversion to methane from methoxyborane is not known.[19]

In the case of hydrogen, the main handicap is its lack of reactivity due to its absence of polarity and the high stability of its σ bond (BDE_{H-H} = 104.2 kcal/mol).[20] This becomes an additional problem, because that implies there would be two inert molecules (H_2 and CO_2) that need to be activated instead of one. Thus, very high pressure of both gases needs to be applied to get some conversion. These disadvantages, along with some complications inherent to the nature of the reduced products remain as problems still to be solved. For instance, reduction of CO_2 to formic acid is not favourable thermodynamically due to entropic factors (ΔH_r = -7.5 kcal/mol and ΔG_r = 7.6 kcal/mol)[21] and the

[19] S. Bontemps, *Coord. Chem. Rev.,* **2016**, *308*, 117-130.
[20] G. Herzberg, A. Monfils, *J. Mol. Spect.,* **1960**, *5*, 482-498.
[21] W. Leitner, *Angew. Chem. Int. Ed. Engl.,* **1995**, *34*, 2207-2221.

most common solution to displace the equilibrium to the products is the addition of Lewis basic additives (usually amines) or solvents so the product can be obtained as a salt or it can be stabilized by hydrogen-bonding, respectively.[22] The use of this type of additives is also extensively used in the methanol synthesis, but in this case it is employed to circumvent kinetic issues: carbon dioxide can be captured by alcohols or amines (Figure 2, diagonal and horizontal reactions) in order to give substrates that are easier to hydrogenate to the methanol stage (Figure 5, pathway B).[23]
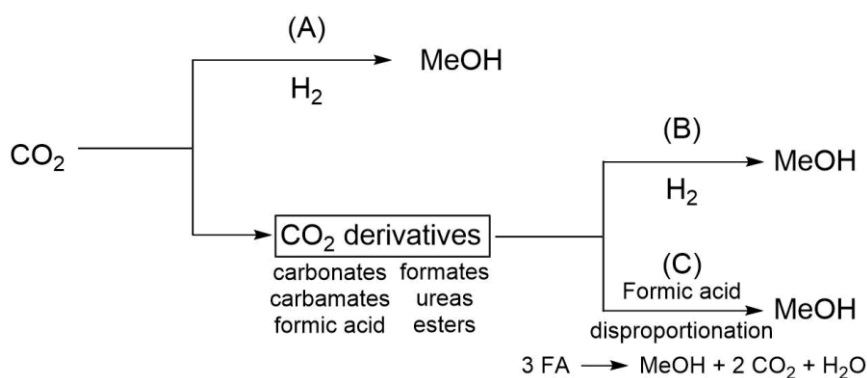

Figure 5. Synthetic pathways for obtaining methanol from carbon dioxide (adapted from reference 23).

Some of the few examples to date in which methanol can be directly obtained by hydrogenation include the one reported by Sanford *et al.* (Scheme 2A), where a system of 3 different catalysts achieve effective cascade transformation to sequentially afford formic acid, methyl formate and finally methanol (Figure 5, pathway B).[24] On the other hand, Klankermayer and Leitner

---

[22] a) J. Klankermayer, S. Wesselbaum, K. Beydoun, W. Leitner, *Angew. Chem. Int. Ed.,* **2016**, *55,* 7296-7343; b) W. H. Bernskoetter, N. Hazari, *Acc. Chem. Res.,* **2017**, *50*, 1049-1058.
[23] K. Sordakis, C. Tang, L. K. Vogt, H. Junge, P. J. Dyson, M. Beller, G. Laurenczy, *Chem. Rev.,* **2018**, *118,* 372-433.
[24] C. A. Huff, M. S. Sanford, *J. Am. Chem. Soc.,* **2011**, *133*, 18122-18125.

in 2012,[25] and Beller in 2017[26] described very similar conditions for CO_2 hydrogenation to methanol, given the similitude in solvent, ligand and acidic additive for the reaction to proceed (Scheme 2B and 2C). In both cases, analogous reaction times (24 h) and considerably harsh conditions are required for achieving low amounts of product. A significant advance was achieved in 2016 by the group of Prakash and Olah.[27] In this work, the authors employed pentaethylenehexamine to capture carbon dioxide, after which the resulting formate was hydrogenated by using a ruthenium catalyst (Scheme 2D). The reported system proved to be robust enough to be recycled 5 times giving TON values superior to 2000, and it turned out to be active enough to capture carbon dioxide from air, transforming it into methanol with good yields.

[25] S. Wesselbaum, T. vom Stein, J. Klankermayer, W. Leitner, *Angew. Chem. Int. Ed.,* **2012**, *51,* 7499-7502.

[26] J. Schneidewind, R. Adam, W. Baumann, R. Jackstell, M. Beller, *Angew. Chem. Int. Ed.,* **2017**, *56*, 1890-1893.

[27] J. Kothandaraman, A. Goeppert, M. Czaun, G. A. Olah, G. K. S. Prakash, *J. Am. Chem. Soc.,* **2016**, *138*, 778-781.
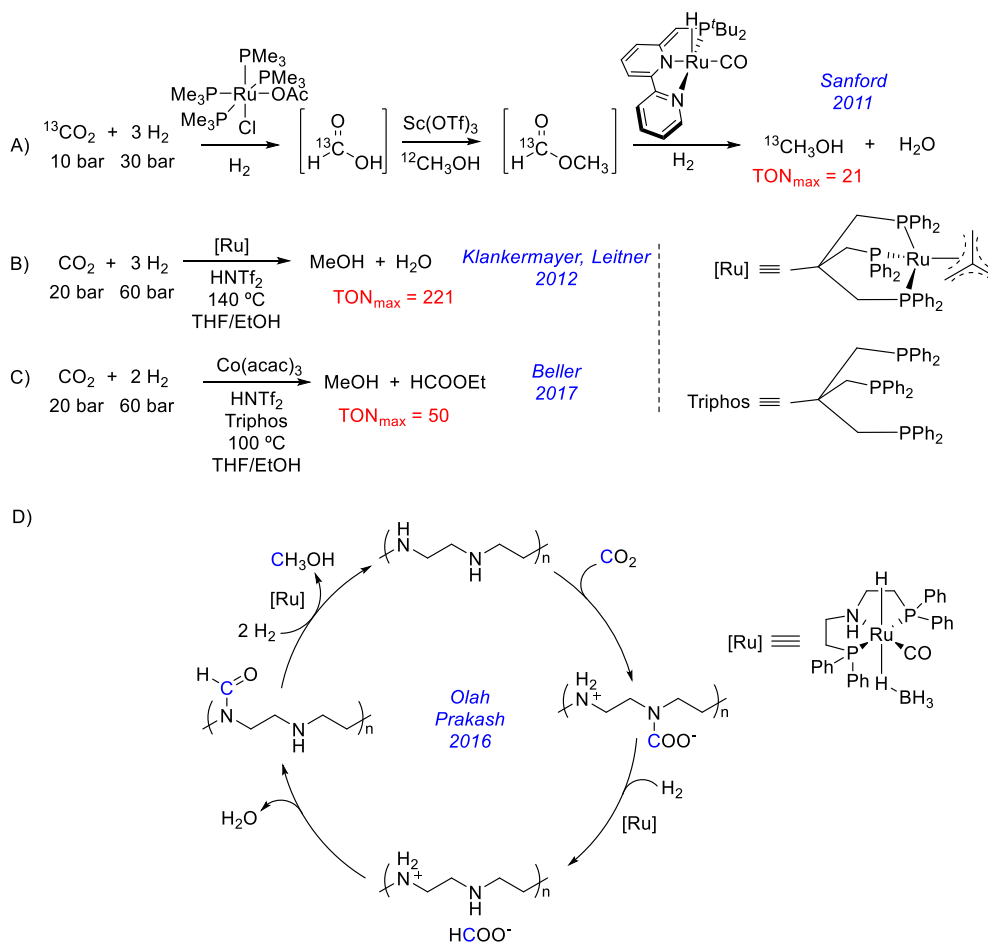
Scheme 2. Current methods to directly obtain methanol from carbon dioxide hydrogenation (adapted from references 24-27).

The obtainment of formaldehyde from CO_2 hydrogenation is even more underdeveloped, given that there are only a few examples reported in the literature.[28] These include a stoichiometric reaction described by Floriani in 1985, in which Schwartz's reagent reacts with CO_2 to afford an oxygen-bridged dimer and formaldehyde,[29] and a catalytic reaction also reported by

[28] L. E. Heim, H. Konnerth, M. H. G. Prechtl, *Green. Chem.,* **2017**, *19*, 2347-2355.

[29] S. Gambarotta, S. Strologo, C. Floriani, A. Chiesi-Villa, C. Guastini, *J. Am. Chem. Soc.,* **1985**, *107*, 6278-6272.

Chapter 1. Introduction

Klankermayer and Leitner in 2016, where their same ruthenium complex described above was combined with aluminium triflate in methanol to yield the acetal (Scheme 1, formaldehyde stage) and the methyl formate derivatives in a 2:1 ratio (Scheme 3, equations A and B respectively).[30]
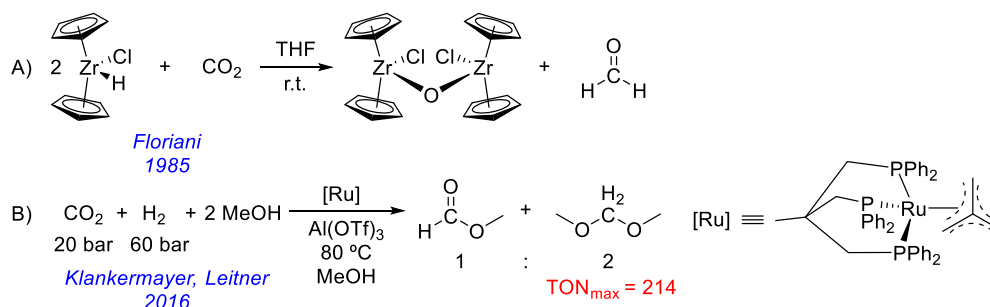
Scheme 3. Different methods to obtain formaldehyde from carbon dioxide hydrogenation (adapted from references 29 and 30).

The scarcity of results (with low turnover numbers and poor selectivity sometimes) from direct hydrogenation of CO_2 to reduced derivatives along with the harsh reaction conditions required reflect once again the challenge in using hydrogen as a reductant, showing that further work needs to be done in this field.

An alternative approach would be the employment of reductants which possess less energy demanding activation barriers, such as boranes or silanes. The polarity of these substrates makes them hydridic enough (BDE_{B-H} = 82.6 kcal/mol and BDE_{Si-H} = 70.2 kcal/mol) to attack the carbon atom of CO_2 once it has been activated by a transition metal. Moreover, the strength of the new resulting bonds (BDE_{B-O} = 193.5 kcal/mol and BDE_{Si-O} = 191.4 kcal/mol) acts as a thermodynamic driving force for the reduction when using these reagents instead of hydrogen (BDE_{H-O} = 102.8 kcal/mol).[31] All these data seems to suggest

---

[30] K. Thenert, K. Beydoun, J. Wiesenthal, W. Leitner, J. Klankermayer, *Angew. Chem. Int. Ed.,* **2016**, *55*, 12266-12269.

[31] Y-R. Luo, *Comprehensive Handbook of Chemical Bond Energies,* CRC Press: Boca Raton, FL, 2007.

that carbon dioxide should undergo reduction reactions under mild conditions when using these hydride sources, which is desirable from the point of view of safety and economy, given that the energy required would be much lower. The only drawback to this method is the generation of boryl ethers or siloxanes; in order to regenerate the corresponding hydroborane or hydrosilane, the employment of a hydride source would be necessary.[16] Nonetheless, siloxanes are very valuable in the polymer industry, and "what may be by-products to organic chemists could be the synthetic target for a polymer chemist".[32] Therefore, the by-products of CO_2 hydrosilation could be useful in the silicone chemistry.

1.3.1 Formaldehyde derivatives

Formaldehyde is synthesized in the chemical industry by means of the *Formox process*. It consists of a 3-step process in which natural gas is transformed to syngas by reaction with water at very high temperatures. Then, the syngas is reduced to methanol, which is later oxidized, affording formaldehyde as the main product at the end of the process (Scheme 4).[28]
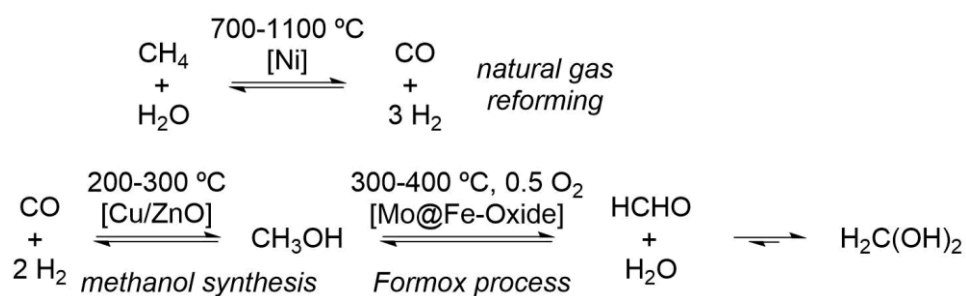
Scheme 4. Current industrial synthesis of formaldehyde (adapted from reference 28).

---

[32] J. B. Grande, *"The Piers-Rubinsztajn Reaction: New Routes to Structured Silicones".* PhD Thesis, McMaster University, 2013.

Following the previous examples, the conditions employed in this process call for an alternative method, less energy-demanding, more economically viable and environmentally friendly. As it will be shown below, the chemistry of hydroboration and hydrosilation to the formaldehyde stage is still somewhat primitive, with only a few systems described on each case.[33]

Bis(boryl)acetal derivatives

Reduction to formatoborane or methoxyborane derivatives is well-known, and there are numerous examples describing such transformations. However, chemoselectivity towards the intermediate bis(boryl)acetal is rare.[33] Hydroboration to the formaldehyde level was firstly described by Sabo-Etienne *et al.* in 2012. In their work, they showed that the ruthenium complex [$RuH_2(\eta^2$-$H_2)_2(PCy_3)_2$] was able to afford the formaldehyde surrogate in the presence of pinacolborane, albeit in very low yield and poor selectivity (26% of methylene products) due to the presence of numerous species in the reaction mixture (Scheme 5).[34] In a subsequent article, they could trap both methylene species by reaction with CD_3OD, yielding the corresponding hemiacetal CD_3OCH_2OD.[35]
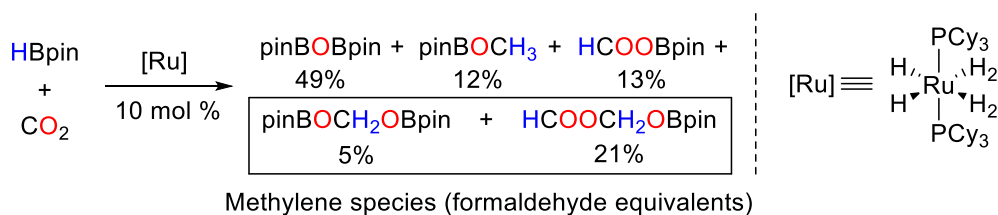
Scheme 5. Hydroboration of carbon dioxide catalyzed by a ruthenium complex (adapted from reference 34).

---

[33] For more examples of carbon dioxide hydroboration, see reference 19. For more examples of carbon dioxide hydrosilation, see: F. J. Fernández-Álvarez, L. A. Oro, *ChemCatChem*, **2018**, *10*, 4783-4796.

[34] S. Bontemps, L. Vendier, S. Sabo-Etienne, *Angew. Chem. Int. Ed.,* **2012**, *51*, 1671-1674.

[35] S. Bontemps, S. Sabo-Etienne, *Angew. Chem. Int. Ed.,* **2013**, *52*, 10253-10255.

In 2014, the same group improved the synthesis of the bis(boryl)acetal by slightly modifying the structure of the ligands and the reaction conditions (solvent, catalyst loading, CO_2 pressure), and they trapped it by means of a bulky amine such as 2,6-diisopropylaniline, achieving yields up to 74% of the resulting imine (Scheme 6A). Such a high yield is in contrast with the observed yield for the acetal species, but the authors attribute the high conversion obtained due to the role of pinacolborane as a dehydrating agent, displacing the equilibrium to the products. In the final step, the imine can undergo hydrolysis to produce formalin.[36] A year later, they explored this type of transformation by using an iron catalyst. This time, the resulting acetal was used as a CH_2 transfer agent in a wide variety of molecules, affording C–C, C–O and C–N bonds (Scheme 6B).[37] A similar strategy was employed by Turculet *et al.* after transforming carbon dioxide to the acetal level with group 10 metals (Scheme 7).[38]
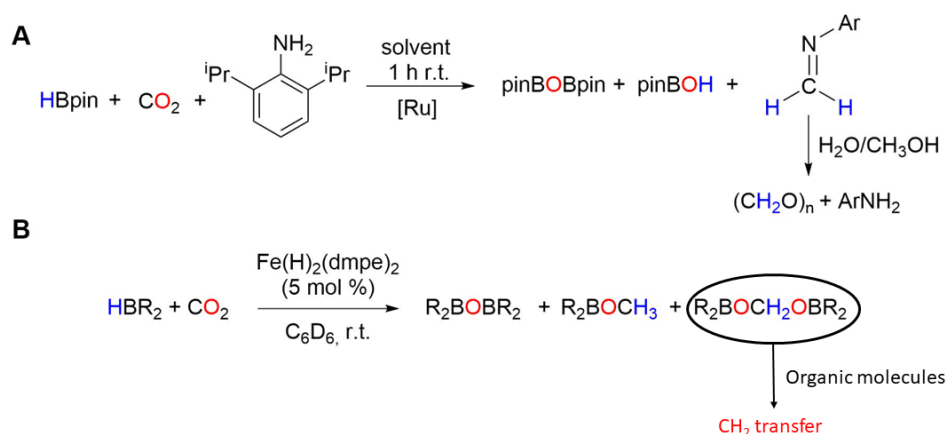

Scheme 6. Different strategies followed by Sabo-Etienne *et al.* to capture formaldehyde from hydroboration of carbon dioxide (adapted from references 36 and 37).

[36] S. Bontemps, L. Vendier, S. Sabo-Etienne, *J. Am. Chem. Soc.,* **2014**, *136*, 4419-4425.

[37] G. Jin, C. G. Werncke, Y. Escudié, S. Sabo-Etienne, S. Bontemps, *J. Am. Chem. Soc.,* **2015**, *137*, 9563-9566.

[38] L. J. Murphy, H. Hollenhorst, R. McDonald, M. Ferguson, M. D. Lumsden, L. Turculet, *Organometallics*, **2017**, *36*, 3709-3720.
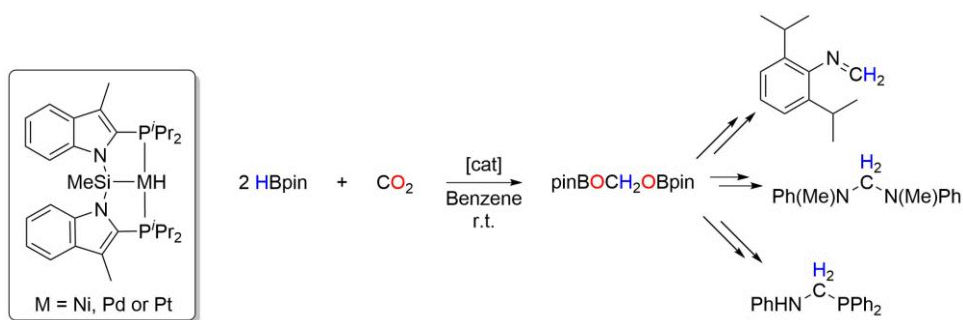
Scheme 7. Approach followed by Turculet *et al.* to transfer a methylene fragment into organic molecules from carbon dioxide (adapted from reference 38).

Another example of CO_2 hydroboration to the formaldehyde level was reported by Berthet and Cantat in 2016. The authors used a set of 1st row transition metal complexes (Cu, Co and Fe) stabilized by silylphosphine ligands as catalysts in the reaction between carbon dioxide and 9-BBN (9-borabicyclo[3.3.1]nonane). Whereas the Co and Fe compounds showed chemoselectivity towards the methoxyborane (up to 100%) at 60 °C, the Cu derivatives gave the acetal species in yields up to 92% in less forcing reaction conditions and faster reactions (Scheme 8).[39]
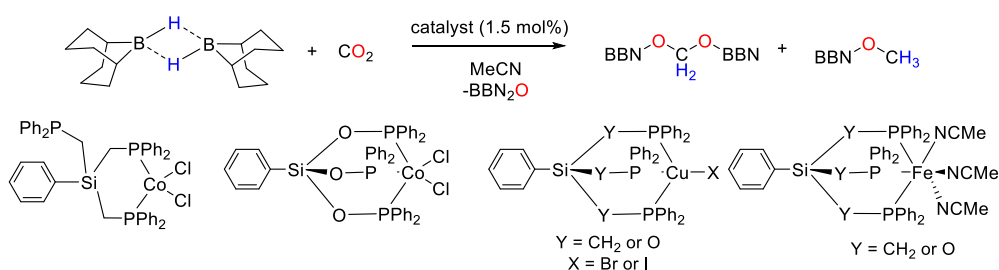

Scheme 8. Catalytic systems developed by Berthet and Cantat for CO_2 hydroboration (adapted from reference 39).

[39] A. Aloisi, J-C. Berthet, C. Genre, P. Thuéry, T. Cantat, *Dalton Trans.,* **2016**, *45*, 14774-14788.

Bis(silyl)acetal derivatives

In the same way as hydroboration, chemoselective partial reduction to intermediate species is also challenging in the case of hydrosilation. In fact, various reports have described the synthesis of silyl formates or the full reduction to methane, yet the controlled reduction to bis(silyl)acetal or methoxysilane derivatives is still uncommon, with only a few examples described (Scheme 9).[40]
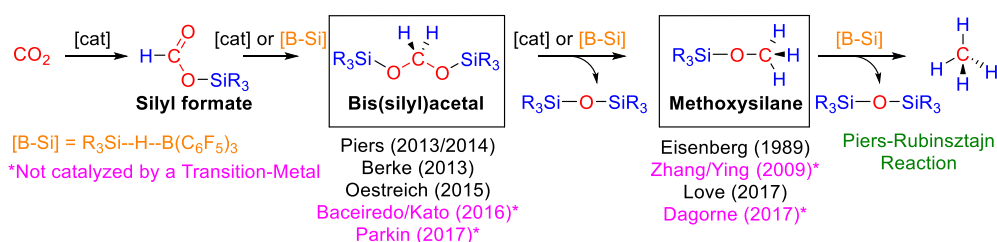
Scheme 9. Overview of the current situation in CO_2 hydrosilation chemistry. *NB*: The last step (*i.e.* over-reduction of alkoxysilanes to alkanes mediated by silanes and $B(C_6F_5)_3$) is called Piers-Rubinsztajn reaction.[41]

In the hydrosilation situation, it is first necessary to mention that activation of the Si−H bond by strong Lewis acids can take place, increasing the hydricity of the reducing agent. As a result, these species are powerful reductants that can achieve full conversion to methane from silyl formates (Scheme 9). One of the most common compounds of this sort is that composed of triethylsilane and tris(pentafluorophenyl)borane (BCF).[42] In fact, these borane-silane complexes have been extensively studied in the hydrosilation of unsaturated molecules such as carbonyl, imine, or alkene functionalizations (Scheme 10), the
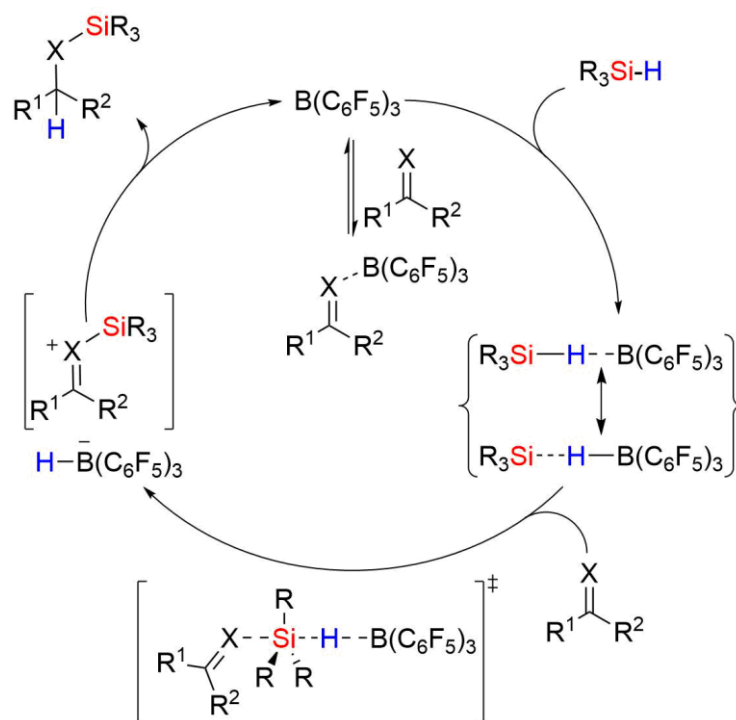
---

[40] T. T. Metsänen, M. Oestreich, *Organometallics*, **2015**, *34*, 543-546.

[41] M. A. Brook, *Chem. Eur. J.,* **2018**, *24*, 8458-8469.

[42] D. J. Parks, J. M. Blackwell, W. E. Piers, *J. Org. Chem.,* **2000**, *65*, 3090-3098.

deoxygenation of alcohols or carbohydrates or even exhaustive reduction of α, β-unsaturated carboxylic acids, to name a few.[43]


Scheme 10. The role of $B(C_6F_5)_3$ in the hydrosilation of unsaturated organic molecules (adapted from reference 43).

This type of molecule has always been elusive to isolation, given that the only way of detecting its existence relied on spectroscopic techniques such as NMR. Nonetheless, Piers, Tuononen *et al.* were able to crystallize one of these derivatives and fully confirm its structure by X-Ray crystallography methods (Scheme 11).[44]

---

[43] M. Oestreich, J. Hermeke, J. Mohr, *Chem. Soc. Rev.,* **2015**, *44*, 2202-2220.
[44] A. Y. Houghton, J. Hurmalainen, A. Mansikkamäki, W. E. Piers, H. M. Tuononen, *Nat. Chem.,* **2014**, *6*, 983-988.

[78]
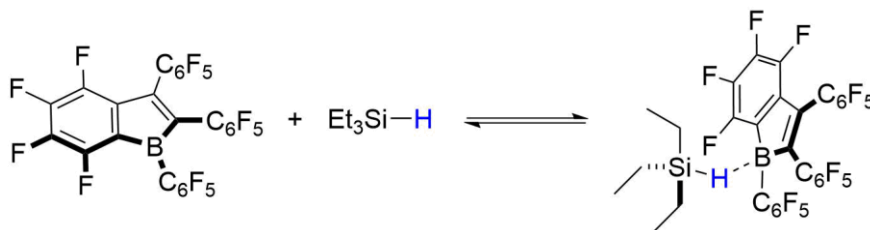
Scheme 11. Borane-silane complex crystallized by Piers and Tuononen (adapted from reference 44).

As one can imagine, the presence of this type of complexes in the reaction medium adds an extra difficulty to the challenge of obtaining chemoselectivity in the partial reduction of carbon dioxide to bis(silyl)acetal or methoxysilane, since the uncontrolled reduction to methane (Piers-Rubinsztajn reaction, Scheme 9) is likely in these cases. For this reason, the concentration of the borane-silane adduct must be limited by effectively reducing the amount of free borane in the reaction.

The first example of some bis(silyl)acetal accumulation during catalysis was observed by Piers, Maron, Eisenstein *et al.* in 2013, when combining the strongly Lewis acidic decamethylscandocinium hydridoborate $[Cp*_2Sc]^+[HB(C_6F_5)_3]^-$ with triethylsilane for the hydrosilation of CO_2 to methane. In this system, the authors take advantage of the high oxophilicity of the scandium center to bind carbon dioxide. Then, the hydridoborate unit transfers the hydride to the carbon atom in order to yield the formate derivative. In this step, some $B(C_6F_5)_3$ is released and it can form the borane-silane complex that performs the full reduction to methane (Scheme 12). The authors emphasize that there is no neutral Cp_2*ScH during catalysis, and that the CO_2 activation takes place through the hydridoborate moiety.[45]

[45] A. Berkefeld, W. E. Piers, M. Parvez, L. Castro, L. Maron, O. Eisenstein, *Chem. Sci.,* **2013**, *4*, 2152-2162.
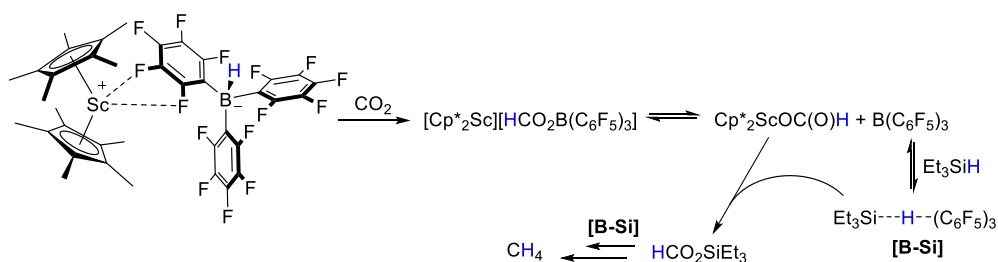
Scheme 12. Mechanism of methane formation from CO_2 by using the scandium system reported by Piers, Maron, Eisenstein *et al.* (adapted from reference 45).

The accumulation of some bis(silyl)acetal during the process made the authors design a different scaffold that could be more effective in capturing the borane and avoiding over-reduction. This led them to synthesize the anilido-bipyridil complex shown in Scheme 13. In this example, they achieve full sequestration of the Lewis acid and obtained the formaldehyde derivative by using triethylsilane as the hydride source, achieving the highest TON to date (~3400).[46]

$Ar = 3,5\text{-}^tBu_2C_6H_3$
$R = CH_2SiMe_2Ph$
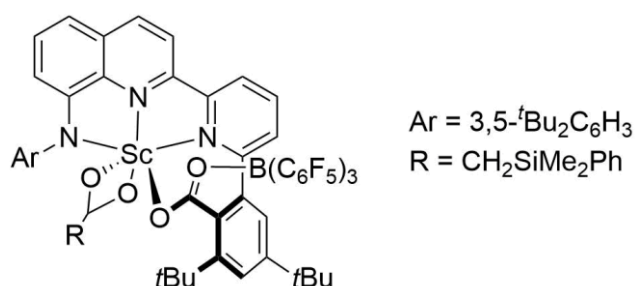
Scheme 13. Piers's system for selective hydrosilation to bis(silyl)acetal (adapted from reference 46).

In 2013, the group of Berke also described the employment of $B(C_6F_5)_3$ as a co-catalyst for this reaction, becoming the first example in achieving selective formation of the methylene derivative. In this work, the Lewis acid showed no

---

46 F. A. Leblanc, W. E. Piers, M. Parvez, *Angew. Chem. Int. Ed.,* **2014**, *53*, 789-792.

reaction upon exposure to the rhenium hydrides [ReHBr(NO)(PR$_3$)$_2$] (where R is either isopropyl or cyclohexyl), but in the presence of CO_2 a couple of borane-bound formato units are observed in a resulting dimer, suggesting a Frustrated Lewis Pair type activation. The dimer can be cleaved by hydrogenation, giving rise to a catalyst that can reduce carbon dioxide in the presence of triethylsilane to yield the acetal species with high selectivity (Scheme 14).[47]
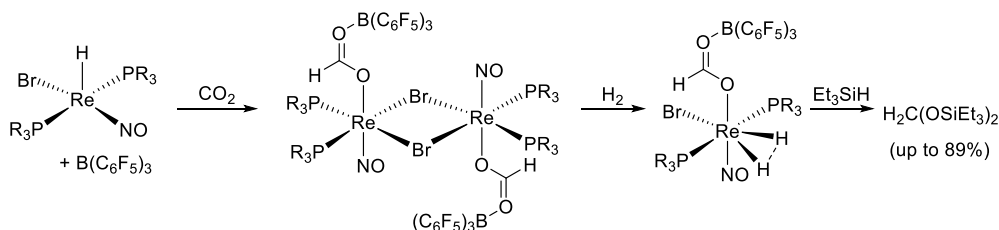

Scheme 14. Frustrated Lewis Pair type activation of carbon dioxide by Berke's system (adapted from reference 47).

Finally, the last and most recent example of transition metal-catalyzed hydrosilation to the aldehyde level was reported by Oestreich *et al.* in 2015. By making use of cationic Ru−S complexes, they were able to tune the selectivity of the process depending on the temperature (Scheme 15): at 80 °C the bis(silyl)acetal compound was observed as the major product (96%), but heating the reaction vessel up to 150 °C gave rise to the methoxysilane as the main species (75%). Alkyl-substituted silanes were used in this study, since the aryl-based ones undergo ligand rearrangement at high temperatures. Additionally, the authors point out that in their mechanism the silyl cation transfer takes place before the hydride attack during the reduction.[40]

---

[47] Y. Jiang, O. Blacque, T. Fox, H. Berke, *J. Am. Chem. Soc.,* **2013**, *135,* 7751-7760.
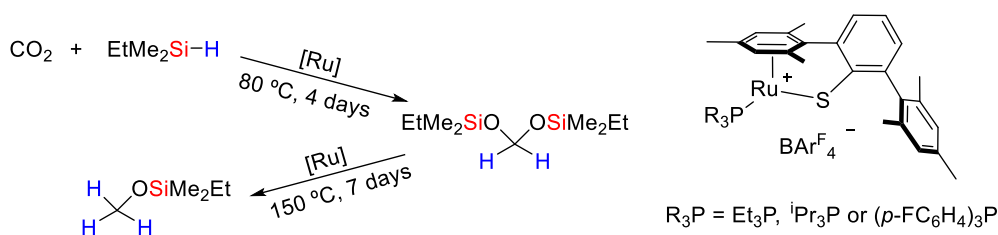
Scheme 15. Temperature dependence of the chemoselectivity in CO_2 hydrosilation when using Oestreich's catalyst.

Although they are not based on transition metals, it is worth mentioning a couple of examples in which selectivity towards the methylene species is achieved as well by using the tris(pentafluorophenyl)borane strategy (Scheme 16). These include the reports by the group of Baceiredo and Kato in 2017, where a N,P-heterocyclic germylene adduct with $B(C_6F_5)_3$ acts as a FLP catalyst in the hydrosilation of CO_2 to the formaldehyde level,[48] and the one reported in the same year by Parkin *et al.*, in which hydrides of Mg and Zn complexes stabilized by benzimidazol-based ligands can react with BCF to afford the corresponding ion pairs, which are effective catalysts for hydrosilation of CO_2 to bis(silyl)acetal or methane, depending on the silane (Ph_3SiH and $PhSiH_3$, respectively).[49]
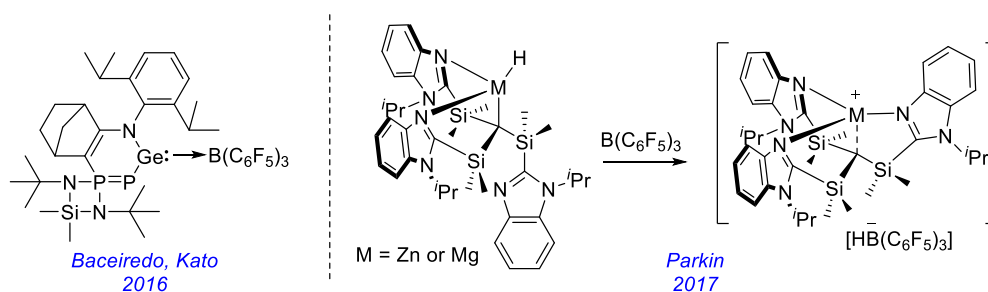
Scheme 16. Non-transition metal based systems that are able to partially reduce carbon dioxide to the aldehyde stage.

[48] N. del Rio, M. Lopez-Reyes, A. Baceiredo, N. Saffon-Merceron, D. Lutters, T. Müller, T. Kato, *Angew. Chem. Int. Ed.,* **2017**, *56,* 1365-1370.

[49] M. Rauch, G. Parkin, *J. Am. Chem. Soc.,* **2017**, *139*, 18162-18165.

In light of these results, it can be deduced that the Lewis acid $B(C_6F_5)_3$ is not able to activate CO_2 by itself. Nonetheless, once it is partially reduced (*e.g.* silyl formate), over-reduction can take place in the presence of a silane as a hydride donor. For this reason, a catalyst capable of activating carbon dioxide and effectively sequestering BCF is necessary in order to achieve chemoselective reduction to intermediate species. As it can be seen above this is not a trivial task, and careful design of the system is needed so as not to get mixture of products during the catalytic reactions.

In this chapter, the synthesis of a Ni(II) complex stabilized by a bis(phosphino)boryl ligand and experimental data showing its performance as a catalyst for carbon dioxide hydrosilation are described. Experimental and theoretical mechanistic studies are also shown, as well as a proposal for a catalytic cycle.

2. Results and discussion

The aim of this work is to exploit the strong *trans* influence exerted by the PBP ligand and apply it in CO_2 activation. A common strategy for activating this molecule involves nucleophilic attack from a ligand of a metal complex to the carbon atom of carbon dioxide, which possesses a slight electrophilic character (the higher contribution of the carbon atom to the LUMO can be observed in Figure 6). If the C−O bond weakens enough, CO_2 can insert into the metal-ligand bond.
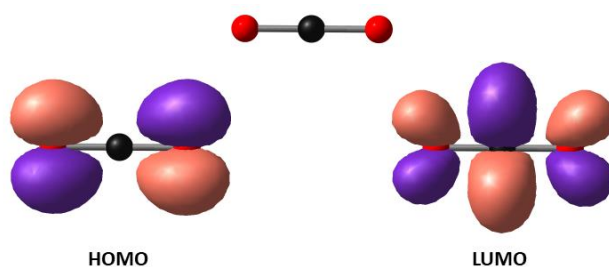
Figure 6. Frontier molecular orbitals of carbon dioxide, showing its ambiphilic character; it can behave as a nucleophile through the oxygen atoms (HOMO) or it can act as an electrophile through the carbon atom (LUMO).

Taking this information into consideration, a hydride ligand in *trans* to the boron atom of the PBP framework would be strongly nucleophilic, given that the M−H bond is weakened by the strong *trans* influence of the boryl moiety. In this way, the hydride could attack a carbon dioxide molecule to yield the

[84]

corresponding formate.[50] Therefore, a complex containing a hydride ligand in *trans* to the PBP scaffold was envisaged as a potential compound for activating carbon dioxide.

2.1. Synthesis of Ni−PBP complexes

The synthesis of Ni(II) complexes stabilized by the ^{tBu}PBP ligand **1** has been previously described in our group: NiBr$_2$(dme) can react with **1** in toluene at room temperature to afford the bromide derivative **2** in very high yields. Et$_3$N is needed in order to neutralize the hydrobromic acid resulting from the activation of the B−H bond (Scheme 17).[51]
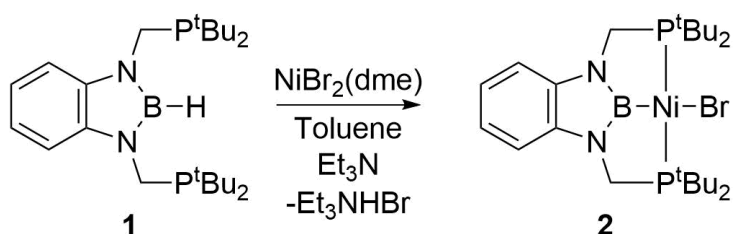
Scheme 17. Utilization of the ^{tBu}PBP ligand **1** in the synthesis of Ni(II) complexes.

In order to test the σ-donation capability of the boryl ligand, the carbonyl derivative **3** was synthesized in dichloromethane by using the halogen abstractor NaBAr$_4$^{F} (sodium tetrakis(3,5-bis(trifluoromethyl)phenyl)borate) in the presence of CO (Scheme 18). The poor coordination ability of the borate anion[52] makes possible the obtainment of a clean product after a few minutes at room temperature. After work-up, X-Ray quality crystals (Figure 7) can be grown by slow diffusion of hexamethyldisiloxane into a dichloromethane solution (10:1 ratio) of **3**.

[50] J. E. Heimann, W. H. Bernskoetter, N. Hazari, J. M. Mayer, *Chem. Sci.,* **2018**, *9*, 6629-6638.
[51] N. Curado, C. Maya, J. López-Serrano, A. Rodriguez, *Chem. Commun.,* **2014**, *50*, 15718-15721.
[52] N. A. Yakelis, R. G. Bergman, *Organometallics,* **2005**, *24*, 3579-3581.
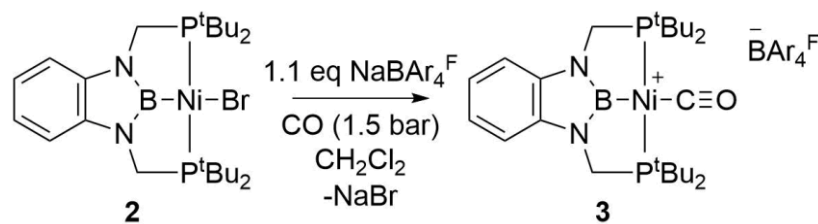
Scheme 18. Synthesis of carbonyl derivative **3**.

The structure of **3** corresponds to a somewhat distorted square-planar Ni(II) complex in which the geometrical features follow the same trend as the previous complexes of this type reported by our group, such as Ni–P distances or P–Ni–P angles.[51]
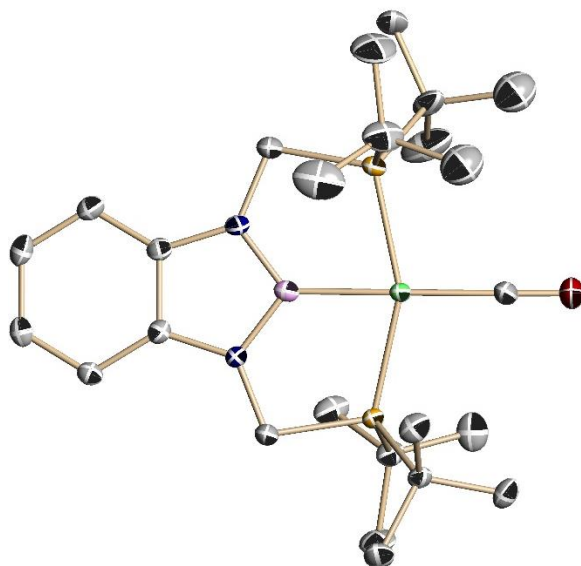
Figure 7. X-Ray structure of complex **3**. Anion and hydrogen atoms have been omitted for clarity.

This complex gives a singlet at 114.5 ppm in the $^{31}P\{^{1}H\}$ NMR spectrum, indicative of the symmetric nature of the resulting square-planar complex in which both phosphine ligands are equivalent. A broad and a sharp peak at 38 and -6.6 ppm in the $^{11}B\{^{1}H\}$ spectrum reveals the presence of a boryl and borate functionalities respectively, in agreement with the structure of **3** (Figure 8).

Unlike the case of some cationic Ni−PCP carbonyl derivatives,[53] we were able to observe the resonance of the CO ligand by $^{13}C\{^{1}H\}$ NMR, showing a singlet at 193.6 ppm. The observation of a singlet (and not a triplet due to coupling with the P atoms) might be attributable to the weak signal to noise ratio because of sensitivity reasons. An IR spectrum (Nujol) was also recorded on the sample, and it showed a $\nu(CO) = 2049$ cm^{-1}, indicative of an appreciable degree of backbonding to the carbonyl ligand ($\nu(CO) = 2143$ cm^{-1} for free CO).[54] As it can be seen in table 1, compound **3** seems to show a higher debilitation of the carbon monoxide fragment in comparison to the aryl based PCP,[53d] pointing out a greater *trans* influence of the PBP ligand. Nevertheless, the alkyl-based PCP ligand displays a similar value,[53c] in accordance with their analogous overall electronic donating abilities.[13] A closer look to both crystal structures reveals some information about the nature of the ligand in *trans* to the carbonyl moiety: whereas both complexes show a similar C−O distance to that observed in free CO ($\sim$1.128 Å),[54] the alkyl-based pincer complex possesses a shorter Ni−C$_{carbonyl}$ bond (1.78 Å) compared to **3** (1.81 Å), denoting a lower *trans* influence than the PBP framework.

[53] a) C. J. Moulton, B. L. Shaw, *J. Chem. Soc. Dalton Trans.,* **1976**, 1020-1024; b) P. Giannoccaro, G. Vasapollo, A. Sacco, *J. Chem. Soc. Chem. Commun.,* **1980**, 1136-1137; c) A. Castonguay, A. L. Beauchamp, D. Zargarian, *Inorg. Chem.,* **2009**, *48*, 3177-3184; d) S. J. Connelly, A. C. Zimmerman, W. Kaminsky, D. M. Heinekey, *Chem. Eur. J.* **2012**, *18*, 15932-15934.
[54] N. N. Greenwood, A. Earnshaw, *Chemistry of the Elements*, 2nd ed. Butterworth-Heinemann: Woburn, MA, 1997.
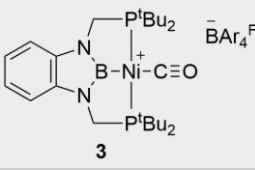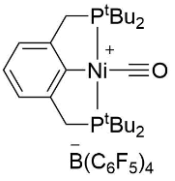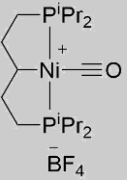
Compound	$\nu(CO)/$ cm^{-1}	C–O distance/Å	Ni–C distance/ Å	$\delta(^{13}C)/$ ppm	Reference
3	2049	1.131(6)	1.810(4)	193.6	This work
	2065	Not given	Not given	Not given	53d
	2040	1.139	1.780	Not found	53c

Table 1. Comparison of some structural data of cationic Ni pincer carbonyl complexes.
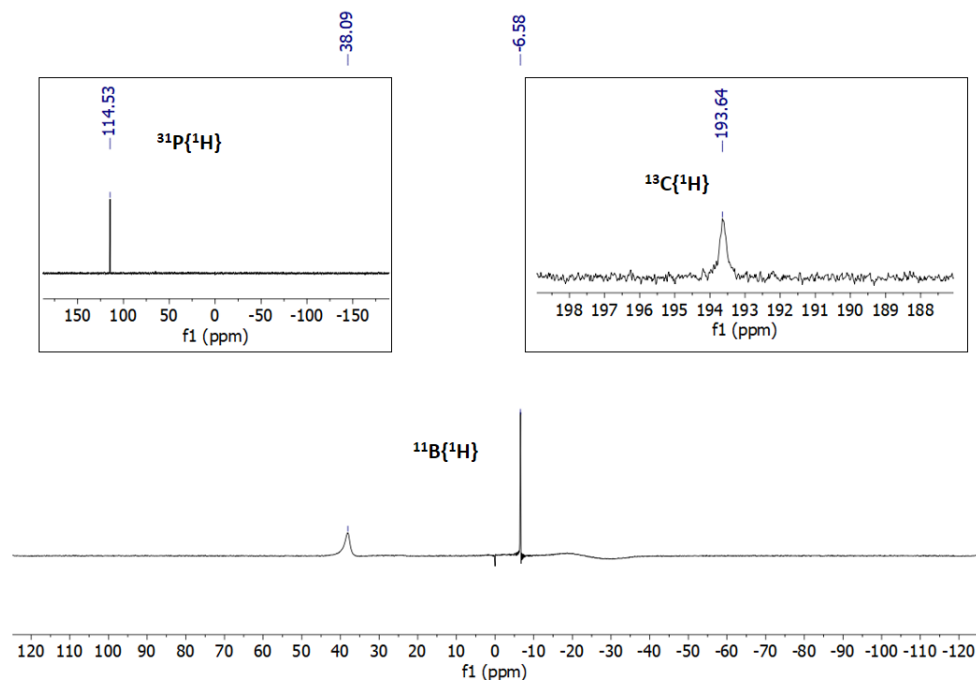
Figure 8. Relevant NMR (400 MHz, CD_2Cl_2) features of complex **3**.

Bromide derivative **2** can serve as a precursor to alkyl compounds such as methyl complex **4** (Scheme 19). Our group previously reported the synthesis of this species by making use of an excess (10 equivalents) of the Grignard reagent MeMgBr in order to achieve full conversion to the desired compound.[51] The need for such a high amount of the reagent might be due to the strong alkylating character of complex **4** because of the presence of the boryl ligand *trans* to it,[55] which would favour the opposite reaction (*i.e.* methylation of $MgBr_2$).

---

[55] J. Zhu, Z. Lin, T. B. Marder, *Inorg. Chem.,* **2005**, *44*, 9384-9390.
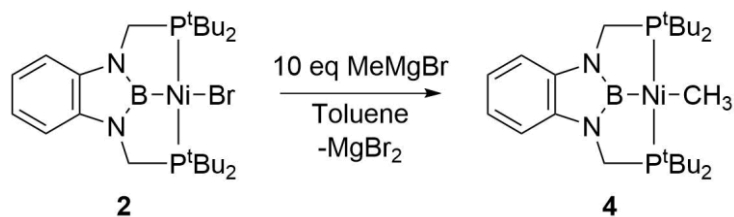
Scheme 19. Synthesis of methyl complex **4**.

Following the synthesis of **4**, our group studied its reactivity towards dihydrogen. In this work, cooperativity of the PBP ligand was demonstrated in the heterolytic cleavage of the hydrogen molecule to yield hydride **6** (Scheme 20): upon coordination of H_2, the methyl group can attack one of the hydrogen atoms (H^+) in order to form methane, whereas the remaining hydrogen atom (hydride) attacks the boron atom of the ligand (transition state of Scheme 20). Thus, the latter behaves as a Lewis acid in this mechanism, in which the Ni(0) intermediate **5** stabilized by a η^2 B−H interaction is formed. Finally, **5** undergoes oxidative addition to give hydride species **6**. Experimental evidence for such intermediate and theoretical calculations support this mechanism.[51] This method is an alternative way to the introduction of hydride ligands in a metal center, given that the strategy of ligand substitution by using numerous hydride reagents proved unfruitful.
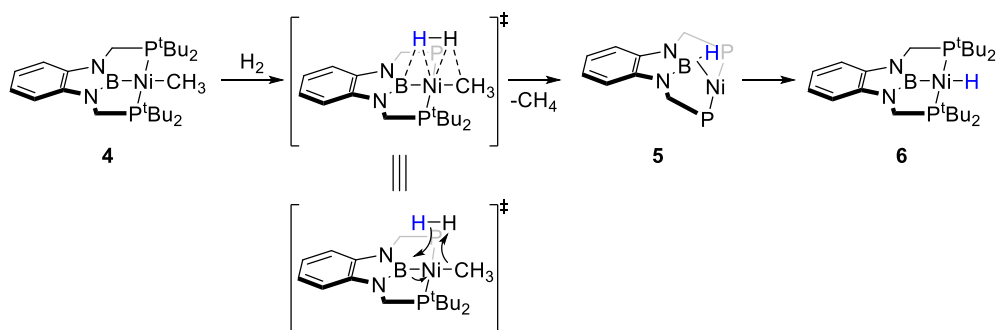
Scheme 20. Hydrogenolysis of the Ni−Me bond assisted by the PBP ligand (adapted from reference 51).

[90]

With hydride **6** in hand, reactivity tests against carbon dioxide could be performed. In this way, exposure of **6** to an atmosphere of CO_2 (1 bar) resulted in the instantaneous clean formation of a new species showing a resonance at 9.11 ppm in the ^{1}H NMR spectrum which correlates in the HSQC spectrum with a new carbon peak in ^{13}C NMR at 167.2 ppm. Given that the hydride signal disappeared in this reaction, the new signals were assigned to the newly formed formate group (Scheme 21).
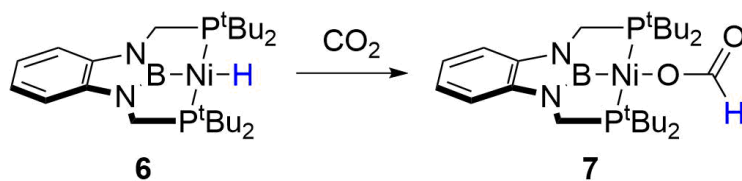
Scheme 21. Formation of formate **7** from hydride **6** upon exposure to CO_2.

Complex **7** also shows a singlet at 85.2 ppm and a broad peak at 37.5 ppm in the ^{31}P{^{1}H} and ^{11}B{^{1}H} NMR spectra, respectively (Figure 9). It is necessary to mention that by the time these studies were taking place in our laboratory, the group of Prof. Jonas C. Peters reported the isolation and characterization of formate **7**.[56]

---

[56] T-P. Lin, J. C. Peters, *J. Am. Chem. Soc.,* **2014**, *136*, 13672-13683.
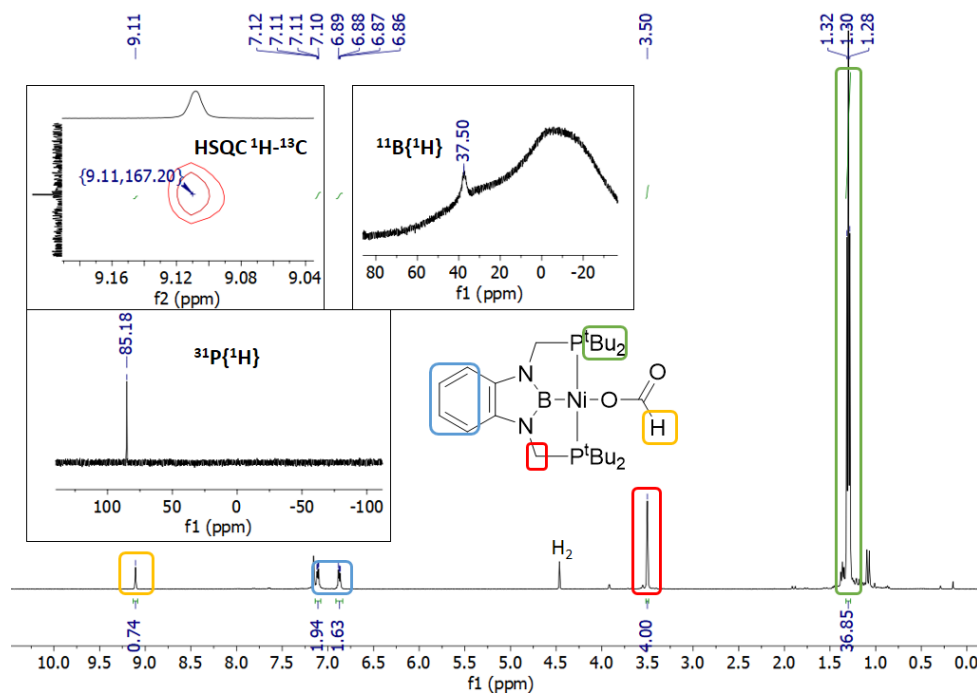
Figure 9. NMR spectra (400 MHz, C_6D_6) of the reaction mixture of the synthesis formate **7**.

2.2. Theoretical study of CO_2 insertion in Ni−H pincer complexes

The influence of the PBP ligand in the carbon dioxide insertion into the Ni−H bond was studied in more detail by means of DFT calculations.[57] For this purpose, several Ni−H complexes were compared (Figure 10), among which some of them have been experimentally synthesized (PCP,[58] POCOP[59] and PSiP[60] derivatives), so the reported results can be compared to the ones we produced

[57] Insertion of CO_2 into different types of metal-element σ bonds has been studied in detail. See: N. Hazari, J. E. Heimann, *Inorg. Chem.,* **2017**, *56*, 13655-13678.

[58] T. J. Schmeier, N. Hazari, C. D. Incarvito, J. A. Raskatov, *Chem. Commun.,* **2011,** *47*, 1824-1826.

[59] a) S. Chakraborty, J. Zhang, J. A. Krause, H. Guan, *J. Am. Chem. Soc.,* **2010**, *132*, 8872-8873 ; b) S. Chakraborty, Y. J. Patel, J. A. Krause, H. Guan, *Polyhedron,* **2012**, *32*, 30-34.

[60] W-H. Suh, M. L. Guard, N. Hazari, *Polyhedron*, **2014**, *84*, 37-43.

in the laboratory using hydride **6**.[61] In this work, model complexes were calculated with methyl moieties on the phosphine or amine groups, and the energy for the transition state (Figure 10, red) of each complex was calculated as well as that corresponding to the resulting formates (Figure 10, pink).
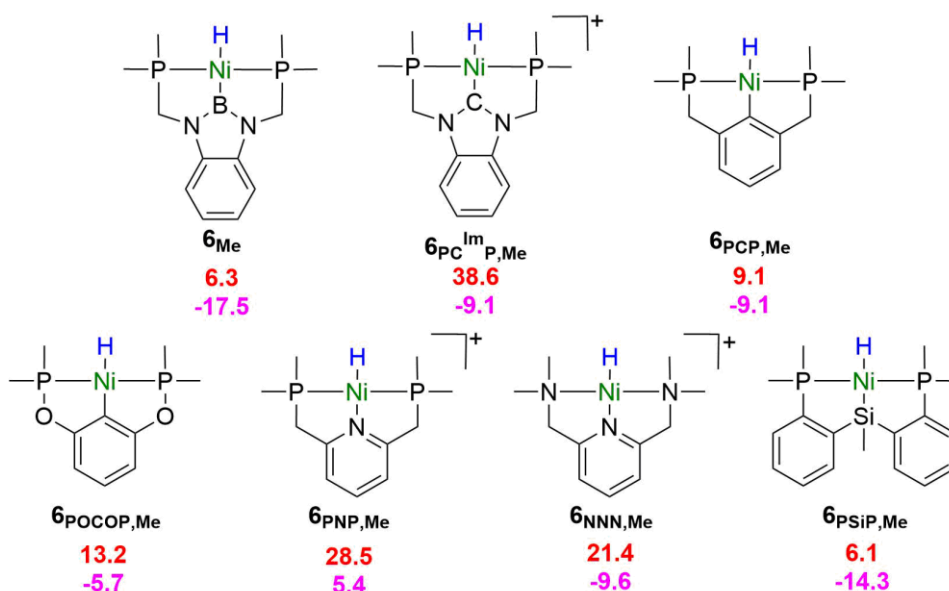
Figure 10. $\Delta G^{\ddagger}$ (red, top) and ΔG^0 (pink, bottom) for the insertion of CO_2 into the Ni−H bond of several pincer complexes. Energies in kcal/mol.

As expected, complexes **6$_{PSiP,Me}$** and **6$_{Me}$** possess the lowest energy barriers for CO_2 insertion, with Gibbs free energies of 6.1 and 6.3 kcal/mol, respectively. This is in excellent agreement with the results published by Marder and Lin in 2005,[55] where they observed the strong *trans* influence exerted by silyl and boryl ligands. Unlike the PNP derivative, all the complexes give stable formates, indicating the thermodynamic feasibility of the process. Cationic

---

[61] Some studies previously reported the energies for CO_2 insertion in Ni−R or Pd−R groups. See: a) T.J. Schmeier, A. Nova, N. Hazari, F. Maseras, *Chem. Eur. J.,* **2012**, *18*, 6915-6927; b) W. H. Suh, T. J. Schmeier, N. Hazari, R. A. Kemp, M. K. Takase, *Organometallics*, **2012**, *31*, 8225-8236.

complexes give the least favourable transition states: replacement of the boryl functionality for a carbene unit results in a very energy-demanding transition state, followed by those obtained in the pincer complexes with amine groups (**6PNP,Me** and **6NNN,Me**) as ancillary ligands.

In the case of PCP and PSiP models, a two-step mechanism was found in which a Ni−H·CO_2 adduct precedes the insertion event. The energies shown in Figure 10 correspond to the highest-energy transition state.

Additionally, the obtained energies for the experimentally reported complexes are consistent with the reaction times required for the insertion to take place (Table 2): while **6** affords the formate species in a few seconds, the PCP and POCOP derivatives require a few minutes and 1 hour, respectively.[58,59b]

Complex	Time	ΔG‡ (kcal/mol)	Reference
6	seconds	6.3	This work
6PCP	minutes	9.1	58
6POCOP	1 hour	13.2	59b

Table 2. Correlation between calculated ΔG‡ values of the transition state for CO_2 insertion into the Ni−H bond and the experimental reaction time.

The hydricity of **6Me** is also evident from the data displayed in Figure 11, where the geometries for the transition states of **6Me**, **6PCP,Me** and **6POCOP,Me** are shown. One of the most striking details is the fold of the CO_2 molecule in the last two cases, where it bends to reach an O−C−O angle of around 133°, a value at which the electronic repulsion is minimal and at the same time, the electrophilic carbon atom is more accessible.[62] In addition, a closer contact between the Ni species and carbon dioxide is required in these two examples, as reflected by the shorter hydride-carbon distance as well as the participation of the metal and one

---

[62] M. Aresta in *Activation of Small Molecules: Organometallic and Bioinorganic perspectives,* W. B. Tolman (Editor), Wiley-VCH, **2006**. Chapter 1: Carbon Dioxide Reduction and Uses as a Chemical Feedstock, pages 1-41.

of the oxygen atoms in the four-membered transition state. Regarding **6**~Me~, a much more linear geometry of the CO_2 molecule and a farther contact is enough for the hydride to attack the carbon atom, without participation of the metal during the transition state.
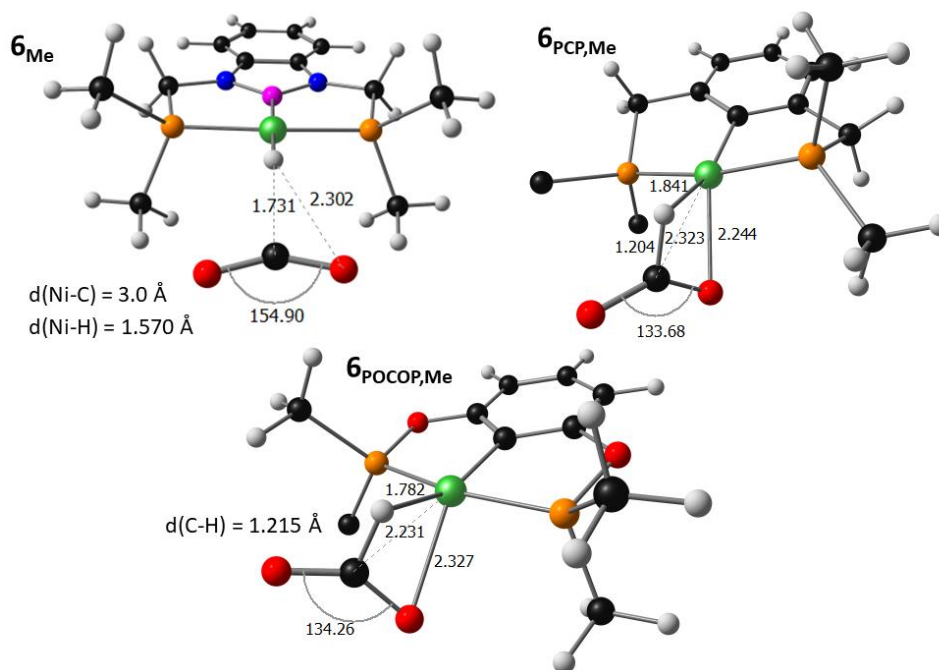
Figure 11. Comparison of the geometrical parameters of the calculated transition states for the CO_2 insertion in the PBP, PCP and POCOP models (some hydrogen atoms have been omitted for clarity).

2.3. Catalytic studies

Formate **7** was tested as catalyst in the hydrosilation of carbon dioxide by using Et_3SiH as a reductant. No change in the NMR spectra was observed at room temperature, and heating up to 40 °C gave rise to the liberation of free PBP ligand and the formation of some other unidentified products. For this reason, and based on the examples discussed in section 1.3.1, we decided to use $B(C_6F_5)_3$ as a co-catalyst.

[95]

Chapter 1. Results and discussion

A stoichiometric reaction in which CO_2 (4 bar) was loaded onto a mixture containing formate **7**, Et_3SiH and $B(C_6F_5)_3$ (1:1:1 ratio) in C_6D_6 showed no evolution at room temperature either. Nonetheless, heating up to 70 °C revealed the consumption of the silane and the formation of the bis(silyl)acetal derivative as the sole product of the reaction after 30 minutes (Figure 12).
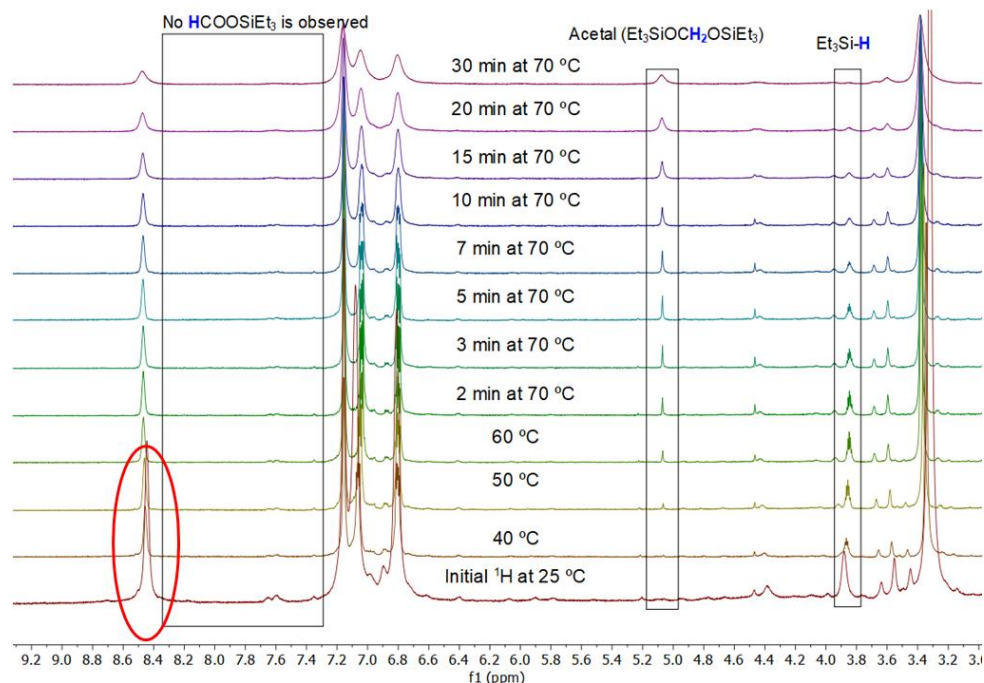
Figure 12. Stoichiometric experiment (400 MHz, C_6D_6) between formate **7**, Et_3SiH and $B(C_6F_5)_3$ in the presence of carbon dioxide (4 bar). The formation of a new Ni species is highlighted in red.

Before warming up the sample, a change in the nature of the Ni species was noticed (Figure 12, red circle), since the peak at 9.11 ppm disappeared in favour of a new singlet at 8.45 ppm. In addition, this peak correlates with a new carbon peak at 173.2 ppm in the HSQC ^1H–^{13}C spectrum. These changes, along with the disappearance of the peak at 167.2 ppm in the ^{13}C NMR spectrum seems to suggest the coordination of the Lewis acid to one of the oxygen atoms of the formate group. A similar downfield shift in the ^{13}C NMR spectrum was observed

[96]

by Piers in their scandium system upon coordination of BCF to the carboxylate group.[46]

Encouraged by the selectivity observed towards the formaldehyde derivative and by the presence of a new Ni species, the synthesis of the catalyst was pursued in order to perform catalytic studies with the certainty of having just 1 equivalent of Lewis acid per Ni complex, so as not to have any free borane that can lead to over-reduction reactions. In this way, the reaction shown in scheme 22 was carried out, affording complex **8** in 88% isolated yield. The purification of this zwitterionic species was possible by its low solubility in pentane. The excess of free borane could be washed away with this solvent, given the high solubility of the Lewis acid in it.
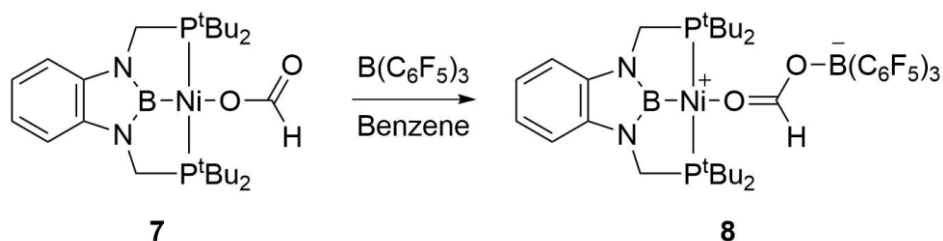
Scheme 22. Synthesis of catalyst **8**.

Complex **8** shows a singlet at 87.7 ppm in the $^{31}P\{^1H\}$ NMR spectrum (Figure 13), proving again the symmetry of the phosphine ligands in the molecule. The $^{11}B\{^1H\}$ NMR spectrum reveals the presence of the boryl ligand with a broad peak at 33.5 ppm and a borate species at -1.4 ppm, indicative of the coordination of the Lewis acid[46,63] (free $B(C_6F_5)_3$ resonates at 60 ppm).[64] Coordination of BCF is also corroborated by the set of signals obtained by $^{19}F\{^1H\}$ NMR.

[63] S. J. Mitton, L. Turculet, *Chem. Eur. J.,* **2012***, 18,* 15258-15262.
[64] A. Willms, H. Schumacher, T. Tabassum, L. Qi, S. L. Scott, P. J. C. Hausoul, M. Rose, *ChemCatChem* **2018**, *10*, 1835-1843.
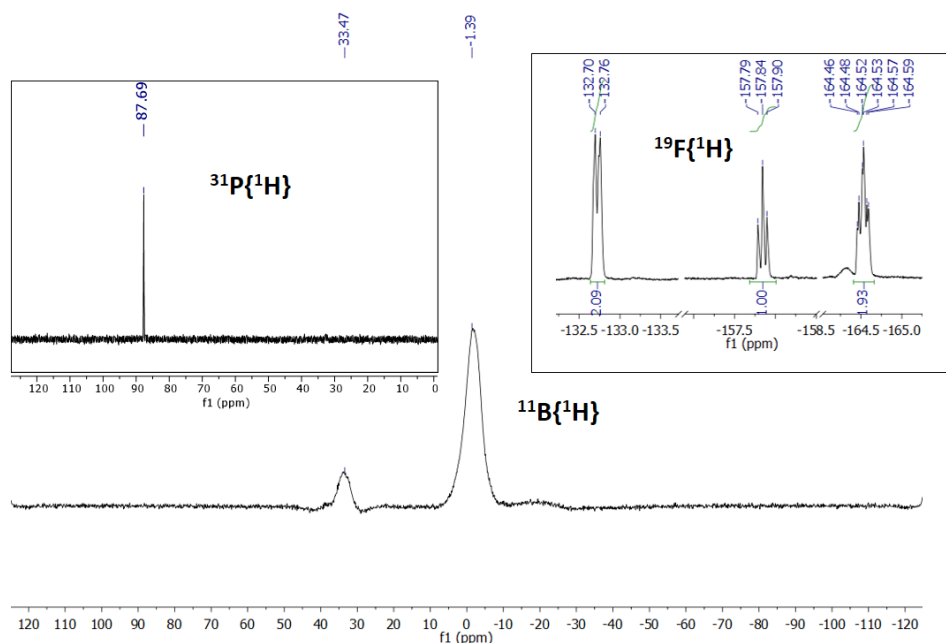
Figure 13. NMR spectra (400 MHz, C_6D_6) of some heteroatoms of complex **8**.

The IR spectrum of **8** also displays a band at a wavelength of 1643 cm^{-1}, which is in excellent agreement with the data reported for scandium[46] and rhenium[47] BCF formatoborates. The complete confirmation of the structure of **8** was possible by X-Ray crystallography thanks to a crop of crystals grown from slow evaporation of a concentrate solution of the Ni complex in toluene (Figure 14). The geometrical data for the formatoborate group gives similar values to related systems,[65] among which it is necessary to mention the difference in the C−O bond lengths: C25−O1 (1.219(2) Å) is considerably shorter than C25−O2 (1.283(2) Å), which agrees with the representation shown in Scheme 22.

---

[65] (a) A. Berkefeld, W. E. Piers, M. Parvez, *J. Am. Chem. Soc.*, **2010**, *132*, 10660-10661; (b) I. Peuser, R. C. Neu, X. Zhao, M. Ulrich, B. Schirmer, J. A. Tannert, G. Kehr, R. Fröhlich, S. Grimme, G. Erker and D. W. Stephan, *Chem. Eur. J.,* **2011**, *17*, 9640-9650; (c) M. Harhausen, R. Fröhlich, G. Kehr and G. Erker, *Organometallics*, **2012**, *31*, 2801-2809; (d) D. W. Stephan, *J. Am. Chem. Soc.,* **2015**, *137*, 10018-10032.

Additionally, Ni1–O1 (1.978(1) Å) is longer than the distance reported for formate **7** with no coordinated borane (1.958(2) Å).[56]
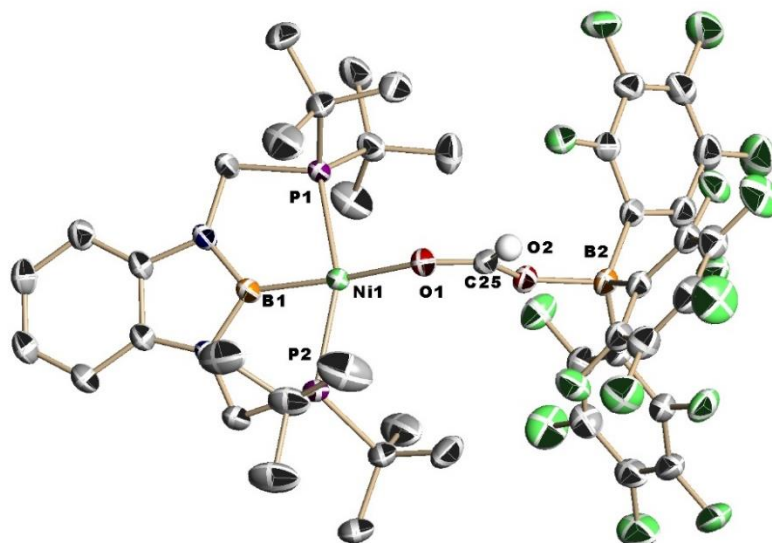
Figure 14. Crystal structure of complex **8**.

The structure of **8** was calculated by means of DFT methods, and the optimized structure was compared to the experimental one. As it can be seen in table 3, both structures agree well in terms of bond distances and angles:

[99]

		Experimental value	Calculated value
Distance (Å)	B1–Ni1	1.903(2)	1.90874
	O1–Ni1	1.978(1)	1.99717
	B2–O2	1.552(2)	1.55803
	O1–C25	1.219(2)	1.23942
	O2–C25	1.283(2)	1.27708
Angle (°)	B1–Ni1–O1	171.34(6)	167.393
	O1–C25–O2	124.1(1)	124.604
	C25–O2–B2	128.0(1)	123.263
	P1–Ni1–P2	158.61(2)	158.124

Table 3. Comparison of experimental and theoretical geometry data of **8**.

With pure complex **8** in hand, catalytic hydrosilation of carbon dioxide was explored by using Et_3SiH under 4 bar of CO_2 at 70 °C in C_6D_6. Selective reduction to the bis(silyl)acetal level was observed during the whole process, as in Figure 12. The catalyst was efficient enough to allow us to lower the catalytic loading down to 0.05% molar (relative to Et_3SiH), achieving turnover numbers (TON) and frequencies (TOF) of 1200 and 56 h^{-1}, respectively. Such a remarkable selectivity can be observed in Figure 15, where only the silane and acetal signals are observed by ^{1}H NMR:
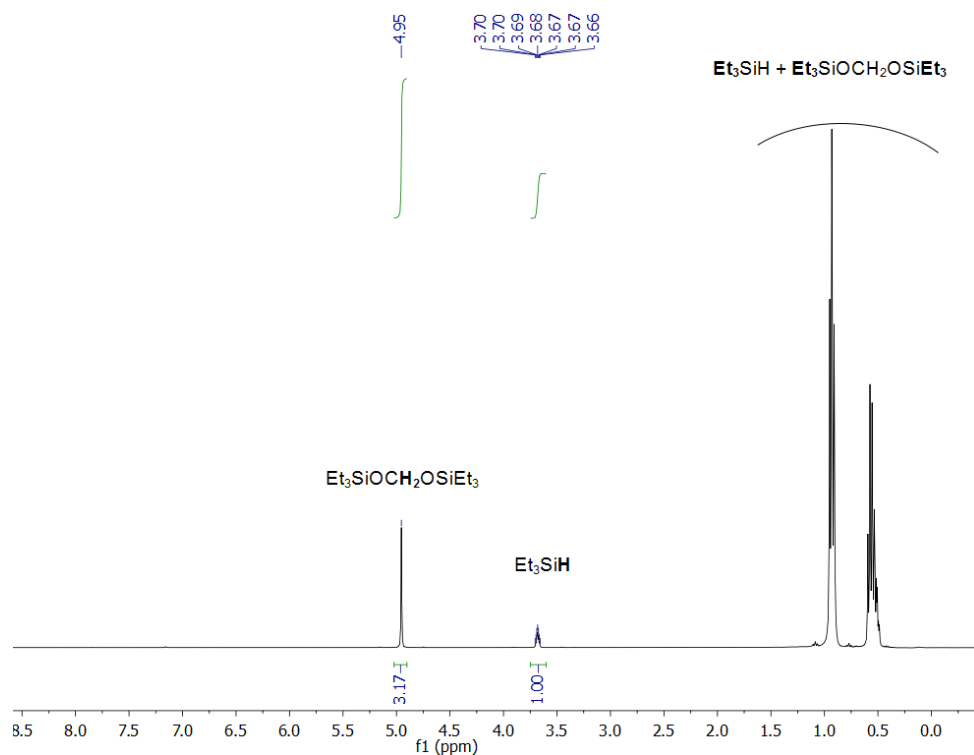
Figure 15. Representative example of catalysis (400 MHz, C_6D_6) with **8** (0.05% mol) and Et_3SiH after 21 hours at 70 °C.

The scope of this catalytic reaction was studied by employing several other silanes such as Ph_2MeSiH (table 4), which also gives the acetal exclusively, with negligible amounts of silyl methyl ether (Figure 16). Faster catalysis can be achieved with the smaller silane Me_2PhSiH, albeit the selectivity is compromised, since some formation of the methoxysilane and methane is observed (Figure 17). It was observed that an increase in the concentration of the reactants was beneficial to the reaction rate, and from table 4 we can conclude that catalyst **8** gives similar turnover numbers and higher turnover frequencies in comparison to the most efficient transition-metal based catalysts reported in the literature.[46]

[101]

Silane	Catalyst loading / % mol	[8] / mM	[Silane] / M	Total volume / µL[a]	Conversion / %	Bis(silyl) acetal / %	t / h	TON[b]	TOF / h[-1]
Et$_2$SiH	0.05	2.36	4.72	304 S + 100 B	60	> 99	21.5	1200	55.8
	0.1	4.77	4.72	304 S + 100 B	91	> 99	34	910	26.8
	0.6	10.9	1.81	101 S + 250 B	86	> 99	15.5	143	9.2
	1	3	0.3	30 S + 600 B	90	> 99	70	90	1.3
Ph$_2$MeSiH	0.1	3.98	4	378 S + 100 B	62	> 99	37.5	620	16.5
	0.1	5	5.04	378 S (Neat)	41	> 99	22	410	18.6
	0.6	10.9	1.81	126 S + 225 B	82	> 99	7.5	137	18.3
	1	3	0.3	38 S + 600 B	90	> 99	45	90	2
Me$_2$PhSiH	0.6	10.9	1.83	97 S + 250 B	90[c]	73 (11% silyl methyl ether / 16 % methane)	3	121	40

Table 4. Summary of the results of the carbon dioxide hydrosilation catalyzed by **8**. Every catalytic experiment has been repeated at least 3 times. Partial decomposition of the catalyst was observed after the conversion values indicated above. [a] S = silane; B = d^6-Benzene [b] (µmoles of silane/ µmoles of catalyst) * acetal ratio [c] Toluene was used as internal standard.
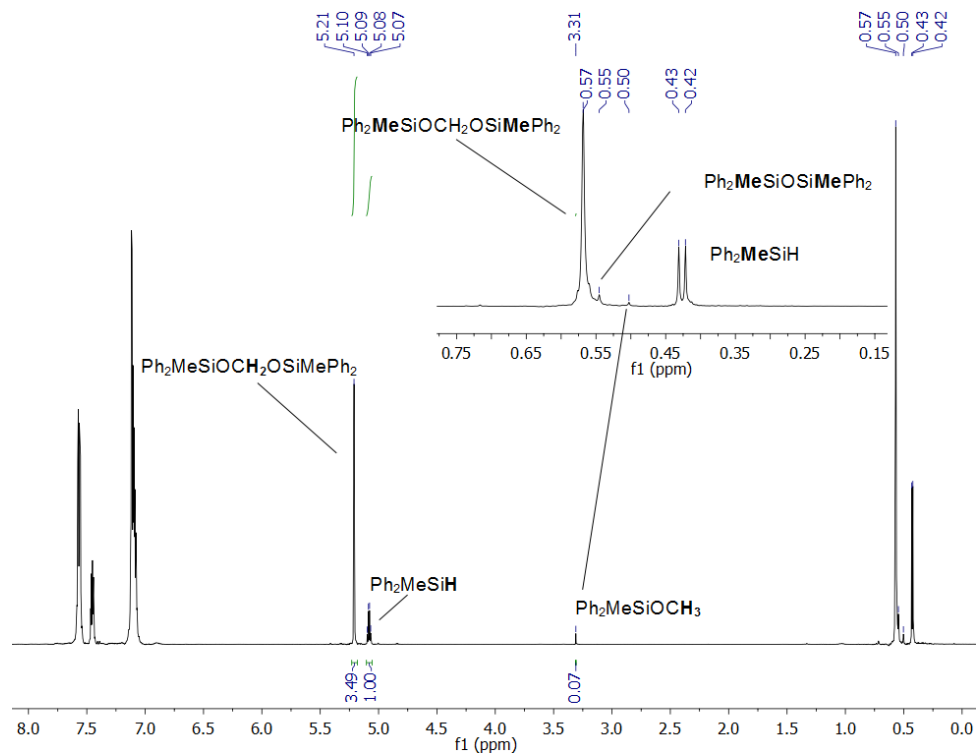
Figure 16. Representative example of catalysis (400 MHz, C_6D_6) with **8** (0.1% mol) and Ph_2MeSiH after 21 hours at 70 °C.
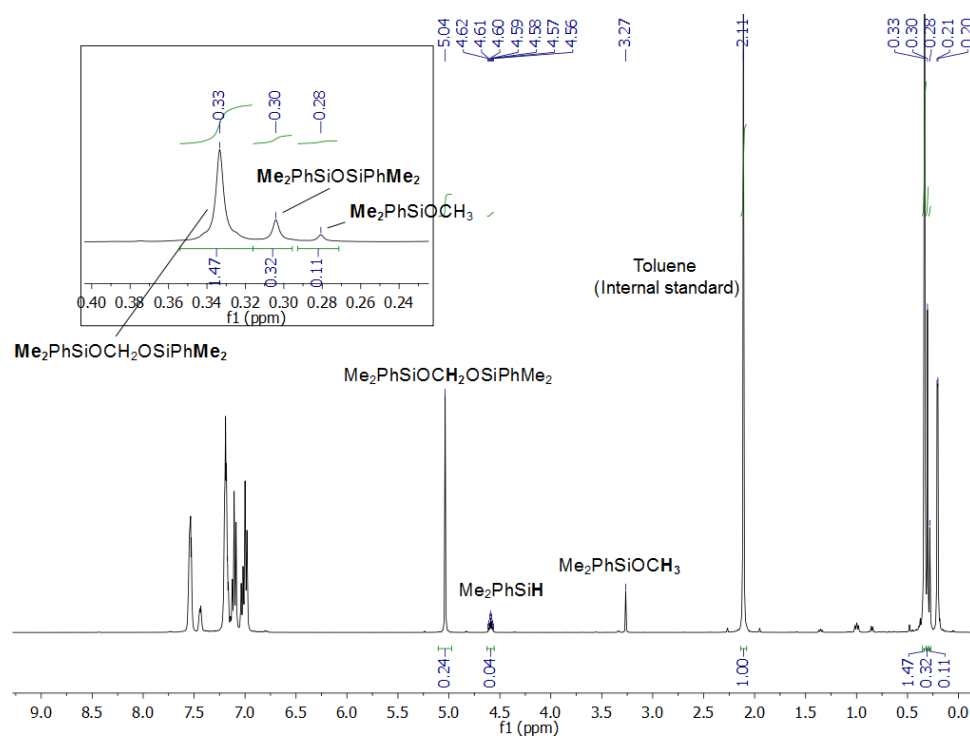
Figure 17. Representative example (400 MHz, C_6D_6) of catalysis with **8** (0.6% mol) and Me₂PhSiH after 3 hours at 70 °C. Toluene was added after the experiment.

2.4. Experimental mechanistic studies

In order to elucidate the mechanism by which the catalytic reactions take place, some experiments were carried out so as to explain the extraordinary selectivity and the good catalytic data. Given that free $B(C_6F_5)_3$ in contact with the silane is responsible for the over-reduction of the intermediates to methane, the first experiment involved the assessment of the equilibrium displayed in scheme 23 in the catalytic conditions.
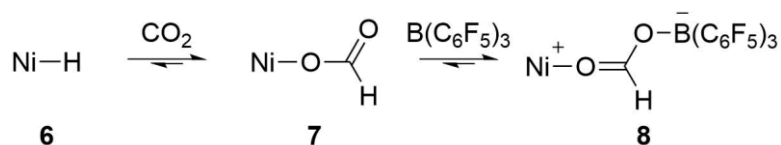
Scheme 23. Equilibrium between complexes **6**, **7** and **8**.

[104]

For this purpose, a sample of **8**-$^{13}CO_2$ (prepared using ^{13}C-labelled carbon dioxide) was heated up to 70 °C in C_6D_6 in a sealed NMR tube. After 4 hours, no evidence of free borane was observed by NMR spectroscopy (^{13}C, ^{19}F, ^{11}B). Nonetheless, when the same NMR tube is charged with $^{12}CO_2$ (1 bar), the insertion of non-labelled carbon dioxide is observed in the ^{1}H NMR spectrum in a 12% ratio after 22 hours at 70 °C (Figure 18), which indicates that the equilibrium shown in scheme 23 is actually taking place at the catalytic conditions, although it is strongly shifted to the right. Therefore, the amount of Lewis acid in the reaction medium is minimal.
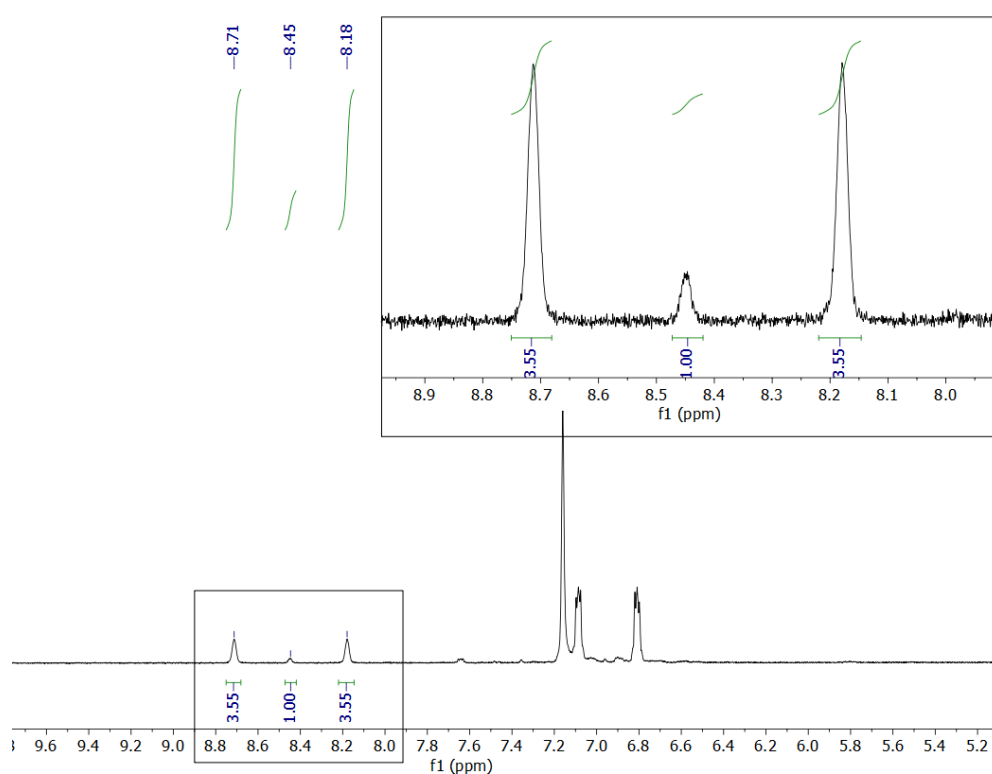
Figure 18. Exchange experiment: ^{1}H NMR spectrum (400 MHz, C_6D_6) of **8**-$^{13}CO_2$ after 22 h heating at 70 °C in the presence of $^{12}CO_2$ (1 bar). Incorporation of $^{12}CO_2$ in a 12% ratio.

These experimental results seem to agree with the Gibbs energy difference found in our calculations for the model complex **8$_{Me}$** (-27 kcal/mol) [105]

and **7** + $B(C_6F_5)_3$ (-11.8 kcal/mol).[66] In comparison to Cp*$_2$Sc,[45] the PBP-Ni framework is more efficient in capturing the Lewis acid, which is consistent with the selectivity observed for both systems (Schemes 12 and 24).
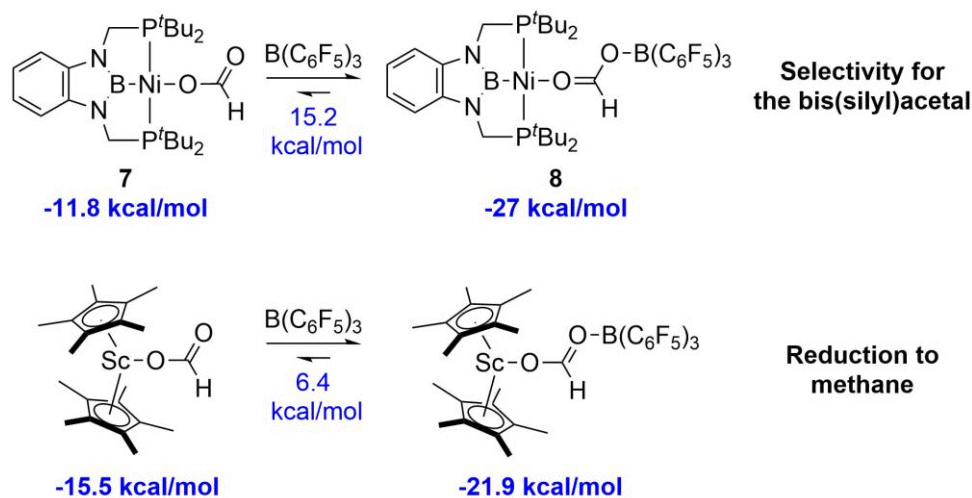
Scheme 24. Comparison of the energies of Ni-PBP and Cp*$_2$Sc complexes and their $B(C_6F_5)_3$ adducts (adapted from reference 45).

^{13}C-labelled carbon dioxide was also employed in a monitoring experiment, where the formation of the formaldehyde derivative as well as the presence of intermediates was analysed over time (Figure 19):

---

[66] Complex **6** + CO_2 + $B(C_6F_5)_3$ were used as the energy reference.

[106]
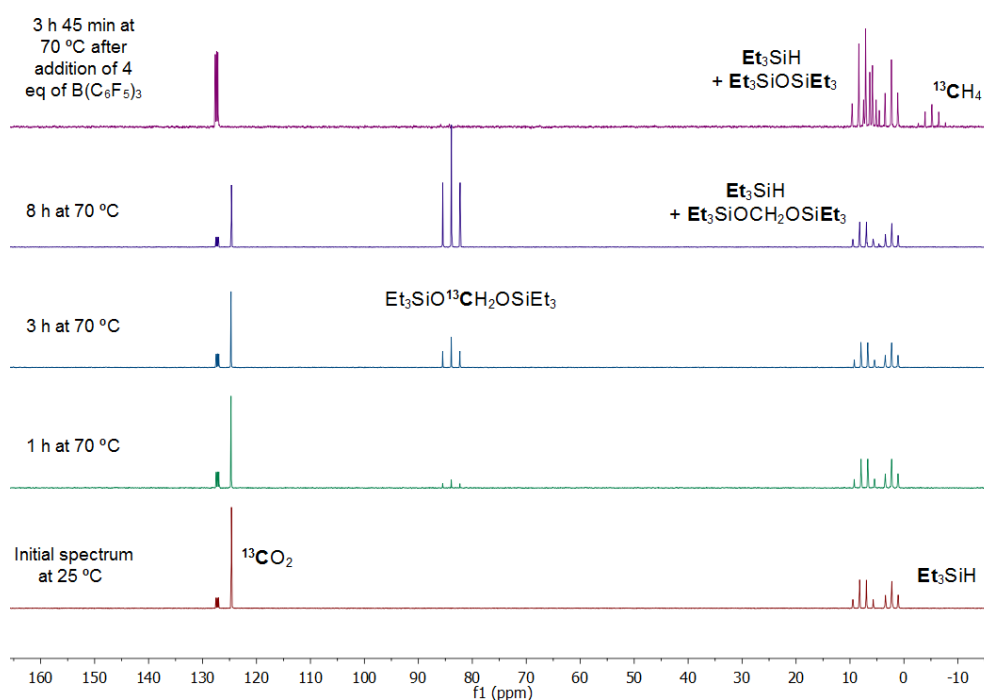
Figure 19. ^{13}C (fully coupled) NMR spectra (400 MHz, C$_6$D$_6$) of the monitoring and over-reduction experiment using **8** and Et$_3$SiH in the presence of ^{13}CO$_2$ (4 bar).

It can be observed that no other product but the bis(silyl)acetal (triplet at 85.5 ppm with $^1J_{CH}$ = 161 Hz) is generated throughout the experiment. After 8 hours, the carbon dioxide peak diminished to some extent and the main observable compound is the formaldehyde derivative. At this point, 4 equivalents of the Lewis acid were added in order to over-reduce the product to methane, to confirm that an excess of tris(pentafluorophenyl)borane with respect to the Ni complex should be avoided if selectivity is desired. Nevertheless, to make sure that the Ni complex was not responsible for this over-reduction and it was only due to the formation of the borane-silane complex, the bis(silyl)acetal was isolated (Figure 20).

[107]
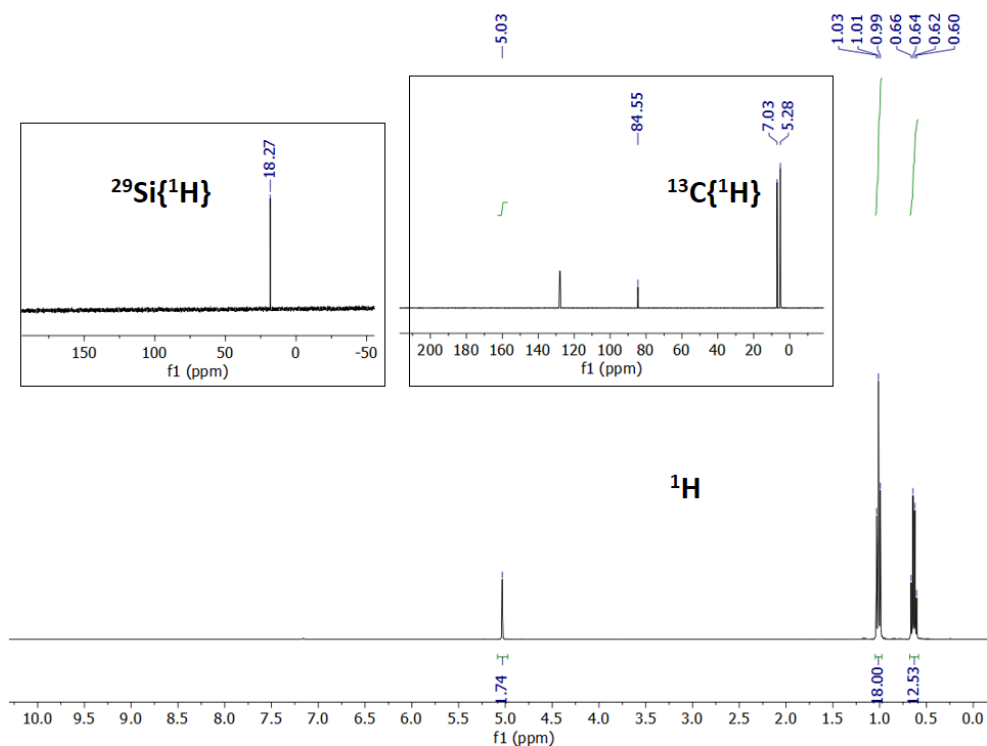
Figure 20. NMR characterization (400 MHz, C_6D_6) of the bis(silyl)acetal $(Et_3SiO)_2CH_2$.

This product can be purified under air using column chromatography techniques, affording a colorless liquid after solvent removal. Once it was isolated, it was mixed with C_6D_6, Et_3SiH and $B(C_6F_5)_3$ and it was analysed by NMR techniques. Figure 21 shows the evolution of the process by using $^{29}Si\{^1H\}$ NMR, where the formation of the siloxane $(Et_3Si)_2O$ is observed upon heating up to 50 °C. No silyl methyl ether is detected, indicating formation of methane.

[108]
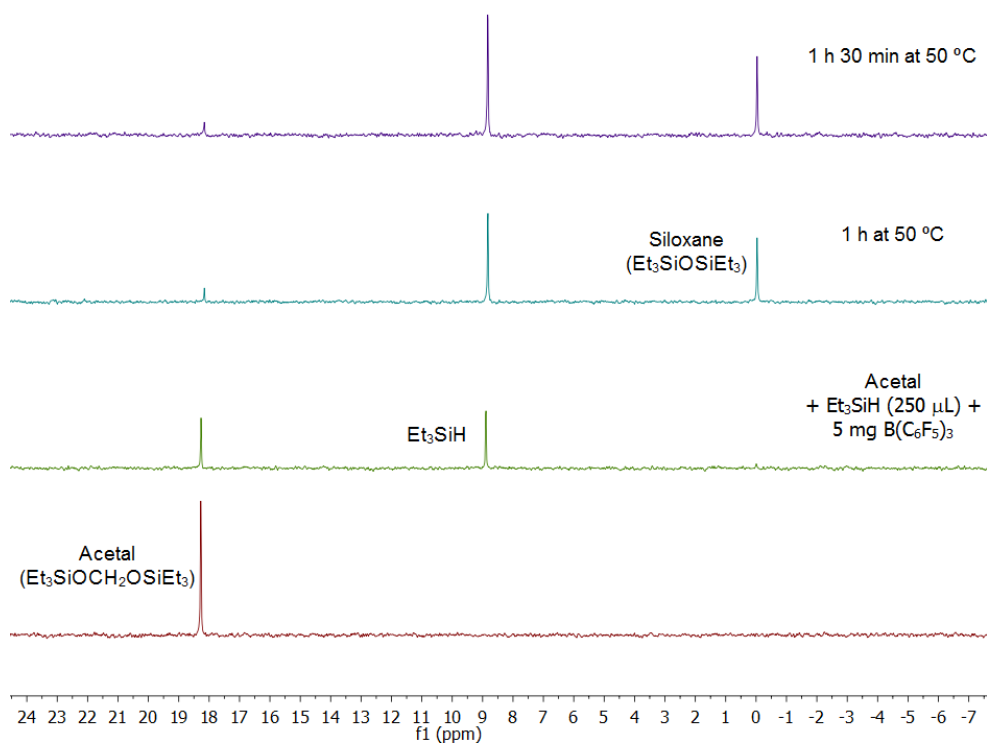
Figure 21. $^{29}Si\{^{1}H\}$ NMR spectra (400 MHz, C_6D_6) of the over-reduction of the isolated acetal species $(Et_3SiO)_2CH_2$ in the absence of Ni complexes.

Finally, it is necessary to mention that studies in which CO_2 is consumed completely, over-reduction to methane is observed and the catalyst changes its nature, since there is no more carbon dioxide to regenerate the formatoborate unit (Figure 22).

[109]
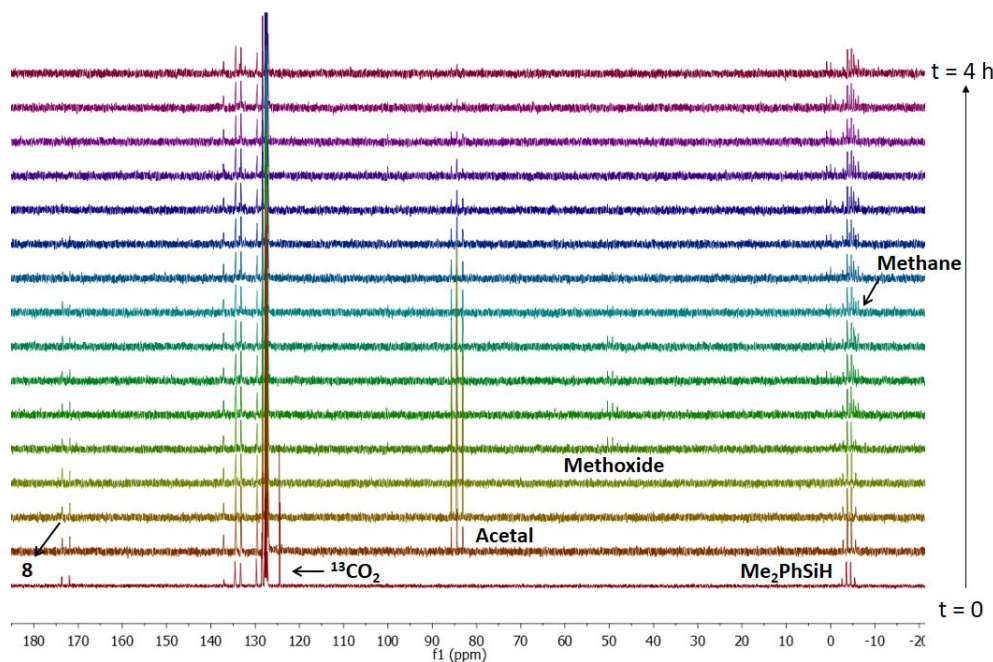
Figure 22. ^{13}C NMR spectra (500 MHz, C$_6$D$_6$) of the catalytic study carried out with ^{13}CO$_2$ and Me$_2$PhSiH in order to analyse the phenomena when carbon dioxide is totally consumed. Although it is overlapping with other signals, methane appears at -5.2 ppm (this signal can be better observed in Figure 19).

Given that no other peak is observed in the ^{13}C NMR spectrum and there is a brown solid at the bottom of the NMR tube once the experiment has finished, it was assumed that the catalyst changed its structure and it precipitated in benzene. Several solvents were tested in order to redissolve the unknown species, and ethereal solvents were effective in achieving such task, despite the risk of getting coordination to the Lewis acid. Thus, NMR characterization of the complex was possible by using toluene and small amounts of THF. Interpretation of the spectra led to the conclusion that the resulting complex was charged species **9**, [(PBP)Ni][HB(C$_6$F$_5$)$_3$] (Figures 23 and 24). It is also necessary to mention that backfilling again the NMR tube with CO$_2$ gives a homogeneous solution back, and NMR analysis shows conversion of complex **9** to species **8**.

[110]
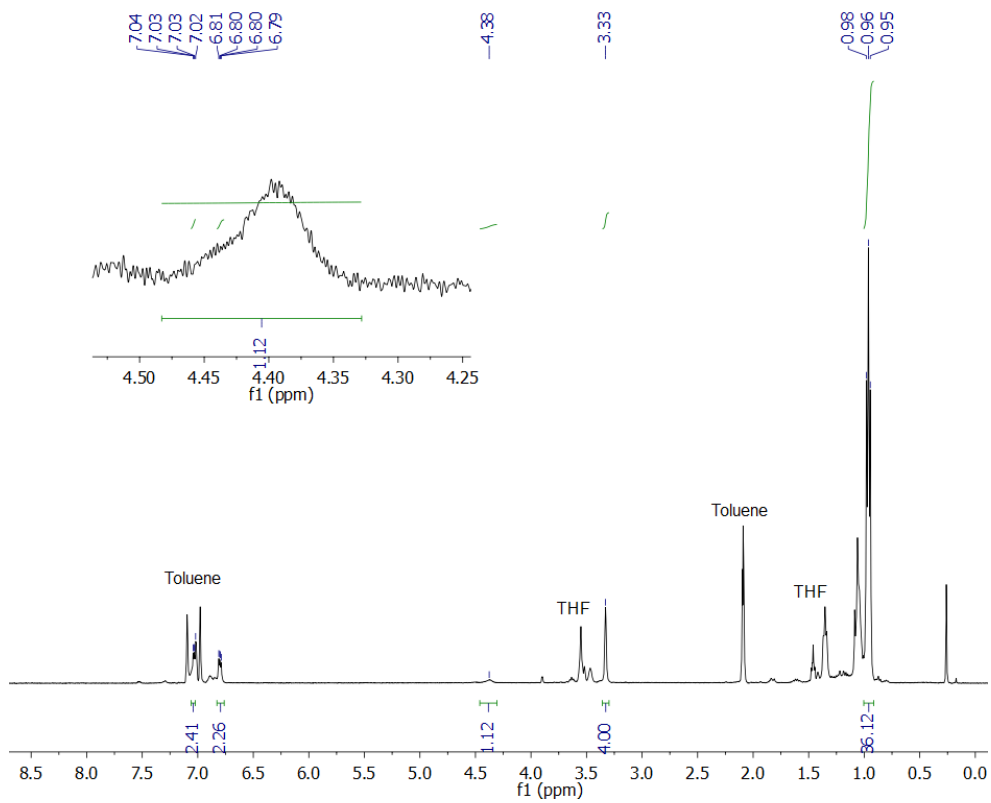
Figure 23. $^1H\{^{11}B\}$ spectrum (400 MHz, d^8-toluene/small amount of THF) of **9**. Inset: broad peak attributed to the B**H** hydrogen, which appeared upon boron decoupling.
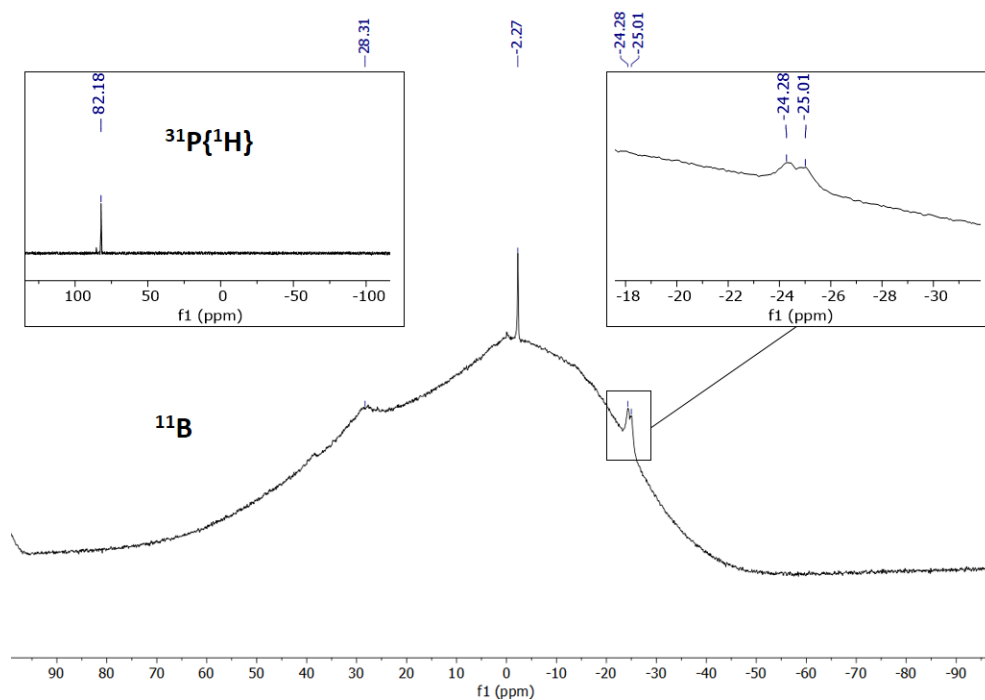
Figure 24. $^{31}P\{^1H\}$ and ^{11}B NMR spectra (400 MHz, d^8-toluene/small amount of THF) of complex **9**. The broad peak at 28.3 ppm corresponds to the boryl ligand, and the doublet at -24.7 ppm ($^1J_{BH}$ = 90 Hz) corresponds to the hydridoborate unit, as previously described in the literature.[63,67] This peak collapses into a singlet upon proton decoupling. The singlet at -2.3 was attributed to the THF·$B(C_6F_5)_3$ adduct, in accordance with literature values.[68]

These data seem to suggest that after CO_2 depletion complex **9** is formed, and it might also be responsible for over-reduction phenomena. Nonetheless, if CO_2 is present, **9** can readily insert carbon dioxide to restore complex **8**, as seen in scheme 25. For this reason, a CO_2 atmosphere is always necessary in order to achieve selective reduction.

---

[67] T. Voss, T. Mahdi, E. Otten, R. Frölich, G. Kehr, D. W. Stephan, G. Erker, *Organometallics*, **2012**, *31*, 2367-2378.

[68] L. H. Doerrer, A. J. Graham, D. Haussinger, M. L. H. Green, *J. Chem. Soc. Dalton Trans.,* **2000**, 813-820.
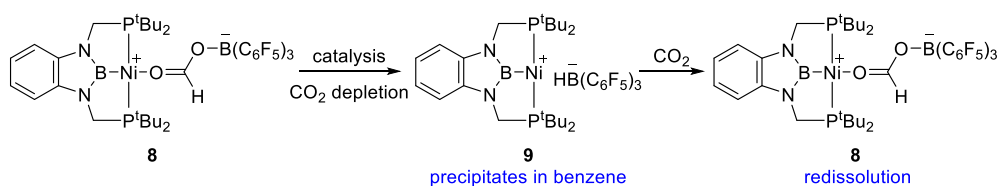
Scheme 25. Reactions of the Ni complexes in the absence and presence of CO_2 during catalysis.

2.5. Computational mechanistic studies[69]

In order to propose a mechanistic pathway, DFT calculations were performed taking into account the experimental observations described in the previous section, such as:

I) During catalysis, the only catalytically active species observed by NMR (^1H, ^{31}P, ^{11}B) is complex **8**.

II) Selectivity towards the formation of the bis(silyl)acetal species is achieved only when 1 equivalent of $B(C_6F_5)_3$ per Ni complex is present. Over-reduction to methane takes place when there is an excess of Lewis acid.

III) CO_2 must always be present during catalysis to ensure the presence of **8**, which is capable of capturing $B(C_6F_5)_3$. Otherwise, complex **9** will precipitate and over-reduction will be observed.

IV) Only a small portion of Lewis acid is released (demonstrated by the exchange experiment), which gives rise to the catalytic process. Then, it needs to be captured back again by complex **8**.

V) Direct reduction to the bis(silyl)acetal is observed without detection of any other intermediate such as silylformates.

With this information in hand, two mechanistic possibilities were considered: **a)** direct hydrosilation on the coordination sphere of the metal with

---

[69] Computational methods are detailed in the Experimental part section.

assistance of the PBP ligand, and **b)** activation of the silane by $B(C_6F_5)_3$ followed by nucleophilic attack of the substituent bound to Ni (*i.e.* formate or silylacetal). In a first exploratory approximation, calculations were carried out using a model of the catalyst, **8$_{Me}$**, with methyl moieties on the phosphine groups. Additionally, Me_3SiH was used as a silane model. However, the employment of the real Lewis acid $B(C_6F_5)_3$ was necessary, since model boranes such as BF_3 or $B(CF_3)_3$ gave very different energy values.

1) Reduction to the formate stage

Model system

In a similar fashion to the hydrogenolysis of the Ni−Me bond reported by our group,[51] Me_3SiH would approach the oxygen atom pointing away from the Lewis acid, as shown in Figure 25 (pathway **a**, blue line). During the transition state (TSa) the formatoborate unit rearranges so the oxygen bound to BCF interacts with the Ni atom ($d_{Ni\cdots O}$ = 2.25 Å), allowing the other oxygen atom to attack the silane molecule ($d_{Si\cdots O}$ = 2.02 Å). At the same time, the hydrogen atom (with hydride character) attacks the boron atom of the PBP ligand. The outcome of this transition state is the σ-B−H stabilized Ni (0) species **5$_{Me}$** and a formate fragment with both oxygen atoms substituted: one of them is bound to the Lewis acid and the other one to the trimethylsilyl moiety. The energy requirement for this step is $\Delta ZPE^{\ddagger}$ = 30.1 kcal/mol (considering **8$_{Me}$** + Me_3SiH the energy reference).
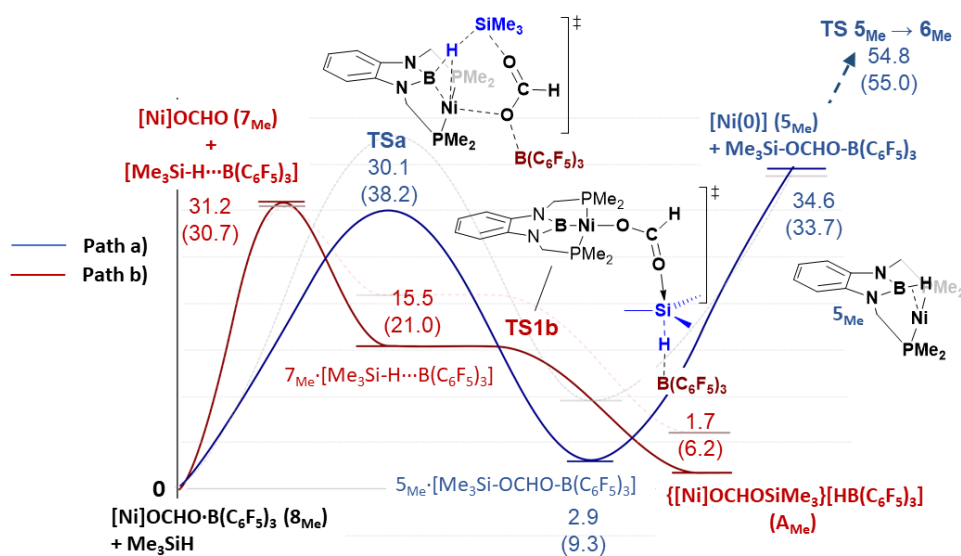
Figure 25. Graphical summary of the energies obtained for the first step of the catalytic process: reduction to the formate stage. ΔZPE in kcal/mol (ΔG_{50} in parentheses).

Pathway **b** (Figure 25, red line) starts with the release of $B(C_6F_5)_3$ and the subsequent activation of Me_3SiH by forming the borane-silane complex. The energy for this step is 31.2 kcal/mol. Then, the oxygen atom of the carbonyl group can attack the activated silane through a virtually barrier-less transition state (TS1b) in which an S_N2 type transfer of the silylium fragment takes place, affording complex A_{Me}, which features the cationic silylformate Ni species and the hydroborate anion. This pair lies 1.7 kcal/mol above the origin.

In pathway **b** the first step is the highest energy barrier for the whole mechanism, whereas pathway **a** is more energy demanding; separation of 5_{Me} and $Me_3SiOCHOB(C_6F_5)_3$ requires 34.6 kcal/mol above the origin, and it is necessary for the Ni(0) complex to undergo oxidative addition in order to yield hydride 6_{Me}, so another CO_2 insertion step can occur. These steps raise the energy of the process up to 54.8 kcal/mol. Therefore, pathway **a** is highly

[115]

unlikely, and the rest of the calculations will be performed for pathway **b** with the real complex.

Calculations with real catalyst 8

The employment of the real catalyst seems to have a negligible effect in the dissociation of the Lewis acid, since similar energy values (30.9 kcal/mol) were obtained (Figure 26). Similarly, this stage is the most energy-demanding of the whole mechanism. No transition state could be found after this step, because the system would either evolve to the reagents (**7** + borane-silane complex) or the products (**A**). The results of a relaxed potential energy surface scan in which the Si−O distance is modified and the energy is evaluated accordingly (Figure 27) along with the almost non-existent barrier in the case of the model complex suggest that the attack of the formate to the activated silane occurs with practically no energy cost.
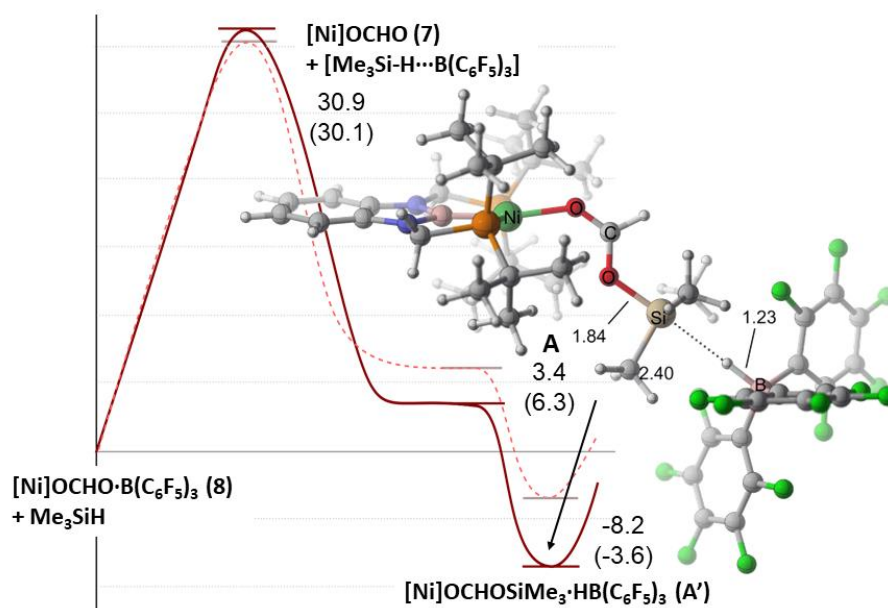
Figure 26. Energy profile of the hydrosilation to the formate stage using real catalyst **8**. ΔZPE in kcal/mol (ΔG$_{50}$ in parentheses).

[116]
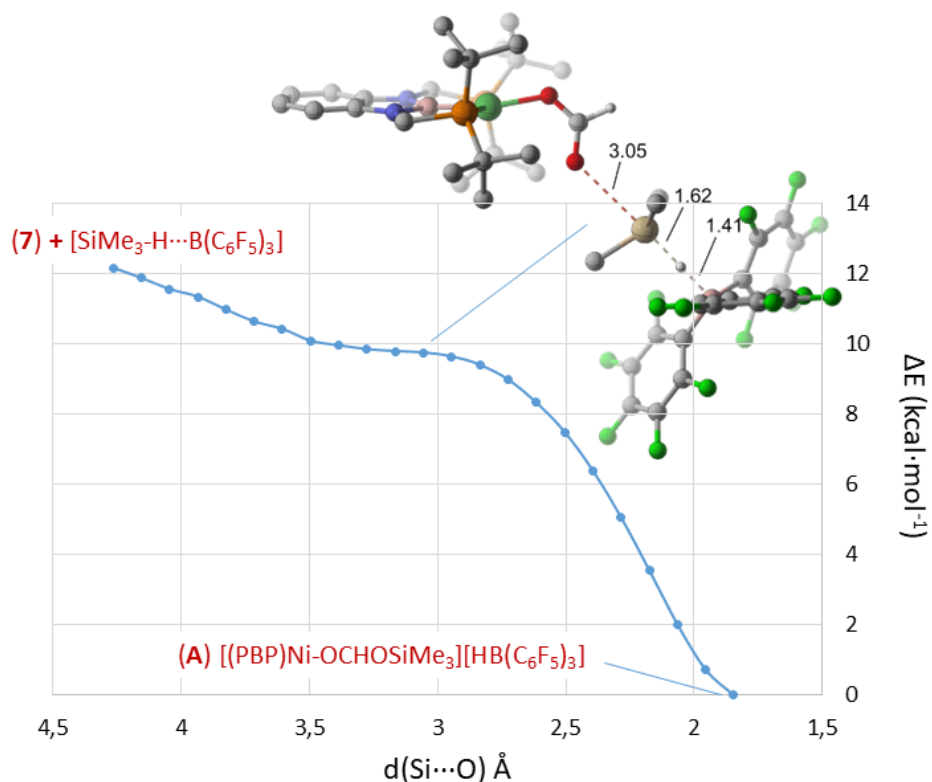
Figure 27. Relaxed Potential Energy Surface scan for the Me_3Si^+ transfer from the borane-silane complex to the formate group. The transition state would be located in the flat region in the middle of the curve.

2) Second Reduction Step

Hydride transfer

It can be observed in Figure 26 that the molecule rearranges after the attack from **A** to a more stable geometry **A'** 8.2 kcal/mol below the origin. At this point, two possibilities arise (Scheme 26): the first one (**i**) involves the displacement of the silylformate unit from the coordination sphere by attack of the hydridoborate anion $[HB(C_6F_5)_3]^-$, and the second possibility (**ii**) consists of the hydride transfer to the carbonyl atom to yield species **B·B(C$_6$F$_5$)$_3$**. Both options are equal in terms of energy (around 25 kcal/mol above **A'**), although the

[117]

experimental results showed no trace of silylformate during catalysis and/or stoichiometric reactions, which seems to point out that step **ii** is much faster than **i**.
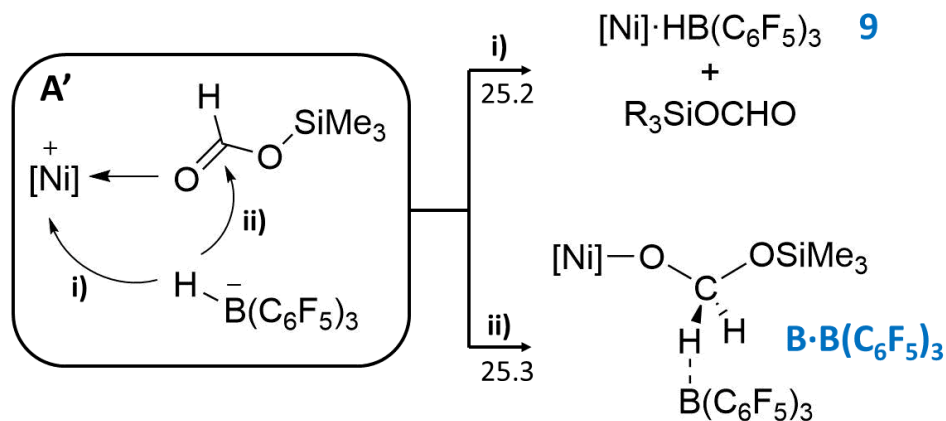
Scheme 26. Possible scenarios of intermediate **A'** for the attack of the hydridoborate unit. ΔZPE in kcal/mol from **A'**.

Again, the transition state for this process using the real catalyst could not be found, but the model system showed that going from **B·B(C₆F₅)₃** to **A'** required no energy to occur. Moreover, a relaxed potential energy surface scan also supports the kinetic ease of the reaction.

Silyl transfer

The interaction that holds the borane and the Ni fragment in **B·B(C₆F₅)₃** is weak, so the Lewis acid can interact with another silane molecule in the reaction medium to give rise to another borane-silane complex (Figure 28, **B·[Me₃Si–H···B(C₆F₅)₃]**). Then, the oxygen atom bound to the metal can attack the activated silane to yield Ni hydridoborate **9** and the bis(silyl)acetal product. It can be observed in Figure 28 that this silylium transfer also proceeds

[118]

kinetically swift since the energy for **T2b** is minuscule.[70] The final product of this reaction is the pair **C** [(PBP)NiO(SiMe$_3$)CH$_2$OSiMe$_3$][HB(C$_6$F$_5$)$_3$].
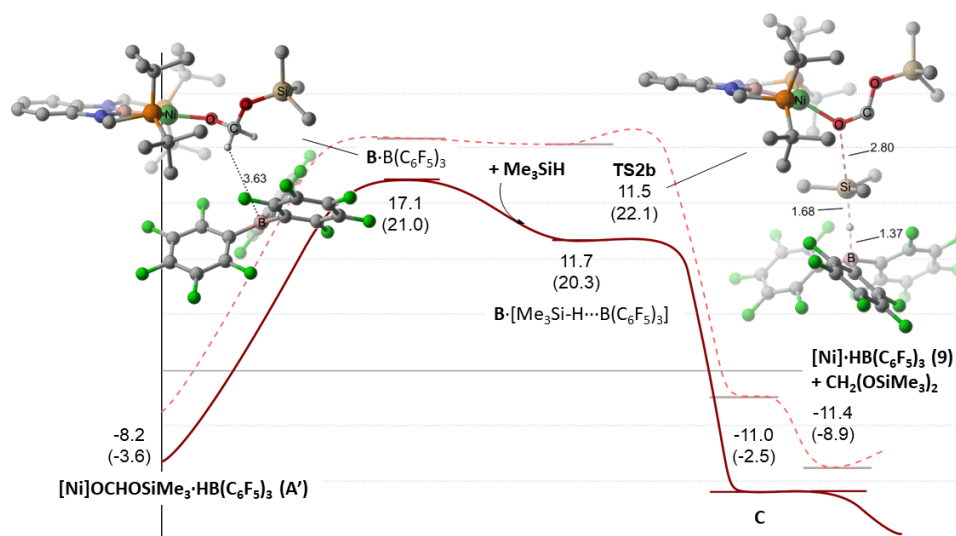
Figure 28. Energy profile of the second reduction stage.

3) Activation of CO$_2$ and catalyst regeneration

The Ni⋯O interaction in **C** can be cleaved by the hydridoborate [HB(C$_6$F$_5$)$_3$]$^-$ to give complex **9** and the free acetal derivative. It can be seen in Figure 28 that this step is also thermodynamically favourable. Given that during catalysis a homogeneous solution is always present, the lifetime of **9** must be rather short so as not to precipitate from the reaction medium.

Two very close minima (1.5 kcal/mol away from each other) were found when calculating the geometry of complex **9**, in which the hydridoborate unit can

---

[70] *NB:* Unless dispersion and entropy corrections are applied, $\Delta G^{\ddagger}$ would be above 50 kcal/mol with respect to the origin. Considering only dispersion corrections, $\Delta G^{\ddagger}$ = 36.9 kcal/mol. This would mean the unfeasibility of this mechanism. Moreover, if it were to be considered as a possibility, it would imply the accumulation of the silyl formate rather than the bis(silyl)acetal, which opposes the experimental facts. This is a clear example that remarks the importance of considering entropy and dispersion effects in the calculations.

interact with Ni via κ^1-*F* or κ^1-*H* arrangements (Figure 29), as in the scandocinium system reported by Piers *et al.*[45]
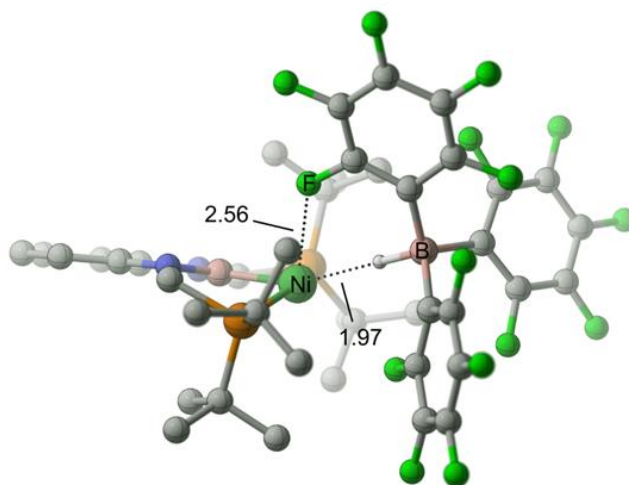
Figure 29. Optimized structure of complex **9**. The two possible interactions with the Ni framework are shown.

In the presence of **9**, carbon dioxide can insert into the cavity created between the 2 ions by stablishing an interaction (2.08 Å) with Ni through one of the oxygen atoms (**D**, Figure 30). At this point, the carbon dioxide molecule is still rather linear (O−C−O angle = 173 °). Then, a first transition state is found (**TS3**, 0.3 kcal/mol away) in which the hydride transfer to the carbon atom takes place. Immediately after, intermediate **E** features a weak H···B interaction (2.36 Å) and a closer O−C−O angle (129 °). Finally, attachment of the borane to the free oxygen of the formate regenerates catalyst **8** after surpassing a second transition state (2.3 kcal/mol from **E**). The whole operation requires practically no energy to overcome the two transition states, and it is quite exothermic, since catalyst **8** is more stable than **9** by 34.9 kcal/mol. These values account for the instantaneous formation of the catalyst after one catalytic cycle and the low degree of CO_2 exchange when using a mixture of labelled and non-labelled carbon dioxide, since the reverse step requires a considerable amount of energy.

[120]
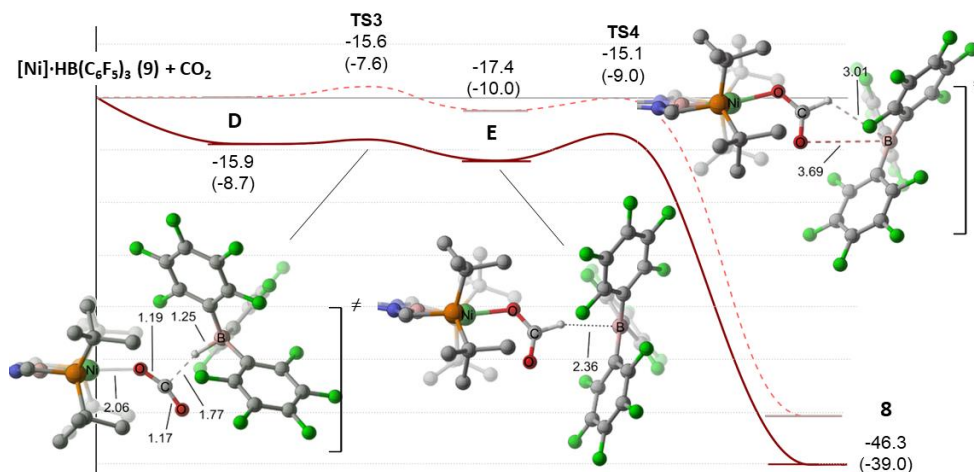
Figure 30. Energy profile for the regeneration of catalyst **8** from hydridoborate **9**.

4) How is selective CO₂ hydrosilation possible?

Efficient sequestration of BCF has been previously postulated as the reason for the selectivity in carbon dioxide hydrosilation.[46] In the Ni-PBP case, liberation of BCF is difficult in all the possible scenarios during the catalytic process:

-Dissociation of the Lewis acid from the catalyst (Scheme 27, equation 1) requires a high amount of energy and the equilibrium is therefore displaced to the left, as well as in the case of the release of $B(C_6F_5)_3$ from complex **9** (equation 2). Besides, **9** reacts more favourably with CO_2 and $Me_3SiOCHO$.

-**B·B(C₆F₅)₃** could also release borane given that it interacts weakly with the Ni framework. Nonetheless, this process is also energy demanding, with ΔG_{50} = 22.3 kcal/mol (considering **8** + 2 Me_3SiH as the reference), as observed in equation 3. Combination of the silyl formate generation (equation 4) with the latter process would give rise to equation 5, which is also extremely energy-demanding.

[121]

-Even if the silyl formate was produced and released during catalysis, its reduction to the bis(silyl)acetal stage with the borane-silane complex [Me$_3$Si–H···B(C$_6$F$_5$)$_3$] would not be irreversible, since formation of the formaldehyde derivative would be only moderately exoergic (ΔG_{50} = -17.7 kcal/mol), *i.e.* the reverse step would be energetically feasible (equation 5).

(Eq. 1) (8) + Me$_3$SiH $\xleftrightarrow{\text{+ 30.1}}$ [Ni]OCHO (7) + [Me$_3$Si-H···B(C$_6$F$_5$)$_3$]

(Eq. 2) [Ni]·HB(C$_6$F$_5$)$_3$ (9) $\xleftrightarrow{\text{+ 24.3}}$ [Ni]-H (6) + B(C$_6$F$_5$)$_3$

(Eq. 3) (8) + 2 Me$_3$SiH $\xrightarrow{}$ B·B(C$_6$F$_5$)$_3$ + Me$_3$SiH $\xleftrightarrow{\text{+ 22.3}}$ [Ni]OCH$_2$OSiMe$_3$ (B) + [Me$_3$Si-H···B(C$_6$F$_5$)$_3$]

(Eq. 4) (8) + Me$_3$SiH $\xleftrightarrow{\text{+16.4}}$ [Ni]·HB(C$_6$F$_5$)$_3$ (9) + Me$_3$SiOCHO

Eq. 5 = Eq.3 + Eq.4

(Eq. 5) 2 (8) + 3 Me$_3$SiH $\xleftrightarrow{\text{+ 38.7}}$ (9) + [Ni]OCH$_2$OSiMe$_3$ (B) + Me$_3$SiOCHO + [Me$_3$Si-H···B(C$_6$F$_5$)$_3$]

(Eq. 6) HCOOSiMe$_3$ + [Me$_3$Si-H···B(C$_6$F$_5$)$_3$] $\xleftrightarrow{\text{-17.7}}$ Me$_3$SiOCH$_2$OSiMe$_3$ + B(C$_6$F$_5$)$_3$
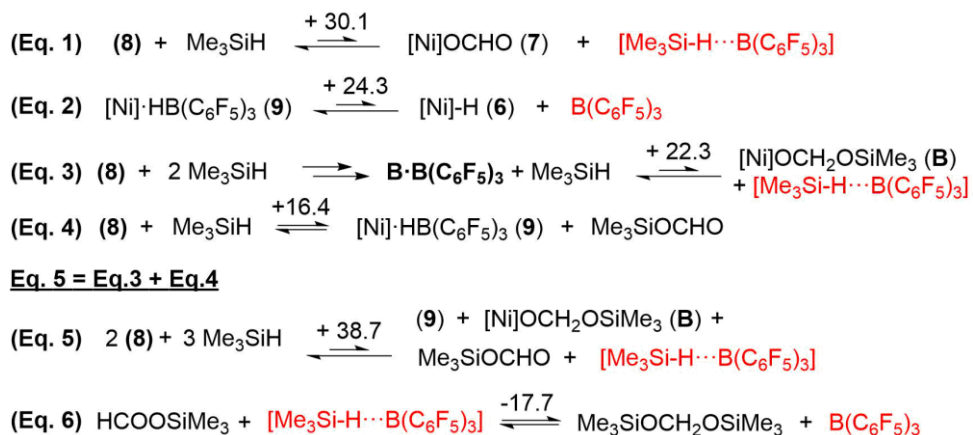
Scheme 27. Possible scenarios in which BCF could be released during catalysis (species with free BCF highlighted in red). ΔG_{50} in kcal/mol.

For all the reasons stated above, the (PBP)Ni complexes are necessary in the proposed mechanism for carbon dioxide reduction, since they are able to activate CO$_2$ efficiently, they mediate the hydrosilation processes and they control the release of the Lewis acid, avoiding in this way over-reduction phenomena. A scheme of the catalytic cycle (Scheme 28) and an overall energy profile (Figure 31) are shown below.
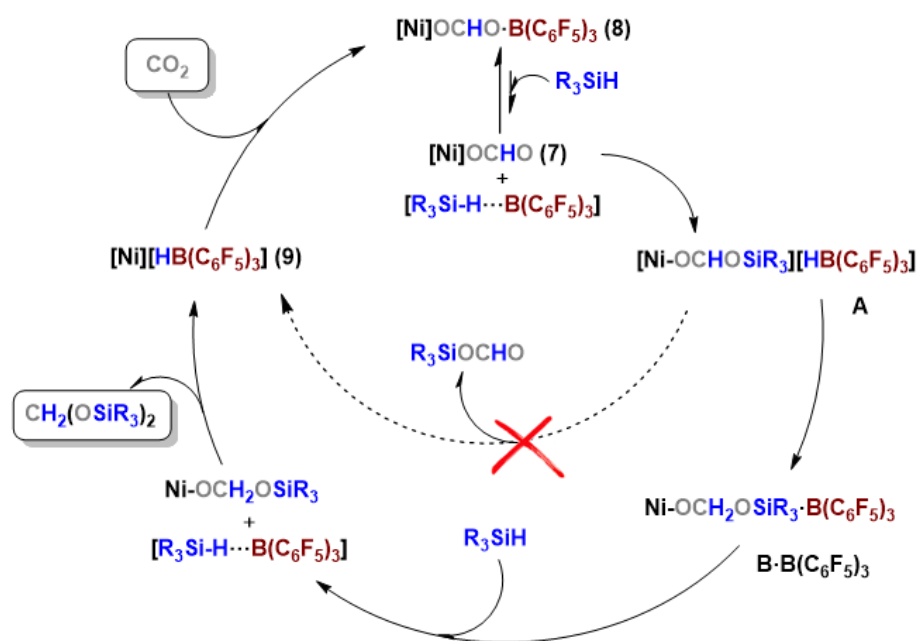
Scheme 28. Proposed catalytic cycle for the carbon dioxide hydrosilation to the bis(silyl)acetal stage based on the experimental and theoretical data.
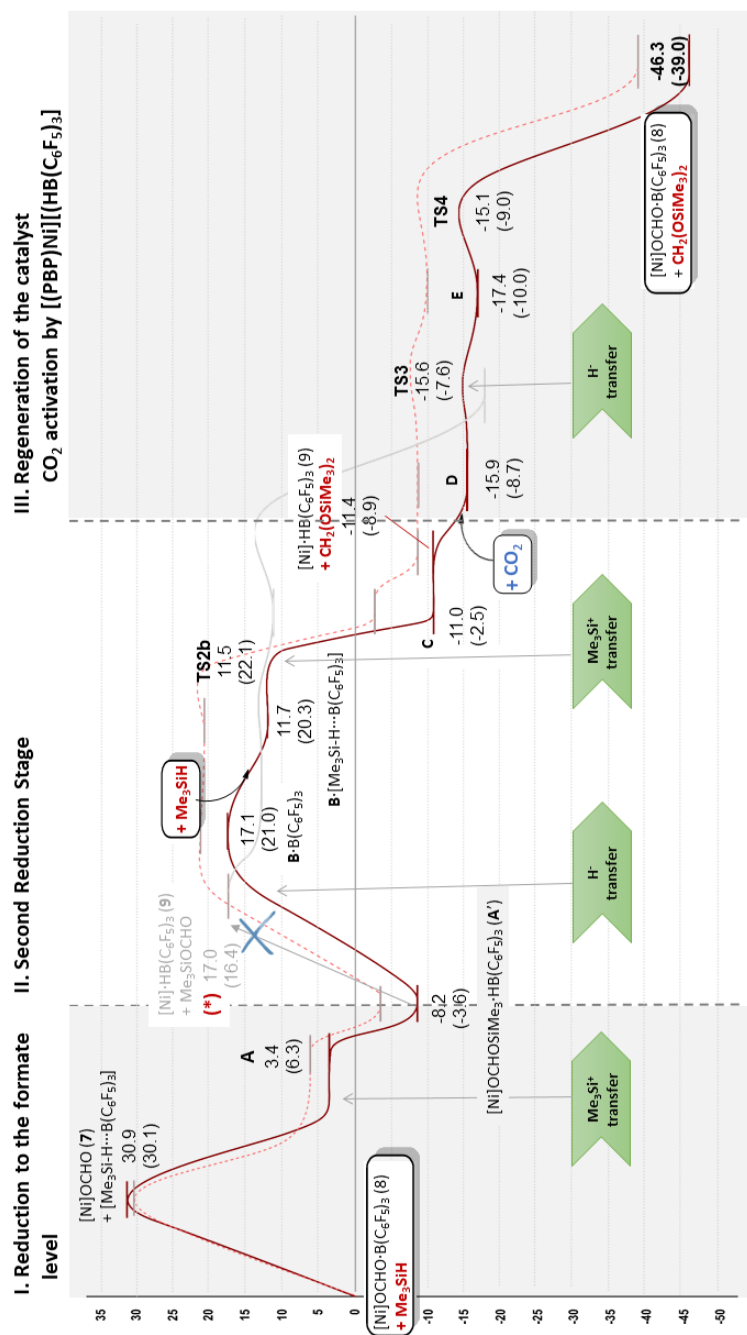
Figure 31. Energy profile for the carbon dioxide hydrosilation to the bis(silyl)acetal stage catalyzed by (PBP)Ni complex **8**. ΔZPE in kcal/mol (ΔG$_{50}$ in parentheses).

It can be observed in Figure 31 that there is a pattern in the reduction process, in which a silylium transfer always precedes the hydride attack, in a similar fashion to the systems described by Oestreich[40] and Müller[71] (Scheme 29), where they describe carbon dioxide hydrosilation by using Ru−S systems and silyl cations, respectively.

$$CO_2 \xrightarrow{\text{2 } R_3SiH} R_3SiOCH_2OSiR_3$$

O=C=O $\xrightarrow{R_3Si^+}$ O=C=O$\diagup^{SiR_3}_+$ $\xrightarrow{H^-}$ O=CH-O$\diagup^{SiR_3}$ $\xrightarrow{R_3Si^+}$ $R_3Si\diagdown\overset{+}{O}$=CH-O$\diagup^{SiR_3}$ $\xrightarrow{H^-}$ $R_3SiOCH_2OSiR_3$

Silylium transfer   Hydride transfer   **Silyl formate**   Silylium transfer   Hydride transfer   **Bis(silyl) acetal**
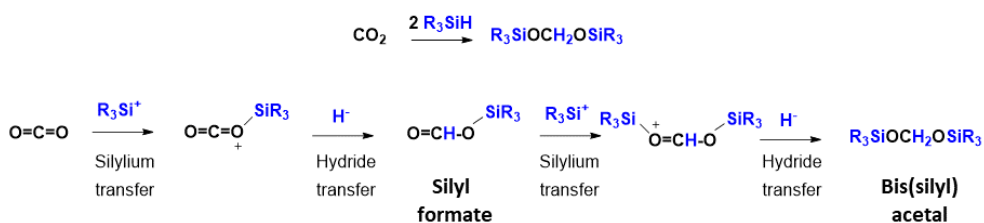
Scheme 29. Reduction steps in the hydrosilation of CO_2 as proposed by Oestreich and Müller (adapted from references 40 and 71).

[71] A. Schäfer, W. Saak, D. Haase, T. Müller, *Angew. Chem. Int. Ed.,* **2012**, *51*, 2981-2984.

References

[1] a) International Energy Agency, Electricity Information 2017, http://www.iea.org/publications/freepublications/publication/ElectricityInformation2017Overview.pdf; b) A. Goeppert, M. Czaun, G.K.S. Prakash, G. A. Olah, *Energy Environ. Sci.*, **2012**, *5*, 7833-7853.

[2] a) J.C. Orr, V. J. Fabry, O. Aumont, L. Bopp, S. C. Doney, R. A. Feely, A. Gnanadesikan, N. Gruber, A. Ishida, F. Joos, R. M. Key, K. Lindsay, E. Maier-Reimer, R. Matear, P. Monfray, A. Mouchet, R. G. Najjar, G-K. Plattner, K. B. Rodgers, C. L. Sabine, J. L. Sarmiento, R. Schlitzer, R. D. Slater, I. J. Totterdell, M-F. Weirig, Y. Yamanaka, A. Yool, *Nature,* **2005**, *437*, 681-686; b) S. C. Doney, V. J. Fabry, R. A. Feely, J. A. Kleypas, *Annu. Rev. Mar. Sci.,* **2009**, *1*, 169-192.

[3] J. Artz, T. E. Müller, K. Thenert, J. Kleinekorte, R. Meys, A. Sternberg, A. Bardow, W. Leitner, *Chem. Rev.,* **2018**, *118*, 434-504.

[4] H. Arakawa, M. Aresta, J. N. Armor, M. A. Barteau, E. J. Beckman, A. T. Bell, J. E. Bercaw, C. Creutz, E. Dinjus, D. A. Dixon, K. Domen, D. L. DuBois, J. Eckert, E. Fujita, D. H. Gibson, W. A. Goddard, D. W. Goodman, J. Keller, G. J. Kubas, H. H. Kung, J. E. Lyons, L. E. Manzer, T. J. Marks, K. Morokuma, K. M. Nicholas, R. Periana, L. Que, J. Rostrup-Nielson, W. M. H. Sachtler, L. D. Schmidt, A. Sen, G. A. Somorjai, P. C. Stair, B. Ray. Stults, W. Tumas, *Chem. Rev.,* **2001**, *101*, 953-996.

[5] J. Meessen, *Chem. Ing. Tech.,* **2014**, *86*, 2180-2189.

[6] Q. Zhang, H-Y. Yuan, N. Fukaya, J-C. Choi, *ACS Sustainable Chem. Eng.,* **2018**, *6*, 6675-6681.

[7] Q. Liu, L. Wi, R. Jackstell, M. Beller, *Nat. Commun.,* **2015**, *6*, 5933.

[8] C. D. N. Gomes, O. Jacquet, C. Villiers, P. Thuéry, M. Ephritikhine, T. Cantat, *Angew. Chem. Int. Ed.,* **2012**, *51*, 187-190.

[9] G. A. Olah, *Angew. Chem. Int. Ed*. **2005**, *44*, 2636-2639. For a recent review on the Methanol Economy, see W-C. Liu, J. Baek, G. A. Somorjai, *Topics in Catalysis,* **2018**, *61*, 530-541.

[126]

[10] K. Huang, C-L. Sun, Z-J. Shi, *Chem. Soc. Rev.*, **2011**, *40*, 2435-2452.

[11] D. W. Stephan, *Org. Biomol. Chem.,* **2008**, *6*, 1535-1539.

[12] B. R. Buckley, M. C. Kimber, N. H. Slater, *Annu. Rep. Prog. Chem. Sect. B: Org. Chem.,* **2012**, *108*, 98-109.

[13] J. F. Hartwig, *Organotransition Metal Chemistry: From Bonding to Catalysis*, University Science Books, Sausalito, CA, **2009**.

[14] D. H. Gibson, *Chem. Rev.,* **1993**, *96*, 2063-2095.

[15] H. Takeda, C. Cometto, O. Ishitani, M. Robert, *ACS Catal.,* **2017**, *7*, 70-88.

[16] C. Chauvier, T. Cantat, *ACS Catal.,* **2017**, *7*, 2107-2115.

[17] R.F. Nystrom, W.H. Yanko, W. Brown, *J. Am. Chem. Soc.,* **1948**, *70,* 441.

[18] J. G. Burr Jr., W. Brown, H. E. Heller, *J. Am. Chem. Soc.,* **1950**, *72*, 2560-2562.

[19] S. Bontemps, *Coord. Chem. Rev.,* **2016**, *308*, 117-130.

[20] G. Herzberg, A. Monfils, *J. Mol. Spect.,* **1960**, *5*, 482-498.

[21] W. Leitner, *Angew. Chem. Int. Ed. Engl.,* **1995**, *34*, 2207-2221.

[22] a) J. Klankermayer, S. Wesselbaum, K. Beydoun, W. Leitner, *Angew. Chem. Int. Ed.,* **2016**, *55,* 7296-7343; b) W. H. Bernskoetter, N. Hazari, *Acc. Chem. Res.,* **2017**, *50*, 1049-1058.

[23] K. Sordakis, C. Tang, L. K. Vogt, H. Junge, P. J. Dyson, M. Beller, G. Laurenczy, *Chem. Rev.,* **2018**, *118,* 372-433.

[24] C. A. Huff, M. S. Sanford, *J. Am. Chem. Soc.,* **2011**, *133*, 18122-18125.

[25] S. Wesselbaum, T. vom Stein, J. Klankermayer, W. Leitner, *Angew. Chem. Int. Ed.,* **2012**, *51,* 7499-7502.

[26] J. Schneidewind, R. Adam, W. Baumann, R. Jackstell, M. Beller, *Angew. Chem. Int. Ed.,* **2017**, *56*, 1890-1893.

[27] J. Kothandaraman, A. Goeppert, M. Czaun, G. A. Olah, G. K. S. Prakash, *J. Am. Chem. Soc.,* **2016**, *138*, 778-781.

[28] L. E. Heim, H. Konnerth, M. H. G. Prechtl, *Green. Chem.,* **2017**, *19*, 2347-2355.

[29] S. Gambarotta, S. Strologo, C. Floriani, A. Chiesi-Villa, C. Guastini, *J. Am. Chem. Soc.,* **1985**, *107*, 6278-6272.

[30] K. Thenert, K. Beydoun, J. Wiesenthal, W. Leitner, J. Klankermayer, *Angew. Chem. Int. Ed.,* **2016**, *55*, 12266-12269.

[31] Y-R. Luo, *Comprehensive Handbook of Chemical Bond Energies,* CRC Press: Boca Raton, FL, 2007.

[32] J. B. Grande, *"The Piers-Rubinsztajn Reaction: New Routes to Structured Silicones".* PhD Thesis, McMaster University, 2013.

[33] For more examples of carbon dioxide hydroboration, see reference 19. For more examples of carbon dioxide hydrosilation, see: F. J. Fernández-Álvarez, L. A. Oro, *ChemCatChem*, **2018**, *10*, 4783-4796.

[34] S. Bontemps, L. Vendier, S. Sabo-Etienne, *Angew. Chem. Int. Ed.,* **2012**, *51*, 1671-1674.

[35] S. Bontemps, S. Sabo-Etienne, *Angew. Chem. Int. Ed.,* **2013**, *52*, 10253-10255.

[36] S. Bontemps, L. Vendier, S. Sabo-Etienne, *J. Am. Chem. Soc.,* **2014**, *136*, 4419-4425.

[37] G. Jin, C. G. Werncke, Y. Escudié, S. Sabo-Etienne, S. Bontemps, *J. Am. Chem. Soc.,* **2015**, *137*, 9563-9566.

[38] L. J. Murphy, H. Hollenhorst, R. McDonald, M. Ferguson, M. D. Lumsden, L. Turculet, *Organometallics*, **2017**, *36*, 3709-3720.

[39] A. Aloisi, J-C. Berthet, C. Genre, P. Thuéry, T. Cantat, *Dalton Trans.,* **2016**, *45*, 14774-14788.

[40] T. T. Metsänen, M. Oestreich, *Organometallics*, **2015**, *34*, 543-546.

[41] M. A. Brook, *Chem. Eur. J.,* **2018**, *24*, 8458-8469.

[42] D. J. Parks, J. M. Blackwell, W. E. Piers, *J. Org. Chem.,* **2000**, *65*, 3090-3098.

[43] M. Oestreich, J. Hermeke, J. Mohr, *Chem. Soc. Rev.,* **2015**, *44*, 2202-2220.

[44] A. Y. Houghton, J. Hurmalainen, A. Mansikkamäki, W. E. Piers, H. M. Tuononen, *Nat. Chem.,* **2014**, *6*, 983-988.

[45] A. Berkefeld, W. E. Piers, M. Parvez, L. Castro, L. Maron, O. Eisenstein, *Chem. Sci.,* **2013**, *4*, 2152-2162.

[46] F. A. Leblanc, W. E. Piers, M. Parvez, *Angew. Chem. Int. Ed.,* **2014**, *53*, 789-792.

[47] Y. Jiang, O. Blacque, T. Fox, H. Berke, *J. Am. Chem. Soc.,* **2013**, *135,* 7751-7760.

[48] N. del Rio, M. Lopez-Reyes, A. Baceiredo, N. Saffon-Merceron, D. Lutters, T. Müller, T. Kato, *Angew. Chem. Int. Ed.,* **2017**, *56,* 1365-1370.

[49] M. Rauch, G. Parkin, *J. Am. Chem. Soc.,* **2017**, *139*, 18162-18165.

[50] J. E. Heimann, W. H. Bernskoetter, N. Hazari, J. M. Mayer, *Chem. Sci.,* **2018**, *9*, 6629-6638.

[51] N. Curado, C. Maya, J. López-Serrano, A. Rodriguez, *Chem. Commun.,* **2014**, *50*, 15718-15721.

[52] N. A. Yakelis, R. G. Bergman, *Organometallics,* **2005**, *24*, 3579-3581.

[53] a) C. J. Moulton, B. L. Shaw, *J. Chem. Soc. Dalton Trans.,* **1976**, 1020-1024; b) P. Giannoccaro, G. Vasapollo, A. Sacco, *J. Chem. Soc. Chem. Commun.,* **1980**, 1136-1137; c) A. Castonguay, A. L. Beauchamp, D. Zargarian, *Inorg. Chem.,* **2009**, *48*, 3177-3184; d) S. J. Connelly, A. C. Zimmerman, W. Kaminsky, D. M. Heinekey, *Chem. Eur. J.* **2012**, *18*, 15932-15934.

[54] N. N. Greenwood, A. Earnshaw, *Chemistry of the Elements*, 2nd ed. Butterworth-Heinemann: Woburn, MA, 1997.

[55] J. Zhu, Z. Lin, T. B. Marder, *Inorg. Chem.,* **2005**, *44*, 9384-9390.

[56] T-P. Lin, J. C. Peters, *J. Am. Chem. Soc.,* **2014**, *136*, 13672-13683.

[57] Insertion of CO_2 into different types of metal-element σ bonds has been studied in detail. See: N. Hazari, J. E. Heimann, *Inorg. Chem.,* **2017**, *56*, 13655-13678.

[58] T. J. Schmeier, N. Hazari, C. D. Incarvito, J. A. Raskatov, *Chem. Commun.,* **2011,** *47*, 1824-1826.

[59] a) S. Chakraborty, J. Zhang, J. A. Krause, H. Guan, *J. Am. Chem. Soc.,* **2010**, *132*, 8872-8873 ; b) S. Chakraborty, Y. J. Patel, J. A. Krause, H. Guan, *Polyhedron,* **2012**, *32*, 30-34.

[60] W-H. Suh, M. L. Guard, N. Hazari, *Polyhedron*, **2014**, *84*, 37-43.

[61] Some studies previously reported the energies for CO_2 insertion in Ni–R or Pd–R groups. See: a) T.J. Schmeier, A. Nova, N. Hazari, F. Maseras, *Chem. Eur. J.,*

2012, *18*, 6915-6927; b) W. H. Suh, T. J. Schmeier, N. Hazari, R. A. Kemp, M. K. Takase, *Organometallics*, **2012**, *31*, 8225-8236.

[62] M. Aresta in *Activation of Small Molecules: Organometallic and Bioinorganic perspectives,* W. B. Tolman (Editor), Wiley-VCH, **2006**. Chapter 1: Carbon Dioxide Reduction and Uses as a Chemical Feedstock, pages 1-41.

[63] S. J. Mitton, L. Turculet, *Chem. Eur. J.,* **2012**, *18,* 15258-15262.

[64] A. Willms, H. Schumacher, T. Tabassum, L. Qi, S. L. Scott, P. J. C. Hausoul, M. Rose, *ChemCatChem* **2018**, *10*, 1835-1843.

[65] (a) A. Berkefeld, W. E. Piers, M. Parvez, *J. Am. Chem. Soc.*, **2010**, *132*, 10660-10661; (b) I. Peuser, R. C. Neu, X. Zhao, M. Ulrich, B. Schirmer, J. A. Tannert, G. Kehr, R. Fröhlich, S. Grimme, G. Erker and D. W. Stephan, *Chem. Eur. J.,* **2011**, *17*, 9640-9650; (c) M. Harhausen, R. Fröhlich, G. Kehr and G. Erker, *Organometallics*, **2012**, *31*, 2801-2809; (d) D. W. Stephan, *J. Am. Chem. Soc.,* **2015**, *137*, 10018-10032.

[66] Complex **6** + CO_2 + $B(C_6F_5)_3$ were used as the energy reference.

[67] T. Voss, T. Mahdi, E. Otten, R. Frölich, G. Kehr, D. W. Stephan, G. Erker, *Organometallics*, **2012**, *31*, 2367-2378.

[68] L. H. Doerrer, A. J. Graham, D. Haussinger, M. L. H. Green, *J. Chem. Soc. Dalton Trans.,* **2000**, 813-820.

[69] Computational methods are detailed in the Experimental part section.

[70] *NB:* Unless dispersion and entropy corrections are applied, $\Delta G^{\ddagger}$ would be above 50 kcal/mol with respect to the origin. Considering only dispersion corrections, $\Delta G^{\ddagger}$ = 36.9 kcal/mol. This would mean the unfeasibility of this mechanism. Moreover, if it were to be considered as a possibility, it would imply the accumulation of the silyl formate rather than the bis(silyl)acetal, which opposes the experimental facts. This is a clear example that remarks the importance of considering entropy and dispersion effects in the calculations.

[71] A. Schäfer, W. Saak, D. Haase, T. Müller, *Angew. Chem. Int. Ed.,* **2012**, *51*, 2981-2984.

[130]

Chapter 2

Nickel(II) boryl complexes as reactive intermediates

1. Introduction

1.1. Transition metal boryl complexes (M–BY$_2$, Y = OR, NR$_2$, alkyl...)

Although the first studies on transition metal boryl complexes date back to the 1960s,[1] there has been a recent increasing interest on these compounds in the last couple of decades, since they have been widely proposed as reactive intermediates in the catalytic borylation or hydroboration of alkenes, alkanes and arenes. Given the high versatility of these resulting organoboron species for making a great diversity of new bonds, it is not surprising that studies on TM boryl complexes are becoming more frequent, so the better understanding on the bonding and reactivity can help in developing more selective and efficient catalytic processes.[2]

1.1.1. Synthesis

Structural features

Before describing the most common approaches to generate metal-boryl bonds, it is worth mentioning that the strong σ-donor properties and *trans* influence of these ligands have consequences on the structure and geometry of the resulting complexes. The main reason for this phenomenon is the tendency of the ligands to rearrange inasmuch as possible to avoid steric hindrance and/or electronic repulsion (*e.g.* two strong *trans* influence ligands in *trans* position to each other).[3]

---

[1] H. Nöth, G. Schmid, *Angew. Chem. Int. Ed.* **1963**, *2*, 623.

[2] a) S. Aldridge, D. L. Coombs, *Coord. Chem. Rev.,* **2004**, *248*, 535-559; b) I. A. I. Mkhalid, J. H. Barnard, T. B. Marder, J. M. Murphy, J. F. Hartwig, *Chem. Rev.* **2010**, *110*, 890-931.

[3] Z. Lin in *Computational Studies in Organometallic Chemistry*, S. A. McGregor & O. Eisenstein (Editors), Springer International Publishing, **2016**. Chapter 2: Reactivities and Electronic Properties of Boryl Ligands, pages 39-58.
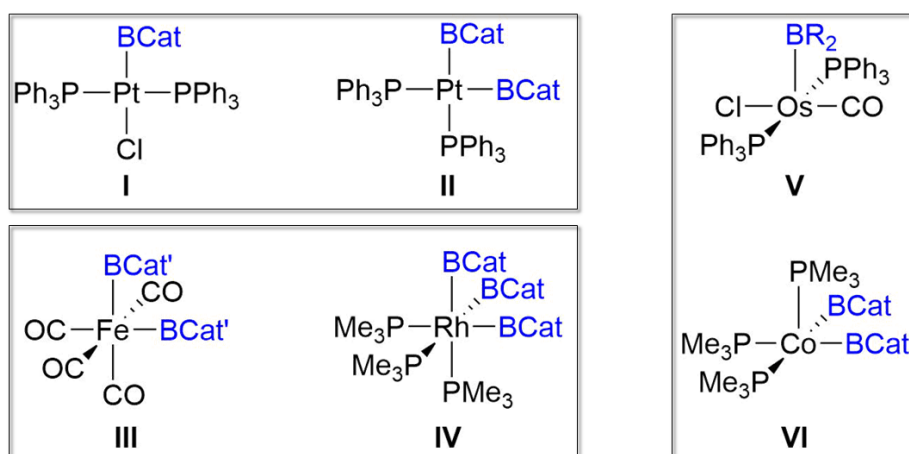
Figure 1. Representative examples of the *trans* influence of boryl ligands and its repercussion on the geometry of transition metal complexes (adapted from reference 3). Bcat = catecholboryl. BCat' = 4-*tert*-butylcatecholboryl.

Figure 1 shows some cases where the presence of boryl ligands forces a certain geometry in a transition metal complex. For instance, platinum square planar complex **I**[4] displays a ligand arrangement in which the boryl moiety is located *trans* to the weakest *trans* influence ligand of the complex (*i.e.* chloride ligand). In this way, the two bulky phosphine groups are far enough from each other not to be sterically constrained. This is not the case for complex **II**,[5] where the electronic effects force the phosphines to be in a *cis* position regardless of the steric bulk. Octahedral complexes **III**[6] and **IV**[7] show the same phenomenon: in **III**, the boryl fragments adopt again a *cis* position, even though the carbonyl ligands are also strong *trans* influence groups. The same effect can be observed

[4] W. Clegg, F. J. Lawlor, G. Lesley, T. B. Marder, N. C. Norman, A. G. Orpen, M. J. Quayle, C. R. Rice, A. J. Scott, F. E. S. Souza, *J. Organomet. Chem.,* **1998**, *550*, 183-192.

[5] G. Lesley, P. Nguyen, N. J. Taylor, T. B. Marder, A. J. Scott, W. Clegg, N. C. Norman, *Organometallics*, **1996**, *15*, 5137-5154.

[6] X. He, J. F. Hartwig, *Organometallics*, **1996**, *15*, 400-407.

[7] C. Dai, G. Stringer, T. B. Marder, A. J. Scott, W. Clegg, N. C. Norman, *Inorg. Chem.,* **1997**, *36*, 272-273.

in **IV**, where the BCat moieties are oriented in a *fac* arrangement. In square pyramidal complex **V**[8] the boryl fragment is placed in the apical position given that there is a vacant *trans* to it. Nonetheless, they occupy basal positions in the 17-electron complex **VI**,[9] since the cobalt atom possesses an electron in the apical position which is located in an orbital with antibonding character, precluding the presence of a boryl ligand in such zone.

To the best of our knowledge, there is no example reported yet for a transition metal complex with two boryl units *trans* to each other.

Synthetic approaches

The most common strategies for the construction of metal−boryl bonds include the following:[10]

- Attack of an anionic transition metal complex to a boron halide to give the corresponding metal−boryl fragment and a salt.

- σ bond metathesis reaction between a M−R bond (*e.g.* M−alkyl, M−alkoxide) and a borane reagent.

- Oxidative addition of a B−X bond to a transition metal, where X = H, Cl, Br, Sn or B.

The last method, and especially the use of diboron(4) reagents is gaining increasing interest in the chemistry community because these species have proven very useful in synthetic chemistry, and they possess attractive features

---

[8] a) C. E. F. Rickard, W. R. Roper, A. Williamson, L. J. Wright, *Organometallics*, **1998**, *17*, 4869-4874; b) G. R. Clark, G. J. Irvine, W. R. Roper, L. J. Wright, *J. Organomet. Chem.,* **2003**, *680*, 81-88.

[9] a) C. Dai, G. Stringer, J. F. Corrigan, N. J. Taylor, T. B. Marder, N. C. Norman, *J. Organomet. Chem.,* **1996**, *513*, 273-275; b) K. C. Lam, W. H. Lam, Z. Lin, T. B. Marder, N. C. Norman, *Inorg. Chem.,* **2004**, *43*, 2541-2547.

[10] C. S. Cundy, H. Nöth, *J. Organomet. Chem.,* **1971**, *30*, 135-143.

such as their ease to manipulate and their stability.[11] Specifically, the stability of diboron(4) Y_2B-BY_2 reagents against disproportionation decreases in the following order: Y = NR$_2$, OR > aryl, alkyl, Cl. The high stability shown by tetraamino and tetra(alkoxy)diborons is due to the π orbital overlap and partial filling of the empty p-orbital of the boron atom. Whereas, B_2Cl_4 is extremely reactive (pyrophoric, and it undergoes partial decomposition to B_4Cl_4 above 0 °C),[12] $B_2(NR_2)_4$ or $B_2(OR)_4$ possess an appropriate stability/reactivity ratio for synthetic purposes.[13] This gradient in reactivity and stability can be observed in Figure 2.
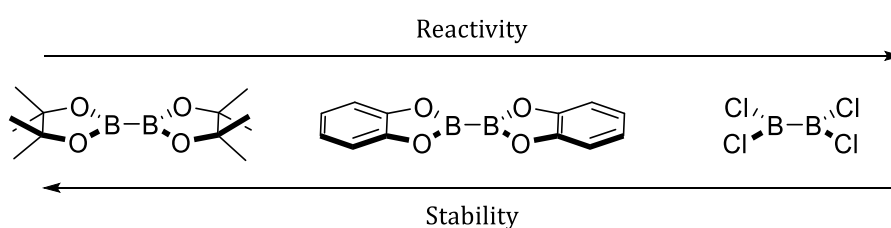
Figure 2. Comparison of the chemical behaviour of some diboron(4) reagents depending on the substituents (adapted from reference 13).

Depending on the environment surrounding them, diboron(4) reagents also react in a variety of modes so the B−B bond undergoes full cleavage. In this way, the presence of a M−R fragment in a transition metal complex can give rise to a metathetic pathway in which there is a ligand exchange, ending up with a metal−boryl bond (Figure 3A). Usually the R group is an alkoxide fragment, so the generation of a new B−O bond drives the reaction towards the products.[13]

Alternatively, the Lewis acidity of the boron atoms in these reagents make the diboron(4) compounds prone to react with Lewis bases. This

[11] E. C. Neeve, S. J. Geier, I. A. I. Mkhalid, S. A. Westcott, T. B. Marder, *Chem. Rev.* **2016**, *116*, 9091-9161.

[12] G. Urry, T. Wartik, R. E. Moore, H. I. Schlesinger, *J. Am. Chem. Soc.,* **1954**, *76*, 5293-5298.

[13] S. A. Westcott, E. Fernández, *Adv. Organomet. Chem.,* **2015**, *63*, 39-89.

interaction polarizes the B−B bond, so the resulting adduct is composed of a sp^3 hybridized boron atom and a boryl-type fragment, characterized by a nucleophilic sp^2 boron (Figure 3B). Several Lewis bases are known to react with these compounds, such as pyridines, alkoxides, amidines, phosphines or NHCs.[11]
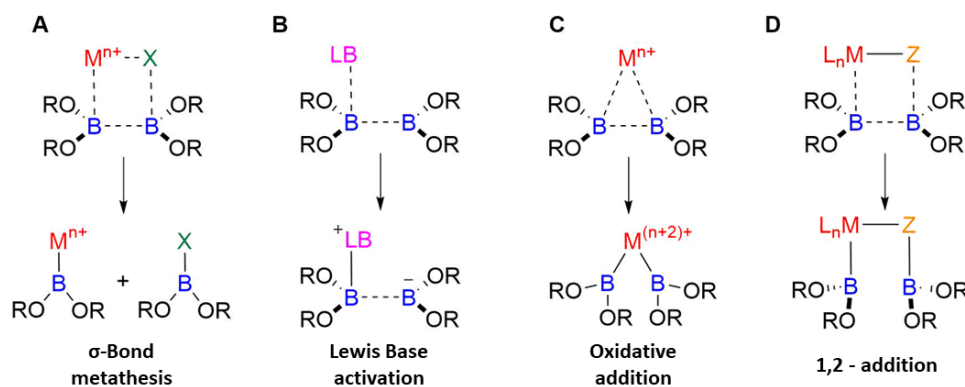
Figure 3. Different methods of activating diboron(4) species (adapted from reference 13).

If the diboron(4) is in the presence of a low-valent transition metal with labile ligands that can dissociate easily, oxidative addition events may take place, affording a metal bis(boryl) complex that might isomerize accordingly so as to avoid steric and electronic repulsions as stated above (Figure 3C). According to some authors, oxidative addition of B−X bonds is the most common strategy for the synthesis of transition metal boryl compounds and 'this route has been exploited for elements of virtually all of the transition metal groups and in the synthesis of mono-, bis- and tris(boryl) derivatives.'[2a,14]

---

[14] According to some references (*e.g.* J. F. Hartwig, *Organotransition Metal Chemistry: From Bonding to Catalysis*, University Science Books, Sausalito, CA, **2009**. Chapter 4, page 186), boryl complexes of all transition metals have been isolated except for group 3 and group 4 elements. However, recent works have reported on the syntheses of group 3 and group 4 boryl complexes. For group 3 boryl compounds, see: L. M. A. Saleh, K. H. Birjkumar, A. V. Protchenko, A. D. Schwarz, S. Aldridge, C. Jones, N. Kaltsoyannis, P. Mountford, *J. Am. Chem. Soc.,* **2011**, *133*, 3836-3839. For group 4 boryl species, see: T. Terabayashi, T. Kajiwara, M. Yamashita, K. Nozaki, *J. Am. Chem. Soc.,* **2009**, *131*, 14162-14163.

Nonetheless, there are obviously some exceptions to this latter statement. For instance, the oxidative addition process is the reason why Pt(0) complexes can catalyse alkyne diboration reactions whereas Pd(0) cannot, even though they are highly active in silyl or stannylmetalation reactions. Following the work of Sakaki,[15] Musaev and Morokuma[16] carried out a DFT study in 1998 where they found a plausible explanation for this discrepancy in reactivity: in both cases the diboration reaction can occur by following the proposed cycle in Scheme 1, in which the first step involves the oxidative addition of the B−B bond. The activation energy for this step is 14.0 kcal/mol for Pt(0) and 8.6 kcal/mol for Pd(0). Although the transition state is easier to access for palladium, the resulting product (*i.e.* bis boryl complex) is 8.5 kcal/mol in energy above the origin, whereas in the case of platinum it is -7.2 kcal/mol. Due to the negligible reverse energy barrier (0.1 kcal/mol), the process does not take place and no catalysis is observed experimentally, given that this difference in energy remains for every intermediate of the catalytic cycle.

[15] S. Sakaki, T. Kikuno, *Organometallics*, **1997**, *36*, 226-229.
[16] Q. Cui, D. G. Musaev, K. Morokuma, *Organometallics*, **1998**, *17*, 742-751.
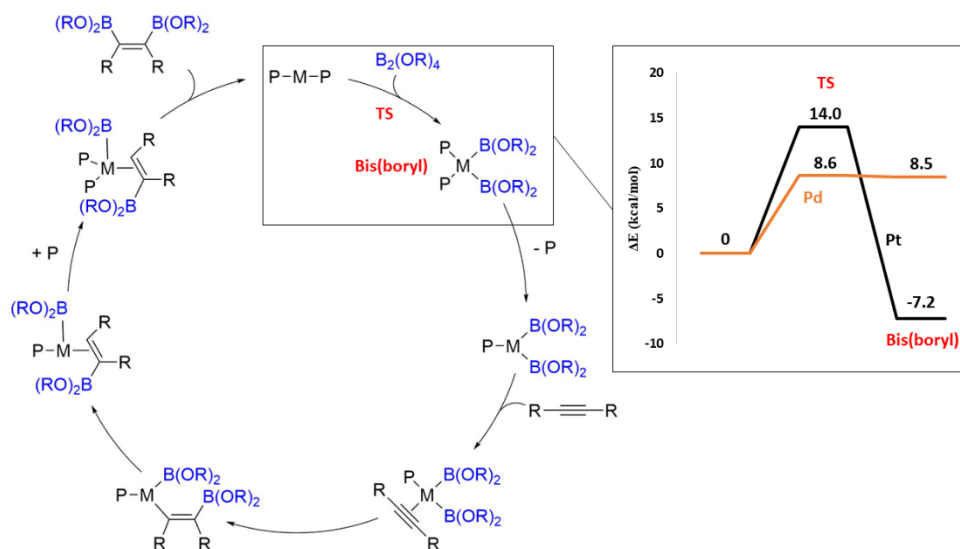
Scheme 1. One of the proposed catalytic cycles for *cis* alkyne diborylation, as proposed by Musaev and Morokuma. Inset: scheme of the energies required for the oxidative addition of the B−B bond (adapted from reference 16).

For this reason, it is more common to find σ-metathesis processes in palladium complexes than in platinum ones. In fact, going up from Pt in group 10 shows a trend in reactivity against tetra(alkoxy)diboron reagents: whereas Pt complexes usually react through oxidative addition processes, Pd[17] and Ni[18] often undergo σ-bond metathesis.[13]

The last approach for activating diboron(4) species by transition metal complexes involve the cooperativity of the ligand, and it is named 1,2 – addition (Figure 3D). In this strategy, the B−B bond is added across a metal-ligand, so each

[17] a) J. Takaya, N. Kirai, N. Iwasawa, *J. Am. Chem. Soc.,* **2011**, *133*, 12980-12983; b) N. Kirai, J. Takaya, N. Iwasawa, *J. Am. Chem. Soc.,* **2013**, *135*, 2493-2496. Oxidative addition events usually take place when a B−X (X= halide, Sn) containing reagent is used. See: c) S. Onozawa, Y. Hatanaka, T. Sakakura, S. Shimada, M. Tanaka, *Organometallics*, **1996**, *15*, 5450-5452; d) S. Onozawa, M. Tanaka, *Organometallics*, **2001**, *20*, 2956-2958; e) H. Braunschweig, K. Gruss, K. Radacki, K. Uttinger, *Eur. J. Inorg. Chem.,* **2008**, 1462-1466.

[18] B. L. Tran, D. Adhikari, H. Fan, M. Pink, D. J. Mindiola, *Dalton Trans.,* **2010**, *39*, 358-360.

fragment of the bond possesses one boryl moiety bound to it. The only examples in the literature of activation of B−X bonds by this mechanism are displayed in Scheme 2. The first two reactions involve the activation of hydroboranes across a metal−oxygen bond to yield the rare peroxoborate (A)[19] and borate (B)[20] species and metal−hydride unions in each case. It can be seen in all of the reactions that monoactivation of B−H species across M−L bonds proceed under mild conditions unlike reaction C, in which B−B cleavage requires some energy to take place. In this example (which is the first case where 1,2 - addition occurs across a M−N bond) it is possible to obtain in one step two boryl functionalities in different regions of the same complex.[21]

[19] M. A. Salomon, T. Braun, A. Penner, *Angew. Chem. Int. Ed.,* **2008**, *47*, 8867-8871.
[20] A. C. Fernandes, J. A. Fernandes, F. A. A. Paz, C. C. Romão, *Dalton Trans.,* **2008**, 6686-6688.
[21] Y. Zhu, C-H. Chen, C. M. Farfard, B. M. Foxman, O. V. Ozerov, *Inorg. Chem.,* **2011**, *50*, 7980-7987.
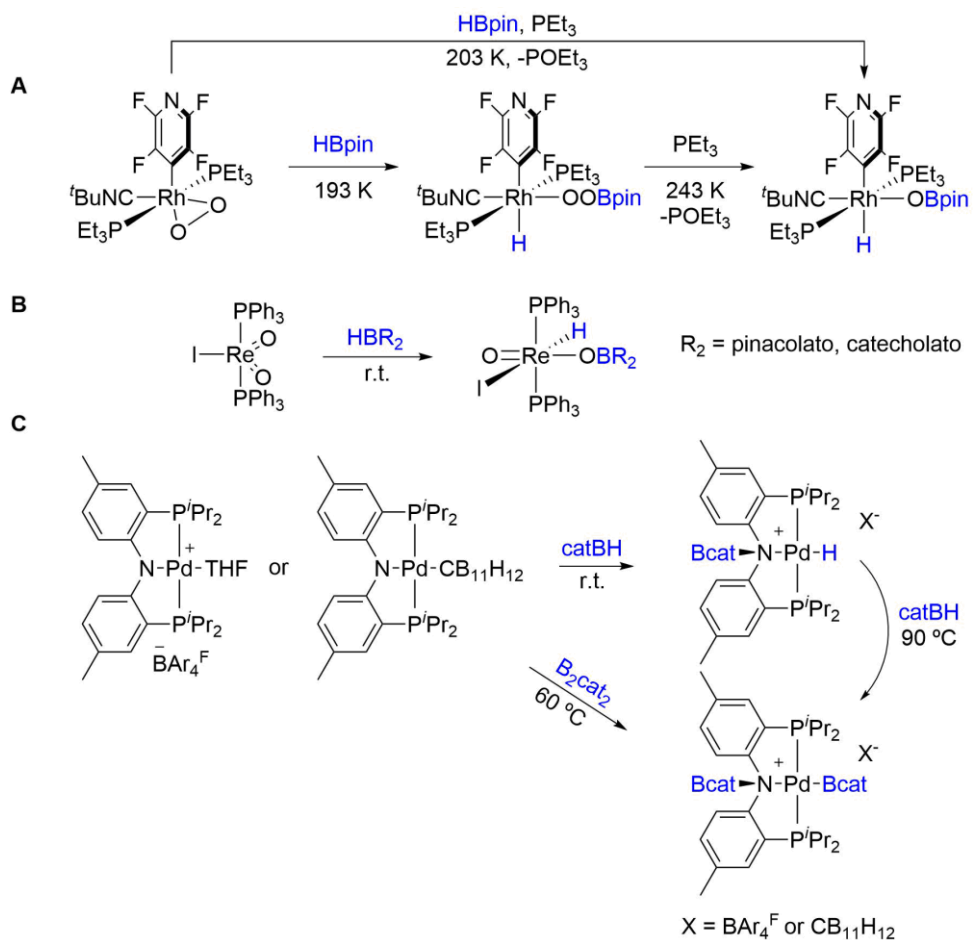
Scheme 2. Examples of B–H or B–B activation by following a 1,2 - addition mechanism (adapted from references 19, 20 and 21).

Some other examples of metal–ligand cooperativity and 1,2 - addition of small molecules like dihydrogen or hydrosilanes can be found in the literature,[22] albeit no B–B activation mediated by a M–B bond has been described to date.

---

[22] a) J. R. Khusnutdinova, D. Milstein, *Angew. Chem. Int. Ed.,* **2015**, *54*, 12236-12273; b) G. R. Owen, *Chem. Commun.,* **2016**, *52*, 10712-10726.

Nickel boryl complexes

The first examples of Nickel boryl complexes were synthesized in the 1960s and 1970s, when Nöth and co-workers obtained the first Ni derivatives of this kind by transmetalation reactions with cobalt complexes[23] and by mixing Ni(0) precursors with alkyl- and haloboranes.[10] However, these compounds lacked exhaustive characterization, and analytical data that could provide conclusive structural confirmation was scarce.

Approximately ten years ago, the group of Prof. Mindiola synthesized the first Ni boryl complex whose structure was completely confirmed by several methods, including X-Ray crystallography. This complex is stabilized by the same PNP scaffold as the Pd species developed by Ozerov *et al.* (Scheme 2C).[21] By mixing catecholborane with a (PNP)Ni−H complex they could obtain **VII**, releasing hydrogen in the process. DFT studies revealed that no backbonding from the metal to the boron atom was occurring, what made the authors think that the boryl fragment could be transferred to other chemicals. In this fashion, they could employ **VII** as a recyclable boryl reagent for the borylation of bromobenzene (Scheme 3).[24]

---

[23] a) G. Schmid, H. Nöth, *Chem. Ber.,* **1967**, *100*, 2899-2907; b) G. Schmid, P. Powell, H. Nöth, *Chem. Ber.,* **1968**, *101*, 1205-1214.

[24] D. Adhikari, J. C. Huffman, D. J. Mindiola, *Chem. Commun.,* **2007**, 4489-4491.
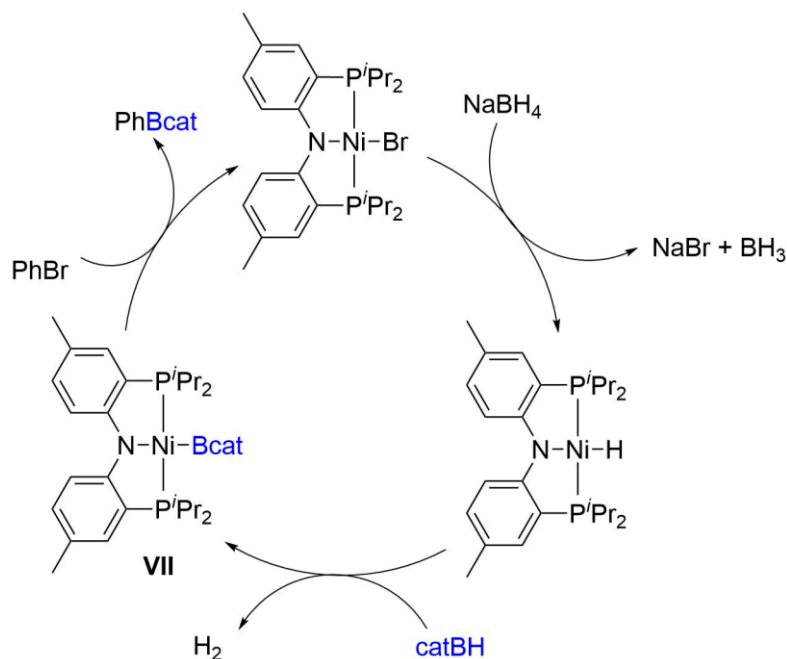
Scheme 3. Borylation of bromobenzene by means of the recyclable Ni(II)Bcat complex **VII** (adapted from reference 24).

The same complex was prepared by the same group by using 2 different methods:

1) Starting from the *tert*-butoxide derivative and B_2cat_2, taking advantage of the B−O bond energy as a driving force for the reaction. In this case, they were able to detect by NMR spectroscopy the intermediate formed during the σ-metathesis reaction and they analysed it by DFT methods. One of the isomers of the intermediate shows a weak Ni−B interaction, as seen in Scheme 4A.[18]

2) Binuclear oxidative addition of B_2cat_2 to a (PNP)Ni(I) dimer (Scheme 4B). Meyer and Mindiola were also able to use this radical dimer as a 2 electron

[142]

reducing agent to transfer the (PNP)Ni fragment when reacting with substrates like H_2, H_2O, MeOH, $PhPH_2$ or catBH.[25]
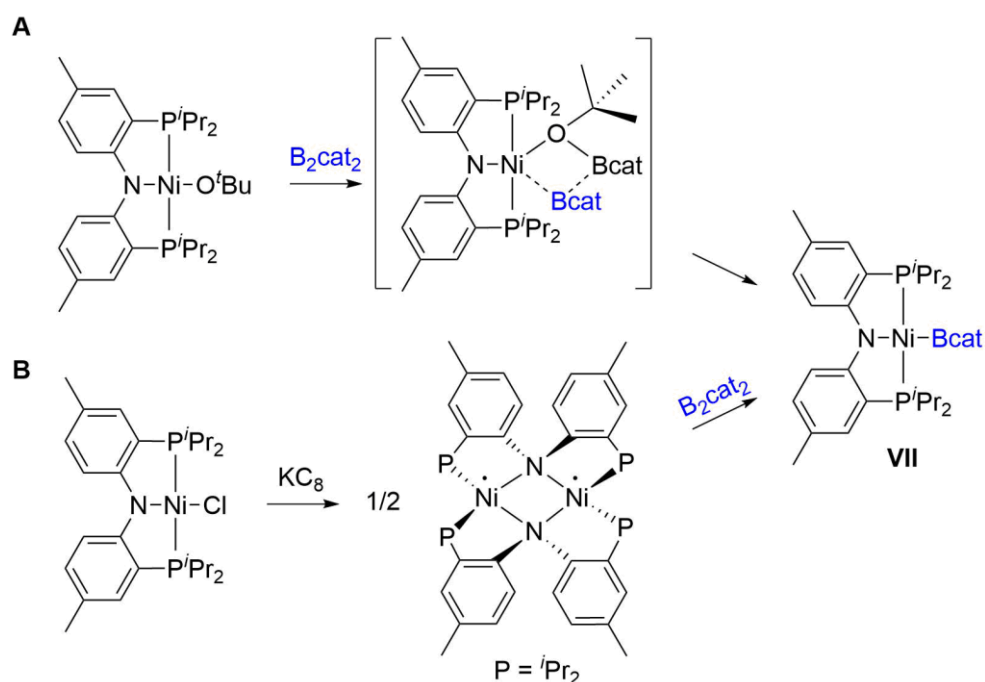
Scheme 4. Alternative pathways to synthesize complex **VII** (adapted from references 18 and 25).

To date, this is the only example of a Nickel boryl complex completely characterized. This is surprising, given the relevance and the advantages that Ni possesses in organometallic catalysis.[26]

1.1.2 Dehydrogenative borylation of styrenes

The versatility of organoboron species in the chemistry community is well known due to the fact that these compounds can operate as precursors to a myriad of organic molecules. A wide range of chemical bonds can be made by

[25] D. Adhikari, S. Mossin, F. Basuli, B. R. Dible, M. Chipara, H. Fan, J. C. Huffman, K. Meyer, D. J. Mindiola, *Inorg. Chem.,* **2008**, *47*, 10479-10490.

[26] a) S. Z. Tasker, E. A. Standley, T. F. Jamison, *Nature*, **2014**, *509*, 299-309; b) V. P. Ananikov, *ACS Catal.,* **2015**, *5*, 1964-1971.

means of cross-coupling reactions, so C–C, C–O, C–N or C–halogen functionalities can be easily achieved under mild conditions. In addition, organoboron derivatives tolerate a great number of functional groups and they are generally stable, which makes them easy to purify by conventional methods like chromatography techniques.[27]

Among them, vinyl boronate esters (VBEs) are especially attractive given their presence in many synthetic processes as building blocks, and they can lead to valuable molecules in many fields of science. Their wide use has then given rise to numerous synthetic approaches by which they can be synthesized (Scheme 5).[28]
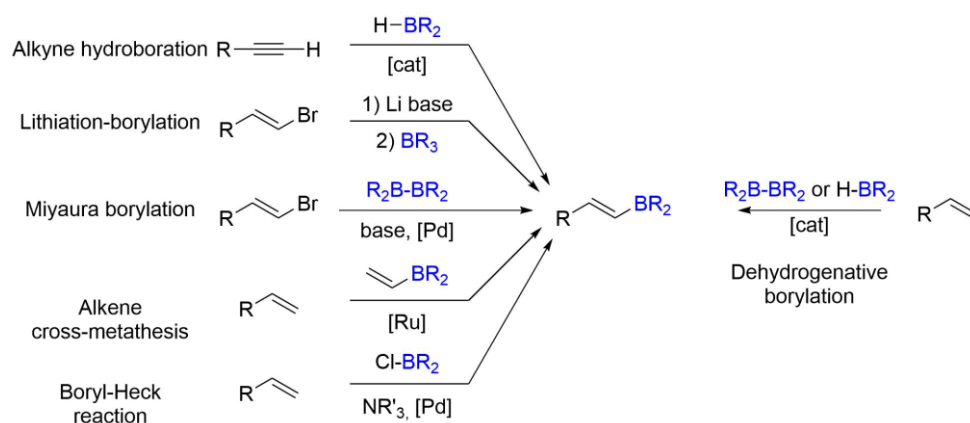
Scheme 5. Synthetic strategies to the formation of VBEs.

Nevertheless, the majority of these methods requires either careful control of the reaction conditions, the previous activation of the vinyl group and/or the degree of substitution is limited, precluding the formation of bis- or triborylated alkenes.[29] In light of this situation, dehydrogenative borylation is a

---

[27] N. Miyaura, A. Suzuki, *Chem. Rev.,* **1995**, *95*, 2457-2483.

[28] A. J. J. Lennox, G. C. Lloyd-Jones, *Chem. Soc. Rev.,* **2014**, *43*, 412-443.

[29] W. B. Reid, J. J. Spillane, S. B. Krause, D. A. Watson, *J. Am. Chem. Soc.,* **2016**, *138*, 5539-5542.

practical alternative which has not been studied and developed in detail until the recent years; in fact, it was formerly considered as a side-reaction during alkene hydroboration.[30] Dehydrogenative borylation of styrenes is of particular interest given that the resulting compounds can be further functionalized to yield polysubstituted olefins or stilbenes, which are valuable compounds in biomedicine or materials science.[31]

(E) - Monoborylation

Metals from the 2nd and 3rd rows of the periodic table are the most employed ones in this type of reaction. In turn, many dehydrogenative borylation reactions are catalyzed by rhodium complexes. In 1993, Marder, Baker *et al.* realised that Wilkinson's catalyst performed the dehydrogenative borylation of 2-phenylpropene using HBcat under typical hydroboration conditions. An extensive scan of reaction conditions led to the conclusion that the VBE ratio was "extremely sensitive to the nature and number of phosphine ligands coordinating to the metal center." By fine tuning of the phosphine ligands, they could obtain the VBE product in yields up to 76%.[32] In subsequent works, the authors slightly modified the catalyst ([RhCl(CO)(PPh$_3$)$_2$]), the borylation agent [tetra(alkoxy)diborons] and the solvent (mixtures of toluene:acetonitrile) to selectively obtain mono or diborylated styrene derivatives depending on the conditions employed (Scheme 6A). The presence of acetonitrile is crucial for the selectivity of the reaction, but another solvent is needed in order to increase the rate, since neat acetonitrile gives rise to very slow reactions.[33]

---

[30] C. Wang, C. Wu, S. Ge., *ACS Catal.,* **2016**, *6*, 7585-7589.

[31] a) T. Shen, X-N. Wang, H-X. Lou, *Nat. Prod. Rep.,* **2009**, *26*, 916-935; b) G. Likhtenshtein, *Stilbenes: Applications in Chemistry, Life Sciences and Materials Science*, Wiley-VCH, **2009**.

[32] S. A. Westcott, T. B. Marder, R. T. Baker, *Organometallics*, **1993**, *12*, 975-979.

[33] a) R. B. Coapes, F. E. S. Souza, R. Ll. Thomas, J. J. Hall, T. B. Marder, *Chem. Commun.,* **2003**, 614-615; b) I. A. I. Mkhalid, R. B. Coapes, S. N. Edes, D. N. Coventry, F. E. S. Souza, R. Ll. Thomas, J. J. Hall, S-W. Bi, Z. Lin, T. B. Marder, *Dalton Trans.,* **2008**, 1055-1064.

Scheme 6. Examples of transition metal catalyzed single dehydrogenative (*E*) borylation.

While Marder and coworkers were doing the first exploratory studies, Lloyd-Jones *et al.* employed phosphine-free rhodium precatalysts in the dehydrogenative borylation of 4-methoxystyrene by using oxazaborolidine derivatives as borylating agents (Scheme 6B). Hydrogenation side-reactions allowed the authors to obtain the monoborylated product in only 50% yield.[34] Extensive experimental mechanistic studies point out at a monomeric rhodium hydride as the active catalytic species (although boryl complexes are also proposed as intermediates).[35] More recent examples also make use of rhodium

---

[34] J. M. Brown, G. C. Lloyd-Jones, *J. Chem. Soc.* **1992**, 710-712.
[35] J. M. Brown, G. C. Lloyd-Jones, *J. Am. Chem. Soc.,* **1994**, *116*, 866-878.

cyclooctadiene precursors for DHB reactions. The groups of Masuda,[36] Suginome[37] and Murakami[38] tested different rhodium precursors, hydroboranes and reaction conditions to obtain monoborylated styrenes in high yields (> 90%). It is worth mentioning the strategies applied by some of the authors where they exploited the robustness and stability of these species to perform one-pot reactions where dehydrogenative borylation and Pd-catalyzed cross-coupling reactions took place in the same procedure (Scheme 7).
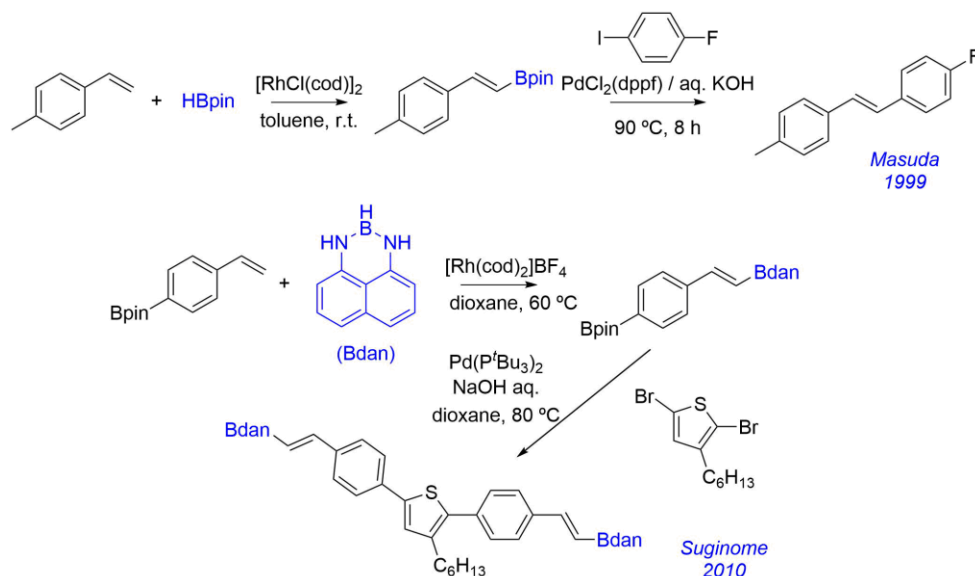
Scheme 7. Examples of one-pot tandem DHB - cross-coupling reactions carried out by means of Rh and Pd complexes, respectively. The different reactivities of some boryl groups (Bdan and Bpin, bottom) can be leveraged when developing synthetic strategies.

Recently, 1st row metals have been successfully applied in DHB processes. Mankad *et al.* achieved highly selective monoborylation of styrenes by using

[36] a) M. Murata, S. Watanabe, Y. Masuda, *Tetrahedron Lett.,* **1999**, *40*, 2585-2588; b) M. Murata, K. Kawakita, T. Asana, S. Watanabe, Y. Masuda, *Bull. Chem. Soc. Jpn.,* **2002**, *75*, 825-829.

[37] N. Iwadate, M. Suginome, *Chem. Lett.,* **2010**, *39*, 558-5060.

[38] M. Morimoto, T. Miura, M. Murakami, *Angew. Chem. Int. Ed.,* **2015**, *54*, 12659-12663.

NHC-stabilized copper complexes (Scheme 6C). A sacrificial ketone was needed though, so as to trap the hydroborane released and preclude hydroboration phenomena (Scheme 6C).[39] Iron-based catalysts have also proven effective in achieving this goal, since the low-valent complex $Fe(PMe_3)_4$ afforded the monoborylated styrene derivatives after reacting with pinacolborane and employing norbornene as a hydrogen acceptor (Scheme 6D).[30] Selectivities up to 90% for the styrene boronate were also achieved by using POCOP pincer stabilized iron hydrides after reacting under UV light (350 nm) in neat pinacolborane (Scheme 6E).[40]

Diborylation

Dehydrogenative borylation to yield diborylalkenes is less common than monoborylation, yet there are a few recent examples in the literature. This method opens up the possibility of obtaining 1,1- and *trans*-diborylalkenes impossible to achieve by other synthetic routes such as alkyne diboration (which would afford *cis* derivatives) or the synthesis assisted by lithiated reagents (which would compromise sensitive functional groups in the molecule of interest).

In this field, the group of Iwasawa developed a system based on a Pd(II) complex stabilized by a PSiP pincer ligand that can perform mono or diborylation of styrenes with complete selectivity achieving yields up to 90% for the (*E*)-styrylboronate and *β,β*-diborylstyrene, respectively. Depending on the substrate, *trans*-1,2-diborylalkenes can also be obtained. The authors attribute the behaviour of the system to the PSiP scaffold; the strong trans influence caused by the Si atom seems to be responsible for the good catalytic activity, whereas the structure of the complex precludes the formation of coordinatively

---

[39] T. J. Mazzacano, N. P. Mankad, *ACS Catal.,* **2017**, *7*, 146-149.
[40] S. Jiang, S. Quintero-Duque, T. Roisnel, V. Dorcet, M. Grellier, S. Sabo-Etienne, C. Darcel, J-B. Sortais, *Dalton Trans.,* **2016**, *45*, 11101-11108.

unsaturated hydrido(boryl) or dihydride species that can lead to hydroboration or hydrogenation side-reactions (Scheme 8).[17a] Moreover, they were able to crystallize and study the catalytically active Pd(II) boryl complex.
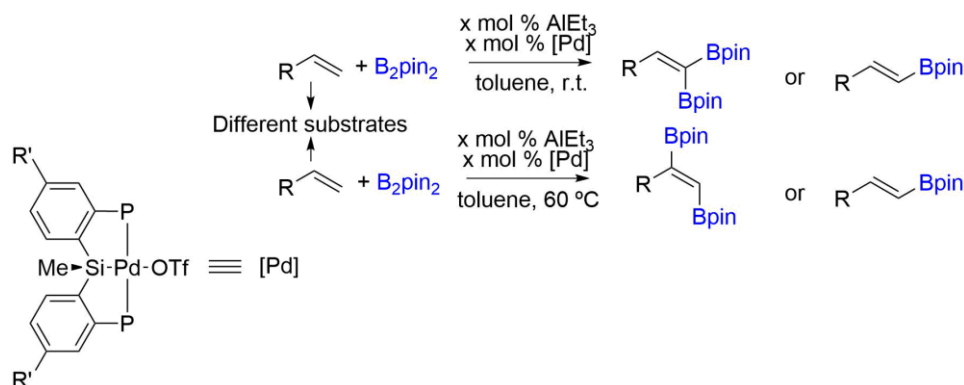
Scheme 8. Dehydrogenative mono and diborylation reactions performed by Iwasawa and coworkers. Triethylaluminum is necessary in order to form the active palladium hydride species from the Pd–OTf complex (adapted from reference 17a).

Additionally, Huang and coworkers came up with the right conditions for efficient double DHB processes by using cobalt complexes in combination with PNN pincer ligands. By combining the corresponding cobalt precursor with sodium triethylborohydride and bis(pinacolato)diboron, the resulting cobalt(II) boryl complex can catalyse the formation of vinylbis(boronate) esters (VBBEs) in a selective manner in the presence of CsF and DMF (Scheme 9, left). The latter serves as a HBpin scavenger, precluding hydroboration phenomena, preserving the selectivity. The former activates the diborane in order to form $[Cs][B_2pin_2F]$, increasing the activity of the whole system.[41] In the absence of these two additives and by using slightly different conditions, the authors achieved a

---

[41] H. Wen, L. Zhang, S. Zhu, G. Liu, Z. Huang, *ACS Catal.,* **2017**, *7*, 6419-6425.

tandem double DHB - hydroboration process by which they can transform styrenes into 1,1,1-tris(boronates) (Scheme 9, right).[42]

[42] L. Zhang, Z. Huang, *J. Am. Chem. Soc.,* **2015**, *137*, 15600-15603.
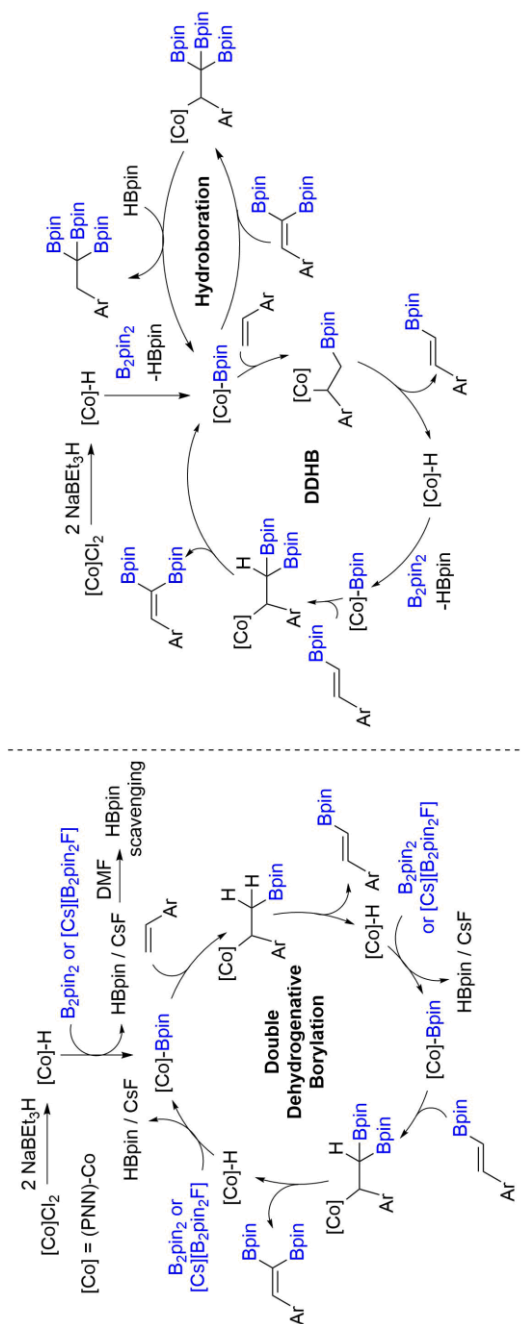
Scheme 9. Double dehydrogenative borylation (left) and tandem DHB - hydroboration systems developed by Huang *et al.* (adapted from references 41 and 42).

[151]

From the antecedents described above, it can be deduced that the development of a complex with an anionic pincer ligand containing a strong *trans* influence central group would provide a platform in which a boryl moiety bound in a *trans* position to it would enhance its nucleophilicity towards unsaturated substrates. Thus, these complexes could be regarded as boryl transfer agents. The employment of a base metal like Ni would also be a practical solution, since it would make the formation of C−B bonds more economically accessible.

This chapter shows the synthesis of Nickel(II) boryl complexes stabilized by the PBP ligand. Theoretical and experimental studies for the rationalization of the mechanism of their formation as well as for analysing their structure are detailed. Last, the chapter concludes with the description of preliminary catalytic studies on the borylation of styrenes.

2. Results and discussion

The aim of this chapter is to take advantage of the PBP ligand in sterically stabilizing the resulting Ni(II) boryl complexes as well as electronically activating them for borylation processes.

2.1 Synthesis and analysis of (PBP)Ni boryl complexes

It was seen in Chapter 1 that the introduction of strong *trans* influence ligands into the (PBP)Ni framework was difficult due to the properties of the boryl moiety. In these cases, a great excess of the reagent or a different mechanistic pathway were necessary to introduce alkyl or hydride groups, respectively,[43] given the unsuccessful attempts of achieving ligand substitution by other methods.

Nonetheless, the method developed by Mindiola and coworkers was attempted, where they synthesize boryl complex **VII** by reacting the PNP-stabilized nickel hydride with catecholborane followed by hydrogen elimination.[24] Thus, hydride **6** was mixed with 1 equivalent of pinacolborane in d^8-toluene at r.t. Right after mixing, the hydride signal in the ^{1}H NMR spectrum (*i.e.* a triplet ($^2J_{\text{H-P}}$ = 34.8 Hz) at -1.8 ppm) disappeared and no new signal was observed but a very broad signal at the same chemical shift. $^{31}P\{^1H\}$ NMR did not reveal any new species, and only the peak corresponding to **6** was observed. This

[43] N. Curado, C. Maya, J. López-Serrano, A. Rodríguez, *Chem Commun.,* **2014**, *50*, 15718-15721.

phenomenon seems to suggest a quick exchange between the hydride and the hydrogen atom of the hydroborane. Cooling down the sample to -30 °C allowed the observation of 2 broad signals at -1.65 and 4.34 ppm, each one of them integrating for 1 hydrogen atom with respect to the pincer ligand (Figure 4). Only the latter showed correlation via HMQC to the sharp singlet in the ^{11}B NMR spectrum at 28.5 ppm, which splits into a doublet in ^{11}B NMR experiments ($^{1}J_{BH}$ = 137.8 Hz) as long as the temperature is below 0 °C (otherwise it is a broad singlet, Figure 5).[44]
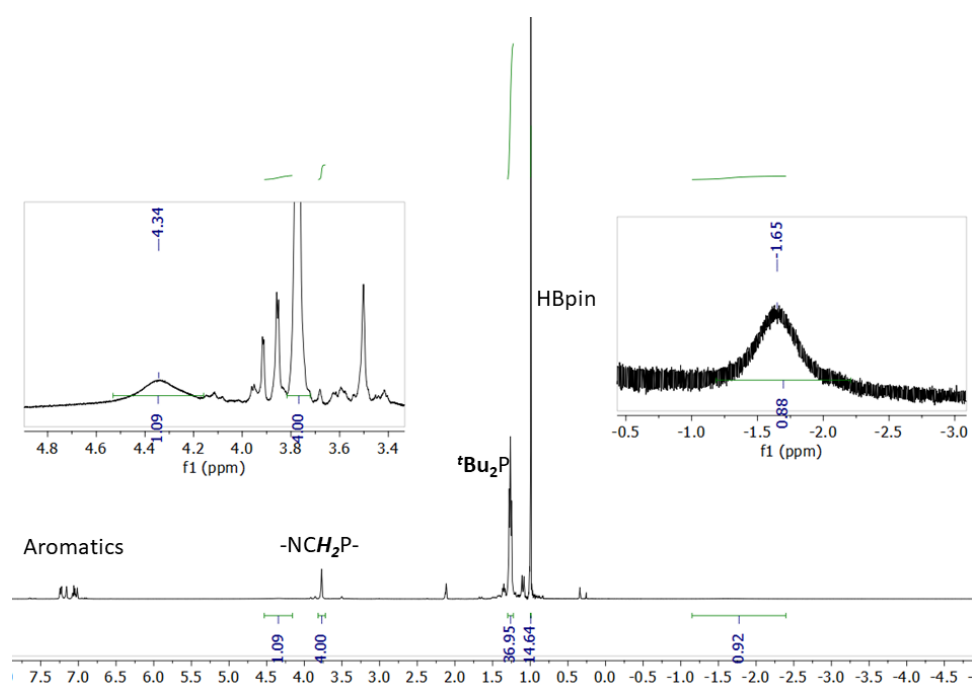
Figure 4. ^{1}H NMR (400 MHz, d^{8}-toluene) spectrum at -30 °C of the reaction between **6** and HBpin.

---

[44] Free HBpin resonates at 28.8 ppm in d^{8}-Toluene, giving a doublet with $^{1}J_{BH}$ = 174.4 Hz.
See: A. Bismuto, S. P. Thomas, M. J. Cowley, *Angew. Chem. Int. Ed.,* **2016**, *55*, 15356-15359.
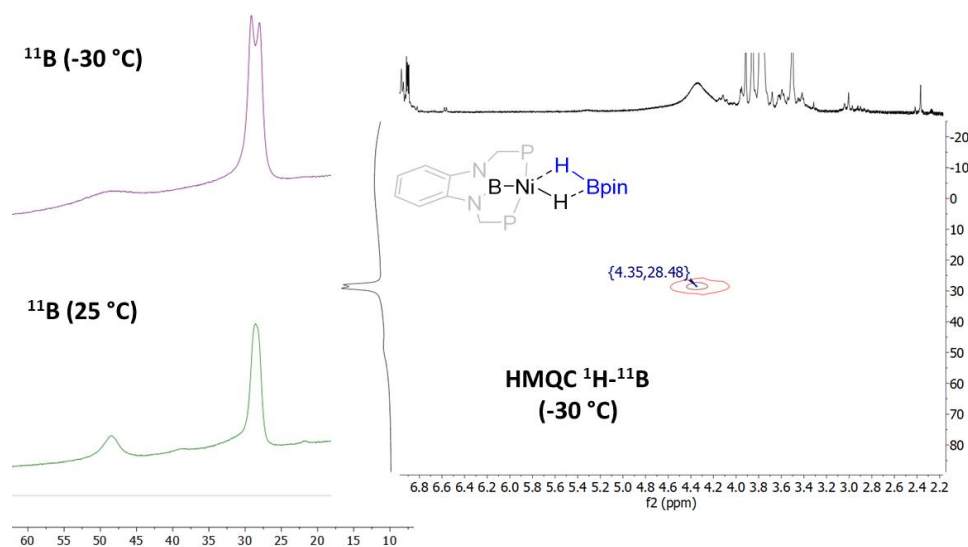
Figure 5. ^{11}B NMR (400 MHz, d^8-toluene) experiments of the reaction between **6** and HBpin.

These data seem to indicate that an interaction between the electron rich hydride ligand and the partially empty p-orbital of the boron atom in HBpin is taking place, similar to that described in the work by Guan and coworkers, where they discovered that dihydroborate species of (POCOP)Ni complexes were responsible for the decrease in the catalytic activity during CO_2 hydroboration.[45] Dihydrogen extrusion was attempted by heating the sample up to 100 °C for 48 h, albeit no change was observed, indicative of the stability of this type of adducts and the need for an alternative method for making (PBP)Ni boryl derivatives (Scheme 10).

---

[45] S. Chakraborty, J. Zhang, Y. J. Patel, J. A. Krause, H. Guan, *Inorg. Chem.,* **2013**, *52*, 37-47.
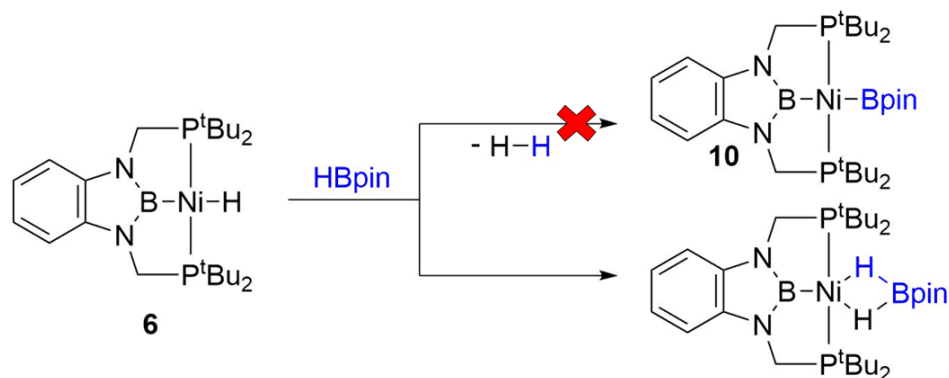
Scheme 10. Outcome of the reaction between hydride **6** and HBpin.

For this reason, it was envisaged that the electronic polarization caused by the pincer ligand could be leveraged in attacking diboranes. Considering bond energies (BDE_{B-H} = 82.6 kcal/mol and BDE_{B-C} = 107.2 kcal/mol),[46] methyl complex **4** was chosen as a candidate for such a reaction instead of hydride **6**.[47] The nucleophilicity of the methyl group in complex **4** was compared to its PCP counterpart (^PCP^**4**),[48] both experimentally and theoretically. Analysis of both crystal structures (Table 1) showed the expected trend: shorter Z−Ni and longer Ni−C bonds for **4**, resulting from the electronic properties of the PBP ligand.

---

[46] Y-R. Luo, *Comprehensive Handbook of Chemical Bond Energies,* CRC Press: Boca Raton, FL, 2007.

[47] The reaction between **6** and B_2pin_2 was attempted anyway, and no apparent change was observed after heating up the sample at 80 °C for 12 hours in benzene. A closer look to the spectrum reveals the absence of the hydride signal by ^1H NMR, in the same way as described above. This, along with catalytic studies where the released HBpin is captured (see section 2.4) seems to point out that the following reactions might be taking place due to the presence of adventitious water in the solvent:

- Ni−H (**6**) + B_2pin_2 → Ni−Bpin (**10**) + HBpin
- Ni−Bpin + H_2O → Ni−H + HOBpin
- Ni−H + HBpin → NiH_2Bpin (stable dihydridoborate described previously)

For this reason, the released HBpin due to hydrolysis is able to inhibit the formation of **10** from **6**.

[48] T. J. Schmeier, N. Hazari, C. D. Incarvito, J. A. Raskatov, *Chem. Commun.,* **2011**, *47*, 1824-1826.

Compound	Z–Ni / Å	Ni–C / Å	(Ni–C)-(Z–Ni)[a] / Å	Reference
4 (Z=B)	1.92	2.06	0.14	43
PCP4 (Z=C)	1.94	2.03	0.09	48

Table 1. Comparison of bond distances between Ni(II) methyl complexes stabilized by pincer ligands (values obtained from crystal structures). [a] It can be seen that even though boron is smaller than carbon, boryl and methyl ligands are further separated in **4** due to electronic effects.

Such a polarization is also distinguishable in the calculated structures by means of DFT methods. Thereby, molecular orbital analysis showed participation of the boryl moiety in the HOMO orbital, where electron delocalization can be observed along the methyl−nickel−borobenzimidazole direction (Figure 6). In contrast, the HOMO in **PCP4** is mainly composed of the dz^2 orbital with a small contribution of the p_y orbital of the carbon from the methyl group.

4   **PCP4**
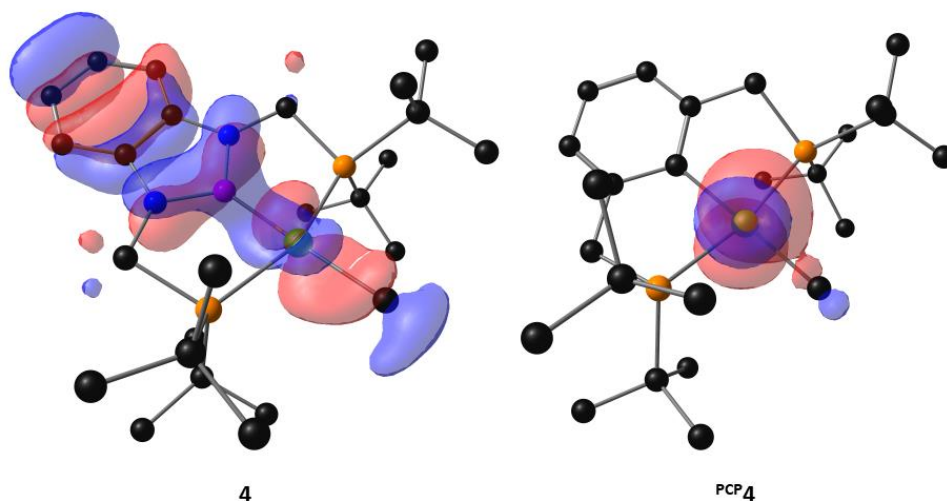
Figure 6. Comparison of the computed HOMO orbitals in **4** and **PCP4**. Hydrogen atoms have been omitted for clarity. Isodensity contour = 0.03 a.u.

This delocalization along the B−Ni−C axis has an impact on the electronic properties of the Ni−CH$_3$ bond. Localized orbital analysis (Figure 7) clearly

[157]

evidenced that the electron pair of the Ni−Me bond is much closer to the CH_3 fragment than to the Ni atom, as a result of the *trans* influence exerted by both pincer ligands. As expected, it is closer in **4** than in **PCP4** (Table 2), indicating a stronger nucleophilic character of the methyl group in the case of the PBP complex.
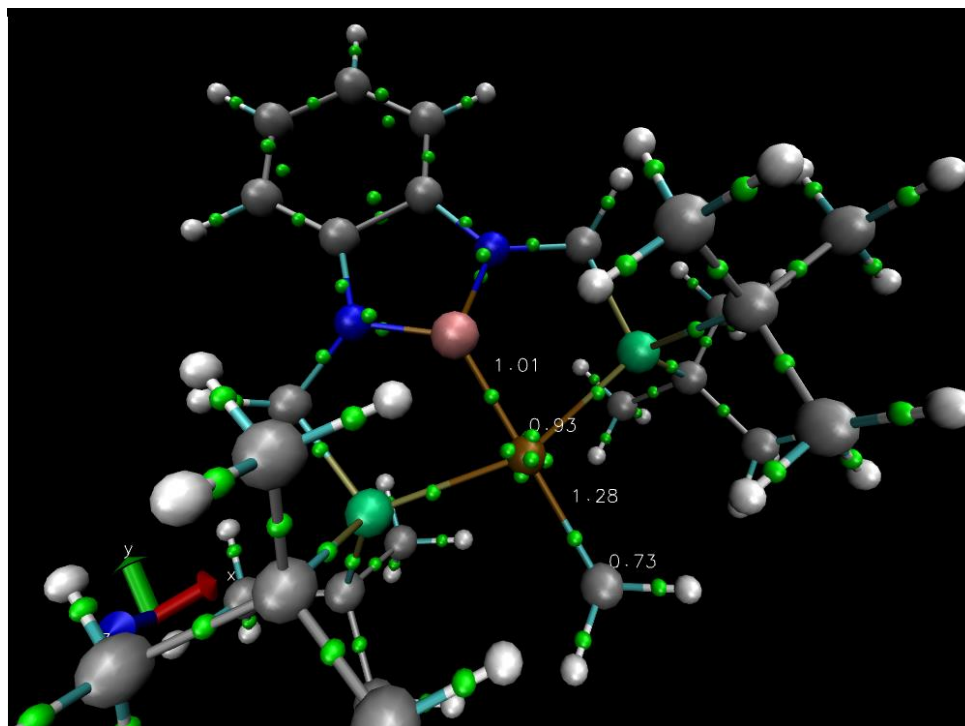
Figure 7. Localized orbital analysis of methyl complex **4**. The molecular structure is overlaid with the centroids of the localized orbitals (small green spheres).

Compound	Ni−X[a] / Å	X−C / Å	Ni−C / Å
4 (Z=B)	1.28	0.73	2.01
PCP4 (Z=C)	1.21	0.78	1.99

Table 2. Comparison of the distances obtained by the localized orbital analysis for complexes **4** and **PCP4**. [a] X is the centroid of the localized orbital of the bond in question.

With these results in hand, the reactivity of **4** against diboron(4) reagents was tested. When **4** was mixed with 5 equivalents of B_2pin_2 in toluene no change

[158]

was observed at room temperature, yet warming the sample up to 70 °C for 7 hours showed full conversion of the methyl complex to a singlet at 116.3 ppm in $^{31}P\{^1H\}$ NMR along with some hydride **6** [(93:7 ratio), Figure 8]. $^{11}B\{^1H\}$ NMR shows a broad peak at 49.5 ppm with a broad shoulder at 53 ppm.[49] These data point to the formation of a symmetrical species with 2 different boryl groups. The fact that some hydride is formed during the synthesis might be attributable to the high sensitivity of the presumed boryl complex towards hydrolysis.[50] The small proportion of **6** persists over time, probably due to the interaction with the released HBpin (see reference 47).

---

[49] There are some other peaks at higher field in the $^{11}B\{^1H\}$ NMR spectrum coming from the excess of diborane, MeBpin and hydrolysis-derived species.

[50] Hydrolysis of metal−boryl bonds to give metal−hydride units has been previously described in the literature: a) J. F. Hartwig, X. He, *Organometallics*, **1996**, *15*, 5350-5358; b) W. Clegg, F. J. Lawlor, T. B. Marder, P. Nguyen, N. C. Norman, A. G. Orpen, M. J. Quayle, C. R. Rice, E. G. Robins, A. J. Scott, F. E. S. Souza,G. Stringer, G. R. Whittell, *J. Chem. Soc. Dalton Trans.,* **1998**, 301-309.
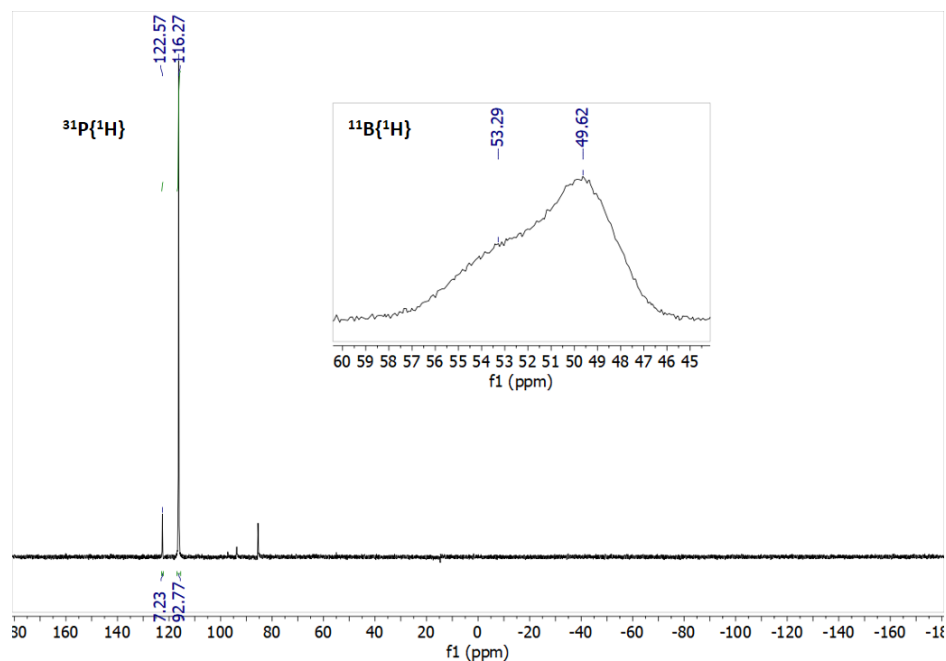
Figure 8. $^{31}P\{^{1}H\}$ NMR spectrum (400 MHz, d^8-toluene) of the reaction between complex **4** and B$_2$pin$_2$ after 7 h at 70 °C. Inset: selected zone of the $^{11}B\{^{1}H\}$ NMR spectrum, indicating the presence of several boryl fragments.

The high sensitivity of this new complex towards hydrolysis precluded its purification by work-up procedures involving solvents. Attempts of purification by sublimating the excess of diborane also proved unfruitful, causing decomposition of the material upon heating. Therefore, bis(catecholato)diboron was used instead. The higher Lewis acidity and smaller volume of the molecule account for the reaction times needed for the reaction to reach completion: whereas suspected boryl complex **10** required heating for several hours, the formation of boryl **11** in THF is instantaneous at room temperature by using 1 equivalent of B$_2$cat$_2$, releasing MeBcat as side-product (Figure 9). This complex shows a singlet at 114.9 ppm by $^{31}P\{^{1}H\}$ NMR and the $^{11}B\{^{1}H\}$ NMR spectrum contains 2 broad peaks in the boryl region at 47.2 and 56.2 ppm (Figure 10). Purification attempts have been performed on this species by crystallization and

precipitation techniques, albeit no pure boryl complex **11** has been obtained yet. Different purification procedures of this compound are currently underway.
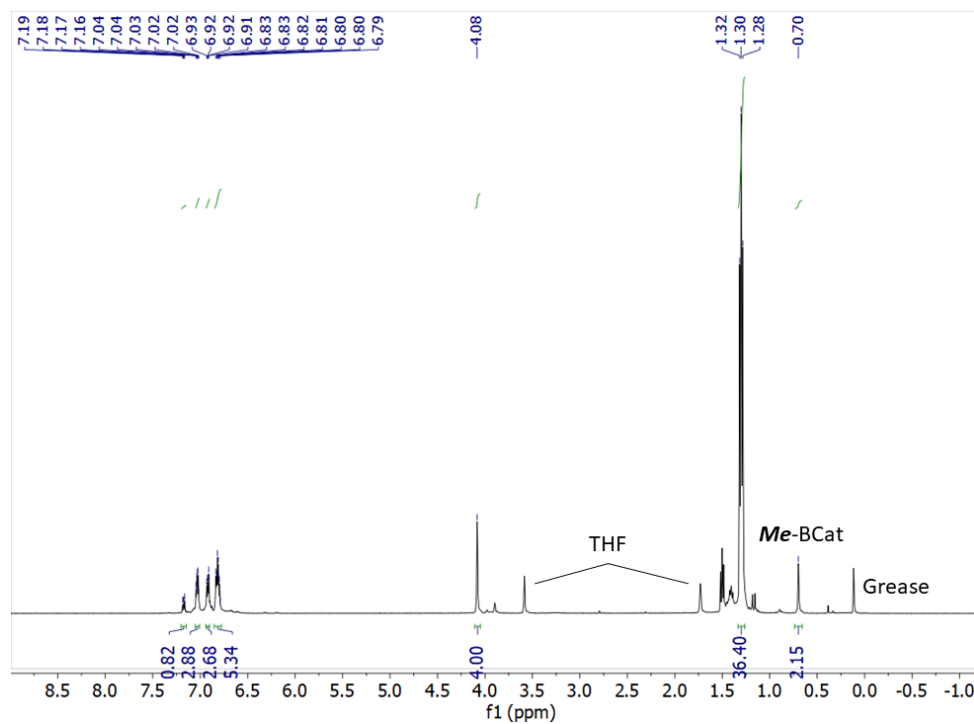
Figure 9. ^{1}H NMR spectrum (400 MHz, d^8-THF) of the reaction mixture between complex **4** and B$_2$cat$_2$ at room temperature, showing the clean formation of **11** and MeBcat.
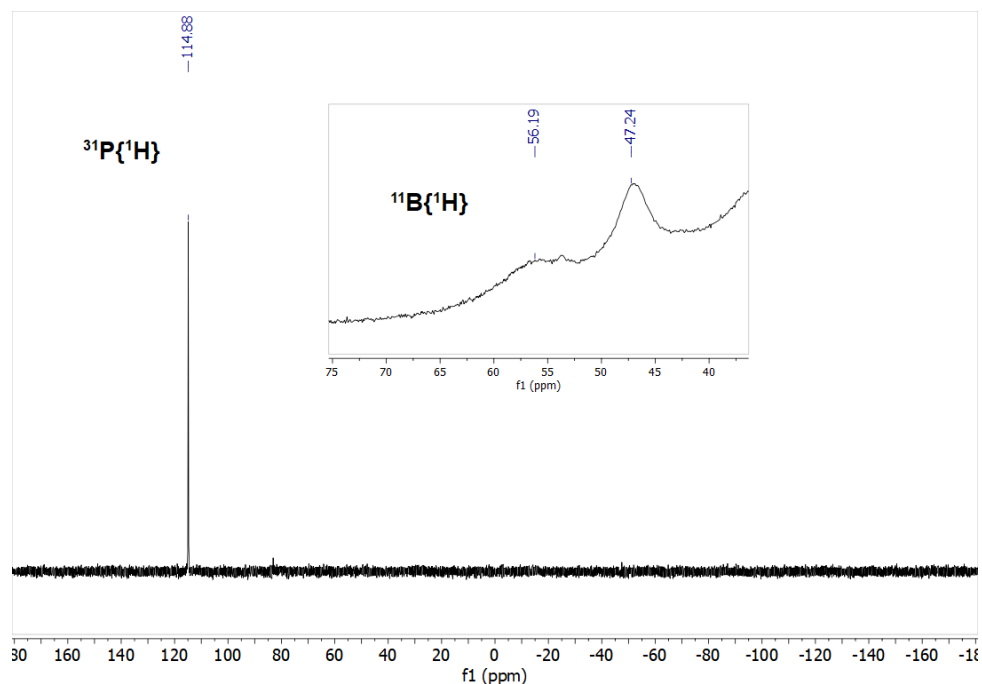
Figure 10. $^{31}P\{^1H\}$ and $^{11}B\{^1H\}$ (inset) NMR spectra (400 MHz, d^8-THF) of the reaction mixture between complex **4** and B_2cat_2 at room temperature.

Fortunately, one of the crystallization attempts in a cold mixture of THF and hexamethyldisiloxane afforded some yellow crystals which could be measured by X-Ray diffraction techniques, confirming the structure of boryl complex **11** (Figure 11).[51]

---

[51] The R-Factor of the measured crystal is 5.63%. Effort is being put at the moment in lowering this value. For the time being, the discussion of the data will be made on these results. Since some parameters might change (although very slightly) upon R lowering, this information must be taken cautiously.

Ni1-B3 = 1.975 Å
Ni1-B2 = 2.135 Å
B3-Ni-B2 =178.04 °
N2-B3-B2-O1 = 7.4 °
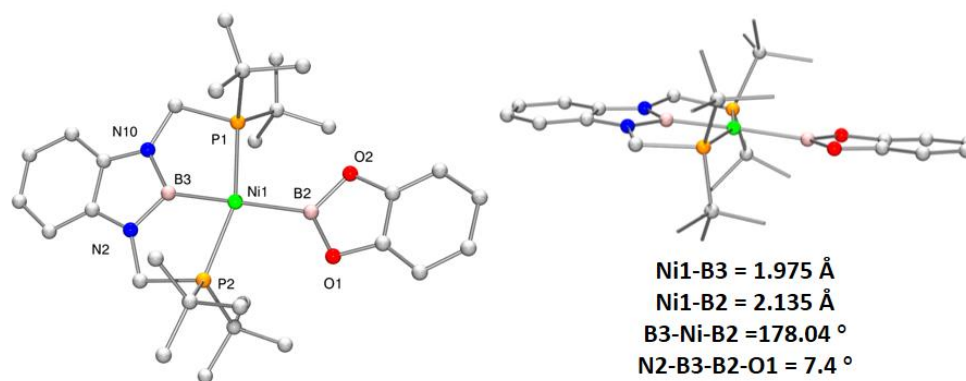
Figure 11. Crystal structure of boryl complex **11** from several points of view. Hydrogen atoms have been omitted for clarity.

The crystal structure of complex **11** reveals some interesting geometrical features, among which three of them are especially relevant: the presence of two strong *trans* influence boryl ligands *trans* to each other, the Ni1−B2 bond length and the orientation of the BCat fragment. The possibility of obtaining such a complex may be explained by the rigid framework imposed by the PBP ligand along with steric protection of the phosphine groups.

Nickel−boron bond distances

Analysis of both Ni−B distances reflects the stronger *trans* influence of diaminoboryl ligands against oxygen-based ones,[52,53,54] given that Ni1−B2 (2.135 Å) is much longer than Ni−B3(1.975 Å). In comparison with other systems, the Ni−BCat distance is remarkably longer than that reported by Mindiola for the (PNP)NiBCat complex **VII** described above (1.909 Å),[24] indicative of the higher σ-donor ability of the PBP ligand. For the purpose of comparison, a molecular orbitals study was performed on the crystal structure of boryl complex **11** (Figure 12). The outcome of this analysis shows some similarities to Mindiola's

[52] G. R. Clark, G. J. Irvine, W. R. Roper, L. J. Wright, *J. Organomet. Chem.,* **2003**, *680*, 81-88.
[53] Y. Segawa, M. Yamashita, K. Nozaki, *J. Am. Chem. Soc.,* **2009**, *131*, 9201-9203.
[54] J. Zhu, Z. Lin, T. B. Marder, *Inorg. Chem.,* **2005**, *44*, 9384-9390.

[163]

system, namely the π* character with contribution from the PBP ligand and the d_{xz} orbital to the HOMO (with no participation of the BCat moiety), and the contribution of the d_{z^2} orbital to HOMO-1. HOMO-2 displays σ-contributions from both Ni−B bonds. However, the LUMO clearly reveals the participation of the p_z orbitals from both boron atoms, pointing to an electrophilic character of this complex (in Mindiola's complex no participation of the BCat ligand is observed in such molecular orbital). A closer examination to more internal molecular orbitals disclosed some π overlap between the d_{xz} orbital from Ni and the p_z orbitals from the boron atoms in HOMO-7, located 1.03 eV (23.7 kcal/mol) below the HOMO (Figure 13). In this molecular orbital, some π overlap between the p_z orbitals of the boron and oxygen atoms can also be observed in the BCat fragment.
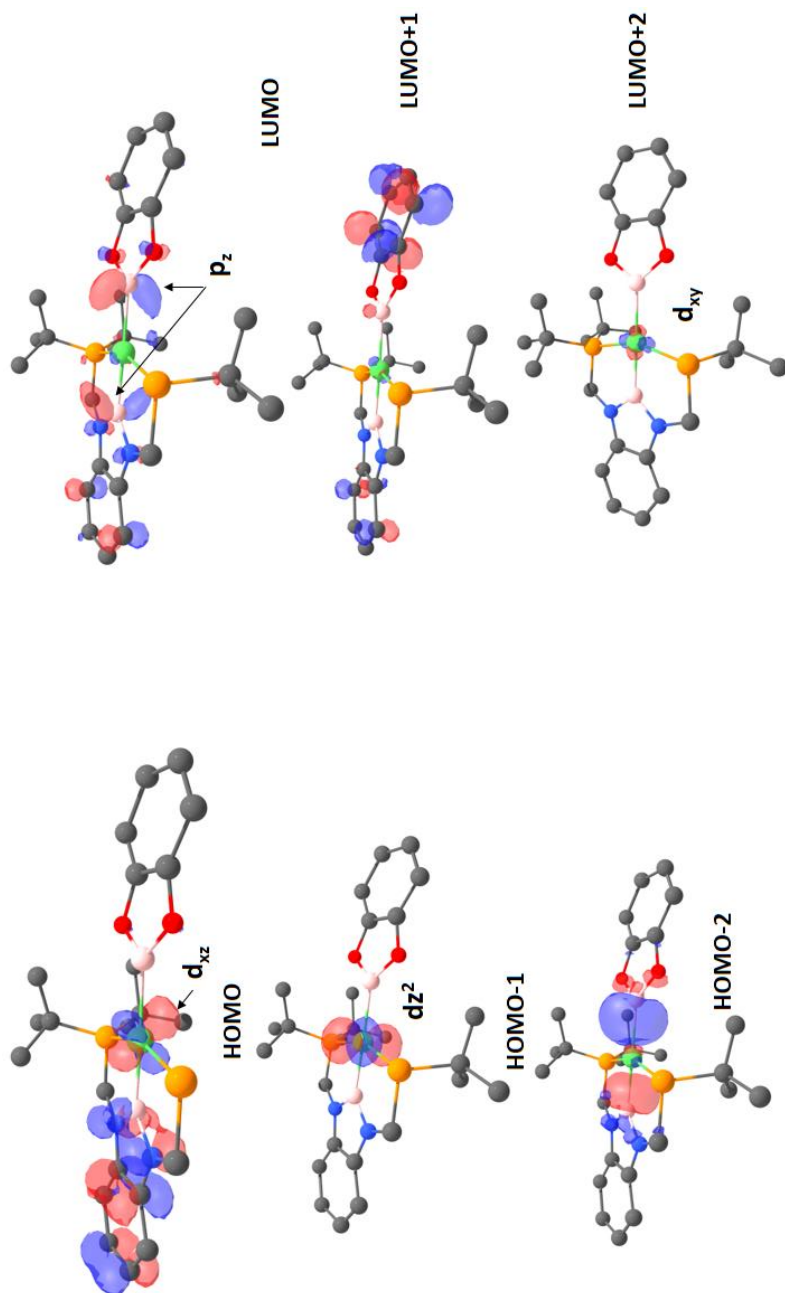
Figure 12. Overview of some molecular orbitals of boryl complex **11**. Isodensity contour = 0.05 a.u. Hydrogen atoms and some fragments of the phosphine ligands have been omitted for clarity.

Isodensity contour: 0.05   Isodensity contour: 0.03
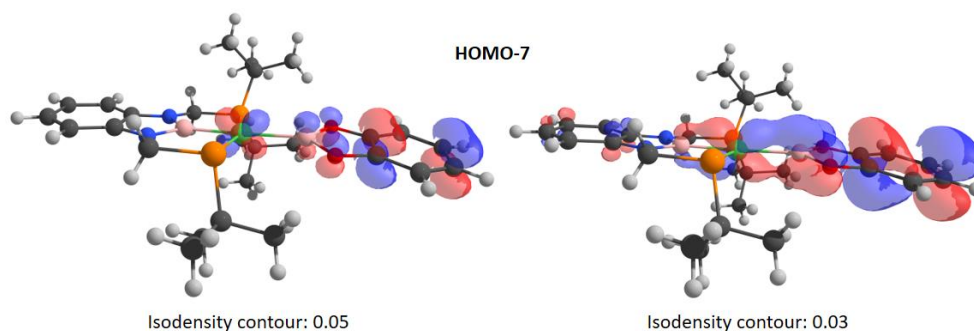
Figure 13. HOMO-7 of boryl complex **11**. The isodensity contour is displayed at different values to increase the intensity and appreciate the π overlap. Hydrogen atoms and some fragments of the phosphine ligands have been omitted for clarity.

Given the oddly long distance of the Ni–BCat bond and the results from the molecular orbitals analysis, the Wiberg Bond Index (WBI) was calculated so as to evaluate some potential degree of back-bonding from nickel to boron as well as a localized orbital analysis. The outcome of these studies is summarized in Table 3 and Figure 14.

	Ni–B(PBP)	Ni–B(cat)	B–N	B–O
Distance (Å)	1.975	2.135	1.437	1.470
WBI	0.768	0.579	1.314	1.456
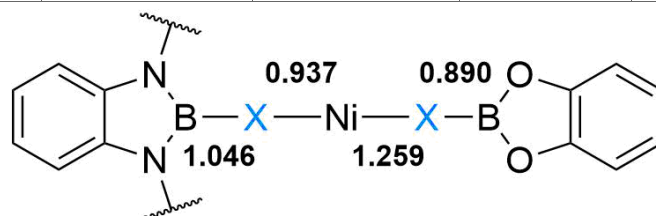
Table 3. Localized orbital analysis (LMO) and Wiberg Bond Index values for some bonds of boryl complex **11**. X is the centroid of the localized orbital of the bond in question (distances in angstroms).
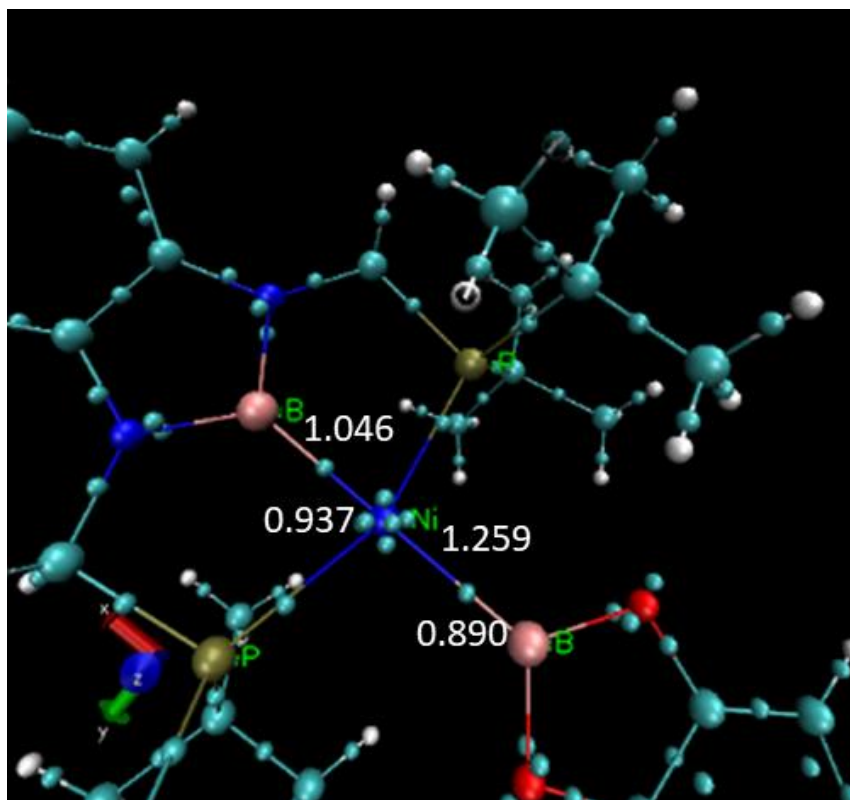
Figure 14. Localized orbital analysis of boryl complex **11**. The molecular structure is overlaid with the centroids of the localized orbitals (small cyan spheres). Numbers in white denote distances (in angstroms).

Wiberg Bond Index calculations seem to indicate that no multiple bond character exists between nickel and any of the boron atoms. In fact, the low WBI found for Ni−BCat is consistent with its remarkable long distance. As expected, the diaminoboryl fragment is more tightly bound to the metal due to chelation by the pincer complex and the higher σ-donor ability previously mentioned. Surprisingly, even though B−O and B−N are almost identical in terms of bond distances, the WBI value is somewhat higher for both B−O bonds. The extra π-

[167]

donation from the oxygen atoms might compensate the lack of electronic stabilization from the metal complex, as opposed to the diaminoboryl moiety.[55]

Localized orbital analysis on the crystal structure is also consistent with the long distances found in the crystal structure, the WBI data and the difference in *trans* influence of both boryl ligands. Table 3 and Figure 14 clearly show how the diaminoboryl group "pushes" the electron pair of the Ni–B bond towards the metal atom, being the electron pair polarized towards Ni. On the contrary, the electron pair in Ni–BCat is very close to the boron atom. However, the observed bond length is greater than the sum of covalent radii.[56] Thus, the Ni–BCat bond seems to be an intermediate bonding scenario of metal–boron bonds, located between Mindiola's system and Nozaki's boryl anion (Figure 15).[57]
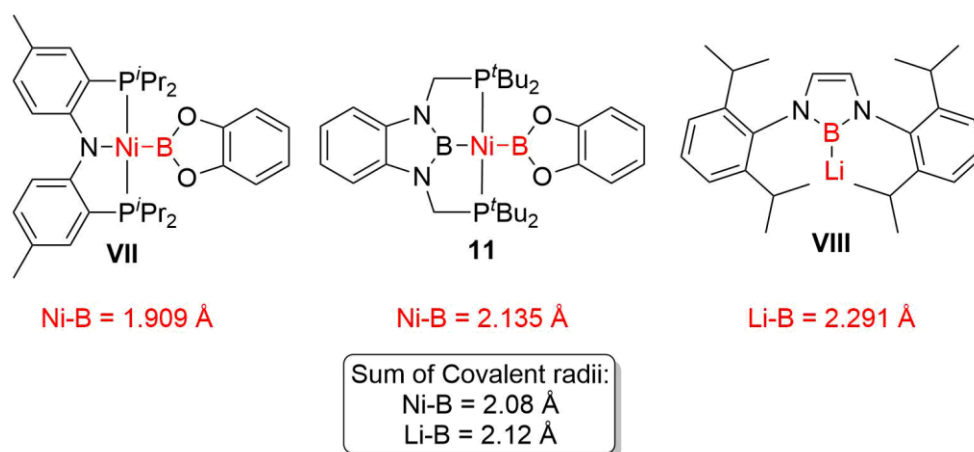
Figure 15. Comparison between different metal–boryl groups. Covalent radii obtained from reference 56.

[55] As a comparison, Mindiola reported bond orders of 0.84 and 0.80 for Ni–B and B–O, respectively (see reference 24).

[56] B. Cordero, V. Gómez, A. E. Platero-Prats, M. Revés, J. Echeverría, E. Cremades, F. Barragán, S. Álvarez, *Dalton Trans.,* **2008**, 2832-2838. Some covalent radii from this reference: B (0.84 Å), Li (1.28 Å), Ni (1.24 Å).

[57] Y. Segawa, M. Yamashita, K. Nozaki, *Science*, **2006**, *314*, 113-115.

Coplanar orientation of the BCat fragment

In order to compare the crystal and theoretical structure, the geometry of complex **11** was calculated by DFT methods. Surprisingly, optimization methods employing different functionals or basis sets always gave a perpendicular orientation of the BCat fragment with respect to the PBP ligand plane (Figure 16). It can be observed that the structural parameters have dramatically changed, although the metal−boron distances follow the same trend, since the Ni−BCat is still longer than the Ni−B bond established with the PBP ligand, in accordance with the difference in *trans* influence previously mentioned.[52-54]

Crystal structure
Ni1-B3 (PBP) = 1.975 Å
Ni1-B2 (Bcat) = 2.135 Å
B3-Ni-B2 =178.04 °
N2-B3-B2-O1 = 7.4 °

DFT (optimized) geometry
Ni1-B3 = 1.95 Å
Ni1-B2 = 2.0 Å
B3-Ni-B2 =180.0 °
N2-B3-B2-O1 = 76.6 °
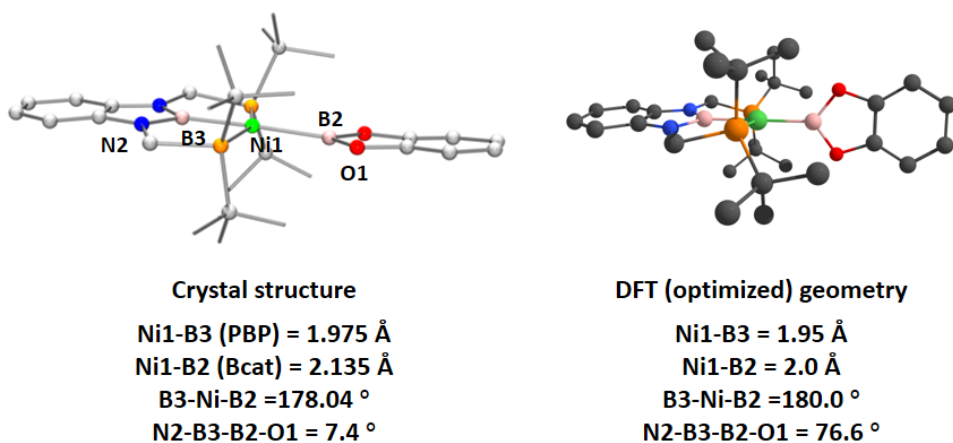
Figure 16. Selected structural differences between the experimental and theoretical structures of complex **11**. Hydrogen atoms have been omitted for clarity.

With the aim of interrogating the rotation energy of the boryl fragment, a relaxed potential energy surface scan was performed varying the dihedral angle formed by the planes of the PBP and BCat ligands. Figure 17 shows the results of this calculation, and the geometry corresponding to that observed in the crystal structure corresponds to the energy maximum around 8 kcal/mol above the calculated geometry.

[169]
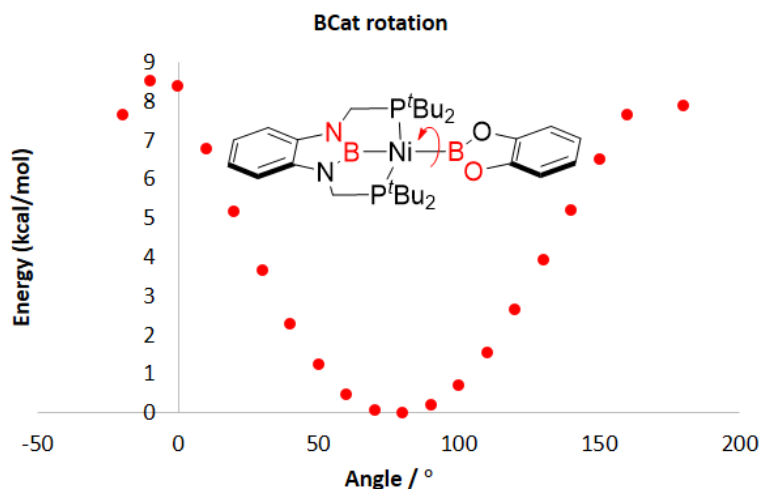
Figure 17. Relaxed Potential Energy Surface Scan (PES) of complex **11** along the dhihedral angle formed by the PBP and BCat planes. The energy minimum is located at 80 degrees.

In the light of these results, and given that the previous data showed that π overlap between the metal and the catecholboryl fragment did not seem to be determinant in the bonding, a different explanation must account for the observation of a coplanar orientation of the BCat ligand (and not perpendicular).

One plausible explanation might find its source in supramolecular interactions taking place in the solid state, which seem to be absent in solution and apparently they are not reproducible by computational methods. As an example, Aldridge and coworkers attributed the unusual conformation of the boryl ligand in $[(\eta^5-C_5H_4Me)Fe(CO)_2(BCat)]$ to a weak C−H···O hydrogen bond between one of the hydrogen atoms from the methyl group and one oxygen atom from BCat, with C···O and O···H distances of 3.279(7) Å and 2.52 Å, respectively.[58] On the other hand, Balcells *et al.* observed the same phenomena (*i.e.* different

---

[58] S. Aldridge, R. J. Calder, R. E. Baghurst, M. E. Light, M. B. Hursthouse, *J. Organomet. Chem.,* **2002**, *649*, 9-14.

conformations between crystal and computational structures) when analysing the structure of $[(\eta^5\text{-}C_5Me_5)Ir(\eta^2\text{-ONCOPh})]$.[59] In this case, packing effects due to noncovalent interactions seem to be responsible for this phenomenon, such as π-π stacking, metal–oxygen interactions and again weak C–H···O hydrogen bonds between the different oxygen atoms from the complex and the methyl groups from the Cp* ligand, with O···H distances of 2.89 Å and 2.68 Å as the shortest ones. A careful examination of the crystal structure of complex **11** revealed numerous C–H···O interactions between the *tert*-butyl groups and the oxygen atoms from the catecholboryl fragment (Figure 18). Some of these distances are close to the shortest O···H (*ca.* 2 Å) and C···O interactions (*ca.* 3 Å) described in the literature.[60] Although both systems are different and not comparable, it is worth mentioning that the Ir system studied by Balcells and coworkers showed an energy barrier of 9.4 kcal/mol required for transforming the experimental structure into the calculated isomer.[59]

[59] J. Chen, J. Campos, B. Q. Mercado, R. H. Crabtree, D. Balcells, *Organometallics*, **2014**, *33*, 4417-4424.

[60] T. Steiner, *Chem. Commun.,* **1997**, 727-734.
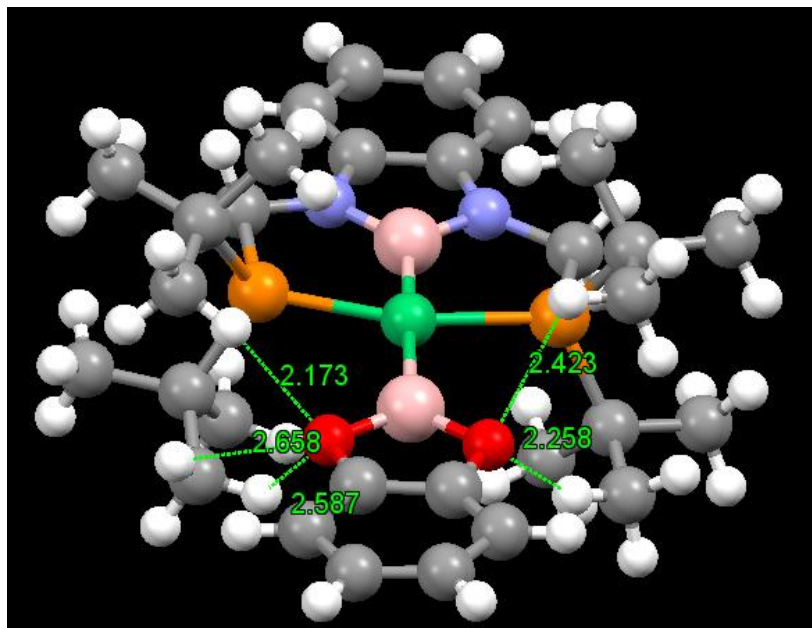
Figure 18. Some C–H⋯O contacts observed in the crystal structure of boryl complex **11**.

Another potential explanation for the conformational difference found in **11** might arise from electronic parameters. Marder, Lin and coworkers attributed the observation of coplanar arrangements of boryl ligands in Rh complexes to the small energy difference between the σ* and π* orbitals of the BO_2 unit, which makes BCat more conformationally flexible than its analogue Bpin (pinacolboryl).[61]

With the purpose of evaluating the influence of the BO_2 fragment in the orientation of the BCat ligand, a substituent with approximately the same steric bulk and without a BO_2 unit was envisaged so as to interrogate its orientation in the (PBP)Ni complex. For this reason, complex **12** was synthesized by using an

[61] a) W. H. Lan, S. Shimada, A. S. Batsanov, Z. Lin, T. B. Marder, J. A. Cowan, J. A. K. Howard, S. A. Mason, G. J. McIntyre, *Organometallics*, **2003**, *22*, 4557-4568; b) L. Dang, H. Zhao, Z. Lin, T. B. Marder, *Organometallics*, **2008**, *27*, 1178-1186.

analogous synthetic protocol to that utilized for the synthesis of methyl complex **4** (Scheme 11).
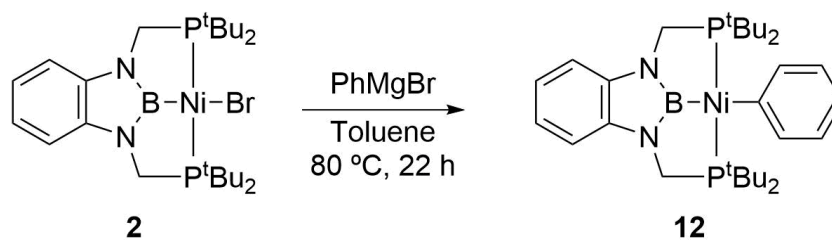
Scheme 11. Synthesis of phenyl complex **12**.

Phenyl complex **12** gives a singlet at 93.8 ppm in the $^{31}P\{^1H\}$ spectrum (Figure 19), indicative of its symmetrical nature. In addition, the boryl signal resonates at ~45 ppm in the $^{11}B\{^1H\}$ spectrum as a broad singlet. The symmetrical character of this compound is also reflected in the ^1H NMR spectrum, since there is only one set of signals for each of the proton groups of the molecule. A concentrated toluene solution of complex **12** afforded yellow crystals that could be measured by X-Ray diffraction techniques (Figure 20).

[173]
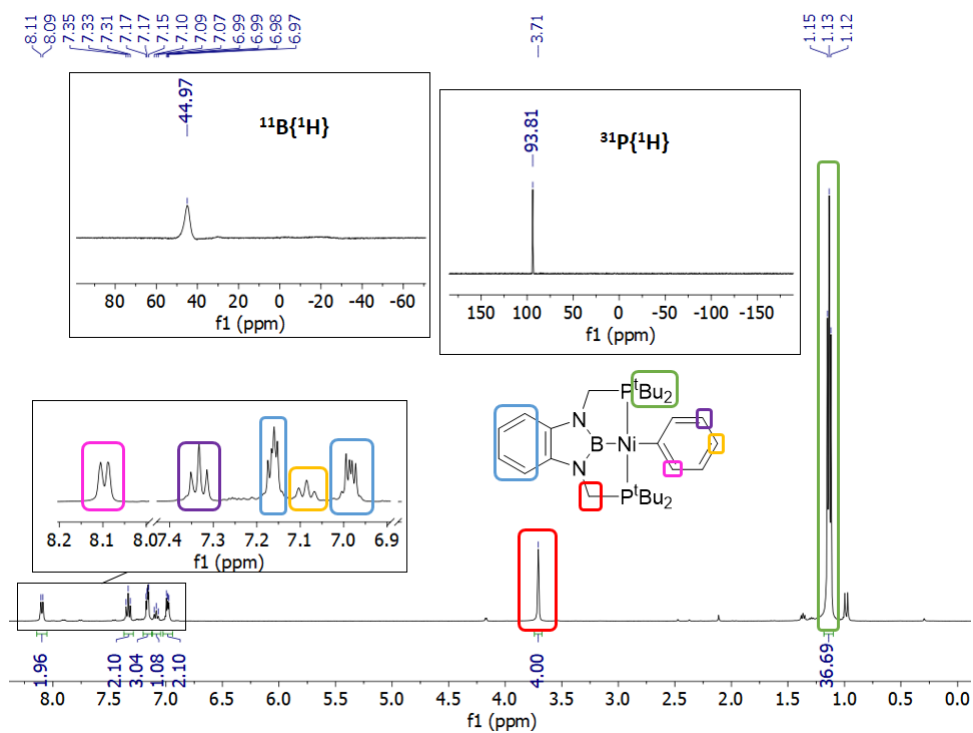
Figure 19. Some characteristic NMR spectra (400 MHz, C_6D_6) of phenyl complex **12**.
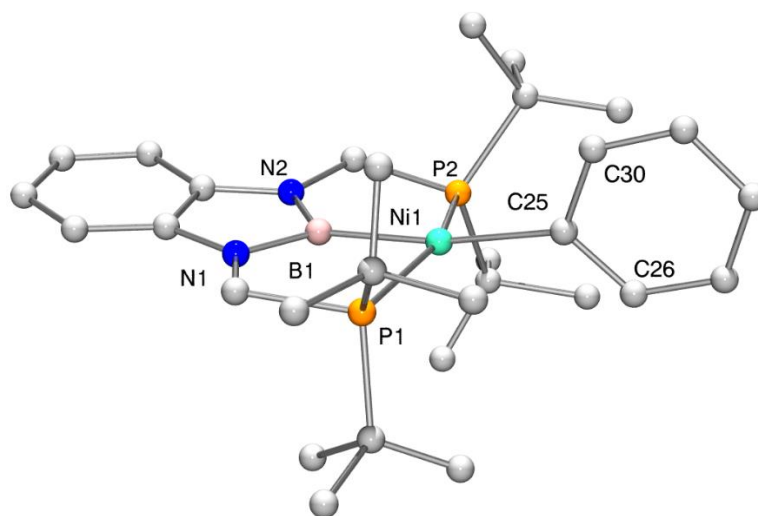
Figure 20. X-Ray structure of phenyl complex **12**. Hydrogen atoms have been omitted for clarity.

[174]

As it can be seen in Figure 20, the phenyl ring adopts a perpendicular orientation with respect to the plane of the pincer ligand as opposed to boryl derivative **11**. Some structural parameters were compared to those of complex **11**, in order to find some explanation to this different behaviour, although no appreciable variation was found. The crystal structure was compared to that obtained by computational methods (Table 4), and an excellent agreement was found between both geometries. For this reason, a potential energy surface scan was performed on this system and compared to that of boryl **11** (Figure 21). It can be observed that in this case, the energy minimum corresponds to a dihedral angle similar to the experimentally observed, and forcing a coplanar arrangement requires almost 15 kcal/mol, which is practically double the amount observed for complex **11**. These high energies found in coplanar arrangements seem to be caused by steric clashes with the *tert*-butyl groups from the phosphine ligands. Therefore, the supramolecular interactions previously described seem to be one plausible possibility for explaining the coplanar disposition of the catecholboryl fragment found in complex **11**.

Parameter	Crystal structure	DFT geometry
B−Ni	1.936(9) Å	1.95 Å
Ni−C	1.991(9) Å	2.01 Å
B−Ni−C	170.6(3) °	179.9 °
P−Ni−P	154.72(9) °	154.0 °
N−B−C−C (Dihedral between PBP and Ph)	77.6(8) °	76.2 °

Table 4. Comparison of some structural parameters between the experimental and calculated geometry of phenyl complex **12**.
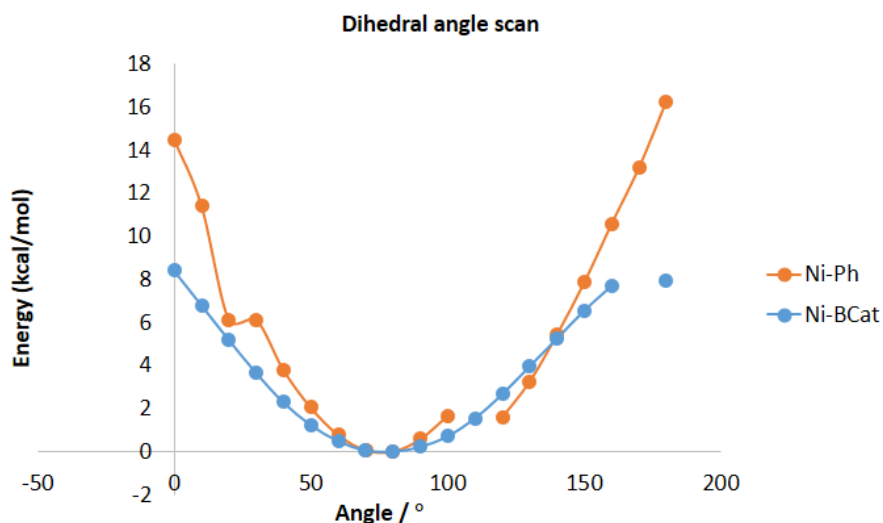
Figure 21. Orange: Relaxed Potential Energy Surface Scan (PES) of complex **12** along the dhihedral angle formed by the PBP and Ph planes. The energy minimum is located at 80 degrees. Some local minima are observed in the curve. Blue: PES of complex **11** for comparison.

2.2 Computational mechanistic studies

DFT calculations were carried out at the Universitat Autonoma de Barcelona in the group of Prof. Agustí Lledós as part of a short internship in his laboratory, in order to elucidate the mechanism by which the Ni(II) boryl complexes are formed.

When considering the mechanistic possibilities that could be taking place during the activation of the B−B bond, several alternatives were conceived and exploratory calculations were performed[62] (Scheme 12). A nucleophilic attack from the methyl group to one of the B atoms was evident given the Lewis acidity of diboron(4) compounds and the increased nucleophilicity of the alkyl group as

---

[62] Exploratory calculations were performed at a lower level of theory (BP97D/6-31g(d,p)/SDD/SMD) for computational time reasons. Then, nucleophilic attack and ligand cooperativity mechanisms were calculated at a higher level of theory. See Experimental Part section for more details.

[176]

mentioned above. Nonetheless, cooperativity of the PBP ligand was also taken into account as in the case of carbon dioxide hydrosilation (Chapter 1), given the antecedents discovered in our group.[43] Initial decoordination of one of the phosphine groups was also studied yet proved to be too energy demanding, and therefore it was not further pursued. Mechanisms involving metathesis processes were studied during the exploratory calculations, although all of them led to the cooperativity pathway, both in the case of B_2pin_2 and B_2cat_2.
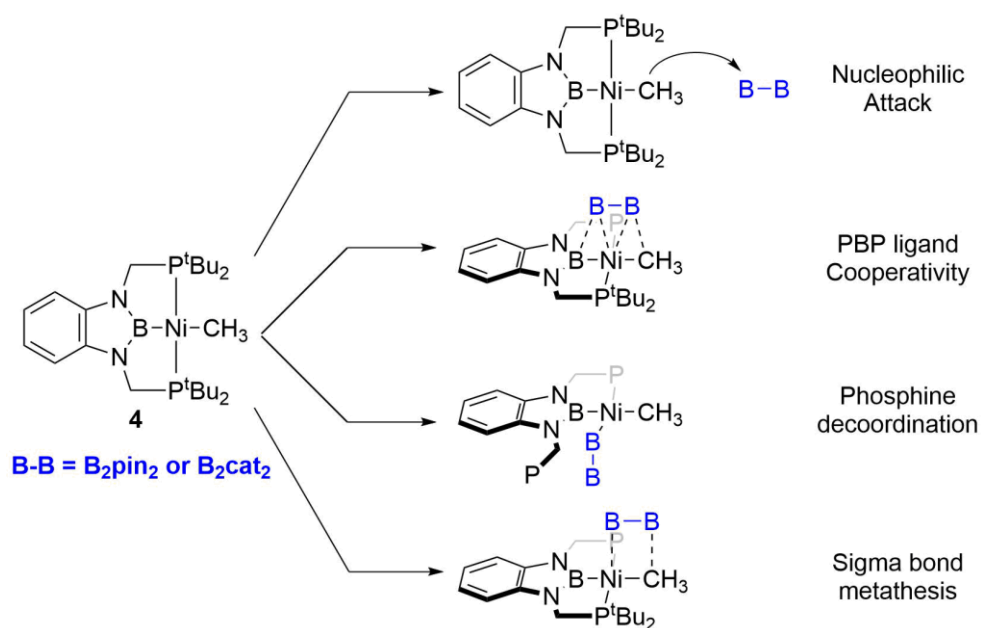
Scheme 12. Mechanistic possibilities considered during the DFT calculations for the formation of the Ni(II) boryl complexes from **4**.

2.2.1 Nucleophilic attack mechanism

The mechanism starts with the approach of the diborane to methyl complex **4** (the whole energy profile is shown in Figure 22). The optimal orientation of the diboron molecule is perpendicular to the P−Ni−P plane in the case of B_2pin_2 (ΔG = 5.7 kcal/mol) and coplanar in the case of B_2cat_2 (1.4 kcal/mol. Bis(pinacolato)diboron is 0.1 Å further away from the methyl group,

[177]

probably due to steric hindrance. Once the boron substrate is close to the complex, the nucleophilic attack takes place. The transition state (**TS1**) for this process shows a change in the geometry of the methyl fragment typical from Walden inversion in S_N2 reactions (*i.e.* in **4**, the hydrogen atoms of the methyl moiety are pointing away from the pincer framework, but after **TS1** they are pointing to the complex, as shown in the balls and stick representation in Figure 22). It can be seen that **TS1** is more energy demanding for B_2pin_2 (24.2 kcal/mol) than for B_2cat_2 (8.6 kcal/mol), which may be attributable to the higher Lewis acidity of the bis(catecholato)diboron compound. Right after this step, a cationic Ni(II) complex results from the Ni−C bond cleavage. This species is stabilized by an agostic interaction (distances range from 1.85 to 2.11 Å, in accordance with the description made by Brookhart, Green and Parkin)[63] from the $[B_2(OR)_2Me]$ anion, in which the B−C distance is 1.68 Å in all cases, identical to that observed in NHC adducts of diboron(4) reagents like the one obtained by mixing CyNHC (3-bis(cyclohexyl)imidazol-2-ylidene) and B_2pin_2, and very similar to the $[B_2pin_2(^nBu)]$ anion described by Hill and McMullin (1.61 Å).[64]

---

[63] M. Brookhart, M. L. H. Green, G. Parkin, *Proc. Natl. Acad. Sci. U. S. A.,* **2007**, *104*, 6908-6914.

[64] a) C. Kleeberg, A. G. Crawford, A. S. Batsanov, P. Hodgkinson, D. C. Apperley, M. S. Cheung, Z. Lin, T. B. Marder, *J. Org. Chem.,* **2012**, *77*, 785-789; b) A-F. Pécharman, A. L. Colebatch, M. S. Hill, C. L. McMullin, M. F. Mahon, C. Weetman, *Nat. Commun.,* **2017**, *8*, 15022-15028.
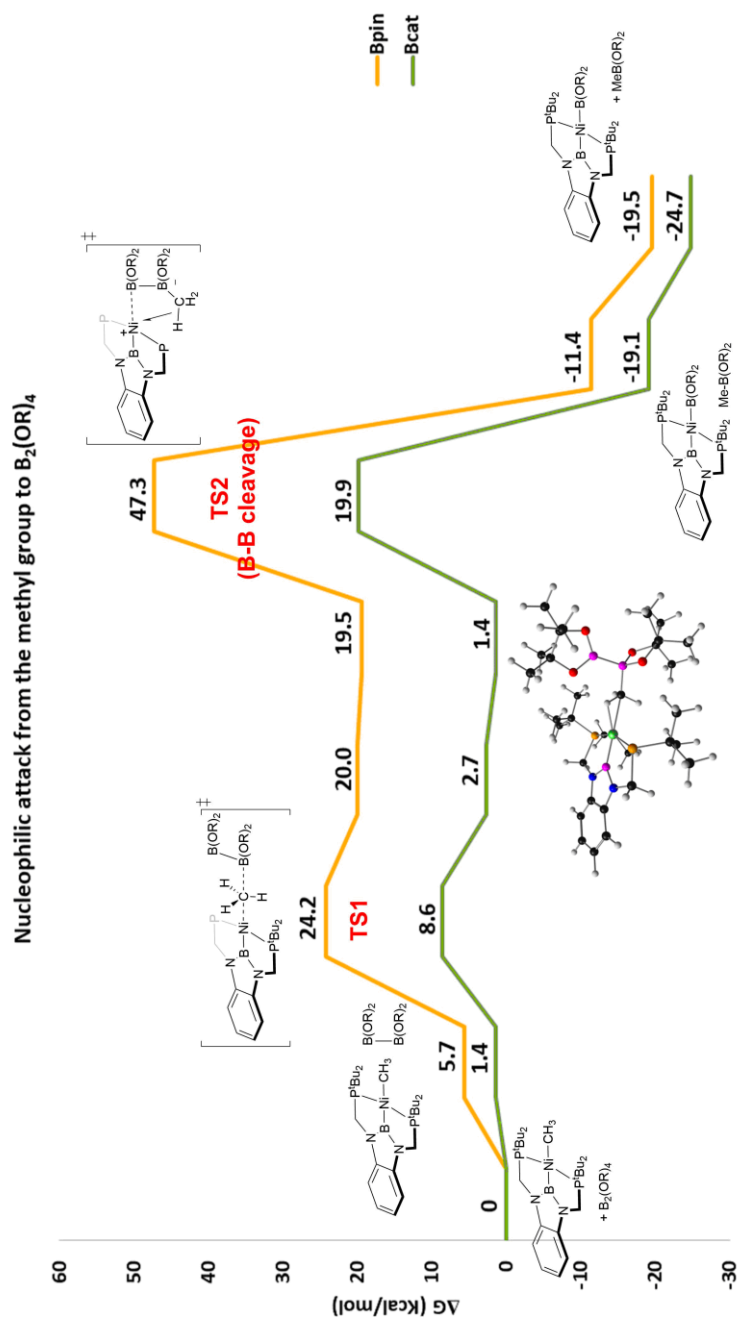
Figure 22. Energy profile for the nucleophilic attack mechanism between **4** and B_2pin_2 or B_2cat_2.

As it can be seen in the energy profile, there are two minima of these complexes with very little variation in energy (around 20 kcal/mol and 2 kcal/mol for B_2pin_2 and B_2cat_2, respectively), corresponding to slight changes in the coordination geometry of the $[B_2(OR)_2Me]$ anion to the Ni atom. At this point, the sp[2] boron attacks the metal during **TS2**, and at the same time the B−B bond becomes weaker. It can be seen that this stage is the most energetic one of the whole mechanistic pathway for both diboranes, and in the case of bis(pinacolato)diboron, the energy is extremely high (47.3 kcal/mol) to be accessible experimentally. Following the transition state, the Ni(II) boryl complexes are formed along with the methylborane derivative. The synthesis is thermodynamically favourable for both diboranes, albeit the kinetic barrier obtained for B_2pin_2 seems to suggest that an alternative mechanism is leading to the nickel boryl species. Nonetheless, the energy difference found for both pathways is in accordance with the experimental rates and conditions required for the reaction to occur. Moreover, this is consistent with the higher flexibility of BCat groups against Bpin ones, as described above.[61]

2.2.2. Cooperativity of the PBP ligand

In this mechanism, the diborane approaches methyl complex **4** from above the pincer plane in order to get close enough to the metal atom to begin the B−B cleavage. However, there is a large difference in the geometry of both adducts, which translates into contrasting energy values. Bis(pinacolato)diboron is not able to form a stable adduct with the Ni atom because of steric repulsions between the bulky substituents on the pinacol fragment and the *tert*-butyl groups on the phosphines (Figure 23, left). Hence, both boron atoms are 5.11 Å away from the metal. This geometry is 4.5 kcal/mol above the origin. In contrast, bis(catecholato)diboron is compact enough to interact with the nickel atom, forming an η^2 complex (17 kcal/mol) in which the boron−nickel distances are much shorter (average of 2.15 Å). In addition, the molecule can bend as shown

[180]

in Figure 23 (right) so the metal−boron contacts are more effective. This results in an elongation of the B−B bond, which is longer than that (1.721 Å) found for the σ complex [Cu(NHC)(σ-catB−Bcat)]+ as reported by Pérez, Fernández *et al.*[65]
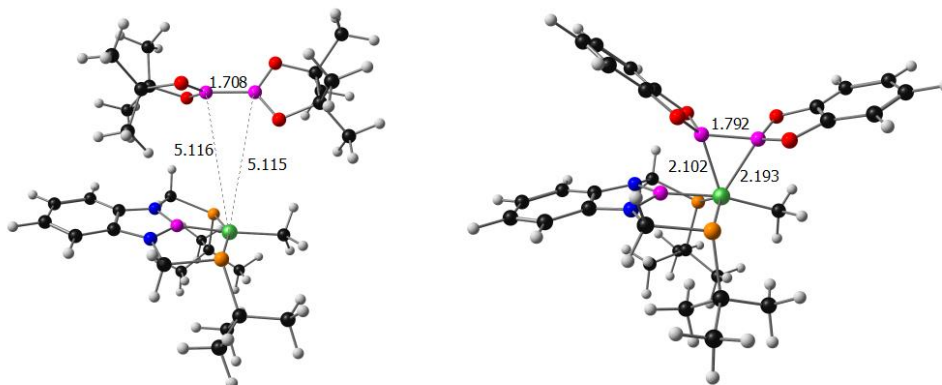
Figure 23. Comparison of the diboron adducts with **4** prior cleavage of the B−B bond (some *tert-butyl* groups have been omitted for clarity).

[65] V. Lillo, M. R. Fructos, J. Ramírez, A. A. C. Braga, F. Maseras, M. M. Díaz-Requejo, P. J. Pérez, E. Fernández, *Chem. Eur. J.,* **2007**, *13*, 2614-2621.
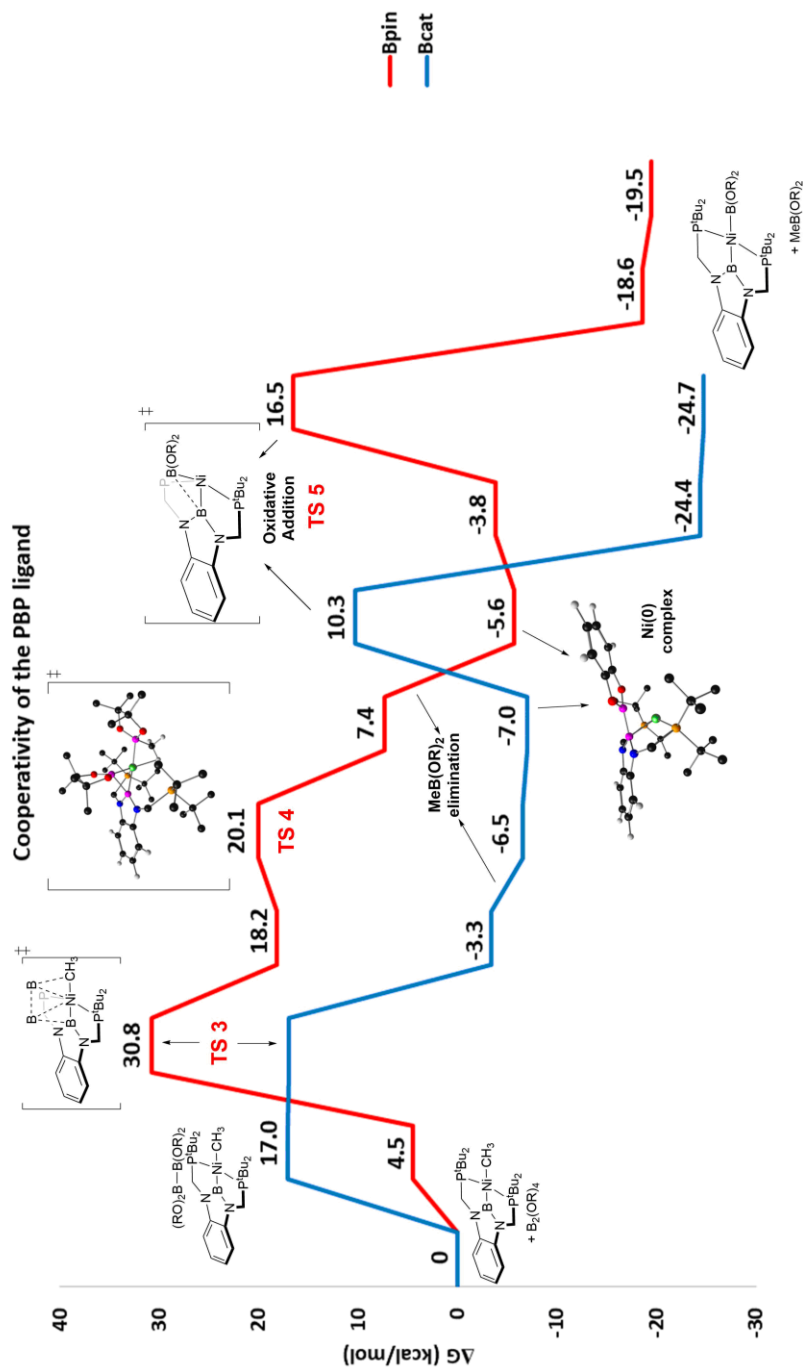
Figure 24. Energy profile for the ligand cooperativity mechanism between **4** and B$_2$pin$_2$ or B$_2$cat$_2$.

[182]

Following this step, the B−B bond breaks through **TS3** (Figure 24), in which the methyl group attacks one of the boron atoms, while the other boron interacts with the boryl fragment of the ligand and the metal atom. For B_2pin_2, a closer contact is needed (around 2.6 Å) in order for these contacts to take place, which might account for the high energy found for this transition state (30.8 kcal/mol). On the contrary, this stage is barrierless for B_2cat_2 probably due to the higher Lewis acidity of the substrate and the smaller volume of the molecule. This steric contrast marks a difference in the fate of the resulting compounds, since the pinacol derivative undergoes some additional steps through this mechanism:

Right after **TS3**, the steric congestion forces one of the phosphine groups to dissociate from the metal. The resulting geometry seems to be that corresponding to a Ni(0) complex stabilized by a η^2 B_{ligand}−B_{Bpin} bond and a η^2 B−C bond (B−Ni = C−Ni = 2.01 Å). In turn, there is an additional agostic interaction which further holds the newly formed MeBpin attached to the metal. Next, a transition state (**TS4**) is found a couple of kcal/mol above the previous geometry, which consists of the rearrangement of the MeBpin unit so it ends up stabilizing the Ni complex through a Ni−O interaction (Figure 25, right). It can be seen in Figure 24 that removal of the methylborane unit affords a symmetrical η^2 B−B stabilized Ni(0) complex upon recoordination of the phosphine ligand (-5.6 kcal/mol). Then, oxidative addition takes place through **TS5** (16.5 kcal/mol), after which complex **10** is formed. The process is thermodynamically favoured (-19.5 kcal/mol after considering both products separately). The high energy needed for the first step (**TS3**, B−B cleavage) is in accordance with the required experimental warming of the sample for several hours.

[183]
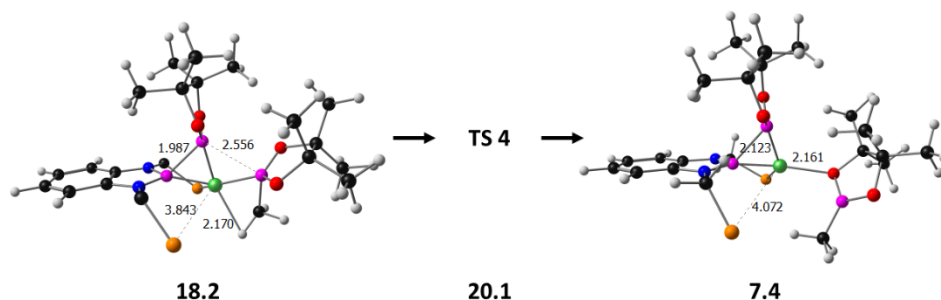
Figure 25. Additional steps obtained by DFT calculations for the formation of complex **10** (Gibbs energy values in kcal/mol). Some hydrogen atoms and the *tert*-butyl groups have been omitted for clarity.

In the case of B_2cat_2, **TS3** leads directly to extrusion of the MeBcat molecule and the formation of the (η^2-B−B)Ni(0) complex (-3.3 kcal/mol), as shown in the energy profile. Removal of the methylborane moiety further stabilizes the system up to -7.0 kcal/mol. At this point, oxidative addition takes place in the same manner as described above (**TS5**, 10.3 kcal/mol) to yield boryl complex **11** (-24.7 kcal/mol). As it can be seen above, the maximum energy required for this mechanism is around 17 kcal/mol, which agrees with the experimental conditions (room temperature, less than 5 minutes) needed for the reaction to take place.

In all cases, splitting the B−B bond is the most energetic stage of the mechanism regardless of the diboron employed. Whereas ligand cooperativity seems to suggest the feasibility of the mechanism, the nucleophilic attack pathway possesses a very high energy demanding barrier for B_2pin_2. In order to detect some of the calculated intermediates, low temperature NMR studies were carried out by using B_2cat_2, since no high temperature is needed.

2.3. Experimental mechanistic studies

Initial low temperature NMR studies performed with **4** and B_2cat_2 in d^8-Toluene were not informative, since no intermediate was observed from -80 °C

[184]

to -15 °C. At the latter temperature, boryl complex **11** started to appear, and its formation was complete after reaching room temperature. Inspired by previous results in our group where the hydride ligand in **6** was able to migrate to the boryl moiety by using 1,5-cyclooctadiene (COD) to yield a Ni(0) complex (Figure 26, left),[43] COD (1 equivalent) was added at room temperature to the sample with the hope of observing the same phenomenon, yet no change was detected.
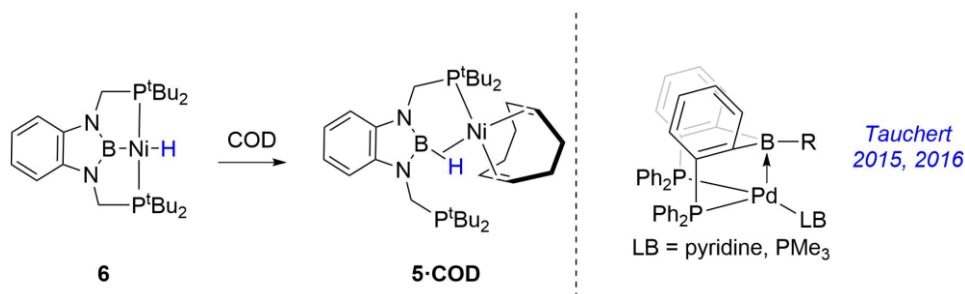
Figure 26. Examples of low-valent PBP-stabilized transition metal complexes. Left: Hydride migration experiment previously performed in our group. Right: Pd(0) complexes stabilized by Lewis bases.

The lack of solubility of B_2cat_2 in toluene raised the question of whether it was in solution at low temperature or not. For this reason, d^8-THF was employed in a different experiment and a new species was detected by $^{31}P\{^1H\}$ NMR at -40 °C (Figure 27), giving a singlet at 81.6 ppm.[66] This, along with the set of signals observed in the ^1H NMR spectrum suggests that both phosphine groups are equivalent and that the intermediate is symmetrical. Such species is stable from -40 to -25 °C, and the **4** : **Intermediate** ratio is dependent on the temperature (see Figure 27, difference between -35 °C and -40 °C). At 0 °C, complex **4** is completely consumed and both **11** and the intermediate coexist

---

[66] The ability of THF to coordinate to Lewis acidic boron species and the partial hydrolysis due to adventitious water in the deuterated solvent gives rise to several species in the $^{11}B\{^1H\}$ NMR spectrum, precluding the follow-up of the experiment by analysing this nucleus.

[185]

temporarily. Warming up the sample to room temperature gives **11** as the sole product again.
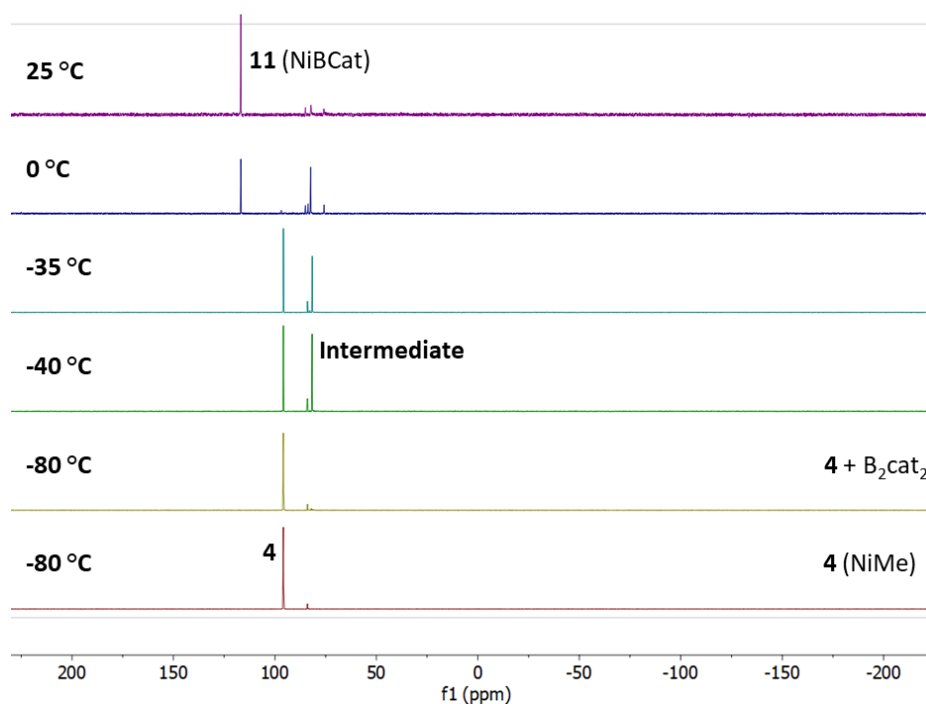
Figure 27. Low temperature $^{31}P\{^{1}H\}$ NMR (400 MHz, d^8-THF) study between **4** and B$_2$cat$_2$.

After observing these results, the same experiment was repeated, but a Lewis base was added at low temperature after detecting the intermediate in order to stabilize the perhaps formed Ni(0) complex, in the same manner as Tauchert *et al.* stabilize their PBP Pd(0) complexes (Figure 26, right).[67]

---

[67] a) T. Schindler, M. Lux, M. Peters, L. T. Scharf, H. Osseili, L. Maron, M. E. Tauchert, *Organometallics*, **2015**, *34*, 1978-1984; b) D. Schuhknecht, F. Ritter, M. E. Tauchert, *Chem. Commun.,* **2016**, *52*, 11823-11826.
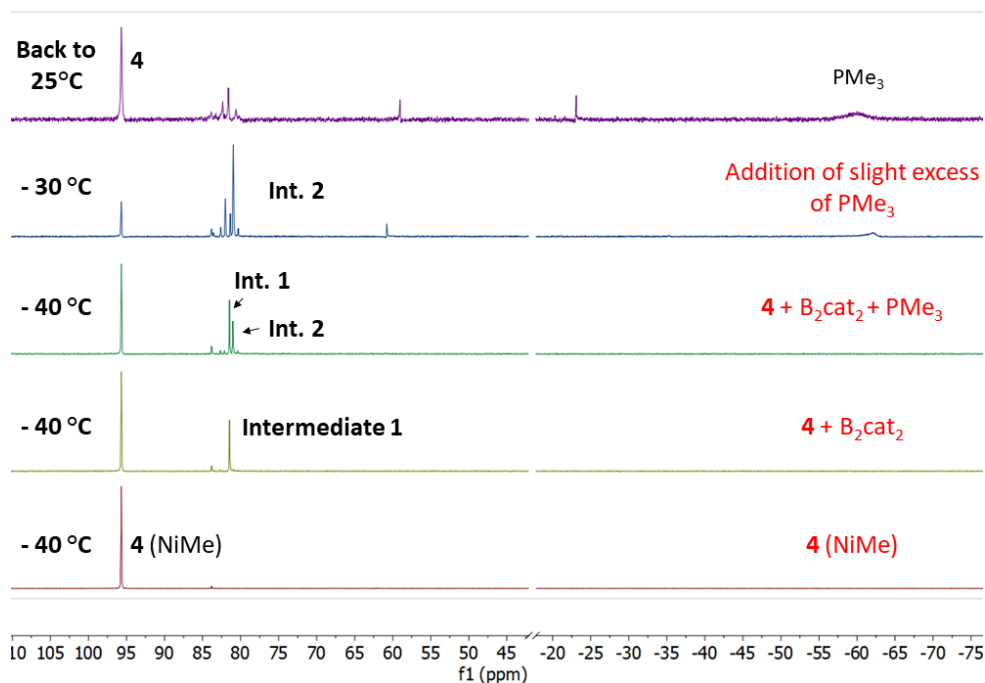
Figure 28. Low temperature $^{31}P\{^{1}H\}$ NMR (400 MHz, d^{8}-THF) study between **4** and B₂cat₂ in the presence of PMe₃.

From figure 28 it can be seen that right after addition of PMe₃ a new intermediate (**intermediate 2**, δ = 80.9 ppm) is formed, and it grows with the amount of phosphine added at the same time that **4** is consumed. Nonetheless, warming up the sample does not increase its proportion in the sample and no boryl complex **11** is observed either; instead, the peak of methyl complex **4** grows back and becomes the major species in the sample. This experiment seems to suggest that the coordination of both B₂cat₂ and PMe₃ is reversible. Upon increasing the temperature, the ability of the diborane to form complex **11** gets somehow inhibited in the presence of the phosphine. A plausible possibility might be the formation of the diborane-phosphine adducts [B₂cat₂(PMe₃)] and [B₂cat₂(PMe₃)₂] (Scheme 13), although more experiments are needed to confirm

[187]

Chapter 2. Results and discussion

this hypothesis. These complexes have been previously reported[68] and detected by NMR.[69]
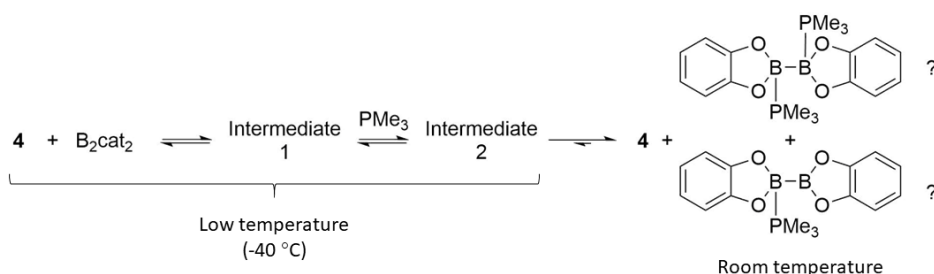
Scheme 13. Possible equilibria that might be taking place during the low temperature NMR experiment in the presence of PMe₃.

Carbon monoxide was employed as a Lewis base in a different experiment with the aim of avoiding the formation of diboron adducts (Figure 29).[70] When **intermediate 1** was detected by $^{31}P\{^1H\}$ NMR, CO (1 bar) was charged at -60 °C and the sample was introduced back into the precooled spectrometer. **Intermediate 1** disappeared at -40 °C in favour of a new species (**species 1**) at 113.4 ppm, slightly different from the chemical shift of boryl **11**. When the temperature was raised to -30 °C, a new singlet was observed at 121.5 ppm (**species 2**) in a small proportion with respect to species 1. These 2 new compounds coexist until the temperature reaches 25 °C. The chemical shift of **species 2** might point out to the formation of some hydride **6** during the process

[68] a) W. Clegg, C. Dai, F. J. Lawlor, T. B. Marder, P. Nguyen, N. C. Norman, N. L. Pickett, W. P. Power, A. J. Scott, *J. Chem. Soc. Dalton Trans.,* **1997**, 839-846 ; b) D. Curtis, M. J. G. Lesley, N. C. Norman, A. G. Orpen, J. Starbuck, *J. Chem. Soc. Dalton Trans.,* **1999**, 1687-1694.

[69] The chemical shifts reported in the reference do not match the peaks observed in the experiment. The solvent in which they are reported is chloroform, which differs from the mixture in which the experiment was carried out (the substrates were dissolved in d^8-THF and PMe₃ was injected as a commercial solution in toluene).

[70] Formation of adducts between diboranes and carbon monoxide is possible, albeit extreme conditions are required. For instance, B₂H₆ reacts with CO at 100 °C and 20 atmospheres to give the following equilibrium: B₂H₆ + 2 CO ↔ H₃B·CO. See: M. W. Rathke, H. C. Brown, *J. Am. Chem. Soc.,* **1966**, *88*, 2606-2607.

coming from hydrolysis events, although the characteristic triplet of the hydride ligand was not observed in the ^{1}H NMR spectrum. On the other hand, the similarity in chemical shifts between **species 1** and carbonyl complex **3** suggests the formation of some type of nickel carbonyl derivative, like [(PBP)Ni(CO)][$B_2cat_2(Me)$].

By the time this thesis is being written, experimental work is being carried out in order to further analyse the nature of these species so the previously calculated mechanisms can be either confirmed or discarded.
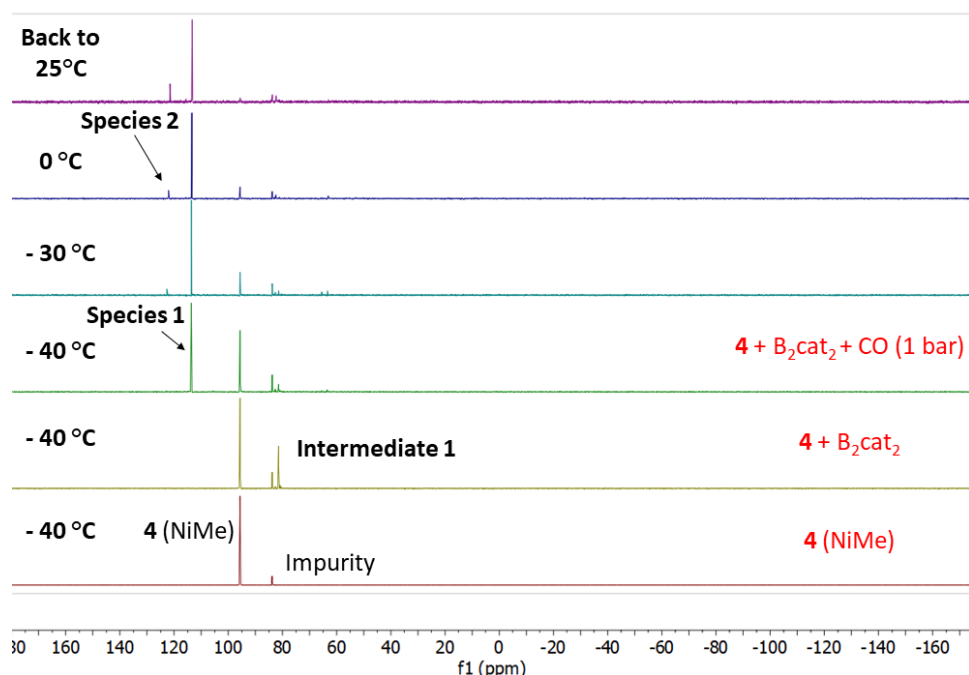
Figure 29. Low temperature $^{31}P\{^1H\}$ NMR (400 MHz, d^8-THF) study between **4** and B_2cat_2 in the presence of CO.

2.4. Catalytic dehydrogenative borylation of styrenes

The enhanced nucleophilicity of the ligand in *trans* to the boryl moiety of the PBP ligand makes it prone to attack unsaturated substrates such as alkynes or alkenes. In this way, compounds **10** and **11** were tested as catalysts for the

dehydrogenative borylation of styrenes in d^8-Toluene.[71] Methyl complex **4** was employed as a pre-catalyst, and the conversion values as well as the selectivities were determined by ^{1}H NMR in combination with GC/MS in some cases. In a typical experiment, the pre-catalyst was mixed in the reaction vessel with diborane in deuterated toluene, and an additive was also added to ensure dehydrogenative borylation and avoid hydroboration reactions. For this purpose, 2-norbornene (NBE) was used as the sacrificial hydroborane acceptor (otherwise, a mixture of DHB and hydroboration products is obtained).[72] Other additives such as DMF and *tert*-butyl ethylene have been employed as well and they prevent hydroboration phenomena too, yet their role is still unknown, since they are not consumed during the whole catalytic process. Once everything is in solution in the sealed reactor, the mixture was heated up to 70 or 80 °C. As a result, monoborylated and diborylated derivatives were obtained. The selectivity of the products depends on the catalytic conditions (Table 5).

---

[71] Early studies with B_2cat_2 are currently taking place. B_2pin_2 was chosen in the first place due to the higher stability of the borylation products.
[72] Some other authors have used 2-norbornene as a sacrificial acceptor for hydrogen (see reference 38) and/or pinacolborane: W. J. Teo, S. Ge, *Angew. Chem. Int. Ed.,* **2018**, *57*, 1654-1658.

Entry	Substrate	Cat. Load. / mol %	Diborane [a]	Conv./%	Monoboryl./%	Diborylated/%	T / °C	t / h	Additive
1	Styrene	10	2 eq B_2cat_2	99	94	-	80	6.5	NBE
2	Styrene	10	1 eq B_2pin_2	75	99	-	70	14	DMF
3	Styrene	10	2 eq B_2pin_2	94	99	-	70	20	^tBu ethylene
4	Styrene	5	2 eq B_2pin_2	99	65	35	70	18	NBE
5	4-CF$_3$ styrene	10	1 eq B_2pin_2	87	97	3	70	3	DMF
6	4-CF$_3$ styrene	5	2 eq B_2pin_2	99	99	-	70	6	NBE
7	4-CF$_3$ styrene	10	4 eq B_2pin_2	99	35	65	80	18	NBE
8	4-CF$_3$ styrene	10	1 eq B_2cat_2	98	70	-	80	18	-
9	α-Me-styrene	10	2 eq B_2pin_2	85	85	-	70	6.5	NBE
10	4-F-styrene	10	2 eq B_2pin_2	99	98	-	70	9	NBE
11	4-F-styrene	10	4 eq B_2pin_2	99	30	70	70	10	NBE
12	4-MeO-styrene	10	2 eq B_2pin_2	70	86	-	70	15	DMF

Table 5. Summary of the catalytic results of the dehydrogenative borylation catalysis by boryl complexes **10** (using B_2pin_2) or **11** (using B_2cat_2). An example of the entry highlighted in blue is shown in Figure 30. [a] Equivalents of diborane with respect to styrene.

[191]

The results displayed in table 5 show that selective DHB towards *E*-monoborylated[73] substrates can be achieved by modifying parameters such as the equivalents of diborane (Scheme 14). There is a trend in the reaction times depending on the substrate employed: whereas electron-withdrawing substituents on the aryl ring require low catalytic loadings and short reaction times (entry 6 and Figure 30), the absence of substituent in it or the presence of electron-donating groups (entries 3 and 12) require a higher loading and longer reaction times to achieve similar conversion values. Additionally, the catalyst loading and the equivalents of diborane can be adjusted to obtain diborylated styrenes with moderate selectivities (up to 70%).
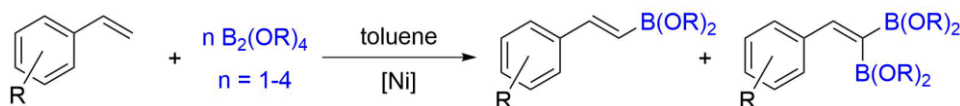
Scheme 14. Ni-catalyzed dehydrogenative borylation of styrenes.

---

[73] The chemical shifts and coupling constants for the alkene protons are characteristic in each geometric isomer, and the ones obtained match the *E*-alkene. Examples on reported data can be found in a) C-C. Tai, M-S. Yu, Y-L. Chen, W-H. Chuang, T-H. Lin, G. P. A. Yap, T-G. Ong, *Chem. Commun.,* **2014**, *50*, 4344-4346 (For (*E*)-boryl alkenes) and b) J. V. Obligacion, J. M. Neely, A. N. Yazdani, I. Pappas, P. J. Chirik, *J. Am. Chem. Soc.,* **2015**, *137*, 5855-5858 (For (*Z*)-boryl alkenes).
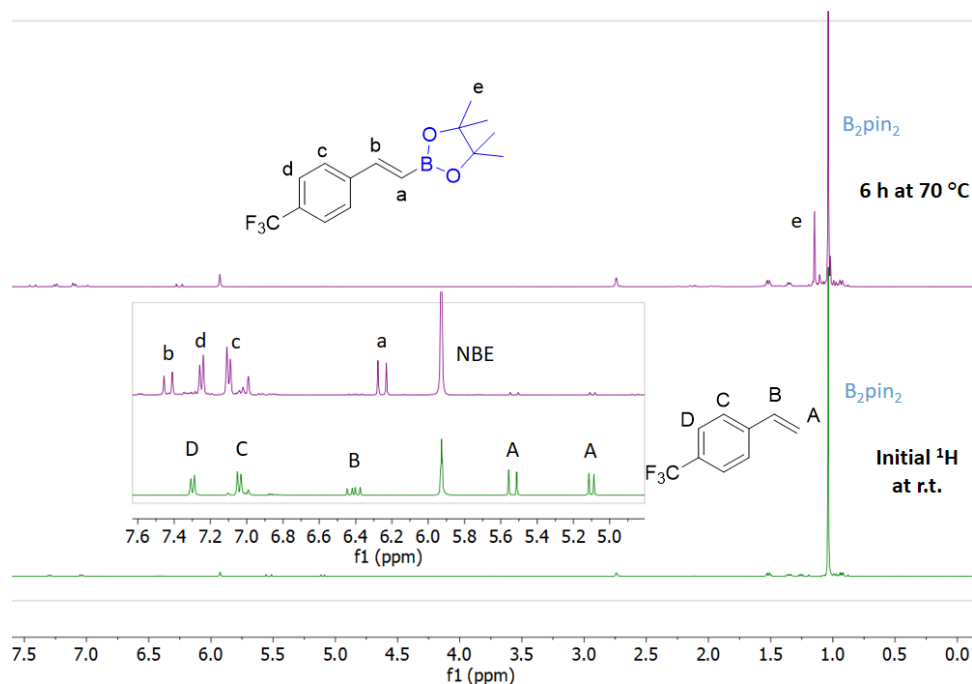
Figure 30. Representative example (400 MHz, d^8-toluene) of a catalytic dehydrogenative monoborylation of *p*-CF$_3$-styrene when using 5% mol of complex **4** and 2 equivalents of B$_2$pin$_2$.

The isolation of the monoborylated products coming from the reaction in the presence of NBE was attempted by column chromatography, HPLC and preparative thin layer chromatography methods. Unfortunately, the similar polarities of the NBE by-products and the styrene derivative made inaccessible the purification of the compounds. When using DMF as an additive, this could be removed by forming an azeotrope with heptane. The azeotropic mixture was then evaporated under vacuum, and the remaining crude purified by column chromatography, affording pure styrene boronic esters like the one shown in Figure 31.
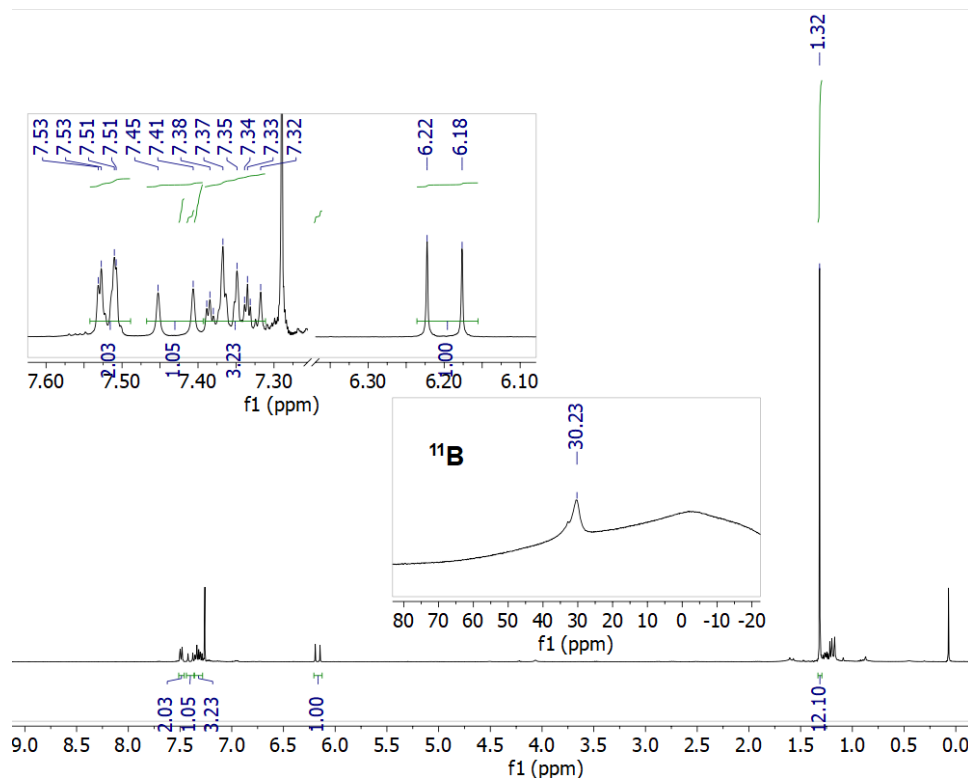
Figure 31. ^{1}H and ^{11}B{^{1}H} NMR spectra (400 MHz, CDCl$_3$) of (*E*)-4,4,5,5-tetramethyl-2-styryl-1,3,2-dioxaborolane. The spectroscopic data match those reported in the literature.[733a]

As deduced from the results above, this work is still preliminary and more work needs to be done so as to explain the structure of boryl complex **11**, to experimentally confirm the mechanistic pathway leading to its formation, to complete the catalytic dehydrogenative borylation of styrene derivatives and to obtain mechanistic evidence for mono- and di-borylation reactions catalysed by complexes **10** and **11**.

[194]

References

[1] H. Nöth, G. Schmid, *Angew. Chem. Int. Ed.* **1963**, *2*, 623.

[2] a) S. Aldridge, D. L. Coombs, *Coord. Chem. Rev.,* **2004**, *248*, 535-559; b) I. A. I. Mkhalid, J. H. Barnard, T. B. Marder, J. M. Murphy, J. F. Hartwig, *Chem. Rev.* **2010**, *110*, 890-931.

[3] Z. Lin in *Computational Studies in Organometallic Chemistry*, S. A. McGregor & O. Eisenstein (Editors), Springer International Publishing, **2016**. Chapter 2: Reactivities and Electronic Properties of Boryl Ligands, pages 39-58.

[4] W. Clegg, F. J. Lawlor, G. Lesley, T. B. Marder, N. C. Norman, A. G. Orpen, M. J. Quayle, C. R. Rice, A. J. Scott, F. E. S. Souza, *J. Organomet. Chem.,* **1998**, *550*, 183-192.

[5] G. Lesley, P. Nguyen, N. J. Taylor, T. B. Marder, A. J. Scott, W. Clegg, N. C. Norman, *Organometallics*, **1996**, *15*, 5137-5154.

[6] X. He, J. F. Hartwig, *Organometallics*, **1996**, *15*, 400-407.

[7] C. Dai, G. Stringer, T. B. Marder, A. J. Scott, W. Clegg, N. C. Norman, *Inorg. Chem.,* **1997**, *36*, 272-273.

[8] a) C. E. F. Rickard, W. R. Roper, A. Williamson, L. J. Wright, *Organometallics*, **1998**, *17*, 4869-4874; b) G. R. Clark, G. J. Irvine, W. R. Roper, L. J. Wright, *J. Organomet. Chem.,* **2003**, *680*, 81-88.

[9] a) C. Dai, G. Stringer, J. F. Corrigan, N. J. Taylor, T. B. Marder, N. C. Norman, *J. Organomet. Chem.,* **1996**, *513*, 273-275; b) K. C. Lam, W. H. Lam, Z. Lin, T. B. Marder, N. C. Norman, *Inorg. Chem.,* **2004**, *43*, 2541-2547.

[10] C. S. Cundy, H. Nöth, *J. Organomet. Chem.,* **1971**, *30*, 135-143.

[11] E. C. Neeve, S. J. Geier, I. A. I. Mkhalid, S. A. Westcott, T. B. Marder, *Chem. Rev.* **2016**, *116*, 9091-9161.

[12] G. Urry, T. Wartik, R. E. Moore, H. I. Schlesinger, *J. Am. Chem. Soc.,* **1954**, *76*, 5293-5298.

[13] S. A. Westcott, E. Fernández, *Adv. Organomet. Chem.,* **2015**, *63*, 39-89.

14 According to some references (*e.g.* J. F. Hartwig, *Organotransition Metal Chemistry: From Bonding to Catalysis*, University Science Books, Sausalito, CA, **2009**. Chapter 4, page 186), boryl complexes of all transition metals have been isolated except for group 3 and group 4 elements. However, recent works have reported on the syntheses of group 3 and group 4 boryl complexes. For group 3 boryl compounds, see: L. M. A. Saleh, K. H. Birjkumar, A. V. Protchenko, A. D. Schwarz, S. Aldridge, C. Jones, N. Kaltsoyannis, P. Mountford, *J. Am. Chem. Soc.,* **2011**, *133*, 3836-3839. For group 4 boryl species, see: T. Terabayashi, T. Kajiwara, M. Yamashita, K. Nozaki, *J. Am. Chem. Soc.,* **2009**, *131*, 14162-14163.

15 S. Sakaki, T. Kikuno, *Organometallics*, **1997**, *36*, 226-229.

16 Q. Cui, D. G. Musaev, K. Morokuma, *Organometallics*, **1998**, *17*, 742-751.

17 a) J. Takaya, N. Kirai, N. Iwasawa, *J. Am. Chem. Soc.,* **2011**, *133*, 12980-12983; b) N. Kirai, J. Takaya, N. Iwasawa, *J. Am. Chem. Soc.,* **2013**, *135*, 2493-2496. Oxidative addition events usually take place when a B–X (X= halide, Sn) containing reagent is used. See: c) S. Onozawa, Y. Hatanaka, T. Sakakura, S. Shimada, M. Tanaka, *Organometallics*, **1996**, *15*, 5450-5452; d) S. Onozawa, M. Tanaka, *Organometallics*, **2001**, *20*, 2956-2958; e) H. Braunschweig, K. Gruss, K. Radacki, K. Uttinger, *Eur. J. Inorg. Chem.,* **2008**, 1462-1466.

18 B. L. Tran, D. Adhikari, H. Fan, M. Pink, D. J. Mindiola, *Dalton Trans.,* **2010**, *39*, 358-360.

19 M. A. Salomon, T. Braun, A. Penner, *Angew. Chem. Int. Ed.,* **2008**, *47*, 8867-8871.

20 A. C. Fernandes, J. A. Fernandes, F. A. A. Paz, C. C. Romão, *Dalton Trans.,* **2008**, 6686-6688.

21 Y. Zhu, C-H. Chen, C. M. Farfard, B. M. Foxman, O. V. Ozerov, *Inorg. Chem.,* **2011**, *50*, 7980-7987.

22 a) J. R. Khusnutdinova, D. Milstein, *Angew. Chem. Int. Ed.,* **2015**, *54*, 12236-12273; b) G. R. Owen, *Chem. Commun.,* **2016**, *52*, 10712-10726.

23 a) G. Schmid, H. Nöth, *Chem. Ber.,* **1967**, *100*, 2899-2907; b) G. Schmid, P. Powell, H. Nöth, *Chem. Ber.,* **1968**, *101*, 1205-1214.

[196]

[24] D. Adhikari, J. C. Huffman, D. J. Mindiola, *Chem. Commun.,* **2007**, 4489-4491.

[25] D. Adhikari, S. Mossin, F. Basuli, B. R. Dible, M. Chipara, H. Fan, J. C. Huffman, K. Meyer, D. J. Mindiola, *Inorg. Chem.,* **2008**, *47*, 10479-10490.

[26] a) S. Z. Tasker, E. A. Standley, T. F. Jamison, *Nature*, **2014**, *509*, 299-309; b) V. P. Ananikov, *ACS Catal.,* **2015**, *5*, 1964-1971.

[27] N. Miyaura, A. Suzuki, *Chem. Rev.,* **1995**, *95*, 2457-2483.

[28] A. J. J. Lennox, G. C. Lloyd-Jones, *Chem. Soc. Rev.,* **2014**, *43*, 412-443.

[29] W. B. Reid, J. J. Spillane, S. B. Krause, D. A. Watson, *J. Am. Chem. Soc.,* **2016**, *138*, 5539-5542.

[30] C. Wang, C. Wu, S. Ge., *ACS Catal.,* **2016**, *6*, 7585-7589.

[31] a) T. Shen, X-N. Wang, H-X. Lou, *Nat. Prod. Rep.,* **2009**, *26*, 916-935; b) G. Likhtenshtein, *Stilbenes: Applications in Chemistry, Life Sciences and Materials Science*, Wiley-VCH, **2009**.

[32] S. A. Westcott, T. B. Marder, R. T. Baker, *Organometallics*, **1993**, *12*, 975-979.

[33] a) R. B. Coapes, F. E. S. Souza, R. Ll. Thomas, J. J. Hall, T. B. Marder, *Chem. Commun.,* **2003**, 614-615; b) I. A. I. Mkhalid, R. B. Coapes, S. N. Edes, D. N. Coventry, F. E. S. Souza, R. Ll. Thomas, J. J. Hall, S-W. Bi, Z. Lin, T. B. Marder, *Dalton Trans.,* **2008**, 1055-1064.

[34] J. M. Brown, G. C. Lloyd-Jones, *J. Chem. Soc.* **1992**, 710-712.

[35] J. M. Brown, G. C. Lloyd-Jones, *J. Am. Chem. Soc.,* **1994**, *116*, 866-878.

[36] a) M. Murata, S. Watanabe, Y. Masuda, *Tetrahedron Lett.,* **1999**, *40*, 2585-2588; b) M. Murata, K. Kawakita, T. Asana, S. Watanabe, Y. Masuda, *Bull. Chem. Soc. Jpn.,* **2002**, *75*, 825-829.

[37] N. Iwadate, M. Suginome, *Chem. Lett.,* **2010**, *39*, 558-5060.

[38] M. Morimoto, T. Miura, M. Murakami, *Angew. Chem. Int. Ed.,* **2015**, *54*, 12659-12663.

[39] T. J. Mazzacano, N. P. Mankad, *ACS Catal.,* **2017**, *7*, 146-149.

[40] S. Jiang, S. Quintero-Duque, T. Roisnel, V. Dorcet, M. Grellier, S. Sabo-Etienne, C. Darcel, J-B. Sortais, *Dalton Trans.,* **2016**, *45*, 11101-11108.

[41] H. Wen, L. Zhang, S. Zhu, G. Liu, Z. Huang, *ACS Catal.,* **2017**, *7*, 6419-6425.

[42] L. Zhang, Z. Huang, *J. Am. Chem. Soc.,* **2015**, *137*, 15600-15603.

[43] N. Curado, C. Maya, J. López-Serrano, A. Rodríguez, *Chem Commun.,* **2014**, *50*, 15718-15721.

[44] Free HBpin resonates at 28.8 ppm in d^8-Toluene, giving a doublet with $^1J_{BH}$ = 174.4 Hz. See: A. Bismuto, S. P. Thomas, M. J. Cowley, *Angew. Chem. Int. Ed.,* **2016**, *55*, 15356-15359.

[45] S. Chakraborty, J. Zhang, Y. J. Patel, J. A. Krause, H. Guan, *Inorg. Chem.,* **2013**, *52*, 37-47.

[46] Y-R. Luo, *Comprehensive Handbook of Chemical Bond Energies,* CRC Press: Boca Raton, FL, 2007.

[47] The reaction between **6** and B_2pin_2 was attempted anyway, and no apparent change was observed after heating up the sample at 80 °C for 12 hours in benzene. A closer look to the spectrum reveals the absence of the hydride signal by ^1H NMR, in the same way as described above. This, along with catalytic studies where the released HBpin is captured (see section 2.4) seems to point out that the following reactions might be taking place due to the presence of adventitious water in the solvent:

- Ni−H (**6**) + B_2pin_2 → Ni−Bpin (**10**) + HBpin
- Ni−Bpin + H_2O → Ni−H + HOBpin
- Ni−H + HBpin → NiH_2Bpin (stable dihydridoborate described previously)

For this reason, the released HBpin due to hydrolysis is able to inhibit the formation of **10** from **6**.

[48] T. J. Schmeier, N. Hazari, C. D. Incarvito, J. A. Raskatov, *Chem. Commun.,* **2011**, *47*, 1824-1826.

[49] There are some other peaks at higher field in the $^{11}B\{^1H\}$ NMR spectrum coming from the excess of diborane, MeBpin and hydrolysis-derived species.

[198]

[50] Hydrolysis of metal–boryl bonds to give metal–hydride units has been previously described in the literature: a) J. F. Hartwig, X. He, *Organometallics*, **1996**, *15*, 5350-5358; b) W. Clegg, F. J. Lawlor, T. B. Marder, P. Nguyen, N. C. Norman, A. G. Orpen, M. J. Quayle, C. R. Rice, E. G. Robins, A. J. Scott, F. E. S. Souza, G. Stringer, G. R. Whittell, *J. Chem. Soc. Dalton Trans.,* **1998**, 301-309.

[51] The R-Factor of the measured crystal is 5.63%. Effort is being put at the moment in lowering this value. For the time being, the discussion of the data will be made on these results. Since some parameters might change (although very slightly) upon R lowering, this information must be taken cautiously.

[52] G. R. Clark, G. J. Irvine, W. R. Roper, L. J. Wright, *J. Organomet. Chem.,* **2003**, *680*, 81-88.

[53] Y. Segawa, M. Yamashita, K. Nozaki, *J. Am. Chem. Soc.,* **2009**, *131*, 9201-9203.

[54] J. Zhu, Z. Lin, T. B. Marder, *Inorg. Chem.,* **2005**, *44*, 9384-9390.

[55] As a comparison, Mindiola reported bond orders of 0.84 and 0.80 for Ni–B and B–O, respectively (see reference 24).

[56] B. Cordero, V. Gómez, A. E. Platero-Prats, M. Revés, J. Echeverría, E. Cremades, F. Barragán, S. Álvarez, *Dalton Trans.,* **2008**, 2832-2838. Some covalent radii from this reference: B (0.84 Å), Li (1.28 Å), Ni (1.24 Å).

[57] Y. Segawa, M. Yamashita, K. Nozaki, *Science*, **2006**, *314*, 113-115.

[58] S. Aldridge, R. J. Calder, R. E. Baghurst, M. E. Light, M. B. Hursthouse, *J. Organomet. Chem.,* **2002**, *649*, 9-14.

[59] J. Chen, J. Campos, B. Q. Mercado, R. H. Crabtree, D. Balcells, *Organometallics*, **2014**, *33*, 4417-4424.

[60] T. Steiner, *Chem. Commun.,* **1997**, 727-734.

[61] a) W. H. Lan, S. Shimada, A. S. Batsanov, Z. Lin, T. B. Marder, J. A. Cowan, J. A. K. Howard, S. A. Mason, G. J. McIntyre, *Organometallics*, **2003**, *22*, 4557-4568; b) L. Dang, H. Zhao, Z. Lin, T. B. Marder, *Organometallics*, **2008**, *27*, 1178-1186.

[62] Exploratory calculations were performed at a lower level of theory (BP97D/6-31g(d,p)/SDD/SMD) for computational time reasons. Then, nucleophilic attack

and ligand cooperativity mechanisms were calculated at a higher level of theory. See Experimental Part section for more details.

[63] M. Brookhart, M. L. H. Green, G. Parkin, *Proc. Natl. Acad. Sci. U. S. A.,* **2007**, *104*, 6908-6914.

[64] a) C. Kleeberg, A. G. Crawford, A. S. Batsanov, P. Hodgkinson, D. C. Apperley, M. S. Cheung, Z. Lin, T. B. Marder, *J. Org. Chem.,* **2012**, *77*, 785-789; b) A-F. Pécharman, A. L. Colebatch, M. S. Hill, C. L. McMullin, M. F. Mahon, C. Weetman, *Nat. Commun.,* **2017**, *8*, 15022-15028.

[65] V. Lillo, M. R. Fructos, J. Ramírez, A. A. C. Braga, F. Maseras, M. M. Díaz-Requejo, P. J. Pérez, E. Fernández, *Chem. Eur. J.,* **2007**, *13*, 2614-2621.

[66] The ability of THF to coordinate to Lewis acidic boron species and the partial hydrolysis due to adventitious water in the deuterated solvent gives rise to several species in the $^{11}B\{^1H\}$ NMR spectrum, precluding the follow-up of the experiment by analysing this nucleus.

[67] a) T. Schindler, M. Lux, M. Peters, L. T. Scharf, H. Osseili, L. Maron, M. E. Tauchert, *Organometallics*, **2015**, *34*, 1978-1984; b) D. Schuhknecht, F. Ritter, M. E. Tauchert, *Chem. Commun.,* **2016**, *52*, 11823-11826.

[68] a) W. Clegg, C. Dai, F. J. Lawlor, T. B. Marder, P. Nguyen, N. C. Norman, N. L. Pickett, W. P. Power, A. J. Scott, *J. Chem. Soc. Dalton Trans.,* **1997**, 839-846 ; b) D. Curtis, M. J. G. Lesley, N. C. Norman, A. G. Orpen, J. Starbuck, *J. Chem. Soc. Dalton Trans.,* **1999**, 1687-1694.

[69] The chemical shifts reported in the reference do not match the peaks observed in the experiment. The solvent in which they are reported is chloroform, which differs from the mixture in which the experiment was carried out (the substrates were dissolved in d^8-THF and PMe$_3$ was injected as a commercial solution in toluene).

[70] Formation of adducts between diboranes and carbon monoxide is possible, albeit extreme conditions are required. For instance, B_2H_6 reacts with CO at 100

°C and 20 atmospheres to give the following equilibrium: $B_2H_6 + 2\ CO \leftrightarrow H_3B{\cdot}CO$. See: M. W. Rathke, H. C. Brown, *J. Am. Chem. Soc.,* **1966**, *88*, 2606-2607.

[71] Early studies with B_2cat_2 are currently taking place. B_2pin_2 was chosen in the first place due to the higher stability of the borylation products.

[72] Some other authors have used 2-norbornene as a sacrificial acceptor for hydrogen (see reference 38) and/or pinacolborane: W. J. Teo, S. Ge, *Angew. Chem. Int. Ed.,* **2018**, *57*, 1654-1658.

[73] The chemical shifts and coupling constants for the alkene protons are characteristic in each geometric isomer, and the ones obtained match the *E*-alkene. Examples on reported data can be found in a) C-C. Tai, M-S. Yu, Y-L. Chen, W-H. Chuang, T-H. Lin, G. P. A. Yap, T-G. Ong, *Chem. Commun.,* **2014**, *50*, 4344-4346 (For (*E*)-boryl alkenes) and b) J. V. Obligacion, J. M. Neely, A. N. Yazdani, I. Pappas, P. J. Chirik, *J. Am. Chem. Soc.,* **2015**, *137*, 5855-5858 (For (*Z*)-boryl alkenes).

Chapter 3

Cationic Pt(II) σ-SiH complexes as reactive intermediates

1. Introduction

1.1. Transition metal catalysed alkene hydrosilation

Context

Hydrosilation consists of the addition of a Si−H fragment across unsaturated bonds (usually C=C bonds). This process is generally catalysed by a transition metal, and it is extensively used in industry for the synthesis of organosilicon derivatives. As a matter of fact, hydrosilation reactions are one of the main applications of industrial homogeneous catalysis due to the versatility of the resulting products as commodity chemicals or in the silicone manufacturing (Figure 1).[1]
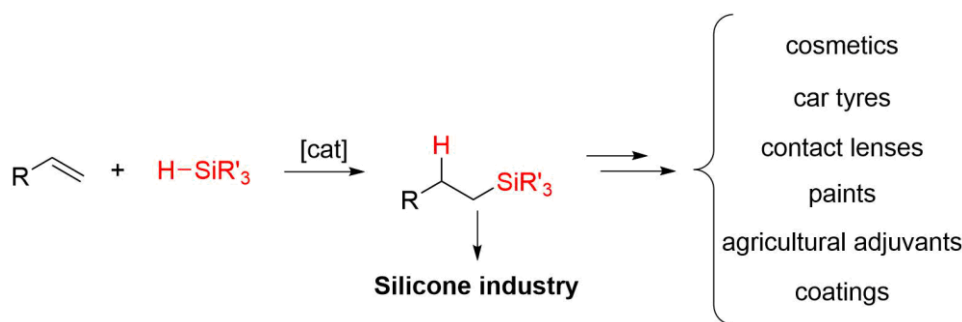
Figure 1. Applications of olefin hydrosilation (adapted from reference 1). *NB*: the great majority of the catalytic methods afford the anti-Markovnikov product, which is the useful substrate in industry.

The reason why commerce with hydrosilation-derived products is economically viable is attributable to the high catalytic activity and efficiency of the complexes involved in such reactions. Among them, platinum is the metal of choice for these processes, since its ability to catalyse these transformations surpasses that of other transition metals. This, in combination with the

---

[1] J. V. Obligacion, P. J. Chirik, *Nat. Rev. Chem.,* **2018**, *2*, 15-34.

remarkable selectivity and robustness shown by the Pt-based complexes, makes them attractive for catalytic hydrosilation purposes.[2] In fact, "hydrosilation reactions are the most important application of platinum in homogeneous catalysis."[3]

This chemistry started to develop in the 1950s, where hexachloroplatinic(IV) acid was found to be a powerful catalyst for the hydrosilation of olefinic compounds by Speier and coworkers from Dow Corning Corporation (Figure 2, left).[4] This event was a landmark in the silicon chemistry, thrusting the growth of the silicone industry. As in every pioneer work, there were some drawbacks that needed solution, such as the lack of solubility of the catalyst in polysiloxane media or the induction times required. These disadvantages were solved in 1973 with Karstedt's catalyst (Figure 2, center), which is a dinuclear Pt(0) complex stabilized by tetramethyldivinylsiloxane ligands that allowed the performance of catalytic reactions in silicone media.[5] Additionally, the activity and selectivity towards hydrosilation products was improved. For these reasons, Karstedt's catalyst is still one of the most commonly used catalysts for this type of transformation.[6]

---

[2] Y. Nakajima, S. Shimada, *RSC Adv.,* **2015**, *5*, 20603-20616.

[3] H. Renner, G. Schlamp, I. Kleinwächter, E. Drost, H. M. Lüschow, P. Tews, P. Panster, M. Diehl, J. Lang, T. Kreuzer, A. Knödler, K. A. Starz, K. Dermann, J. Rothaut, R. Drieselmann, C. Peter, R. Schiele. Platinum Group Metals and Compounds. *Ullmann's Encyclopedia of Industrial Chemistry,* **2001**, doi:10.1002/14356007.a21_075.

[4] J. L. Speier, J. A. Webster, G. H. Barnes, *J. Am. Chem. Soc.,* **1956**, *78*, 2278-2281.

[5] B. D. Karstedt, General Electric Company, US3775452A, **1973**.

[6] L. N. Lewis, J. Stein, Y. Gao, R. E. Colborn, G. Hutchins, *Platinum Metals Rev.,* **1997**, *41*, 66-75.

Figure 2. Temporal overview of the development of Pt-based hydrosilation catalysts.

The vinyl ligands must dissociate for the catalysis to take place. This can lead to the formation of platinum nanoparticles or platinum black, which increases the possibility of observing side-products derived from isomerization, dehydrogenative silylation, silane redistribution, oligo- and polymerization or hydrogenation phenomena.[1,7] In addition, liberation of elemental platinum can cause contamination of the final products, especially in the curation of silicones (Scheme 1), where the metal atoms can end up trapped.[2,8]
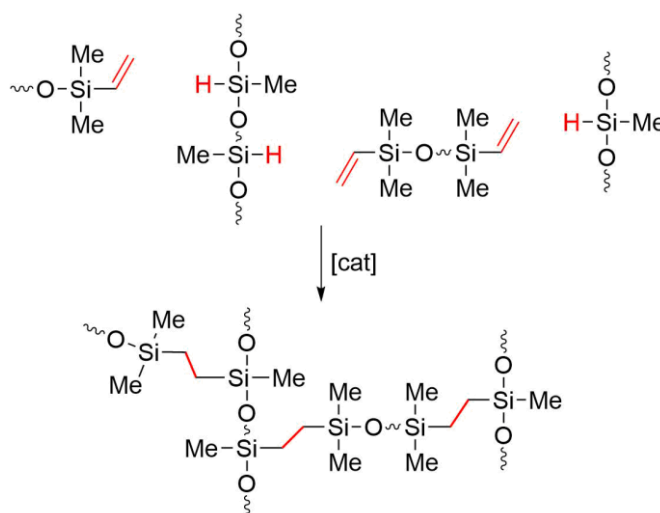
Scheme 1. Cross-linking hydrosilation reactions for the formation of siloxane-containing polymers (adapted from reference 8).

[7] B. Marciniec, *Coord. Chem. Rev.,* **2005**, *249*, 2374-2390.

[8] D. Troegel, J. Stohrer, *Coord. Chem. Rev.,* **2011**, *255*, 1440-1459.

The problems derived from the lability of the ligands stabilizing the platinum atoms were solved around thirty years later by the group of Markó *et al.*, when they proved that strong coordinating ligands such as *N*-heterocyclic carbenes (NHCs) were able to stabilize the catalyst enough not to observe any formation of colloidal platinum (Figure 2, right). As a result, no Pt precipitate was formed and the amount of side-products was greatly reduced even in the case of substrates containing sensitive functional groups such as epoxides.[9] An impressive comparison of this improvement can be observed in Scheme 2:
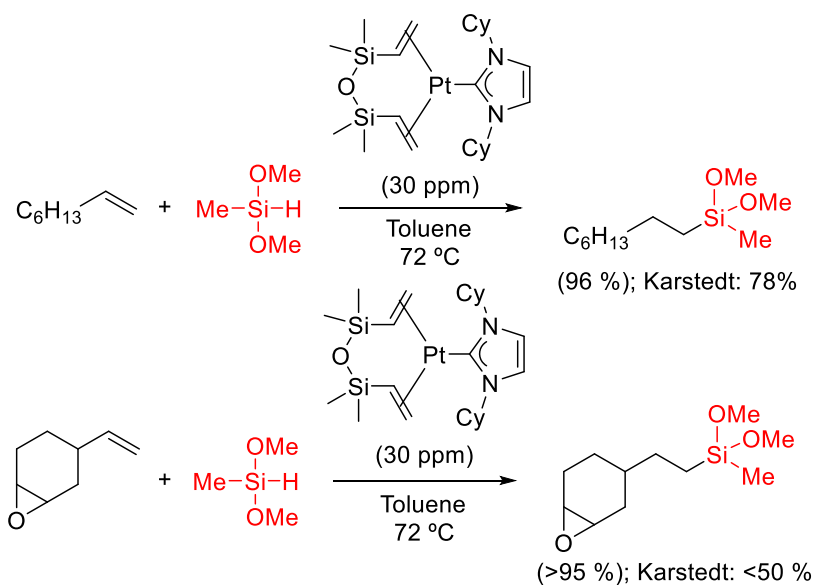
Scheme 2. Comparison of the regio- and chemoselectivity between Markó's and Karstedt's catalysts (adapted from reference 9).

The benefitial properties conferred by the NHCs to the Pt complexes opens up the possibility of further exploiting the role of these ligands in hydrosilation chemistry, since the steric and electronic properties of the

---

[9] I. E. Markó, S. Stérin, O. Buisine, G. Mignani, P. Branlard, B. Tinant, J-P. Declercq, *Science*, **2002**, *298*, 204-206.

resulting catalysts can be modulated by changing the substituents on the nitrogen atoms and/or the backbone of the imidazole ring.

Mechanistic features

Pt-catalyzed olefin hydrosilation is frequently rationalized by the Chalk-Harrod mechanism (Scheme 3): initial Si−H oxidative addition to the metal affords the hydride-silyl metal complex. Then, the alkene coordinates to the platinum atom, after which it inserts into the M−H unit, giving the alkyl-silyl derivative. Reductive elimination of both groups yields the anti-Markovnikov C−Si product along with recycled catalyst.[10] In several occasions, experimental results, like the formation of vinylsilanes along with the hydrosilation product, made some authors propose a slightly different mechanistic cycle, namely modified Chalk-Harrod mechanism. In this pathway, the alkene inserts into the M−Si bond, after which reductive elimination or β-hydride elimination would give the hydrosilation or dehydrogenative silylation products, respectively.[11] Although it depends on the employed substrates, the modified Chalk-Harrod mechanism is less likely to occur, since the insertion of the olefin into the M−Si fragment is usually much higher in energy than the rate-determining step of the Chalk-Harrod mechanism (*i.e.* isomerization of the alkyl fragment to end up in a *cis* position to the silyl ligand), as in the case of ethylene, for example.[12]

---

[10] A. J. Chalk, J. F. Harrod, *J. Am. Chem. Soc.,* **1965**, *87*, 16-21.

[11] a) M. A. Schroeder, M. S. Wrighton, *J. Organomet. Chem.,* **1977**, *128*, 345-358; b) I. Ojima, T. Fuchikami, M. Yatabe, *J. Organomet. Chem.,* **1984**, *260*, 335-346.

[12] S. Sakaki, N. Mizoe, M. Sugimoto, *Organometallics*, **1998**, *17*, 2510-2523.
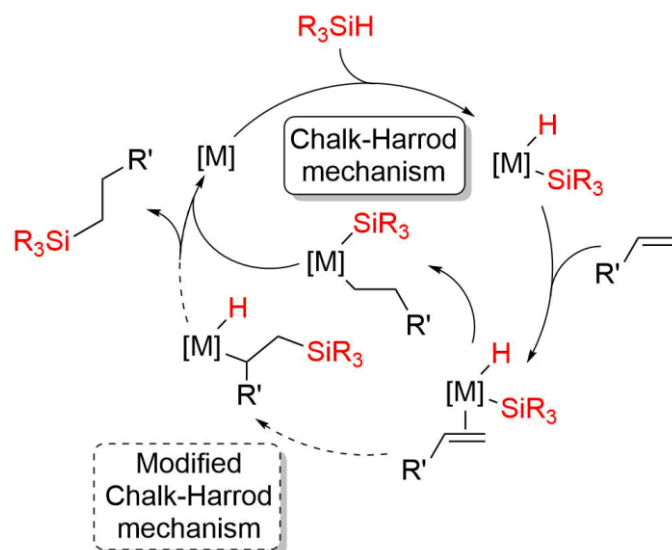
Scheme 3. Chalk-Harrod mechanisms for the hydrosilation of alkenes (adapted from reference 8).

The above mentioned mechanisms are commonly found in transition metal complexes. However, transition metal-free alkene hydrosilation is also possible in the presence of Lewis acidic species.[13] The last few decades have witnessed a development in this area with the discovery of perfluoroarene-based main-group compounds such as $B(C_6F_5)_3$.[14] The increased Lewis acidity of such species makes them able to activate silanes, forming the same kind of complexes as the borane-silane derivatives mentioned in Chapter 1 which are responsible for CO_2 over-reduction to methane. In the presence of an unsaturated molecule like an olefin, the latter can attack the silane (now with silylium character) as depicted in Scheme 4. The resulting carbenium can receive

---

[13] Some representative examples include: a) M. Rubin, T. Schwier, V. Gevorgyan, *J. Org. Chem.,* **2002**, *67*, 1936-1940; b) M. Pérez, L. J. Hounjet, C. B. Caputo, R. Dobrovetsky, D. W. Stephan, *J. Am. Chem. Soc.,* **2013**, *135*, 18308-18310; c) J. Chen, E. Y.-X. Chen, *Angew. Chem. Int. Ed.,* **2015**, *54*, 6842-6846.

[14] W. E. Piers, T. Chivers, *Chem. Soc. Rev.,* **1997**, *26*, 345-354.

then the attack of the E–hydride (E = main-group element) so as to form the hydrosilation product and regenerate the perfluoroarene catalyst.
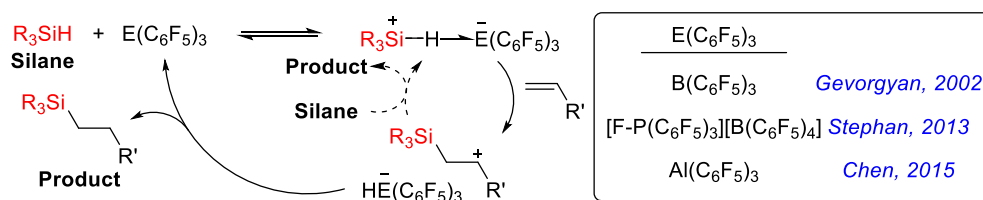
Scheme 4. Main-group element catalysed alkene hydrosilation (adapted from reference 13).

Although metal and non-metal mediated alkene hydrosilation seem to be very different mechanistically, they have one common aspect, which is the approach of the silane towards the metal or Lewis acid prior activation of the Si–H bond. The understanding of the silane-catalyst interaction in the first stages of this process can contribute to the comprehension about how the silane becomes activated. By doing so, the knowledge acquired can help in the design of more efficient catalysts for silane-based reduction phenomena.

σ-Silane complexes

Nonclassical σ-compounds are those which contain delocalized σ-bonds over at least three atoms, and their structure cannot be represented by Lewis forms. Among these, σ-silane complexes are the most studied ones along with dihydrogen species.[15]

---

[15] G. I. Nikonov, *Adv. Organomet. Chem.,* **2005**, *53*, 217-309.
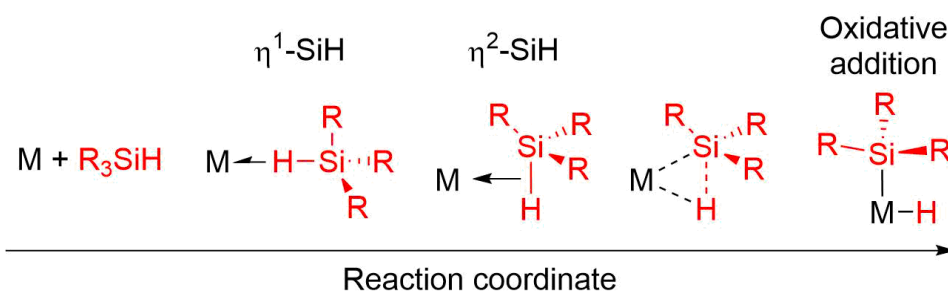
Scheme 5. Sequential steps into the oxidative addition of a Si–H bond, including η^1 and η^2 σ-silane complexes.

Regarding their nature, they can be considered as captured intermediates in the oxidative addition process of a Si–H bond to a transition metal complex (Scheme 5): compared to H–H or C–H bonds, Si–H units are more basic (their Si–H bonding orbital is higher in energy) and better σ-donors. At the same time, their low energy σ* Si–H orbital makes them better π-acceptors.[15] As a consequence, the silane molecule will approach the metal to interact through the hydrogen center first, since the electronic charge is mainly located on the H atom due to the electronegativity difference (Figure 3). This interaction gives a η^1-silane complex. Then, it will pivot to place the Si atom close enough to the metal, making possible the interaction through the Si–H bond (η^2-silane complex). At this point, the degree of backbonding from M to the Si–H bond will depend on the substituents on the silane and the nature and oxidation state of the metallic atom. The more electron density on the antibonding Si–H orbital, the higher the splitting of the Si–H unit. The ultimate situation would render the oxidative addition product (*i.e.* silyl and hydride ligands) if the backbonding is enough to cleave the bond.[16] It is necessary to mention that the closer the geometry to a η^1 coordination mode is, the higher the silylium character on the

---

[16] J. Y. Corey, *Chem. Rev.,* **2011**, *111*, 863-1071.

silane and it will be more electrophilic , since the antibonding σ* Si−H orbital is less occupied.
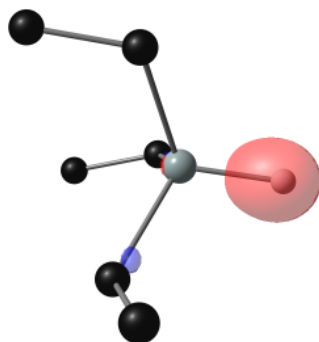
Figure 3. HOMO-2 of Et$_3$SiH. Isodensity contour: 0.12 a.u. Hydrogen atoms on the ethyl chains have been omitted for clarity.

The methods for synthesizing this kind of complexes include the protonation of metal−silyl bonds or mixing a silane molecule with a transition metal complex which contains a vacant orbital available for interaction. The first σ-SiH complex was synthesized in 1969 by the latter method, upon mixing Re$_2$(CO)$_{10}$ and Ph$_2$SiH$_2$ under ultraviolet irradiation (promoting CO loss).[17] In the resulting compound (Figure 4) each rhenium atom is bound to a Si−H bond in a 3-center-2-electron interaction. The hydrogen atoms were not found in the crystal structure, yet the spectroscopic experimental evidence allowed the assignment of the geometry shown below.

---

[17] J. K. Hoyano, M. Elder, W. A. G. Graham, *J. Am. Chem. Soc.,* **1969**, *91*, 4568-4569.
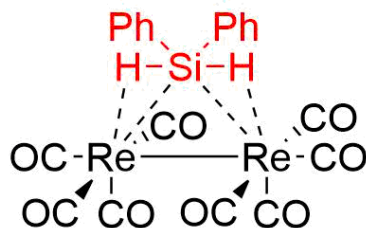
Figure 4. Structure of the first σ-silane complex, synthesized by Graham and coworkers. *NB*: The Re−Re distance was found to be 3.121 Å, excluding the possibility of multiple bonding between the metal atoms.

In fact, this type of experimental limitations partly account for the moderate rate in which this chemistry developed at that time. However, several advances such as detailed NMR analyses on the Si−H bonding to transition metals[18] and neutron diffraction studies on sigma-silane complexes[19] paved the way for subsequent work on this field, and contributed to the faster development of this area. Indeed, there are numerous non-classical silane complexes nowadays, yet most of them are neutral species.[20] In comparison, there are very few cationic transition metal σ-silane complexes described in the literature. The reason for this lack of compounds might be related to the increased reactivity of the silane moiety, which is now activated to receive the attack from nucleophiles. A recent work has stablished a 'sililicity' scale where TM cationic σ-SiH complexes are on top of it (*i.e.* the silane fragment possesses a great silylium character).[21] Therefore, these complexes are elusive to isolation, given that the majority of the cationic compounds (Figure 5) have only been detected and

[18] E. Colomer, R. J. P. Corriu, C. Marzin, A. Vioux, *Inorg. Chem.,* **1982**, *21*, 368-373.

[19] U. Schubert, K. Ackermann, B. Wörle, *J. Am. Chem. Soc.,* **1982**, *104*, 7378-7380.

[20] J. Y. Corey, *Chem. Rev.,* **2016**, *116*, 11291-11435.

[21] D. H. Binh, M. Milovanović, J. Puertes-Mico, M. Hamdaoui, S. D. Zarić, J-P. Djukic, *Chem. Eur. J.,* **2017**, *23*, 17058-17069.

analysed by spectroscopic methods by a few groups, like Crabtree's,[22] Brookhart's,[23] Kubas's[24] and Nikonov's.[25]
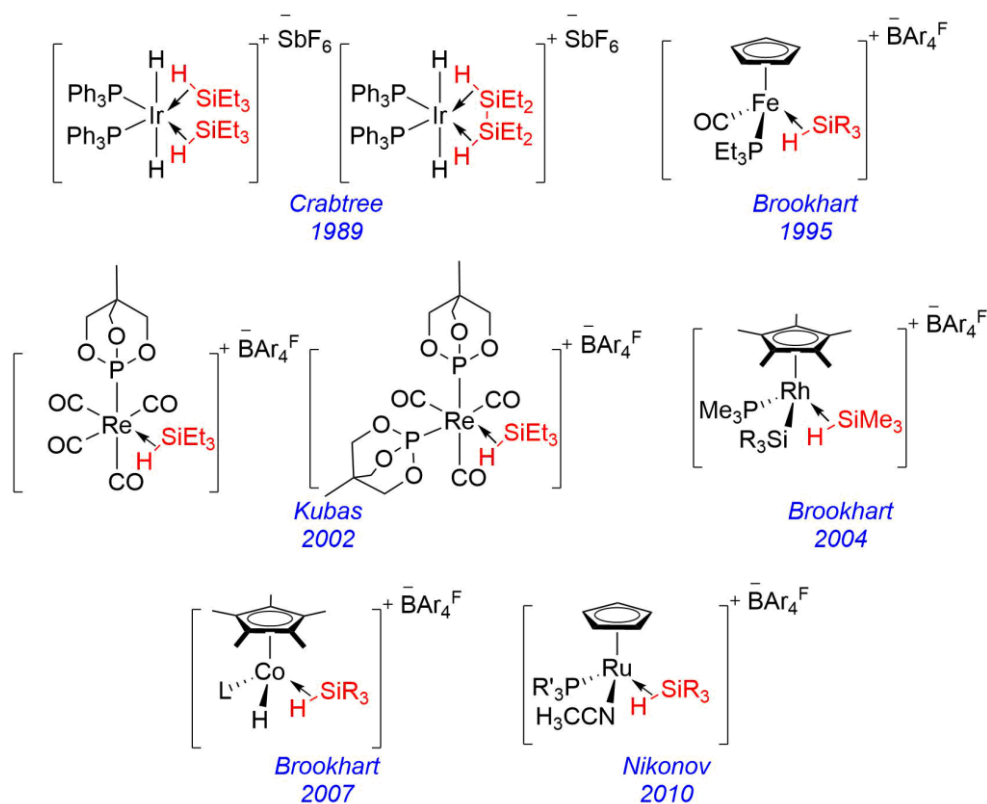
Figure 5. Detected cationic σ-silane transition metal complexes described in the literature.

To date, only two compounds have been successfully isolated and analysed by X-Ray crystallography apart from NMR spectroscopy. The first one to be crystallized was the Ru(II) η²-silane complex **Ru·HSiCl₃** described by

---

[22] X-L. Luo, R. H. Crabtree, *J. Am. Chem. Soc.,* **1989**, *111*, 2527-2535.

[23] a) E. Scharrer, S. Chang, M. Brookhart, *Organometallics,* **1995**, *14*, 5686-5694; b) F. L. Taw, R. G. Bergman, M. Brookhart, *Organometallics,* **2004**, *23*, 886-890; c) M. D. Doherty, B. Grant, P. S. White, M. Brookhart, *Organometallics*, **2007**, *26*, 5950-5960.

[24] X. Fang, B. L. Scott, K. D. John, G. J. Kubas, *Organometallics*, **2000**, *19*, 4141-4149.

[25] D. V. Gutsulyak, S. F. Vyboishchikov, G. I. Nikonov, *J. Am. Chem. Soc.,* **2010**, *132*, 5950-5951.

Lemke and coworkers in 2002 (Figure 6, left),[26] which is rather similar to those compounds stabilized by Cp and phosphine ligands described above. The second one is the (POCOP)Ir(III) complex **Ir·HSiEt$_3$** synthesized by Brookhart *et al.*, which is the only transition metal complex containing a η^1 coordination mode of a silane molecule (Figure 6, right).[27] In both cases, the hydrogen atom from the Si–H bond was located in the Fourier map, thus both structures could be completely characterized.

All these complexes have in common the weakly coordinating anions (usually BAr$_4$^{F})[28] so the vacant coordination site is available for the interaction with silane. It is remarkable that the hexafluoroantimonate anion[22] does not react to form Si–F bonds, considering that their formation is greatly favoured from a thermodynamic point of view (BDE$_{Si-F}$ = 137.9 kcal/mol).[29]
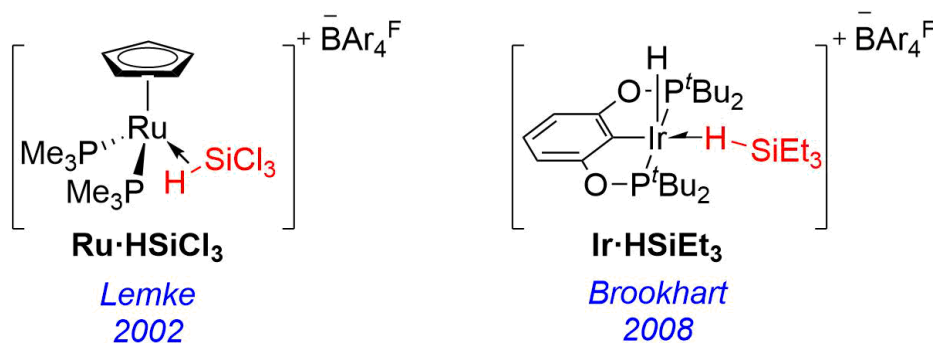
Figure 6. Cationic TM σ-silane complexes crystallographically characterized.

[26] S. T. N. Freeman, F. R. Lemke, *Organometallics,* **2002**, *21*, 2030-2032. This complex was previously synthesized and analysed before its crystallization: F. R. Lemke, *J. Am. Chem. Soc.,* **1994**, *116*, 11183-11184.

[27] J. Yang, P. S. White, C. K. Schauer, M. Brookhart, *Angew. Chem. Int. Ed.,* **2008**, *47*, 4141-4143.

[28] N. A. Yakelis, R. G. Bergman, *Organometallics,* **2005**, *24*, 3579-3581.

[29] Y-R. Luo, *Comprehensive Handbook of Chemical Bond Energies,* CRC Press: Boca Raton, FL, 2007.

As in the case of alkene hydrosilation, non-transition metal compounds can also form σ-silane complexes. In these species, wider E–H–Si angles (*i.e.* closer geometries to pure η^1 coordination modes) are found due to the almost non-existent backdonation to the antibonding σ* Si–H orbital (Table 1). There are some examples of crystal structures in the literature (Figure 7), like the borane-silane complex mentioned in Scheme 10 of Chapter 1,[30] the $Al(C_6F_5)_3$ Lewis acid mentioned above in Scheme 4 (which interacts with Et_3SiH)[13c] or the silane-stabilized silylium ion described by Reed *et al.*[31]
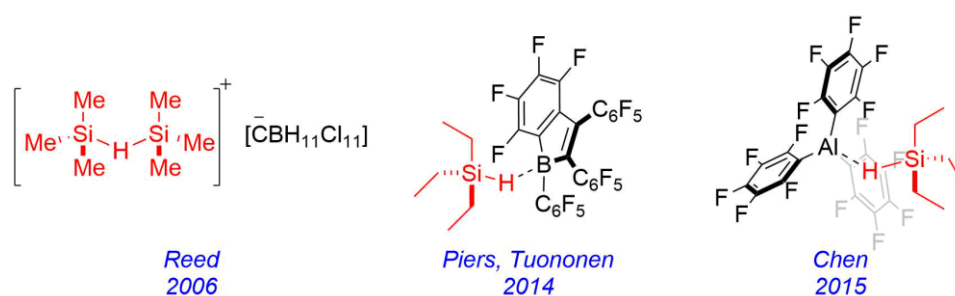
Figure 7. Examples of main-group σ-silane complexes crystallographically characterized.

Table 1 shows the Si–H–E angles for the species displayed in Figure 7 and complex **Ir·HSiEt₃** for comparison. The higher degree of silane activation is evident in the silylium-silane and alane-silane cases, where the angle is wider. For instance, the latter example had to be crystallized in hexanes, since toluene was basic enough to coordinate to the aluminium atom, precluding the formation of the complex. In the former, a carborane group had to be used as a non-coordinating anion so the silane was the most basic species in the reaction medium. All these examples reflect the difficulty in forming and isolating σ-silane complexes.

---

[30] A. Y. Houghton, J. Hurmalainen, A. Mansikkamäki, W. E. Piers, H. M. Tuononen, *Nat. Chem.,* **2014**, *6*, 983-988.

[31] S. P. Hoffmann, T. Kato, F. S. Tham, C. A. Reed, *Chem. Commun.,* **2006**, 767-769.

Species	E–H–Si / degrees	Reference
[(POCOP)Ir-HSiEt$_3$]$^+$	157	27
Borane-Silane	157	30
Silylium-Silane	160	31
Alane-Silane	174	13c

Table 1. Comparison of the angle in the E–H–Si fragment in some crystalized σ-silane complexes.

The vast majority of the complexes described above are composed of strong Lewis acids, so the silane can donate some electron density to them in the initial stages of the adduct formation. In fact, some authors have stated that the electrophilicity of the Lewis acid and/or transition metal complex is transferred to the silicon atom upon the development of the σ-SiH complex.[32]

Nonetheless, in light of all the information above, it is rather surprising that no mononuclear Pt σ-silane complexes have ever been reported in the literature regardless of the charge (neutral or cationic),[33] despite the great relevance of this metal in the hydrosilation and silicone industry.[1]

1.2. NHC-stabilized Pt(II) cationic complexes

Our group has extensive experience in the synthesis and characterization of cationic Pt(II) complexes stabilized by *N*-heterocyclic ligands.[34] These are strong Lewis acids, and its role in C–H[35] and H–H[36] activation processes has been

---

[32] M. C. Lipke, A. L. Liberman-Martin, T. D. Tilley, *Angew. Chem. Int. Ed.,* **2017**, *56*, 2260-2294.

[33] A Pt(0) agostic Si–H complex has been synthesized, though: S. J. Mitton, R. McDonald, L. Turculet, *Organometallics*, **2009**, *28*, 5122-5136.

[34] a) O. Rivada-Wheelaghan, B. Donnadieu, C. Maya, S. Conejero, *Chem. Eur. J.,* **2010**, *16*, 10323-10326; b) M. Roselló-Merino, O. Rivada-Wheelaghan, M. A. Ortuño, P. Vidossich, J. Díez, A. Lledós, S. Conejero, *Organometallics*, **2014**, *33*, 3746-3756.

[35] a) O. Rivada-Wheelaghan, M. A. Ortuño, J. Díez, A. Lledós, S. Conejero, *Angew. Chem. Int. Ed.,* **2012**, *51*, 3936-3939; b) M. A. Ortuño, S. Conejero, A. Lledós, *Beilstein J. Org. Chem.,* **2013**, *9*, 1352-1382.

[36] O. Rivada-Wheelaghan, M. Roselló-Merino, M. A. Ortuño, P. Vidossich, E. Gutiérrez-Puebla, A. Lledós, S. Conejero, *Inorg. Chem.,* **2014**, *53*, 4257-4268.

deeply studied by experimental and theoretical methods. More recently, the Lewis acidity of these compounds has been exploited in the dehydrocoupling of dimethylamine-borane when using cationic complex [Pt(I^{t}Bu')(I^{t}Bu)][BAr$_4^F$][37] **13** as a catalyst. Stoichiometric reactions and low temperature NMR studies along with DFT calculations disclosed a novel mechanism that involves the deprotonation of boronium cations (Scheme 6): first, the basicity of dimethylamine-borane makes it interact with **13**, in order to form a Shimoi-type, η^1-BH complex. Upon coordination, activation of the borane takes place and the electrophilicity is transferred to the boron atom, which can receive a nucleophilic attack from dimethylamine. The outcome of this step is the formation of neutral hydride **14** along with the boronium cation [(NHMe$_2$)$_2$BH$_2$]$^+$. The latter can dissociate an amine group in the presence of THF, which stabilizes the resulting new boronium species. In turn, this can protonate hydride **14** to release hydrogen and H$_2$B−NMe$_2$, regenerating catalyst **13**.[38]

---

[37] I^{t}Bu stands for 1,3-di-*tert*-butylimidazol-2-ylidene, whereas I^{t}Bu' represents the cyclometalated version of the NHC ligand.

[38] M. Roselló-Merino, J. López-Serrano, S. Conejero, *J. Am. Chem. Soc.,* **2013**, *135*, 10910-10913.
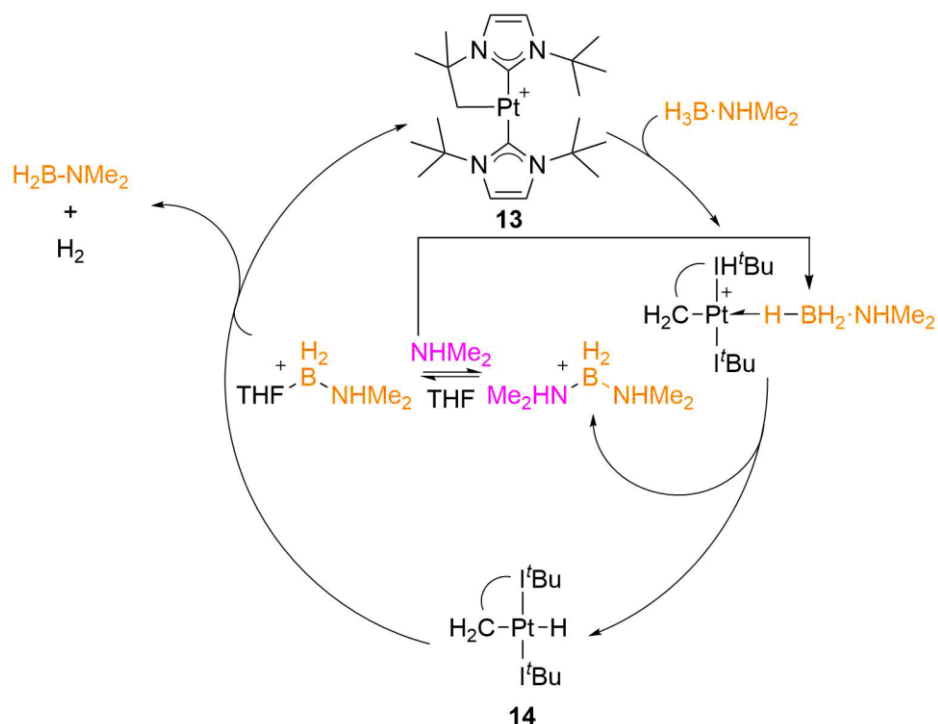
Scheme 6. Mechanism of the dehydrocoupling of dimethylamine-borane catalysed by Pt(II) complexes.

Although the formation of the Shimoi-type, η^1-BH complex was confirmed by spectroscopic methods, the high reactivity of $Me_2NH \cdot BH_3$ and $^tBuNH_2 \cdot BH_3$ towards dehydrocoupling prevented the isolation of such species even at low temperature. The employment of tertiary amines like $Me_3N \cdot BH_3$ also proved unfruitful, since it was too bulky to interact with catalyst **13**. However, the pyridine adduct $C_5H_5N \cdot BH_3$ was basic and compact enough to interact with the Pt atom, and the compound was crystallized, showing a η^1-BH coordination mode that supports the mechanism displayed above (Figure 8).[39]

---

[39] M. Roselló-Merino, R. J. Rama, J. Díez, S. Conejero, *Chem. Commun.,* **2016**, *52*, 8389-8392.
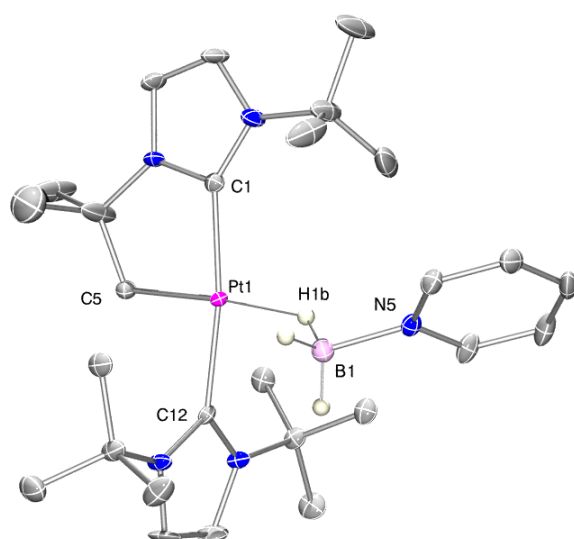
Figure 8. X-Ray structure of **13·C₅H₅N·BH₃**. Most of the hydrogen atoms have been omitted for clarity.

In this chapter, the interaction between NHC-stabilized Pt(II) complexes and hydrosilanes will be described. The resulting σ-SiH complexes derived from these contacts will be studied and their structure analysed in detail by experimental and theoretical methods. Similarly, the role of these species as intermediates in the formation of Pt–silyl derivatives (with or without concomitant formation of C−Si bonds) will be demonstrated.

2. Results and discussion

The aim of this work is to take advantage of the Lewis acidity shown by the Pt(II) compounds previously described in our group to promote the formation of σ-silane complexes.

2.1. Exploratory studies using Pt I^{t}Bu complexes

Experimental studies

In light of the results obtained from the interaction of **13** with amine-boranes, several hydrosilanes were added to **13** to evaluate their interaction by means of ^{1}H NMR spectroscopy (Scheme 7).

$R^a = R^b = R^c = Et$ (**13·Et$_3$SiH**)
$R^a = {}^nBu; R^b = R^c = H$ (**13·BuSiH$_3$**)
$R^a = R^b = Et; R^c = H$ (**13·Et$_2$SiH$_2$**)
$R^a = Ph; R^b = R^c = H$ (**13·PhSiH$_3$**)
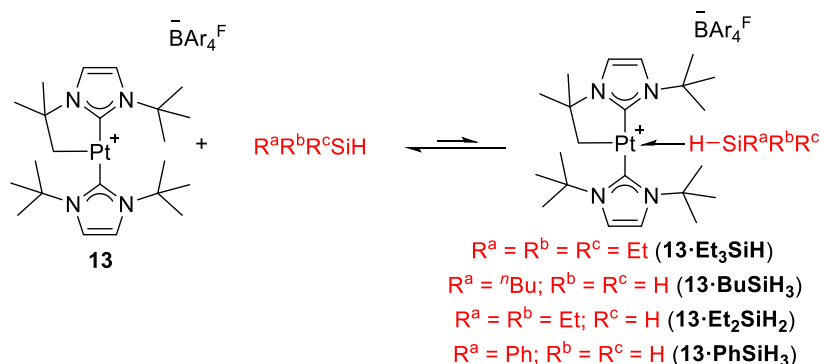
Scheme 7. Interaction between hydrosilanes and I^{t}Bu complex **13**.

Addition of Et$_3$SiH to the NMR tube containing a solution of the Pt complex in CD$_2$Cl$_2$ showed no evolution of the system regardless of the

[220]

temperature, since the bulkiness of the silane prevents the approach towards the metal center because of steric hindrance with the *tert*-butyl groups of the carbene ligands. In a different experiment, *n*-butylsilane (a smaller silane) did not show any difference at room temperature either, but upon lowering the temperature the Si−H protons started to shift to lower frequencies (from 3.5 ppm at r.t. to 2.2 ppm at -50 °C) along with the protons of the methylene group bound to Pt (Figure 9). At -50 °C, a ^{1}H-^{29}Si HMQC experiment revealed the deshielding of the Si atom upon silane coordination, since a cross-peak was observed at -48 ppm (free butylsilane resonates at -60 ppm).[40] Further cooling of the sample made the signals disappear in the baseline, yet a couple of broad peaks in a 2:1 ratio were detected at -90 °C at 3.9 and -4.4 ppm (Figure 10) that have been assigned to the terminal and bridging SiH protons, respectively, indicative of the slowdown of a dynamic event at the NMR timescale. No silicon satellites were observed because of the broadness of both peaks. However, NOESY experiments confirmed the exchange between the terminal and bridging protons of the silane molecule (Figure 11). These data seem to suggest the formation of a σ-silane complex between ^{n}BuSiH$_3$ and **13** (**13·BuSiH$_3$**). Similar shifts to lower frequencies were obtained when using PhSiH$_3$, albeit coalescence phenomena precluded the identification of terminal and bridging protons even at -90 °C. Warming up both samples to r.t. eventually gave rise to a mixture of unidentified products.

---

[40] The cross-peak between H and Si was lost at lower temperatures due to signal broadening and coalescence phenomena.
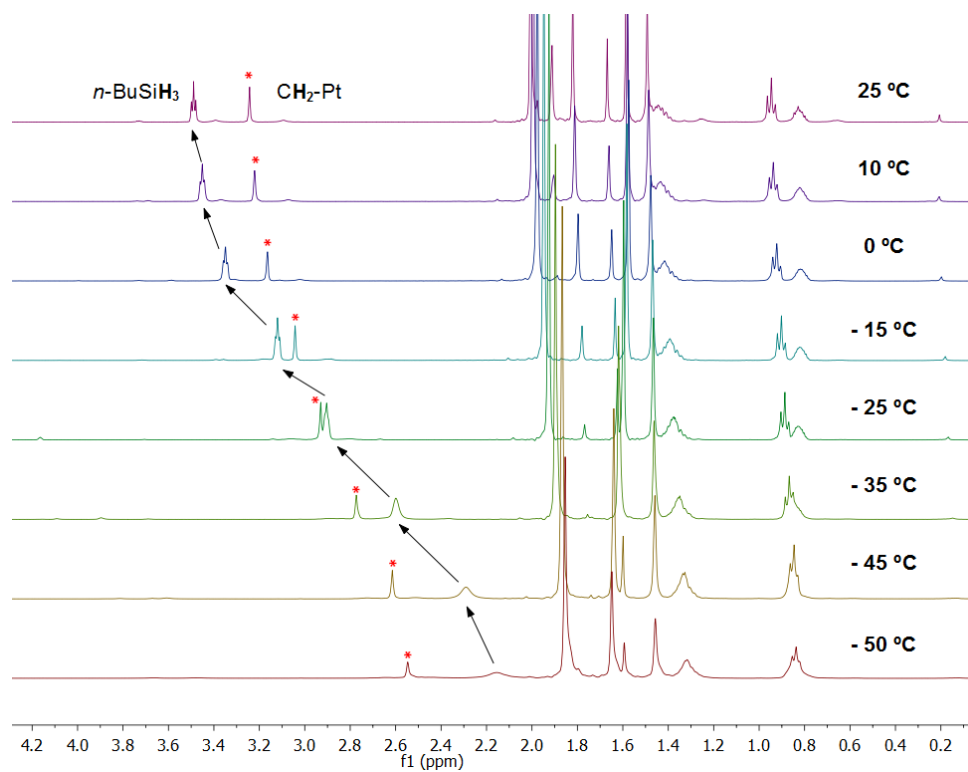
Figure 9. Portion of the ^{1}H NMR spectra (400 MHz, CD$_2$Cl$_2$) of the interaction between **13** and ^{n}BuSiH$_3$ from 25 to -50 °C.
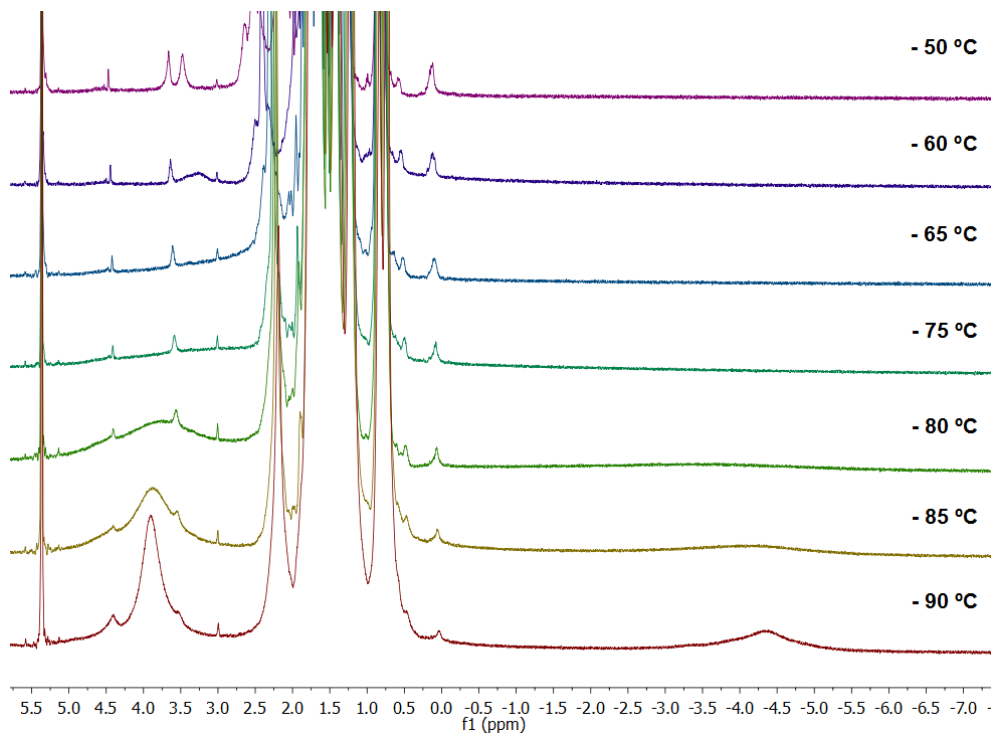
Figure 10. Portion of the ^{1}H NMR spectra (400 MHz, CD_2Cl_2) of the interaction between **13** and $^nBuSiH_3$ from -50 °C to -90 °C.
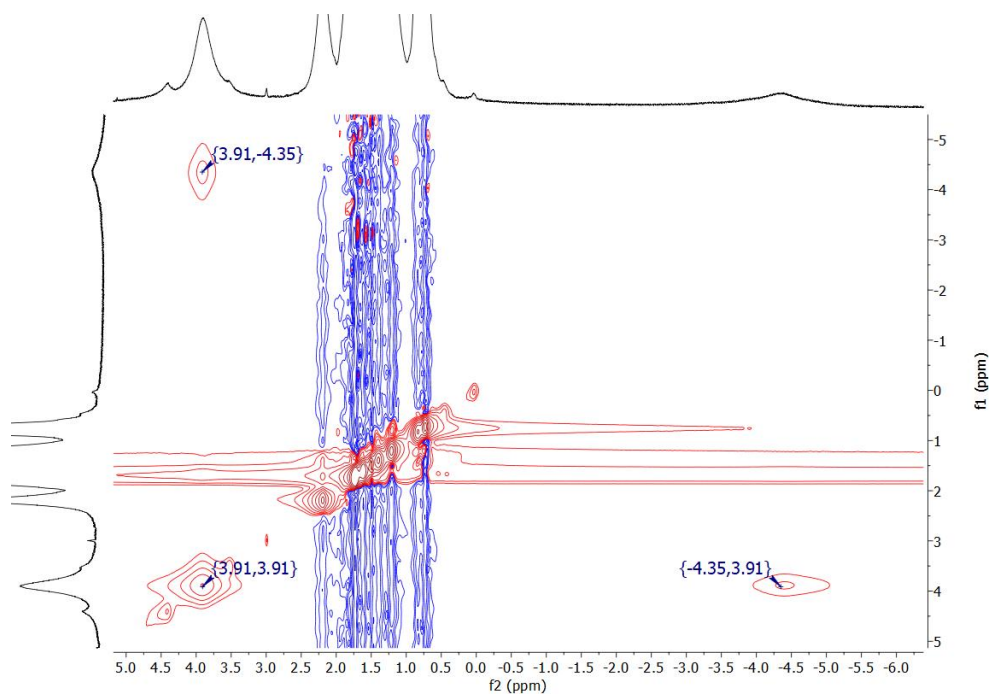
Figure 11. NOESY experiment (400 MHz, CD$_2$Cl$_2$) showing the inequivalence of the silane protons and its exchange on the NMR timescale.

Mixing Et$_2$SiH$_2$ and **13** showed the same evolution as with PhSiH$_3$ (*i.e.* upfield shift of the silane protons and loss of the peaks because of signal broadening):

[224]
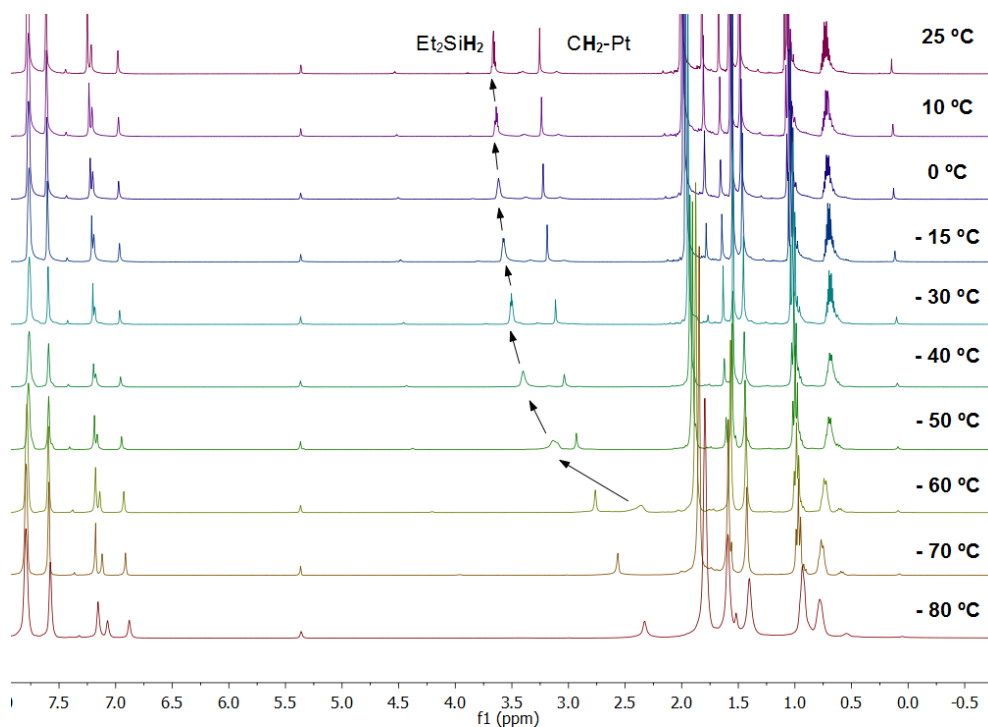
Figure 12. ^{1}H NMR spectra (400 MHz, CD2Cl2) of the interaction between **13** and Et2SiH2 from 25 °C to -80 °C.

Nevertheless, when the NMR tube containing **13** and 1 equivalent of diethylsilane was warmed up to room temperature, a slow but clean evolution was observed for several days to form two symmetrical species according to the NMR signals. These are hydride complex **15** and silyl derivative **16** (Scheme 8). The former was previously synthesized in our group by hydrogenation of **13**,[36] and its presence during this reaction might be due to the same process as a consequence of partial hydrolysis of the silane by adventitious water in the solvent that leads to the formation of dihydrogen, ending up in the partial formation of **15**. Indeed, the yield of silyl complex **16** can be increased and the reaction time shortened by using a large excess of Et2SiH2. Thus, when 30 equivalents of the silane are added, ^{1}H NMR shows full conversion of **13** after 15

[225]

minutes to give complex **16** with very small amounts of hydride **15** (typically around 5%, Figure 13).
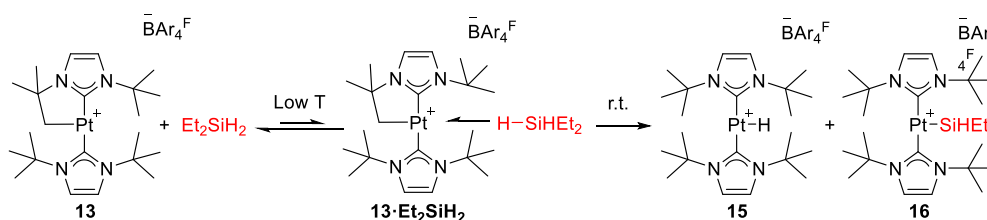
Scheme 8. Reaction between Et₂SiH₂ and complex **13**.
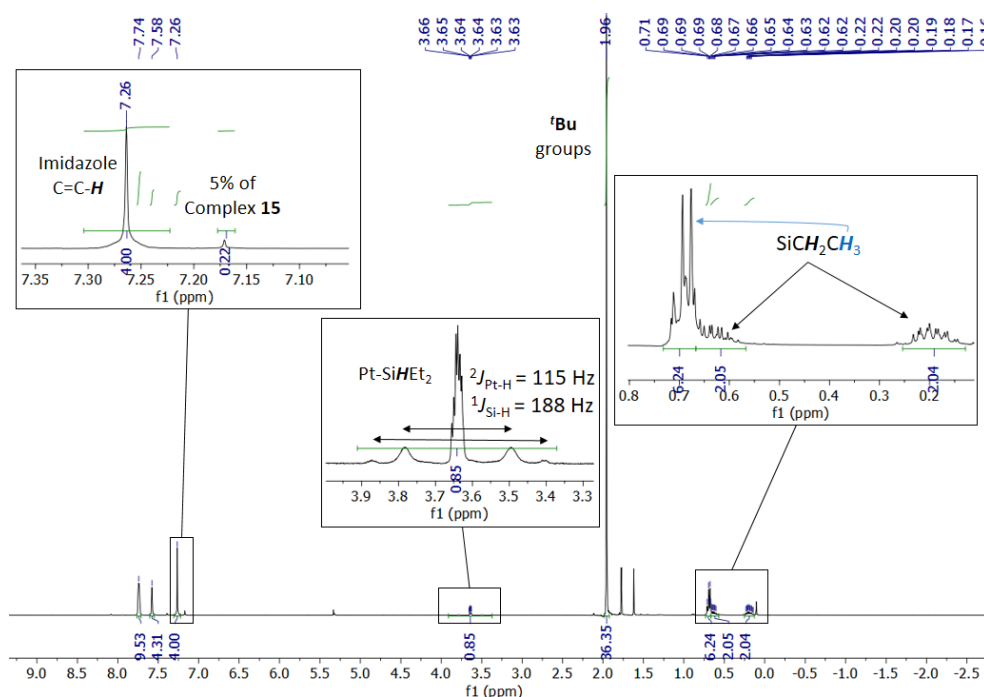
Figure 13. ¹H NMR spectrum (400 MHz, CD₂Cl₂) of complex **16** with small amounts of hydride **15**.

Silyl complex **16** is an unusual kind of compound. Cationic Pt(II)-silyl species have been barely studied experimentally[41] and theoretically.[42] The

[41] J. Voigt, T. Braun, *Dalton Trans.,* **2011**, *40*, 12699-12704
[42] M. Besora, F. Maseras, A. Lledós, O. Eisenstein, *Inorg. Chem.,* **2002**, *41*, 7105-7112.

formation of the Pt–Si bond in **16** is clearly evidenced by the characteristic peak in ^{1}H NMR at 3.64 ppm that corresponds to the SiH proton, which shows satellites to ^{195}Pt ($^2J_{\text{Pt-H}}$ = 115 Hz) and to ^{29}Si ($^1J_{\text{H-Si}}$ = 188 Hz). This signal also correlates with a peak at 18.1 ppm in the ^{1}H–^{29}Si HMQC NMR spectrum. With respect to the I^{t}Bu ligands, both of them appear equivalent according to NMR spectroscopy, clearly indicating that the CH$_2$–Pt unit in the original cyclometallated I^{t}Bu' ligand in **13** is no longer present. The proposed structure was confirmed by X-ray crystallography, showing the silyl ligand bound to the Pt atom (Pt–Si bond distance = 2.314(3) Å) and the *trans* arrangement of the NHC ligands (Figure 14). As seen below, a close contact between H9a and Pt (2.207(2) Å) and C9 and Pt (2.950(8) Å) points to an agostic interaction, which seems to stabilize the strong Lewis acidic Pt(II) center. Besides, Figure 14 shows the steric pressure of the ethyl chains on the carbene ligands, deviating the C12-Pt1-C1 angle from linearity (192.6 °). In contrast to complex **13**, which readily hydrogenates to yield hydride **15**,[36] complex **16** does not react with H$_2$, and it can be stored at -20°C without changing its chemical nature. However, it is thermally unstable towards cyclometalation, since appearance of cyclometalated species **13** along with Et$_2$SiH$_2$ was observed (25% conversion) after keeping the complex at room temperature for 5 days.

[227]
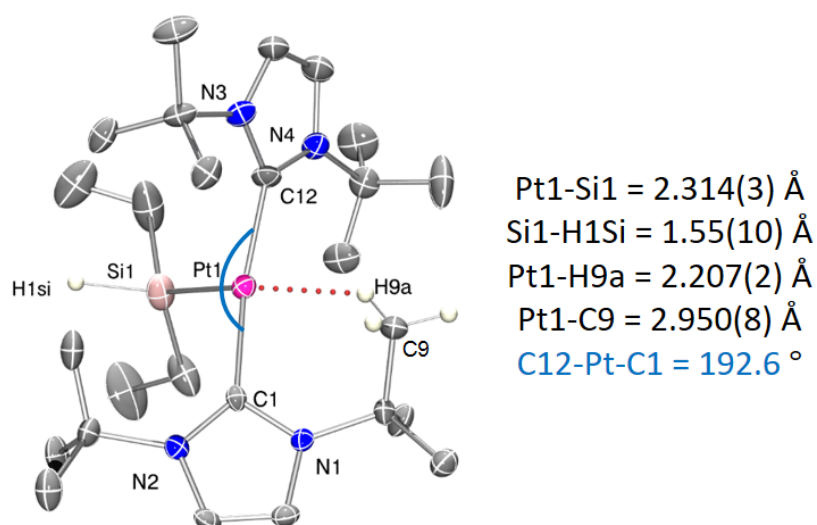
Figure 14. Crystal structure of silyl complex **16** and some selected structural parameters. BAr$_4^F$ anion and most of the hydrogen atoms have been omitted for clarity. The C$_{carbene}$−Pt−C$_{carbene}$ angle has been highlighted in blue.

Complexes **15** and **16** were also tested as Pt-based Lewis acids for the formation of σ-silane complexes. In this way, Et$_2$SiH$_2$ and ^{n}BuSiH$_3$ were added to dichloromethane solutions of the aforementioned compounds and their behaviour was evaluated by ^{1}H and ^{29}Si (HMQC) NMR spectroscopy at different temperatures. Nevertheless, no significant interaction was detected even at -90 °C, as observed in the example in Figures 15 and 16, showing the ^{1}H NMR spectra of a mixture of complexes **15** and **16** and *n*-butylsilane at different temperatures. It is also necessary to mention that neither **15** nor **16** react with silanes at room temperature.

[228]
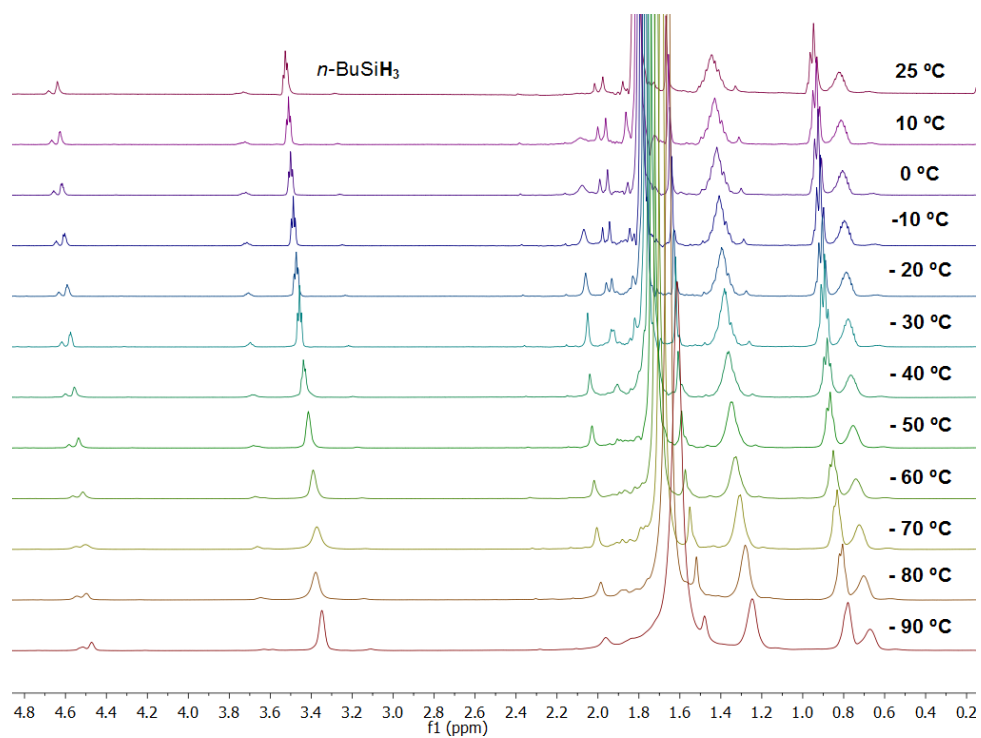
Figure 15. Portion of the ^{1}H NMR spectra (400 MHz, CD$_2$Cl$_2$) of the mixture of **15** and ^{n}BuSiH$_3$ from 25 °C to -90 °C.
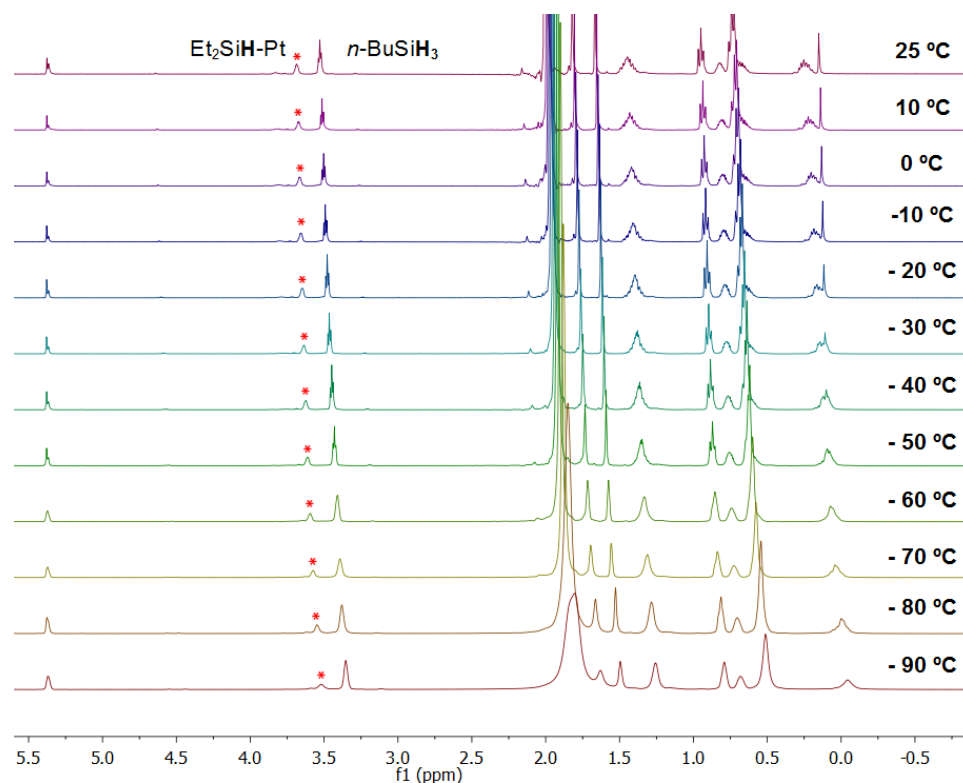
Figure 16. ^{1}H NMR spectra (400 MHz, CD_2Cl_2) of the mixture of **16** and ^{n}BuSiH$_3$ from 25 °C to -90 °C.

The lack of interaction between the Pt centre (in **15** and **16**) and the hydrosilane reminisces the different behaviour of **13** and **15** against $C_5H_5N \cdot BH_3$: whereas **13** reacted at r.t. to give the η^1-BH complex quantitatively, **15** only interacted at low temperatures, showing a mixture of bound and unbound amine-borane.[39] Chapter 4 also describes the greater activation of the silane in the case of **13** in comparison to **15** and **16** when exposing the σ-SiH complexes to a carbon dioxide atmosphere. In order to find an explanation for the higher degree of silane activation by **13**, computational DFT studies were performed on these systems.

[230]

Computational studies

The geometries of the σ-silane complexes of systems **13**, **15** and **16** with either Et_2SiH_2 or $^nBuSiH_3$ were optimized so as to evaluate the resulting structure and the coordination mode of the silanes, as well as the energy of the process (Figure 17). Regarding the latter aspect, the formation of all σ-complexes is exothermic, being the coordination to the cyclometalated complex **13** the most stable one, in agreement with the experimental observations. The calculated enthalpy values (from -12.8 to -8.2 kcal/mol, gas phase) are also in accordance with the absence of appreciable interaction at room temperature due to entropy loss.[43] As the temperature decreases, the entropic factor becomes smaller and the bonding more favourable. This was confirmed by calculating the Gibbs free energy (gas phase) of the complexes at different temperatures (Table 2).

13·BuSiH₃   **15·BuSiH₃**   **16·BuSiH₃**
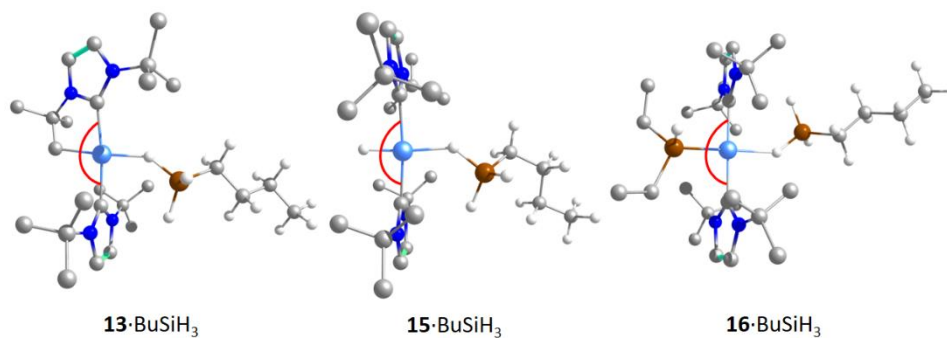
Figure 17. DFT-optimized structures for the σ-SiH complexes of **13, 15** and **16** upon coordination of $^nBuSiH_3$. Hydrogen atoms on the NHC ligands have been omitted for clarity. The $C_{carbene}-Pt-C_{carbene}$ angle has been highlighted in red.

---

[43] L. A. Watson, O. Eisenstein, *J. Chem. Educ.*, **2002**, *79*, 1269-1277.

Temperature	13·BuSiH$_3$	15·BuSiH$_3$	16·BuSiH$_3$	13·Et$_2$SiH$_2$	15·Et$_2$SiH$_2$	16·Et$_2$SiH$_2$
298 K (25 °C)	4.3	6.3	4.4	2.2	3.7	4.7
273 K (0 °C)	3.1	5.0	3.3	0.9	2.5	3.4
243 K (-30 °C)	1.6	3.6	2.0	-0.6	1.0	1.9
213 K (-60 °C)	0.1	2.1	0.6	-2.1	-0.5	0.4
183 K (-90 °C)	-1.4	0.6	-0.7	-3.7	-2.0	-1.1

Table 2. Calculated ΔG values for the formation of the σ-SiH complexes at different temperatures.

Concerning the geometry of the compounds, the calculated structures result in a η^1 coordination mode of the silane according to the wide Pt−H−Si angles[44] and the long Pt−Si distances (Table 3).[45] Complex **13** seems to give geometries closer to η^1 binding modes, where the cationic (silylium) character of the silane is increased according to the values of the natural charge on Si obtained by NBO analysis. The Pt−H distance is oddly long for derivatives of **16**, but it can be explained by the C−Pt−C angle as mentioned earlier: the angle of 182° evidences how the silyl group pushes one of the carbene ligands towards the silane, in the same manner as in the crystal structure of **16**. For this reason, steric factors force the silane to interact with the metal center in a more distant way.

---

[44] The Ir−H−Si angle in the only η^1 σ-silane complex crystallographically described is 157 ° (Reference 27).

[45] The sum of the covalent radii for Si (1.11 Å) and Pt (1.36 Å) is 2.47 Å. See: B. Cordero, V. Gómez, A. E. Platero-Prats, M. Revés, J. Echeverría, E. Cremades, F. Barragán, S. Alvarez, *Dalton Trans.,* **2008**, 2832-2838.

Species	Pt··H / Å	Pt··Si / Å	Si···H / Å	Pt–H– Si / °	C–Pt– C / °	Natural charge on Pt	Nat. charge on Si	Nat. charge on H(Si)	ΔH$_f$ (kcal/ mol)
13·BuSiH₃	1.97	3.33	1.53	145.25	173.28	0.08	1.10	-0.25	-10.5
15·BuSiH₃	1.95	3.24	1.53	137.09	174.75	-0.15	1.08	-0.23	-8.2
16·BuSiH₃	2.24	3.54	1.51	140.73	182.52	-0.18	1.04	-0.23	-8.7
13·Et₂SiH₂	1.96	3.44	1.53	159.07	171.46	0.10	1.41	-0.27	-12.8
15·Et₂SiH₂	1.94	3.39	1.53	154.82	175.45	-0.13	1.42	-0.27	-10.7
16·Et₂SiH₂	2.18	3.63	1.52	157.25	182.35	-0.17	1.35	-0.26	-10.2

Table 3. Calculated geometrical, electronic and energetic parameters of the optimized structures obtained for the σ-silane complexes derived from species **13**, **15** and **16**. ΔH$_f$ = enthalpy of formation.

Analysis of the calculated geometries reveals some differences between the studied systems. Figure 18A shows the dihedral angle formed by both carbene planes. Whereas in **15·BuSiH₃** and **16·BuSiH₃** both carbene ligands are practically eclipsed (dihedral angles close to 0°), complex **13** displays a perpendicular or staggered arrangement of the carbene fragments (dihedral angle = -100.8°) . In principle, this situation would render a more accessible platinum atom in hydride **15** or silyl **16**, favouring a stronger binding of the hydrosilane**,** contrary to the experimental and the previous theoretical data. Nonetheless, the cyclometalated fragment in **13·BuSiH₃** is greatly distorted, as evidenced from the M−C$_{carbene}$−C$_{centroid}$ angle (Θ, Figure 18B) as described by Chaplin, Tonner *et al.*[46] In comparison to numerous examples in the literature, the value of this angle in complex **13·BuSiH₃** (Θ = 165.9 °) is considerably deviated from linearity, unlike derivatives **15·BuSiH₃** and **16·BuSiH₃** (Θ ∼176 °). This distortion is mainly due to yawing (in-plane) tilting (Figure 18B), given that |∠PtC$_{carbene}$N-∠PtC$_{carbene}$N'| = 27.5 ° and the almost linear C−Pt−C arrangement (173 °), which rules out major contributions from pitching (out-of-plane) phenomena. A closer look to the calculated structures without silane

---

46 J-N. Luy, S. A. Hauser, A. B. Chaplin, R. Tonner, *Organometallics*, **2015**, *34*, 5099-5112.

(Figure 18C) indicates that, unlike complexes **15** and **16**, cyclometallated species **13** retains its structure to a greater extent with and without silane, minimizing any entropic penalty due to conformational rigidity that might arise during adduct formation (*i.e.* the preorganization degree in compound **13** is higher). This means that **13** does not need to rearrange its ligands in order to accommodate a silane molecule, which requires less energy. Whereas these steric reasons might explain the different behaviour between these systems, the strong *trans* influence exerted by silyl and hydride ligands[47] surely play a role as well during the coordination of silanes, hampering the interaction between the platinum center and the Si−H unit.

---

[47] J. Zhu, Z. Lin, T. B. Marder, *Inorg. Chem.,* **2005**, *44*, 9384-9390.
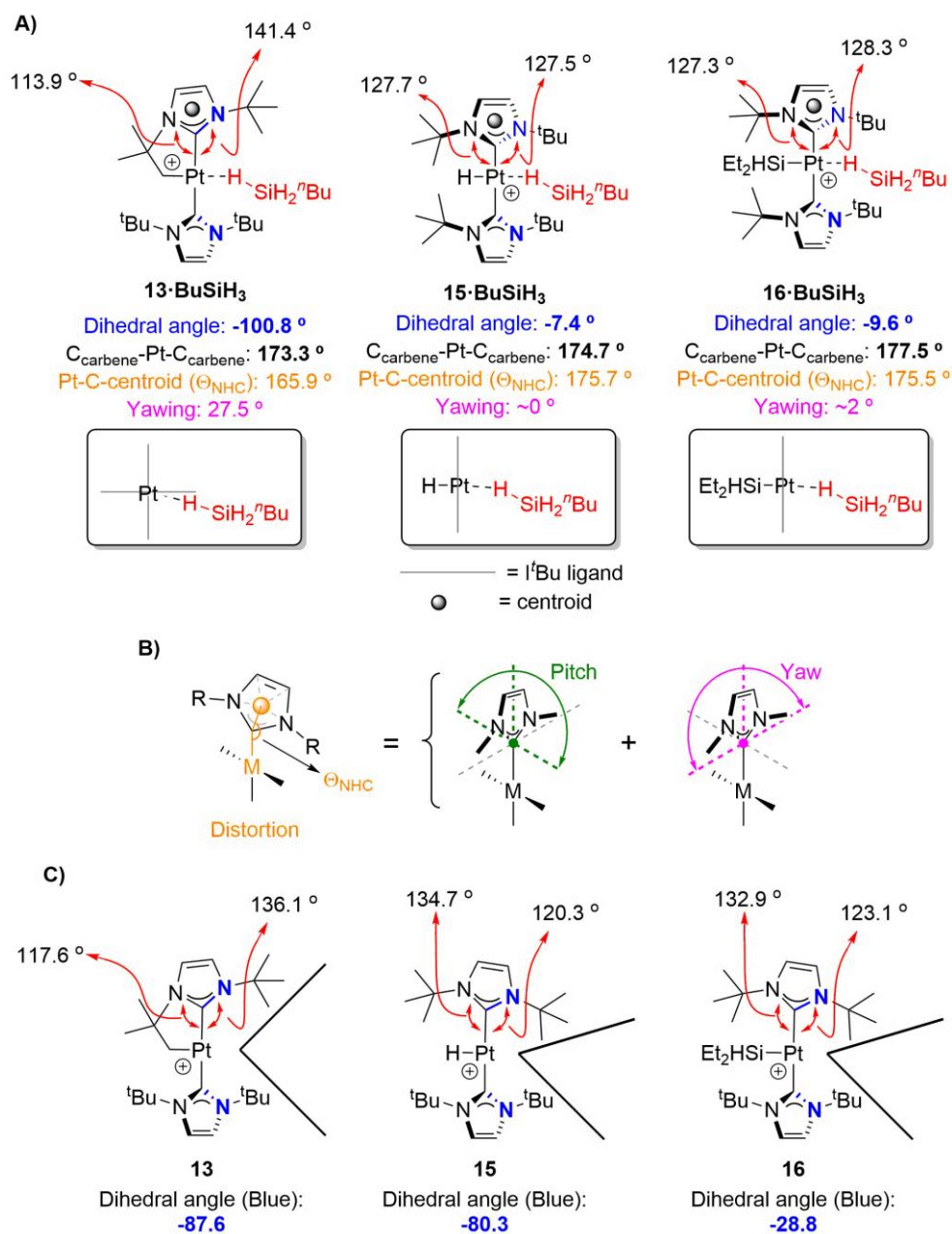
Figure 18. Steric differences between DFT calculated structures of **13·BuSiH₃**, **15·BuSiH₃** and **16·BuSiH₃** (A) and **13**, **15** and **16** (C) that may account for the different reactivity against silanes. B) Contributions of pitching and yawing motions to the M−C_carbene−C_centroid angle (Θ) (adapted from reference 46).

[235]

Finally, it is necessary to mention that numerous attempts were carried out to crystallize σ-silane complexes derived from species **13**. Unfortunately, the majority of the experiments led to the formation of oils, or they afforded no crystals. This is consistent with the weak interaction observed by low temperature NMR studies. However, crystals of complex **15** were accidentally obtained in several cases. The crystal structure of hydride **15** (elusive so far) was determined by X-Ray diffraction techniques, and it will be discussed at the end of this chapter.

2.2. Carbene modifications for improvement of Pt-silane interactions

Section 2.1. showed how weak the interactions between hydrosilanes and Pt(II) I^{t}Bu complexes are. These results seemed to indicate that the *tert*-butyl groups on the carbene ligands are probably too bulky to accommodate a silane molecule close to the platinum atom. For this reason, less hindered carbenes are likely required to provide more room for the reagent to interact with the metal, but we knew from previous results that the use of smaller carbenes such as I^{i}Pr$_2$Me$_2$ (I^{i}Pr = 1,3-diisopropyl-4,5-dimethylimidazol-2-ylidene) might compromise the stability and reactivity of their platinum complexes.[34b] Therefore, the unsymmetrical carbene I^{t}Bu^{i}Pr (containing *tert*-butyl and *iso*-propyl groups as substituents) was designed. In order to synthesize unsaturated 14-electron Pt(II) complexes similar to **13**, the strategy previously followed in our group was attempted, which involved the use of the Pt reagent [PtMe$_3$I]$_4$.[48] Reaction of the NHC ligands with the Pt tetramer usually affords PtMeI(NHC)$_2$ species upon release of ethane. Halide abstraction by reagents such as NaBAr$_4$^{F} (Sodium Tetrakis[(3,5-trifluoromethyl)phenyl]borate)[28] would yield the electron-deficient cationic species that undergo cyclometalation at r.t. or upon heating[34a] (Scheme 9):

---

[48] J. C. Baldwin, W. C. Kaska, *Inorg. Chem.,* **1979**, *18*, 686-691.
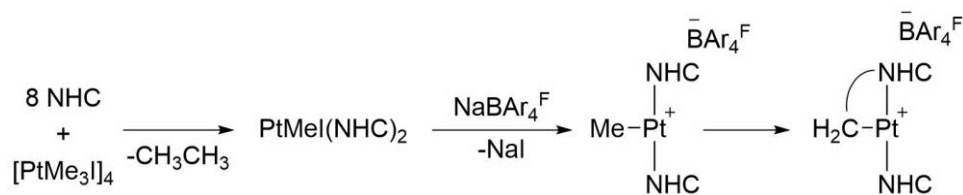
Scheme 9. General strategy for the obtainment of unsaturated 14-electron Pt(II) species stabilized by NHC ligands.

However, this strategy failed, since reaction with the Pt tetramer gave a mixture of unidentified compounds. This has also been observed in our group for some carbenes,[34b] so a different approach was adopted, which involves the use of $PtMe_2(COD)$[49] as a platinum precursor (Scheme 10A). This methodology has already been described by the group of Nolan for the synthesis of dimethyl Pt(II) complexes stabilized by small NHCs.[50] Then, protonation of the dimethyl complex with 1 equivalent of $H(Et_2O)_2BAr_4^F$ would produce the cationic species upon methane release, as previously described in our group.[34b] Thus, the synthetic pathway depicted in Scheme 10B was envisaged:

---

[49] R. Bassan, K. H. Bryars, L. Judd, A. W. G. Platt, P. G. Pringle, *Inorg. Chim. Acta*, **1986**, *121*, L41-L42.

[50] G. C. Fortman, N. M. Scott, A. Linden, E. D. Stevens, R. Dorta, S. P. Nolan, *Chem. Commun.,* **2010**, *46*, 1050-1052.
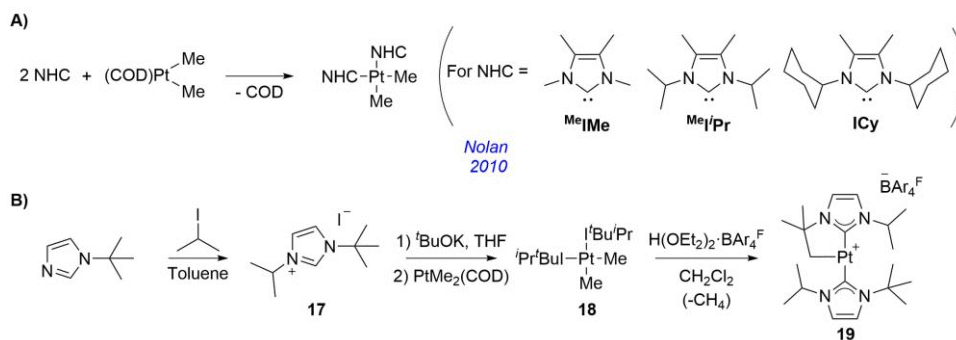
Scheme 10. A) General strategy employed by Nolan *et al.* for the synthesis of dimethyl Pt(II) complexes stabilized by small NHCs (adapted from reference 50). B) Synthetic pathway of coordinatively unsaturated complex **19**.

Starting from 1-*tert*-butylimidazole, reaction with 2-iodopropane for 24 h in toluene at 100 °C makes imidazolium salt **17** precipitate in the reaction medium in almost quantitative yield (Scheme 10B). Subsequent deprotonation with potassium *tert*-butoxide yields the corresponding carbene, which reacts *in situ* with the platinum precursor PtMe$_2$(COD) affording *cis*-[Pt(CH$_3$)$_2$(I^{t}Bu^{i}Pr)$_2$] **18** in 67% yield. This solid contains small amounts of what seems to be either the isomer *trans*-[Pt(CH$_3$)$_2$(I^{t}Bu^{i}Pr)$_2$] or a conformational isomer (Figure 19). Stirring the mixture of isomers in dichloromethane for a few hours gives only one species with a *cis* arrangement of the ligands. There are some characteristic spectroscopic features of this complex: one of them is the presence of satellite peaks for the methyl groups bound to the metal due to coupling with ^{195}Pt ($^2J_{Pt-H}$ = 68 Hz), which are similar to those observed for similar carbenes such as I^{i}Pr$_2$Me$_2$ ($^2J_{Pt-H}$ = 65 Hz).[51] On the other hand, the methine protons of the *iso*-propyl groups are strongly deshielded (they resonate at 6.52 ppm). This phenomenon might be attributable to the presence of an anagostic interaction

---

[51] *"Complejos de metals de transición conteniendo ligandos de tipo carbeno N-heterocíclico de 5 y 6 miembros. Síntesis y estudios de reactividad."* M. Roselló-Merino. PhD Thesis. **2013**.

(Figure 20).[52] In fact, the methine carbon shows satellite peaks due to coupling with ^{195}Pt ($^3J_{Pt-C}$ = 52 Hz) in the ^{13}C{^{1}H} NMR spectrum (Figure 21), in the same way as observed in other Pt(II) systems.[53]
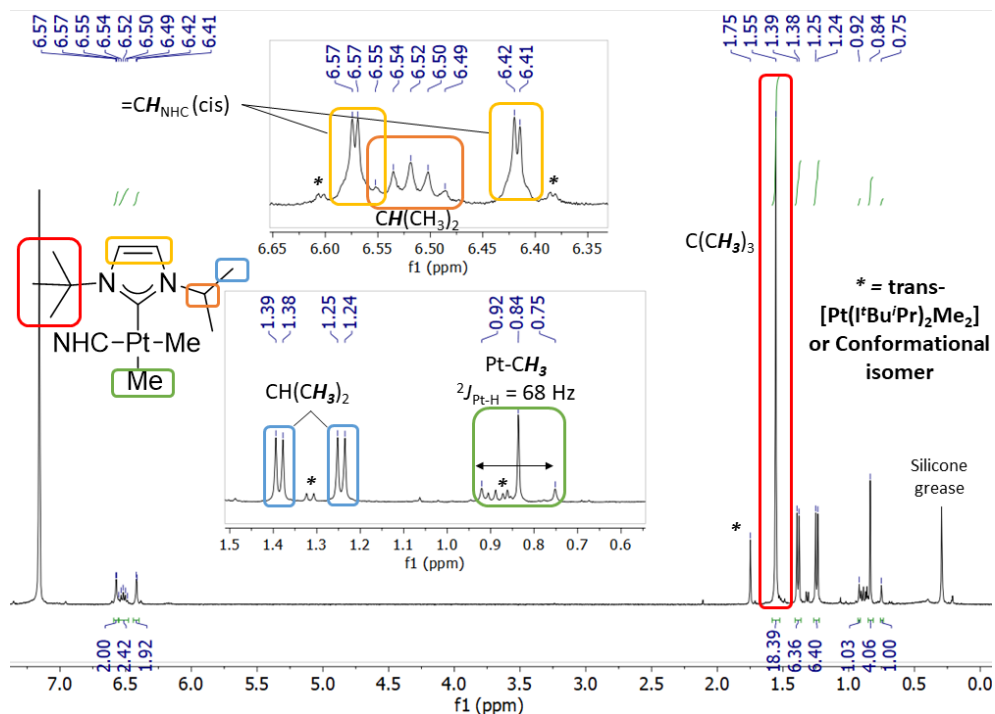
Figure 19. ^{1}H NMR spectrum (400 MHz, C$_6$D$_6$) of the synthesis of complex **18**, showing the presence of both geometrical or conformational isomers.

[52] M. Brookhart, M. L. H. Green, G. Parkin, *Proc. Natl. Acad. Sci. U. S. A.,* **2007**, *104*, 6908-6914.

[53] E. S. Tabei, H. Samouei, M. Rashidi, *Dalton Trans.,* **2011**, *40*, 11385-11388.
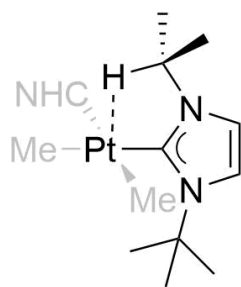
Figure 20. Visualization of the anagostic interaction observed in complex **18**.
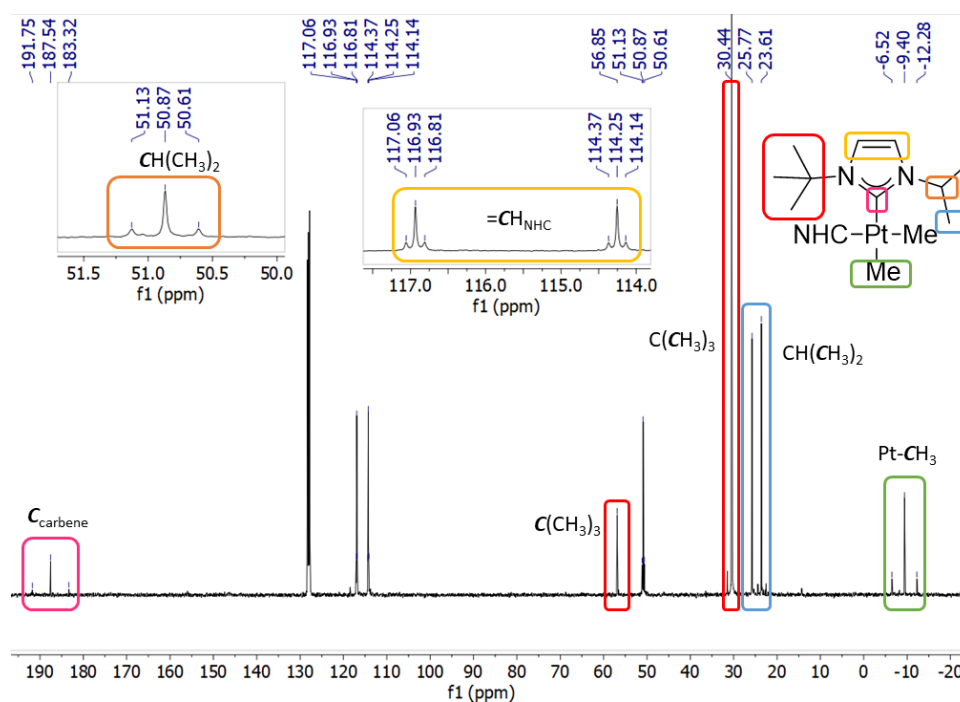
Figure 21. ^{13}C{^{1}H} NMR spectrum (400 MHz, C$_6$D$_6$) of complex **18**, where the satellite peaks to ^{195}Pt ($^3J_{Pt-C}$ = 52 Hz) of the methine carbons (inset, orange square) can be observed.

The last step for the synthesis of complex **19** is the protonation of **18**. This process takes place through a platinum-methyl intermediate [Pt(Me)(I^{t}Bu^{i}Pr)$_2$]$^+$, but at this point cyclometalation leading to **19** might take place, in principle, either at the *tert*-butyl or the *iso*-propyl groups. However, previous work in our group showed that cyclometalation of *tert*-butyl groups in

[240]

these complexes is much more favoured over *iso*-propyl ones, since the former takes place at low temperatures[34a] and the latter requires heating.[34b] Therefore, protonation of one of the methyl groups in complex **18** with Brookhart's acid[54] in dichloromethane leads to a very clean and selective reaction with the cyclometalation at one of the *tert*-butyl groups (with concomitant release of methane). As previously observed for some other complexes, coordinating solvents can bind to the metal, observing a decrease in the magnitude of the $^2J_{Pt-H}$ of the methylene protons.[55] For this reason, the remaining diethyl ether was removed by dissolving the complex in dichloromethane and evaporating the solvents under vacuum several times. The resulting species gives NMR data consistent with the proposed cyclometalation mode (Figure 22). As a result, a methylene group coming from the *tert*-butyl fragment is bound to the metal, with coupling constants ($^2J_{Pt-H}$ = 103 Hz in ^{1}H NMR and $^1J_{Pt-C}$ = 860 Hz in ^{13}C{^{1}H} NMR), slightly smaller than those observed in similar compounds like **13** ($^2J_{Pt-H}$ = 120 Hz and $^1J_{Pt-C}$ = 975 Hz).[55] Crystalline material can be obtained by solvent diffusion methods, yet the crystals are not of enough quality for X-Ray diffraction analysis.

[54] M. Brookhart, B. Grant, A. F. Volpe Jr., *Organometallics*, **1992**, *11*, 3920-3922.
[55] *"Síntesis de complejos coordinativamente insaturados de Pt(II) estabilizados por ligandos carbeno N-heterocíclicos. Activación y funcionalización de enlaces C−H."* O. Rivada-Wheelaghan. PhD Thesis. **2013**.
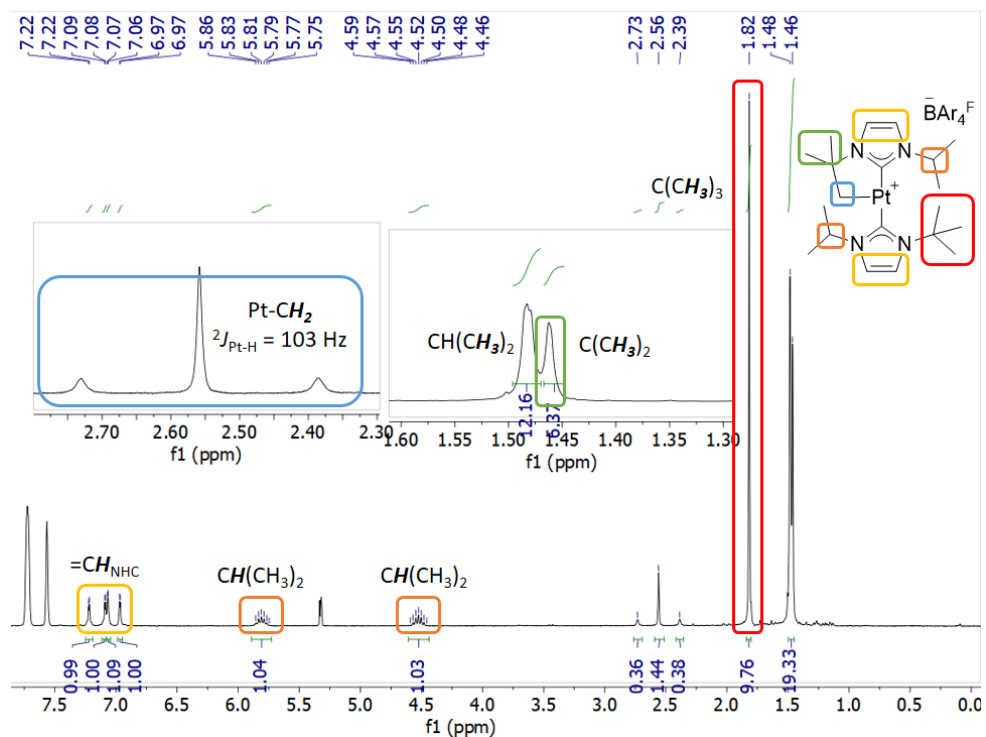
Figure 22. ^{1}H NMR spectrum (400 MHz, CD$_2$Cl$_2$) of complex **19**.

With the less bulky complex **19** in hand, low-temperature NMR studies with several silanes were performed so as to evaluate the behaviour of the newly synthesized system (Scheme 11).
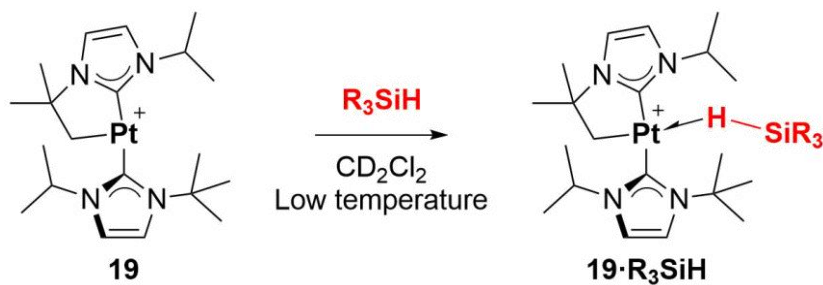
Scheme 11. Formation of σ-silane complexes derived from **19**.

Clean formation of a single species was observed in all cases when 1 equivalent of silane was added at low temperature (-30 °C), consistent with the

[242]

formation of a σ-SiH complex. Removal of just one methyl group from the substituent on the NHC was enough to get a stronger interaction of the silane: much sharper signals were obtained at higher temperatures than those required for **13**, indicative of a tighter binding. In addition, the peaks are sharp enough to observe satellite peaks of the bridging hydrogen atom due to coupling to [195]Pt and [29]Si (Table 4 and Figure 23). Another evidence indicative of silane coordination comes from the decrease in the $^2J_{Pt-H}$ coupling constant of the methylene fragment Pt−CH$_2$, which is typically observed when a ligand is bound in a *trans* position to the CH$_2$ group.[55] As an example, $^2J_{Pt-H}$ has a value of 103 Hz in complex **19**, but coordination of Et$_3$SiH makes this parameter drop to 87.5 Hz and 65 Hz (inequivalent protons) in **19·Et$_3$SiH**. Moreover, an upfield shift is obtained in all cases for the bridging hydrogen atoms, consistent with the increase in hydride character upon polarization of the Si−H bond.

Complex	δ ^1H (ppm)	δ ^{29}Si (ppm)	$^1J_{Pt-H}$ (Hz)	$^1J_{Si-H}$ (Hz)	Free silane (25°C)
					δ ^1H/δ ^{29}Si
19·Et$_3$SiH	-4.9	11.5	398	79	3.50 / 0 ppm (-60°C)
19·Me$_2$PhSiH	-4.3	-8.6	410	85	4.53 / 0.5 ppm
19·Ph$_3$SiH	-4.0	-15.6	410	-[a]	5.48 / -19 ppm
19·PhSiH$_3$	-4.8	-51.4	435	74	4.23 / -60.2 ppm
19·nBuSiH$_3$	-5.4	-48.2[b]	444	-[a]	3.52 / -60 ppm

Table 4. Selected spectroscopic parameters of the σ-Silane complexes obtained with species **19** at -30 °C. [a] Not determined because of signal broadness. [b] Determined at -50 °C.

[243]
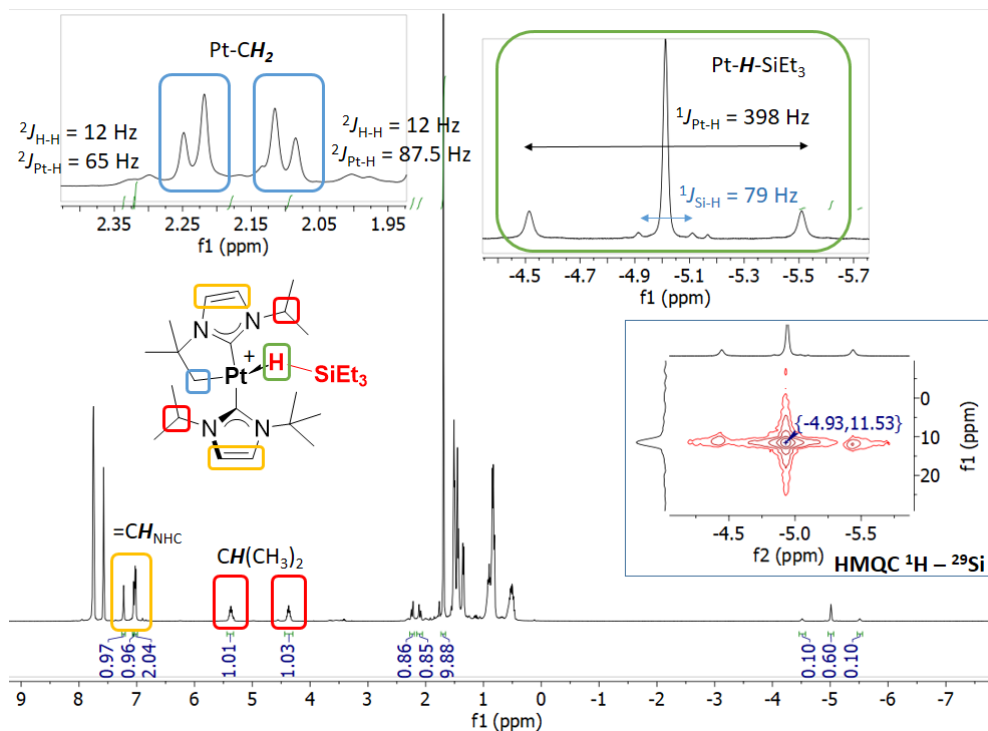
Figure 23. ^{1}H NMR spectrum (400 MHz, CD$_2$Cl$_2$, -30 °C) of complex **19·Et$_3$SiH**. Inset (bottom right): HMQC [1]H−[29]Si experiment, where the cross-peak of the bridging hydride with the Si atom can be observed.

Complex **19·Et$_3$SiH** is an excellent example to be compared to the previously reported complex **Ir·HSiEt$_3$** described by Brookhart *et al.,*[27] given that in both cases Et$_3$SiH is employed as silane. The [1]H−[29]Si HMQC spectrum shows a cross-peak of the bridging hydride with a signal at 11.5 ppm, which is shifted 11.5 ppm downfield with respect to that of the free silane.[56] This phenomenon reflects the deshielding of the Si atom in the presence of the Lewis-acidic Pt(II) species, which enhances the electrophilicity of the silane.[32] In addition, both Pt and Ir systems display the same ^{1}H chemical shifts for the bridging hydride (-4.9

---

[56] Free Et$_3$SiH: ^{1}H NMR (600 MHz, 213 K, CD$_2$Cl$_2$): δ 3.50 (sept, 1 H, [1]J_{Si-H} = 173.6 Hz) ppm, ^{29}Si NMR (119 MHz, 213 K, CD$_2$Cl$_2$): δ 0.0 (s) ppm. See: M. Hamdaoui, C. Desrousseaux, H. Habbita, J-P. Djukic, *Organometallics*, **2017**, *36*, 4864-4882.

ppm) with identical coupling constants to ^{29}Si ($^1J_{\text{Si-H}}$ = 79 Hz), which points out to a η^1 coordination mode, since a smaller J value would suggest a stronger debilitation of the Si−H bond resulting from a higher degree of backbonding from the metal atom, typical for η^2 Si−H compounds.[57]

These adducts are stable at low temperatures (usually below 0 °C). Therefore, in order to isolate any of these species and to confirm their geometry, numerous crystallization attempts were performed by trying different silanes, solvents and crystallization conditions. Fortunately, crystals of **19·Et₃SiH** were stable enough to be measured by X-Ray diffraction methods (Figure 24).

Experimental (X-Ray)   **Calculated (DFT)**
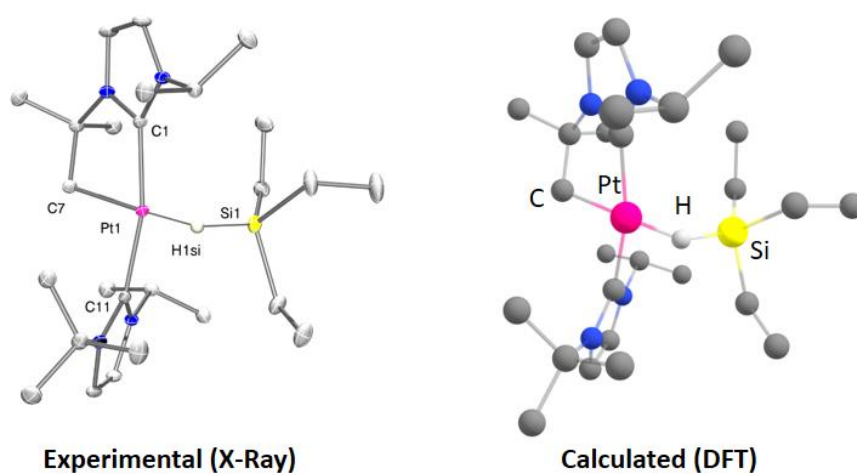
Figure 24. X-Ray and calculated structures of **19·Et₃SiH**. BAr₄^F anion and all hydrogen atoms except the bridging hydride have been omitted for clarity.

As previously observed by NMR experiments, the crystal structure shows a *trans* arrangement of both NHCs, being one of them cyclometalated. The methylene moiety is located trans to the hydrogen atom of Et₃SiH (C7−Pt1−H1Si: 173.1(1)°), which was located in the Fourier map. It is bound to Si (H1$_\text{Si}$−Si1:

---

[57] W. Scherer, P. Meixner, K. Batke, J. E. Barquera-Lozada, K. Ruhland, A. Fischer, G. Eickerling, K. Eichele, *Angew. Chem. Int. Ed.,* **2016**, *55*, 11673-11677.

1.66(3) Å) and Pt (Pt1–H1$_{Si}$: 1.58(3) Å) forming an angle of 103(2)°. This value suggests that **19·Et$_3$SiH** possesses a silane geometry intermediate between η^1 and η^2 coordination modes. However, there seems to be no formal Pt–Si bond since the distance found (2.53(1) Å) is longer than the sum of the covalent radii for Pt and Si (2.47 Å)[45] and that found for Pt(II)–silyl derivatives (~2.3 Å, Figure 14). Moreover, the formation of an η^2 complex would place the C–Pt bond in the bisection of the Si–H linkage (Figure 25, right). Instead, the experimental structure shows the initial stage of this process (given the C–Pt–Si angle), since the first step involves the approach of the silane through the hydrogen atom (with hydride character, Figure 3) prior to the pivoting motion around such bridging hydride (Figure 25).[15]
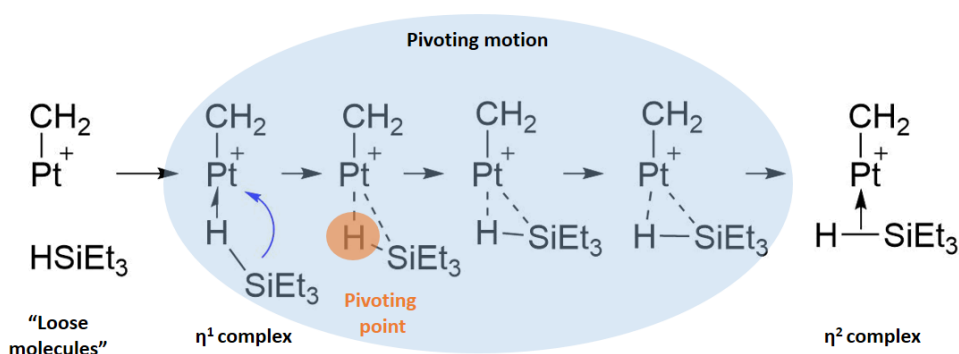
Figure 25. Schematic view of the motion between η^1 and η^2 coordination modes in a σ-SiH complex.

The detection and isolation of this type of complexes demonstrates that ligand design and the Lewis acidity of the metal are crucial. In fact, this contradicts several other strategies employed for avoiding η^2 geometries and/or Si–H bond cleavage, such as a) the use of 1st row transition metals (since their contracted d-orbitals do not overlap enough with the ligand orbitals); b) the presence of π acidic auxiliary ligands like CO or PF$_3$ (which delocalize the metal electrons); c) high oxidation states on the metal (which contract the d-orbitals).[15]

[246]

Computational studies

Nonetheless, DFT studies[58] were carried out on this system in order to gather additional data that could help to explain the interaction between Et_3SiH and complex **19**. In a first approach, the geometry of **19·Et₃SiH** was optimized, and an excellent agreement between the calculated and the experimental structure was observed (Figure 24 and Table 5), with slight disparity in the Pt–Si and Pt–H bond lengths. Thus, the selected functional and basis set accurately reproduce this system. The presence of the non-coordinating anion BAr_4^F produces an insignificant effect on the geometrical parameters of the sigma complex (Table 5).

	X-Ray	DFT (no BAr_4^F)	DFT (BAr_4^F)
C–Pt (Å)	2.082(2)	2.084	2.082
Pt–H (Å)	1.58(3)	1.716	1.726
Si–H (Å)	1.66(3)	1.651	1.642
Pt–Si (Å)	2.532(2)	2.631	2.642
Pt–H–Si (°)	102.9	102.8	103.3
C7–Pt–H (°)	173.1(11)	171.3	172.2
C–Pt–C (°)	166.74(9)	166.9	167.3

Table 5. Comparison of the experimental and calculated geometrical parameters of complex **19·Et₃SiH** in the presence and absence of the BAr_4^F anion.

The QTAIM methodology (Quantum Theory of Atoms In Molecules) was applied to perform a topological analysis of the electron density of this complex. However, studying the electron density function is not appropriate, since it does not define spatial regions beyond the atomic center. Instead, the laplacian of the electron density ($\nabla^2\rho(r)$) is usually interrogated, given that it measures its local

---

[58] Calculations were carried out at the TPSSh-D3/6-31g(d,p)/SDD//TPSSh-D3/6-311++G(2d,p)/def2QZVP level of theory. SMD (Dichloromethane) continuum was used to model the solvent.

[247]

concentration or depletion. Thus, it can be employed to identify electron pair localization. In fact, correlation between QTAIM analysis and the VSEPR model (Valence Shell Electron Pair Repulsion) is accurate enough (yet not perfect) to explain different chemical phenomena.[59] Therefore, the laplacian of the electron density was studied on **19·Et₃SiH** and the two other crystallographically characterized σ-SiH complexes **Ru·HSiCl₃** and **Ir·HSiEt₃** for comparison reasons. The outcome of this investigation is shown in Figure 26:
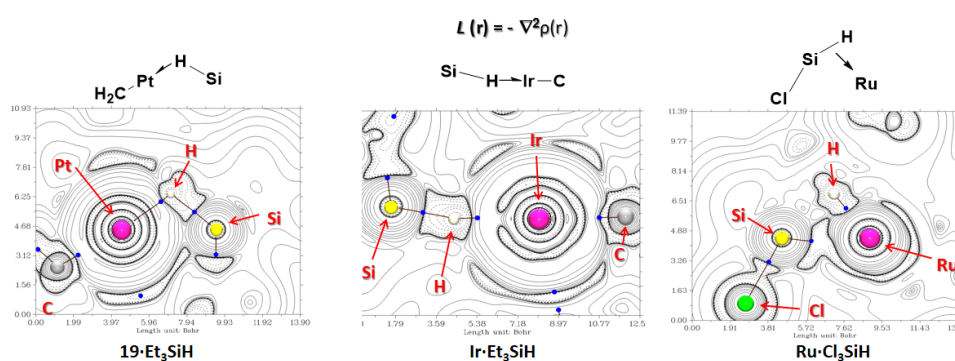
Figure 26. DFT calculated $\nabla^2\rho(r)$ maps of σ-SiH complexes **19·Et₃SiH**, **Ir·Et₃SiH** and **Ru·Cl₃SiH** in the plane defined by the metal, silicon, and hydrogen atoms. Bond paths are displayed as black solid lines and bond critical points (BCP) as blue circles.

As it can be seen above, the Pt and Ir complexes contain atomic interaction lines between Pt and H, and Si and H, each of them containing in turn a bond critical point (BCP).[60] On the other hand, there is neither bond path nor critical point between Pt and Si.[61] The electron density at the BCPs (M−H: $\rho(r)$ = 1.06/0.62 e·Å⁻³, Si−H: $\rho(r)$ = 0.65/0.70 e·Å⁻³ for **19·Et₃SiH** and **Ir·Et₃SiH**, respectively), combined with the aforementioned data, point out to η¹

---

[59] P. L. A. Popelier, *Coord. Chem. Rev.,* **2000**, *197*, 169-189.

[60] A BCP indicates a bonding situation between two nuclei. See reference 59 for more details.

[61] The same study was performed on the experimental structure derived from X-Ray diffraction studies, and the same topological map was obtained (*i.e.* no BCP was found between Pt and Si).

coordination modes in both complexes. However, the Pt complex shows the initial stage of the pivoting motion leading to a η^2 binding fashion, which is in agreement with the experimentally found bond lengths and angles, like the one formed by Pt, H and Si (102.9 °), for example. In the Ru complex, the opposite situation is found: there is no BCP or bond path between Si and H, and there seems to be a Pt−Si and a Pt−H bond. This suggests a complete cleavage of the Si−H bond (*i.e.* oxidative addition), and not a η^2 σ-SiH complex. All these data are in accordance with the calculated Wiberg Bond Indices and natural charges resulting from NBO analysis (Table 6), which clearly show that coordination modes close to η^1 geometries enhance the electrophilicity of the silane.

	Wiberg Bond Index	**Natural Charge**
19·Et₃SiH	**Si−H:** 0.45	**Si:** 1.682
	Si−Pt: 0.53	**Pt:** -0.078
	Pt−H: 0.58	**H:** -0.123
Ir·Et₃SiH	**Si−H:** 0.58	**Si:** 1.738
	Si−Ir: 0.23	**Ir:** -0.334
	Ir−H: 0.39	**H:** -0.266
Ru·Cl₃SiH	**Si−H:** 0.24	**Si:** 1.341
	Si−Ru: 1.22	**Ru:** -1.406
	Ru−H: 0.70	**H:** 0.140

Table 6. Wiberg Bond Indices and Natural Charges of the atoms involved in the interactions describing the σ-SiH complex formation of the different compounds.

Influence of the silane

The influence of the silane in the coordination mode was also explored by testing the coordination capabilities of Ph₃SiH to complex **19**. Single crystals of the σ-SiH complex **19·Ph₃SiH** could be grown by solvent diffusion techniques (dichloromethane/pentane) at -30 °C. The crystals were of enough quality to perform X-Ray diffraction studies. Interestingly, overlap of two different

[249]

structures was found in the unit cell: sigma complex **19·Ph₃SiH** and silyl derivative **21** [Pt(SiPh$_3$)(I^{t}BuiPr)$_2$][BAr$_4^F$][62] (Figure 27, left).

---

[62] Formation of silyl complex **21** is a consequence of the reactivity patterns displayed by the σ-silane complexes studied in this thesis. This behaviour will be described in detail in the next section of the chapter.

19·Ph₃SiH

N^1-C-C-N^3 = 113.71°
N^2-C-C-N^4 = 152.46°
Pt-Si = 2.3568 Å
R-Factor = 3.34 %

21

N^1-C-C-N^3 = 114.64°
N^2-C-C-N^4 = 154.94°
Pt-Si = 2.3045 Å
R-Factor = 2.77 %
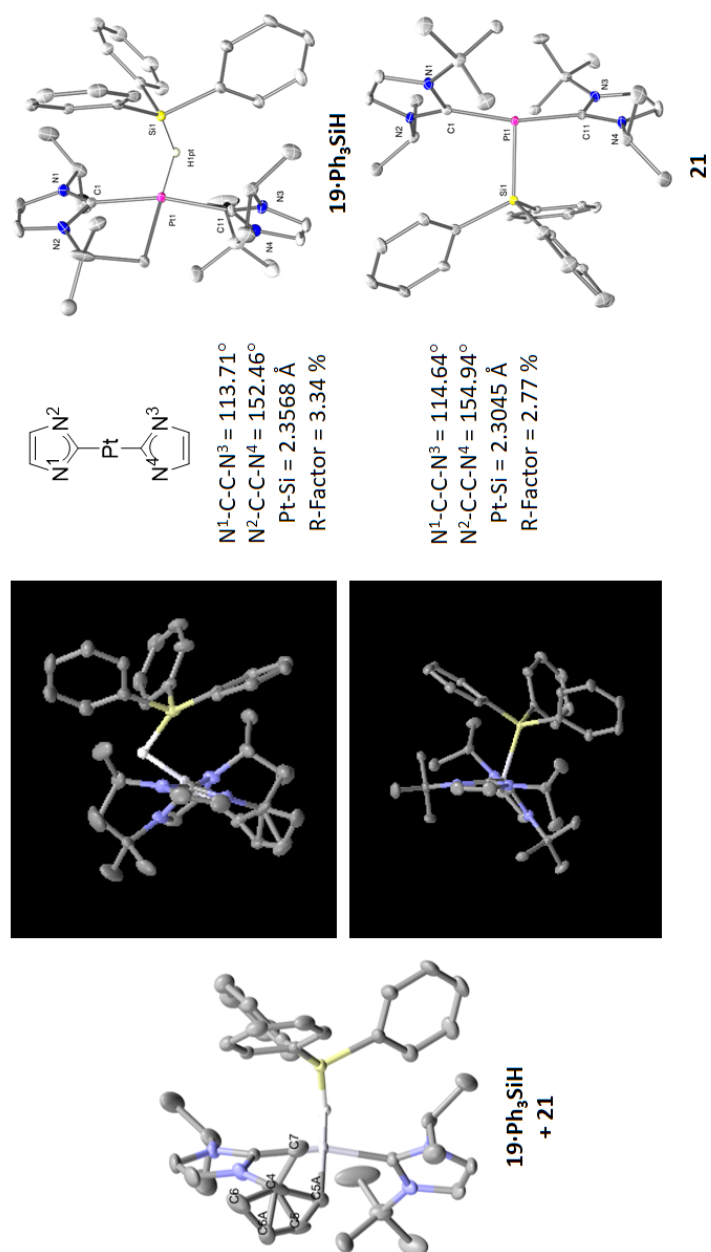
**19·Ph₃SiH
+ 21**

Figure 27. Left: Overlaid experimental crystal structure of complexes **19·Ph₃SiH** and **21**. Center: Top view of both complexes, comparison of dihedral angles and Pt–Si bond lengths. Right: ORTEP representations of complex **19·Ph₃SiH** (after removal of atoms C5 and C6) and complex **21** (independently prepared and crystallized).

[251]

Although the crystal structure might look as crystallographically disordered at a first glance, a closer look seems to point out to the presence of two overlaid structures, in which the only variations are the presence or absence of the bridging hydride and the labeled carbon atoms in Figure 27 (left) corresponding to one of the *tert*-butyl groups of one NHC ligand. A careful examination of the angles between them suggests that C5, C6 and C7 belong to one of the non-cyclometalated carbenes of complex **21**, and C5A, C6A and C7 belong to the cyclometalated arm of the σ-SiH complex **19·Ph₃SiH**. Analysis of the independently synthesized and crystallized silyl complex **21** (Figure 27, right) provides additional support to this theory. Three other structural parameters back the hypothesis of having two overlaid geometries: a) The bridging hydride could be found in the Fourier map, *trans* to the methylene group (C5A–Pt–H angle: 177.99°); b) Both Pt–Si distances only differ in 0.05 Å; c) The dihedral angles between the NHC ligands are almost identical. It can be seen that the Pt–Si distance and the Pt–H–Si angle in **19·Ph₃SiH** (2.357 Å and 87.7°) considerably vary from those obtained by DFT methods (2.534 Å and 97.5°, Table 7), probably because of the overlap effect of both structures. In any case, topological analysis was performed on the experimental geometry to check the presence of BCP between Pt–Si, in order to discern the binding mode of the silane. It is interesting to notice that despite having the same Pt–Si bond length, experimental **19·Ph₃SiH** does not show any BCP between the metal and silicon, but complex **21** does (Figure 28).[63]

---

[63] A BCP is observed between Pt and Si in the calculated structure of **19·Ph₃SiH** upon further closing the Pt−H−Si angle to around 80°, which suggests that the situation observed above is close to the threshold for a BCP to appear.

[252]
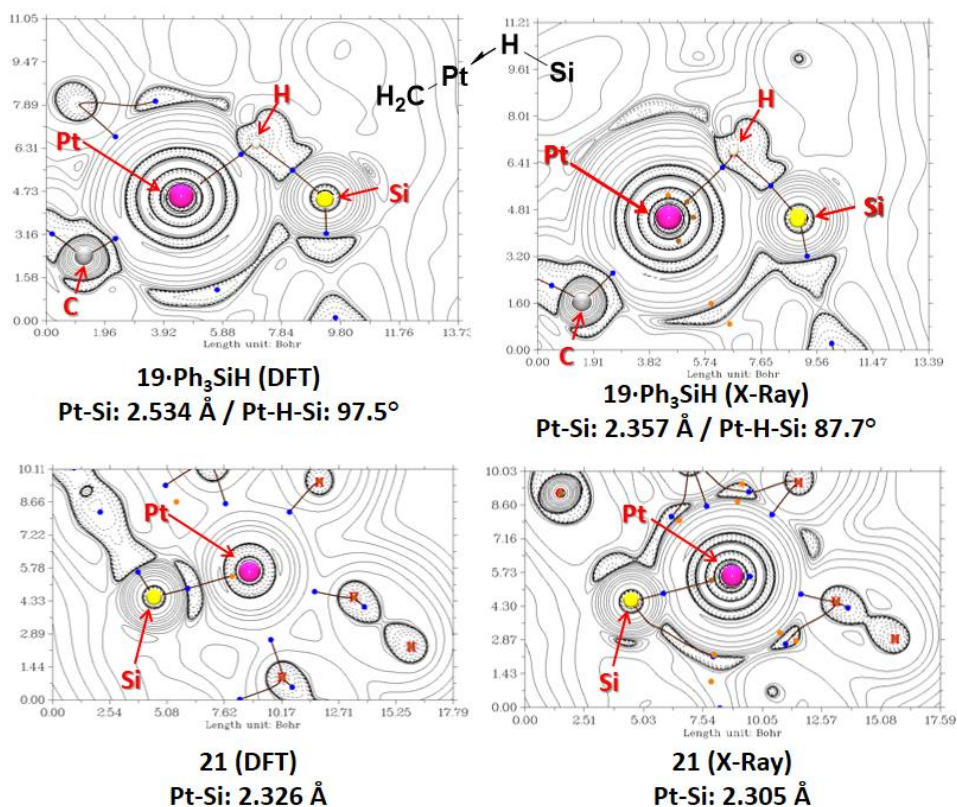
Figure 28. DFT calculated ∇²ρ(r) maps of σ-SiH complexes **19·Ph₃SiH** and **21** in the plane defined by the metal, silicon, and hydrogen atoms. Bond paths are displayed as black solid lines and bond critical points (BCP) as blue circles.

Following the study of the influence of the silane in the coordination mode of the resulting σ-SiH complexes, DFT calculations on different **19·R₃SiH** complexes (R = Et, Ph or Cl) showed that electron-withdrawing substituents on the Si atom induce a higher degree of backbonding from the metal (following the trend SiCl₃ > SiPh₃ > SiEt₃), hence there is a lower positive charge on Si and the Si−H bond is weakened in favour of the formation of Pt−Si and Pt−H bonds. This transition can be observed in Table 7, where smaller Pt−H−Si angles and Pt−Si distances and longer Si−H bond lengths can be found with increasing electronegative substituents on the silane. This situation is extreme in the case

[253]

of **19·Cl₃SiH**, where a BCP appears between Pt and Si as well as a Ring Critical Point (RCP),[64] which suggests that the Si−H bond is close to splitting (Figure 29).
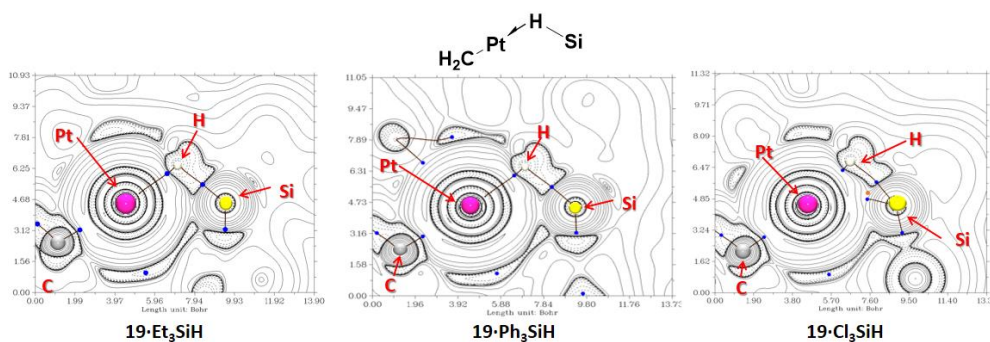
Figure 29. DFT calculated $\nabla^2\rho(r)$ maps of σ-SiH complexes **19·Et₃SiH**, **19·Ph₃SiH** and **19·Cl₃SiH** (optimized structures) in the plane defined by the metal, silicon, and hydrogen atoms. Bond paths are displayed as black solid lines, bond critical points (BCP) as blue circles and ring critical points (RCP) as orange circles.

---

[64] Some studies have shown that the presence of a RCP close to a BCP is indicative of the instability of the latter. See: P. Meixner, K. Batke, A. Fischer, D. Schmitz, G. Eickerling, M. Kalter, K. Ruhland, K. Eichele, J. E. Barquera-Lozada, N. P. M. Casati, F. Montisci, P. Macchi, W. Scherer, *J.Phys. Chem. A*, **2017**, *121*, 7219.

	Wiberg Bond Index	Natural Charge	Geometrical Parameters[a]
19·Et₃SiH	**Si–H:** 0.45	**Si:** 1.682	**Pt–Si:** 2.631 Å
	Si–Pt: 0.53	**Pt:** -0.078	**Si–H:** 1.651 Å
	Pt–H: 0.58	**H:** -0.123	**Pt–H–Si:** 102.8°
19·Ph₃SiH	**Si–H:** 0.42	**Si:** 1.673	**Pt–Si:** 2.534 Å
	Si–Pt: 0.60	**Pt:** -0.073	**Si–H:** 1.668 Å
	Pt–H: 0.59	**H:** -0.100	**Pt–H–Si:** 97.5°
19·Cl₃SiH	**Si–H:** 0.39	**Si:** 1.285	**Pt–Si:** 2.313 Å
	Si–Pt: 0.88	**Pt:** -0.22	**Si–H:** 1.736 Å
	Pt–H: 0.64	**H:** -0.012	**Pt–H–Si:** 85.1°

Table 7. Wiberg Bond Indices and Natural Charges of the atoms involved in the interactions describing the σ-SiH complex formation of the different compounds. [a] Obtained from DFT calculations.

The interactions between the platinum atom and the different silanes were additionally evaluated by means of a localized orbital analysis,[65] so the bonding interactions can accurately be established by locating the centroids of charge of the different bonds involved in the process.[66] This study was possible thanks to a collaboration with Dr. Pietro Vidossich and Prof. Agustí Lledós, from the Universitat Autónoma de Barcelona (UAB). As an example, Figure 30 shows the analysis on **19·Et₃SiH**, where the centroid of charge of the Si–H bond (X_{SiH}) is displaced from the Si–H bisection towards the H atom (in agreement with the molecular orbital of Et₃SiH depicted in Figure 3) and pointing to the metal center. Similar distortions have been described by our group for agostic interactions of Pt(II) complexes.[67] On the other hand, one centroid from the platinum atom (X_{outer}) is displaced away from the metal, and it points to the Si center. Both

---

[65] Calculations were carried out at the PBE/DZVP/GTH level of theory.

[66] P. Vidossich, A. Lledós, *Dalton Trans.,* **2014**, *43*, 11145-11151.

[67] M. A. Ortuño, P. Vidossich, G. Ujaque, S. Conejero, A. Lledós, *Dalton Trans.,* **2013**, *42*, 12165-12172.

distances become longer with the electronegativity of the substituents on the silane, as shown in Table 8, in agreement with the trend described above. Moreover, the rearrangement of the centroids of the different fragments obtained by this localized orbital analysis[68] shows how the Si−H bond cleaves upon closing the Pt−H−Si angle. This implies that the Si−H cleavage mechanism is different from that observed in C−H activation reactions by the Pt Shilov system; in the Shilov system, the centroid of the C−H bond gives rise to a Pt−C linkage, and the Pt center catches the resulting H atom.[69] In our system, the centroid from the Si−H bond produces the Pt−H bond, and the metal catches the Si moiety (Scheme 12). These results suggest that the Si fragment acts as a silylium species.
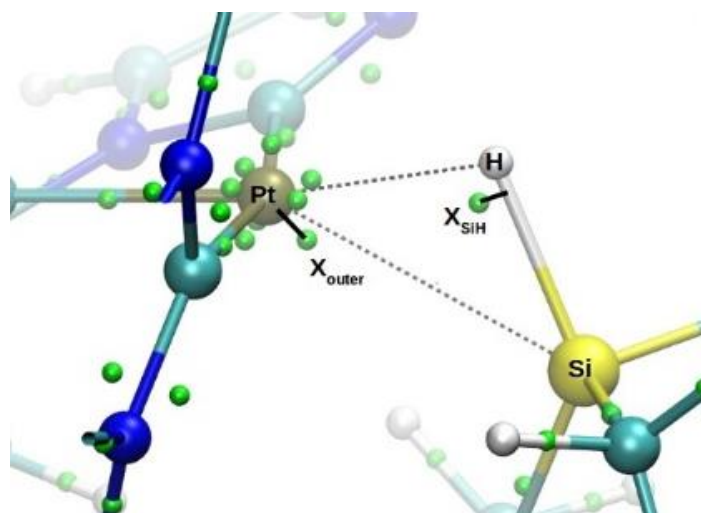
Figure 30. Localized orbital analysis of **19·Et₃SiH**. The centroids of the localized orbitals are shown as green spheres.

---

[68] This rearrangement can be observed in the video file included in the CD attached to this thesis.

[69] P. Vidossich, G. Ujaque, A. Lledós. *Chem. Commun.,* **2012**, *48*, 1979-1981.

	d(Si, H) (Å)	d(X_{SiH}, Si−H axis) (Å)	d(Pt, X_{outer}) (Å)
19·Et₃SiH	1.651	0.235	0.435 (0.347-0.401)
19·Ph₃SiH	1.668	0.245	0.468 (0.342-0.405)
19·Cl₃SiH	1.736	0.276	0.603 (0.337-0.407)

Table 8. Distances of the analysed centroids from the Pt center and the Si−H bond in each of the Pt(II) σ-SiH complex studied. For d(Pt, X_{outer}), the range of the distance of the Pt atom to the other centroids is shown in parentheses.
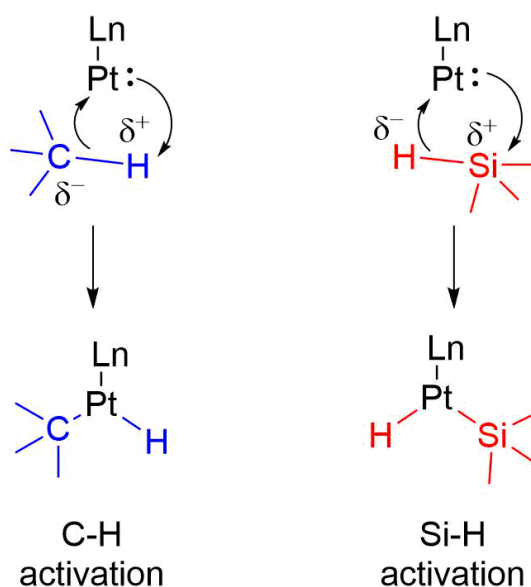
Scheme 12. Comparison between C−H activation and Si−H activation in platinum complexes.

Potential Energy Scans

The computational results on **19·Et₃SiH** along with the observed experimental data (*e.g.* the high electron density value $\rho(r) = 1.06$ e·Å⁻³ on the Pt−H bond or its short distance (1.53 Å)) indicate that the η^1-SiH geometry is the most stable one, but the complex tends to pivot towards a η^2-SiH binding fashion, eventually leading to the cleavage of the Si−H bond. In order to confirm this hypothesis, a potential energy scan was performed, in which the electronic

[257]

energy of the system was evaluated upon deformation of the Pt–H–Si angle, so as to examine which is the most stable geometry. In agreement with the experimental observations, the minimum is located at an angle of 102.8°, and opening the angle up to a lineal arrangement (Pt–H–Si = 170°) requires only 4.7 kcal/mol (Figure 31). Reaching a value similar to that reported by Brookhart for **Ir·Et₃SiH** (150°) takes only 3 kcal/mol, yet closing the angle down to 55° is much more energy demanding, since it requires 11.4 kcal/mol. These data are in agreement with our hypothesis, and suggest that Si–H cleavage would take place at higher temperatures. Additionally, complex **13·BuSiH₃** was subjected to this study to corroborate our initial interpretations (Figure 32). Again, η¹-SiH coordination seems to be the preferred geometry, since going from the minimum (at 145°) to a linear arrangement only demands 1.5 kcal/mol, but more acute angles increase the required energy up to 25.9 kcal/mol (at 52°). This is logical, since the bulkier carbene IᵗBu precludes the approach of the Si moiety to the metal center due to steric hindrance.
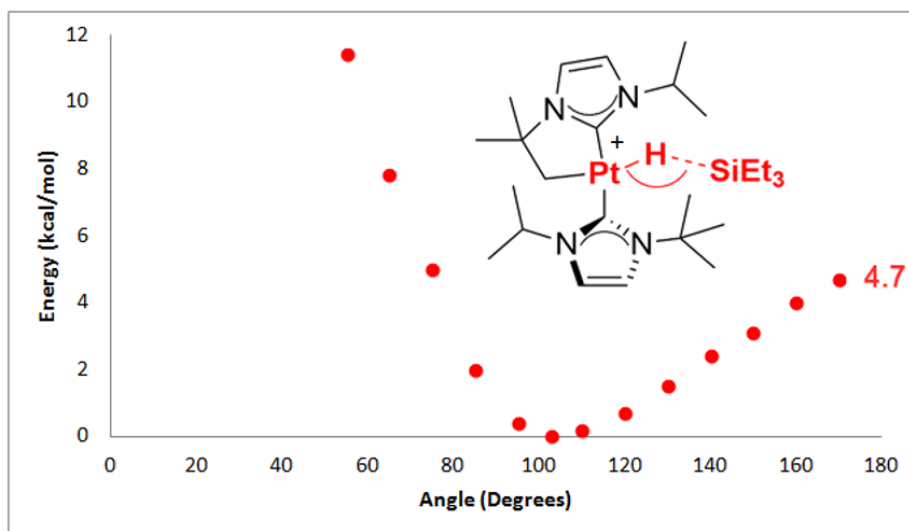
Figure 31. Relaxed Potential Energy Surface (PES) Scan of complex **19·Et₃SiH** along the Pt–H–Si coordinate. The energy minimum is located at 102.8 degrees.

[258]
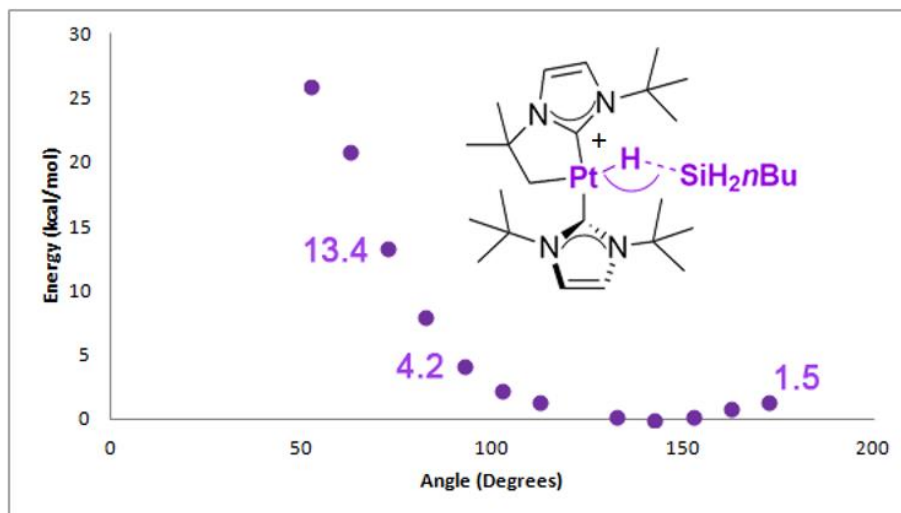
Figure 32. Relaxed Potential Energy Surface (PES) Scan of complex **13·BuSiH₃** along the Pt−H−Si coordinate. The energy minimum is located at 142.3 degrees.

For the sake of comparison, **Ir·Et₃SiH** and **Ru·Cl₃SiH** were also evaluated, since their crystallographic structures are available and their data can be contrasted with our systems (Figures 33 and 34). As it can be seen, **Ir·Et₃SiH** shows a similar plot to that obtained for **13·BuSiH₃** and it agrees well with the experimental findings, for the most stable geometry is very similar to the crystal structure. This accuracy also prevails for **Ru·Cl₃SiH**, where the opposite scenario is found: linear arrangements are very energetic (33.8 kcal/mol), yet the energy minimum (at 83°) is located very close to the experimental angle (87°).

[259]
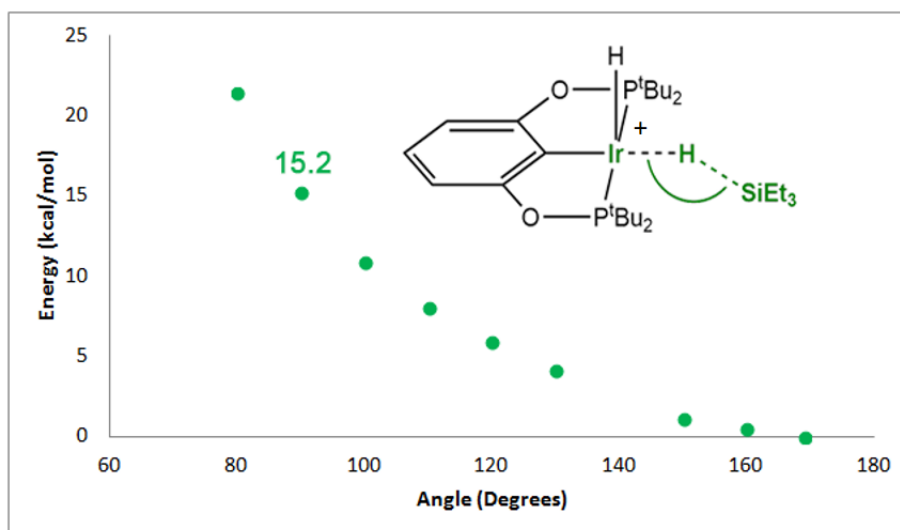
Figure 33. Relaxed Potential Energy Surface (PES) Scan of complex **Ir·Et₃SiH** along the Ir−H−Si coordinate. The energy minimum is located at 169° (The X-Ray structure showed a Ir−H−Si angle of 157°, which requires less than 1 kcal/mol).
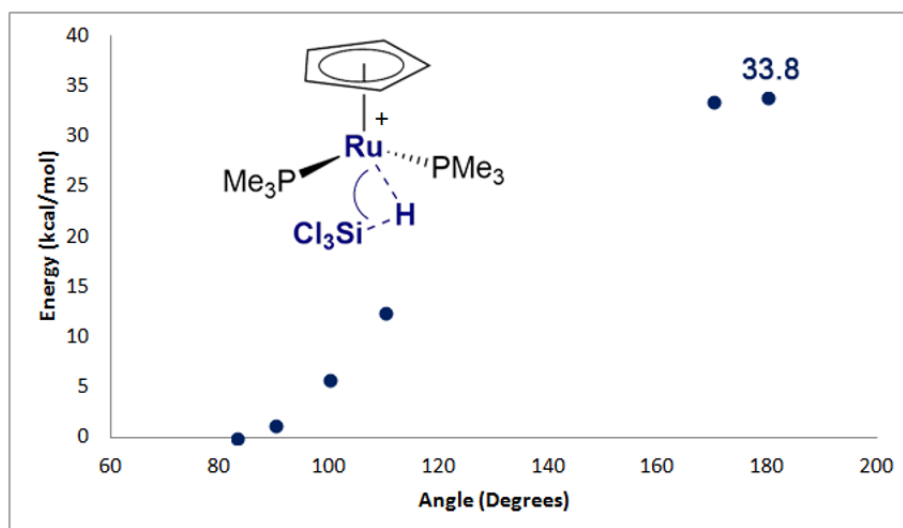
Figure 34. Relaxed Potential Energy Surface (PES) Scan of complex **Ru·Cl₃SiH** along the Ru−H−Si coordinate. The energy minimum is located at 83°. (The X-Ray structure showed a Ru−H−Si angle of 87°, which requires less than 1 kcal/mol). The absence of data between 120° and 160° is due to the fact that convergence criteria were not reached during the PES calculation.

[260]

This section has shown how minor and subtle modifications on the structure of the NHC ligands can dramatically change the stability of the corresponding Pt(II) σ-SiH species. However, these compounds are only stable at low temperatures (usually below 0 °C), and they are reactive intermediates that evolve at room temperature to different products depending on the silane used. The following sections will describe in detail the nature of these resulting derivatives (Scheme 13). Although Scheme 13 shows the example of cyclometalated I^{t}Bu^{i}Pr complexes, it will be shown below that different compounds such as hydride species containing different types of NHC ligands can also give rise to σ-SiH complexes which undergo subsequent transformations.
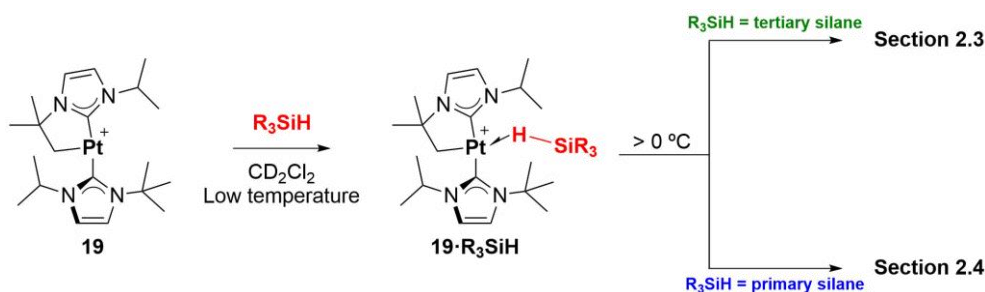
Scheme 13. σ-silane complexes as reactive intermediates in the formation of different silicon-containing Pt(II) species.

2.3. Reactivity of the σ-SiH complexes using tertiary silanes

Substitution of the I^{t}Bu carbene for the smaller version I^{t}Bu^{i}Pr gave rise to more stable σ-SiH complexes, which allowed their study and characterization at temperatures below 0 °C. In agreement with the theoretical predictions, tertiary silane-based σ-complexes rearrange above this temperature into the 14-electron Pt(II) silyl species (Scheme 14), in the same way as **13** reacts with Et$_2$SiH$_2$ to yield complex **16**.

[261]
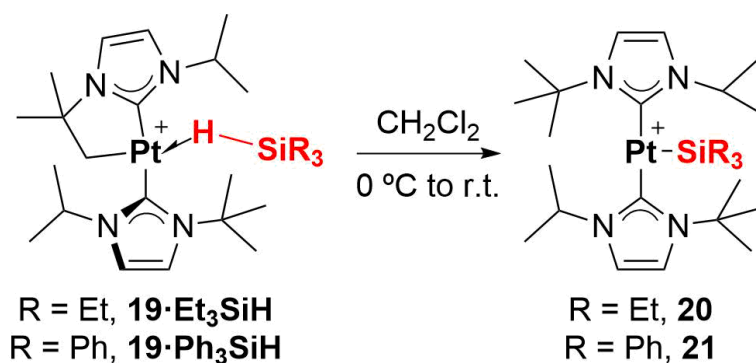
Scheme 14. Evolution of the tertiary silane-based σ-SiH complexes **19** into the corresponding 14-electron Pt(II) silyl derivatives **20** and **21**.

When **19·Et₃SiH** was left to warm to r.t., a color change to intense yellow was observed. This change in appearance was accompanied by the emergence of a new set of signals by ^{1}H NMR, which corresponded to a complex possessing equivalent NHC ligands (Figure 35). Complex **20** can be made by stirring complex **19** with 1.1 equivalents of Et₃SiH in dichloromethane at room temperature for 5 hours, and it can be purified by crystallization techniques through solvent diffusion at 0 °C. Unfortunately, the resulting crystals were not adequate for X-Ray diffraction studies.
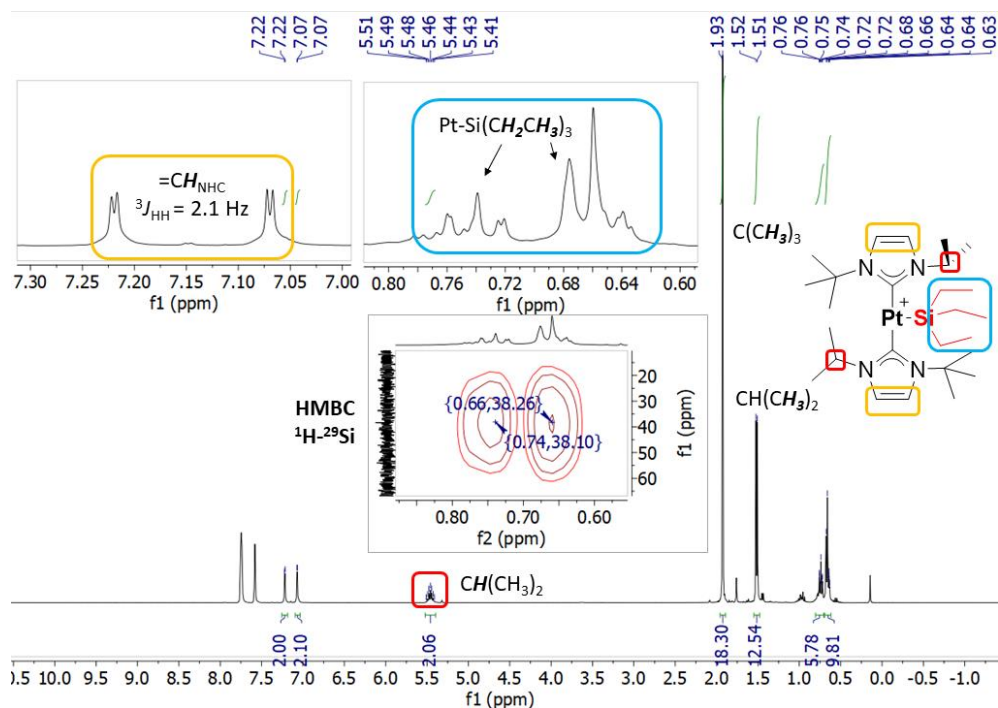
Figure 35. ^{1}H NMR spectrum (400 MHz, CD₂Cl₂) of the reaction mixture to obtain complex **20**. Inset (bottom): HMBC [1]H−[29]Si experiment, where the cross-peaks of the ethyl chains with the Si atom can be observed.

As shown above, the reaction is extremely clean and selective towards the formation of C−H and Pt−Si bonds, which is rather surprising considering the possibility of obtaining mixtures of C−Si and C−H products, as reported for Ir(III) species,[70] (Figure 36A) or observing selective C−Si coupling phenomena, as described by Milstein *et al.* for a different class of Pt(II) complexes in the presence of tertiary alkyl and aryl silanes[71] (Figure 36B).

---

[70] M. Aizenberg, D. Milstein, *J. Am. Chem. Soc.,* **1995**, *117*, 6456-6464.

[71] M. E. van der Boom, J. Ott, D. Milstein, *Organometallics,* **1998**, *17*, 4263-4266.
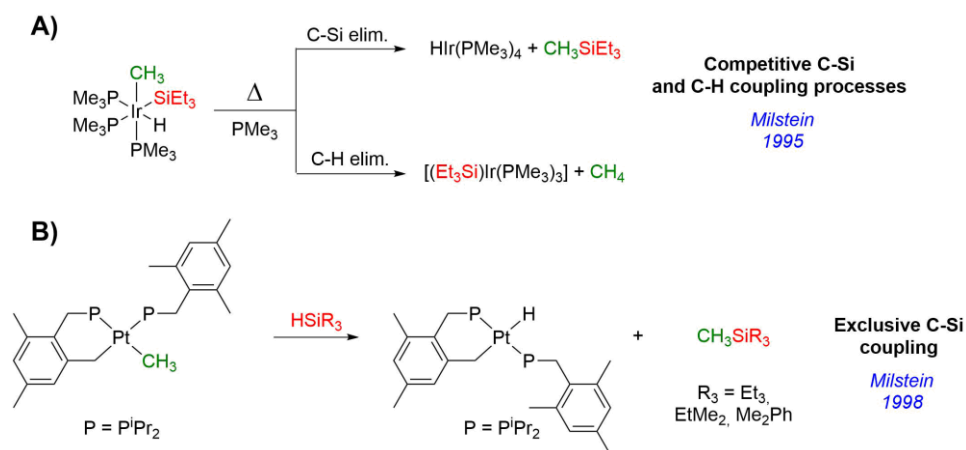
Figure 36. Competitive C−H and C−Si coupling (A) and selective C−Si coupling (B) displayed by Pt(II) complexes, as described by Milstein *et al.* (adapted from references 70 and 71).

It has also been described that the selectivity towards either C−H or C−Si coupling can be modulated depending on the silane employed (*e.g.* alkylsilanes and arylsilanes behave differently).[72] For this reason, Ph_3SiH was used so as to explore a potential different outcome. A similar behavior was found, since the Pt(II) silyl derivative **21** was exclusively formed in two hours by using similar experimental conditions as with Et_3SiH (Figure 37).[73] Although the patterns governing the selectivity of this type of reactions are not clear yet, a plausible explanation might be attributed to steric bulk: in **13** the I*t*Bu groups are too large to accommodate any tertiary silane, given that no interaction or reaction is experimentally observed. Perhaps, I*t*Bu*i*Pr provides enough space for the hydride to migrate to the carbon atom, but not enough for the silane, regardless of the orientation of the NHC ligands (Figure 38).

---

[72] M. Aizenberg, D. Milstein, *Angew. Chem. Int. Ed.,* **1994**, *33*, 317-319.
[73] As shown above in section 2.2, complex **21** could be crystallized and analyzed by X-Ray diffraction methods (Figure 27).
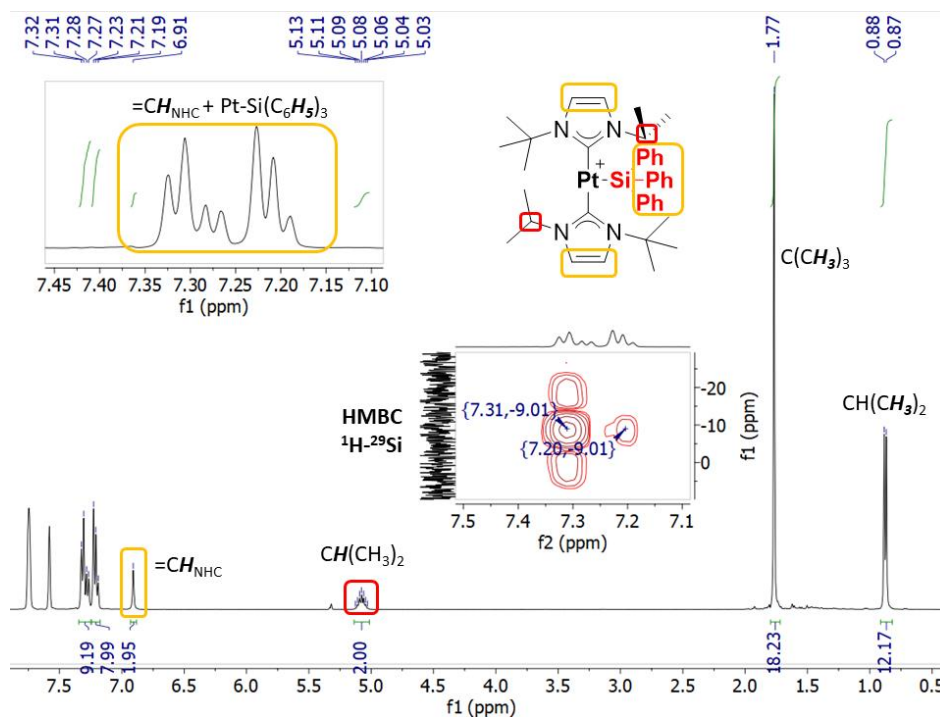
Figure 37. ^{1}H NMR spectrum (400 MHz, CD$_2$Cl$_2$) of complex **21**. Inset (bottom): HMBC ^{1}H−^{29}Si experiment, where the cross-peaks of the phenyl protons with the Si atom can be observed.
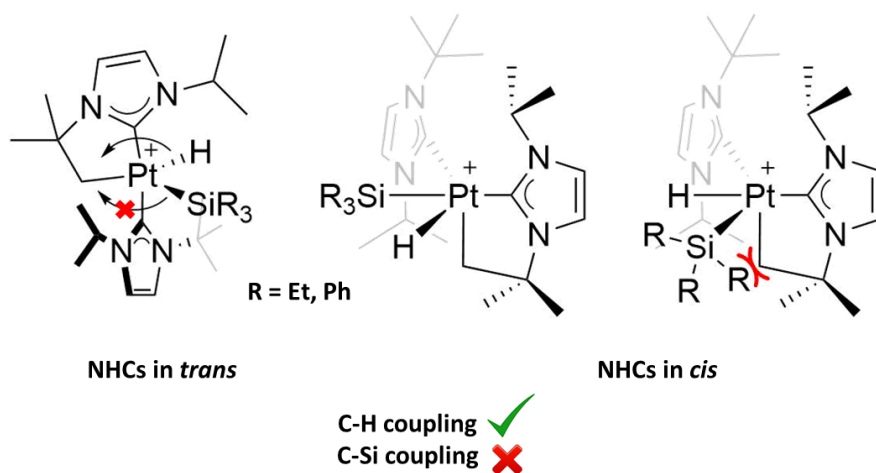
Figure 38. Plausible explanation based on steric hindrance for the selective formation of the cationic Pt(II) silyl derivatives stabilized by I^{t}Bu^{i}Pr ligands.

2.4. Reactivity of the σ-SiH complexes using primary silanes

Whereas the use of I^{t}Bu^{i}Pr-stabilized Pt(II) complexes with tertiary silanes could only lead to the formation of either Pt–silyl derivatives or Pt–hydride compounds with the silane moiety attached to one of the carbenes (not observed), the availability of additional Si–H bonds in primary silanes allowed us to explore new potential patterns of reactivity by using these complexes.

Cyclometalated cationic Pt(II) silyl complexes

When complex **19** was mixed with either ^{n}BuSiH$_3$ or PhSiH$_3$ in CH$_2$Cl$_2$ at room temperature, a quick change of colour was observed from orange to intense yellow along with bubble formation, indicative of gas release. NMR analysis of both reactions revealed the clean and selective formation of an asymmetric species, in which one of the NHC ligands seems to be cyclometalated, according to the signals observed by ^{1}H NMR for the *tert*-butyl and *iso*-propyl peaks, the inequivalence of the imidazole protons and the presence of a methylene signal directly attached to Si (example of the reaction between **19** and ^{n}BuSiH$_3$ in Figures 39 and 40). The ^{1}H NMR spectrum also shows a peak at 4.60 ppm that has been attributed to H$_2$. All these data suggest that the silane molecule has inserted into the Pt–C bond, releasing hydrogen gas during the process (coming from the two other protons of the silane) to give complexes **22** and **23**, as depicted in Scheme 15. The signal for the SiH proton correlates via HMQC ^{1}H–^{29}Si with a silicon peak at -1.2 ppm, and it shows satellite peaks due to coupling with ^{195}Pt ($^2J_{Pt-H}$ = 120 Hz), similar to those described for complex **16** (Figure 13).[74] Additionally, the SiH proton of complex **23** appears as a triplet ($^3J_{H-}$

[74] For NMR data regarding neutral silyl Pt(II) complexes, see: a) D. Chan, S. B. Duckett, S. L. Heath, I. G. Khazal, R. N. Perutz, S. Sabo-Etienne, P. L. Timmins, *Organometallics*, **2004**, *23*, 5744-5756; b) J. C. DeMott, W. Gu, B. J. McCulloch, D. E. Herbert, M. D. Goshert, J. R.

$_H$ = 3 Hz), consistent with the proximity of the CH$_2$ group of the cyclometalated arm.
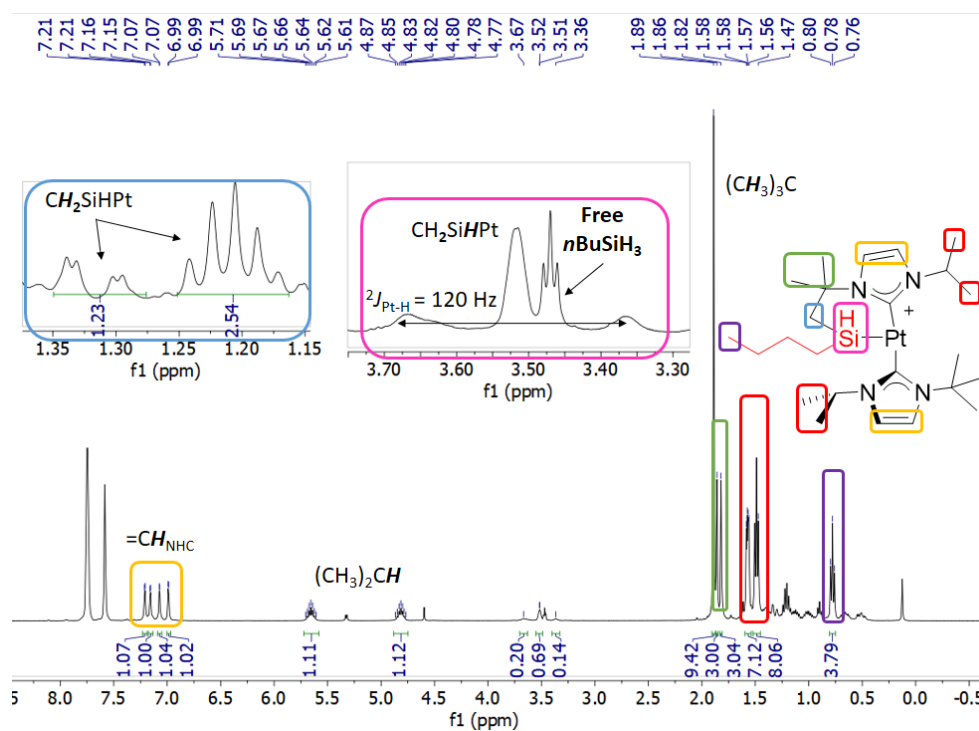
Figure 39. ^{1}H NMR spectrum (400 MHz, CD$_2$Cl$_2$) of complex **22** from the crude reaction mixture.

Walensky, J. Zhou, O. V. Ozerov, *Organometallics*, **2015**, *34*, 3930-3933; c) C. Mitzenheim, T. Braun, R. Laubenstein, B. Braun, R. Herrmann, *Dalton Trans.,* **2016**, *45*, 6394-6404.
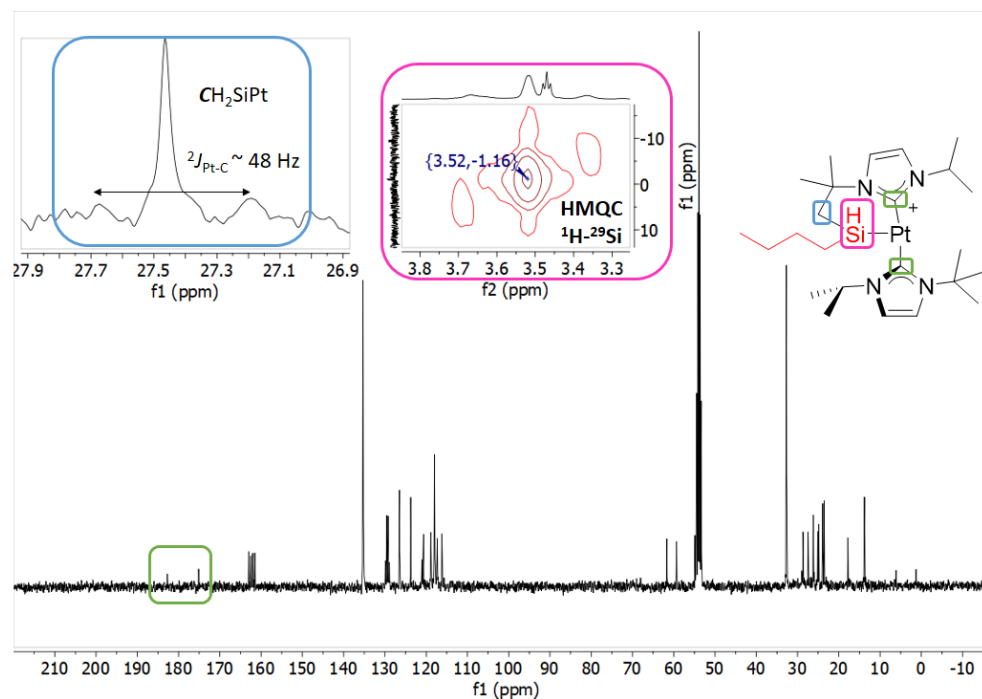
Figure 40. $^{13}C\{^1H\}$ NMR spectrum (400 MHz, CD_2Cl_2) of complex **22** from the crude reaction mixture. (Top left): $^{13}C\{^1H\}$ NMR spectrum, showing the region of the methylene unit bound to Si, which displays satellite peaks due to coupling with ^{195}Pt. (Top center): HMQC $^1H-^{29}Si$ experiment, where the cross-peak of the Si*H* proton with the Si atom can be observed (free $^nBuSiH_3$ resonates at -60.1 ppm in ^{29}Si NMR).
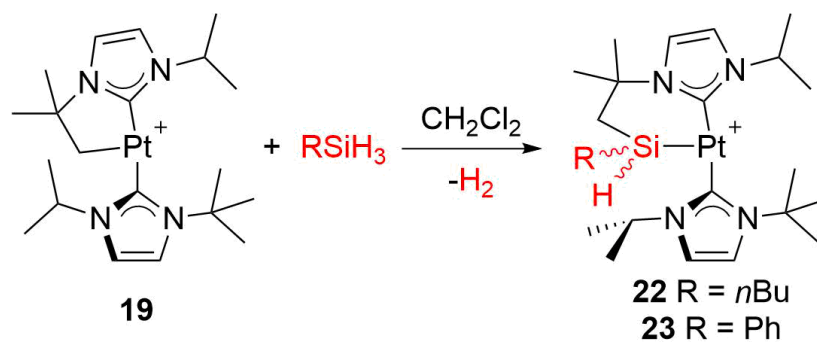
Scheme 15. Reaction of complex **19** with primary silanes to give silyl-cyclometalated complexes **22** and **23**.

[268]

As shown in Figures 39 and 40, there seems to be only one species, with none or negligible trace of C–H coupling resulting derivatives, which highlights the drastic difference in reactivity depending on the type of silane employed, regardless of the nature of the substituents on the Si atom. As it can be seen, this process is rather complex and requires the cleavage of two Si–H bonds and the formation of a C–Si and a Pt–Si bonds with release of a H_2 molecule. The structure of phenylsilane derivative **23** could also be confirmed by X-Ray crystallography (Figure 41). It can be seen that a dichloromethane molecule (coming from the crystallization solvent) interacts with the platinum atom (Pt···Cl distance: 2.803 Å), although in a weak manner, since elemental analysis does not reveal the presence of any solvent molecule in the results. The insertion of the silane molecule into the Pt–C bond gives rise to a 6-membered metalacycle that forces the carbene ligands to be almost coplanar (∼18°). The Pt–Si bond length (2.269 Å) is comparable to that displayed by similar cationic silyl Pt(II) systems like complex **16** or complex **21** despite the metalacycle constraint.
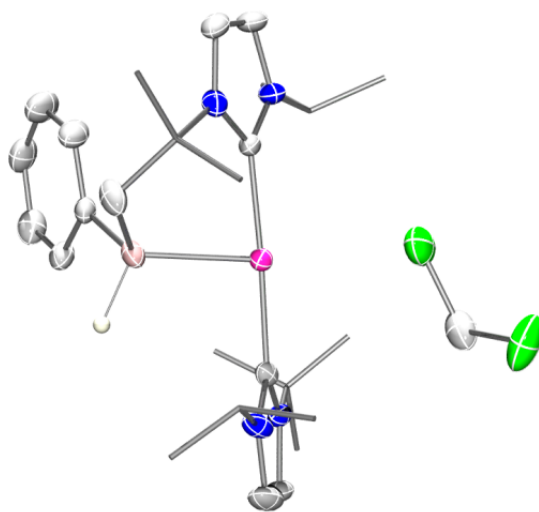
Figure 41. X-Ray structure of **23**. BAr₄F anion, all hydrogen atoms except the SiH proton have been omitted and some carbon atoms are shown in a wireframe format for clarity.

[269]

C–Si bond formation has not only been observed in I^{t}Bu^{i}Pr derivatives. Mesityl-based carbene ligands like IMes (1,3-bis-(2,4,6-trimethylphenyl)imidazol-2-ylidene) or IMes* (4,5-Dimethyl-1,3-bis-(2,4,6-trimethylphenyl)-imidazol-2-ylidene) lead to the cationic cyclometalated complexes **24** and **25** previously described in our group,[35,55] which can undergo similar processes in the presence of ^{n}BuSiH$_3$ or PhSiH$_3$ to yield the corresponding unsymmetrical complexes **26-29** (Scheme 16).[75] This type of complexes stabilized by silane-functionalized NHC ligands have previously been described in the literature for cobalt[76] and iron derivatives,[77] where the authors underline the distinctive nature of these ligands, since combining a Lewis acidic silane fragment with a nucleophilic carbene is synthetically challenging. The reaction and work-up conditions are similar to those employed for complexes **22** and **23**. NMR analysis of the samples reveals some characteristic signals like the SiH proton (Figures 42 and 43), which displays coupling to ^{29}Si (chemical shifts range from -1.6 to 9.0 ppm, similar to complexes **22** and **23**), ^{195}Pt and one of the methylene hydrogen atoms (CH$_2$–Si), showing the asymmetry of the compound. It is worth mentioning that the robustness of these complexes is remarkable, since they are stable under air in solution and in the solid state at room temperature.

---

[75] A small amount (~5%) of complex **37** ([Pt(IMes*)$_2$SiH$_2$^{n}Bu][BAr$_4$^{F}], see below) is observed in the synthesis of species **28**. See Experimental part for more details.

[76] a) Z. Mo, Y. Liu, L. Deng, *Angew. Chem. Int. Ed.,* **2013**, *52*, 10845-10849; b) J. Sun, C. Ou, C. Wang, M. Uchiyama, L. Deng, *Organometallics*, **2015**, *34*, 1546-1551; c) J. Sun, L. Luo, Y. Luo, L. Deng, *Angew. Chem. Int. Ed.,* **2017**, *56*, 2720-2724.

[77] Z. Ouyang, L. Deng, *Organometallics*, **2013**, *32*, 7268-7271.
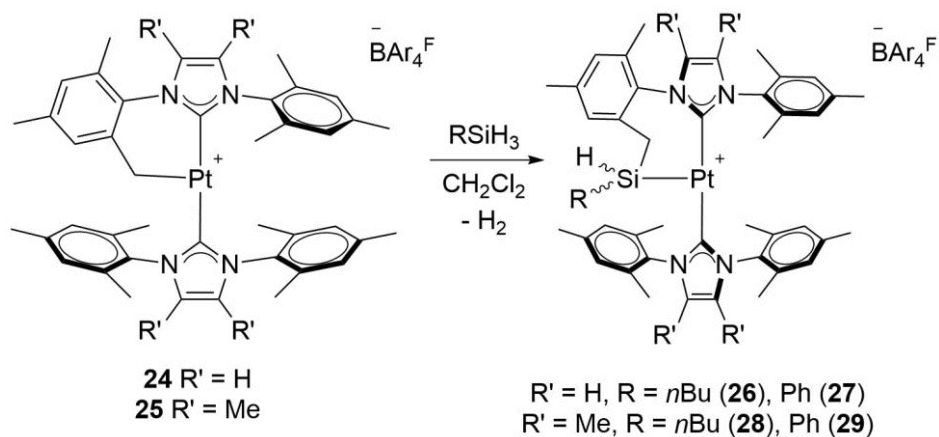
Scheme 16. Reaction of complexes **24** and **25** with primary silanes to give silyl-cyclometalated complexes **26-29**.
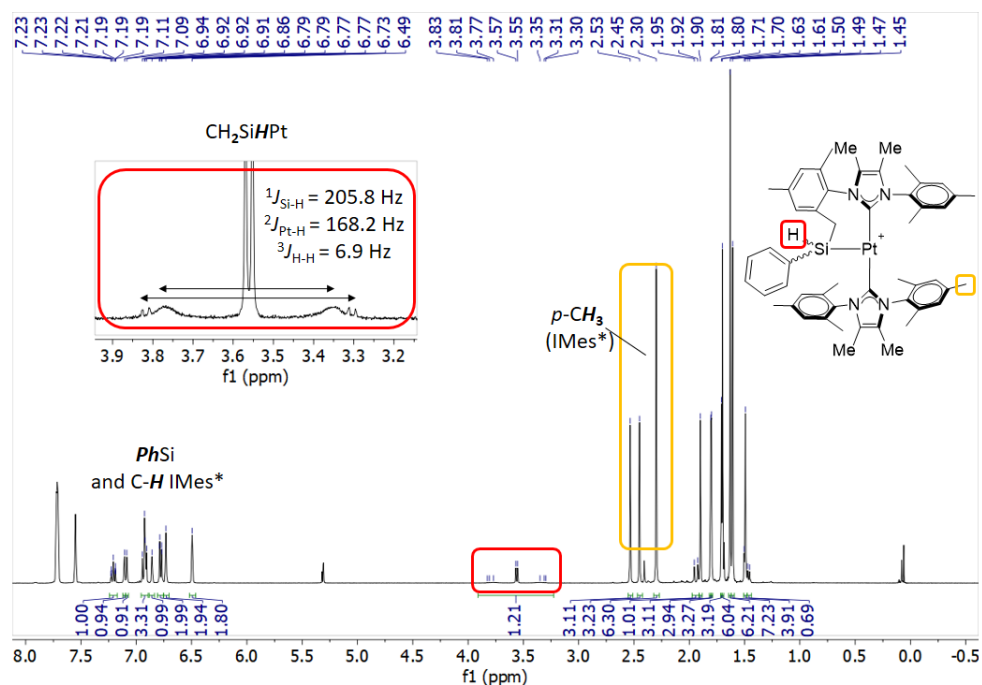
Figure 42. ^{1}H NMR spectrum (400 MHz, CD$_2$Cl$_2$) of complex **29**. Inset: (Top left) Zoom-in of the signal corresponding to the SiH proton, which shows coupling to different nuclei.

[271]
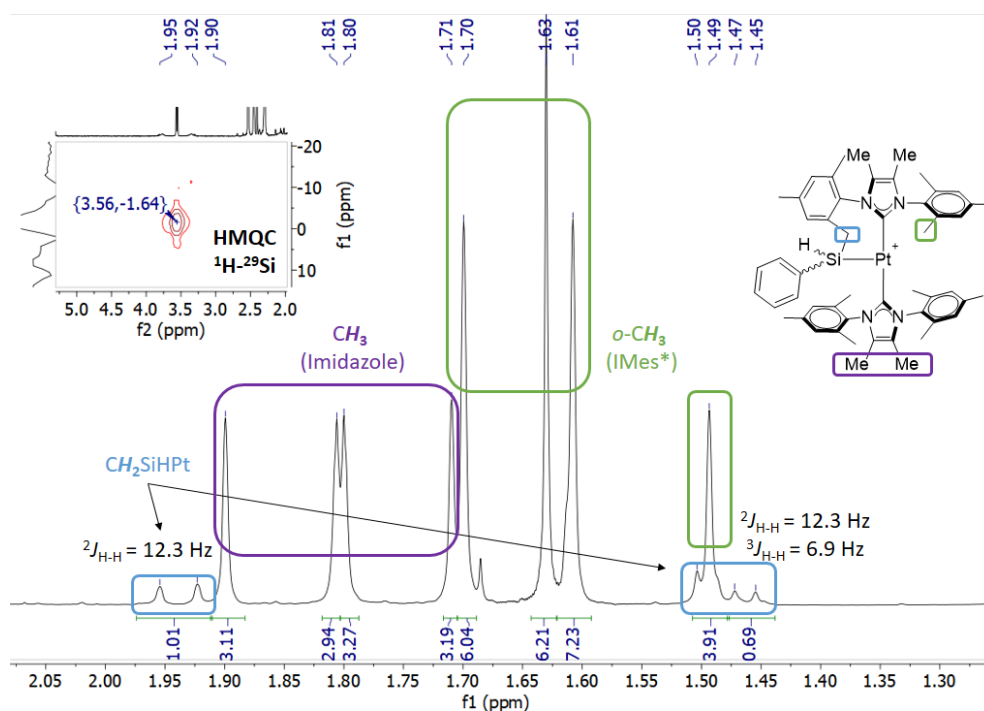
Figure 43. Portion of the ^{1}H NMR spectrum (400 MHz, CD$_2$Cl$_2$) of complex **29**. Inset: (Top left) HMQC ^{1}H-^{29}Si experiment, where the cross-peak of the Si*H* proton with the Si atom can be observed.

The majority of these complexes can be crystallized by diffusion of either pentane or hexamethyldisiloxane into a concentrated solution of the platinum species in dichloromethane, and X-Ray diffraction studies could be performed on some of them, as shown in Figure 44. In **26** and **27**, there is neither solvent molecule nor C−H bond in close proximity to the metal atom (generally > 3 Å), so these molecules can be regarded as 14-electron T-shaped Pt(II) complexes, just like their cyclometalated precursor.[55] The Pt−Si bond length is identical for both compounds and for complex **23** (2.26 Å, Table 9), and it is very similar to those displayed by complexes **16** and **21**, which suggests that this parameter is not affected by the presence or absence of a silane-containing metalacycle, the carbene or the type of silane employed in these cases. However, the bigger size of the IMes NHCs in comparison to I^{t}Bu^{i}Pr forces a wider dihedral angle (defined

[272]

by the imidazole-ylidene fragment) between both ligands (up to 125°) so as to minimize steric hindrance.
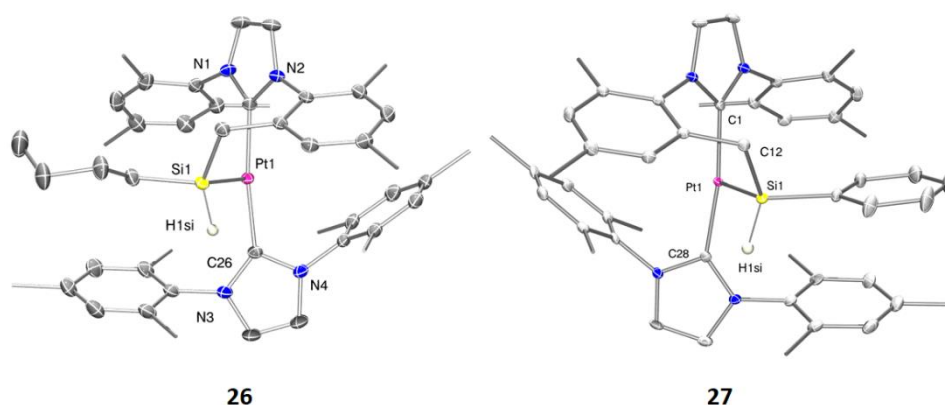
Figure 44. X-Ray structures of complexes **26** and **27**. BAr$_4$^{F} anion, all hydrogen atoms except the SiH proton and some methyl carbon atoms have been omitted for clarity.

	26	**27**
Pt−Si (Å)	2.2619(6)	2.2609(8)
Si−H1$_{si}$ (Å)	1.44(3)	1.39(3)
C$_{carbene}$−Pt−C$_{carbene}$ (°)	172.37(9)	171.85(11)
C12−Pt−Si (°)	109.17(7)	109.52(9)
Dihedral angle (NHCs) (°)	125.8	67.7

Table 9. Selected structural parameters from complexes **26** and **27**.

Cationic Pt(II) hydride complexes

In contrast to the cyclometalated cationic Pt(II) species described above, hydride Pt(II) derivatives [Pt(H)(IMes)$_2$][BAr$_4$^{F}] and [Pt(H)(IMes*)$_2$][BAr$_4$^{F}] (previously synthesized in our group)[36] or the mixed carbene [Pt(H)(I^{t}Bu^{i}Pr)$_2$][BAr$_4$^{F}] can react with primary silanes to afford the corresponding silyl complexes, releasing H$_2$ in the reaction (Scheme 17). No C−Si products are detected even after prolonged reaction times, which seems to

[273]

suggest that these Pt(II) silyl complexes are not intermediates in the formation of the cyclometalated C−Si analogues.
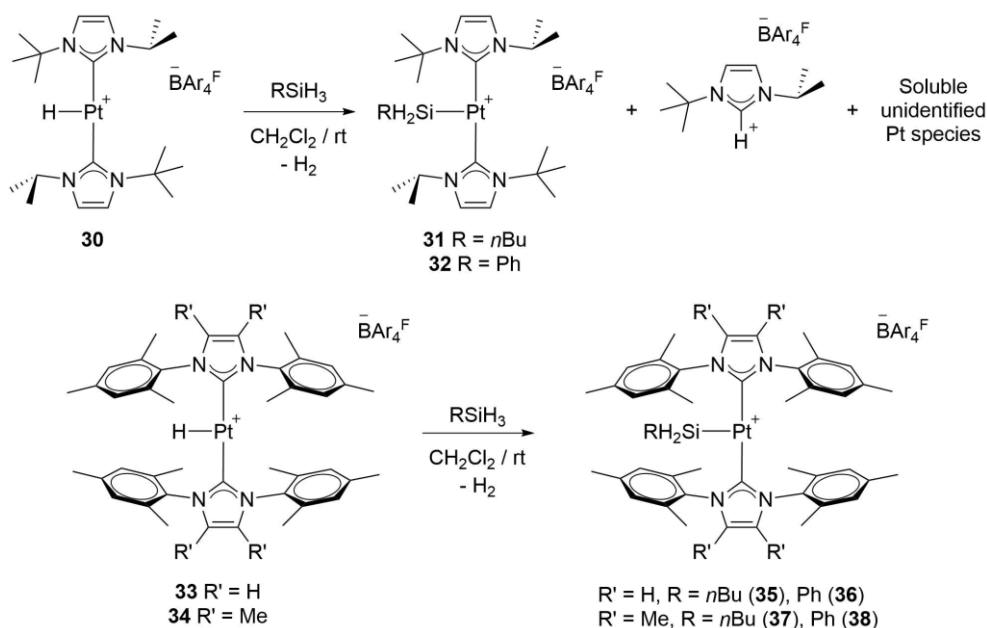
Scheme 17. Reaction of hydride complexes **30**, **33** and **34** with primary silanes to give silyl species **31** and **32** and **35-38**.

Reaction of hydride **30** with ^{n}BuSiH$_3$ and PhSiH$_3$ respectively gave rise to the silyl derivatives **31** and **32** with considerable amounts (~15-20%) of the corresponding imidazolium salt I^{t}Bu^{i}Pr·HBAr$_4^F$ and unidentified soluble platinum species. The formation of these by-products was inevitable, given that their formation took place even if the reaction was carried out at low temperature (0 °C). Crystallization of these species always came accompanied with imidazolium salt, so purification of silyl complexes **31** and **32** was not possible. However, mesityl derivatives **33** and **34** react (around 30 minutes) at room temperature with primary silanes to cleanly give silyl complexes **35-38** as intense yellow solids. Again, these complexes are stable under air both in solution and in the solid state, and they do not react with hydrogen or upon

[274]

heating, which makes them easy to handle. Their NMR analysis is much simpler than their cyclometalated counterparts, since their symmetrical nature produces only one set of signals for the carbene ligands, as shown in Figure 45. Besides, ^{29}Si chemical shifts appear in a different zone of the spectrum (higher fields, around -30 ppm) to those described above, given their different substitution degree.
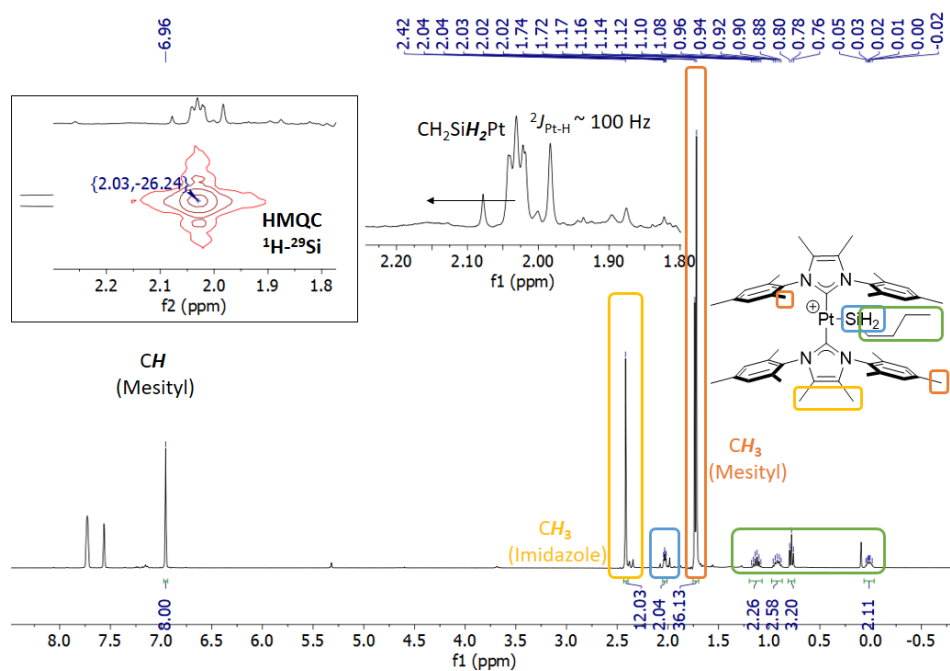
Figure 45. ^{1}H NMR spectrum (400 MHz, CD$_2$Cl$_2$) of complex **37**. Inset: (Top left) HMQC ^{1}H–^{29}Si experiment, where the cross-peak of the Si*H* proton with the Si atom can be observed. (Top center) Zoom-in of the signal corresponding to the SiH proton, which shows coupling to ^{195}Pt.

In a similar manner to the cyclometalated C–Si coupling products, these complexes can be crystallized by solvent diffusion methods. X-Ray quality crystals of species **36** confirmed the proposed structure based on NMR analysis (Figure 46). The same features observed for the complexes shown in Figure 44 were detected, like the *trans* arrangement of the carbene ligands, with the silyl moiety occupying the third coordination site. One more time, there seems to be

[275]

no CH group in a close position to the metal center to consider the possibility of agostic interactions stabilizing the complex. The Pt–Si bond length possesses the same value (2.270 Å) as that observed for the aforementioned silyl compounds and again, the NHCs arrange themselves with a wide dihedral angle (up to 123°) so as to diminish steric hindrance.
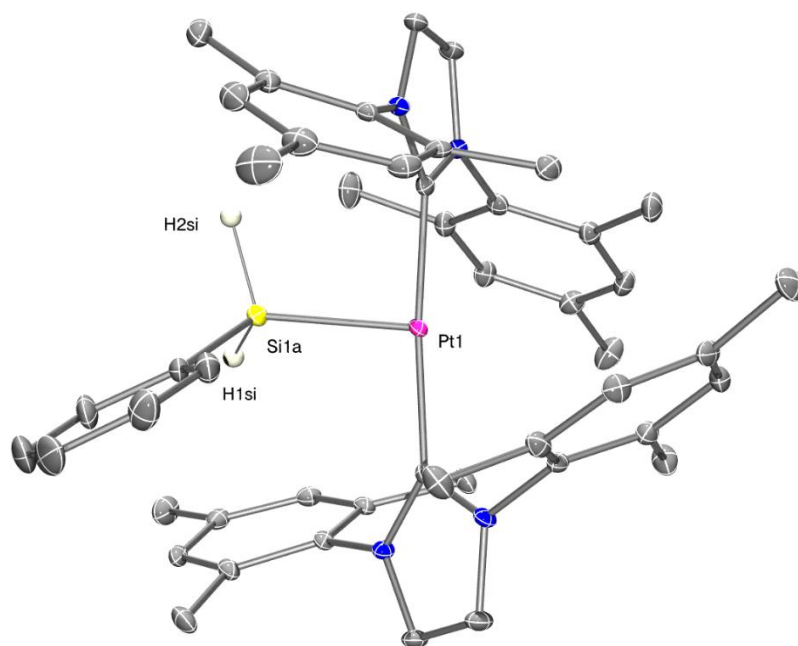
Figure 46. X-Ray structure of complex **36**. BAr$_4^F$ anion and all hydrogen atoms except the SiH protons have been omitted for clarity. Selected bond lengths (Å) and angles (°): Pt1–Si1: 2.2703(9); Si1–H1$_{si}$: 1.39(3); Si1-H2$_{si}$: 1.44(3); C$_{carbene}$–Pt–C$_{carbene}$: 174.78(12); Dihedral angle (NHC planes): 123.4.

2.5. Mechanistic studies on the C–Si and/or Pt–Si bond formation mediated by σ-SiH complexes

Low temperature NMR experiments

In order to get insight about the mechanism by which the C–Si and/or Pt–Si coupling events take place, several cationic Pt(II) complexes were

[276]

evaluated by means of low temperature NMR experiments. Among them, the results obtained with cyclometalated species [Pt(IMes*')(IMes*)][BAr$_4$^{F}], **25**, and ^{n}BuSiH$_3$ are very informative: first, addition of ^{n}BuSiH$_3$ to a solution of **25** in CD$_2$Cl$_2$ at -80 °C leads to the formation of the σ-SiH complex **25·^{n}BuSiH$_3$**. As shown in Figure 47, the bridging hydride resonates around -8 ppm in the ^{1}H NMR spectrum,[78] and it shows satellite peaks due to coupling with ^{29}Si ($^1J_{Si-H}$ = 67 Hz) and ^{195}Pt ($^1J_{Pt-H}$ = 500 Hz). The latter coupling constant is somewhat higher than that observed for **19·Et$_3$SiH** ($^1J_{Pt-H}$ = 396 Hz), which suggests a stronger interaction with the metal center. Figure 47 also shows that the σ complex is stable from -80 °C up to -15 °C, where an intermediate species (**Intermediate A**) appears.

---

[78] The terminal hydrogen atoms resonate at 3 and 3.84 ppm. The three SiH protons correlate with a peak at -53.5 ppm in the ^{29}Si spectrum (HMQC ^{1}H−^{29}Si). Additionally, NOESY experiments reveal exchange between bridging and terminal protons, suggesting a fluxional process.
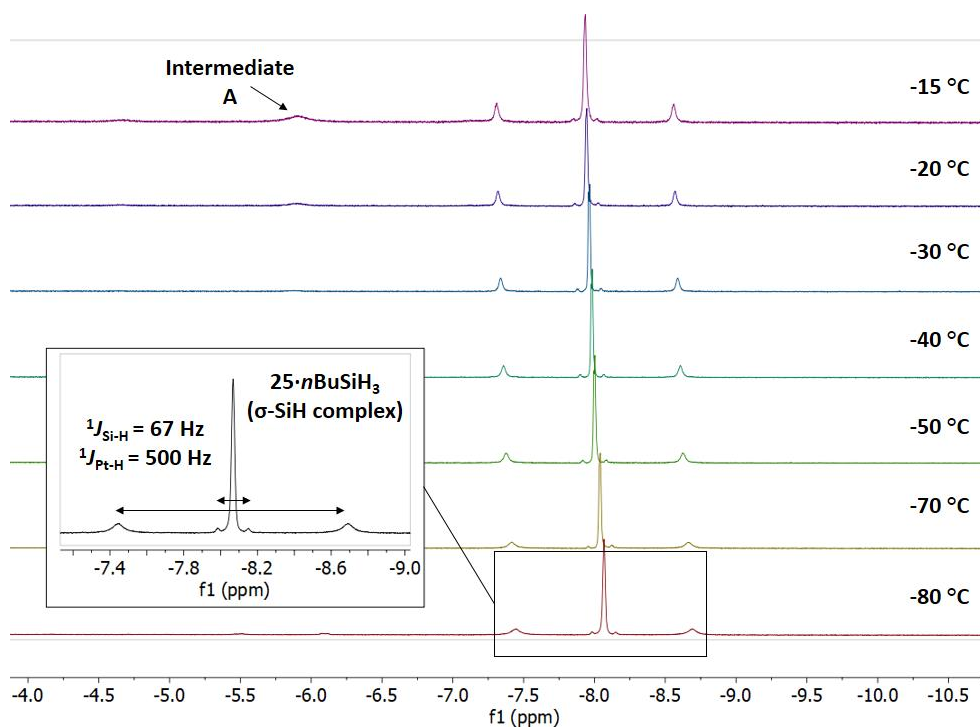
Figure 47. ^{1}H NMR spectra (400 MHz, CD$_2$Cl$_2$) of the mixture of **25** and *n*BuSiH$_3$ from -80 °C to -15 °C, showing the formation of the σ-SiH complex **25·BuSiH$_3$** and the appearance of **Intermediate A** at -15 °C.

The sample was kept to this temperature (*ca*. 1h) so as to observe the transformation of **25·BuSiH$_3$** into **A** (Figure 48), which shows a broad signal with Pt satellites integrating for 2 protons at -5.9 ppm ([1]J_{Pt-H} = 990 Hz). A NOESY experiment reveals that this signal exchanges with a multiplet (which integrates for 1 proton) at ~4 ppm. Unfortunately, additional information of the new appearing intermediate **A** was not possible since HMQC [1]H−[29]Si did not show any cross-peak at that temperature (probably due to signal broadening) and the rest of the spectrum was too complex to extract any information from it. Nevertheless, DFT calculations (see below in this section) indicated that intermediate **A** seems to be the agostic SiH platinum hydride shown in Scheme 18.

[278]
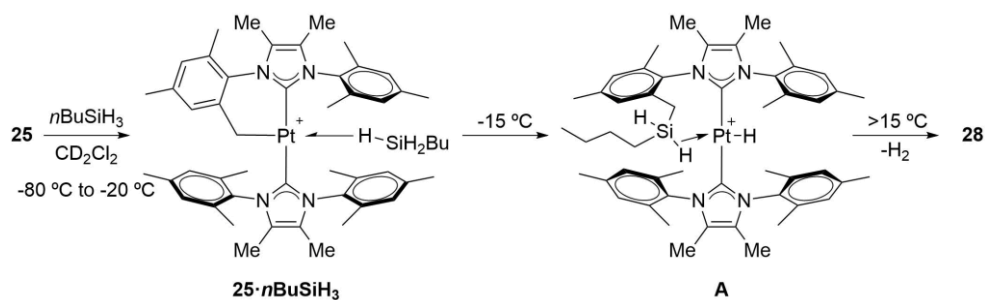
Scheme 18. Intermediates observed during the low temperature NMR experiment in the reaction between **25** and ^{n}BuSiH$_3$.
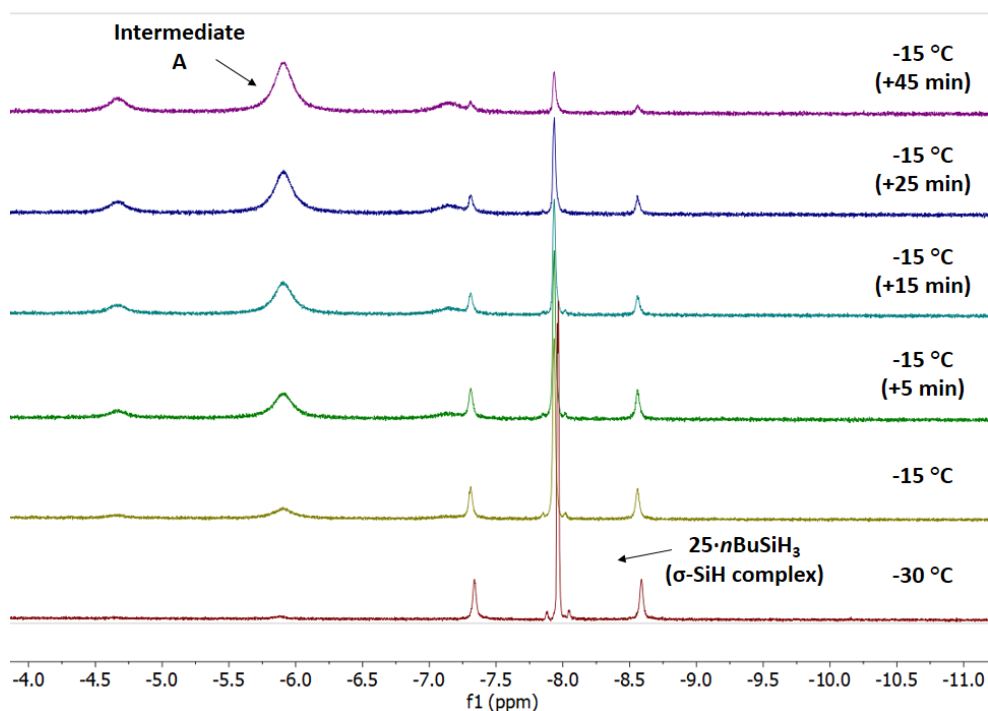
Figure 48. ^{1}H NMR spectra (400 MHz, CD$_2$Cl$_2$) of the mixture of **25** and ^{n}BuSiH$_3$ from -30 °C to -15 °C, showing the growth of intermediate **A** and the disappearance of **25·^{n}BuSiH$_3$** at -15 °C.

In fact, cooling back the sample down to -80 °C makes the signal of intermediate **A** split into two different broad peaks, each one of them with satellite peaks to platinum (Figure 49). The first one, at -4.74 ppm, possesses a $^1J_{Pt-H} \approx 390$ Hz and it shows (along with the signal a 3.97 ppm) a cross-peak in the

[279]

HMQC ^{1}H$-^{29}$Si spectrum with a signal at -21.0 ppm. The values of the chemical shift and the coupling constant are similar to those shown by the bridging hydrides of the σ-SiH complexes displayed in Table 4. Thus, it seems reasonable to assign the signal at 3.97 ppm to proton H^a and the signal at -4.74 ppm to proton H^b (Figure 49). Regarding the peak resonating at -6.88 ppm, it also integrates for one proton, yet it does not show any appreciable correlation on the HMQC ^{1}H$-^{29}$Si experiment. Besides, its coupling constant to platinum is much higher ($^1J_{Pt-H} \approx 1500$ Hz), typical from a cationic Pt(II) hydride with the coordination site *trans* to the hydride occupied by another ligand,[35a,36] as shown in the examples of Figure 50. Therefore, the signal at -6.88 ppm was assigned to proton H^c.
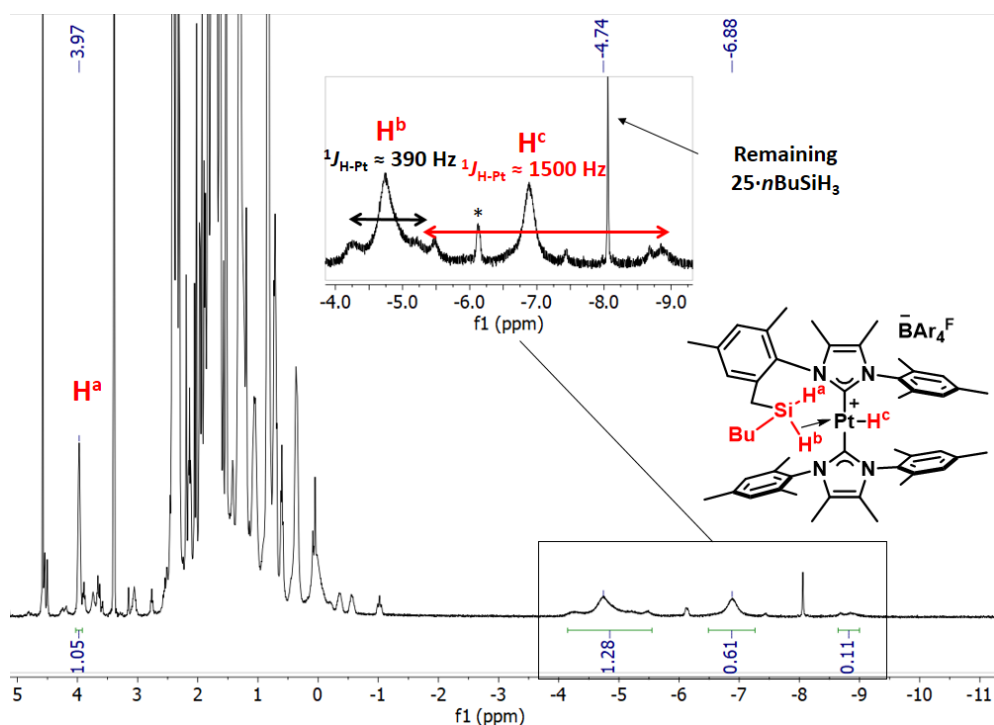
Figure 49. Portion of the ^{1}H NMR spectrum (400 MHz, CD$_2$Cl$_2$) of the mixture of **25** and ^{n}BuSiH$_3$ at -80 °C after consuming most of **25·BuSiH$_3$** into intermediate **A** at -15 °C. Inset: zoom-in of the signals assigned to protons H^b and H^c, showing satellite peaks due to coupling with ^{195}Pt.

^{1}H NMR (500 MHz, CD$_2$Cl$_2$, 25 °C)
δ -10.48 ppm
$^1J_{Pt-H}$ = 1429 Hz

^{1}H NMR (400 MHz, CD$_2$Cl$_2$, -40 °C)
δ -12.28 ppm
$^1J_{Pt-H}$ = 1818 Hz
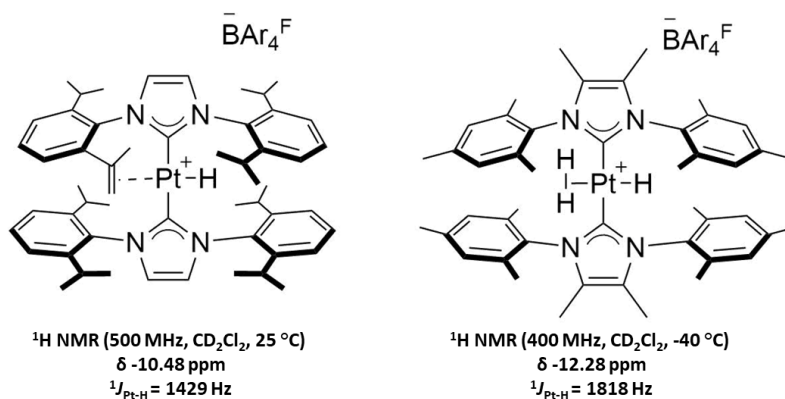
Figure 50. Cationic Pt(II) hydrides previously synthesized in our group with the coordination site *trans* to the hydride involved in π or σ interactions.

Nevertheless, an additional experiment was performed so as to get more NMR data supporting the assignment of intermediate **A**. Hydride **34** was mixed with ^{n}BuSiH$_3$ in order to form the corresponding σ-SiH complex **34·BuSiH$_3$** (which resembles the proposed structure for intermediate **A**). Three different signals were observed when the temperature reached -90 °C. The first one, a broad singlet at 3.71 ppm, integrates for 2 protons and it shows a cross-peak with a signal at -49.80 ppm in the HMQC ^{1}H–^{29}Si. This signal was attributed to terminal protons H^{te} (Figure 51). The second one, a doublet (integrates for 1 H) at -5.55 ppm, correlating with the same Si signal in the HMQC experiment, is coupled to ^{195}Pt ($^1J_{Pt-H}$ = 423 Hz) and to another proton ($^2J_{H-H}$ = 17 Hz). The similarity in the chemical shift and the Pt–H coupling constant bear resemblance to H^b in intermediate **A**. Based on this, this signal was attributed to the bridging proton H^{br}. Finally, a doublet integrating for 1 H at -6.08 ppm does not show any correlation in the HMQC experiment, it shows the same H–H coupling constant than proton H^{br} (17 Hz) and it is coupled to the metal with a greater coupling constant ($^1J_{Pt-H}$ = 1544 Hz). These data suggest that this signal corresponds to the hydride directly bound to the platinum atom, analogous to proton H^c in intermediate **A**. Additionally, all three signals show exchange in the NOESY

[281]

experiment, which is in accordance with the proposed structure depicted in Figure 51 for the σ-SiH complex **34·BuSiH₃**. As the temperature increases, the two signals in the hydride region collapse into a single broad signal at -60 °C (with coupling to ^{195}Pt of 1544 Hz) until it coalesces at about -40 °C. This behaviour, and all NMR data discussed above, provides additional support for the previous assignment of intermediate **A** as a platinum hydride agostic SiH complex. Complex **34·BuSiH₃** was transformed into silyl derivative **37** upon warming to room temperature, with concomitant loss of H_2.
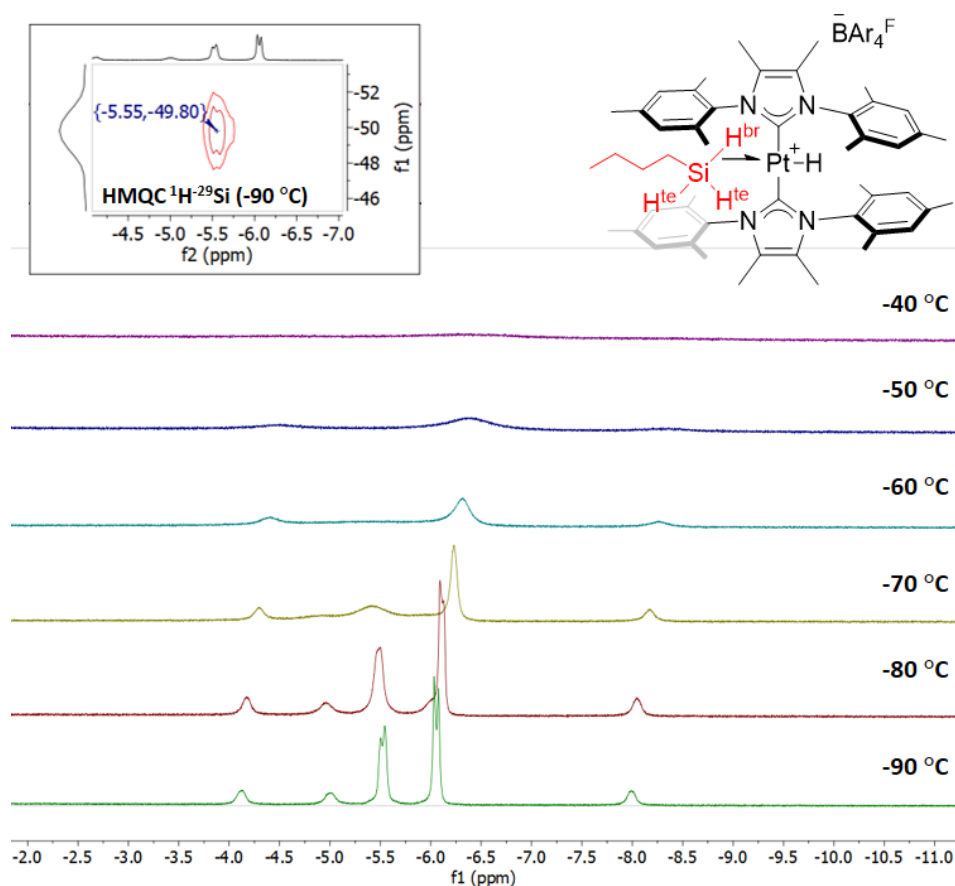
Figure 51. Hydride region of the ^1H NMR spectra (400 MHz, CD_2Cl_2) of the mixture of **34** and $^nBuSiH_3$ from -90 °C to -40 °C, where the formation of the σ-SiH complex **34·BuSiH₃** can be observed. Inset: HMQC ^1H–^{29}Si experiment performed at -90 °C.

[282]

DFT calculations

The mechanism of the formation of C−Si/Pt−Si complexes **26-29**, **31-32** and **35-38** was investigated by DFT methods[79] in order to gather additional information that can complement the experimental observations so as to propose a pathway by which these phenomena might be taking place, and to explain the remarkable selectivity experimentally obtained. This work was made in collaboration with Prof. Agustí Lledós from Universitat Autónoma de Barcelona (UAB), who ran the calculations.

Cyclometalated Pt(II) complexes with primary silanes

In this study, IMes derivative **24** and ^{n}BuSiH$_3$ were chosen as models, since the experimental outcome is known (*i.e.* formation of complex **26**). Four different alternatives were considered, which consist of either C−H bond formation with concomitant generation of silyl complex **35** or C−Si coupling to yield the cyclometalated C−Si derivative **26**.[80] Both of them were calculated by considering pathways in which the NHC ligands initially adopt a *trans* or a *cis* arrangement in the course of the reaction. The four alternative pathways are summarized in Scheme 19, and might involve σ-bond metathesis processes or Pt(IV) intermediates:

---

[79] Calculations were carried out at the M06/6-31g(d,p)/SDD//M06/6-311++g(d,p)/SDD level of theory. SMD (Dichloromethane) continuum was used to model the solvent.
[80] Mechanistic pathways involving silylene species were also taken into account, yet their energy barriers were too high to be considered as experimentally feasible. For the sake of simplicity, these preliminary results are not included in this thesis.
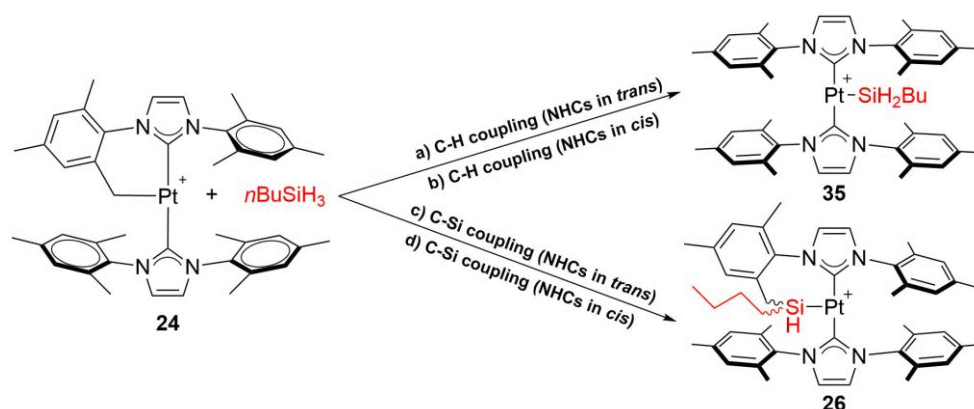
Scheme 19. Summary of the 4 different pathways calculated in this work for the reaction between **24** and ^{n}BuSiH$_3$.

- a) C−H coupling (NHCs in *trans*)

Considering cyclometalated complex **24** and butylsilane as the energy reference (Figure 52), formation of the σ-SiH complex **24·BuSiH$_3$** (Pt−H$_{bridging}$ distance = 1.859 Å; Si−H = 1.549 Å; Pt−H−Si angle = 121.2°) only requires 0.4 kcal/mol ($\Delta G_{273\text{ K}}$),[81] after which oxidative addition of one of the Si−H bonds of ^{n}BuSiH$_3$ can take place through transition state **TS1**, demanding 29.7 kcal/mol for the process to occur. No Pt(IV) species was found after the transition state as a local energy minimum, but the system directly evolved towards the formation of silyl complex **35**, which is 22.2 kcal/mol more stable than the reagents.

- b) C−H coupling (NHCs in *cis*)

Starting from the same energy reference, this pathway is slightly more complex due to the initial isomerization step required to achieve a *cis* orientation of the carbene ligands (Figure 53). In this process, isomerization of **24** (C−Pt−C angle of 175.1°) to **24$_{cis}$** (C−Pt−C = 118.6°) requires 13.9 kcal/mol (**TS$_{isom1}$**,

---

[81] It is worth remembering that the formation of the σ-SiH complexes is slightly endergonic due to entropic factors (see section 2.1) but exothermic enough to observe their formation at low temperature.

C–Pt–C angle = 135.5°) and formation of the σ-SiH complex **24$_{cis}$·BuSiH$_3$** (Pt–H$_{bridging}$ distance = 1.633 Å; Si–H = 1.824 Å; Pt–H–Si angle = 90.6°) leaves the system 12.1 kcal/mol above the origin. It can be observed from both systems that the complex with a *cis* arrangement gives rise to a σ-SiH complex with much more η^2 character and greater weakening and elongation of the Si–H bond, probably due to the bigger size of the cavity available for the metal–silane interaction. From here, one of the protons of the silane is close to the methylene group of the cyclometalated carbene (C–H$_{silane}$ distance = 1.795 Å) and it can bounce to form a methyl fragment at the same time that the silane establishes a new bond with the metal (Pt–Si = 2.403 Å). This step (**TS2**) has an energy cost of 26.4 kcal/mol, after which the complex rearranges itself to the *trans* isomer back again to yield silyl species **35**.

[285]

Figure 52. Energy profile for the formation of complex **35** from **24** considering a *trans* arrangement of the carbene ligands.

[286]

Figure 53. Energy profile for the formation of complex **35** from **24** considering a *cis* arrangement of the carbene ligands.

[287]

- c) C−Si coupling (NHCs in *trans*)

In this pathway, the formation of the σ-SiH species is identical to that shown in pathway a). From there, the only difference from the C−H coupling mechanism is the relative position of the silyl group after the formation of the sigma complex (Figure 54), which is *trans* with respect to the Pt−CH$_2$ moiety in **TS1** (leading to a C−H bond) or *cis* in **TS3** leading to the C−Si bond (Si···C$_{methylene}$ = 3.639 Å, Figure 54 right).

TS1
(C-H coupling)

TS3
(leads to C-Si coupling)
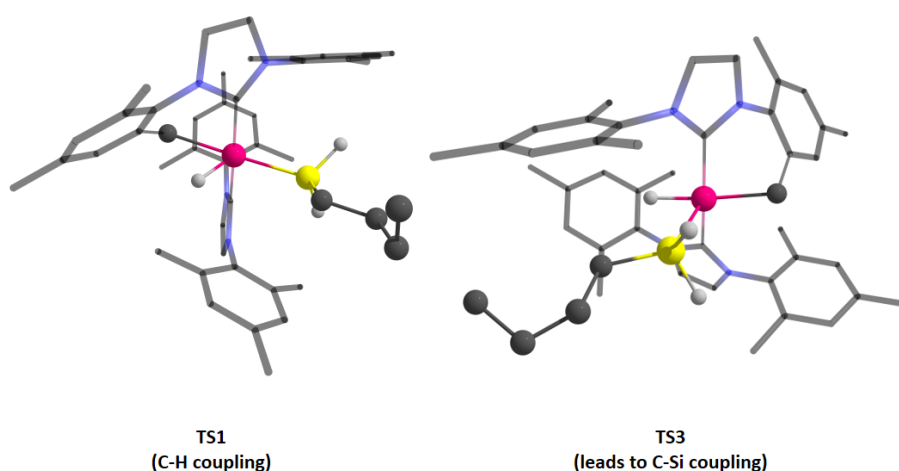
Figure 54. Representation of the two different transition states derived from the oxidative addition of ^{n}BuSiH$_3$ to complex **24**. Depending on the orientation of the silane, either C−H (**TS1**, Figure 52) or C−Si coupling events may take place.

In the latter case, this step requires 22.9 kcal/mol and it leads to intermediate **I1** (17.8 kcal/mol), which consists of a Pt(IV) complex with a distorted trigonal bipyramidal geometry composed by the two NHC ligands in the axial positions and the cyclometalated group, the silyl and hydride ligands occupying equatorial positions. In intermediate **I1**, the Si and C atoms are close to each other (2.46 Å) due to the acute Si−Pt−C angle (63.6°), which prepares both ligands for the coupling event. This phenomenon takes place during **TS4** (18.8 kcal/mol), which is only 1 kcal/mol above **I1**, probably because of the

[288]

preorganization of the complex. This transition state leads to intermediate **I2** (-6.0 kcal/mol), which consists of a cationic platinum(II) hydride where one of the mesityl rings of the carbene possesses one ^{n}BuSiH$_2$– chain dangling away from platinum without showing any appreciable interaction with the metal (Figure 55), given the long distance observed (Pt–Si distance = 4.657 Å), which precludes any stabilization through agostic interactions (the closest proton is 2.769 Å away). This situation changes in intermediate **I3** (-18.6 kcal/mol), which, according to the geometry and the energy observed, might be the intermediate **A** experimentally detected by NMR. In it, a platinum(II) hydride was obtained, where an agostic Si–H interaction with the metal center (Pt–H$_{bridging}$ = 1.884 Å; Pt–Si distance = 2.929 Å; Pt–H–Si angle = 116.6°; H$_{bridging}$–Pt–H$_{hydride}$ angle = 172.3°) could also be observed, in agreement with the ^{1}H-NMR data and the proposed structure depicted in Scheme 18 and Figure 49.
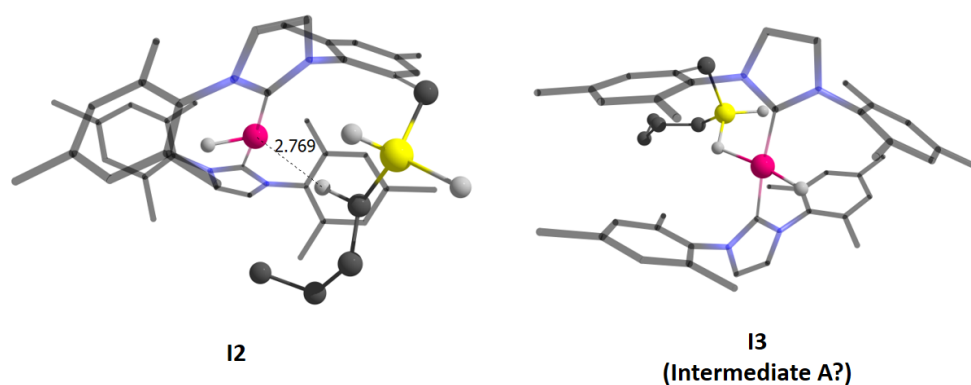
Figure 55. Representation of the intermediates **I2** and **I3** calculated during the C–Si coupling process between butylsilane and complex **24**.

Intermediate **I3** can evolve towards transition state **TS5**, where the second Si–H oxidative addition takes place. This step is 11.0 kcal/mol above the origin, yet it has a total energy cost of 29.6 kcal/mol given that the previous geometry was very exergonic. In this transition state, the bridging hydride migrates from the silicon atom to a position which is very close to the hydride ligand directly

[289]

bound to the metal, describing an orbiting motion around the metal atom. The outcome of this event is intermediate **I4** (-17.9 kcal/mol), which displays the Pt(II) cyclometalated silyl species (Pt–Si distance = 2.336 Å) derived from the insertion of the silane into the Pt–C bond of **24**, and it also contains a dihydrogen molecule bound to the metal via σ interaction, with Pt–H distances of 2.317 Å and 2.385 Å. Release of the H_2 molecule gives complex **26** as the most stable geometry (-28.4 kcal/mol) of the energy profile, as shown in Figure 56.

- d) C–Si coupling (NHCs in *cis*)

This mechanism has the same initial stages than b), so discussion will start from **24$_{cis}$·BuSiH$_3$**. Again, the approach of the silane can be different to that observed in pathway b), so this time the Si atom is closer to the methylene unit than any of the SiH protons. This gives rise to transition state **TS6**, 23.5 kcal/mol above the energy reference, where the C–Si bond formation and the Si–H cleavage take place simultaneously (Figure 57). The resulting intermediates coming from this reaction, **I5** and **I6** (8.8 and -6.4 kcal/mol, respectively) are similar to their *trans* isomers **I2** and **I3**. Nonetheless, analysis of the calculated structure reveals parameters suggesting a η^2 agostic SiH complex (Pt–H$_{bridging}$ = 1.649 Å; Pt–Si distance = 2.518 Å; Pt–H–Si angle = 96.6°; H$_{bridging}$–Pt–H$_{hydride}$ angle = 90.1°) in comparison to **I3**. In a similar way to its *trans* counterpart, the second oxidative addition takes place through transition state **TS7** (5.6 kcal/mol above the reference, 12.0 kcal/mol overall energy barrier) to give the σ-dihydrogen complex **I7** (-1.3 kcal/mol). Extrusion of H_2 leads to the formation of complex **26** after carbene rearrangement to a *trans* disposition once again.

Although the NMR data (*e.g.* coupling constants of intermediate **A**, see Figures 49-51) indicate a *trans* arrangement of the carbene ligands, DFT calculations suggest that a *cis* geometry pathway is less energy demanding. This

is currently being investigated by computational methods, where participation of both mechanisms might be involved in the process.
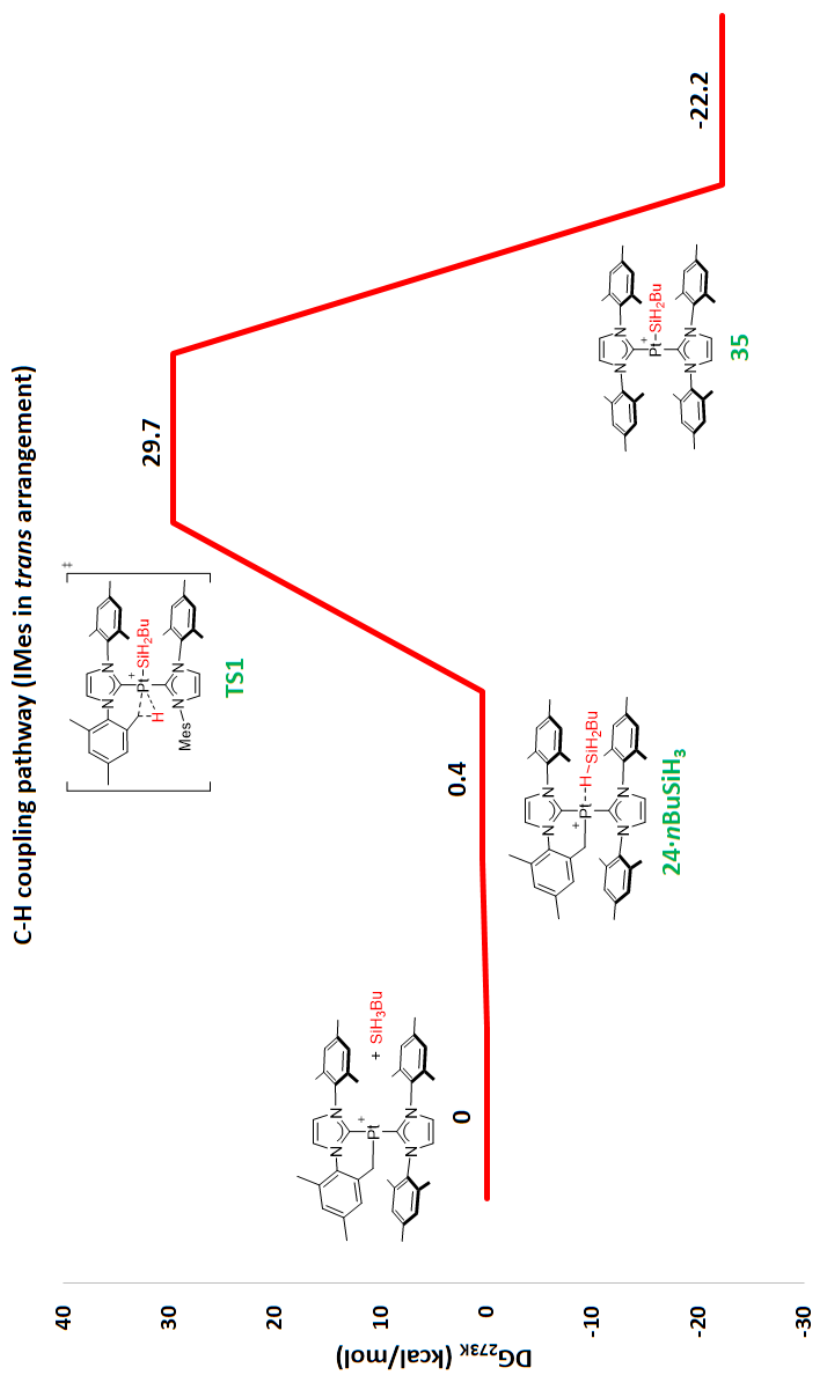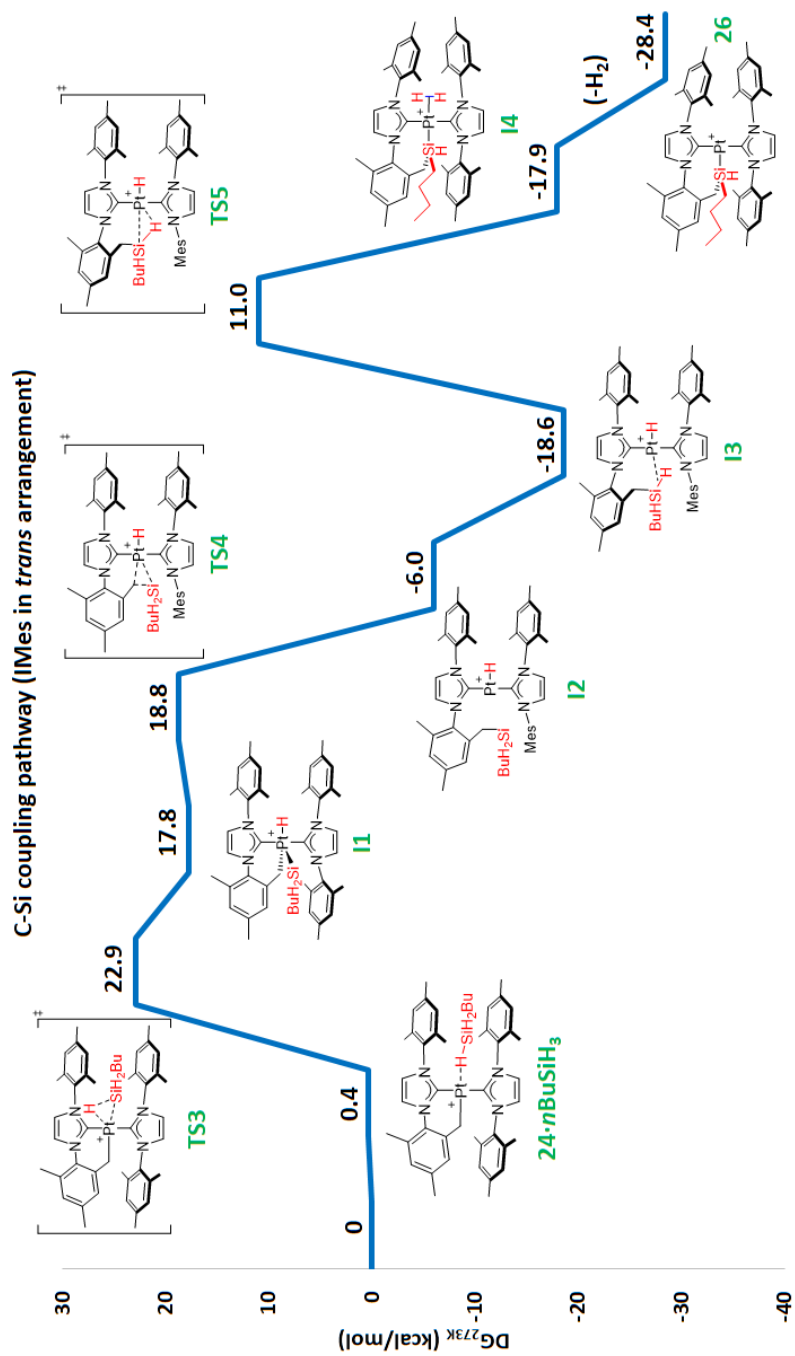
Figure 56. Energy profile for the formation of complex **26** from **24** considering a *trans* arrangement of the carbene ligands.

[292]
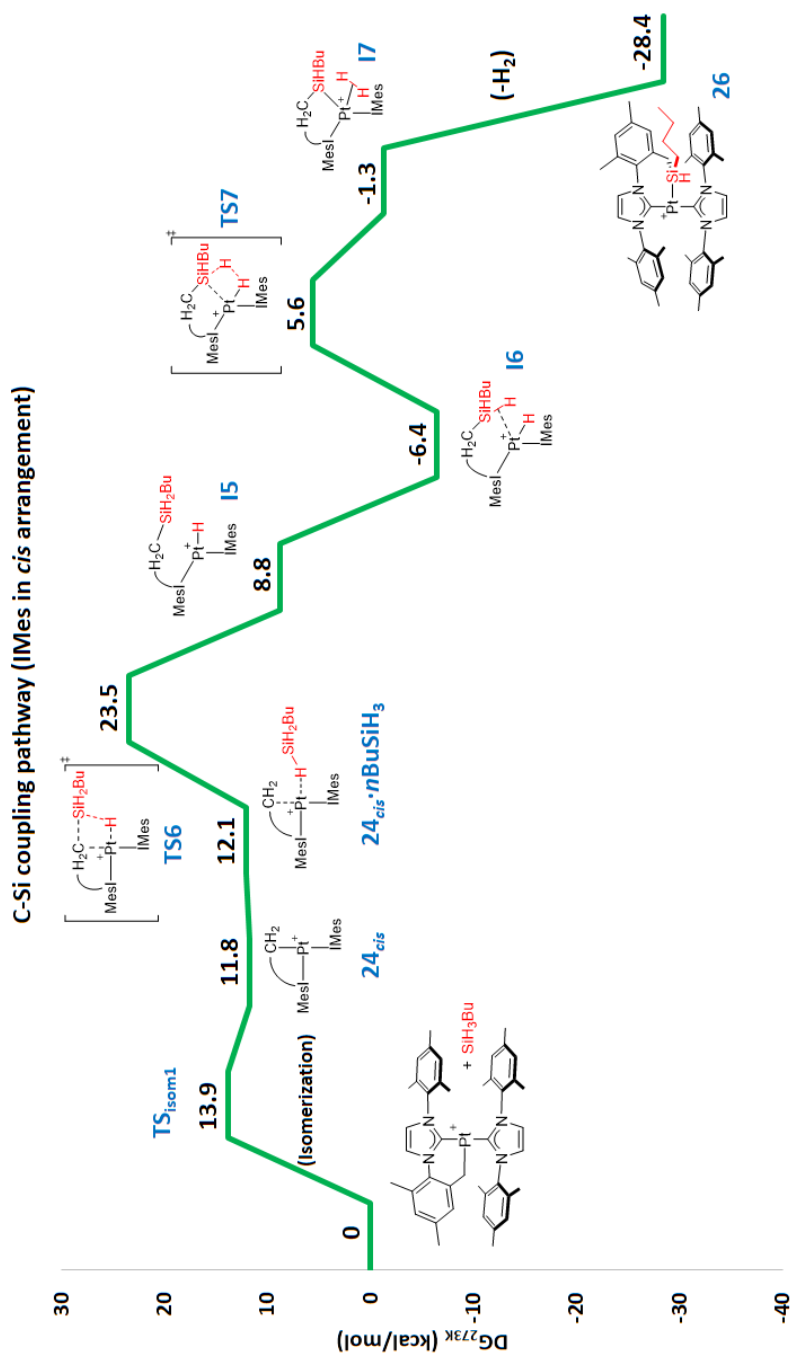
Figure 57. Energy profile for the formation of complex **26** from **24** considering an initial *cis* arrangement of the carbene ligands.

[293]

Chapter 3. Results and discussion

<u>Pt(II) hydride complexes with primary silanes</u>

In this study, I^{t}Bu^{i}Pr derivative [Pt(H)(I^{t}BuiPr)$_2$][BAr$_4^F$], **30**, and ^{n}BuSiH$_3$ were used in calculations where the formation of silyl complex **31** was analysed by considering two mechanistic alternatives: the reaction with the NHC ligands in a *trans* arrangement, or a scenario where both carbenes are *cis* to each other.

- a) Pt−Si coupling (NHCs in *trans*)

Starting with complex [Pt(H)(I^{t}BuiPr)$_2$][BAr$_4^F$] (**30**) and ^{n}BuSiH$_3$ as the energy reference, formation of the σ-SiH complex **30·BuSiH₃** is once again slightly endergonic (2.7 kcal/mol) due to entropic factors (Figure 58). Then, this species evolves towards the oxidative addition of one of the Si−H bonds of the silane to give transition state **TS8**, which is 35.2 kcal/mol above the origin. As described above, an orbiting-like motion of the bridging hydride places the SiH proton close to the hydride ligand bound to the metal center. The outcome of this transition state is intermediate **I8**, which shows the formation of the Pt−Si bond as well as the dihydrogen σ-complex. This geometry is almost isoenergetic to the reagents, with 0.2 kcal/mol. Stabilization of the system (-6.4 kcal/mol) comes from the liberation of the H$_2$ molecule, releasing silyl complex [Pt(SiH$_2$$n$Bu)(I^{t}Bu$i$Pr)$_2$][BAr$_4^F$] (**31**) in the process. As can be deduced, the high energy observed for transition state **TS8** makes this pathway unlikely to happen.

- b) Pt−Si coupling (NHCs in *cis*)

In a similar manner to the previously described mechanisms, isomerization of the platinum precursor is necessary for the reaction to be conducted. This comes about through transition state **TS$_{isom2}$**, which requires 16.8 kcal/mol (Figure 59). Carbene rearrangement gives isomer **30$_{cis}$**, 8.8 kcal/mol less stable than its *trans* counterpart. Approach of one molecule of butylsilane produces **30$_{cis}$·BuSiH₃**, whose formation is again somewhat endergonic to almost the same extent as the *trans* isomer, given that this complex is 2.6 kcal/mol above the

cyclometalated species. The *cis* arrangement of the carbene ligands places the bridging SiH hydrogen close enough to bounce to the position where the platinum hydride is located so as to form the σ-dihydrogen complex. This migration takes place through transition state **TS9**, requiring 20.0 kcal/mol, making this mechanism a feasible possibility by which this reaction takes place. Final formation of the Pt−Si bond yields the dihydrogen intermediate **I9**. Extrusion of H_2 gives silyl derivative [Pt(SiH$_2$*n*Bu)(I*t*Bu*i*Pr)$_2$][BAr$_4^F$] (**31**) 6.4 kcal/mol below the reagents.

In the light of the energy data obtained for both pathways, it seems reasonable to think that this transformation takes place through the mechanism where both carbene ligands are located *cis* to each other.
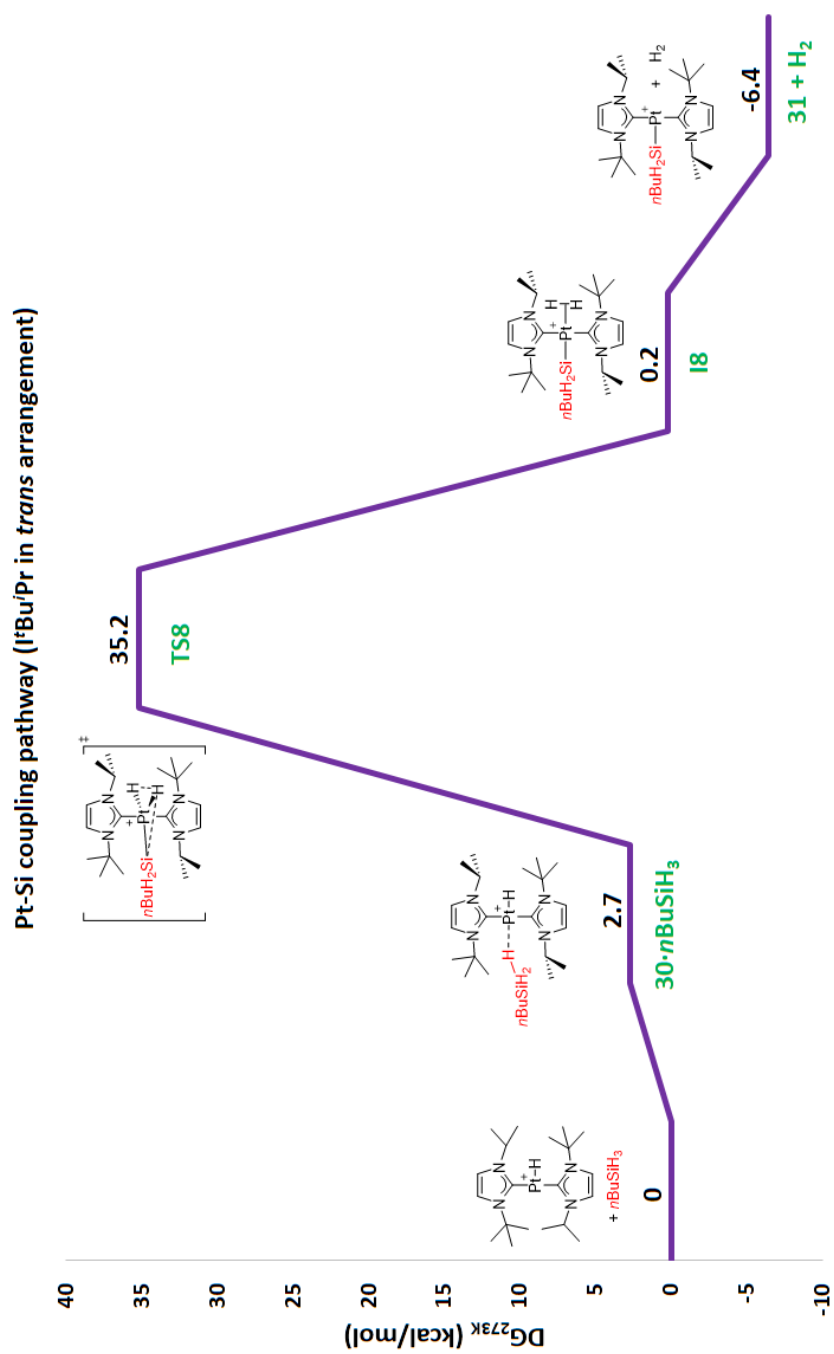
Figure 58. Energy profile for the formation of complex **31** from **30** considering a *trans* arrangement of the carbene ligands.

[296]

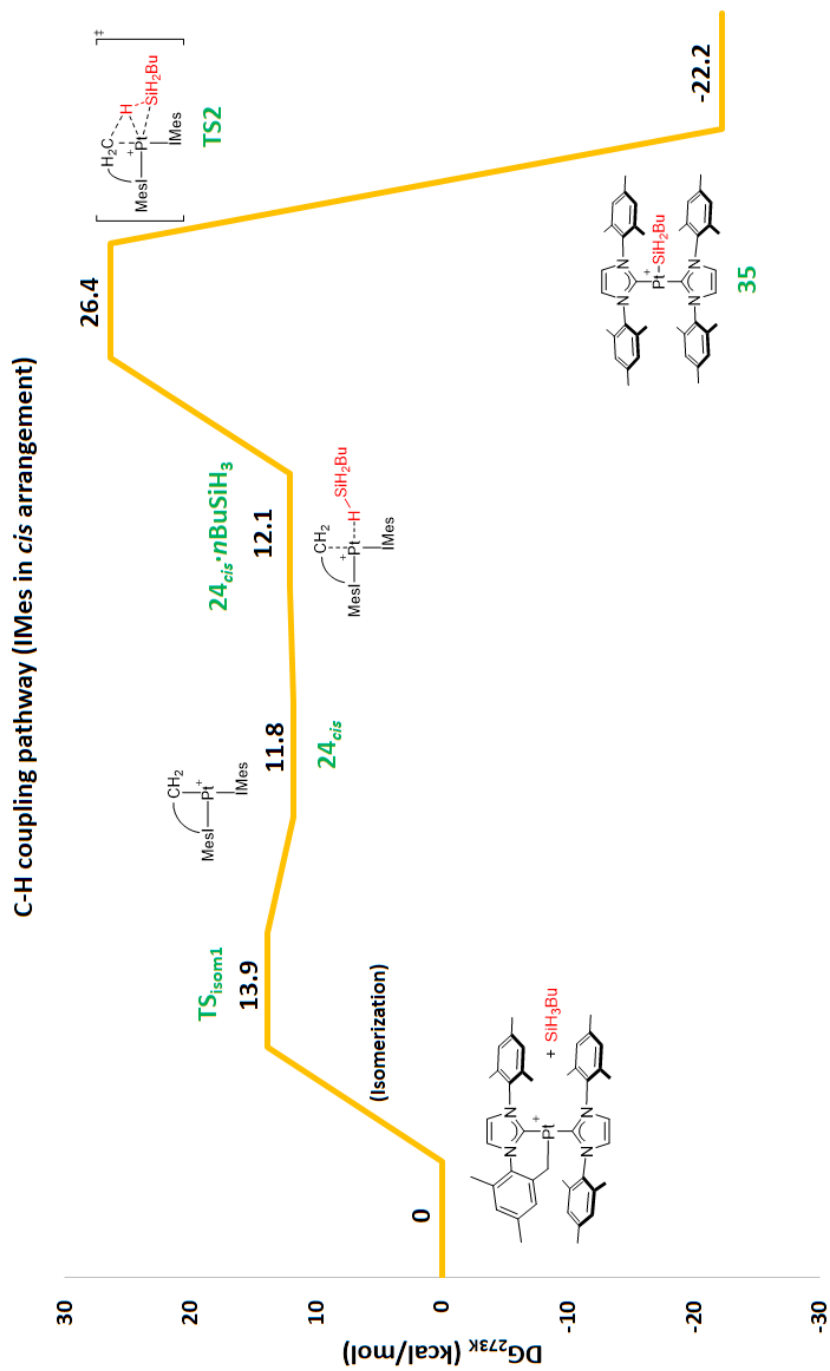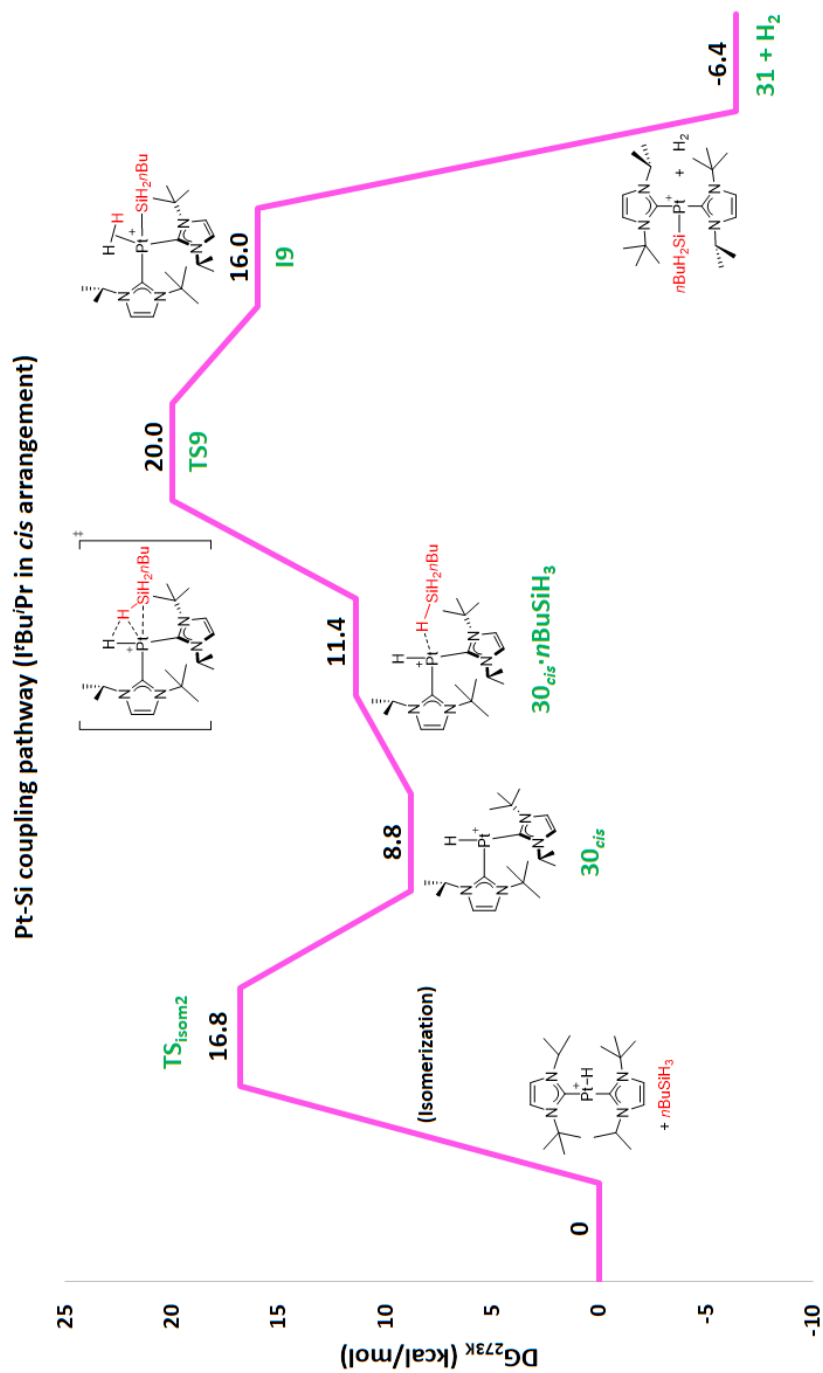**Figure 59.** Energy profile for the formation of complex **31** from **30** considering an initial *cis* arrangement of the carbene ligands.

[297]

2.6. Crystallization of Pt(II) hydride and/or deuteride complexes. Molecular rotors

Numerous attempts of crystallizing the σ-SiH complexes with I^tBu ligands were performed yet all of them proved unfruitful as no crystals were obtained, or precipitate or oils were formed instead. This is not surprising, given the broad signals displayed in the NMR spectra, which indicate that the interaction is not strong enough to hold both chemical entities together. Nonetheless, a crystal obtained in one of the few presumed successful experiments was measured by X-Ray diffraction techniques and turned out to be hydride complex **15** (Figure 60). The solid-state structure of this species could not be elucidated in the past since this molecule is unstable towards cyclometalation to give **13** when exposed to vacuum or mild heating, and attempts to crystallize it under an atmosphere of H_2 failed.[55] However, the unintentional hydrolysis of the silane during crystallization of the mixture of complex **13** and $^nBuSiH_3$ provided a *reservoir* of H_2 leading to hydride derivative **15**.

Pt1-H1pt = 1.254 Å
Pt1-H5c = 1.971(1) Å
Pt1-C5 = 2.639(5) Å
C1-Pt-C12 = 178.2(1) °
N2-C1-C12-N3 = 74.1(4) °
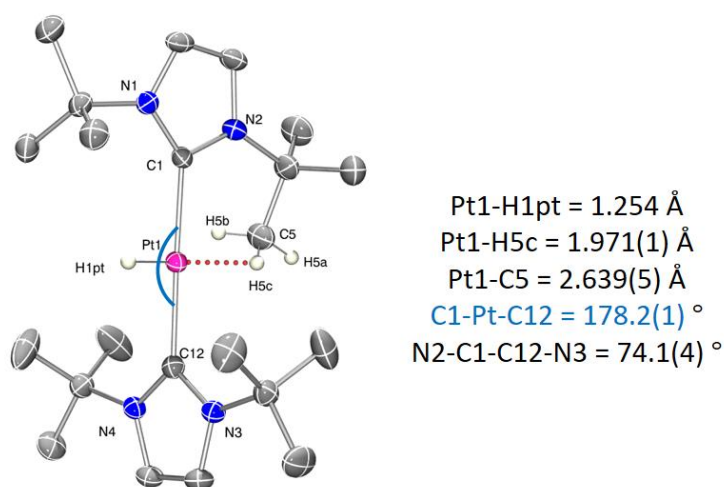
Figure 60. Crystal structure of hydride complex **15**. BAr_4^F anion and most of the hydrogen atoms have been omitted for clarity.

[298]

In the same way as in complex **16**, the crystal structure shows a *trans* arrangement of the carbene groups, and the hydride has no ligand in the opposite direction to it, although there is an agostic interaction stabilizing the Pt(II) center. The shorter distance between Pt and H5c (1.971(1) Å) and Pt and C5 (2.639(5) Å) with respect to silyl complex **16** can be explained by the weaker *trans* influence of hydride ligands in comparison to silyl groups.[47] These structural parameters perfectly fit those previously reported in our group in collaboration with Prof. Agustí Lledós (UAB) by DFT calculations.[36,82] Moreover, these calculations revealed an unexpected fluxional behaviour of the hydride ligands, which are able to move around the metal center in an orbital fashion while the NHCs are static (Scheme 20), similar to that described in the previous section. These results explain the reasons for the unobserved agostic interaction of the platinum center with the *tert*-butyl groups by ^{1}H NMR spectroscopy. Unfortunately, solution NMR spectroscopy is not a convenient technique to demonstrate this fluxional process. However, soon after publishing our results, the groups of Ulrich Fekl and Robert W. Schurko at the Universities of Toronto and Windsor, respectively, were able to determine the capability of deuteride ligands in *trans*-D(L)-Pt(P^{t}Bu$_3$)$_2$ (L = deuteride or chloride) complexes to behave as rotors by combining ^{2}H and [195]Pt solid-state NMR studies with theoretical calculations.[83]

[82] M. A. Ortuño, P. Vidossich, S. Conejero, A. Lledós, *Angew. Chem. Int. Ed.,* **2014**, *53*, 14158-14161.

[83] E. Prack, C. A. O'Keefe, J. K. Moore, A. Lai, A. J. Lough, P. M. Macdonald, M. S. Conradi, R. W. Schurko, U. Fekl, *J. Am. Chem. Soc.,* **2015**, *137*, 13464-13467.
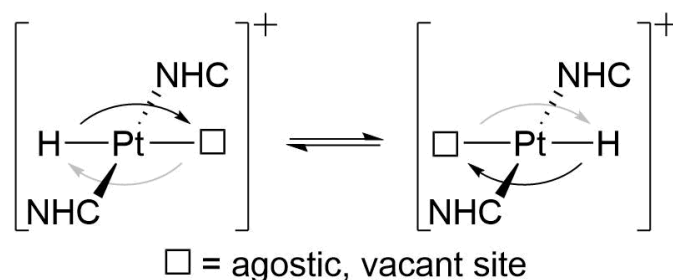
Scheme 20. Orbital-like motion of hydride ligands around the metal center (adapted from reference 82).

The fact that it is possible to isolate complex **15** in the solid state raised the question of whether it is possible to determine experimentally such a fluxional process. For this reason, a collaboration has been stablished with these researchers, and several *trans*-D(L)-Pt(NHC)$_2$ compounds containing I^{t}Bu and IPr[84] carbenes (Figure 61) have been prepared through modified procedures.
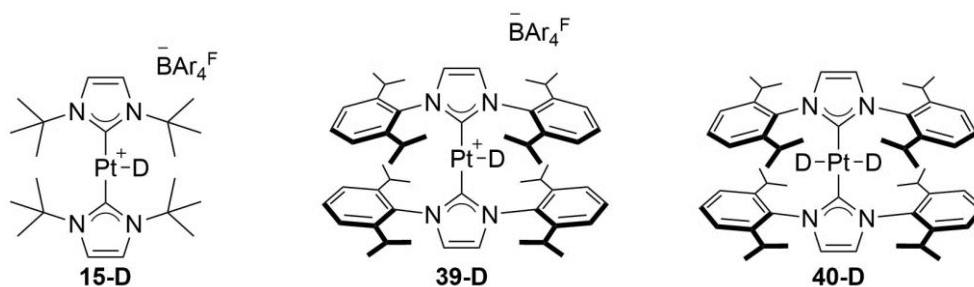
Figure 61. Platinum deuteride complexes employed in the molecular rotors investigation.

The reason for the selection of these compounds is the availability of their corresponding crystal structures,[55,85] so they can be employed in the molecular dynamics calculations to evaluate their rotor behaviour. Complex **39-D** was previously synthesized in our group by H/D exchange using the

---

[84] IPr stands for 1,3-bis-(2,6-diisopropylphenyl)-imidazol-2-ylidene.
[85] The crystal structure of complex **39** contained hexafluoroantimonate(V) as a non-coordinating anion.

corresponding hydride derivatives.[36] With respect to complex **15-D**, as mentioned before, it is unstable towards cyclometalation under vacuum or mild heating, but we have found that it can be prepared in the solid state (without solvent) by pressurizing the cyclometalated derivative **13** under D_2. This compound is stable under a D_2 atmosphere, but undergoes cyclometalation even in the solid state at r.t. after a few hours under air. However, it is stable enough for studying it by solid state NMR spectroscopy at low temperatures. Complex **40** was also prepared in our group, but only in the dihydride form.[51] The synthetic procedure for the dideuteride complex **40-D**, that entails the reaction of complex **39-H** with NaH, has now been modified and the yield improved: when searching for commercially available anionic sources of deuterium that could transform **39-D** into **40-D**, alkali salts such as LiD or $LiAlD_4$ were unsuccessful to achieve such transformation.[86] However, $NaBD_4$ was reactive enough to transform **39-D** into adduct **41** in 1 hour in excellent yield (Scheme 21). Subsequent removal of the BD_3 unit was possible by using a large excess (85 eq) of Et_3N at 70 °C for 19 hours, affording the corresponding amino-borane $Et_3N·BD_3$ and clean **40-D** in good yield (Figure 62).
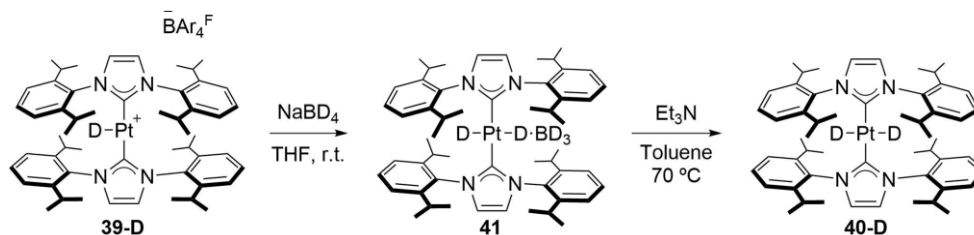
Scheme 21. Synthetic route for platinum dideuteride **40–D**.

---

[86] NaD was not commercially available by the time the synthesis of **40-D** was performed.
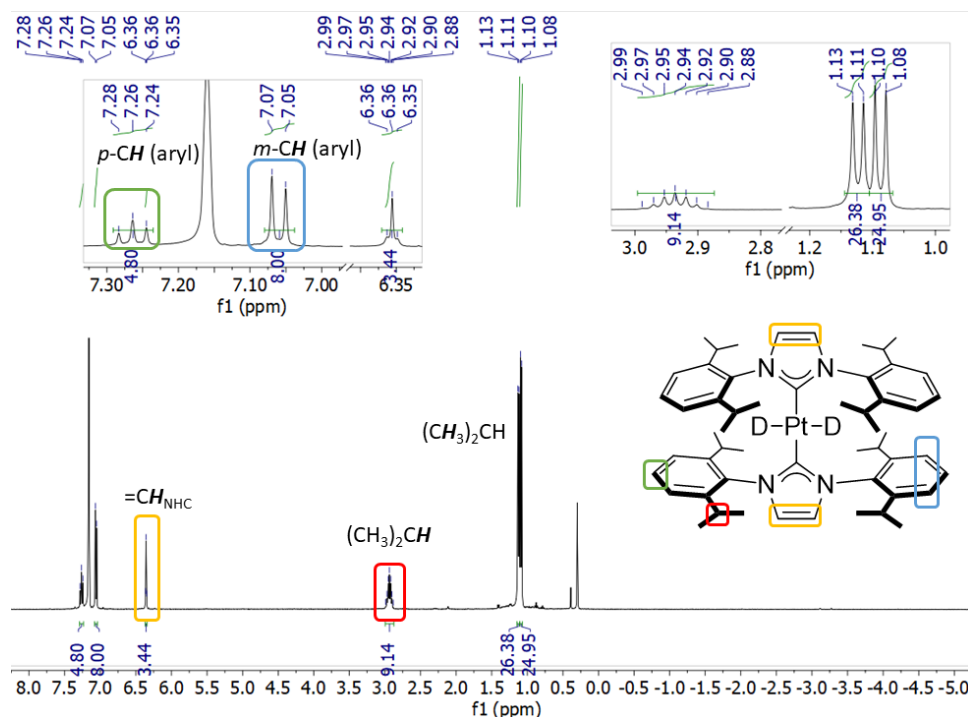
Figure 62. ^{1}H NMR spectrum (400 MHz, C_6D_6) of complex **40−D**. It can be observed that the hydride region shows that no isotopologue **40** is formed during the synthesis.

Dideuteride **40-D** was crystallized by solvent diffusion techniques, giving colorless crystals that were measured by X-Ray diffraction. The crystal structure (Figure 63) confirms the arrangement of ligands previously observed by NMR, and it completes the characterization of this compound. The geometrical parameters of dihydride **40-D** are very similar to those observed for cationic species **39**.[36] The Pt−H1pt distances (1.703(5) Å for **40-D**[87] and 1.67(2) Å for **39**) are in accordance with reported Pt−H lengths, which are in the order of 1.5-1.8

---

[87] The other Pt−D distance is 1.961(9) Å, which is oddly long. This might be due to the difficulties found when locating the electron density of the deuteride ligand during refinement of the structure. DFT calculations on **40** (Level of theory: M06/6-31g(d,p/SDD) gave a length of 1.68 Å, in agreement with the experimental findings (1.703(5) Å).

Å.[88] The C1–Pt1 (2.001(6) Å) and C28–Pt1 (1.990(0) Å) distances are almost identical to those observed for the cationic derivative, as well as the dihedral angle formed by N2–C1–C28–N4 (41.58 °). The crystal structure of **40-D** geometry serves as a starting point for molecular dynamics calculations on the molecular rotors project. By the time this thesis is being written, measurements on the complexes shown in Figure 61 are underway.

Pt1-H1pt = 1.704 Å
Pt1-H2pt = 1.962 Å
H1pt-Pt1-H2pt = 176.4 °
C1-Pt-C28 = 178.7 °
N2-C1-C28-N4 = 41.6 °
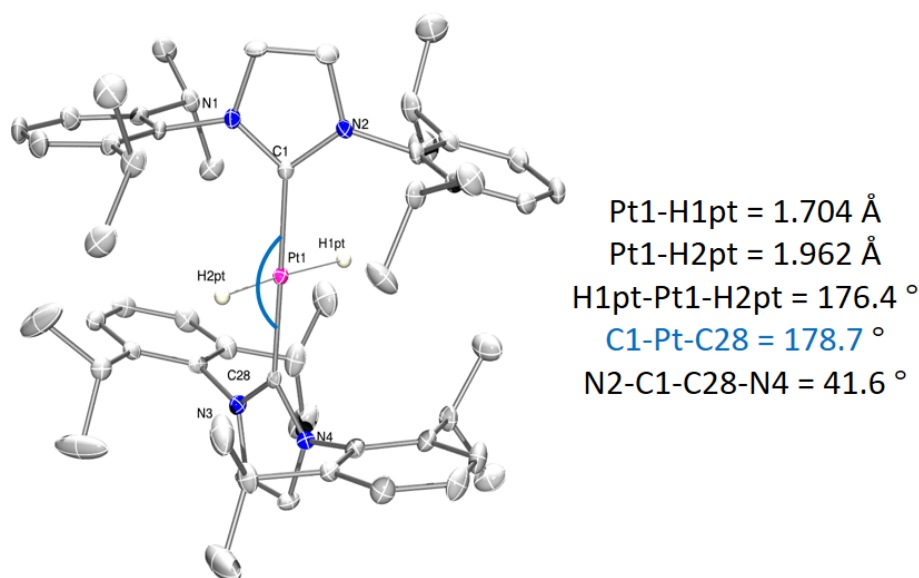
Figure 63. Crystal structure of dideuteride complex **40-D**. Most of the hydrogen atoms have been omitted for clarity.

[88] a) P. G. Owston, J. M. Partridge, J. M. Rowe, *Acta Crystallogr.,* **1960**, *13*, 246-252; b) G. B. Robertson, P. A. Tucker, W. A. Wickramasinghe, *Aust. J. Chem.,* **1986**, *39*, 1495-1507; c) A. Albinati, G. Bracher, D. Carmona, J. H. P. Jans, W. T. Klooster, T. F. Koetzle, A. Macchioni, J. S. Ricci, R. Thouvenot, L. M. Venanzi, *Inorg. Chim. Acta*, **1997**, *265*, 255-265.

References

[1] J. V. Obligacion, P. J. Chirik, *Nat. Rev. Chem.,* **2018**, *2*, 15-34.

[2] Y. Nakajima, S. Shimada, *RSC Adv.,* **2015**, *5*, 20603-20616.

[3] H. Renner, G. Schlamp, I. Kleinwächter, E. Drost, H. M. Lüschow, P. Tews, P. Panster, M. Diehl, J. Lang, T. Kreuzer, A. Knödler, K. A. Starz, K. Dermann, J. Rothaut, R. Drieselmann, C. Peter, R. Schiele. Platinum Group Metals and Compounds. *Ullmann's Encyclopedia of Industrial Chemistry,* **2001**, doi:10.1002/14356007.a21_075.

[4] J. L. Speier, J. A. Webster, G. H. Barnes, *J. Am. Chem. Soc.,* **1956**, *78*, 2278-2281.

[5] B. D. Karstedt, General Electric Company, US3775452A, **1973**.

[6] L. N. Lewis, J. Stein, Y. Gao, R. E. Colborn, G. Hutchins, *Platinum Metals Rev.,* **1997**, *41*, 66-75.

[7] B. Marciniec, *Coord. Chem. Rev.,* **2005**, *249*, 2374-2390.

[8] D. Troegel, J. Stohrer, *Coord. Chem. Rev.,* **2011**, *255*, 1440-1459.

[9] I. E. Markó, S. Stérin, O. Buisine, G. Mignani, P. Branlard, B. Tinant, J-P. Declercq, *Science*, **2002**, *298*, 204-206.

[10] A. J. Chalk, J. F. Harrod, *J. Am. Chem. Soc.,* **1965**, *87*, 16-21.

[11] a) M. A. Schroeder, M. S. Wrighton, *J. Organomet. Chem.,* **1977**, *128*, 345-358; b) I. Ojima, T. Fuchikami, M. Yatabe, *J. Organomet. Chem.,* **1984**, *260*, 335-346.

[12] S. Sakaki, N. Mizoe, M. Sugimoto, *Organometallics*, **1998**, *17*, 2510-2523.

[13] Some representative examples include: a) M. Rubin, T. Schwier, V. Gevorgyan, *J. Org. Chem.,* **2002**, *67*, 1936-1940; b) M. Pérez, L. J. Hounjet, C. B. Caputo, R. Dobrovetsky, D. W. Stephan, *J. Am. Chem. Soc.,* **2013**, *135*, 18308-18310; c) J. Chen, E. Y.-X. Chen, *Angew. Chem. Int. Ed.,* **2015**, *54*, 6842-6846.

[14] W. E. Piers, T. Chivers, *Chem. Soc. Rev.,* **1997**, *26*, 345-354.

[15] G. I. Nikonov, *Adv. Organomet. Chem.,* **2005**, *53*, 217-309.

[16] J. Y. Corey, *Chem. Rev.,* **2011**, *111*, 863-1071.

[17] J. K. Hoyano, M. Elder, W. A. G. Graham, *J. Am. Chem. Soc.,* **1969**, *91*, 4568-4569.

[18] E. Colomer, R. J. P. Corriu, C. Marzin, A. Vioux, *Inorg. Chem.,* **1982**, *21*, 368-373.

[304]

[19] U. Schubert, K. Ackermann, B. Wörle, *J. Am. Chem. Soc.,* **1982**, *104*, 7378-7380.

[20] J. Y. Corey, *Chem. Rev.,* **2016**, *116*, 11291-11435.

[21] D. H. Binh, M. Milovanović, J. Puertes-Mico, M. Hamdaoui, S. D. Zarić, J-P. Djukic, *Chem. Eur. J.,* **2017**, *23*, 17058-17069.

[22] X-L. Luo, R. H. Crabtree, *J. Am. Chem. Soc.,* **1989**, *111*, 2527-2535.

[23] a) E. Scharrer, S. Chang, M. Brookhart, *Organometallics,* **1995**, *14*, 5686-5694; b) F. L. Taw, R. G. Bergman, M. Brookhart, *Organometallics,* **2004**, *23*, 886-890; c) M. D. Doherty, B. Grant, P. S. White, M. Brookhart, *Organometallics*, **2007**, *26*, 5950-5960.

[24] X. Fang, B. L. Scott, K. D. John, G. J. Kubas, *Organometallics*, **2000**, *19*, 4141-4149.

[25] D. V. Gutsulyak, S. F. Vyboishchikov, G. I. Nikonov, *J. Am. Chem. Soc.,* **2010**, *132*, 5950-5951.

[26] S. T. N. Freeman, F. R. Lemke, *Organometallics,* **2002**, *21*, 2030-2032. This complex was previously synthesized and analysed before its crystallization: F. R. Lemke, *J. Am. Chem. Soc.,* **1994**, *116*, 11183-11184.

[27] J. Yang, P. S. White, C. K. Schauer, M. Brookhart, *Angew. Chem. Int. Ed.,* **2008**, *47*, 4141-4143.

[28] N. A. Yakelis, R. G. Bergman, *Organometallics,* **2005**, *24*, 3579-3581.

[29] Y-R. Luo, *Comprehensive Handbook of Chemical Bond Energies,* CRC Press: Boca Raton, FL, 2007.

[30] A. Y. Houghton, J. Hurmalainen, A. Mansikkamäki, W. E. Piers, H. M. Tuononen, *Nat. Chem.,* **2014**, *6*, 983-988.

[31] S. P. Hoffmann, T. Kato, F. S. Tham, C. A. Reed, *Chem. Commun.,* **2006**, 767-769.

[32] M. C. Lipke, A. L. Liberman-Martin, T. D. Tilley, *Angew. Chem. Int. Ed.,* **2017**, *56*, 2260-2294.

[33] A Pt(0) agostic Si−H complex has been synthesized, though: S. J. Mitton, R. McDonald, L. Turculet, *Organometallics*, **2009**, *28*, 5122-5136.

[34] a) O. Rivada-Wheelaghan, B. Donnadieu, C. Maya, S. Conejero, *Chem. Eur. J.,* **2010**, *16*, 10323-10326; b) M. Roselló-Merino, O. Rivada-Wheelaghan, M. A. Ortuño, P. Vidossich, J. Díez, A. Lledós, S. Conejero, *Organometallics*, **2014**, *33*, 3746-3756.

[35] a) O. Rivada-Wheelaghan, M. A. Ortuño, J. Díez, A. Lledós, S. Conejero, *Angew. Chem. Int. Ed.,* **2012**, *51*, 3936-3939; b) M. A. Ortuño, S. Conejero, A. Lledós, *Beilstein J. Org. Chem.,* **2013**, *9*, 1352-1382.

[36] O. Rivada-Wheelaghan, M. Roselló-Merino, M. A. Ortuño, P. Vidossich, E. Gutiérrez-Puebla, A. Lledós, S. Conejero, *Inorg. Chem.,* **2014**, *53*, 4257-4268.

[37] ItBu stands for 1,3-di-*tert*-butylimidazol-2-ylidene, whereas ItBu' represents the cyclometalated version of the NHC ligand.

[38] M. Roselló-Merino, J. López-Serrano, S. Conejero, *J. Am. Chem. Soc.,* **2013**, *135*, 10910-10913.

[39] M. Roselló-Merino, R. J. Rama, J. Díez, S. Conejero, *Chem. Commun.,* **2016**, *52*, 8389-8392.

[40] The cross-peak between H and Si was lost at lower temperatures due to signal broadening and coalescence phenomena.

[41] J. Voigt, T. Braun, *Dalton Trans.,* **2011**, *40*, 12699-12704

[42] M. Besora, F. Maseras, A. Lledós, O. Eisenstein, *Inorg. Chem.,* **2002**, *41*, 7105-7112.

[43] L. A. Watson, O. Eisenstein, *J. Chem. Educ.*, **2002**, *79*, 1269-1277.

[44] The Ir–H–Si angle in the only η^1 σ-silane complex crystallographically described is 157 ° (Reference 27).

[45] The sum of the covalent radii for Si (1.11 Å) and Pt (1.36 Å) is 2.47 Å. See: B. Cordero, V. Gómez, A. E. Platero-Prats, M. Revés, J. Echeverría, E. Cremades, F. Barragán, S. Alvarez, *Dalton Trans.,* **2008**, 2832-2838.

[46] J-N. Luy, S. A. Hauser, A. B. Chaplin, R. Tonner, *Organometallics*, **2015**, *34*, 5099-5112.

[47] J. Zhu, Z. Lin, T. B. Marder, *Inorg. Chem.,* **2005**, *44*, 9384-9390.

[306]

[48] J. C. Baldwin, W. C. Kaska, *Inorg. Chem.,* **1979**, *18*, 686-691.

[49] R. Bassan, K. H. Bryars, L. Judd, A. W. G. Platt, P. G. Pringle, *Inorg. Chim. Acta*, **1986**, *121*, L41-L42.

[50] G. C. Fortman, N. M. Scott, A. Linden, E. D. Stevens, R. Dorta, S. P. Nolan, *Chem. Commun.,* **2010**, *46*, 1050-1052.

[51] *"Complejos de metals de transición conteniendo ligandos de tipo carbeno N-heterocíclico de 5 y 6 miembros. Síntesis y estudios de reactividad."* M. Roselló-Merino. PhD Thesis. **2013**.

[52] M. Brookhart, M. L. H. Green, G. Parkin, *Proc. Natl. Acad. Sci. U. S. A.,* **2007**, *104*, 6908-6914.

[53] E. S. Tabei, H. Samouei, M. Rashidi, *Dalton Trans.,* **2011**, *40*, 11385-11388.

[54] M. Brookhart, B. Grant, A. F. Volpe Jr., *Organometallics*, **1992**, *11*, 3920-3922.

[55] *"Síntesis de complejos coordinativamente insaturados de Pt(II) estabilizados por ligandos carbeno N-heterocíclicos. Activación y funcionalización de enlaces C−H."* O. Rivada-Wheelaghan. PhD Thesis. **2013**.

[56] Free Et_3SiH: ^1H NMR (600 MHz, 213 K, CD_2Cl_2): δ 3.50 (sept, 1 H, $^1J_{Si-H}$ = 173.6 Hz) ppm, ^{29}Si NMR (119 MHz, 213 K, CD_2Cl_2): δ 0.0 (s) ppm. See: M. Hamdaoui, C. Desrousseaux, H. Habbita, J-P. Djukic, *Organometallics*, **2017**, *36*, 4864-4882.

[57] W. Scherer, P. Meixner, K. Batke, J. E. Barquera-Lozada, K. Ruhland, A. Fischer, G. Eickerling, K. Eichele, *Angew. Chem. Int. Ed.,* **2016**, *55*, 11673-11677.

[58] Calculations were carried out at the TPSSh-D3/6-31g(d,p)/SDD//TPSSh-D3/6-311++G(2d,p)/def2QZVP level of theory. SMD (Dichloromethane) continuum was used to model the solvent.

[59] P. L. A. Popelier, *Coord. Chem. Rev.,* **2000**, *197*, 169-189.

[60] A BCP indicates a bonding situation between two nuclei. See reference 59 for more details.

[61] The same study was performed on the experimental structure derived from X-Ray diffraction studies, and the same topological map was obtained (*i.e.* no BCP was found between Pt and Si).

[62] Formation of silyl complex **21** is a consequence of the reactivity patterns displayed by the σ-silane complexes studied in this thesis. This behaviour will be described in detail in the next section of the chapter.

[63] A BCP is observed between Pt and Si in the calculated structure of **19·Ph₃SiH** upon further closing the Pt−H−Si angle to around 80°, which suggests that the situation observed above is close to the threshold for a BCP to appear.

[64] Some studies have shown that the presence of a RCP close to a BCP is indicative of the instability of the latter. See: P. Meixner, K. Batke, A. Fischer, D. Schmitz, G. Eickerling, M. Kalter, K. Ruhland, K. Eichele, J. E. Barquera-Lozada, N. P. M. Casati, F. Montisci, P. Macchi, W. Scherer, *J.Phys. Chem. A*, **2017**, *121*, 7219.

[65] Calculations were carried out at the PBE/DZVP/GTH level of theory.

[66] P. Vidossich, A. Lledós, *Dalton Trans.,* **2014**, *43*, 11145-11151.

[67] M. A. Ortuño, P. Vidossich, G. Ujaque, S. Conejero, A. Lledós, *Dalton Trans.,* **2013**, *42*, 12165-12172.

[68] This rearrangement can be observed in the video file included in the CD attached to this thesis.

[69] P. Vidossich, G. Ujaque, A. Lledós. *Chem. Commun.,* **2012**, *48*, 1979-1981.

[70] M. Aizenberg, D. Milstein, *J. Am. Chem. Soc.,* **1995**, *117*, 6456-6464.

[71] M. E. van der Boom, J. Ott, D. Milstein, *Organometallics,* **1998**, *17*, 4263-4266.

[72] M. Aizenberg, D. Milstein, *Angew. Chem. Int. Ed.,* **1994**, *33*, 317-319.

[73] As shown above in section 2.2, complex **21** could be crystallized and analyzed by X-Ray diffraction methods (Figure 27).

[74] For NMR data regarding neutral silyl Pt(II) complexes, see: a) D. Chan, S. B. Duckett, S. L. Heath, I. G. Khazal, R. N. Perutz, S. Sabo-Etienne, P. L. Timmins, *Organometallics*, **2004**, *23*, 5744-5756; b) J. C. DeMott, W. Gu, B. J. McCulloch, D. E. Herbert, M. D. Goshert, J. R. Walensky, J. Zhou, O. V. Ozerov, *Organometallics*, **2015**, *34*, 3930-3933; c) C. Mitzenheim, T. Braun, R. Laubenstein, B. Braun, R. Herrmann, *Dalton Trans.,* **2016**, *45*, 6394-6404.

[308]

[75] A small amount (∼5%) of complex **37** ([Pt(IMes*)$_2$SiH$_2^n$Bu][BAr$_4^F$], see below) is observed in the synthesis of species **28**. See Experimental part for more details.

[76] a) Z. Mo, Y. Liu, L. Deng, *Angew. Chem. Int. Ed.,* **2013**, *52*, 10845-10849; b) J. Sun, C. Ou, C. Wang, M. Uchiyama, L. Deng, *Organometallics*, **2015**, *34*, 1546-1551; c) J. Sun, L. Luo, Y. Luo, L. Deng, *Angew. Chem. Int. Ed.,* **2017**, *56*, 2720-2724.

[77] Z. Ouyang, L. Deng, *Organometallics*, **2013**, *32*, 7268-7271.

[78] The terminal hydrogen atoms resonate at 3 and 3.84 ppm. The three SiH protons correlate with a peak at -53.5 ppm in the ^{29}Si spectrum (HMQC ^{1}H–^{29}Si). Additionally, NOESY experiments reveal exchange between bridging and terminal protons, suggesting a fluxional process.

[79] Calculations were carried out at the M06/6-31g(d,p)/SDD//M06/6-311++g(d,p)/SDD level of theory. SMD (Dichloromethane) continuum was used to model the solvent.

[80] Mechanistic pathways involving silylene species were also taken into account, yet their energy barriers were too high to be considered as experimentally feasible. For the sake of simplicity, these preliminary results are not included in this thesis.

[81] It is worth remembering that the formation of the σ-SiH complexes is slightly endergonic due to entropic factors (see section 2.1) but exothermic enough to observe their formation at low temperature.

[82] M. A. Ortuño, P. Vidossich, S. Conejero, A. Lledós, *Angew. Chem. Int. Ed.,* **2014**, *53*, 14158-14161.

[83] E. Prack, C. A. O'Keefe, J. K. Moore, A. Lai, A. J. Lough, P. M. Macdonald, M. S. Conradi, R. W. Schurko, U. Fekl, *J. Am. Chem. Soc.,* **2015**, *137*, 13464-13467.

[84] IPr stands for 1,3-bis-(2,6-diisopropylphenyl)-imidazol-2-ylidene.

[85] The crystal structure of complex **39** contained hexafluoroantimonate(V) as a non-coordinating anion.

[86] NaD was not commercially available by the time the synthesis of **40-D** was performed.

[309]

[87] The other Pt–D distance is 1.961(9) Å, which is oddly long. This might be due to the difficulties found when locating the electron density of the deuteride ligand during refinement of the structure. DFT calculations on **40** (Level of theory: M06/6-31g(d,p/SDD) gave a length of 1.68 Å, in agreement with the experimental findings (1.703(5) Å).

[88] a) P. G. Owston, J. M. Partridge, J. M. Rowe, *Acta Crystallogr.,* **1960**, *13*, 246-252; b) G. B. Robertson, P. A. Tucker, W. A. Wickramasinghe, *Aust. J. Chem.,* **1986**, *39*, 1495-1507; c) A. Albinati, G. Bracher, D. Carmona, J. H. P. Jans, W. T. Klooster, T. F. Koetzle, A. Macchioni, J. S. Ricci, R. Thouvenot, L. M. Venanzi, *Inorg. Chim. Acta*, **1997**, *265*, 255-265.

Chapter 4

Catalytic processes assisted by cationic Pt(II) σ-SiH complexes

1. Introduction

1.1. Reactivity with electrophilic sources of Silicon

As described throughout this thesis, activation of hydrosilanes by Lewis acids can lead to an increase in the electrophilicity of the silicon atom. This process can be mediated by main-group Lewis acids or electrophilic transition-metal complexes, in which silylene species may be involved.[1] Depending on the degree of activation, partial or total exposure of the silicon atom (and silylium character)[2] might be observed.

Silylium cations

R_3Si^+ species are extremely strong Lewis acids due to their empty *p*-orbital and their unfilled valence shell with only six electrons in it. In spite of having properties that would suggest a higher stabilization over their carbon analogues (*i.e.* carbenium ions) such as bigger size, lower electronegativity (2.55 for C vs 1.90 for Si) and greater polarizability, they are indeed much more unstable. This is because of kinetic reasons, which make silylium cations exceptionally reactive and susceptible to nucleophiles in comparison to their carbon counterparts.[3] For this reason, the presence of even weak Lewis bases (like coordinating solvents) must be avoided in the synthesis of this type of species. One of the most common methods for preparing them takes advantage of the polarization of the Si–H bond to abstract the hydrogen atom (with hydride character) by using strong electrophiles containing weak-coordinating anions

[1] M. C. Lipke, A. L. Liberman-Martin, T. D. Tilley, *Angew. Chem. Int. Ed.,* **2017**, *56*, 2260-2294.

[2] D. H. Binh, M. Milovanović, J. Puertes-Mico, M. Hamdaoui, S. D. Zarić, J-P. Djukic, *Chem. Eur. J.,* **2017**, *23*, 17058-17069.

[3] V. Y. Lee, A. Sekiguchi in *Organosilicon Compounds*, **2017**, Academic Press. *Chapter 5: Silicon-centered cations*, 197-230.

such as the trityl salt [Ph$_3$C][B(C$_6$F$_5$)$_4$]. This procedure is frequently referred to as Bartlett-Condon-Schneider *hydride-transfer reaction* (Scheme 1).[4]

$$\underset{\substack{R\\|\\R}}{R-Si-H} \;+\; E^{+} \;\longrightarrow\; \underset{\substack{R\\|\\R}}{\overset{R}{R-\overset{+}{Si}}} \;+\; EH$$
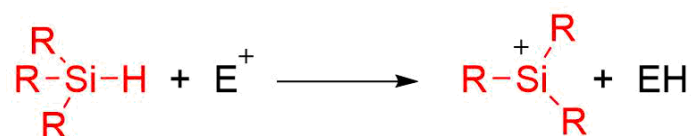
Scheme 1. Hydride-transfer reaction to give silylium cations (adapted from reference 3).

In fact, this methodology was adopted by the group of Oestreich several years ago, where they synthesized the ferrocene-stabilized silylium ion displayed in Scheme 2 (top), which was able to effectively carry out Diels-Alder reactions at low temperature[5] as well as hydrosilation of carbonyl groups (Scheme 2, bottom).[6]

---

[4] P. D. Bartlett, F. E. Condon, A. Schneider, *J. Am. Chem. Soc.,* **1944**, *66*, 1531-1539.

[5] H. F. T. Klare, K. Bergander, M. Oestreich, *Angew. Chem. Int. Ed.,* **2009**, *48*, 9077-9079.

[6] K. Müther, M. Oestreich, *Chem. Commun.,* **2011**, *47*, 334-336.
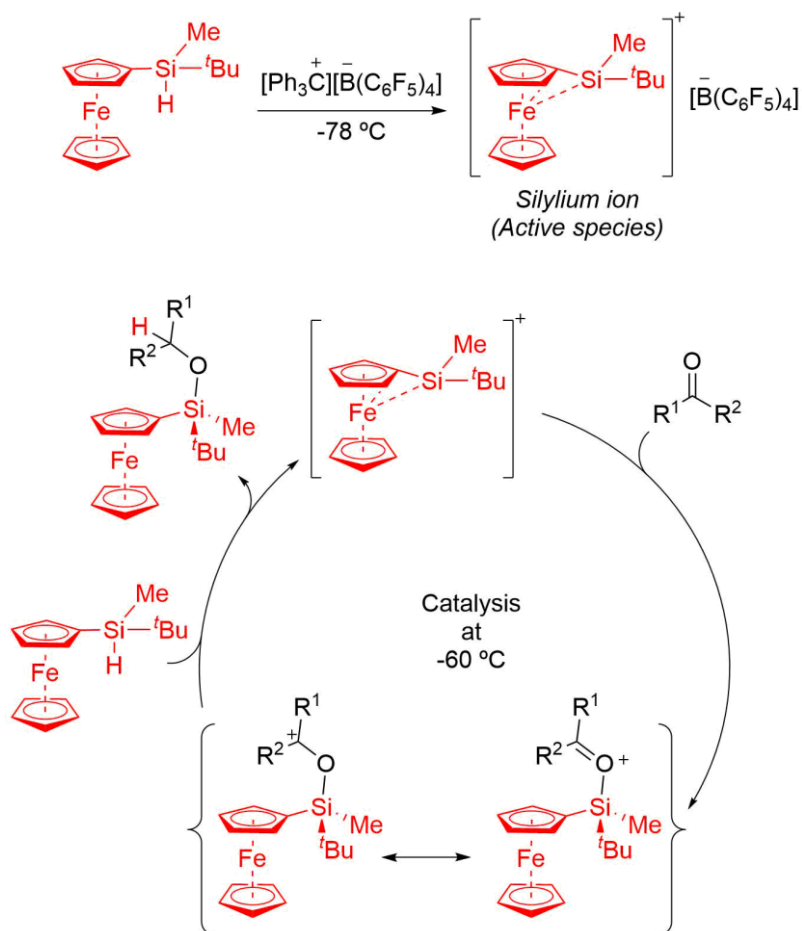
Scheme 2. Top: hydride-transfer reaction to give the ferrocenium stabilized silylium ion described by Oestreich *et al*. Bottom: proposed catalytic cycle for the silylium-assisted hydrosilation of carbonyl groups (adapted from reference 6).

The short reaction times and low temperatures required for performing such reactions reflects the high reactivity of these derivatives. Moreover, the powerful Lewis acidity of silylium cations allows them to activate inert entities such as carbon dioxide. Examples of CO_2 activation by silylium species include those in which these cations are forming part of silylium/phosphane,[7]

---

[7] M. Reissmann, A. Schafer, S. Jung, T. Müller, *Organometallics*, **2013**, *32*, 6736-6744.

silylium/NHCs[8] or silylium/guanidine[9] Frustrated Lewis Pairs, to name a few. The formation of a FLP is not unavoidable, given that "naked" silylium ions can transform carbon dioxide by themselves, as reported by Müller *et al*., since they can convert CO_2 into different products by changing the conditions of the stoichiometric reactions they carry out (Scheme 3, top).[10] By using the same strategy as Oestreich (*i.e.* hydrogen abstraction assisted by the trityl cation), the resulting silylium ion can react with hydrosilanes in chlorobenzene to give disilylated formate **A**, which can undergo hydrolysis to formic acid. In the specific case of Et_3SiH, more equivalents of hydrosilane can react with **A** to afford disilyl methyl oxonium ion **B**, which can in turn be hydrolyzed to methanol. On the other hand, reactions carried out in benzene lead to the formation of cation **C**. In this situation, two alternative pathways were described by the authors: deprotonation with 2,4,6-collidine to give silyl ester **D** or hydrolysis to benzoic acid **E**. The group demonstrated the role of the solvents and their participation in the different mechanisms originating such a variety of species from the same reagents. Additionally, a silylium-assisted version of the Gatterman-Koch reaction to produce aromatic silyl carboxonium compounds from silyl cations, benzene and CO was published very recently, where a similarity between protons and silylium ions ("*fat" protons*, according to the article) was made, establishing a new chemical point of view for this reactive species (Scheme 3, bottom).[11]

---

[8] M. F. S. Valverde, E. Theuergarten, T. Bannenberg, M. Freytag, P. G. Jones, M. Tamm, *Dalton Trans.,* **2015**, *44*, 9400-9408.

[9] N. von Wolff, G. Lefèvre, J.-C. Berthet, P. Thuéry, T. Cantat, *ACS Catal.,* **2016**, *6*, 4526-4535.

[10] A. Schäfer, W. Saak, D. Haase, T. Müller, *Angew. Chem. Int. Ed.,* **2012**, *51*, 2981-2984.

[11] L. Omann, Z-W. Qu, E. Irran, H. F. T. Klare, S. Grimme, M. Oestreich, *Angew. Chem. Int. Ed.,* **2018**, *57*, 8301-8305.
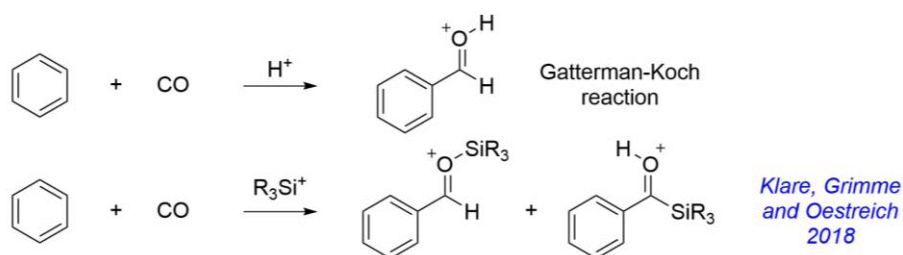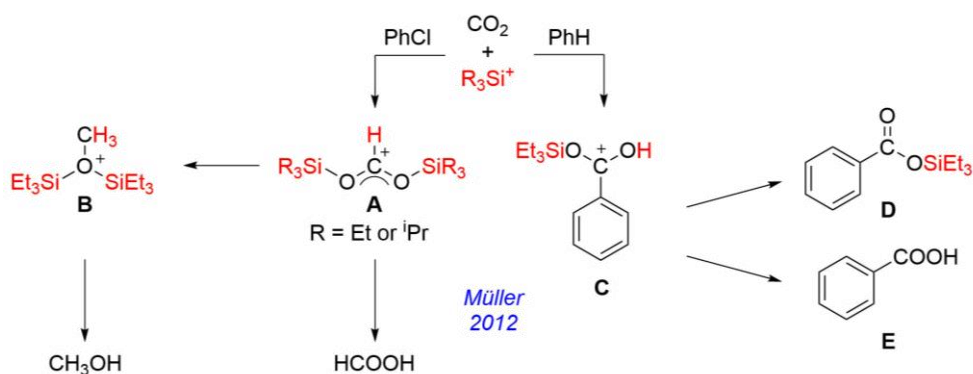
Scheme 3. Silylium-assisted carbon dioxide (top) and carbon monoxide reduction (bottom). Adapted from references 10 and 11.

In some of the previous cases, CO_2 activation takes place through the oxygen atom which attacks the electrophilic silylium species, opposed to the carbon dioxide insertion mechanisms described in chapter 1, where a hydride ligand usually attacked the electrophilic carbon atom. This activation mechanism has been described for other processes where extremely Lewis acidic species are involved, like the protonation of CO_2 by the carborane superacid $H(CHB_{11}F_{11})$.[12] In this case, the resulting product is the proton di-solvate $H(CO_2)_2^+$ (Scheme 4) and not the monoprotonated salt $[HCO_2][CHB_{11}F_{11}]$. This is not surprising, given

---

[12] S. Cummings, H. P. Hratchian, C. A. Reed, *Angew. Chem. Int. Ed.,* **2016**, *55*, 1382-1386.

the prevalence of proton disolvates[13] like in the case of Brookhart's acid, $[H(Et_2O)_2][BAr_4^F]$.[14]
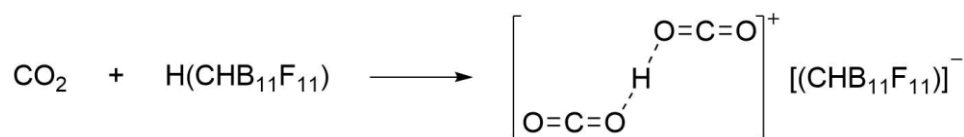
Scheme 4. Protonation of CO_2 to give the proton disolvate $[H(CO_2)_2][CHB_{11}F_{11}]$ (adapted from reference 12).

σ-SiH complexes

It has been shown throughout this thesis that sigma-silane complexes can also carry out catalytic processes in which silyl group transfers are involved. Even though they do not give rise to fully "naked" silylium ions, they render the silicon atom with enough electrophilic character to perform this type of reactions. The degree of electrophilicity is related to the coordination mode of the silane (*i.e.* η^1 or η^2 fashion), as previously seen in chapter 3.

σ-SiH complexes have been proposed as intermediates in silane alcoholysis reactions (Scheme 5), where a Si−O bond is forged at the same time dihydrogen is released.[15]

Scheme 5. Silane alcoholysis reaction.

Crabtree *et al.* observed that the kinetic and mechanistic data obtained with Ir(III) complexes of the type $[Ir(H)_2(PPh_3)_2S_2][SbF_6]$ (where S = THF, H_2O, MeOH or Me_2CO) suggested an alternative mechanism to the oxidative addition pathway, in which the silane was bound to the metal through the Si−H bond in a

[13] C. A. Reed, *Acc. Chem. Res.,* **2013**, *46*, 2567-2575.
[14] M. Brookhart, B. Grant, A. F. Volpe Jr., *Organometallics*, **1992**, *11*, 3920-3922.
[15] E. Lukevics, M. Dzintara, *J. Organomet. Chem.,* **1985**, *295*, 265-315.

η^2 fashion ("adduct formation", according to the authors) before undergoing nucleophilic attack from the alcohol. In addition, they state that this attack takes place inside the coordination sphere upon formation of species like $[Ir(H)_2(PPh_3)_2(MeOH)(\eta^2\text{-}HSiEt_3)]^+$.[16]

Ten years later, the group of Piers found that the sterically hindered Lewis acid tris(pentafluorophenyl)borane could equally catalyse this reaction by following the mechanism depicted in Scheme 6, showing that this reaction can proceed in the absence of metal atoms.[17] There, $B(C_6F_5)_3$ must dissociate from any Lewis base present in the reaction medium so the activation of the silane can take place, in a similar way to the calculated reaction pathway detailed in chapter 1 for CO_2 hydrosilation by PBP-stabilized Ni(II) species. Then, attack by the alcohol yields an oxonium cation that undergoes deprotonation by the newly formed borohydride species. As a result, the silyl ether and dihydrogen are produced.

---

[16] X-L. Luo, R. H. Crabtree, *J. Am. Chem. Soc.,* **1989**, *111*, 2527-2535.

[17] J. M. Blackwell, K. L. Foster, V. H. Beck, W. E. Piers, *J. Org. Chem.,* **1999**, *64*, 4887-4892.
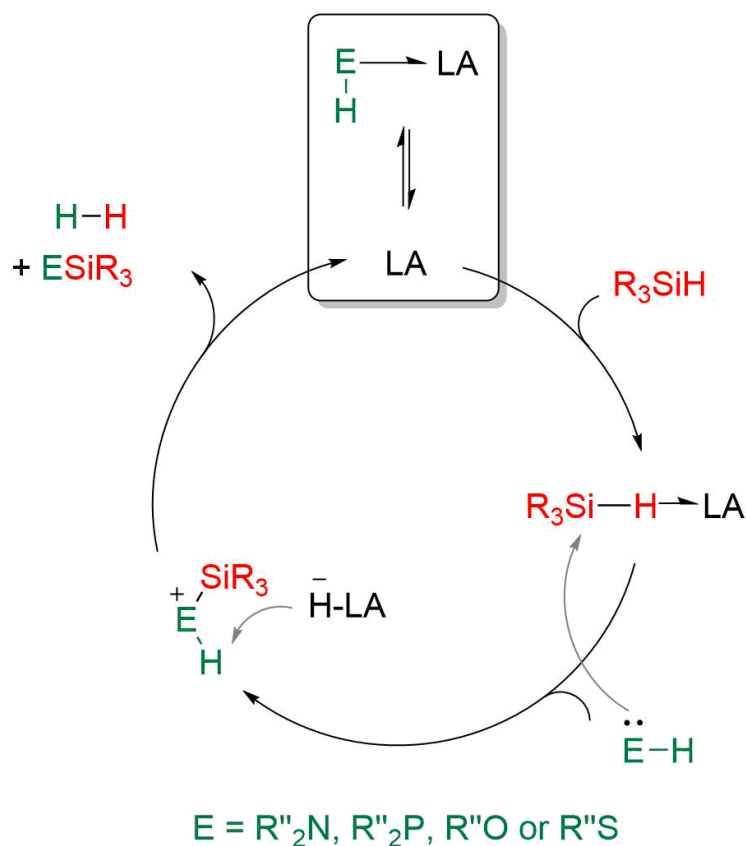
Scheme 6. General mechanism for the dehydrogenative coupling of hydrosilanes, where LA stands for an electrophilic transition metal complex or a main-group based Lewis acid. The box shows the dissociation step required for the reaction to proceed.

The tolerance of this system towards numerous functional groups (*e.g.* alkenes, alkynes, lactones, nitro groups, etc.) is remarkable. Interestingly, primary alcohols undergo silylation in a slower fashion than secondary or tertiary ones. This is due to their increased ability of coordinating to the sterically considerable Lewis acid, which is superior to bulky secondary or tertiary alcohols. Thus, primary alcohols release a smaller amount of $B(C_6F_5)_3$ available for reaction. However, competition experiments show that primary alcohols are silylated selectively over secondary ones, since they coordinate to the activated silane faster than their competitors.[17]

[319]

The strategy displayed in Scheme 6 for the metal or metal-free Lewis acid catalysed dehydrogenative coupling of silanes has been widely used for multiple processes involving different main-group based nucleophiles such as amines, phosphines, thiols or alcohols, given its versatility.[18] One of the methodologies for which this approach is applied is the catalytic reductive cleavage of ethers. Scheme 7 shows a general catalytic cycle, analogous to the dehydrocoupling one described in Scheme 6:
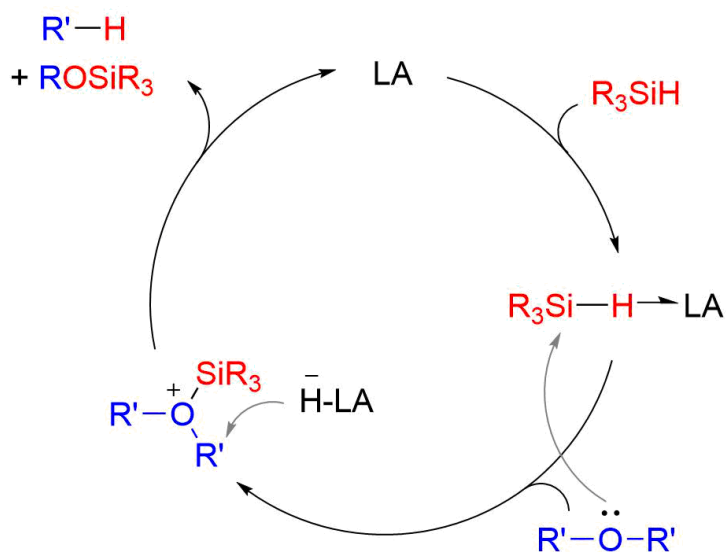
Scheme 7. General mechanism for the cleavage of ethers catalyzed by the Lewis acid/hydrosilane system.

Gevorgyan and coworkers demonstrated that metal-free catalysis is possible by using again $B(C_6F_5)_3$,[19] whereas Brookhart *et al.* employed Ir(III)

[18] a) B-H. Kim, M-S. Cho, H-G. Woo, *Synlett*, **2004**, *5*, 761-772; b) D. J. Harrison, D. R. Edwards, R. McDonald, L. Rosenberg, *Dalton Trans.,* **2008**, 3401-3411; c) E. M. Leitao, T. Jurca, I. Manners, *Nat. Chem.,* **2013**, *5*, 817-829; d) R. L. Melen, *Chem. Soc. Rev.,* **2016**, *45*, 775-788.
[19] a) V. Gevorgyan, J-X. Liu, M. Rubin, S. Benson, Y. Yamamoto, *Tetrahedron Lett.,* **1999**, *40*, 8919-8922; b) V. Gevorgyan, M. Rubin, S. Benson, J-X. Liu, Y. Yamamoto, *J. Org. Chem.,* **2000**, *65*, 6179-6186.

complexes for this purpose.[20] A report published a few years ago compared both systems (Scheme 8), concluding that their behavior during catalysis is identical, since both species act as mere Lewis acids so as to partially abstract the hydrogen atom from the hydrosilane.[21] In fact, the isolation of a σ-SiH complex derived from the iridium compound (see chapter 3, complex **Ir·Et₃SiH**) proved that sigma silane species are indeed reactive intermediates of these reactions, and that they can be isolated.
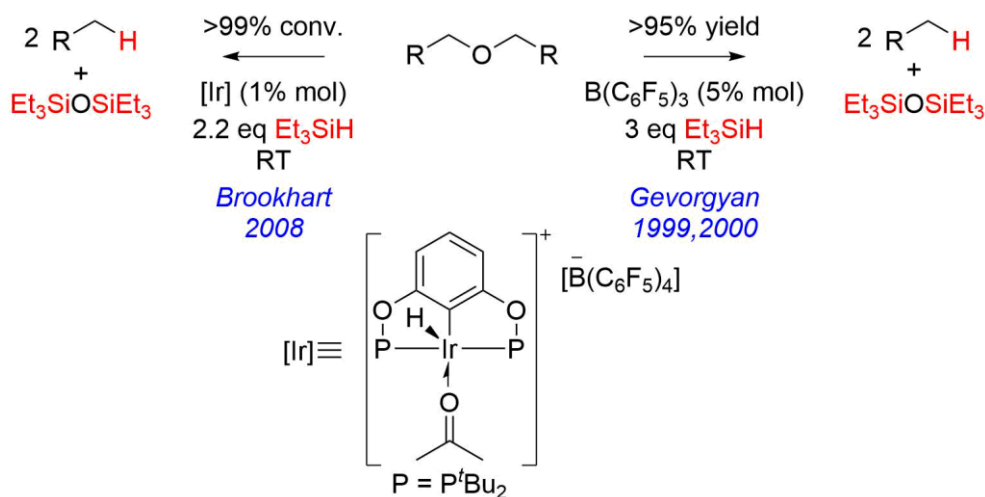
Scheme 8. Comparison of metal and metal-free systems for the catalytic reductive cleavage of ethers (adapted from reference 21).

1.2. Carbon dioxide hydrosilation to the formic acid stage

In chapter 1, carbon dioxide activation and its selective transformation to its different reduction stages was discussed, where a special focus was put on the selective hydrosilation to the bis(silyl)acetal species (formaldehyde level) catalyzed by Ni(II) complexes stabilized by bis(phosphino)boryl pincer ligands. In this chapter, part of the attention will be devoted to the selective catalytic

[20] J. Yang, P. S. White, M. Brookhart, *J. Am. Chem. Soc.,* **2008**, *130*, 17509-17518.

[21] T. Robert, M. Oestreich, *Angew. Chem. Int. Ed.,* **2013**, *52*, 5216-5218.

synthesis of silyl formate derivatives (formic acid stage) from CO_2 by means of some of the Pt(II) complexes stabilized by NHC ligands described previously in chapter 3.

Although the first examples of catalytic reduction of carbon dioxide to silyl esters date back to the 1980s,[22] this chemistry is still a matter of interest nowadays given the challenge in transforming such a stable and inert substrate, its availability and the utility of the resulting products derived from its chemical transformation. In fact, scientific reviews specialized on the hydrosilation of CO_2 to the formic acid stage keep appearing in the literature nowadays.[23] Recent examples included in such reports comprise complexes like the accessible ruthenium isomers *mer*-[RuX$_3$(MeCN)$_3$] and *cis/trans*-[RuX$_2$(MeCN)$_4$] (where X is either Br or Cl) described in Figure 1A, which are able to generate silyl formate derivatives at 85 °C in acetonitrile and silane mixtures.[24] The authors state that the presence of carbon dioxide during the process is fundamental, since otherwise hydrosilation of the solvent is observed. The nature of the halide ligands is important too, for there is a difference in the catalytic activity when going down in the group: Cl (most active catalysts) > Br > I (inactive). However, high temperature and CO_2 pressure (from 20 to 40 bar) were necessary to achieve the high TOF values obtained (up to 3700).

Much higher TON (up to 70000) and TOF values were observed by Baba *et al.*, who employed Cu(OAc)$_2$ as a precatalyst in combination with a great excess

---

[22] a) H. Koinuma, F. Kawakami, H. Kato, H. Hirai, *J. Chem. Soc. Chem. Commun.,* **1981**, 213-214; b) G. Süss-Fink, J. Reiner, *J. Organomet. Chem.,* **1981**, *221*, C36-C38.

[23] Some recent reports include the following: a) F. J. Fernández-Álvarez, A. M. Aitani, L. A. Oro, *Catal. Sci. Technol.,* **2014**, *4*, 611-624; b) C. Chauvier, T. Cantat, *ACS Catal.,* **2017**, *7*, 2107-2115; c) F. J. Fernández-Álvarez, L. A. Oro, *ChemCatChem*, **2018**, *10*, 4783-4796

[24] P. Deglmann, E. Ember, P. Hofmann, S. Pitter, O. Walter, *Chem. Eur. J.,* **2007**, *13*, 2864-2879.

of chelating diphosphines (up to 50 equivalents).[25] The resulting Cu derivatives yielded the corresponding copper hydrides upon reaction with hydrosilane (Figure 1B). One atmosphere of carbon dioxide was enough to afford the silyl formate species at room temperature after 24 hours of reaction. The same year, a similar strategy based on copper(I) complexes was adopted by Hou *et al.*, yet from a different approach. NHC ligands were shown to provide robust catalysts (Figure 1C) that can afford silyl formates at high temperatures (up to 100 °C).[26] Additionally, multigram scale reactions can be performed by using these systems, obtaining around 7 grams of the product. In both copper processes, the mechanism seems to proceed by insertion of the CO_2 molecule into the Cu−H fragment followed by activation of the Si−H bond to regenerate the catalyst and release the formic acid derivative.

---

[25] K. Motokura, D. Kashiwame, N. Takahashi, A. Miyaji, T. Baba, *Chem. Eur. J.*, **2013**, *19*, 10030-10037.
[26] L. Zhang, J. Cheng, Z. Hou, *Chem. Commun.,* **2013**, *49*, 4782-4784.
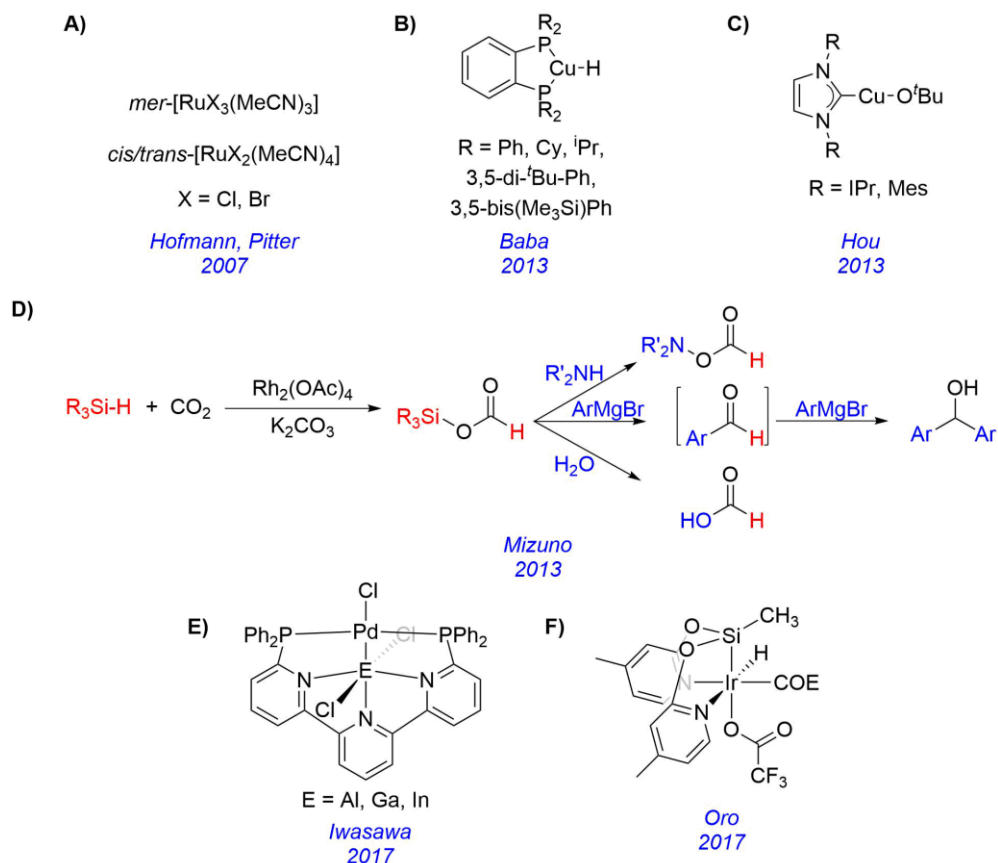
Figure 1. Some selected recent examples of transition metal complexes able to selectively transform CO_2 into silyl formates by using hydrosilanes.

Also in 2013, the group of Mizuno achieved successful chemical manipulation of the silyl formate products after its catalytic synthesis. After testing a set of commercially available metal salts, bases and solvents, the authors concluded that the best catalytic results were those obtained by using $Rh_2(OAc)_4$, inorganic O-donor bases like K_2CO_3 and acetonitrile (Figure 1D).[27] Then, the catalysis products were subjected to hydrolysis (to give formic acid) or they were exposed to Grignard reagents (to give benzhydrol derivatives) or

---

[27] S. Itagaki, K. Yamaguchi, N. Mizuno, *J. Mol. Catal. A: Chem.,* **2013**, *366*, 347-352.

amines (to give formylamines). Other groups also make use of formoxysilanes as formylating agents[28] or as surrogates of silanes.[29]

More recent examples of selective carbon dioxide hydrosilation include the bimetallic Pd-based system developed in the group of Iwasawa (Figure 1E). The Al−metalloligand complex achieved the highest TOF value (19300) reported so far, working at room temperature in DMF under 1 atmosphere of CO_2 (balloon) and in the presence of cesium pivalate as an additive.[30] On the other hand, Oro and co-workers have studied the carbon dioxide hydrosilation reaction by using Ir(III) complexes stabilized by NSiN ligands (Figure 1F).[31] As a result, selective reduction to the formic acid stage was observed, and experimental and theoretical (DFT) studies led to the conclusion that different mechanisms (*e.g.* outer or inner-sphere pathways) were taking place depending on the iridium species employed. In addition, the trifluoroacetate ligand proved to be non-innocent from a certain temperature (55 °C), since hydrosilation to the silyl ether $CF_3CH_2OSiR_3$ was observed. Moreover, the authors noticed a great dependence on the hydrosilane in terms of reaction rates by means of kinetic analysis.

It is worth mentioning that all the cases described above employed tertiary silanes, in which only one Si−H bond is chemically available. If secondary or primary silanes were to be used, the selectivity challenge found in carbon dioxide reduction (*i.e.* selective transformation towards formic acid, formaldehyde, methanol or methane) would find an additional issue, since mono-, di- or trisubstituted species could be formed (Scheme 9). Indeed,

---

[28] L. González-Sebastián, M. Flores-Alamo, J. J. García, *Organometallics*, **2013**, *32*, 7186-7194.

[29] C. Chauvier, P. Thuéry, T. Cantat, *Angew. Chem. Int. Ed.,* **2016**, *55*, 14096-14100.

[30] J. Takaya, N. Iwasawa, *J. Am. Chem. Soc.,* **2017**, *139*, 6074-6077.

[31] A. Julián, J. Guzmán, E. A. Jaseer, F. J. Fernández-Álvarez, R. Royo, V. Polo, P. García-Orduña, F. J. Lahoz, L. A. Oro, *Chem. Eur. J.,* **2017**, *23*, 11898-11907.

insertion of CO_2 into multiple Si−H bonds has been experimentally observed in some cases.[32]
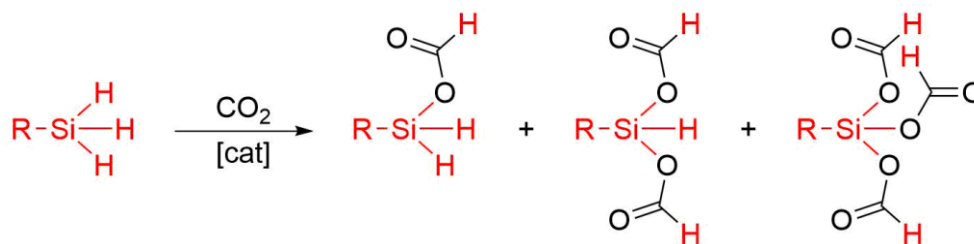
Scheme 9. Mixture of products that can be obtained during catalytic CO_2 hydrosilation when using primary silanes.

1.3. Synthesis of silazanes via dehydrogenative coupling reactions

Silazanes and polysilazanes

Contrary to their organic counterparts, inorganic polymers have remained elusive for a long time until recently, since the synthesis of inorganic molecular chains is much more challenging due to several reasons. For instance, addition mechanisms (*e.g.* polymerization of alkenes, alkynes, nitriles, etc) are not easy to achieve in inorganic entities, given that isolating the hypothetical monomers with multiple bonds between inorganic elements frequently involves the use of bulky substituents so as to kinetically overcome the "double-bond rule"[33] and prevent the uncontrolled oligomerization.[34] In this regard, some of the first stable dinuclear species like disilenes or iminoboranes date back to the 1980s, which evidences that this chemistry is still very young (Figure 2A).[35]

---

[32] a) A. Jansen, H. Görls, S. Pitter, *Organometallics*, **2000**, *19*, 135-138; b) M. L. Scheuermann, S. P. Semproni, I. Pappas, P. J. Chirik, *Inorg. Chem.,* **2014**, *53*, 9463-9465.

[33] L. E. Gusel'nikov, N. S. Nametkin, *Chem. Rev.,* **1979**, *79*, 529-577.

[34] I. Manners, *Angew. Chem. Int. Ed.,* **1996**, *35*, 1602-1621.

[35] a) Information about disilenes: R. West, *Angew. Chem. Int. Ed.,* **1987**, *26*, 1201-1211; b) Information about iminoboranes: P. Paetzold, *Adv. Inorg. Chem.,* **1987**, *31*, 123-170.
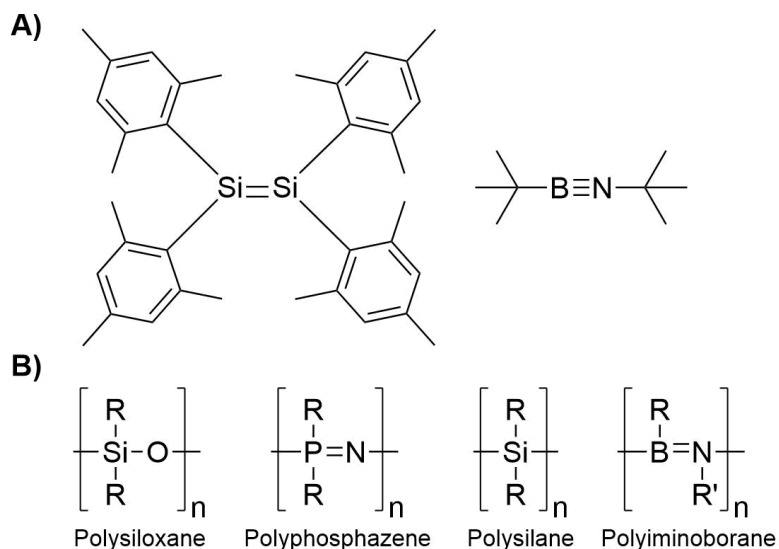
Figure 2. A) Examples of disilane and iminoborane as kinetically stable unsaturated inorganic molecules (adapted from references 35a and 35b). B) General formula of the first inorganic polymers synthesized (adapted from reference 34).

The drawbacks in the synthesis of inorganic polymers narrowed the scope of this type of materials, limiting their variety to polysiloxanes, polyphosphazenes, polysilanes and polyiminoboranes (Figure 2B). Thus, the formation of different polymers such as those with Si−N bonds as the main repeating unit (polysilazanes) has been underdeveloped. In addition, the chemical instability of the primitive structures of silazanes and polysilazanes towards water, oxygen or protic species made their investigation even more difficult. Nonetheless, their relevance as precursors in the synthesis of silicon nitride (Si_3N_4) or silicon carbonitride ($Si_xN_yC_z$) boosted the research in this field, given that these materials are extensively employed in the production of ceramics[36] due to their exceptional stability properties under extreme temperatures and oxidation environments, making them ideal candidates for

---

[36] A. Soum in *Silicon-containing Polymers. The Science and Technology of their Synthesis and Applications*, **2000**, Springer Netherlands. *Chapter 11: Polysilazanes*, 323-349.

abrasives or highly resistant components of many devices.[37] As a matter of fact, recent developments on this area have led to the creation of a new family of polymers which serve as extremely resistant coatings for a number of surfaces at the same time they provide protection against stains, inks and paints due to their hydrophobic nature.[38] Moreover, silazanes are useful compounds that can serve as ligands, protecting groups or bases.[18c] Regarding their structure, silazanes or amino-silanes are entities in which a silane molecule is bound to one, two or three amine groups, forming mono-, di- or trisilazanes respectively (Scheme 10). The binding and cross-linking of these species give rise to the corresponding polysilazanes. These polymers are often referred to as organopolysilazanes when hydrocarbon chains are present as substituents across the Si−N backbone.[36]
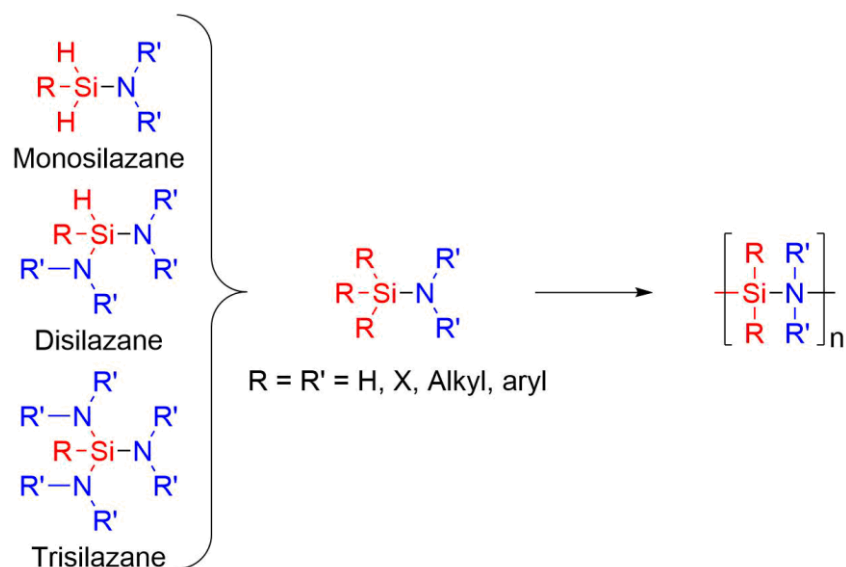
Scheme 10. General formulae of silazanes and polysilazanes.

---

[37] M. Birot, J-P. Pillot, J. Dunoguès, *Chem. Rev.,* **1995**, *95*, 1443-1477.

[38] This family of polysilazanes has been commercialized by Merck KGaA under the name Durazane® . For more information, see: https://www.merckgroup.com/en/brands/pm/durazane.html.

The most common method for the synthesis of silazanes and oligosilazanes is the aminolysis of chlorosilanes. In this process, hydrochloric acid is formed as a by-product and it is usually neutralized by an excess of the amine involved in the reaction, forming an equilibrium between the involved species (Scheme 11A).[18d,39] In addition, the presence of a strong acid in the reaction medium limits the functional group tolerance. These disadvantages, along with the toxic, irritant and corrosive nature of HCl,[40] demand for alternative methods of synthesizing Si−N derivatives. In the light of this situation, dehydrogenative coupling of hydrosilanes and amines arises as a clean alternative (Scheme 11B) given that the only by-product is dihydrogen, which can be leveraged for several other purposes.[41]

A)

$$R_3SiCl \ + \ 2 \ R'NH_2 \ \rightleftharpoons \ R_3SiNHR' \ + \ R'NH_3Cl$$

B)

$$R_3SiH \ + \ R'NH_2 \ \xrightarrow{[cat]} \ R_3SiNHR' \ + \ H_2$$
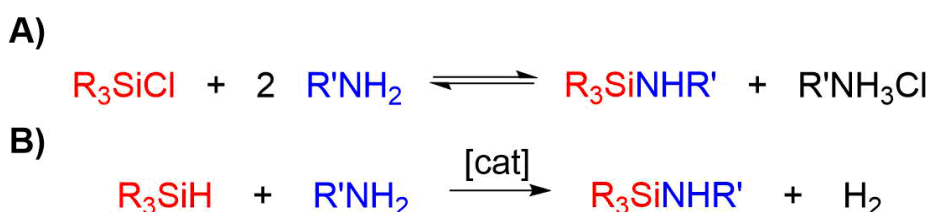
Scheme 11. Synthetic methods for the preparation of silazanes. A) Aminolysis of chlorosilanes. B) Dehydrogenative coupling of hydrosilanes and amines.

Metal-assisted dehydrogenative Si−N formation

The development of homogeneous catalytic methods to forge Si−N bonds from hydrosilanes and amines has gained interest during the last couple of decades.[42] This transformation is challenging because of the wide variety of

---

[39] R. Fessenden, J. S. Fessenden, *Chem. Rev.,* **1961**, *61*, 361-388.

[40] S. Austin, A. Glowacki. Hydrochloric acid. *Ullmann's Encyclopedia of Industrial Chemistry*, **2000**, doi: 10.1002/14356007.a13_283.

[41] a) R. Noyori, T. Ohkuma, *Angew. Chem. Int. Ed.,* **2001**, *40*, 40-73; b) S. Werkmeister, K. Junge, M. Beller, *Org. Process Res. Dev.,* **2014**, *18,* 289-302; c) G. A. Filonenko, R. V. Putten, E. J. M. Hensen, E. A. Pidko, *Chem. Soc. Rev.,* **2018**, *47*, 1459-1483.

[42] Metal-free catalytic systems have also been described in the literature (see reference 18d).

species that might arise from the reaction, since mixtures of products with diverse Si / N ratios, oligo- or polysilazanes may be found. Thus, aside from high activities, selective systems capable of leading to just one type of amino-silane are desirable.

Alkaline earth based systems proved to be efficient for this type of transformation, as shown by the work of Harder *et al.* in 2007, where the calcium azacyclopropane depicted in Scheme 12 (left) is able to give monosilazanes out of the bulky silane Ph_3SiH and aliphatic and aromatic amines at room temperature and catalyst loadings of around 5-10 mol %.[43] A few years later, the group of Sadow employed magnesium complexes stabilized by tris(oxazolinyl)borato ligands (To^M) to selectively transform primary and secondary hydrosilanes into amino-silanes (Scheme 12, right).[44] The degree of substitution on the Si atom (*i.e.* the amount of amine groups bound to silicon) depends on the type and stoichiometry of the reagents. Interestingly, the Mg complex is effective even in the transformation of NH_3, which affords monosilazanes upon reaction with tertiary silanes. This phenomenon is remarkable, as incorporation of silyl groups in ammonia makes the rest of the N−H bonds more acidic, turning the monosilation reaction difficult to achieve.

---

[43] F. Buch, S. Harder, *Organometallics*, **2007**, *26*, 5132-5135.
[44] J. F. Dunne, S. R. Neal, J. Engelkemier, A. Ellern, A. D. Sadow, *J. Am. Chem. Soc.,* **2011**, *133*, 16782-16785.
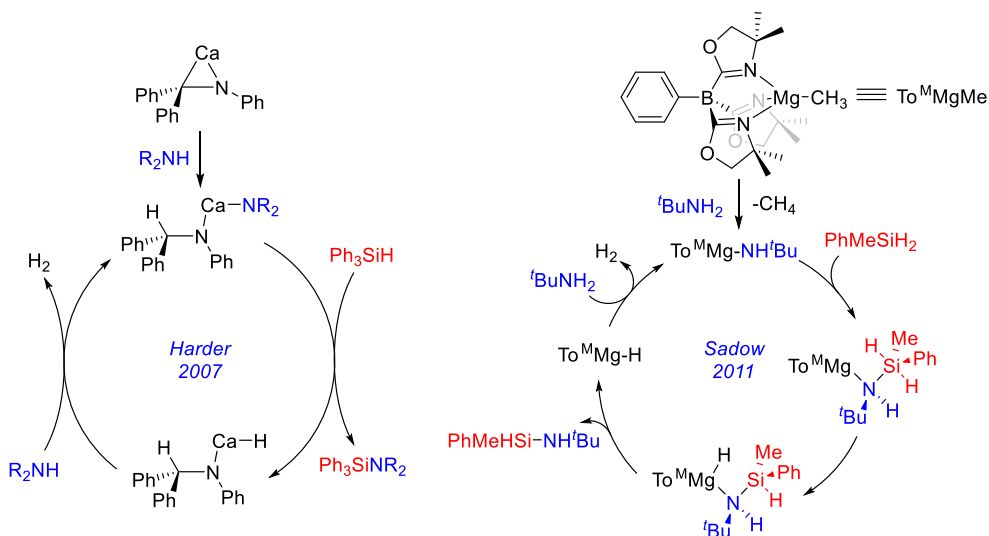
Scheme 12. Examples of alkaline earth-based catalysts and their proposed catalytic cycles for the formation of monosilazanes. (adapted from references 43 and 44).

Although the mechanisms by which these processes take place are not completely clear, the authors propose analogous catalytic cycles that involve nucleophilic attack of the amide group to the silane followed by hydrogen transfer from Si to the metal, in a process that resembles β-elimination. Elimination of the silazane and protonation of the resulting hydride finish the cycle by releasing H_2 and regenerating the metal–amide bond.[43,44]

This transformation is not limited to group 2 elements, given that transition metal-based catalysts can also be found in the literature, like the rhodium system described by Eisenberg *et al.*, which consisted of binuclear complexes of the type $Rh_2(H)_2(CO)_2(dppm)_2$ or $Rh_2(\mu\text{-}SiRH)_2(CO)_2(dppm)_2$[45] that are capable of producing small oligosilazanes (up to Si–N–Si–N–Si–N products). The nature of the resulting chain depends on the size of the substituents: bulky groups like *i*Bu give linear products, whereas small alkyl fragments like CH_3

---

[45] R = Ph, Et or C_6H_{13}. dppm stands for bis(diphenylphosphino)methane.

produce branched oligomers.[46] Binuclear rhodium derivatives have also been used in the silylation of indoles, pyrroles and carbazoles, by means of $Rh_2(OAc)_4$ accompanied by the base TBA_2WO_4 (TBA = tetrabutylammonium), as described by the group of Mizuno.[47] These heterocyclic substrates were also used by Oestreich and coworkers for the same purpose, extending the scope to indolines and anilines, which undergo Si−N coupling by means of catalytic loadings of 1 mol % of the same Ru complex described in chapter 1 for CO_2 reduction to the bis(silyl)acetal stage (Figure 3).[48]
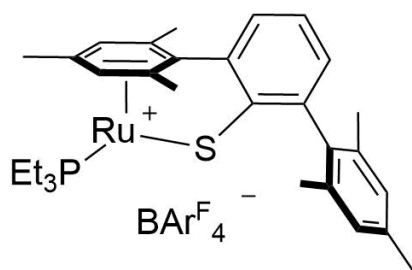
Figure 3. Ruthenium system described by the group of Oestreich for Si−N dehydrogenative coupling and CO_2 hydrosilation (adapted from reference 48).

Curiously, many of the precatalysts reported in the literature contain the bis(trimethylsilyl)amide or hexamethyldisilazide (HMDS) ligand, probably due to the solubility and steric stability that they provide (Figure 4). This makes possible the stabilization of lanthanide-based compounds such as the ytterbium species reported by Cui (Figure 4, top left), which also possess an NHC ligand that modulates the reactivity of the complex (preliminary studies in the absence of NHCs led to the conclusion that an ancillary ligand was necessary). For instance, coupling $PhSiH_3$ to Et_2NH by using 5 mol % of the I^iPr derivative gives a 1:1 mixture of the mono- and disilazane products, yet it yields quantitative

---

[46] W-D. Wang, R. Eisenberg, *Organometallics*, **1991**, *10*, 2222-2227.
[47] S. Itagaki, K. Kamata, K. Yamaguchi, N. Mizuno, *Chem. Commun.,* **2012**, *48*, 9269-9271.
[48] C. D. F. Königs, M. F. Müller, N. Aiguabella, H. F. T. Klare, M. Oestreich, *Chem. Commun.,* **2013**, *49*, 1506-1508.

formation of the disilazane in the presence of the IMes complex.[49] Similar enhancements due to auxiliary ligands were observed in the group of Crimmin for the yttrium precatalysts depicted in Figure 4 (top right). Whereas both complexes similarly catalyze the dehydrocoupling reaction of primary or secondary phenylsilanes with primary or sterically accessible secondary amines (*e.g.* dibenzylamine, piperidine), there is a dramatic difference in the reaction with bulky amines such as diisopropylamine: the complex bearing a cyclometalated phosphonium methylide ligand is able to achieve 95% yield of the desired monosilazane after 44 h, but [Y{N(SiMe$_3$)$_2$}$_3$] gives no product after 262 hours of reaction under the same conditions (10 mol % of catalyst at room temperature).[50] On the contrary, Waterman *et al*. showed that no auxiliary ligands were needed when using the lanthanum precatalyst shown in Figure 4 (bottom right), that turned out to be the most active lanthanide-based one for this type of reaction, given that even trisilazanes can be obtained with catalyst loadings as low as 0.8 mol % by slightly increasing the amine/silane ratio (up to 4 equivalents) and the temperature up to 90 °C.[51]

[49] W. Xie, H. Hu, C. Cui, *Angew. Chem. Int. Ed.,* **2012**, *51*, 11141-11144.
[50] A. E. Nako, W. Chen, A. J. P. White, M. R. Crimmin, *Organometallics*, **2015**, *34*, 4369-4375.
[51] M. P. Cibuzar, R. Waterman, *Organometallics*, **2018**, *37*, 4395-4401.
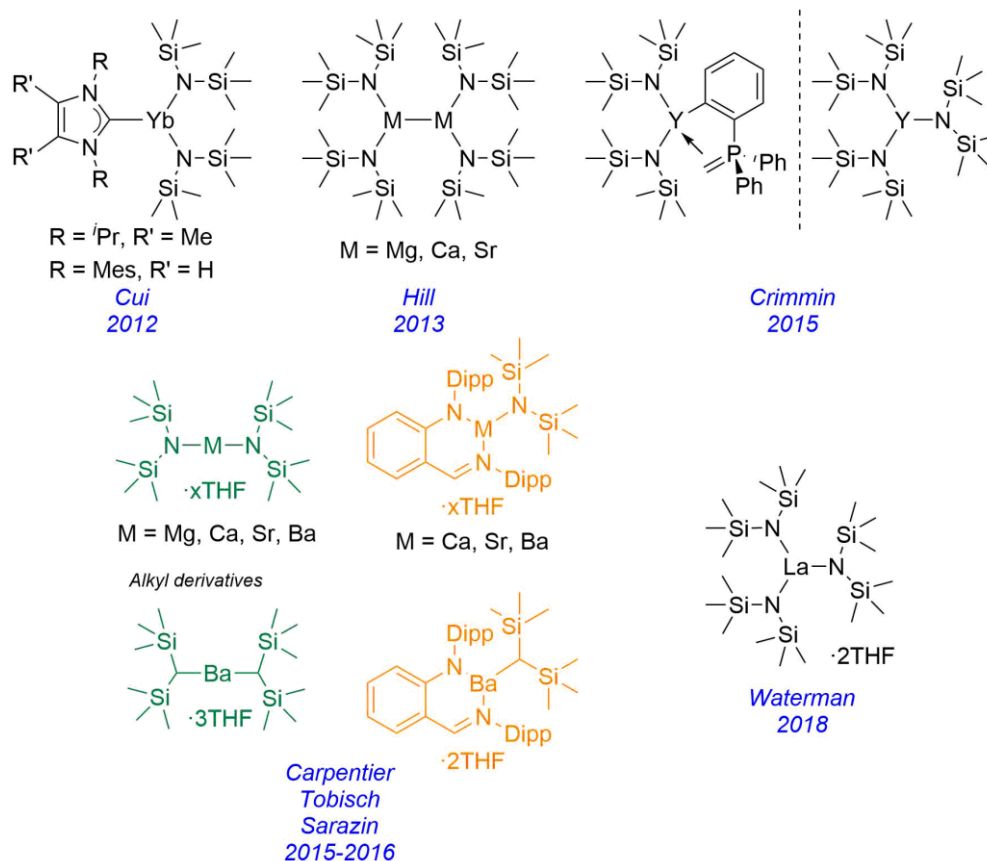
Figure 4. Some recent examples of HMDS-stabilized complexes which are capable of performing Si–H dehydrogenative coupling reactions (bottom left: carbon analogues of some HMDS complexes).

Alkaline earth elements are widely employed in Si–N dehydrogenative coupling, as it can be observed in Figure 4 and Scheme 12. Hill and coworkers also observed a kinetic dependence on the steric volume of the reagents when using the homoleptic complexes [M{N(SiMe$_3$)$_2$}$_2$] (M = Mg, Ca, Sr).[52] As an example, Ph$_3$SiH did not react with any of the precatalysts when it was combined with the sterically hindered amine 2,6-di-*iso*-propylaniline. However, all of them

---

readily reacted with small substrates like $PhSiH_3$ and $BnNH_2$, for which intractable mixtures of oligosilazanes were obtained, demonstrating the simplicity in the activation of these entities when they are accessible enough to establish contact with the catalyst. The authors attribute this difference in reactivity to the size of the metal atom: magnesium is smaller, and therefore large substrates will influence its activity to a great extent. On the contrary, a bigger atom like strontium will be less influenced by bulky amines and silanes, and it will exhibit better catalytic results. Carpentier, Sarazin, Tobisch and coworkers confirmed this reactivity trend after testing the precatalysts shown in Figure 4 (bottom left) against a range of substrates. In fact, they proved how going down in group 2 improved the catalytic activity in the following fashion: Ba > Sr > Ca >> Mg.[53] Additionally, it was shown that the presence of ancillary ligands in this type of complexes is not required to enhance the catalytic performance, just like in the case of the lanthanide derivative described above.[51] This was assessed by comparing the HMDS derivatives (Figure 4, green) with the iminoanilide-stabilized species (Figure 4, orange). Besides, alkyl versions of the ligands proved even more efficient due to their increased basicity, which generate a higher amount of the Ba-amido species (upon deprotonation of the amine), which is thought to be the actual catalyst. Low concentrations of catalyst (down to 0.25 mol %, 2500 ppm) yielded a variety of silazanes with excellent chemoselectivity by adjusting the stoichiometry of the reagents, and even though the proposed catalytic cycle is identical to that reported in the work of Sadow,[44] kinetic studies and DFT calculations indicate that the Si−H cleavage step is the rate-determinant stage in this mechanism, and not the nucleophilic attack from

---

[53] C. Bellini, J-F. Carpentier, S. Tobisch, Y. Sarazin, *Angew. Chem. Int. Ed.,* **2015**, *54*, 7679-7683.

the amine to the silane (Scheme 13).[53] Further improvements to these systems were developed by the authors in subsequent works.[54]
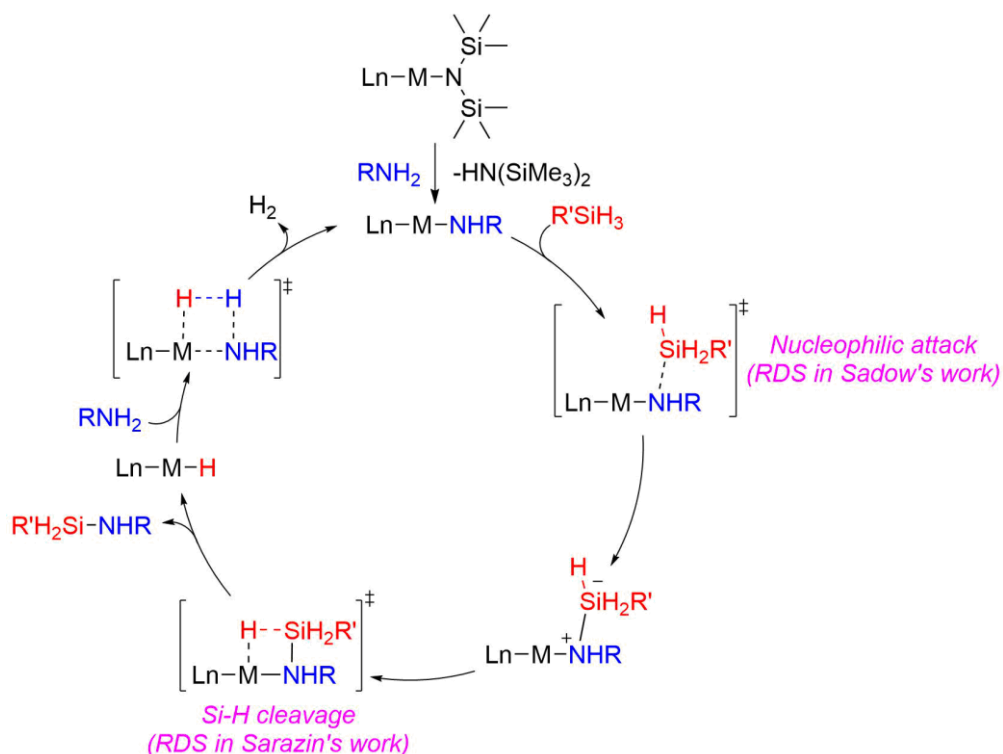
Scheme 13. General catalytic cycle for the Si–N dehydrogenative coupling by HMDS-stabilized alkaline earth catalysts (adapted from reference 53). RDS = rate-determining step.

---

[54] a) C. Bellini, V. Dorcet, J-F. Carpentier, S. Tobisch, Y. Sarazin, *Chem. Eur. J.,* **2016**, *22*, 4564-4583; b) C. Bellini, T. Roisnel, J-F. Carpentier, S. Tobisch, Y. Sarazin, *Chem. Eur. J.,* **2016**, *22*, 15733-15744.

2. Results and discussion

The goal of this work is to employ the cationic Pt(II) σ-SiH complexes described in chapter 3 as catalysts in CO_2 hydrosilation and Si–N dehydrogenative coupling processes, taking advantage of the increased electrophilicity of the silane upon coordination to the Lewis acidic organometallic complex. In addition, the influence of the ligands on the chemoselectivity of the resulting products will be explored. By modifying them, specific selectivity patterns not available by other methods (such as in the case of naked silylium cations) can be achieved.

2.1. Carbon dioxide hydrosilation to silyl formates

Given that the (POCOP)Ir(III) σ-silane complex described by Brookhart *et al.*[55] turned out to be a proficient catalyst for CO_2 hydrosilation to methane (Scheme 14),[56] our Pt(II) complexes were also evaluated as potential catalysts for this process.

[55] J. Yang, P. S. White, C. K. Schauer, M. Brookhart, *Angew. Chem. Int. Ed.,* **2008**, *47*, 4141-4143.
[56] S. Park, D. Bézier, M. Brookhart, *J. Am. Chem. Soc.,* **2012**, *134*, 11404-11407.
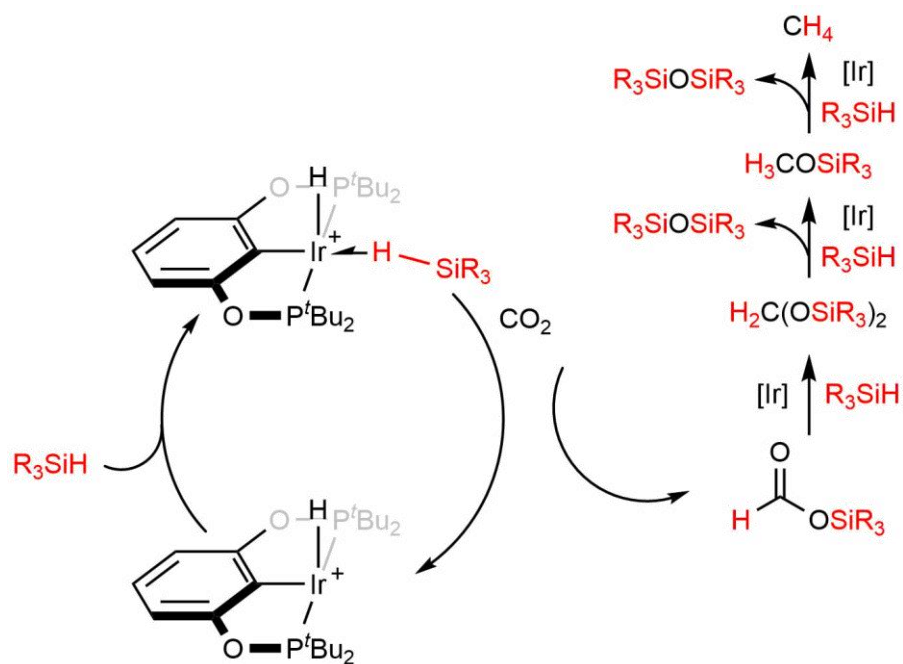
Scheme 14. Proposed catalytic cycle for the hydrosilation of CO_2 to methane by (POCOP)Ir(III) complexes (adapted from reference 56).

Since the most linear Pt–H–Si arrangement was obtained with I^{t}Bu complexes (up to 159°, see chapter 3), these derivatives were subjected to analysis in carbon dioxide hydrosilation reactions. Complexes **13, 15** and **16** are stable in a CO_2 atmosphere. However, their presence in mixtures of CO_2 and hydrosilanes leads to the selective formation of the corresponding silyl formates, as shown in Scheme 15:

[338]
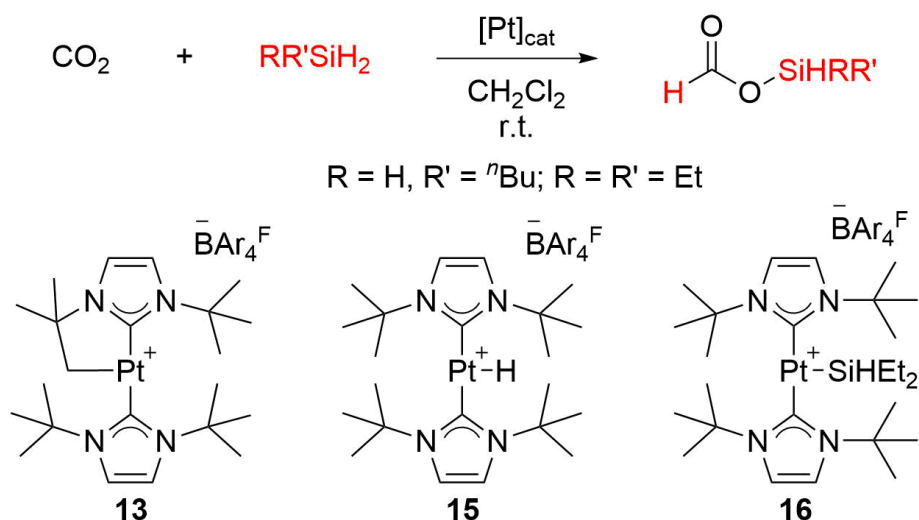
Scheme 15. Top: carbon dioxide hydrosilation to the formic acid stage. Bottom: I^{t}Bu stabilized Pt(II) catalysts used in this transformation.

Cyclometalated species **13** proved to be the most efficient catalyst due to the short times required when 0.5 mol % of the complex is in the presence of ^{n}BuSiH$_3$ and 5 bar of CO$_2$. As a result, silane consumption and selective formation of the silyl formate HCOOSiH$_2$^{n}Bu was obtained after 15 minutes (Figure 5).[57] The same product was observed when using hydride **15** or silyl derivative **16**, although much longer reaction times were needed (Figure 6).

---

[57] The conversion was measured by ^{1}H NMR integration of the silane and silyl formate peaks.
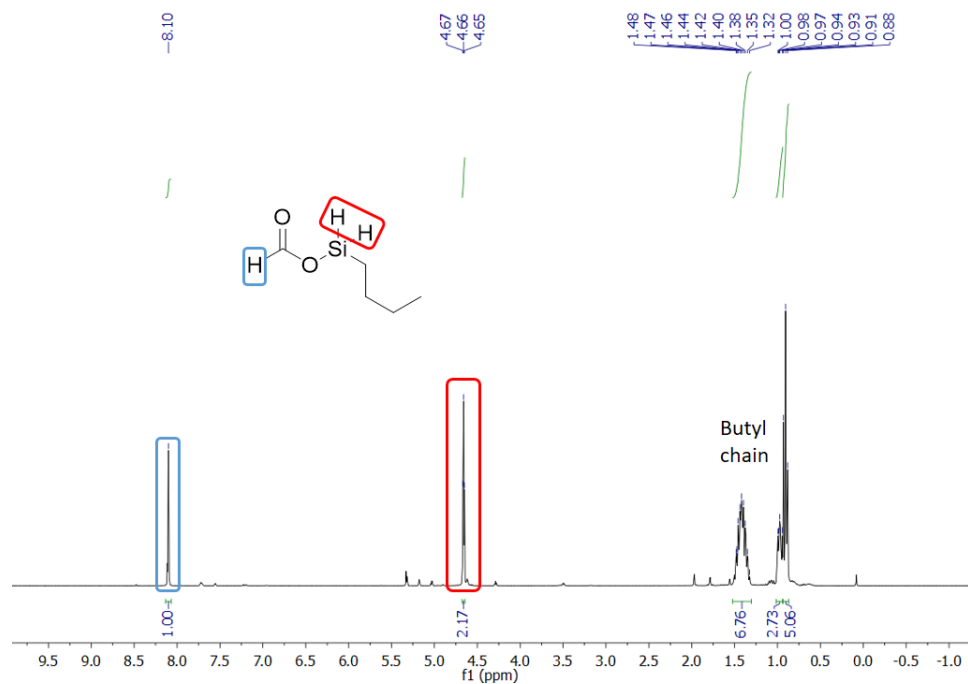
Figure 5. Typical ¹H NMR spectrum (400 MHz, CD₂Cl₂) of a catalytic experiment with **13** (0.5 mol %), ⁿBuSiH₃ and CO₂ (5 bar) after consumption of the silane.
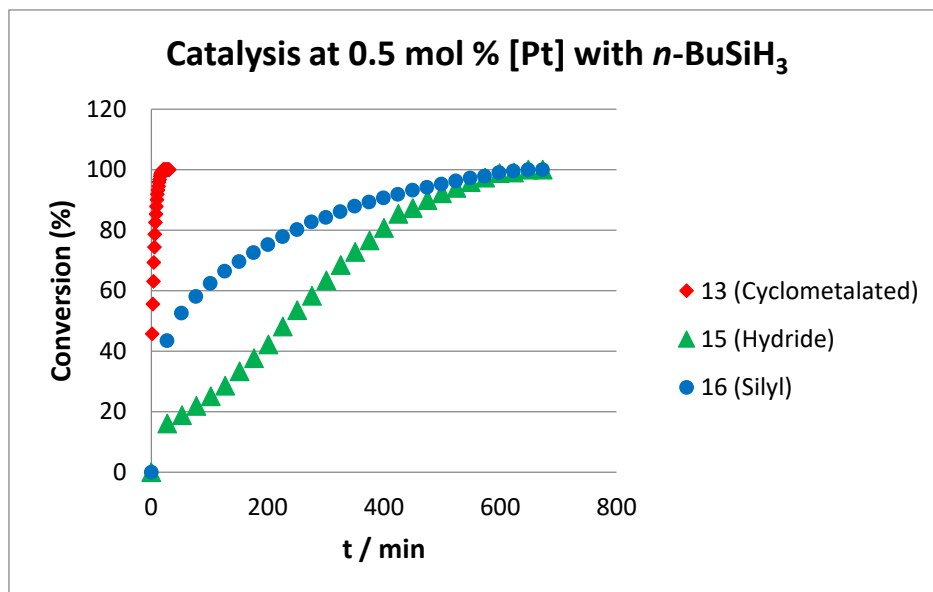
Figure 6. Comparison of the different plots when using platinum complexes **13**, **15** and **16** (0.5 mol %) and $^{n}BuSiH_3$ in the presence of CO_2 (5 bar) for the formation of $HCOOSiH_2 nBu$.

The use of secondary silanes such as Et_2SiH_2 also gives monoformates as products, but in this occasion longer reaction times are needed in all cases (Figures 7 and 8), despite the fact that higher catalytic loadings of **13** are necessary (3 mol %) due to partial hydrolysis (and concomitant formation of hydride **15**, which is less efficient) due to the presence of adventitious water in the reaction media. Tertiary silanes such as Et_3SiH seemed to be too bulky to interact with the platinum center, since no evolution was observed after prolonged reaction times and mild heating (45 °C).[58]

---

[58] Aromatic silanes like $PhSiH_3$ were also studied, although several unidentified species were observed rather than silyl formate derivatives.
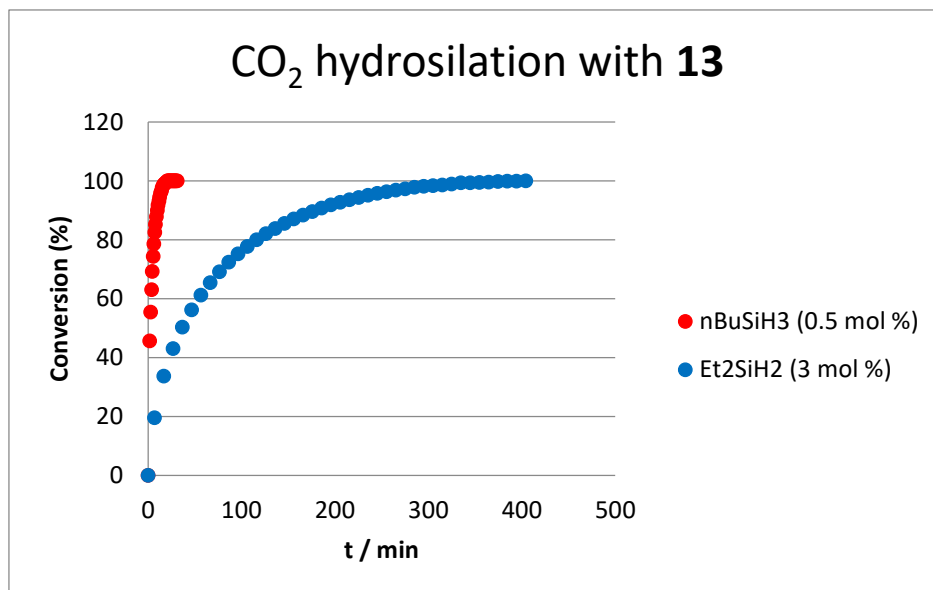
Figure 7. Comparison of the different plots when using **13** and different hydrosilanes in the presence of CO_2 (5 bar) for the formation of the corresponding silyl formate.
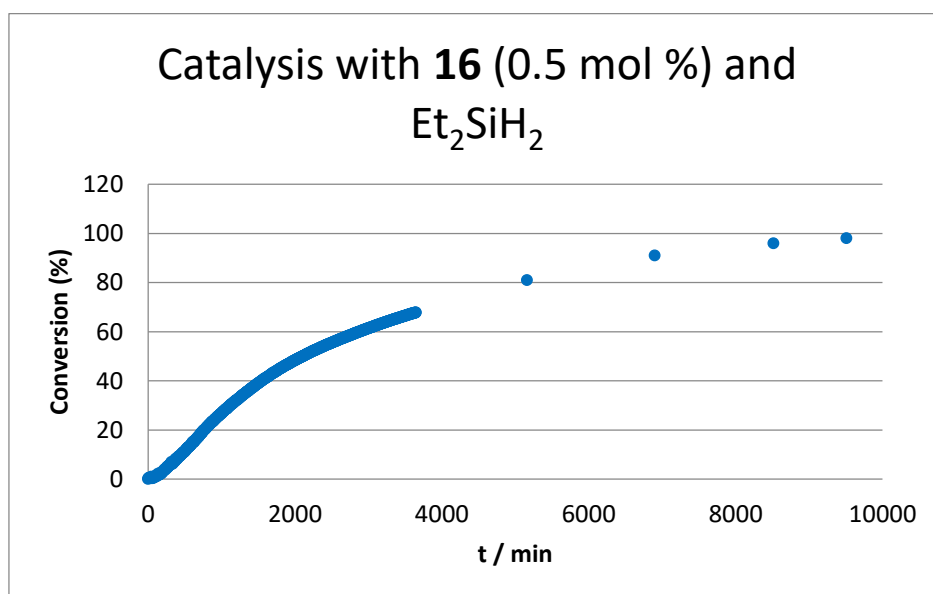
Figure 8. Monitoring of the amount of $HCOOSiHEt_2$ produced when using **16** (0.5 mol %) and Et_2SiH_2 in the presence of 5 bar of CO_2.

[342]

Nonetheless, the mild conditions (room temperature, 5 bar of CO_2) at which these reactions are carried out and the resulting catalytic activities obtained (Table 1) make these Pt(II) complexes competitive catalysts for carbon dioxide hydrosilation to the formic acid stage. Moreover, the excellent chemoselectivity observed towards monoformates in spite of using primary or secondary silanes is remarkable and uncommon, given that the usual strategy is to employ tertiary silanes so as to avoid mixtures of products (Scheme 9),[32] as stated in the introduction of this chapter. Although steric hindrance may account for the kinetic differences experimentally observed (primary silanes like butylsilane rapidly react to yield the monoformate, yet secondary silanes undergo between 6 and 15 times longer reactions to get the same conversion values), several reasons might be behind the observation of silyl monoformate derivatives (Figure 9): a) formation of a second formate unit on the product might require longer reaction times; b) the electron-withdrawing nature of the formate group on the silane might favour a η^2-coordination mode (less electrophilic than η^1 SiH complexes) when interacting with the platinum atom, similar to the results obtained with Cl_3SiH in chapter 3; c) the silyl monoformate may interact with the metal through one of the oxygen atoms, competing with the hydrosilane. As a consequence, the corresponding silyl monoformate builds up in the reaction mixture, becoming the only product of the catalytic process.

[Pt]	Silane	Loading (mol %)	time (h)	T (°C)	TON	TOF (h^{-1})
13	^{n}BuSiH$_3$	0.5	0.28	25	200	714
13	Et$_2$SiH$_2$	3	4.2	25	33.33	8
15	^{n}BuSiH$_3$	0.5	10.8	25	200	18.5
15	Et$_2$SiH$_2$	0.5	60.3	25	177[a]	3
16	^{n}BuSiH$_3$	0.5	10.8	25	200	18.5
16	Et$_2$SiH$_2$	0.5	158.5	25	196[b]	3

Table 1. Reaction conditions and results for the Pt-catalyzed CO_2 hydrosilation to silyl formate derivatives. Every catalytic experiment has been repeated at least twice. TON = (μmoles of silane/μmoles of catalyst)*formate ratio. [a] Value determined at a conversion of 88.4%. [b] Value determined at a conversion of 98%.
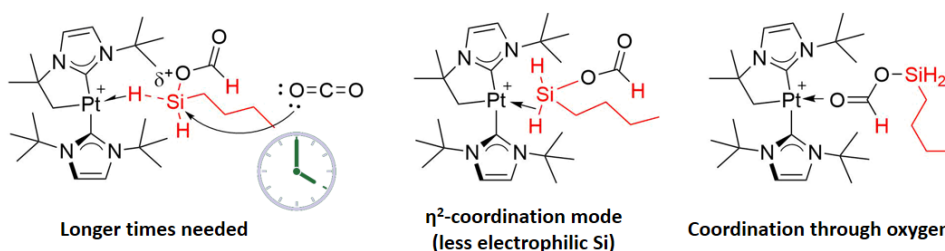
Figure 9. Plausible explanations for the observed chemoselectivity during carbon dioxide hydrosilation by using complexes **13**, **15** and **16**.

On the other hand, the superior activity of **13** in comparison to **15** and **16** may be explained in terms of stereoelectronic properties, as described in chapter 3: the bigger cavity of **13** with respect to **15** and **16**, its preorganization towards interaction with hydrosilanes and the weaker *trans* influence of the methylene moiety against hydride or silyl ligands[59] may contribute to the stronger σ-silane species observed for complex **13** by experimental and theoretical methods, thus leading to a higher activation of the silane and consequently a faster catalytic transformation when CO_2 is present. This is in

---

[59] J. Zhu, Z. Lin, T. B. Marder, *Inorg. Chem.,* **2005**, *44*, 9384-9390.

agreement with the observed experimental trend when the catalysts were subjected to an atmosphere of carbon dioxide and diethylsilane, since the required reaction times follow the sequence **13** (4 hours) > **15** (60 hours) > **16** (158 hours).

2.2. Dehydrogenative coupling of silanes and amines

The mechanistic evidence shown by Crabtree *et al.* for the alcoholysis of silanes[16] (assisted by σ-SiH complexes, see section 1.1 and Scheme 5) and by our group for dehydrocoupling reactions leading to amino-[60] and diaminoboranes[61] point to an initial step in which the Lewis base (*i.e.* silane or amine-borane) approaches the metal atom to undergo electrophilic activation so as to start the catalytic process. Thus, we rationalized that amine groups could in principle react with the Pt(II) σ-silane complexes observed in the laboratory to give rise to silazane derivatives.

Dehydrocoupling of primary silanes

Initial studies were performed by using $PhSiH_3$ and $^tBuNH_2$ (1:1 ratio) in the presence of 0.5 mol % of complex **13** in dichloromethane (Scheme 16). This system gave rise to an extremely intense bubbling and the formation of the monosilazane $PhSiH_2(NH^tBu)$ after a few seconds (Figure 10). At the end of the process, hydride **15** was observed as the only detected species, produced from the hydrogenation of **13** due to the H_2 produced during the dehydrocoupling event. Whereas the selectivity is identical to that reported by the group of Sadow for the same substrates, their Mg system needs 24 h and a catalyst loading of 5 mol %.[44]

[60] M. Roselló-Merino, J. López-Serrano, S. Conejero, *J. Am. Chem. Soc.,* **2013**, *135*, 10910-10913.

[61] M. Roselló-Merino, R. J. Rama, J. Díez, S. Conejero, *Chem. Commun.,* **2016**, *52*, 8389-8392.
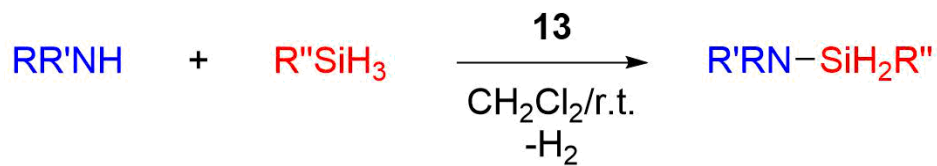
Scheme 16. Si−N dehydrogenative coupling of primary silanes with amines catalyzed by **13** to give monosilazanes.
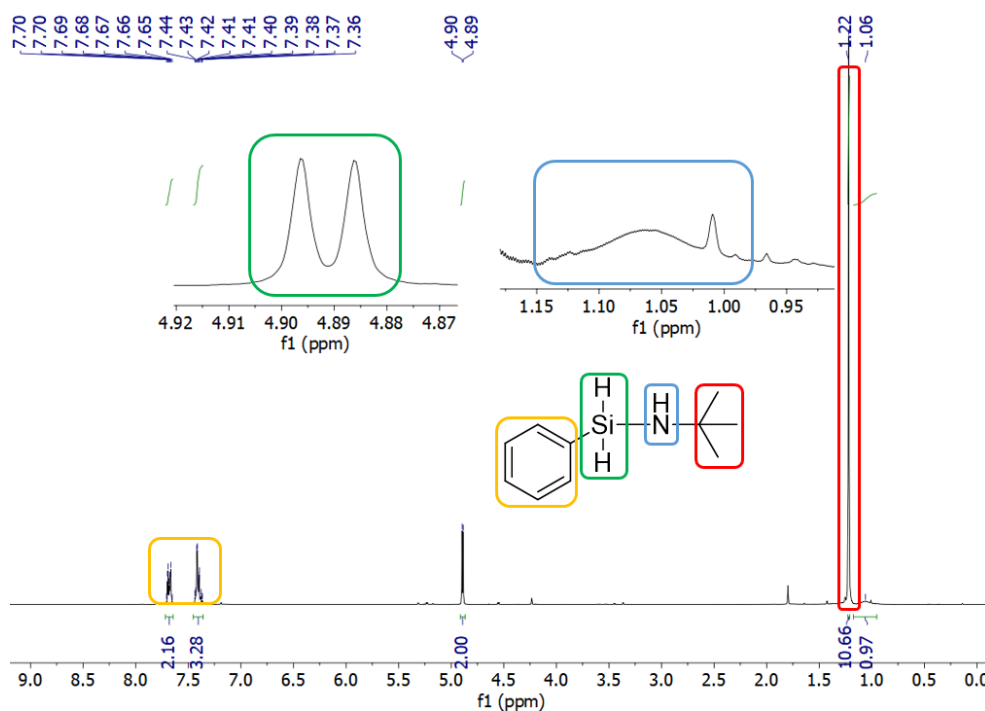
Figure 10. ^{1}H NMR spectrum (400 MHz, CD$_2$Cl$_2$) of the crude reaction between PhSiH$_3$ and ^{t}BuNH$_2$ catalyzed by **13** (0.5 mol %).

In the light of these encouraging results, the Pt loading was decreased to 0.005 mol % (50 ppm, Table 2, entry 1) and 0.003 mol % (30 ppm, Table 2, entry 2). In these reactions, **13** consumed the reactants in 12 and 35 min, respectively. The latter experiment afforded TON and TOF values of 3.3x10^4 and 5.7x10^4 h^{-1} respectively, which are much higher than those reported for the uranium system

[346]

[(Et$_2$N)$_3$U][BPh$_4$] for the same product (TON = 167, TOF = 24 h^{-1}).[62] The employment of Et$_2$NH produced even faster reactions, since 50 ppm of **13** completely converted the silane into PhSiH$_2$(NEt$_2$) in 3.6 minutes (TON = 2x10^4, TOF = 3.3x10^5 h^{-1}, entry 3 of Table 2), giving the highest activity values reported to date so far (as a comparison, previous works reported TON values of 20 and TOF values of 0.83-1.6 h^{-1}).[44,63] The extremely fast catalysis observed allowed us to decrease the loading even more, down to 10 ppm (Table 2, entry 4), achieving 98% conversion in 3 hours.

Several other amines also react with PhSiH$_3$ in the presence of **13**, such as the selectivity challenging substrate pyrrolidine, giving the corresponding monosilazane PhSiH$_2$[N(CH$_2$)$_4$] in 35 min under 50 ppm of catalyst (Table 2, entry 6). However, bigger amines such as ^{i}Pr$_2$NH or less basic ones like MesNH$_2$ need higher loadings in order to give similar conversions and reaction times (Table 2, entries 7-10). Nonetheless, the activities observed are still much higher than those reported for other methods (*e.g.* TON and TOF values of 20 and 20 h^{-1} for a 5 mol % loading of the NHC-stabilized Yb system described in Figure 4).[49]

Alkyl silanes such as ^{n}BuSiH$_3$ can also successfully undergo dehydrocoupling with amines with similar reaction times and catalyst loadings (50 ppm, entries 12-15 of Table 2). Nevertheless, the employment of ^{i}Pr$_2$NH gave rise to a rate increase of an order of magnitude compared to the reaction with PhSiH$_3$ (entries 8 *vs.* 15). A plausible explanation for this phenomenon is explained below.

[62] J. X. Wang, A. K. Dash, J. C. Berthet, M. Ephritikhine, M. S. Eisen, *J. Organomet. Chem.,* **2000**, *610*, 49-57.

[63] S. Anga, Y. Sarazin, J-F. Carpentier, T. K. Panda, *ChemCatChem,* **2016**, *8*, 1373-1378.

Entry	Silane	Amine (equiv.)	mol % (ppm) cat.[a]	Product	% yield[b] (isol.)	TON	TOF (h⁻¹)
1	PhSiH$_3$	^{t}BuNH$_2$ (1)	0.005 (50)	PhSiH$_2$(^{t}BuNH)	99(90)	2x10^4	9.6x10^4
2	PhSiH$_3$	^{t}BuNH$_2$ (1)	0.003 (30)	PhSiH$_2$(^{t}BuNH)	99	3.3x10^4	5.7x10^4
3	PhSiH$_3$	Et$_2$NH (1)	0.005 (50)	PhSiH$_2$(NEt$_2$)	99(88)	2x10^4	3.3x10^5
4	PhSiH$_3$	Et$_2$NH (1)	0.001 (10)	PhSiH$_2$(NEt$_2$)	98	9.8x10^4	2.9x10^4
5	PhSiH$_3$	(CH$_2$)$_4$NH (1)	0.01 (100)	PhSiH$_2$[N(CH$_2$)$_4$]	99	1x10^4	6.4x10^4
6	PhSiH$_3$	(CH$_2$)$_4$NH (1)	0.005 (50)	PhSiH$_2$[N(CH$_2$)$_4$]	99	2x10^4	3.4x10^4
7	PhSiH$_3$	^{i}Pr$_2$NH (1)	0.3 (3000)	PhSiH$_2$(N^{i}Pr$_2$)	99(93)	333	1600
8	PhSiH$_3$	^{i}Pr$_2$NH (1)	0.1 (1000)	PhSiH$_2$(N^{i}Pr$_2$)	99	1000	667
9	PhSiH$_3$	^{i}Pr$_2$NH (4)	0.1 (1000)	PhSiH$_2$(N^{i}Pr$_2$)	99	1000	1.7x10^4
10	PhSiH$_3$	MesNH$_2$ (2)	0.1 (1000)	PhSiH$_2$(NHMes)	95	950	840
11	PhSiH$_3$	MesNH$_2$ (4)	0.1 (1000)	PhSiH$_2$(NHMes)	99	1000	2300
12	^{n}BuSiH$_3$	^{t}BuNH$_2$ (1)	0.005 (50)	^{n}BuSiH$_2$(^{t}BuNH)	99(90)	2x10^4	1.3x10^5
13	^{n}BuSiH$_3$	Et$_2$NH (1)	0.005 (50)	^{n}BuSiH$_2$(NEt$_2$)	99(88)	2x10^4	1.2x10^5
14[c]	^{n}BuSiH$_3$	(CH$_2$)$_4$NH (1)	0.005 (50)	^{n}BuSiH$_2$[N(CH$_2$)$_4$]	99(91)	2x10^4	3x10^4
15	^{n}BuSiH$_3$	^{i}Pr$_2$NH (1)	0.1 (1000)	^{n}BuSiH$_2$(N^{i}Pr$_2$)	96(86)	1000	3.5x10^4

Table 2. Summary of the catalytic dehydrocoupling Si−N reactions performed by **13** with primary silanes to give monosilazanes. [a] Catalyst loadings were determined with respect to silane. [b] Determined by ^{1}H NMR. [c] Around 5% of disilazane ^{n}BuSiH[N(CH$_2$)$_4$]$_2$ has been detected by NMR.

Although the majority of these products are cleanly formed, their volatility makes possible their purification and isolation by vacuum distillation techniques or extraction with pentane, removing the catalyst in this way (Figure 11):
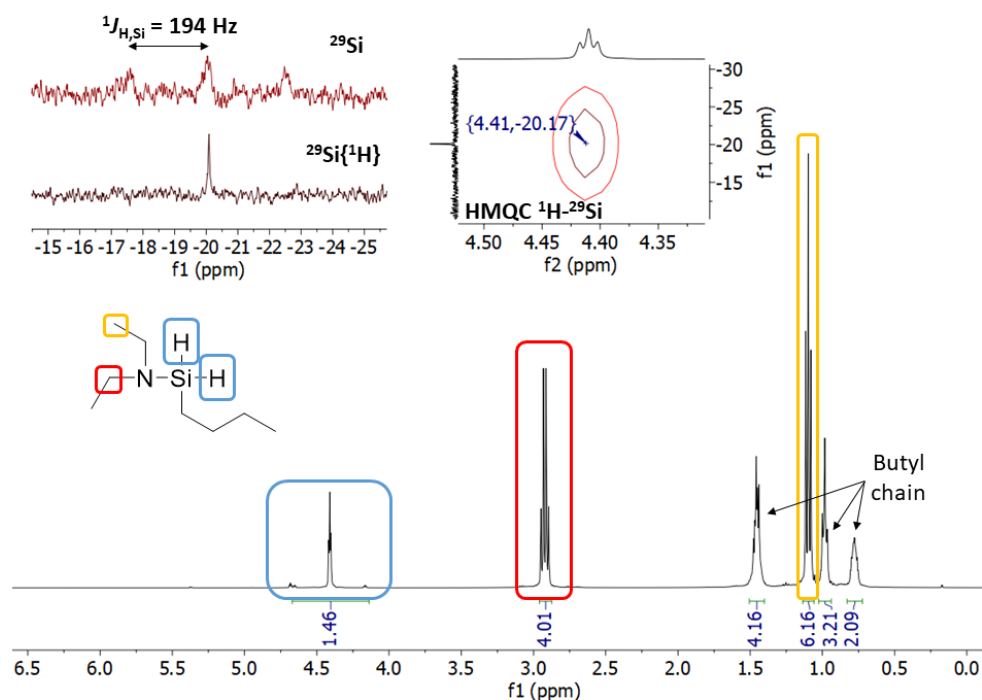
Figure 11. ^{1}H NMR spectrum (400 MHz, CD$_2$Cl$_2$) of ^{n}BuSiH$_2$(NEt$_2$). Inset: Monodimensional and bidimensional ^{29}Si NMR (400 MHz, CD$_2$Cl$_2$) experiments.

Dehydrocoupling of secondary silanes

Regarding secondary silanes, arylsilanes like Ph$_2$SiH$_2$ need higher catalyst loadings (0.1 mol %) in order to react with relatively small amines (Scheme 17) like ^{t}BuNH$_2$, Et$_2$NH or (CH$_2$)$_4$NH to yield the corresponding Ph$_2$SiH(NR$_2$) at short reaction times (entries 1-3 of Table 3). Bulkier amines such as ^{i}Pr$_2$NH show no reaction at room temperature, and heating the mixture to 60 °C for 4 days yields a mixture of multiple species. Alkylsilanes like Et$_2$SiH$_2$ react faster than their aromatic counterparts under the same conditions, giving activities up to two orders of magnitude higher (Table 3, entries 4-6 *vs.* 1-3).

[349]

$$RR'NH \quad + \quad R''_2SiH_2 \xrightarrow[\substack{CH_2Cl_2/r.t. \\ -H_2}]{\substack{\textbf{13} \\ \geq 0.1 \ mol \ \%}} R'RN-SiHR''_2$$

$$R'' = Et \ or \ Ph$$
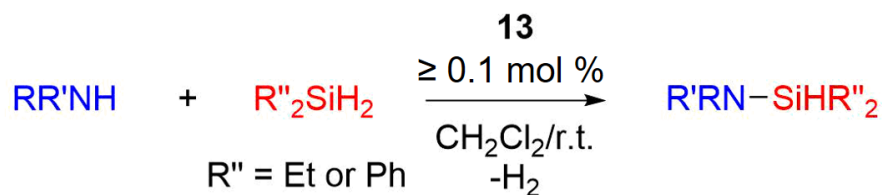
Scheme 17. Si–N dehydrogenative coupling of secondary silanes with amines catalyzed by **13** to give monosilazanes.

Entry	Silane	Amine (equiv.)	mol % (ppm) cat.[a]	Product	% yield[b] (isol.)	TON	TOF (h^{-1})
1	Ph$_2$SiH$_2$	^{t}BuNH$_2$ (1)	0.1 (1000)	Ph$_2$SiH(^{t}BuNH)	99(97)	1000	2000
2	Ph$_2$SiH$_2$	Et$_2$NH (1)	0.1 (1000)	Ph$_2$SiH(NEt$_2$)	99(91)	1000	1300
3	Ph$_2$SiH$_2$	(CH$_2$)$_4$NH (1)	0.1 (1000)	Ph$_2$SiH[N(CH$_2$)$_4$]	99(92)	1000	1330
4	Et$_2$SiH$_2$	^{t}BuNH$_2$ (1)	0.1 (1000)	Et$_2$SiH(^{t}BuNH)	99(98)	1000	3.3x10^5
5	Et$_2$SiH$_2$	Et$_2$NH (1)	0.1 (1000)	Et$_2$SiH(NEt$_2$)	99(96)	1000	5.3x10^4
6	Et$_2$SiH$_2$	(CH$_2$)$_4$NH (1)	0.1 (1000)	Et$_2$SiH[N(CH$_2$)$_4$]	99(98)	1000	9.4x10^3

Table 3. Summary of the catalytic dehydrocoupling Si–N reactions performed by **13** with secondary silanes to give monosilazanes. [a] Catalyst loadings were determined with respect to silane. [b] Determined by ^{1}H NMR.

In accordance with the results observed in chapter 3, tertiary silanes like Ph$_3$SiH are too bulky to interact with the metal. Thus, no reaction was observed in any case.

Synthesis of disilazanes

In the case of primary silanes, silane:amine ratios of 1:2 produce the corresponding bis(amino)silanes or disilazanes at room temperature for amines like ^{t}BuNH$_2$, Et$_2$NH or (CH$_2$)$_4$NH (Table 4), although a catalyst loading of at least

[350]

0.2 mol % is necessary in order to achieve the corresponding products (Scheme 18). Entries 1-3 show TON and TOF numbers up to 1000 and 8450 h^{-1}, respectively, which are still higher than those described in the literature for similar substrates (TON = 40, TOF = 40 h^{-1}).[49,53] Other amines, like $^{i}Pr_2NH$ or $MesNH_2$ do not afford disilazanes even when using high catalytic loadings. Adding more equivalents of amine does not make any difference on the nature of the product, yet shorter reaction times are observed (Table 2, entries 8-11).

Again, alkylsilanes seem to give faster reaction than aromatic ones, as it can be seen in Table 4 (entries 4 and 6 *vs*. 1 and 3).

$$2 \; RR'NH \quad + \quad R''SiH_3 \quad \xrightarrow[\substack{CH_2Cl_2/r.t. \\ -H_2}]{\substack{\textbf{13} \\ \geq 0.2 \; mol \; \%}} \quad \underset{\substack{| \\ NRR'}}{R'RN-SiHR''}$$

$$R'' = {}^{n}Bu \; or \; Ph$$
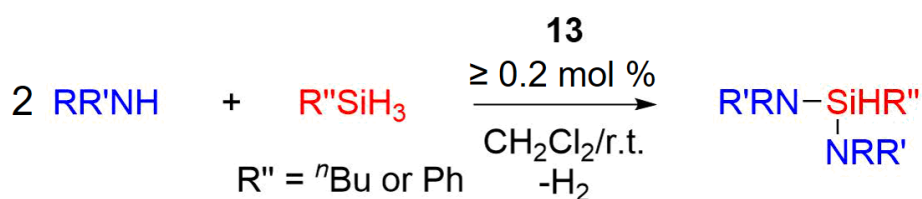
Scheme 18. Si−N dehydrogenative coupling of primary silanes with amines catalyzed by **13** to give disilazanes.

Entry	Silane	Amine (equiv.)	mol % (ppm) cat.[a]	Product	% yield[b] (isol.)	TON	TOF (h[-1])
1	$PhSiH_3$	$^{t}BuNH_2$ (2)	0.2 (2000)	$PhSiH(^{t}BuNH)_2$	92(90)	920	540
2	$PhSiH_3$	Et_2NH (2)	0.3 (3000)	$PhSiH(NEt_2)_2$	99(86)	666	595
3	$PhSiH_3$	$(CH_2)_4NH$ (2)	0.2 (2000)	$PhSiH[N(CH_2)_4]_2$	99(96)	1000	8450
4	$^{n}BuSiH_3$	$^{t}BuNH_2$ (2)	0.2 (2000)	$^{n}BuSiH(^{t}BuNH)_2$	96(91)	1000	1.9×10^4
5	$^{n}BuSiH_3$	Et_2NH (2)	0.2 (2000)	$^{n}BuSiH(NEt_2)_2$	99(89)	1000	5.7×10^3
6	$^{n}BuSiH_3$	$(CH_2)_4NH$ (2)	0.2 (2000)	$^{n}BuSiH[N(CH_2)_4]_2$	99(95)	1000	1.3×10^4

Table 4. Summary of the catalytic dehydrocoupling Si−N reactions performed by **13** with primary silanes to give disilazanes. [a] Catalyst loadings were determined with respect to silane. [b] Determined by ^{1}H NMR.

[351]

Chapter 4. Results and discussion

Experiments with >1 equivalent of amine: rationalization of the reaction rates

The nature and steric volume of the amine turned out to be rather influential on the reaction rates when an excess of amine is present with primary silanes and **13**. Whereas ^{t}BuNH$_2$, Et$_2$NH and (CH$_2$)$_4$NH required longer reaction times, ^{i}Pr$_2$NH and MesNH$_2$ gave faster reaction rates. This phenomenon finds its explanation in the size of the amines: smaller ones can coordinate to the metal, occupying the coordination vacant site and precluding the formation of the σ-SiH complex. On the contrary, bulky or poorly nucleophilic amines cannot approach the platinum center, thus the vacant is available for the silane to establish an interaction. This hypothesis was confirmed by analyzing the kinetic profiles of the reactions between these amines and phenylsilane, in which the amount of hydrogen produced was measured over time. This was possible thanks to a device named Man on the Moon series X102 kit, which measures the changes in pressure and temperature of the headspace in a closed reaction vessel (Figure 12).[64] In addition, a change of color from yellow to colorless was observed in the reaction of the small, coordinating amines with complex **13** along with a decrease in the $^2J_{H,Pt}$ coupling constant of the methylene protons (Pt−CH$_2$) when an excess of amine was used ($^2J_{H,Pt}$ diminished 15 and 7 Hz when 5 equivalents of ^{t}BuNH$_2$ or Et$_2$NH were added, respectively), indicative of the coordination of some Lewis base in a *trans* position to the CH$_2$ group, as previously observed for complex **13**·THF of **13**·CH$_3$CN.[65,66]

---

[64] http://www.manonthemoontech.com/x102-gas-evolution.html.

[65] *"Síntesis de complejos coordinativamente insaturados de Pt(II) estabilizados por ligandos carbeno N-heterocíclicos. Activación y funcionalización de enlaces C−H"*. O. Rivada-Wheelaghan. PhD Thesis, **2013**.

[66] M. A. Ortuño, S. Conejero, A. Lledós, *Beilstein J. Org. Chem.,* **2013**, *9*, 1352-1382.

Figure 12. Assembly of the Man on the Moon X102 kinetic kit (obtained from reference 64).

As a result, it can be seen in Figure 13 that increasing amounts of coordinating amines like Et_2NH produce slower rates in the dehydrocoupling reaction with phenylsilane, whereas bulky substrates such as $^iPr_2NH$ lead to the opposite effect (*i.e.* faster rates with more equivalents of the amine).

[353]
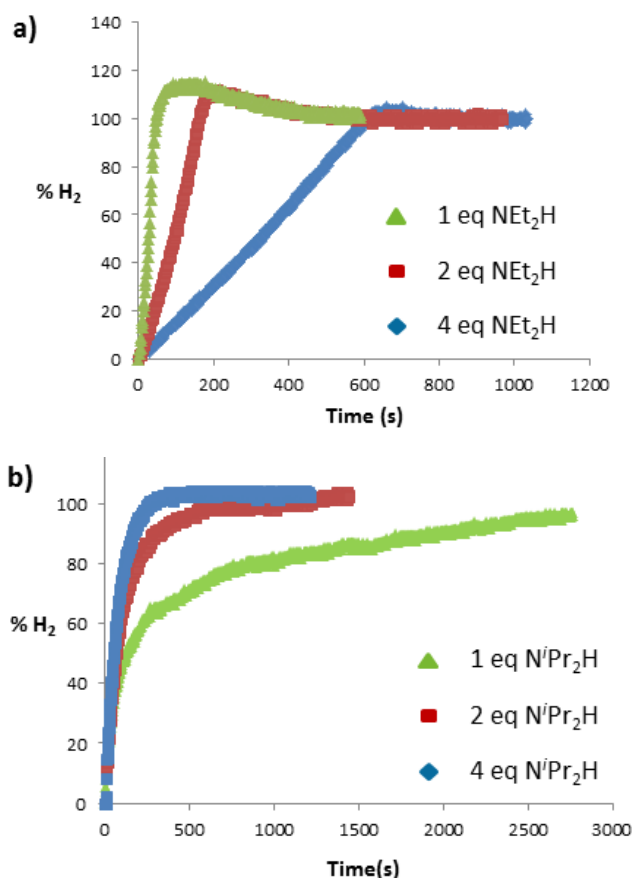
Figure 13. Kinetic profiles (H_2 pressure *vs.* time) of the dehydrocoupling of $PhSiH_3$ with a) Et_2NH and b) $^iPr_2NH$ catalyzed by **13**. It can be observed that both amines produce inverse effects depending on their coordination capabilities to **13**.[67]

A comparison of different amines is also displayed in Figure 14, where their coordination efficiencies to **13** follow the trend $^tBuNH_2 > Et_2NH > {}^iPr_2NH$. The plot reveals an exponential curve for the non-coordinating amine and sigmoidal shapes for less hindered, coordinating ones. Given that sigmoidal curves are sometimes associated with the formation of metal nanoparticles,

---

[67] The initial increase of pressure above 100% in the plot on the left is attributed to the partial evaporation of the low-boiling point solvent (CH_2Cl_2) due to the exothermic nature of the reaction. When the process is slower (plot on the right) the heat is gradually released, avoiding solvent evaporation.

[354]

poisoning experiments using Hg (~1000 equivalents) discarded this possibility upon observation of the same kinetic data. Therefore, the initial stage of the sigmoid may be attributable to the time required for the amine to decoordinate from the catalyst.
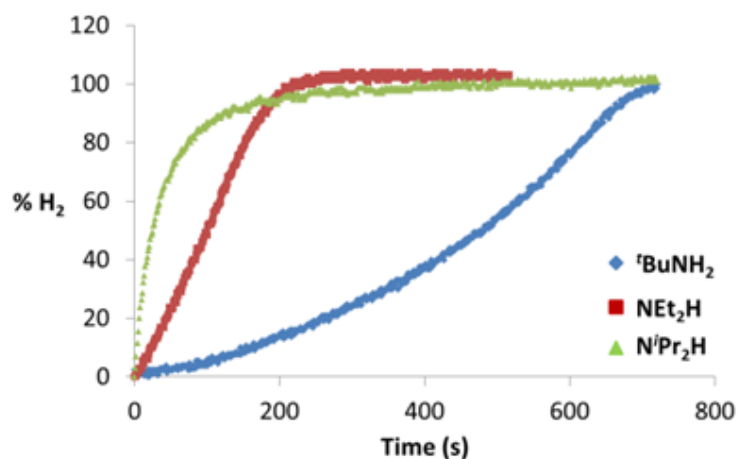
Figure 14. Kinetic profile (H$_2$ evolution) of the reaction of PhSiH$_3$ with ^{t}BuNH$_2$, Et$_2$NH and ^{i}Pr$_2$NH (catalyst loadings of 0.005, 0.005 and 0.3 mol %, respectively).

Figure 15 summarizes the aforementioned phenomena related to the nature of the amines and their influence on the dehydrocoupling reaction rates upon coordination to the metal center:

[355]
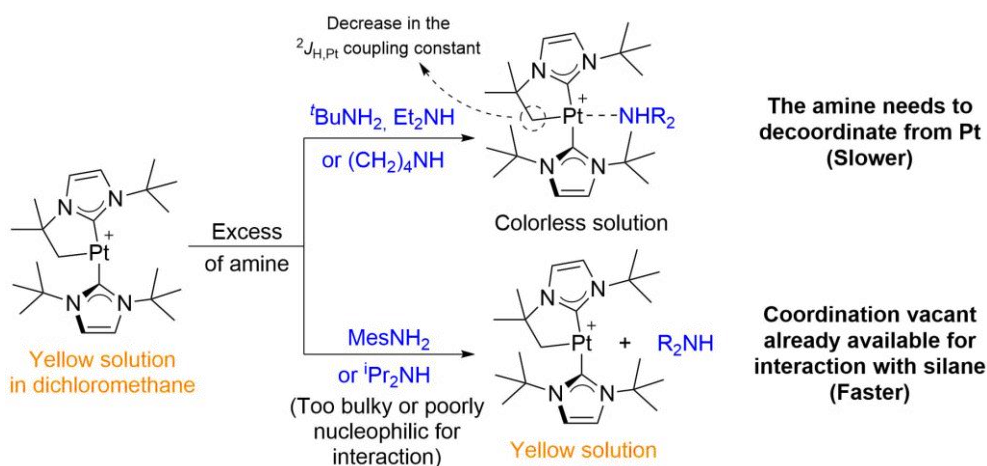
Figure 15. Plausible explanation for the observed experimental differences depending on the amine used in the dehydrocoupling reaction.

The obtainment of reliable kinetic plots made possible the kinetic analysis so as to determine partial orders in the species involved in the reaction (see Experimental Part for more details). The reaction between $PhSiH_3$ and Et_2NH was chosen for this purpose. Unfortunately, partial order in amine could not be determined because of the reactivity between **13** and silanes, as described in chapter 3. At any rate, a negative partial order is expected, given the deceleration of the dehydrocoupling process with increasing amounts of Et_2NH. Notwithstanding, the reaction proved to be zero-order in silane (similar to the calcium and magnesium systems described by Hill *et al.*)[52] and second order (2.2) in catalyst (similar to the strontium systems described by the same group). This latter result will be discussed later on this chapter.

Finally, it is interesting to mention that secondary silanes cause a different behaviour than primary ones. For instance, reactions carried out with Ph_2SiH_2 give exponential profiles in all cases, as indicated in Figure 16. This behavior is observed even when an excess of amine is present (Figure 17).

[356]
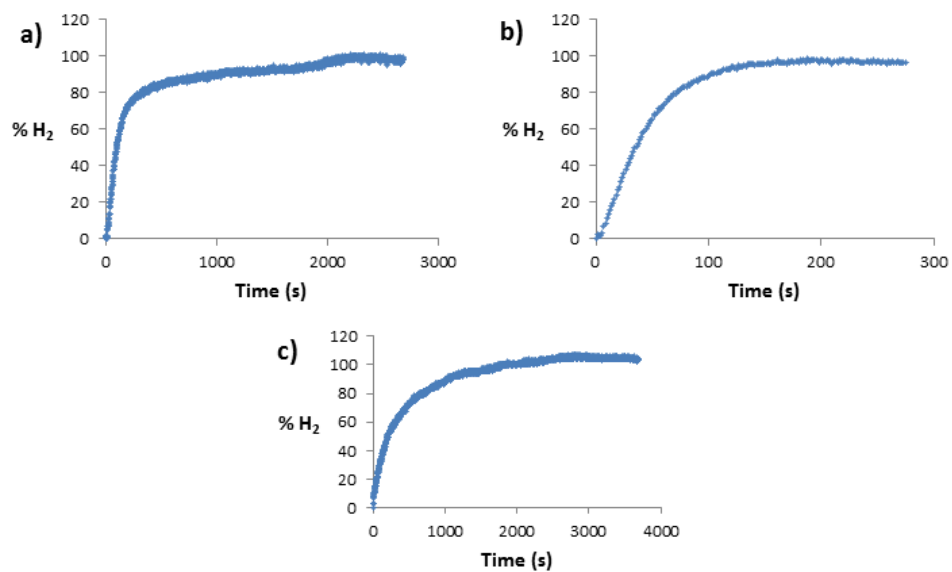
Figure 16. Kinetic profile (H_2 evolution) of the reaction of Ph_2SiH_2 with 1 equivalent of: (a) $^tBuNH_2$, (b) Et_2NH and (c) $(CH_2)_4NH$ (catalyst loadings of 0.1, 0.2 and 0.3 mol % respectively).
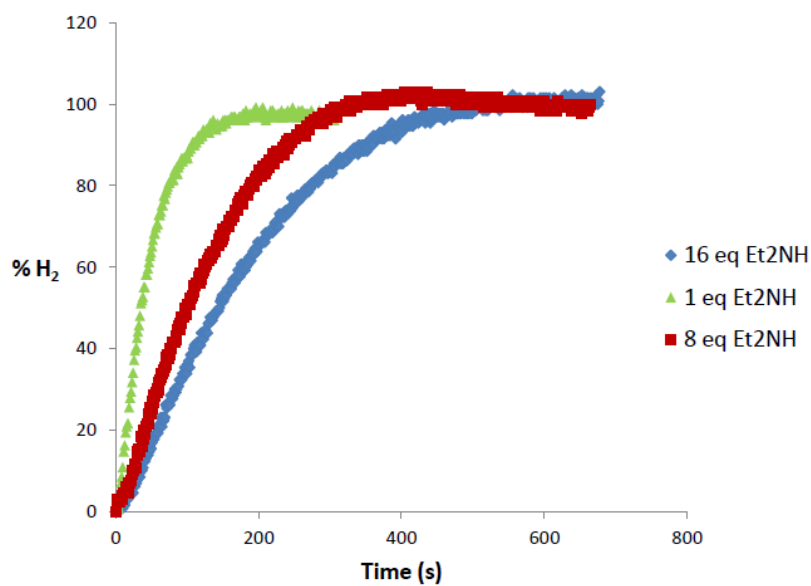
Figure 17. Effect of the concentration of Et_2NH on the rate of H_2 evolution in the reaction of Ph_2SiH_2 and Et_2NH with 0.3 % of catalyst **13**.

[357]

In order to find an explanation to this disparity, a collaboration was established with Prof. Joaquín López-Serrano from the University of Seville, who performed DFT calculations on the interaction between $PhSiH_3$ and Ph_2SiH_2 with **13**.[68] Scheme 19 shows the energy breakdown of the bonding between the silanes and the metal complex. As it can be seen, the overall bonding electronic energy (ΔE_b) is composed of two terms: the deformation energy (ΔE_{def}) that the fragments undergo upon their approach and the interaction energy (ΔE_{int}) between the entities with the geometry that they adopt in the adducts.
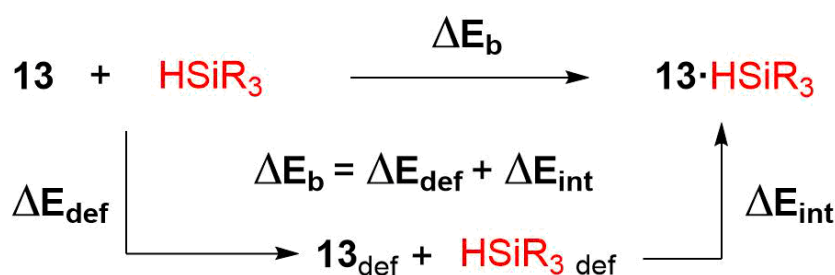
Scheme 19. Electronic energy breakdown of the overall bonding energy in the formation of **13**·$PhSiH_3$ and **13**·Ph_2SiH_2

Table 3 displays the energies extracted from these calculations, and it clearly shows how diphenylsilane interacts more strongly than phenylsilane by 4.8 kcal/mol. This accounts for the stronger interaction of Ph_2SiH_2 with complex **13**, and it may explain why there is no induction period when using these substrate regardless of the amine, giving rise to exponential (and not sigmoidal) kinetic plots.

---

[68] Calculations were carried out at the M06/6-31g(d,p)/SDD level of theory. SMD (Dichloromethane) continuum was used to model the solvent.

	PhSiH$_3$	Ph$_2$SiH$_2$	ΔΔE
ΔE$_{def}$ (13)	4.2	5.3	1.1
ΔE$_{def}$ (silane)	0.8	1.2	0.4
ΔE$_{int}$	-18.3	-23.1	**_-4.8_**
ΔE$_b$	-13.3	-16.6	-3.3
ΔE$_b$^{DCM}	-7.9	-8.8	**_-0.9_**

Table 3. Electronic energies (kcal/mol) obtained from the DFT analysis of the interaction between **13** and PhSiH$_3$ and Ph$_2$SiH$_2$. The interaction and bonding energies include basis set superposition error (BSSE, Counterpoise method) corrections.

Origin of the selectivity

Table 4 showed that catalyst loadings of at least 0.2 mol % are able to catalyse the formation of disilazanes when a silane:amine ratio of 1:2 is employed for non-coordinating amines such as ^{t}BuNH$_2$, Et$_2$NH or (CH$_2$)$_4$NH, being the process faster for ^{n}BuSiH$_3$ than for PhSiH$_3$. However, mixtures are observed in some cases depending on the reaction conditions. For instance, 0.5 mol % of **13** catalyses the reaction between phenylsilane and pyrrolidine in a 1:1 proportion, giving the mono- and disilazane in a 1:5.7 ratio along with unreacted silane. Addition of a second equivalent of amine selectively affords the product PhSiH[N(CH$_2$)$_4$]$_2$. Nonetheless, entry 6 of Table 2 reveals that the selective formation of the monosilazane PhSiH$_2$N[(CH$_2$)$_4$] is possible if the catalyst loading is decreased down to 50 ppm.

The explanation behind this divergent behavior might be found in the nature of the active catalyst. It was mentioned at the beginning of Section 2.2 (see *Dehydrocoupling of primary silanes*) that the only Pt species remaining after the catalytic process was hydride **15**.[69] Previously, it has been discussed in chapter 3 that **13** forms stronger σ-SiH complexes than **15**, and indeed, this phenomenon

---

[69] No decomposition was observed in any case, discarding the formation of solid platinum or any type of colloid or nanoparticles.

has consequences that influence the outcome of some catalytic events such as carbon dioxide hydrosilation, as shown in section 2.1 (*i.e.* **15** is a less active catalyst than **13**, since the degree of electrophilic activation on the silane is lower). In order to compare these facts with the Pt-assisted Si−N dehydrogenative coupling, a series of experiments were performed so as to obtain more information about the system:

Hindered amines

- Entries 7 and 8 of Table 2 demonstrate that **13** requires 12 min and 1.5 h (catalyst loadings of 0.3 and 0.1 mol %, respectively) to transform a 1:1 mixture of $PhSiH_3$ and $^iPr_2NH$ into the monosilazane $PhSiH_2(N^iPr_2)$. If this reaction is carried out with 0.5 mol % of **15** (generated *in situ* by reaction of **13** with H_2), 65% conversion is observed after 5 hours, and 10 hours are needed to achieve full conversion.

- Two consecutive additions of $PhSiH_3$ and $^iPr_2NH$ were carried out in a reaction flask initially containing **13**. It was observed that the second run was much slower than the first one, indicative of a change in the nature of the catalyst.

Non-hindered amines

- The reaction between $PhSiH_3$ and Et_2NH catalyzed by 50 ppm of **13** (entry 3 of Table 2) was carried out in 3 consecutive runs. In this case, the rates of the first, second and third runs are practically the same, exhibiting similar kinetic plots (Figure 18). This suggests that the whole process is catalysed by the same species (presumably complex **15**, given that **13** is readily hydrogenated to hydride **15** in the presence of H_2).

[360]
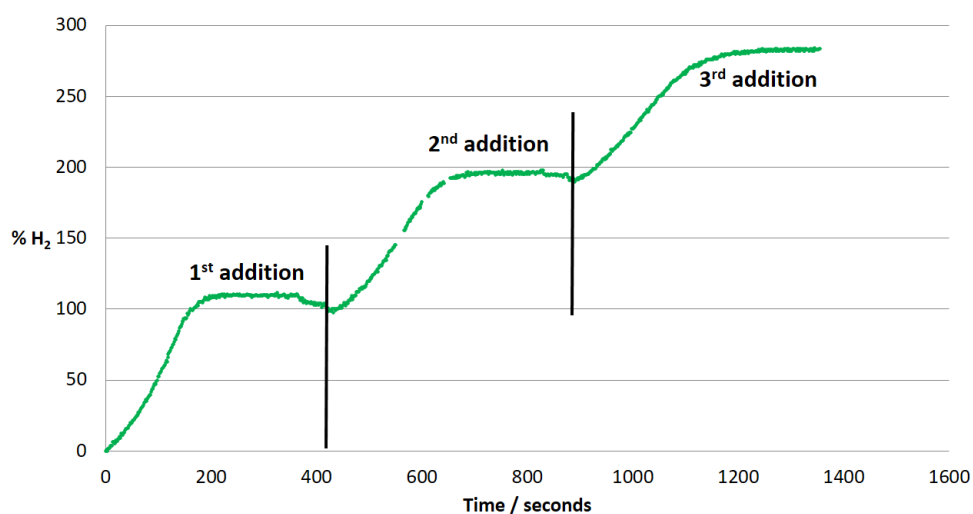
Figure 18. Kinetic profile (H_2 evolution) of the reaction (3 consecutive additions) between $PhSiH_3$ and Et_2NH (1 equivalent) under 50 ppm of catalyst **13**.

- An interesting result was observed when monitoring the released H_2 during the reaction between $PhSiH_3$ and pyrrolidine (2 equivalents) under 0.2 mol % of **13** (Entry 3 of Table 4). As it can be seen in Figure 19, there are two clear kinetic profiles. The first one corresponds to the first dehydrogenation event, and the second one, starting at ~50-60% of the expected amount of H_2, corresponds to the dehydrocoupling of the newly formed monosilazane $PhSiH_2[N(CH_2)_4]$. As expected for the employed substrates, the first kinetic profile is sigmoidal (pyrrolidine is a coordinating amine) and the second kinetic profile is exponential (as expected for a secondary silane, according to the previously mentioned experimental and theoretical results).

[361]
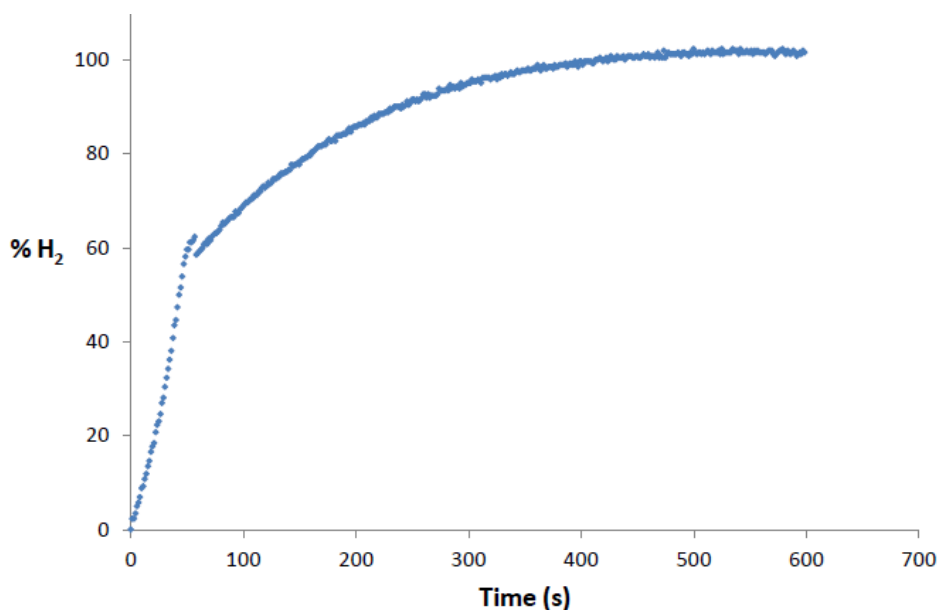
Figure 19. Kinetic profile (H$_2$ evolution) of the reaction of PhSiH$_3$ with 2 equivalents of (CH$_2$)$_4$NH under 0.2 mol % of catalyst **13**.

These experiments seem to suggest that at low catalytic loadings (ppm), cyclometalated catalyst **13** is easily transformed into hydride complex **15** because of the formed H$_2$, and **15** is responsible for the observed selectivity towards monosilazanes, given that the second Si−N dehydrogenative coupling is so extremely slow that no disilazane is detected. At higher catalytic loadings (from 0.2 mol % upwards), the amount of catalyst present in the reaction (either **13** or **15**) is enough to carry out the mono and/or disubstitution at an appreciable reaction time. As shown above, these processes occur much faster when **13** is present, and the reaction rates will vary depending on the nature and amount of amine added.

Mechanistic investigations: Low temperature NMR studies

With the purpose of obtaining more experimental evidence about the mechanism by which these reactions occur, the reaction between Ph$_2$SiH$_2$ and

[362]

Et$_2$NH was analysed at low temperature through ^{1}H NMR spectroscopy. Initial studies in CD$_2$Cl$_2$ showed no trace of any intermediate from -80 °C to 25 °C. Thus, the solvent was switched to d^8-THF due to its ability to coordinate to the metal and to lead to slower reaction rates. At -30 °C, a stoichiometric mixture of **13**, Ph$_2$SiH$_2$ and Et$_2$NH showed the presence of some unreacted complex **13** and neutral hydride **14** (Figure 20), which is presumably formed after hydride transfer from the η^1 σ-SiH complex right after the nucleophilic attack of the amine, in the same way as the amine-borane dehydrocoupling mechanism described by our group (see Scheme 6 of chapter 3).[60]
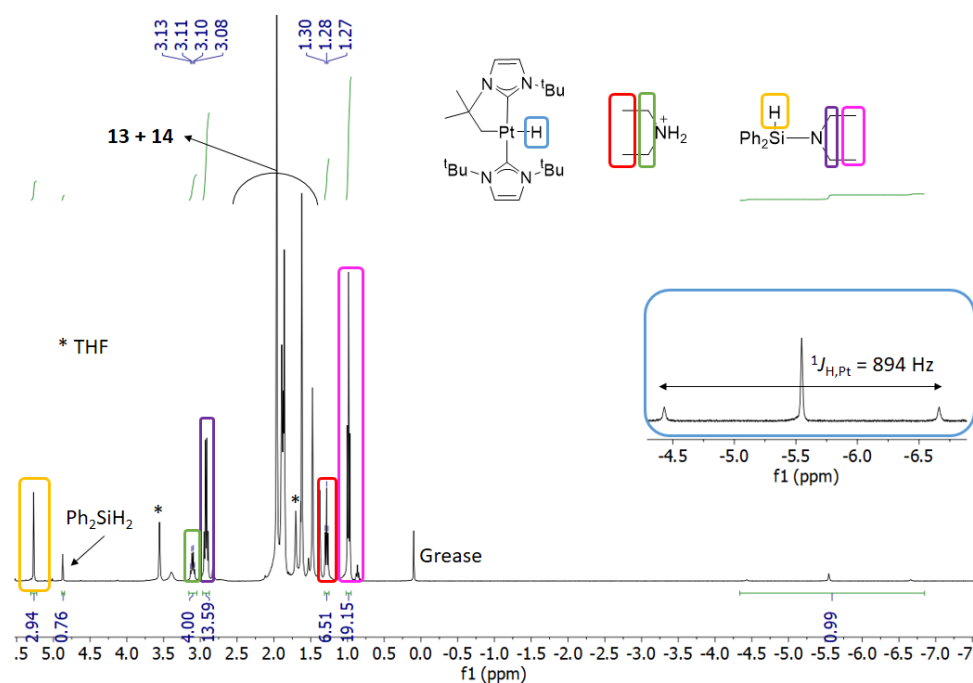
Figure 20. Portion of the ^{1}H NMR spectrum (400 MHz, d^8-THF) of the reaction between **13**, Ph$_2$SiH$_2$ and Et$_2$NH (1 equivalent) acquired at -30 °C.

Apart from **13** and **14**, monosilazane Ph$_2$SiH(NEt$_2$) is also observed, and another unknown species (**A**) which seems to be present in a 1:1 ratio with

[363]

complex **14**. Regarding **A**, it shows signals that point to a NEt_2 fragment, and it possesses no Si atom in close proximity according to ^1H-^{29}Si HMBC experiments, given that the only compounds with silicon are the some unreacted diphenylsilane and the previously mentioned monosilazane. The ethyl chains of **A** correlate (COSY) with a signal at around 7.6 ppm at -40 °C. Upon warming up the sample, the peaks corresponding to **14** and **A** simultaneously decrease until they disappear at 25 °C. Although our first tempting thought was to identify **A** as the silylium intermediate $Ph_2SiH(NHEt_2)^+$ (in analogy to the boronium cation $BH_2(NHMe_2)_2^+$ observed during the dehydrocoupling of $NMe_2H \cdot BH_3$),[60] the lack of correlating signals of any proton of this intermediate with a silicon atom in the ^1H–^{29}Si HMBC experiments led us to propose a different type of ammonium cation. One reasonable possibility would be that species **A** corresponds to the cationic derivative $[Et_2NH_2][BAr_4^F]$, generated from the deprotonation reaction of the short-lived cation $Ph_2SiH(NEt_2H)^+$ by free diethylamine. In order to confirm this hypothesis, the ammonium salt $[Et_2NH_2][BAr_4^F]$ was synthesized by reaction of Et_2NH and $[H(Et_2O)_2][BAr_4^F]$, and to our delight, the low temperature ^1H NMR spectrum[70] of pure $[Et_2NH_2][BAr_4^F]$ was nearly identical to that observed for intermediate **A**:

---

[70] The NH_2 protons of the ammonium cation are only visible below -30 °C.
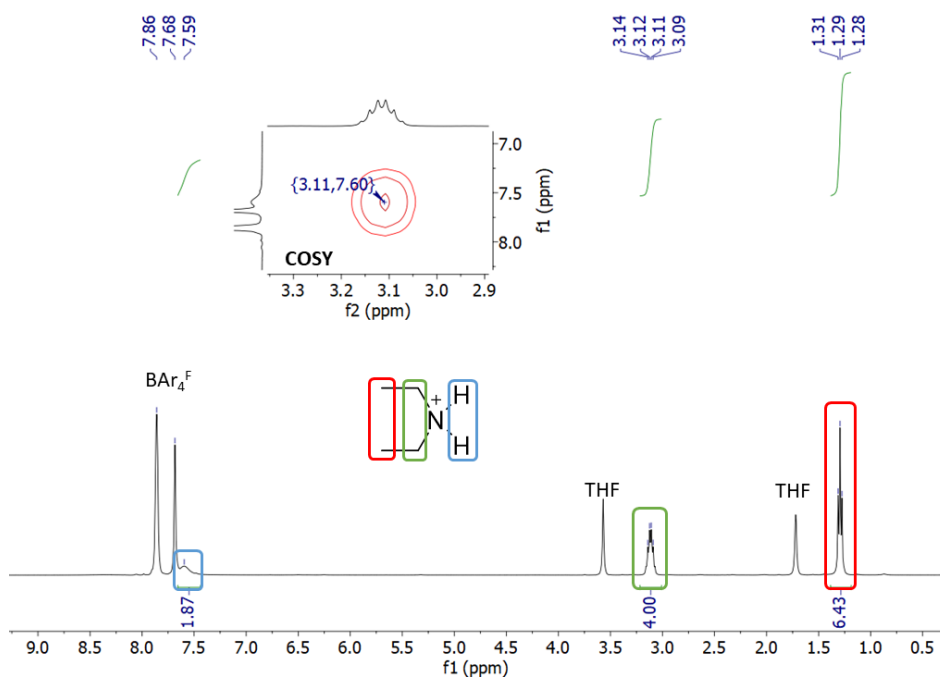
Figure 21. ^{1}H NMR of [Et$_2$NH$_2$][BAr$_4$^{F}] (400 MHz, d^8-THF) at -50 °C. It can be seen that the chemical shifts of the alkyl chains perfectly match those highlighted in Figure 20.

Moreover, the chemical shifts of the ^{15}N NMR spectrum (obtained from a ^{1}H-^{15}N HMBC experiment) of both [Et$_2$NH$_2$][BAr$_4$^{F}] and intermediate **A** are nearly the same (49.4 and 49.1 ppm, respectively) thus providing further evidence of intermediate **A** being the ammonium salt [Et$_2$NH$_2$][BAr$_4$^{F}].

Therefore, all these data indicate that two NEt$_2$H molecules are needed to generate the aminosilane Ph$_2$SiH(NEt$_2$) in the experiment carried out at low temperature, explaining the reasons why we observed some unreacted free Ph$_2$SiH$_2$ and complex **13** (that are only consumed when reaching room temperature). In fact, another identical experiment with 2 equivalents of amine instead of 1 led to the observation of species **14**, **A** and Ph$_2$SiH(NEt$_2$), but neither free Ph$_2$SiH$_2$ nor **13** were detected, corroborating the need of 2 equivalents of amine per catalytic cycle. At the end of the experiment (room temperature), cationic hydride **15** is observed. This is in agreement with the formation of H$_2$

[365]

from the protonation of **14** by **A**, regenerating complex **13** which is subsequently hydrogenated. A summary of the results experimentally observed is depicted in Scheme 20:
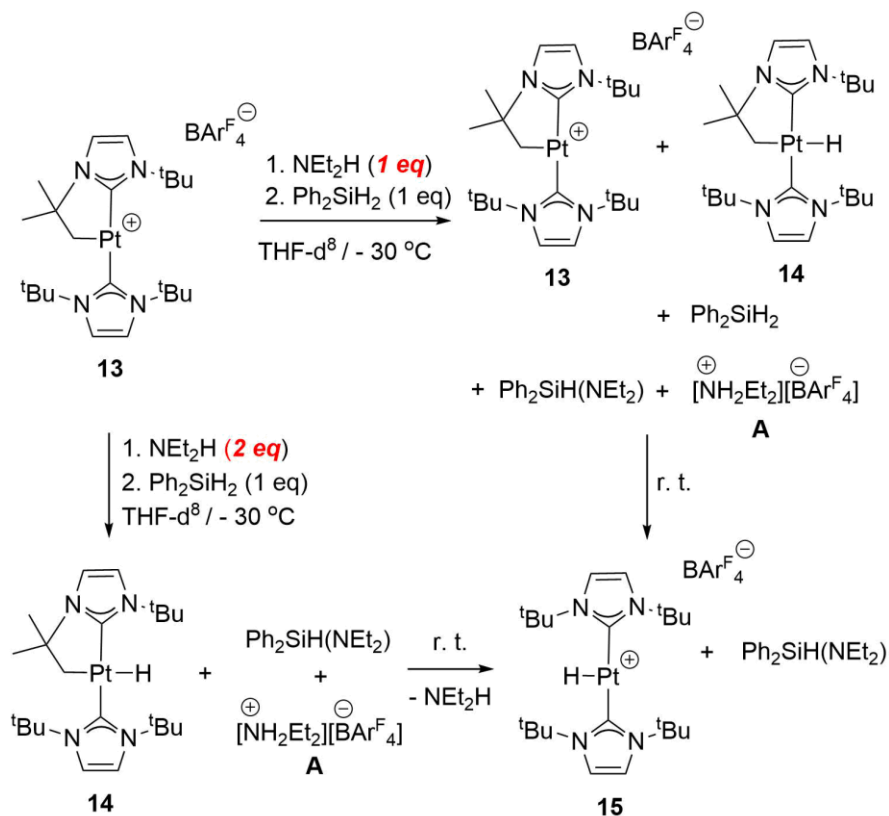
Scheme 20. Summary of the observed species during low temperature NMR experiments of the stoichiometric reactions between **13**, Ph₂SiH₂ and Et₂NH.

Mechanistic investigations: DFT calculations

Computational studies also support the experimental observations.[71] Thanks to the collaboration with Prof. Joaquín López-Serrano, it was possible to obtain the energy values corresponding to each stage of our proposed

---

[71] Calculations were carried out at the PBE0-D3/6-31g(d,p)/SDD level of theory. SMD (Dichloromethane) continuum was used to model the solvent.

mechanism. Given that some amines are able to coordinate to **13**, the first step would be the evaluation of the amine-silane exchange in the coordination sphere of the platinum catalyst, in order to assess that the equilibrium between the σ-SiH complex and the Pt-amine adduct is indeed energetically feasible (Figure 22). For this purpose, phenylsilane was chosen as the model silane, $^tBuNH_2$ and Me_2NH (model for Et_2NH) were selected as model coordinating amines and $^iPr_2NH$ as a hindered amine. In agreement with the experimental results, N-adducts of the coordinating amines $^tBuNH_2$ and Me_2NH are more stable than the corresponding σ complex **13·PhSiH₃**. However, bulky species like $^iPr_2NH$ give rise to less stable adducts than the silane ones. These data support the presence of an induction period in some of the kinetic plots shown above in the case of the less hindered amines.
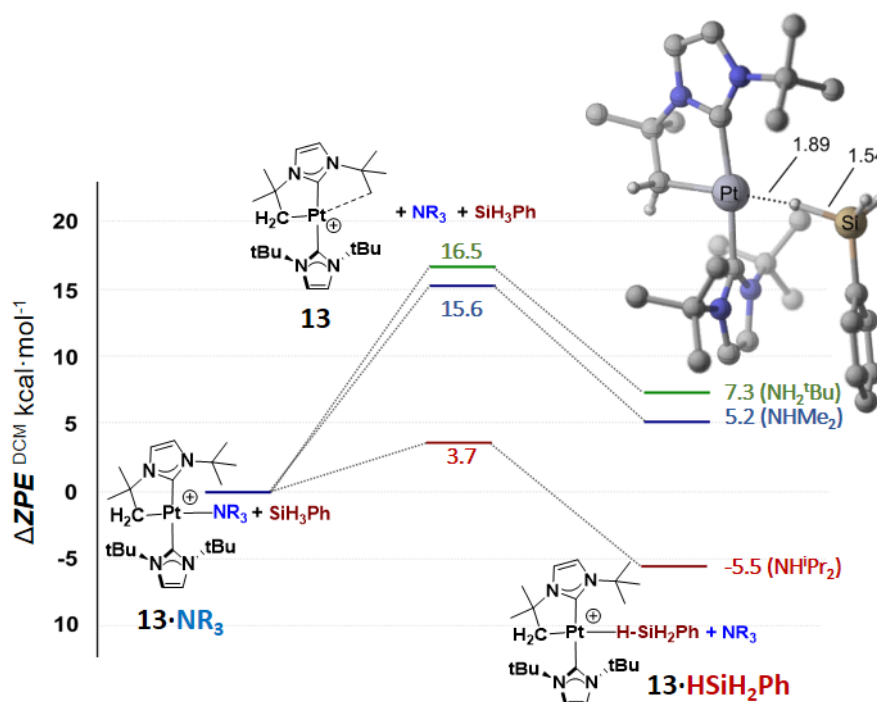
Figure 22. Stability of the σ-complex **13·PhSiH₃** relative to various N-amine adducts of **13**. Most of the hydrogen atoms have been omitted for clarity.

[367]

Then, the mechanistic pathway for the Si−N dehydrogenative coupling reaction has been calculated. For simplicity reasons and computational time, Me_2NH was chosen as the model amine and $PhSiH_3$ as the model silane. Figure 23 displays the first stage of the mechanism, which consists of the hydride abstraction from phenylsilane by **13** in a process assisted by Me_2NH, which attacks the Si atom in the σ-SiH complex to give the corresponding cation $PhH_2Si−NHMe_2^+$.[72] This takes place through intermediate **B** (ΔG^{DCM} = 0.2 kcal/mol), where the Si−H bond elongates and the Si−N and Pt−H bonds are partially formed. Si−H cleavage and separation of the **14** and silyl cation fragments is only 4.6 kcal/mol (ΔE^{DCM} = 18.8 kcal/mol) above the origin. It is worth mentioning that Figure 23 also shows the energies corresponding to the same pathway, albeit catalysed by hydride complex **15** (ΔG^{DCM} values in parentheses). The higher free energies obtained for this system are also in agreement with the slower catalytic reactions performed by **15** in comparison to **13**.

---

[72] Calculations discard mechanisms involving Si−H oxidative addition.
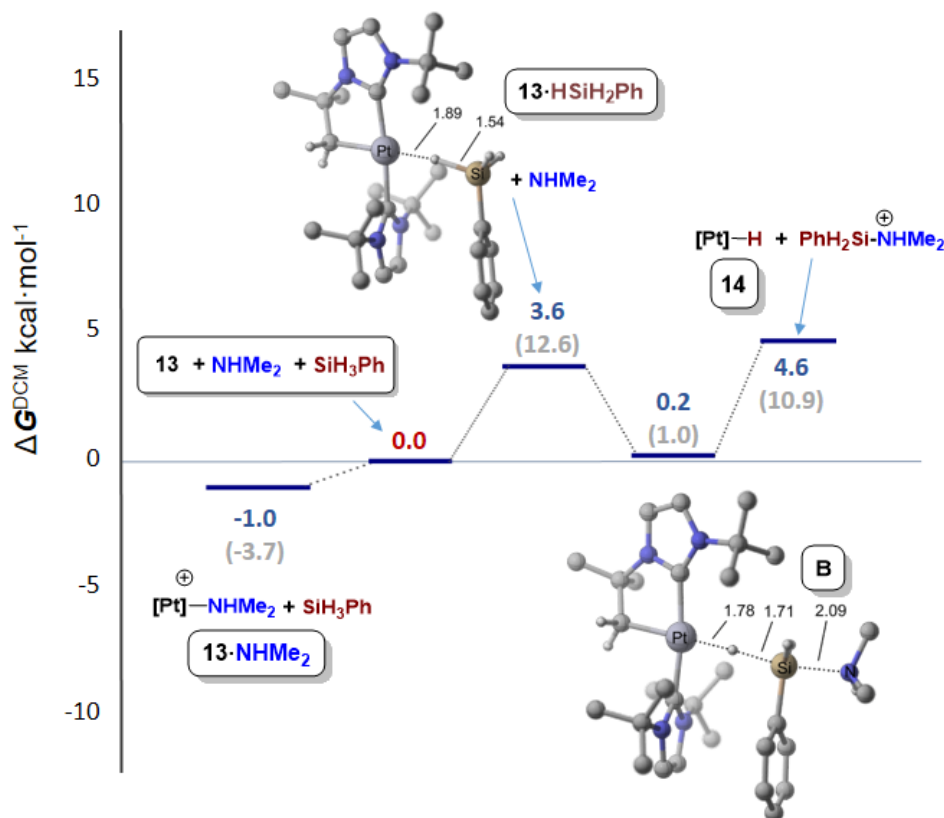
Figure 23. Calculated Free Energy profile of the nucleophilic attack of Me₂NH to σ-silane complex **13·HSiH₂Ph**. Data in parentheses correspond to the reactions catalyzed by hydride complex **15**. Most of the hydrogen atoms have been omitted for clarity.

At this point, complex **14** can give rise to a dihydrogen complex due to protonation[73] from the PhH₂Si−NHMe₂⁺ cation. This is illustrated in Figure 24 (orange numbers), where the resulting adduct **14·H−N(Me₂)SiH₂Ph⁺** is 3.1 kcal/mol above the reference. The protonation event requires 9.5 kcal/mol and leads to the adduct composed of the platinum dihydrogen derivative and the monosilazane PhH₂Si−NMe₂ (ΔG^{DCM} = 4.5 kcal/mol). Nevertheless, this sequence would not explain the experimental results obtained from the low temperature

---

[73] M. Besora, A. Lledós, F. Maseras, *Chem. Soc. Rev.,* **2009***, 38*, 957-966.

NMR experiments, since no $PhH_2Si-NHMe_2^+$ was detected in any case. Also, only one equivalent of amine would be needed, in contradiction with the experiment using a silane:amine stoichiometry of 1:2. This route does not include the formation of species **A** either.

An alternative protonation route was then conceived (blue numbers in Figure 24). This involves the deprotonation of the silyl cation by Me_2NH (Figure 24, inset), whose transition state is located 3.0 kcal/mol below the reagents. It is necessary to mention that this transition state is practically barrierless (0.1 kcal/mol) and explains the absence of the cationic species $PhH_2Si-NHMe_2^+$ in the reaction mixture at low temperature. This gives the experimentally observed mixture **14 + A ($Me_2NH_2^+$ in the model) + $PhH_2Si-NMe_2$** (ΔG^{DCM} = -3.5 kcal/mol), as noticed in the ^1H NMR spectrum at -30 °C. Then, the ammonium cation **A** can protonate neutral hydride **14** through a transition state which is located 3.0 kcal/mol above the reference. The overall free energy for this step is 8.2 kcal/mol, making the N–H cleavage event the rate determining step in the mechanism. This is in agreement with the kinetic isotope effect (KIE) obtained when using Et_2ND (k_H/k_D = 1.67).[74] Liberation of neutral Me_2NH and irreversible H_2 release gives back catalyst **13** along with the monosilazane with a free energy value of 3.8 kcal/mol below the reagents. All these data account for the mechanistic proposal initially envisaged and the experimental results obtained in the laboratory. Hydrogenation of **13** to yield hydride **15** has been computationally described in our group already.[75] Again, all these steps were also calculated for the reaction catalysed by **15**, and the energies turned out to be much higher, in accordance with the slower rates experimentally observed.

---

[74] This KIE was obtained in the reaction Ph_2SiH_2 + Et_2ND (due to the availability of deuterated reagents). No KIE was detected when using Ph_2SiD_2 (k_H/k_D = 0.88).
[75] O. Rivada-Wheelaghan, M. Roselló-Merino, M. A. Ortuño, P. Vidossich, E. Gutiérrez-Puebla, A. Lledós, S. Conejero, *Inorg. Chem.,* **2014**, *53*, 4257-4268.
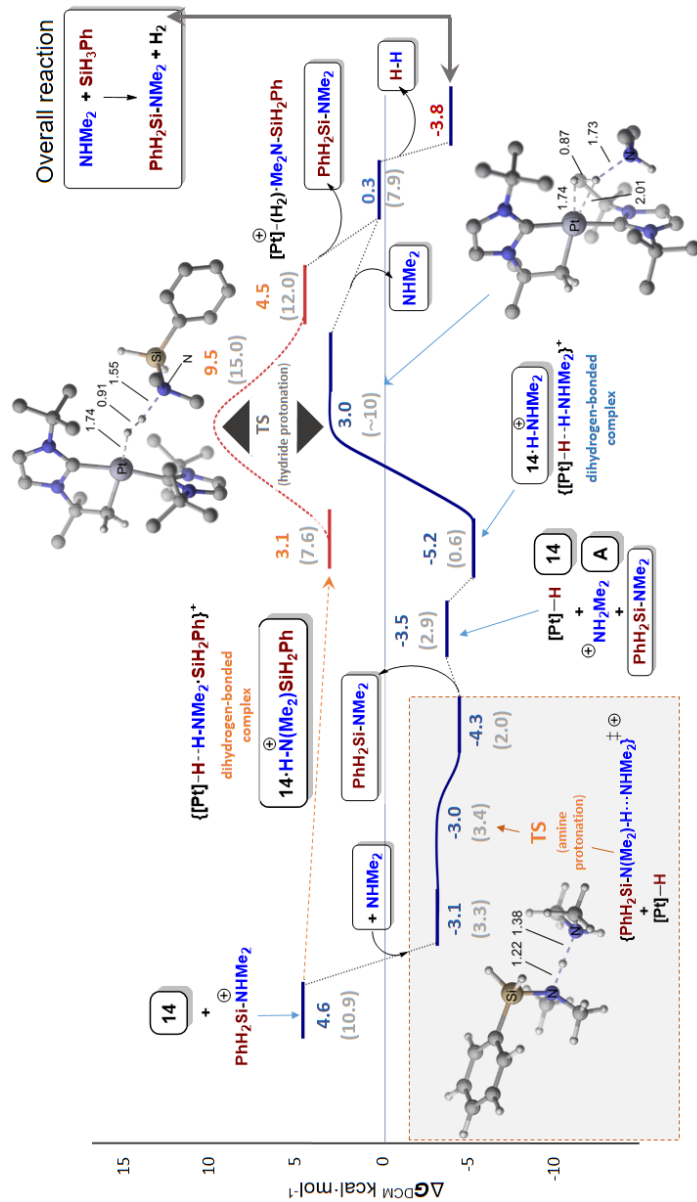
Figure 24. Calculated Free Energy profile of the protonation reaction of **14**. Blue (solid) trace corresponds to NMe₂H protonation by PhH₂SiH(NMe₂H)⁺ and formation of the dihydrogen bonded species **14·**H−NMe₂H⁺. Red (dashed) trace corresponds to the dihydrogen bonded species **14·**H−NMe₂(SiH₂Ph)⁺. Data in parentheses correspond to the pathway catalyzed by system **15**.

[371]

As a final comment, it is necessary to mention that the catalytic process studied in this section is highly complex due to the multiple phenomena that can take place simultaneously, since complex **13** transforms into **15** during the reaction as a consequence of the newly formed H_2. Moreover, both complexes can efficiently catalyse the dehydrocoupling reaction, making the analysis even more difficult. For these reasons, kinetic data such as the KIE values or the partial orders must be cautiously taken. For instance, the partial order of 2.2 in catalyst is usually related to the involvement of 2 metal atoms in the reaction. However, neither experimental nor computational studies seem to lead in this direction. Instead, this value must be associated with a different phenomenon, such as the progressive change in the nature of the active catalyst from **13** to **15** (Scheme 21A).[76] In light of these results, and taking into consideration the complexity of this process, a plausible catalytic cycle can be proposed (Scheme 21B):

---

[76] T. Rosner, J. L. Bars, A. Pfaltz, D. G. Blackmond, *J. Am. Chem. Soc.,* **2001**, *123*, 1848-1855. In this example, the role of an inactive Pd species in the partial order determination is described.
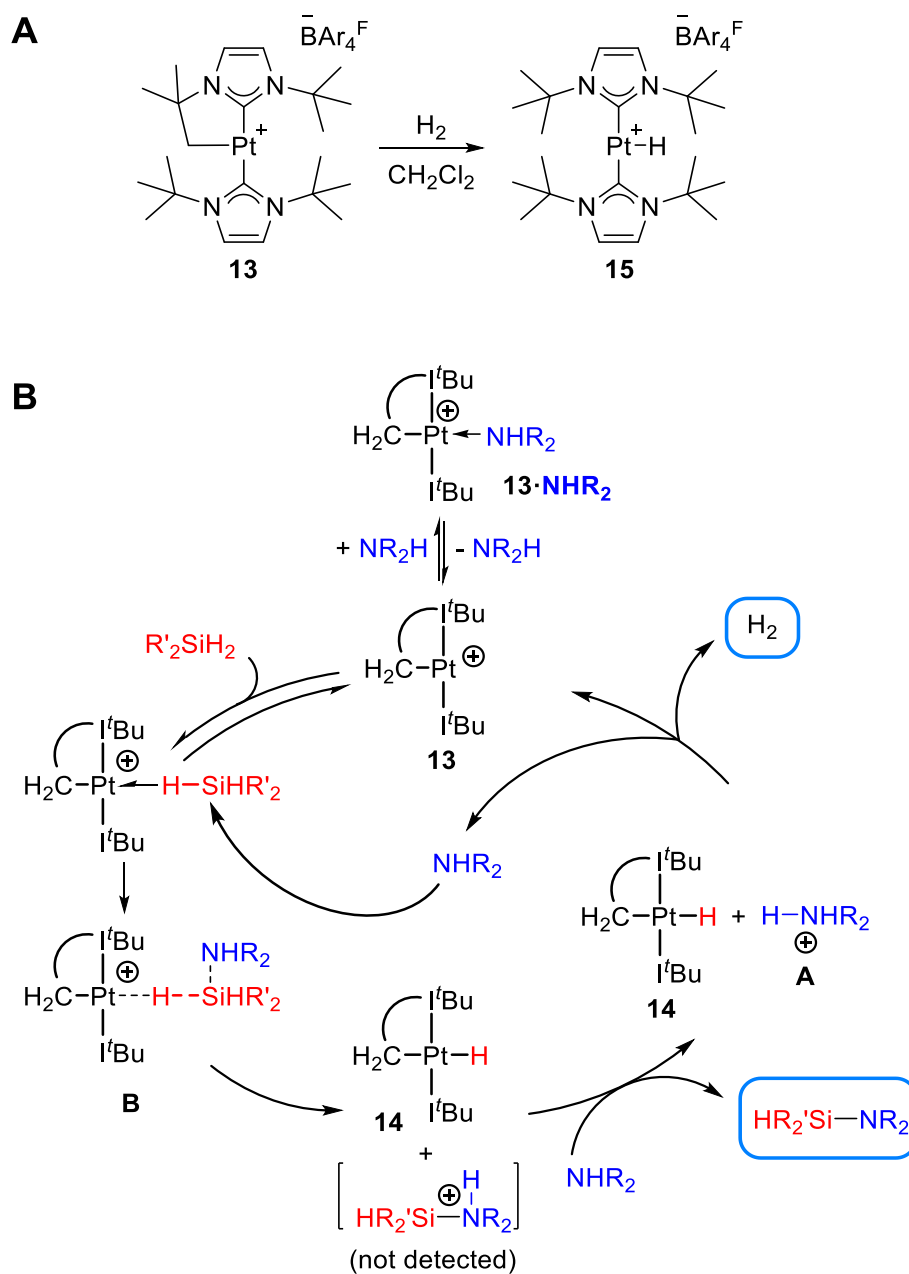
Scheme 21. Proposed overall catalytic cycle of the Si–N dehydrogenative coupling catalyzed by complex **13**.

[373]

References

[1] M. C. Lipke, A. L. Liberman-Martin, T. D. Tilley, *Angew. Chem. Int. Ed.,* **2017**, *56*, 2260-2294.

[2] D. H. Binh, M. Milovanović, J. Puertes-Mico, M. Hamdaoui, S. D. Zarić, J-P. Djukic, *Chem. Eur. J.,* **2017**, *23*, 17058-17069.

[3] V. Y. Lee, A. Sekiguchi in *Organosilicon Compounds*, **2017**, Academic Press. *Chapter 5: Silicon-centered cations*, 197-230.

[4] P. D. Bartlett, F. E. Condon, A. Schneider, *J. Am. Chem. Soc.,* **1944**, *66*, 1531-1539.

[5] H. F. T. Klare, K. Bergander, M. Oestreich, *Angew. Chem. Int. Ed.,* **2009**, *48*, 9077-9079.

[6] K. Müther, M. Oestreich, *Chem. Commun.,* **2011**, *47*, 334-336.

[7] M. Reissmann, A. Schafer, S. Jung, T. Müller, *Organometallics*, **2013**, *32*, 6736-6744.

[8] M. F. S. Valverde, E. Theuergarten, T. Bannenberg, M. Freytag, P. G. Jones, M. Tamm, *Dalton Trans.,* **2015**, *44*, 9400-9408.

[9] N. von Wolff, G. Lefèvre, J.-C. Berthet, P. Thuéry, T. Cantat, *ACS Catal.,* **2016**, *6*, 4526-4535.

[10] A. Schäfer, W. Saak, D. Haase, T. Müller, *Angew. Chem. Int. Ed.,* **2012**, *51*, 2981-2984.

[11] L. Omann, Z-W. Qu, E. Irran, H. F. T. Klare, S. Grimme, M. Oestreich, *Angew. Chem. Int. Ed.,* **2018**, *57*, 8301-8305.

[12] S. Cummings, H. P. Hratchian, C. A. Reed, *Angew. Chem. Int. Ed.,* **2016**, *55*, 1382-1386.

[13] C. A. Reed, *Acc. Chem. Res.,* **2013**, *46*, 2567-2575.

[14] M. Brookhart, B. Grant, A. F. Volpe Jr., *Organometallics*, **1992**, *11*, 3920-3922.

[15] E. Lukevics, M. Dzintara, *J. Organomet. Chem.,* **1985**, *295*, 265-315.

[16] X-L. Luo, R. H. Crabtree, *J. Am. Chem. Soc.,* **1989**, *111*, 2527-2535.

[17] J. M. Blackwell, K. L. Foster, V. H. Beck, W. E. Piers, *J. Org. Chem.,* **1999**, *64*, 4887-4892.

[18] a) B-H. Kim, M-S. Cho, H-G. Woo, *Synlett*, **2004**, *5*, 761-772; b) D. J. Harrison, D. R. Edwards, R. McDonald, L. Rosenberg, *Dalton Trans.,* **2008**, 3401-3411; c) E. M. Leitao, T. Jurca, I. Manners, *Nat. Chem.,* **2013**, *5*, 817-829; d) R. L. Melen, *Chem. Soc. Rev.,* **2016**, *45*, 775-788.

[19] a) V. Gevorgyan, J-X. Liu, M. Rubin, S. Benson, Y. Yamamoto, *Tetrahedron Lett.,* **1999**, *40*, 8919-8922; b) V. Gevorgyan, M. Rubin, S. Benson, J-X. Liu, Y. Yamamoto, *J. Org. Chem.,* **2000**, *65*, 6179-6186.

[20] J. Yang, P. S. White, M. Brookhart, *J. Am. Chem. Soc.,* **2008**, *130*, 17509-17518.

[21] T. Robert, M. Oestreich, *Angew. Chem. Int. Ed.,* **2013**, *52*, 5216-5218.

[22] a) H. Koinuma, F. Kawakami, H. Kato, H. Hirai, *J. Chem. Soc. Chem. Commun.,* **1981**, 213-214; b) G. Süss-Fink, J. Reiner, *J. Organomet. Chem.,* **1981**, *221*, C36-C38.

[23] Some recent reports include the following: a) F. J. Fernández-Álvarez, A. M. Aitani, L. A. Oro, *Catal. Sci. Technol.,* **2014**, *4*, 611-624; b) C. Chauvier, T. Cantat, *ACS Catal.,* **2017**, *7*, 2107-2115; c) F. J. Fernández-Álvarez, L. A. Oro, *ChemCatChem*, **2018**, *10*, 4783-4796

[24] P. Deglmann, E. Ember, P. Hofmann, S. Pitter, O. Walter, *Chem. Eur. J.,* **2007**, *13*, 2864-2879.

[25] K. Motokura, D. Kashiwame, N. Takahashi, A. Miyaji, T. Baba, *Chem. Eur. J.,* **2013**, *19*, 10030-10037.

[26] L. Zhang, J. Cheng, Z. Hou, *Chem. Commun.,* **2013**, *49*, 4782-4784.

[27] S. Itagaki, K. Yamaguchi, N. Mizuno, *J. Mol. Catal. A: Chem.,* **2013**, *366*, 347-352.

[28] L. González-Sebastián, M. Flores-Alamo, J. J. García, *Organometallics*, **2013**, *32*, 7186-7194.

[29] C. Chauvier, P. Thuéry, T. Cantat, *Angew. Chem. Int. Ed.,* **2016**, *55*, 14096-14100.

[30] J. Takaya, N. Iwasawa, *J. Am. Chem. Soc.,* **2017**, *139*, 6074-6077.

[31] A. Julián, J. Guzmán, E. A. Jaseer, F. J. Fernández-Álvarez, R. Royo, V. Polo, P. García-Orduña, F. J. Lahoz, L. A. Oro, *Chem. Eur. J.,* **2017**, *23*, 11898-11907.

[32] a) A. Jansen, H. Görls, S. Pitter, *Organometallics*, **2000**, *19*, 135-138; b) M. L. Scheuermann, S. P. Semproni, I. Pappas, P. J. Chirik, *Inorg. Chem.,* **2014**, *53*, 9463-9465.

[33] L. E. Gusel'nikov, N. S. Nametkin, *Chem. Rev.,* **1979**, *79*, 529-577.

[34] I. Manners, *Angew. Chem. Int. Ed.,* **1996**, *35*, 1602-1621.

[35] a) Information about disilenes: R. West, *Angew. Chem. Int. Ed.,* **1987**, *26*, 1201-1211; b) Information about iminoboranes: P. Paetzold, *Adv. Inorg. Chem.,* **1987**, *31*, 123-170.

[36] A. Soum in *Silicon-containing Polymers. The Science and Technology of their Synthesis and Applications*, **2000**, Springer Netherlands. *Chapter 11: Polysilazanes*, 323-349.

[37] M. Birot, J-P. Pillot, J. Dunoguès, *Chem. Rev.,* **1995**, *95*, 1443-1477.

[38] This family of polysilazanes has been commercialized by Merck KGaA under the name Durazane® . For more information, see: https://www.merckgroup.com/en/brands/pm/durazane.html.

[39] R. Fessenden, J. S. Fessenden, *Chem. Rev.,* **1961**, *61*, 361-388.

[40] S. Austin, A. Glowacki. Hydrochloric acid. *Ullmann's Encyclopedia of Industrial Chemistry*, **2000**, doi: 10.1002/14356007.a13_283.

[41] a) R. Noyori, T. Ohkuma, *Angew. Chem. Int. Ed.,* **2001**, *40*, 40-73; b) S. Werkmeister, K. Junge, M. Beller, *Org. Process Res. Dev.,* **2014**, *18,* 289-302; c) G. A. Filonenko, R. V. Putten, E. J. M. Hensen, E. A. Pidko, *Chem. Soc. Rev.,* **2018**, *47*, 1459-1483.

[42] Metal-free catalytic systems have also been described in the literature (see reference 18d).

[43] F. Buch, S. Harder, *Organometallics*, **2007**, *26*, 5132-5135.

[44] J. F. Dunne, S. R. Neal, J. Engelkemier, A. Ellern, A. D. Sadow, *J. Am. Chem. Soc.,* **2011**, *133*, 16782-16785.

[376]

[45] R = Ph, Et or C_6H_{13}. dppm stands for bis(diphenylphosphino)methane.

[46] W-D. Wang, R. Eisenberg, *Organometallics*, **1991**, *10*, 2222-2227.

[47] S. Itagaki, K. Kamata, K. Yamaguchi, N. Mizuno, *Chem. Commun.,* **2012**, *48*, 9269-9271.

[48] C. D. F. Königs, M. F. Müller, N. Aiguabella, H. F. T. Klare, M. Oestreich, *Chem. Commun.,* **2013**, *49*, 1506-1508.

[49] W. Xie, H. Hu, C. Cui, *Angew. Chem. Int. Ed.,* **2012**, *51*, 11141-11144.

[50] A. E. Nako, W. Chen, A. J. P. White, M. R. Crimmin, *Organometallics*, **2015**, *34*, 4369-4375.

[51] M. P. Cibuzar, R. Waterman, *Organometallics*, **2018**, *37*, 4395-4401.

[52] M. S. Hill, D. J. Liptrot, D. J. MacDougall, M. F. Mahon, T. P. Robinson, *Chem. Sci.,* **2013**, *4*, 4212-4222.

[53] C. Bellini, J-F. Carpentier, S. Tobisch, Y. Sarazin, *Angew. Chem. Int. Ed.,* **2015**, *54*, 7679-7683.

[54] a) C. Bellini, V. Dorcet, J-F. Carpentier, S. Tobisch, Y. Sarazin, *Chem. Eur. J.,* **2016**, *22*, 4564-4583; b) C. Bellini, T. Roisnel, J-F. Carpentier, S. Tobisch, Y. Sarazin, *Chem. Eur. J.,* **2016**, *22*, 15733-15744.

[55] J. Yang, P. S. White, C. K. Schauer, M. Brookhart, *Angew. Chem. Int. Ed.,* **2008**, *47*, 4141-4143.

[56] S. Park, D. Bézier, M. Brookhart, *J. Am. Chem. Soc.,* **2012**, *134*, 11404-11407.

[57] The conversion was measured by ^{1}H NMR integration of the silane and silyl formate peaks.

[58] Aromatic silanes like $PhSiH_3$ were also studied, although several unidentified species were observed rather than silyl formate derivatives.

[59] J. Zhu, Z. Lin, T. B. Marder, *Inorg. Chem.,* **2005**, *44*, 9384-9390.

[60] M. Roselló-Merino, J. López-Serrano, S. Conejero, *J. Am. Chem. Soc.,* **2013**, *135*, 10910-10913.

[61] M. Roselló-Merino, R. J. Rama, J. Díez, S. Conejero, *Chem. Commun.,* **2016**, *52*, 8389-8392.

[62] J. X. Wang, A. K. Dash, J. C. Berthet, M. Ephritikhine, M. S. Eisen, *J. Organomet. Chem.,* **2000**, *610*, 49-57.

[63] S. Anga, Y. Sarazin, J-F. Carpentier, T. K. Panda, *ChemCatChem,* **2016**, *8*, 1373-1378.

[64] http://www.manonthemoontech.com/x102-gas-evolution.html.

[65] *"Síntesis de complejos coordinativamente insaturados de Pt(II) estabilizados por ligandos carbeno N-heterocíclicos. Activación y funcionalización de enlaces C−H"*. O. Rivada-Wheelaghan. PhD Thesis, **2013**.

[66] M. A. Ortuño, S. Conejero, A. Lledós, *Beilstein J. Org. Chem.,* **2013**, *9*, 1352-1382.

[67] The initial increase of pressure above 100% in the plot on the left is attributed to the partial evaporation of the low-boiling point solvent (CH_2Cl_2) due to the exothermic nature of the reaction. When the process is slower (plot on the right) the heat is gradually released, avoiding solvent evaporation.

[68] Calculations were carried out at the M06/6-31g(d,p)/SDD level of theory. SMD (Dichloromethane) continuum was used to model the solvent.

[69] No decomposition was observed in any case, discarding the formation of solid platinum or any type of colloid or nanoparticles.

[70] The NH_2 protons of the ammonium cation are only visible below -30 °C.

[71] Calculations were carried out at the PBE0-D3/6-31g(d,p)/SDD level of theory. SMD (Dichloromethane) continuum was used to model the solvent.

[72] Calculations discard mechanisms involving Si−H oxidative addition.

[73] M. Besora, A. Lledós, F. Maseras, *Chem. Soc. Rev.,* **2009**, *38*, 957-966.

[74] This KIE was obtained in the reaction Ph_2SiH_2 + Et_2ND (due to the availability of deuterated reagents). No KIE was detected when using Ph_2SiD_2 (k_H/k_D = 0.88).

[75] O. Rivada-Wheelaghan, M. Roselló-Merino, M. A. Ortuño, P. Vidossich, E. Gutiérrez-Puebla, A. Lledós, S. Conejero, *Inorg. Chem.,* **2014**, *53*, 4257-4268.

[76] T. Rosner, J. L. Bars, A. Pfaltz, D. G. Blackmond, *J. Am. Chem. Soc.,* **2001**, *123*, 1848-1855. In this example, the role of an inactive Pd species in the partial order determination is described.

[378]

Experimental Part

Experimental Part

General Methods

All manipulations were carried out using standard Schlenk and glovebox techniques, under an atmosphere of argon and of high purity nitrogen, respectively. All solvents were dried and degassed prior to use. *n*-pentane, toluene and tetrahydrofuran were distilled under nitrogen over sodium and stored under Na/K alloy. Dichloromethane was distilled under nitrogen over calcium hydride and stored under 3 Å activated molecular sieves. Hexamethyldisiloxane was degassed (freeze-pump-thaw) and stored under 3 Å activated molecular sieves.

Benzene-d_6, toluene-d_8 and tetrahydrofuran-d_8 were distilled under argon over sodium/benzophenone and stored under 3 Å activated molecular sieves. Dichloromethane-d_2 was heated under reflux over calcium hydride for several hours, distilled under argon and stored under 3 Å activated molecular sieves.

Solution NMR spectra were acquired on Bruker AMX-300, DRX-400 and DRX-500 spectrometers at 298 K unless otherwise specified. ^{1}H and ^{13}C chemical shifts were referenced to the residual solvent peak. ^{31}P NMR spectra were referenced to an external 85% solution of H_3PO_4. ^{19}F NMR spectra were referenced to an external standard of $CFCl_3$. ^{11}B NMR spectra were referenced to an external standard of $BF_3 \cdot Et_2O$. ^{29}Si chemical shifts were referenced to an external standard of $Si(CH_3)_4$. Spectral assignments were made by means of 1D and 2D NMR experiments (^{1}H, ^{13}C, ^{13}C{^{1}H}, COSY, NOESY, HSQC and HMBC).

Elemental analysis was carried out with a LECO TruSpec CHN elementary analyser.

Infra-red spectra (Nujol on NaCl plates) were measured on a Bruker Vector 22 instrument.

[380]

Mass spectra were recorded on a Bruker Esquire 6000 instrument with an ESI ion source and ion trap analyser. HR-MS spectra were recorded on a QExactive mass spectrometer with an APCI (Atmospheric Pressure Chemical Ionization) source in positive mode at the CITIUS central services of the University of Seville.

Flash column chromatography was carried out on Merck Silica Gel 60 (0.063-0.200 mm), and the process was monitored by using TLC pre-coated silica gel plates (Merck Silica Gel 60 F254). Spots were visualized by means of UV light (254 nm) or using a solution of potassium permanganate or cerium molybdate (Hanessian's stain).

Tris(pentaflorophenyl)borane was purchased from TCI and sublimed at 100 °C under static vacuum. Bis(catecholato)diboron and bis(pinacolato)diboron were purchased from Sigma-Aldrich and sublimed at 100 °C (former) and 70 °C (latter) under dynamic vacuum. Triethylsilane, dimethylphenylsilane, diphenylmethylsilane, diethylsilane and n-butylsilane were distilled from CaH_2 and stored under 3 Å activated molecular sieves. All other commercially available reagents were purchased from Sigma-Aldrich, TCI or Alfa Aesar and used as received.

Carbon dioxide, carbon monoxide and ^{13}C-labeled carbon dioxide (99.05% [13]C) were supplied by Air Liquide ([12]CO_2 and CO) and Euriso-top (^{13}C), and used as received.

[381]

Experimental Part

Compounds **2**, **4**, **6**,[1] **13**,[2] **24**, **25**[3] **15**, **33**, **34** and **39**[4] were prepared according to procedures previously described by our group. *Tert*-butylimidazol,[5] [H(OEt$_2$)][BAr$_4^F$][6], NaBAr$_4^F$[7] and complex [PtMe$_2$(COD)],[8] were prepared according to procedures previously described in the literature.

[1] N. Curado, C. Maya, J. López-Serrano, A. Rodríguez, *Chem. Commun.,* **2014**, *50*, 15718-15721.

[2] O. Rivada-Wheelaghan, B. Donnadieu, C. Maya, S. Conejero, *Chem. Eur. J.,* **2010**, *16*, 10323-10326.

[3] O. Rivada-Wheelaghan, M. A. Ortuño, J. Díez, A. Lledós, S. Conejero, *Angew. Chem. Int. Ed.,* **2012**, *51*, 3936-3939.

[4] O. Rivada-Wheelaghan, M. Rosselló-Merino, M. A. Ortuño, P. Vidossich, E. Gutiérrez-Puebla, A. Lledós, S. Conejero, *Inorg. Chem.,* **2014**, *53*, 4257-4268.

[5] R. E. Cowley, R. P. Bontchev, E. N. Duesler, J. M. Smith, *Inorg. Chem.,* **2006**, *45*, 9771-9779.

[6] M. Brookhart, B. Grant, A. F. Volpe. Jr, *Organometallics*, **1992**, *11*, 3920-3922.

[7] N. A. Yakelis, R. G. Bergman, *Organometallics*, **2005**, *24*, 3579-3581.

Given that the BAr$_4^F$ anion is present in several compounds throughout this thesis, its NMR signals are the following: **^{1}H-NMR (400 MHz, CD$_2$Cl$_2$, 298 K): δ** 7.58 (bs, 4 H, C*H*$_{para}$), 7.74 (bs, 8 H, C*H*$_{ortho}$) ppm. **^{13}C-NMR (100 MHz, CD$_2$Cl$_2$, 298 K): δ** 117.9 (bs, *C*$_{para}$), 124.9 (q, $^1J_{C-F}$ = 272 Hz, *C*F$_3$), 129.2 (br q, $^2J_{C-F}$ = 31 Hz, *C*$_{meta}$), 135.2 (bs, *C*$_{ortho}$), 162.2 (q, $^1J_{C-B}$ = 50 Hz, *C*$_{ipso}$) ppm.

[8] R. Bassan, K. H. Bryars, L. Judd, A. W. G. Platt, P. G. Pringle, *Inorg. Chim. Acta*, **1986**, *121*, L41-L42.

Experimental Part for Chapter 1

Synthesis of PBP-stabilized Ni(II) complexes

Complex [(^{tBu}PBP)Ni−CO][BAr₄^F] (3)

Complex [(^{tBu}PBP)Ni−CO][BAr$_4$^{F}] (3)
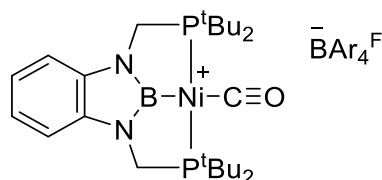
Synthesis

In the glovebox, complex **2** (34 mg, 59.4 μmol) and NaBAr$_4$^{F} (58 mg, 65.3 μmol, 1.1 eq) were added to a J. Young NMR tube. CD$_2$Cl$_2$ (0.5 mL) was added to the mixture of solids, and CO (1.5 bar) was charged to the tube outside the glovebox, after which the tube was vigorously shaken. After 5 min at room temperature, the formation of the carbonyl compound was confirmed by NMR. At this point, the resulting yellow suspension was transferred to a Schlenk flask. Dichloromethane (2 x 1 mL) was added to the tube in order to recover the material left in the cannula. The suspension in the Schlenk was filtered via cannula to a J. Young flask, and the resulting yellow-green solution was evaporated in vacuo, affording a yellow solid (82 mg, 57.8 μmol, 99% yield). X-Ray quality yellow crystals can be grown by slow diffusion of hexamethyldisiloxane in dichloromethane (10:1).

Spectroscopic and analytical data

Yellow solid.

Molecular weight: 1383.31 g/mol.

^{1}H-NMR (400 MHz, CD$_2$Cl$_2$, 298 K) δ 1.43 (m, 36 H, ^{t}Bu), 3.70 (vt, 4 H, $^2J_{H\text{-}P}$ = 2 Hz, C*H*$_2$), 7.17 (m, 4 H, ligand aromatic C*H*), 7.56 (s, 4 H, BAr$_4$^{F} aromatic *p*-C*H*), 7.73 (s, 8 H, BAr$_4$^{F} aromatic *o*-C*H*) ppm.

[383]

13C{1H}-NMR (100 MHz, CD2Cl2, 298 K) δ 29.7 ((*C*H)3C), 37.7 (t, $^1J_{\text{C-P}}$ = 7.6 Hz, (CH)3*C*), 40.4 (t, $^1J_{\text{C-P}}$ = 19.7 Hz, *C*H2), 111.1 (ligand aromatic *C*H), 121.3 (ligand aromatic *C*H), 137.5 (t, $^3J_{\text{C-P}}$ = 8.4 Hz, ligand aromatic *C*q), 193.6 (*C*O) ppm.

31P{1H}-NMR (161 MHz, CD2Cl2, 298 K) δ 114.5 (s) ppm

11B{1H}-NMR (128 MHz, CD2Cl2, 298 K) δ 38.1 (bs, boryl), -6.6 (s, BAr4F) ppm.
Elem. Anal. Calcd. for $C_{57}H_{56}B_2F_{24}N_2NiOP_2$**:** C, 49.49; H, 4.08; N, 2.03. **Found:** C, 49.27; H, 4.45; N, 1.91.

IR ν(Nujol) 2049 (ν_{CO}) cm^{-1}.

Complex (tBuPBP)Ni−OC(H)O·B(C6F5)3 (8)
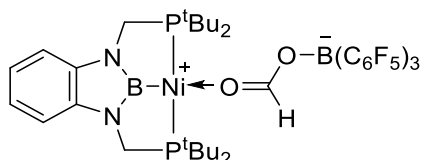
Synthesis

A J. Young valve NMR tube containing a solution of **6** (26 mg, 0.053 mmol) in C6D6 (0.5 mL) was charged with CO2 (2 bar). The NMR tube was shaken at r.t., and instantaneous CO2 insertion was confirmed by 31P and 1H NMR analysis. In the glovebox, a solution of B(C6F5)3 (30 mg, 0.058 mmol, 1.1 eq) in C6D6 (0.2 mL) was added to the tube. Instantaneous formation of **8** was confirmed again by NMR. The mixture was filtered via cannula to a previously flame-dried Schlenk flask. The solvent was removed under vacuum, and pentane (2 mL) was added to remove the remaining benzene; the mixture was vigorously stirred until a powdery suspension was observed, after which the mixture was dried in vacuo. Then, the solid was washed with pentane (2 x 2 mL) at -20^{0}C and the solid was

dried under vacuum, affording complex **8** as a yellowish solid (48.9 mg, 0.046 mmol, 88%).

Spectroscopic and analytical data

Ochre solid.

Molecular weight: 1049.08 g/mol.

¹H-NMR (400 MHz, C₆D₆, 298 K) δ 0.99 (vt, 36 H, $^3J_{\text{H-P}}$= 6.8 Hz, ᵗBu), 3.31 (vt, 4 H, $^2J_{\text{H-P}}$ = 2.1 Hz, C*H*₂), 6.81 (dd, 2 H, $^3J_{\text{H-H}}$ = 5.7 Hz, $^4J_{\text{H-H}}$ = 3.1 Hz, arom C*H*), 7.09 (dd, 2 H, $^3J_{\text{H-H}}$ = 5.7 Hz, $^4J_{\text{H-H}}$ = 3.1 Hz, arom C*H*), 8.45 ppm (s, 1 H, *H*COO) ppm.

¹³C{¹H}-NMR (100 MHz, C₆D₆, 298 K) δ 29.1 (t, $^2J_{\text{C-P}}$ = 2.5 Hz, (*C*H)₃C), 35.0 (t, $^1J_{\text{C-P}}$ = 5.4 Hz, (CH)₃*C*), 39.0 (t, $^1J_{\text{C-P}}$ = 19.2 Hz, *C*H₂), 109.1 (arom *C*H), 119.6 (arom *C*H), 137.1 (dm, $^1J_{\text{C-F}}$ ~ 249 Hz, *C*₆F₅), 138.6 (t, $^3J_{\text{C-P}}$ = 7.3 Hz, arom *C*q), 140.0 (dm, $^1J_{\text{C-F}}$ ~ 249 Hz, *C*₆F₅), 148.5 (dm, $^1J_{\text{C-F}}$ ~ 243 Hz, *C*₆F₅), 173.2 (H*C*OO) ppm**.** ¹³C resonances of C$_{\text{ipso}}$ of C₆F₅ rings were not detected.

³¹P{¹H}-NMR (161 MHz, C₆D₆, 298 K) δ 87.7 (s, *P*ᵗBu₂) ppm

¹¹B{¹H}-NMR (128 MHz, C₆D₆, 298 K) δ -1.4 (bs, *B*(C₆F₅)₃), 33.5 (bs, boryl) ppm.

¹⁹F{¹H}-NMR (376 MHz, C₆D₆, 298 K) δ -164.5 (d, $^3J_{\text{F-F}}$ = 24 Hz, ortho C-*F*), -157.8 (t, $^3J_{\text{F-F}}$ = 21 Hz, para C-*F*), -132.7 (td, $^3J_{\text{F-F}}$ = 23.3 Hz, $^4J_{\text{F-F}}$ = 5.4 Hz, meta C-*F*) ppm.

IR ν(Nujol) 1643 (ν$_{\text{C=O}}$) cm⁻¹.

Elem. Anal. Calcd. for C₄₃H₄₅B₂F₁₅N₂NiO₂P₂: C, 49.23; H, 4.32; N, 2.67. **Found**: C, 49.14; H, 4.18; N, 2.85.

[385]

Experimental evidences of the formation of [(^{tBu}PBP)Ni][HB(C$_6$F$_5$)$_3$] (9)

       Complex **9** was identified from the solid that precipitates in benzene after CO$_2$ is used up in reactions with **8** and silanes. A number of solubility studies led to the conclusion that ethereal solvents are needed in some extent to dissolve **9**. For this reason, some coordination to the borane is always observed in the ^{11}B NMR spectra. Nonetheless, the rest of NMR experiments are consistent with the formation of **9**.

^{1}H{^{11}B}-NMR (400 MHz, C$_7$D$_8$, 298 K) δ 0.96 (vt, 36 H, $^3J_{H\text{-}P}$= 7 Hz, ^{t}Bu), 3.33 (s, 4 H, C$\boldsymbol{H_2}$), 4.38 (bs, 1H, B$\boldsymbol{H}$), 6.80 (dd, 2 H, $^3J_{H\text{-}H}$ = 5.6 Hz, $^4J_{H\text{-}H}$ = 3.1 Hz, arom C$\boldsymbol{H}$), 7.09 (dd, 2 H, $^3J_{H\text{-}H}$ = 5.6 Hz, $^4J_{H\text{-}H}$ = 3.2 Hz, arom C$\boldsymbol{H}$).

^{13}C{^{1}H}-NMR* (100 MHz, C$_7$D$_8$, 298 K) δ 28.0 ((**C**H$_3$)$_3$C), 32.8 ((CH$_3$)$_3$**C**), 37.4 (**C**H$_2$), 107.5 (arom **C**H), 118.9 (arom **C**H), 127.6 (arom **C**$_q$)

^{31}P{^{1}H}-NMR (161 MHz, C$_7$D$_8$, 298 K) δ 82.2 (s, **P**^{t}Bu$_2$) ppm.

^{11}B-NMR (128 MHz, C$_7$D$_8$, 298 K) δ -24.7 (d, $^1J_{B\text{-}H}$ = 93 Hz), 28.3 (bs, boryl) ppm.

*^{13}C NMR data has been obtained via ^{1}H-^{13}C heteronuclear correlations, therefore the C$_6$F$_5$ fragments could not be assigned.

General procedure for a catalytic experiment using a 0.05 mol % catalyst loading

       In a glovebox, a J. Young valve NMR tube was charged with a solution of **8** (1 mg, 0.95 µmol) in C$_6$D$_6$ (100 µL), after which silane (1.91 mmol) was added with a microsyringe. Outside the glovebox, CO$_2$ (4 bar) was charged and the tube was heated up to 70 °C in an oil bath. Conversion to bis(silyl)acetal was obtained from the integration values in the ^{1}H NMR spectra by using a relaxation delay

[386]

(D1) of 10 seconds in the acquisition process. A similar procedure was followed for the experiments with ^{13}C-labeled CO_2.

*Stoichiometric reaction between Et₃SiH and **8***

In the glovebox, a solution of **8** (20 mg, 0.019 mmol) in C_6D_6 (0.3 mL) and a solution of Et_3SiH (3 μL, 0.019 mmol) in C_6D_6 (0.1 mL) were added to a J. Young valve NMR tube by means of microsyringes. Outside the glovebox, the NMR tube was charged with CO_2 (4 bar) and the temperature was gradually increased in the NMR spectrometer while the process was being monitored by ^{1}H NMR.

Isolation of acetal derived from Et₃SiH (Et₃SiOCH₂OSiEt3) and over-reduction to methane

The reaction mixture obtained after the catalysis was packed onto a silica column (ø = 1.2 cm, 40 g) in pentane, which was flushed with pentane to give 3,3,7,7-tetraethyl-3,7-disila-4,6-dioxanonane (R_f=0.64) as a colorless liquid after removing the solvent in vacuo.

^{1}H-NMR (400 MHz, C₆D₆, 298 K) δ 0.63 (q, 12 H, $^3J_{H\text{-}H}$= 8 Hz, CH₃C**H**₂), 1.01 (t, 18H, $^3J_{H\text{-}H}$ = 8 Hz, C**H**₃CH₂), 5.03 (s, 2 H, OC**H**₂O) ppm.
^{13}C{^{1}H}-NMR (100 MHz, C₆D₆, 298 K) δ 5.3 (CH₃**C**H₂), 7.0 (**C**H₃CH₂), 84.6 (O**C**H₂O) ppm.

^{29}Si{^{1}H}-NMR (79 MHz, C₆D₆, 298 K) δ 18.3 (s, **Si**OCH₂O**Si**) ppm.

After isolating 3,3,7,7-tetraethyl-3,7-disila-4,6-dioxanonane, conversion to methane was achieved by adding $B(C_6F_5)_3$ (5 mg) and Et_3SiH (250 μL) to the NMR tube that contains it. The process was monitored by multinuclear (^{1}H, ^{13}C, [29]Si) NMR.

[387]

Experimental Part for Chapter 2

Synthesis of PBP-stabilized Ni (II) complexes

(tBuPBP)Ni−BCat (11)
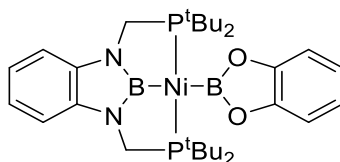
Synthesis

In the glovebox, a solution of complex **4** (31 mg, 0.061 mmol) in dry tetrahydrofuran (0.5 mL) was added to a vial that contains B_2cat_2 (16 mg, 0.067 mmol, 1.1 eq). The resulting suspension was manually stirred until a clear yellow solution was observed (*i.e.* until both reagents are completely dissolved). At this point, hexamethyldisiloxane was slowly added with manual stirring until a cloudy solution/precipitate in suspension was formed. Then, the minimum amount of tetrahydrofuran (a few drops) was added so as to redissolve the sample. The vial was closed and placed into the freezer of the glovebox. After 2-3 days, yellow crystals of complex **11** were formed. By the time this thesis is being written, isolation of the crystals to determine a yield and complete the characterization is ongoing.

Spectroscopic and analytical data

Yellow crystals.

Molecular weight: 610.99 g/mol.

1H-NMR (400 MHz, d^8-THF, 298 K) δ 1.30 (vt, 36H, $^3J_{H-P}$ = 6.5 Hz, *tBu*), 4.08 (s, 4H, C*H*$_2$), 6.80, 6.92, 7.03 and 7.18 (m, 8 H, arom C*H*) ppm.

[388]

^{13}C{^{1}H}-NMR (100 MHz, d^8-THF, 298 K) δ 30.2 ((**C**H)$_3$C), 36.4 (t, $^1J_{C-P}$ = 7.5 Hz, (CH)$_3$**C**), 43.7 (t, $^1J_{C-P}$ = 17.3 Hz, **C**H$_2$), 109.7, 111.1, 118.6, 120.8 (aromatic **C**H), 140.2 (t, $^3J_{C-P}$ = 7.3 Hz, ligand **C**$_q$), 151.6 (BCat **C**$_q$) ppm.

^{31}P{^{1}H}-NMR (161 MHz, d^8-THF, 298 K) δ 114.9 (s, **P**^{t}Bu$_2$) ppm.

^{11}B-NMR (128 MHz d^8-THF, 298 K) δ 47.24 and 56.2 (bs, **boryl**) ppm.

(^{tBu}PBP)Ni−Ph (12)
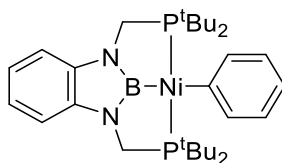
In the glovebox, a previously flame-dried J. Young flask was charged with complex **2** (100 mg, 0.175 mmol) and a stirrer bar. Toluene (12 mL) was added under argon, after which a yellow solution was obtained. Then, a solution of PhMgBr (0.23 mL, 3 M in Et$_2$O, 0.7 mmol) was added, and the resulting orange solution was stirred at 80 ^{0}C for 22 h. The solvent was removed under reduced pressure, and the dark solid obtained was extracted with pentane (20 mL) and filtered via cannula. The resulting yellow solution was evaporated under vacuum to obtain a yellow solid which was washed with hexamethyldisiloxane (3 mL) at -40 ^{0}C, affording a bright yellow solid (51 mg, 0.090 mmol, 51% yield). Yellow crystals suitable for X-Ray diffraction analysis were obtained by cooling at -25 ^{0}C a concentrated solution in toluene.

Spectroscopic and analytical data

Yellow crystals or solid.

Molecular weight: 569.19 g/mol.

[389]

Experimental Part

¹H-NMR (400 MHz, C₆D₆, 298 K) δ 1.13 (vt, 36 H, $^3J_{HP}$= 6.2 Hz, ***t**Bu*), 3.70 (m, 4 H, C**H**₂), 6.98 (dd, 2 H, $^3J_{HH}$ = 5.6 Hz, $^4J_{HH}$ = 3.4 Hz, ligand aromatic C**H**), 7.08 (t, 1H, $^3J_{HH}$ = 7.3 Hz, C**H**-Ph$_{para}$) 7.16 (dd, 2 H, $^3J_{HH}$ = 5.4 Hz, $^4J_{HH}$ = 3.4 Hz, ligand aromatic C**H**), 7.33 (t, 2H, $^3J_{HH}$ = 7.3 Hz, C**H**-Ph$_{meta}$), 8.09 (d, 2H, $^3J_{HH}$ = 7.1 Hz, C**H**-Ph$_{ortho}$).

¹³C{¹H}-NMR (100 MHz, C₆D₆, 298 K) δ 30.1 (t, $^2J_{CP}$ = 2.5 Hz, (**C**H)₃C), 36.5 (t, $^1J_{CP}$ = 5.5 Hz, (CH)₃**C**), 42.3 (t, $^1J_{CP}$ = 17.2 Hz, **C**H₂), 109.0 (ligand aromatic **C**H), 118.6 (ligand aromatic **C**H), 121.0 (**C**H-Ph$_{para}$), 125.4 (**C**H-Ph$_{meta}$), 139.6 (t, $^3J_{CP}$ = 7.3 Hz, ligand aromatic **C**$_q$), 143.4 (**C**H-Ph$_{ortho}$), 176.2 (t, $^2J_{CP}$ = 14 Hz, Ph-**C**$_{ipso}$).

³¹P{¹H}-NMR (161 MHz, C₆D₆, 298 K) δ 93.8 (s, **P**^{t}Bu₂) ppm.

¹¹B{¹H}-NMR (128 MHz, C₆D₆, 298 K) δ 44.9 (bs, boryl) ppm.

Anal. Calcd. for C₃₀H₄₉BN₂NiP₂: C, 63.31; H, 8.68; N, 4.92. Found: C, 63.22; H, 8.52; N, 4.79.

General procedure for low temperature NMR experiments
In the glovebox, a solution of **4** (15 mg, 0.030 mmol) was dissolved in d^8-THF (0.4 mL) and placed into a J. Young NMR tube. The same was repeated for a solution of B₂cat₂ (8.4 mg, 0.035 mmol, 1.1 eq) in d^8-THF (0.2 mL) in a different NMR tube. In the Schlenk line, both tubes were cooled down to -60 °C and the solution of diborane was transferred under argon via cannula to the NMR tube containing the nickel complex. The NMR tube was closed and shaken in the cold bath, after which it was introduced into the pre-cooled (-60 °C) NMR spectrometer. Once the mixture of **4** + Intermediate was observed by NMR, PMe₃ (up to 4 equivalents) or CO (1 bar) was added to the sample under inert atmosphere at low temperature (-60 °C, cold bath). The NMR tube was brought back to the NMR spectrometer to monitor the evolution of the sample at different temperatures.

[390]

General procedure for the borylation of styrenes and isolation of the products. Example of styrene and B₂pin₂ (1 equivalent) using DMF as additive (entry 2 of Table 5)

In the glovebox, a vial was charged with complex **4** (4 mg, 0.008 mmol, 10 mol %), B_2pin_2 (20.3 mg, 0.08 mmol), styrene (9.2 μL, 0.08 mmol), and dry DMF (12.4 μL, 0.16 mmol). The resulting yellow solution was transferred to a J. Young NMR tube, which was heated to 70 °C for 14 hours. Then, the sample was placed into an HPLC vial, and the solvent was removed under vacuum. Heptane (2 mL) was added to the brown residue and the solvents were removed again under vacuum. This process was repeated 2 more times. The resulting brown solid was purified by column chromatography (ø = 1.2 cm, 11 cm of silica), eluting with Et_2O-Hexane 1:9, affording the pure (*E*)-monoborylated styrene.

Dehydrogenative borylation products
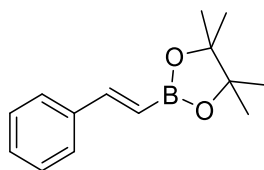
(*E*)-4,4,5,5-tetramethyl-2-styryl-1,3,2-dioxaborolane

¹H-NMR (400 MHz, CDCl₃, 298 K): δ 1.32 (s, 12H, C*H₃*), 6.18 (d, $^3J_{H-H}$ = 18.6 Hz, 1H, =C*H*), 7.32 (m, 3H, arom C*H*), 7.40 (d, $^3J_{H-H}$ = 18.7 Hz, 1H, =C*H*), 7.50 (m, 2H, arom C*H*) ppm.

¹¹B-NMR (128 MHz CDCl₃, 298 K) δ 30.2 (*B*pin) ppm.
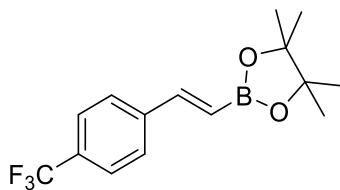
(*E*)-4,4,5,5-tetramethyl-2-(4-(trifluoromethyl)styryl)-1,3,2-dioxaborolane

[391]

Experimental Part

^{1}H-NMR (400 MHz, *d*[8]-Toluene, 298 K): δ 1.13 (s, 12H, C*H*₃), 6.24 (d, $^3J_{\text{H-H}}$ = 18.4 Hz, 1H, =C*H*), 7.07 (d, $^3J_{\text{H-H}}$ = 8.1 Hz, 2H, arom C*H*), 7.23 (d, $^3J_{\text{H-H}}$ = 8.1 Hz, 2H, arom C*H*), 7.40 (d, $^3J_{\text{H-H}}$ = 18.2 Hz, 1H, =C*H*) ppm.
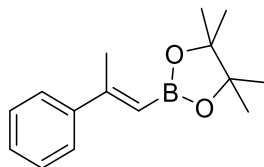
(*E*)-4,4,5,5-tetramethyl-2-(2-phenylprop-1-en-1-yl)-1,3,2-dioxaborolane[9]

^{1}H-NMR (400 MHz, CDCl₃, 298 K): δ 1.32 (s, 12H, OCC*H*₃), 2.41 (d, $^4J_{\text{H-H}}$ = 0.9 Hz, 3H, C=CC*H*₃), 5.76 (broad quartet, $^4J_{\text{H-H}}$ = 0.9 Hz, 1H, =C*H*), 7.31 (m, 3H, arom C*H*), 7.50 (m, 2H, arom C*H*) ppm.
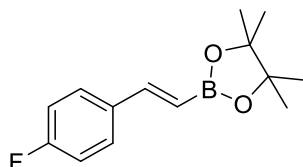
(*E*)-2-(4-fluorostyryl)-4,4,5,5-tetramethyl-1,3,2-dioxaborolane

^{1}H-NMR (400 MHz, *d*[8]-Toluene, 298 K): δ 1.15 (s, 12H, C*H*₃), 6.13 (d, $^3J_{\text{H-H}}$ = 18.4 Hz, 1H, =C*H*), 6.68 (m, 2H, arom C*H*), 7.06 (m, 2H, arom C*H*), 7.45 (d, $^3J_{\text{H-H}}$ = 18.5 Hz, 1H, =C*H*) ppm.
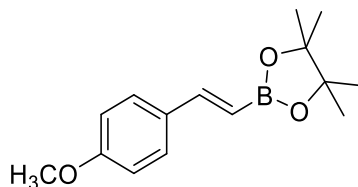
(*E*)-2-(4-methoxystyryl)-4,4,5,5-tetramethyl-1,3,2-dioxaborolane

---

[9] The assignation of the *E*-isomer was made based on the coupling constants and chemical shifts observed by ^{1}H NMR, which match those described in the literature. See: S. Tanaka, Y. Saito, T. Yamamoto, T. Hattori, *Org. Lett.,* **2018**, *20*, 1828-1831 (Supporting information).

¹H-NMR (400 MHz, *d*⁸-Toluene, 298 K): δ 1.13 (s, 12H, C*H*₃), 3.31 (s, 3H, OC*H*₃) 6.14 (d, ³*J*H-H = 18.4 Hz, 1H, =C*H*), 6.60 (d, ³*J*H-H = 8.5 Hz, 2H, arom C*H*), 7.22 (d, ³*J*H-H = 8.8 Hz, 2H, arom C*H*), 7.54 (d, ³*J*H-H = 18.5 Hz, 1H, =C*H*) ppm.
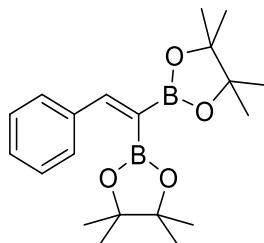
2,2'-(2-phenylethene-1,1-diyl)bis(4,4,5,5-tetramethyl-1,3,2-dioxaborolane)

¹H-NMR (500 MHz, CDCl₃, 298 K): δ 1.27 (s, 12H, C*H*₃), 1.31 (s, 12H, C*H*₃), 7.33 (m, 3H, arom C*H*), 7.47 (m, 2H, arom C*H*), 7.70 (s, 1H, =C*H*) ppm.
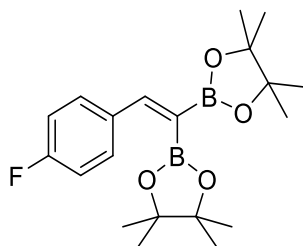
2,2'-(2-(4-fluorophenyl)ethene-1,1-diyl)bis(4,4,5,5-tetramethyl-1,3,2-dioxaborolane)

¹H-NMR (400 MHz, *d*⁸-Toluene, 298 K): δ 1.07 (s, 12H, C*H*₃), 1.15 (s, 12H, C*H*₃), 6.99 (m, 2H, arom C*H*), 7.46 (m, 2H, arom C*H*), 7.88 (s, 1H, =C*H*) ppm.

[393]
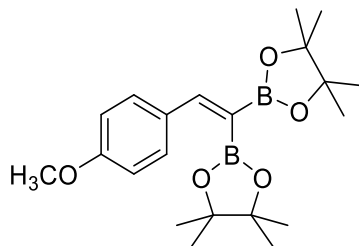
Experimental Part

2,2'-(2-(4-methoxyphenyl)ethene-1,1-diyl)bis(4,4,5,5-tetramethyl-1,3,2-dioxaborolane)

^{1}H-NMR (400 MHz, d^8-Toluene, 298 K): δ 1.15 (s, 24H, CH_3), 3.31 (s, 3H, OCH_3), 6.67 (d, $^3J_{H-H}$ = 8.6 Hz, 2H, arom CH), 7.47 (d, $^3J_{H-H}$ = 8.7 Hz, 2H, arom CH), 7.98 (s, 1H, =CH) ppm.

[394]

Experimental Part for Chapter 3

Synthesis of Pt I^{t}Bu complexes

Complex [Pt(SiHEt$_2$)(I^{t}Bu)$_2$][BAr$_4$^{F}] (16)
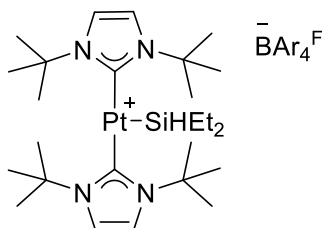
Synthesis

A J. Young flask was charged with a stirrer bar, complex [Pt(I^{t}Bu')(I^{t}Bu)][BAr$_4$^{F}], **13**, (190 mg, 134 μmol) and CH$_2$Cl$_2$ (3 mL). Et$_2$SiH$_2$ (0.52 mL, 4.02 mmol, 30 eq) was added to the solution, and the mixture was stirred at room temperature for 15 min, after which a change of color from orange to yellow was observed. A layer of pentane was then added (30 mL), and slow mixing of both solvents yielded yellow crystals suitable for X-Ray analysis. The solution was removed via cannula, the crystals were dried under vacuum at -40 °C and stored at -20 °C in the glovebox (170 mg, 113 μmol, 84% yield). Complex **16** is thermally unstable towards cyclometalation, but it can be stored for months at -20 °C without decomposition.

Spectroscopic and analytical data

Yellow crystals.

Molecular weight: 1506.11 g/mol.

^{1}H-NMR (400 MHz, CD$_2$Cl$_2$, 298 K): δ 0.19 (m, 2H, C*H$_2$*CH$_3$), 0.63 (m, 2H, C*H$_2$*CH$_3$), 0.69 (m, 6H, CH$_2$C*H$_3$*), 1.96 (s, 36H, (C*H$_3$*)$_3$C), 3.64 (m + d + d, $^2J_{Pt-H}$ = 115 Hz, $^1J_{H-Si}$ = 188 Hz, 1H, Si*H*), 7.26 (s, 4H, =C*H*) ppm.

[395]

13C{1H}-NMR (100 MHz, CD$_2$Cl$_2$, 298 K): δ 10.1 (*C*H$_3$CH$_2$), 10.5 (CH$_3$*C*H$_2$), 33.4 ((*C*H$_3$)$_3$C), 60.7 ((CH$_3$)$_3$*C*), 120.1 (=*C*H), 173.8 (*C*$_{carbene}$-Pt) ppm**.**

29Si{1H}-NMR (79 MHz, CD$_2$Cl$_2$, 298 K): δ 18.12 (*Si*HEt$_2$) ppm.

LRMS (ESI): *m/z* **calculated** for C$_{26}$H$_{51}$N$_4$PtSi [M$^+$]: 642.35. **Found:** 642.4

Elem. Anal. Calcd. for C$_{58}$H$_{63}$BF$_{24}$N$_4$PtSi: C, 46.25; H, 4.22; N, 3.72. **Found**: C, 46.45; H, 3.97; N, 3.47.

Variable Temperature NMR experiments using Pt I^{t}Bu complexes (**13, 15** and **16**)

A J. Young NMR tube was charged with [Pt] (around 40 mg) and dissolved in CD$_2$Cl$_2$ (0.4 mL). The system was brought to the NMR spectrometer, where it was analysed (1H NMR) at room temperature before lowering the temperature to -80 °C. At this point, the tube was taken out of the spectrometer and introduced in a cold (-78 °C) bath. 1 equivalent of silane was added under argon, and the tube was then introduced again in the precooled NMR spectrometer. The behavior of the system was monitored by 1H NMR spectroscopy at different temperatures.

In the case of [Pt(H)(I^{t}Bu)$_2$][BAr$_4$^{F}], **15**, the J. Young NMR tube was initially charged with [Pt(I^{t}Bu')(I^{t}Bu)][BAr$_4$^{F}], **13**, CD$_2$Cl$_2$ and H$_2$ (2 bar). Once the hydride complex was formed, the solution was degassed with 4 freeze-pump-thaw cycles and brought to the NMR spectrometer as in the other cases.

[396]

Synthesis of Pt I^{t}Bu^{i}Pr complexes

1-(*tert*-butyl)-3-(*iso*-propyl)-1*H*-imidazolium iodide, I^{t}Bu^{i}Pr·HI (17)
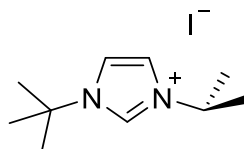
Synthesis

In the Schlenk line, a J. Young flask was charged with a stirrer bar, 1-(*tert*-butyl)-1*H*-imidazol (3.2 g, 25.8 mmol) and 2-iodopropane (5.44 g, 32 mmol). Toluene (30 mL) was added, and the mixture was heated up to 100 °C for 24 hours, after which the resulting white solid was filtered off and washed with diethyl ether (3 x 30 mL). 7.1 g (24.1 mmol, 94 % yield) of an analytically pure white solid was obtained.

Spectroscopic and analytical data

White solid.

Molecular weight: 294.18 g/mol.

^{1}H-NMR (400 MHz, CD$_2$Cl$_2$, 298 K): δ 1.62 (d, $^3J_{H-H}$ = 6.8 Hz, 6H, CH(C*H*$_3$)$_2$), 1.73 (s, 9H, C(CH$_3$)$_3$), 5.11 (sept, $^3J_{H-H}$ = 6.8 Hz , 1H, C*H*(CH$_3$)$_2$), 7.48 (br, 2H, =C*H*), 10.06 (s, 1H, =C*H*) ppm.

^{13}C{^{1}H}-NMR (100 MHz, CD$_2$Cl$_2$, 298 K): δ 23.2 (CH(*C*H$_3$)$_2$), 30.3 (C(*C*H$_3$)$_3$), 53.6 (*C*H(CH$_3$)$_2$), 61.0 (*C*(CH$_3$)$_3$), 119.9 and 120.0 (=*C*H), 134.5 (=*C*H) ppm.

Elem. Anal. Calcd. for C$_{10}$H$_{19}$IN$_2$: C, 40.83; H, 6.51; N, 9.52. **Found**: C, 40.9; H, 6.3; N, 9.7.

[397]

Experimental Part

Complex *cis*-[Pt(CH$_3$)$_2$(I^{t}Bu^{i}Pr)$_2$] (18)
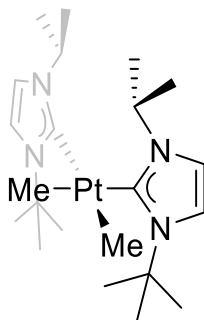
Synthesis

In the glovebox, a J. Young flask was charged with a stirrer bar, I^{t}Bu^{i}Pr·HI (**17**) (705 mg, 2.4 mmol) and ^{t}BuOK (300 mg, 2.7 mmol). In the Schlenk line, the solids were suspended in dry THF (7 mL) under argon at – 30 °C. The mixture was stirred for 10 min at this temperature and for 2h at r.t. Then, the mixture was cooled to – 30 °C and a solution of complex [Pt(CH$_3$)$_2$(COD)] (400 mg, 1.2 mmol) in THF (3 mL) was slowly added via cannula. The mixture was left to reach r.t. and stirred for 1 h. The solvent was then removed under vacuum and the resulting residue was suspended in 10 mL of pentane. Pentane was then evaporated and complex **18** was extracted with toluene (10 + 5 mL), filtering it via cannula. The solvent was removed under vacuum yielding a viscous oil. Pentane (10 mL) was added and the suspension was vigorously stirred until a white precipitate appears. The solid was filtered off yielding a white solid. We have noticed that this solid contains complex *cis*-[Pt(CH$_3$)$_2$(I^{t}Bu^{i}Pr)$_2$] and minor amounts of *trans*-[Pt(CH$_3$)$_2$(I^{t}Bu^{i}Pr)$_2$] or some other conformational isomer. Complete isomerization to the *cis* isomer can be carried out by dissolving the mixture in CH$_2$Cl$_2$ while stirring for a few hours. 450 mg (0. 81 mmol, 67 % yield) of complex **18** were obtained.

Spectroscopic and analytical data

White solid.

[398]

Molecular weight: 557.69 g/mol.

^{1}H-NMR (400 MHz, C$_6$D$_6$, 298 K): δ 0.81 (s+d, $^2J_{\text{Pt-H}}$ = 68 Hz, 6H, Pt-CH$_3$), 1.25 (d, $^3J_{\text{H-H}}$ = 6.8 Hz, 6H, CH(C**H**$_3$)$_2$), 1.39 (d, $^3J_{\text{H-H}}$ = 6.5 Hz, 6H, CH(C**H**$_3$)$_2$), 1.56 (s, 18H, C(C**H**$_3$)$_3$), 6.44 (d, $^3J_{\text{H-H}}$ = 2.2 Hz, 2H, =C**H**), 6.51 (sept, $^3J_{\text{H-H}}$ = 6.5 Hz, 2H, C**H**(CH$_3$)$_2$), 6.59 (d, $^3J_{\text{H-H}}$ = 2.2Hz, 2H, =C**H**) ppm.

^{13}C{^{1}H}-NMR (100 MHz, C$_6$D$_6$, 298 K): δ −9.3 (s + d, $^1J_{\text{Pt-C}}$ = 579 Hz, Pt-**C**H$_3$), 23.7 and 25.9 (CH(**C**H$_3$)$_2$), 30.5 (C(**C**H$_3$)$_3$), 51.0 (s + d, $^3J_{\text{Pt-C}}$ = 52 Hz, **C**H(CH$_3$)$_2$), 57.0 (**C**(CH$_3$)$_3$), 114.4 (s + d, $^4J_{\text{Pt-C}}$ = 23 Hz, =**C**H), 117.0 (s + d, $^4J_{\text{Pt-C}}$ = 25 Hz, =**C**H), 187.5 (s + d, $^1J_{\text{Pt-C}}$ = 848, Hz Pt-**C**$_{\text{carbene}}$) ppm.

Elem. Anal. Calcd. for C$_{22}$H$_{42}$N$_4$Pt: C, 47.38; H, 7.59; N, 10.05. **Found**: C, 47.4; H, 7.6; N, 9.8.

Complex [Pt(I^{t}Bu^{i}Pr')(I^{t}Bu^{i}Pr)][BAr$_4^F$] (19)
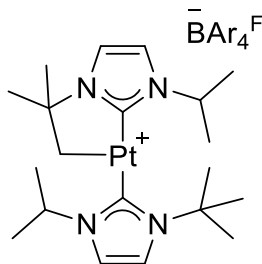
Synthesis

In the glovebox, a Schlenk flask was charged with a stirrer bar, complex **18** (330 mg, 0.59 mmol) and [H(OEt$_2$)$_2$][BAr$_4^F$] (600 mg, 0.59 mmol). In the Schlenk line, both solids were dissolved in 6 mL of CH$_2$Cl$_2$, under argon, at -78 °C. After 5 minutes, the cold bath was removed allowing the flask to reach room temperature. After 30 minutes, the solvent was evaporated under vacuum. The resulting yellow solid was washed with pentane (2 x 12 mL), re-dissolved in

[399]

CH$_2$Cl$_2$ (6 mL) and evaporated under vacuum in order to remove the remaining diethyl ether. This last process (dissolution/evaporation in CH$_2$Cl$_2$) was repeated leading to a pale yellow-orange fine powder that was dried under vacuum for 2 h yielding complex **19** (750 mg, 0.54 mmol, 91% yield). Complex **19** can be stored in a glove-box or under an inert atmosphere indefinitely.

Spectroscopic and analytical data

Pale yellow-orange solid.

Molecular weight: 1389.83 g/mol.

^{1}H-NMR (400 MHz, CD$_2$Cl$_2$, 298 K): δ 1.46 (d, $^3J_{\text{H-H}}$ = 7.1 Hz, 12H, CH(CH_3)$_2$), 1.47 (s, 6H, 2 CH_3), 1.81 (s, 9H, (CH_3)$_3$), 2.55 (s+d, $^2J_{\text{Pt-H}}$ = 103 Hz, 2H, Pt-CH_2), 4.53 (sept, $^3J_{\text{H-H}}$ = 7.1 Hz, 1H, CH(CH$_3$)$_2$), 5.83 (sept, $^3J_{\text{H-H}}$ = 7.1 Hz 1H, CH(CH$_3$)$_2$), 6.95 and 7.05 (d, $^3J_{\text{H-H}}$ = 1.9 Hz, 1H each, =CH), 7.07 and 7.20 (d, $^3J_{\text{H-H}}$ = 2.1 Hz, 1H each, =CH) ppm.

^{13}C{^{1}H}-NMR (100 MHz, CD$_2$Cl$_2$, 298 K): δ 19.7 (s+d, $^1J_{\text{Pt-C}}$ = 860 Hz, Pt-CH$_2$), 23.6 and 23.7 (CH(CH$_3$)$_2$), 30.0 (s+d, $^3J_{\text{Pt-C}}$ = 50 Hz, 2 CH$_3$), 31.6 (C(CH$_3$)$_3$), 51.4 and 53.9 (CH(CH$_3$)$_2$), 59.3 and 65.1 (C(CH$_3$)$_3$), 116.4, 116.6 and 117.1 (=CH), 120.8 (s+d, $^3J_{\text{Pt-C}}$ = 31 Hz, =CH), 169.9 and 173.4 (Pt-$C$$_{\text{carbene}}$) ppm.

Elem. Anal. Calcd. for C$_{52}$H$_{47}$BF$_{24}$N$_4$Pt: C, 44.94; H, 3.41; N, 4.03. **Found**: C, 44.8; H, 3.5; N, 4.1.

Synthesis of Pt I^{t}Bu^{i}Pr σ-SiH complexes

Complex [Pt(I^{t}Bu^{i}Pr')(I^{t}Bu^{i}Pr)(HSiEt$_3$)][BAr$_4$^{F}] (19·Et$_3$SiH)

Synthesis

In the Schlenk line, complex **19** (80 mg, 0.057 mmol) was dissolved in 0.6 mL of CD$_2$Cl$_2$ in a screw-cap NMR tube under argon. The solution was cooled to -78 °C and Et$_3$SiH (10 μL, 0.063 mol) was injected. The sample was analysed by NMR in a pre-cooled (0 °C) NMR apparatus. X-Ray quality crystals can be grown by slow diffusion of pentane into a concentrated solution of **19·Et$_3$SiH** in dichloromethane (10:1) at -20 °C.

Spectroscopic and analytical data

Pale-yellow crystals.

Molecular weight: 1506.11 g/mol.

^{1}H-NMR (400 MHz, CD$_2$Cl$_2$, 273 K): δ -4.98 (s+d+d, $^1J_{Pt-H}$ = 398 Hz, $^1J_{Si-H}$ = 79 Hz, Pt-***H***-Si), 0.49-0.58 (m, 4H, Si***Et***$_3$), 0.83-0.93 (m, 11 H, Si***Et***$_3$), 1.36 (d, $^3J_{H-H}$ = 6.6 Hz, 3H, CH(C***H***$_3$)$_2$), 1.43-1.46 (m, 6H, CH(C***H***$_3$)$_2$ and C***H***$_3$C$_q$), 1.52 (m, 9H, CH(C***H***$_3$)$_2$ and C***H***$_3$C$_q$), 1.70 (s, 9H,C(C***H***$_3$)$_3$), 2.11 (d+d, $^2J_{H-H}$ = 12.0 Hz, $^2J_{Pt-H}$ = 87.5 Hz, 1H, Pt-C***H****$_a$*H$_b$), 2.24 (d+d, $^2J_{H-H}$ = 12.0 Hz, $^2J_{Pt-H}$ = 65.0 Hz, 1H, Pt-CH$_a$***H****$_b$*), 4.38 and 5.38 (sept, $^3J_{H-H}$ = 6.6 Hz, 1H each, C***H***(CH$_3$)$_2$), 7.02 and 7.03 (d, $^3J_{H-H}$ = 1.8 Hz, 1H each, =C***H***), 7.05 (d, $^3J_{H-H}$ = 2.1 Hz, 1H each, =C***H***), 7.05 and 7.23 (d, $^3J_{H-H}$ = 2.1 Hz, 1H each, =C***H***) ppm.

[401]

^{13}**C{^{1}H}-NMR (100 MHz, CD$_2$Cl$_2$, 273 K): δ** 6.8 and 7.6 (Si***Et***$_3$), 21.4, 22.8, 24.90, 24.94 (CH(**C**H$_3$)$_2$ and **C**H$_3$C$_q$), 28.4 (s, **C**H$_3$), 31.1 (C(**C**H$_3$)$_3$), 32.3 (CH(**C**H$_3$)$_2$), 33.6 (s+d, $^1J_{\text{Pt-C}}$ = 694 Hz, Pt-**C**H$_2$), 52.4 and 53.3 (**C**H(CH$_3$)$_2$), 59.0 (**C**(CH$_3$)$_3$), 65.4 (s+d, $^3J_{\text{Pt-C}}$ = 27 Hz, **C**(CH$_3$)$_3$), 116.0 (s+d, $^3J_{\text{Pt-C}}$ = 27 Hz, 2 =**C**H), 117.7 (=**C**H), 121.1 (s+d, $^3J_{\text{Pt-C}}$ = 31 Hz, =**C**H), 167.0 and 168.7 (Pt-**C**$_{\text{carbene}}$) ppm.

^{29}**Si{^{1}H}-NMR (79 MHz, CD$_2$Cl$_2$, 273 K): δ** 11.7 (***Si***Et$_3$) ppm.

Elemental analysis was not possible due to the instability of the sample above 0 °C.

Complex [Pt(I^{t}Bu^{i}Pr')(I^{t}Bu^{i}Pr)(HSiPh$_3$)][BAr$_4$^{F}] (19·Ph$_3$SiH)

Synthesis

In the Schlenk line, complex **19** (80 mg, 0.057 mmol) and Ph$_3$SiH (15 mg, 0.057 mmol) were dissolved in 0.6 mL of CD$_2$Cl$_2$ in a screw-cap NMR tube at -78 °C under argon. The sample was analysed by NMR in a pre-cooled (0 °C) NMR apparatus. X-Ray quality crystals can be grown by slow diffusion of pentane into a concentrated solution of **19·Ph$_3$SiH** in dichloromethane (10:1) at -20 °C.

Spectroscopic and analytical data
Pale-yellow crystals.
Molecular weight: 1650.24 g/mol.

[402]

¹H-NMR (400 MHz, CD₂Cl₂, 273 K): δ -4.01 (s+d, $^1J_{\text{Pt-H}}$ = 416.2 Hz, Pt-**H**-Si), 0.30, 0.40 and 0.70 (bs, 3H each, CH(C**H**₃)₂ and C**H**₃C_q), 1.01-1.58 (m, 9H, CH(C**H**₃)₂ and C**H**₃C_q), 1.94 (s, 9H, C(C**H**₃)₃), 2.00-2.35 (m, 2H, Pt-C**H**₂), 4.46 (sept, $^3J_{\text{H-H}}$ = 6.6Hz, 1H, C**H**(CH₃)₂), 4.74 (bs, 1H, C**H**(CH₃)₂), 6.90 (d, $^3J_{\text{H-H}}$ = 1.6 Hz, 1H, =C**H**), 6.92 and 6.94 (d, $^3J_{\text{H-H}}$ = 1.9 Hz, 1H each, =C**H**), 7.20-7.40 (br m, 15H, **Ph**), 7.41 (d, $^3J_{\text{H-H}}$ = 1.6 Hz, 1H, =C**H**) ppm.

¹³C{¹H}-NMR (100 MHz, CD₂Cl₂, 273 K): δ 19.3, 21.2, 24.9, 28.5 and 29.2 (br, 1:1:2:1:1 ratio, CH(**C**H₃)₂ and **C**H₃C_q), 31.7 (C(**C**H₃)₃), 52.8 and 53.1 (**C**H(CH₃)₂), 59.5 and 65.7 (**C**(CH₃)₃), 116.6 and 116.7 (=**C**H), 118.2 and 121.4 (=**C**H), 128.1, 128.6, 130.3, 135.1 (**Ph**), 164.2 and 166.4 (Pt-**C**_carbene) ppm. The Pt-CH₂ signal was too broad to be observed.

²⁹Si{¹H}-NMR (79 MHz, CD₂Cl₂, 273 K): δ -15.6 (**Si**Ph₃) ppm.

Elemental analysis was not possible due to the instability of the sample above 0 °C.

Synthesis of Pt I^tBu^iPr silyl complexes from cyclometalated complexes and tertiary silanes

Complexes [Pt(SiR₃)(I^tBu^iPr)₂][BAr₄^F] [20 (R =Et) and 21 (R=Ph)]

Syntheses

Since NHC-stabilized Pt(II) σ-SiH complexes are reactive intermediates in the synthesis of silyl derivatives, these complexes were obtained by using the same synthetic protocols described for the preparation of complexes **19·Et₃SiH** and **19·Ph₃SiH** and allowing the sample to warm up to r.t.: in a J. Young flask, the sample was stirred for 5 h (complex **20**) or 2 h (complex **21**), followed by evaporation of the solvent. The resulting yellow solid was washed with dry

[403]

pentane (2 x 5 mL), and the solid was dried under vacuum. Both complexes can be crystallized by slow diffusion of a solution of the sample in CH_2Cl_2 into pentane at 0 °C (**20**, 72 mg, 0.048 mmol, 83% yield); **21**, 71 mg, 0.043 mmol, 75% yield).

Complex [Pt(SiEt₃)(I^{t}Bu^{i}Pr)₂][BAr₄^F] (20)

Spectroscopic and analytical data

Bright yellow solid.

Molecular weight: 1506.11 g/mol.

¹H-NMR (400 MHz, CD₂Cl₂, 298 K): δ 0.62-0.75 (m, 15H, Si***Et***₃), 1.52 (d, $^3J_{H-H}$ = 6.7 Hz, 12H, CH(C***H***₃)₂), 1.93 (s, 18H, C(C***H***₃)₃), 5.45 (sept, $^3J_{H-H}$ = 6.7 Hz, 2H, C***H***(CH₃)₂), 7.08 and 7.23 (d, $^3J_{H-H}$ = 2.1 Hz, 2H each, =C***H***) ppm.

¹³C{¹H}-NMR (100 MHz, CD₂Cl₂, 298 K): δ 8.2 (Si-CH₂***C***H₃), 10.1 (s+d, $^2J_{Pt-C}$ = 93 Hz, Si-***C***H₂CH₃), 23.9 (CH(***C***H₃)₂), 33.3 (C(***C***H₃)₃), 54.4 (***C***H(CH₃)₂), 59.8 (***C***(CH₃)₃), 116.0 (s+d, $^3J_{Pt-C}$ = 38 Hz, =***C***H), 121.1 (s+d, 3J_{Pt-C} = 36 Hz, =***C***H), 181.1 (Pt-***C***_carbene) ppm.

²⁹Si{¹H}-NMR (79 MHz, CD₂Cl₂, 298 K): δ 38.2 (***Si***Et₃) ppm.

Elem. Anal. Calcd. for C₅₈H₆₃BF₂₄N₄PtSi: C, 46.25; H, 4.22; N, 3.72. **Found**: C, 46.2; H, 4.3; N, 3.7

Complex [Pt(SiPh₃)(I^tBu^iPr)₂][BAr₄^F] (21)

Spectroscopic and analytical data

Bright yellow solid.

Molecular weight: 1650.24 g/mol.

¹H-NMR (400 MHz, CD₂Cl₂, 298 K): δ 0.87 (d, $^3J_{H\text{-}H}$ = 6.6 Hz, 12H, CH(C**H₃**)₂), 1.77 (s, 18H, C(C**H₃**)₃), 5.08 (sept, $^3J_{H\text{-}H}$ = 6.6 Hz, 2H, C**H**(CH₃)₂), 6.91 (d, $^3J_{H\text{-}H}$ = 1.8 Hz, 2H, =C**H**), 7.18-7.24 (m, 8H, Ph), 7.25-7.32 (m, 9H, **Ph** and =C**H**) ppm.

¹³C{¹H}-NMR (100 MHz, CD₂Cl2, 298 K): δ 22.9 (CH(**C**H₃)₂), 33.4 (C(**C**H₃)₃), 54.8 (**C**H(CH₃)₂), 59.8 (**C**(CH₃)₃), 116.2 (s+d, $^3J_{Pt\text{-}C}$ = 40 Hz, =**C**H), 121.0 (s+d, $^3J_{Pt\text{-}C}$ = 28 Hz, =**C**H), 128.5, 129.5, 130.3, 135.3 (**Ph**), 137.9 (Ph-**C**ipso), 178.0 (Pt-**C**carbene) ppm.

²⁹Si{¹H}-NMR (79 MHz, CD₂Cl₂, 273 K): δ – 9.0 ($^1J_{Pt\text{-}Si}$ = 1690 Hz, **Si**Ph₃) ppm.

Elem. Anal. Calcd. for C₇₀H₆₃BF₂₄N₄PtSi: C, 50.95; H, 3.85; N, 3.40. Found: C, 50.9; H, 3.9; N, 3.4.

Synthesis of Pt cyclometalated silyl complexes

General synthesis

Complexes **19**, **24** or **25** (0.057 mmol) were dissolved in 0.7 mL of CH₂Cl₂ (or CD₂Cl₂) under argon, after which the corresponding silane was injected (0.058 mmol, 1 equivalent). The reaction mixture was stirred at r.t. for 30 min

Experimental Part

and the solvent was evaporated under vacuum. The resulting yellow solid was washed with pentane (2 x 4 mL), and dried under vacuum. In most of the cases crystals suitable for X-ray diffraction studies can be obtained by slow diffusion of a concentrated solution of the complex in CH_2Cl_2 into pentane (1:10).

Complex [Pt(I^{t}Bu^{i}PrSiH^{n}Bu')(I^{t}Bu^{i}Pr)][BAr$_4^F$] (22)

Spectroscopic and analytical data

Yellow solid.

Molecular weight: 1476.04 g/mol.

Yield: 80 % (67 mg, 0.046 mmol).

^{1}H-NMR (400 MHz, CD$_2$Cl$_2$, 298 K): δ 0.50 and 0.66 (m, 1H each, SiCH_2), 0.78 (t, $^3J_{H-H}$ = 7.2 Hz, CH_3(CH$_2$)$_3$Si), 1.01 and 1.12 (m, 1H each, CH_2), 1.20 (m, 2H, CH_2), 1.32 (dd, $^2J_{H,H}$ = 14.6 Hz, $^3J_{H-H}$ = 3.0 Hz, 1H, Si-CH_aH$_b$), 1.47-1.50 (m, 7H, Si-CH$_a$$H_b$ + CH(CH_3)$_2$), 1.52 and 1.57 (d, $^3J_{H-H}$ = 6.7 Hz, 3H each, CH(CH_3)$_2$), 1.82 and 1.86 (s, 3H each, CH_3), 1.89 (s, 9H, (CH_3)$_3$), 3.52 (br+d, $^2J_{Pt-H}$ = 120 Hz, 1H, SiH), 4.81 (sept, $^3J_{H-H}$ = 6.7 Hz, 1H, CH(CH$_3$)$_2$), 5.65 (sept, $^3J_{H-H}$ = 6.7 Hz, 1H, CH(CH$_3$)$_2$), 6.99 (d, $^3J_{H-H}$ = 2.0 Hz, 1H, =CH), 7.07 (d, $^3J_{H-H}$ = 2.0 Hz, 1H, =CH), 7.16 (d, $^3J_{H-H}$ = 2.0 Hz, 1H, =CH), 7.21 (d, $^3J_{H-H}$ = 2.0 Hz, 1H, =CH) ppm.
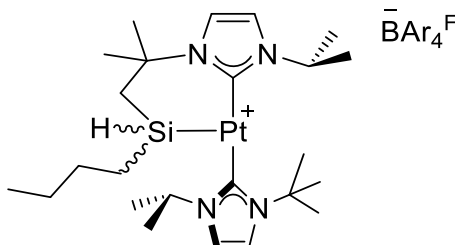
^{13}C{^{1}H} NMR (100 MHz, CD$_2$Cl$_2$, 298 K): δ 13.7 (CH$_3$(CH$_2$)$_3$Si), 17.8 (CH$_2$$CH_2$Si), 23.5, 23.8, 24.8 and 25.1 (CH(CH$_3$)$_2$), 26.1 (CH$_2$), 27.4 (s+d, $^2J_{Pt-C}$ ~ 48 Hz, CCH$_2$Si), 28.6 (CH$_2$), 32.6 (C(CH$_3$)$_3$ + 2 CH$_3$), 54.5 and 54.8 (CH(CH$_3$)$_2$), 59.3 and 61.6 (C(CH$_3$)$_3$), 116.1, 117.3, 118.8 and 120.6 (=CH), 175.1 and 182.7 (Pt-$C$$_{carbene}$) ppm.

^{29}Si{^{1}H} NMR (79 MHz, CD$_2$Cl$_2$, 298 K) δ = -1.5 ppm (^{n}BuSiHPt) ppm.

Elem. Anal. Calcd. for $C_{56}H_{57}BF_{24}N_4PtSi$: C, 45.57; H, 3.89; N, 3.80. **Found**: C, 45.3; H, 4.2; N, 3.7

Complex [Pt(I^{t}Bu^{i}PrSiHPh')(I^{t}Bu^{i}Pr)][BAr$_4^F$] (23)
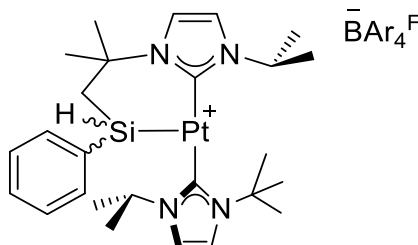
Spectroscopic and analytical data

Yellow solid.

Molecular weight: 1496.03 g/mol.

Yield: 95 % (80.9 mg, 0.054 mmol).

^{1}H-NMR (400 MHz, CD$_2$Cl$_2$, 298 K): δ 1.05 (d, $^3J_{H-H}$ = 6.7 Hz, 3H, CH(C**H**$_3$)$_2$), 1.42 (d, $^3J_{H-H}$ = 6.7 Hz, 3H, CH(C**H**$_3$)$_2$), 1.51 (d, $^3J_{H-H}$ = 7.0 Hz, 3H, CH(C**H**$_3$)$_2$), 1.61 (d, $^3J_{H-H}$ = 6.5 Hz, 3H, CH(C**H**$_3$)$_2$), 1.66 (t, $^3J_{H-H}$ = 3 Hz, 2H, C**H**$_2$-Si), 1.80 (s, 9H, (C**H**$_3$)$_3$), 1.83 (s, 3H, CC**H**$_3$), 2.04 (s, 3H, CC**H**$_3$), 4.04 (t+d, $^3J_{H-H}$ = 3 Hz, $^2J_{Pt-H}$ = 123 Hz, 1H, Si**H**), 4.77 (sept, $^3J_{H-H}$ = 6.7 Hz, 1H, C**H**(CH$_3$)$_2$), 5.37 (sept, $^3J_{H-H}$ = 6.7 Hz, 1H, C**H**(CH$_3$)$_2$), 6.99 (d, $^3J_{H-H}$ = 1.8 Hz, 1H, =C**H**), 7.06 (d, $^3J_{H-H}$ = 2.1 Hz, 1H, =C**H**), 7.12 (d, $^3J_{H-H}$ = 7.3 Hz, 2H, C**H**-Ph$_{ortho}$), 7.18 (d, $^3J_{H-H}$ = 2.1 Hz, 1H, =C**H**), 7.24 (t, $^3J_{H-H}$ = 7.3 Hz, 2H, C**H**-Ph$_{meta}$), 7.26 (d, $^3J_{H-H}$ = 1.8 Hz, 1H, =C**H**), 7.33 (t, $^3J_{H-H}$ = 7.1 Hz, 1H, C**H**-Ph$_{para}$) ppm.

^{13}C{^{1}H} NMR (100 MHz, CD$_2$Cl$_2$, 298 K): δ 22.7, 24.1, 24.6 and 25.7 (CH(C**C**H$_3$)$_2$), 29.9 (s+d, $^2J_{Pt-C}$ = 44 Hz, **C**H$_2$-Si), 32.4 (C**C**H$_3$), 32.5 (C(**C**H$_3$)$_3$), 32.9 (C**C**H$_3$), 54.5 and 54.8 (**C**H(CH$_3$)$_2$), 59.4 and 61.7 (**C**(CH$_3$)$_3$), 116.6,

[407]

Experimental Part

117.8, 118.9 and 120.8 (=CH), 128.6 ($\mathbf{Ph}_{meta}$), 130.4 ($\mathbf{Ph}_{para}$), 134.4 ($\mathbf{Ph}_{ortho}$), 136.8 ($\mathbf{Ph}_{ipso}$), 174.9 and 181.7 (Pt-$\mathbf{C}_{carbene}$) ppm.

^{29}Si{^{1}H} NMR (79 MHz, CD$_2$Cl$_2$, 298 K) δ -10.8 (s+d, $^1J_{Pt-Si}$ = 1577 Hz, Ph$\mathbf{Si}$HPt) ppm.

Elem. Anal. Calcd. for C$_{58}$H$_{53}$BF$_{24}$N$_4$PtSi: C, 46.57; H, 3.57; N, 3.75. Found: C, 46.4; H, 3.7; N, 3.7

Complex [Pt(IMesSiH^{n}Bu')(IMes)][BAr$_4^F$] (26)
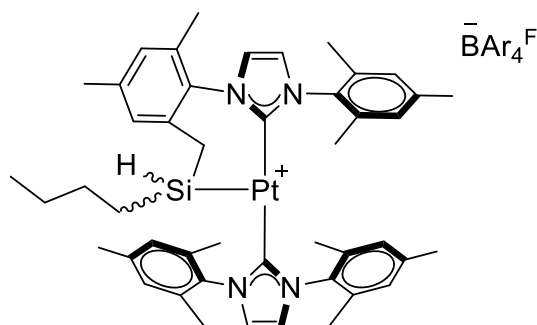
Spectroscopic and analytical data

Yellow solid.

Molecular weight: 1752.38 g/mol.

Yield: 68 % (68 mg, 0.039 mmol).

^{1}H-NMR (400 MHz, CD$_2$Cl$_2$, 298 K) δ -0.58 and 0.14 (m, 1H each, SiCH_2(CH$_2$)$_2$CH$_3$), 0.79 (t, $^3J_{H-H}$ = 7.2 Hz, 3H, CH_3(CH$_2$)$_3$Si), 0.95 (m, 2H, CH_2), 1.08 (m, 2H, CH_2), 1.52 (dd, $^2J_{H-H}$ = 12.7 Hz, $^3J_{H-H}$ = 6.3 Hz, 1H, Si-CH_aH_b), 1.64 (s, 6H, CH_3), 1.77 and 1.82 (s, 3H each, CH_3), 1.89 (m, 1H, Si-CH$_a$$H_b$), 1.95 (s, 6H, C$H_3$), 2.05 (s, 3H, C$H_3$), 2.36 (s, 6H, C$H_3$), 2.43 and 2.44 (s, 3H each, CH_3), 2.91 (t+d, $^3J_{H-H}$ = 6.3 Hz, $^2J_{Pt-H}$ = 160 Hz, 1H, SiH), 6.78 (s, 2H, CH-Mes), 6.87 (s, 1H, CH-Mes),

6.93 (s, 2H, C*H*-Mes), 6.95 (s, 1H, C*H*-Mes), 7.00 (br, 3H, 2=C*H* + C*H*-Mes), 7.05 (d, $^3J_{H-H}$ = 1.3 Hz, 1H, =C*H*), 7.09 (d, $^3J_{H-H}$ = 1.3 Hz, 1H, =C*H*), 7.14 (s, 1H, C*H*-Mes) ppm.

^{13}C{^{1}H} NMR (100 MHz, CD$_2$Cl$_2$, 298 K) δ 13.8 (*C*H$_3$(CH$_2$)$_3$Si), 16.3 (CH$_2$*C*H$_2$Si), 17.8 and 18.2 (*C*H$_3$), 18.3 (3 *C*H$_3$), 18.7 and 21.2 (*C*H$_3$), 21.2 (3 *C*H$_3$), 22.7 (Si-*C*H$_2$), 26.3 and 28.0 (*C*H$_2$), 122.8 (=*C*H), 123.7 (br, 3 =*C*H), 127.2 and 128.7 (*C*H-Mes), 129.5 (2 *C*H-Mes), 129.7 (*C*H-Mes), 130.0 (2 *C*H-Mes), 130.2 (*C*H-Mes), 133.2, 133.9, 134.5, 134.6 (*C*$_q$-Mes), 134.8 (3 *C*$_q$-Mes), 134.9 (*C*$_q$-Mes), 135.3 (br, C$_{ortho}$-BAr$_4$^{F} + *C*$_q$-Mes), 135.6 (2 *C*$_q$-Mes) 137.3 and 139.7 (*C*$_q$-Mes), 140.1 (2 *C*$_q$-Mes), 140.5 (*C*$_q$-Mes), 181.8 and 186.5 (Pt-*C*$_{carbene}$) ppm.

^{29}Si{^{1}H} NMR (79 MHz, CD$_2$Cl$_2$, 298 K) δ 9.0 (s+d, $^1J_{Pt-Si}$ ∼ 1360 Hz, ^{n}Bu*Si*HPt) ppm.

Elem. Anal. Calcd. for C$_{78}$H$_{69}$BF$_{24}$N$_4$PtSi: C, 53.46; H, 3.97; N, 3.20. **Found**: C, 53.3; H, 4.3; N, 3.1

Complex [Pt(IMesSiHPh')(IMes)][BAr$_4$^{F}] (27)

Spectroscopic and analytical data

Yellow solid.

Molecular weight: 1772.37 g/mol.

[409]

Experimental Part

Yield: 70 % (71 mg, 0.040 mmol).

^{1}H-NMR (400 MHz, CD$_2$Cl$_2$, 298 K) δ 1.49 (dd, $^2J_{\text{H-H}}$ = 12.8 Hz, $^3J_{\text{H-H}}$ = 6.9 Hz, Si-C$\boldsymbol{H}_a$H$_b$), 1.68 (s, 3H, C$\boldsymbol{H}_3$), 1.80 and 1.81 (s, 6H each, C$\boldsymbol{H}_3$), 1.91 (s, 3H, C$\boldsymbol{H}_3$), 2.0-2.03 (m, 4H, C$\boldsymbol{H}_3$ + Si-CH$_a\boldsymbol{H}_b$), 2.26 (s, 6H, C$\boldsymbol{H}_3$), 2.47 and 2.55 (s, 3H each, C$\boldsymbol{H}_3$), 3.57 (d+d, $^3J_{\text{H-H}}$ = 6.9 Hz, $^2J_{\text{Pt-H}}$ = 165 Hz, 1H, Si$\boldsymbol{H}$), 6.53 and 6.69 (s, 2H each, C$\boldsymbol{H}$-Mes), 6.81 (d, $^3J_{\text{H-H}}$ = 7.3 Hz, 2H, C$\boldsymbol{H}$-Ph$_{ortho}$), 6.95 (t, $^3J_{\text{H-H}}$ = 7.3 Hz, 2H, C$\boldsymbol{H}$-Ph$_{meta}$), 6.97 (br, 4H, 2 =C$\boldsymbol{H}$ + 2 C$\boldsymbol{H}$-Mes), 7.06 (s, 2H, =C$\boldsymbol{H}$), 7.16 (s, 2H, C$\boldsymbol{H}$-Mes), 7.23 (t, $^3J_{\text{H,H}}$ = 7.3 Hz, 1H, C$\boldsymbol{H}$-Ph$_{para}$) ppm.

^{13}C{^{1}H} NMR (100 MHz, CD$_2$Cl$_2$, 298 K) δ 19.9 ($\boldsymbol{C}$H$_3$), 18.1 and 18.4 (2 $\boldsymbol{C}$H$_3$ each), 18.9 and 19.9 ($\boldsymbol{C}$H$_3$), 21.3 (4 $\boldsymbol{C}$H$_3$), 25.2 (Si-$\boldsymbol{C}$H$_2$), 123.0 and 123.9 (=$\boldsymbol{C}$H), 124.1 (2 =$\boldsymbol{C}$H), 126.4 ($\boldsymbol{C}$H-Mes), 127.5 ($\boldsymbol{C}$H-Ph$_{meta}$), 129.0 (=$\boldsymbol{C}$H), 129.1 ($\boldsymbol{C}$H-Ph$_{para}$), 129.5 (3 $\boldsymbol{C}$H-Mes), 129.8 (2 $\boldsymbol{C}$H-Mes), 130.5 and 130.9 ($\boldsymbol{C}$H-Mes), 133.1, 133.6 and 133.7 ($\boldsymbol{C}_q$-Mes), 134.0 ($\boldsymbol{C}_q$-Mes), 134.1 ($\boldsymbol{C}$H-Mes), 134.2 ($\boldsymbol{C}$H-Ph$_{ortho}$), 134.3 ($\boldsymbol{C}_q$-Mes), 134.5 and 134.6 (2 $\boldsymbol{C}_q$-Mes), 135.0 ($\boldsymbol{C}_q$), 136.3 ($\boldsymbol{C}_q$-Mes), 139.8 (3 $\boldsymbol{C}_q$-Mes), 140.5 (1 $\boldsymbol{C}_q$-Mes), 181.6 and 185.4 (Pt-$\boldsymbol{C}_{carbene}$) ppm.

^{29}Si{^{1}H} NMR (79 MHz, CD$_2$Cl$_2$, 298 K) δ -0.5 (s+d, $^1J_{\text{Pt-Si}}$ ∼ 1500 Hz, Ph$\boldsymbol{Si}$HPt) ppm.

Elem. Anal. Calcd. for C$_{80}$H$_{65}$BF$_{24}$N$_4$PtSi: C, 54.21; H, 3.70; N, 3.16. **Found**: C, 54.0; H, 3.9; N, 3.1.

[410]

Complex [Pt(IMes*SiH*n*Bu')(IMes*)][BAr₄*F*] (28)

Spectroscopic and analytical data

Yellow solid.

Molecular weight: 1808.49 g/mol.

Yield: 91 % (94 mg, 0.052 mmol).

¹H-NMR (400 MHz, CD₂Cl₂, 298 K): δ -0.53 and 0.18 (m, 1H, CH₂C*H₂*Si), 0.80 (t, 3H, $^3J_{H\text{-}H}$=7.3 Hz, C*H₃*CH₂), 1.00 and 1.13 (m, 2H each, CH₃C*H₂*CH₂), 1.48 (dd, 1H, $^2J_{H\text{-}H}$=12.2 Hz, $^3J_{H\text{-}H}$=6.6 Hz, MesC*H*ₐHᵦSi), 1.54 and 1.63 (s, 3H each, C*H₃*), 1.67 (s, 3H, =CC*H₃*), 1.72 (s, 6H, =CC*H₃*), 1.81 (br, 10H, C*H₃* + MesCHₐ*H*ᵦSi), 1.86 (s, 3H, =CC*H₃*), 1.97 (s, 3H, C*H₃*), 2.37 (s, 6H, C*H₃*), 2.41 and 2.43 (s, 3H each, C*H₃*), 2.90 (t+d, 1H, $^1J_{Si\text{-}H}$=165 Hz, $^3J_{H\text{-}H}$=6.5 Hz, Si*H*), 6.79 (s, 2H, C*H*-Mes), 6.83 and 6.85 (s, 1H each, C*H*-Mes), 6.91 (s, 2H, C*H*-Mes), 6.98 and 7.13 (s, 1H, C*H*-Mes) ppm.

¹³C{¹H}-NMR (100 MHz, CD₂Cl₂, 298 K) δ 9.2 (2 =CC*H₃*), 9.2 (=CC*H₃*), 9.6 (=CC*H₃*), 14.0 (C*H₃*CH₂) , 17.0 (C*H₃*), 17.5 (CH₂C*H₂*Si), 18.1 (2 C*H₃*), 18.3 (2 C*H₃*), 18.4 (2 C*H₃*), 21.5 (2 C*H₃*), 21.5 (2 C*H₃*), 22.8 (MesC*H₂*Si), 26.5 (C*H₃*CH₂), 28.3 (C*H₂*CH₂Si), 126.9, 127.0, 127.1 and 127.2 (=C*C*H₃), 128.5 (C*H*-Mes), 129.6 (3 C*H*-Mes), 129.7 (C*H*-Mes), 130.1 (2 C*H*-Mes), 130.2 (C*H*-Mes), 131.7 (C*q*-Mes), 133.2

[411]

Experimental Part

(2 C_q-Mes), 133.5, 134.8, 135.7, 135.8 (C_q-Mes), 136.1 (2 C_q-Mes), 138.1, 139.4 (C_q-Mes), 139.8 (2 C_q-Mes), 140.3 (C_q-Mes), 179.0 and 184.8 (Pt-$C_{carbene}$) ppm.

^{29}Si{^{1}H}-NMR (79 MHz, CD$_2$Cl$_2$, 298 K) δ 7.9 (^{n}BuSiHPt) ppm.

Elem. Anal. Calcd. for C$_{82}$H$_{77}$BF$_{24}$N$_4$PtSi: C, 54.46; H, 4.29; N, 3.10. **Found**: C, 54.2; H, 4.4; N, 2.9 (There is 5% of silyl complex **37** in the sample, see below).

A small amount (~5%) of complex **37** ([Pt(IMes*)$_2$SiH$_2$^{n}Bu][BAr$_4$^{F}], see below) is observed in the synthesis of species **28**. This phenomenon can be explained by a) C−H coupling process competing with the C−Si formation reaction, or b) Partial hydrogenation of **25** in the presence of small amounts of hydrogen generated from adventitious water in the solvent (which originates hydride **34**) followed by reaction with ^{n}BuSiH$_3$ to give complex **37**.

Complex [Pt(IMes*SiHPh')(IMes*)][BAr$_4$^{F}] (29)

Spectroscopic and analytical data
Yellow solid.
Molecular weight: 1828.48 g/mol.
Yield: 98 % (104 mg, 0.057 mmol).

¹H-NMR (400 MHz, CD₂Cl₂, 298 K) δ 1.46 (dd, 1H, $^2J_{H-H}$=12.3 Hz, $^3J_{H-H}$=6.9 Hz, MesCH_aH$_b$Si), 1.49 (s, 3H, CH_3), 1.61, 1.63 and 1.70 (s, 6H each, CH_3), 1.71, 1.80, 1.81 and 1.90 (s, 3H each, =CCH_3), 1.94 (d, 1H, $^2J_{H-H}$=12.3 Hz Hz, MesCH$_a$$H_b$Si), 2.30 (s, 6H, C$H_3$), 2.45 and 2.53 (s, 3H each, CH_3), 3.56 (d+d+d, 1H, $^1J_{Si-H}$=205.8 Hz, $^2J_{Pt-H}$=168.2 Hz, $^3J_{H-H}$=6.3 Hz, SiH), 6.49 (s, 2H, CH-Mes), 6.73 (s, 2H, CH-Mes), 6.78 (m, 2H, CH-Ph$_{ortho}$) 6.86 and 6.92 (s, 1H, CH-Mes), 6.92 (t, 2H, $^3J_{H-H}$ = 7.5 Hz, CH-Ph$_{meta}$) 7.09 and 7.11 (s, 1H, CH-Mes), 7.21 (tt, 1H, $^3J_{H-H}$=7.4 Hz, $^4J_{H-H}$=1.2 Hz, CH-Ph$_{para}$) ppm.
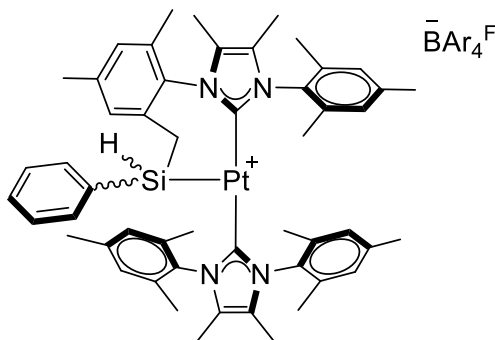
¹³C{¹H}-NMR (100 MHz, CD₂Cl₂, 298 K) δ 9.2 (2 =CCH_3), 9.3 (=CCH_3), 9.6 (=CCH_3), 17.6 (CH_3), 18.1 (2 CH_3), 18.4 (2 CH_3), 19.1 (CH_3), 19.4 (CH_3), 21.6 (4 CH_3), 25.5 (MesCH_2Si), 127.2 (=CCH$_3$), 127.4 (CH-Ph$_{meta}$), 127.6 (2 =CCH$_3$), 127.7 (=CCH$_3$), 128.9 (2 CH-Mes), 128.9 (CH-Ph$_{para}$), 129.8 (2 CH-Mes), 129.9 (2 CH-Mes), 130.1 (CH-Mes), 130.4 (CH-Mes), 131.6 (C_q-Mes), 133.1 (C_q-Mes), 133.7 (C-Ph$_{ipso}$), 134.7 (4 C_q-Mes), 134.8 (CH-Ph$_{ortho}$), 135.2 (4 C_q-Mes), 136.2 (C_q-Mes), 136.9 (C_q-Mes), 139.5 (C_q-Mes), 139.6 (2 C_q-Mes), 140.3 (C_q-Mes), 178.9 and 183.8 (Pt-$C_{carbene}$) ppm.

²⁹Si-NMR (79 MHz, CD₂Cl₂, 298 K) δ -1.6 (PhSiHPt) ppm.

Elem. Anal. Calcd. for $C_{84}H_{73}BF_{24}N_4PtSi$: C, 55.18; H, 4.02; N, 3.06. **Found**: C, 55.3; H, 4.1; N, 3.0.

[413]

Experimental Part

Synthesis of Pt hydride complexes

Complex [Pt(H)(I*t*Bu*i*Pr)₂][BAr₄*F*] (30)
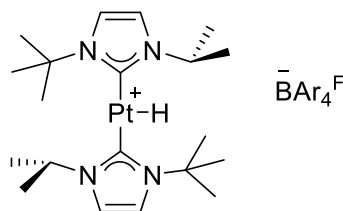
Synthesis

Complex [Pt(I*t*Bu*i*Pr')(I*t*Bu*i*Pr)][BAr₄*F*], **19**, (80 mg, 0.057 mmol) was dissolved in 0.6 mL of CD_2Cl_2 in a J. Young NMR tube with a screw cap, after which it was charged with H_2 (3 bar). The initial yellow solution became nearly colourless in around 20 min. The ¹H NMR spectrum, recorded at room temperature, indicated full conversion to complex **30**. This compound is unstable under vacuum (releasing a molecule of H_2 and regenerating compound **19**) and has been characterized in solution by NMR.

Spectroscopic and analytical data

Colourless solution in dichlorometane.

Molecular weight: 1391.85 g/mol.

¹H-NMR (400 MHz, CD₂Cl₂, 298 K) δ -25.06 (s+d, 1H, $^1J_{Pt-H}$ = 2496 Hz, Pt-*H*), 1.45 (d, $^3J_{H-H}$ = 6.8 Hz, 12H, CH(C*H₃*)₂), 1.76 (s, 18H, (C*H₃*)₃), 5.37 (sept, $^3J_{H-H}$ = 6.8 Hz, 2H, C*H*(CH₃)₂), 7.06 (d, $^3J_{H-H}$ = 1.8 Hz, 2H, =C*H*), 7.15 (d, $^3J_{H-H}$ = 1.8 Hz, 2H, =C*H*) ppm.

[414]

^{13}C{^{1}H} NMR (100 MHz, CD$_2$Cl$_2$, 298 K) δ 23.1 (CH(CH$_3$)$_2$), 30.0 (C(CH$_3$)$_3$), 55.0 (s+d, $^3J_{Pt-C}$ = 31 Hz, CH(CH$_3$)$_2$), 58.8 (C(CH$_3$)$_3$), 116.3 (s+d, $^3J_{Pt-C}$ = 14 Hz, 2 =CH), 119.8 (s+d, $^3J_{Pt-C}$ = 15 Hz, 2 =CH), 171.2 (Pt-C$_{carbene}$) ppm.

Synthesis of Pt silyl complexes from hydride complexes and primary silanes

General Synthesis

Cyclometallated complex **19** (0.058 mmol) was dissolved in 0.4 mL of CD$_2$Cl$_2$ in a J. Young NMR tube with a screw cap. Then, H$_2$ (3 bar) was charged so as to form the corresponding platinum hydride derivative [Pt(H)(NHC)$_2$][BAr$_4$^{F}]. After 30 min, this solution was transferred via cannula to a solution of the silane RSiH$_3$ (0.059 mmol) in 0.2 mL of CD$_2$Cl$_2$. Gas evolution (H$_2$) is then observed and the solution became progressively bright yellow. After stirring for 30 min (**32**), 4h (**31**) or 30 min (**35-38**) the volatiles were removed under vacuum and the yellow residue washed with pentane (2 x 5 mL) to give the corresponding platinum silyl compound [Pt(SiR$_3$)(NHC)$_2$][BAr$_4$^{F}] as an intense yellow solid. [Pt(SiR$_3$)(IMes)$_2$][BAr$_4$^{F}] and [Pt(SiR$_3$)(IMes*)$_2$][BAr$_4$^{F}] complexes can be crystalized by slow diffusion of pentane (for the former ones) or hexamethyldisiloxane (for the latter ones) into a concentrated solution of the corresponding complex in dichloromethane.

Complex [Pt(SiH$_2$^{n}Bu)(I^{t}Bu^{i}Pr)$_2$][BAr$_4$^{F}] (31)

[415]
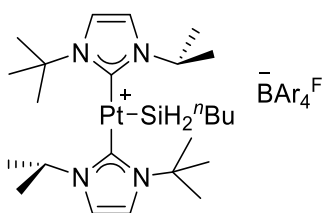
Experimental Part

Spectroscopic and analytical data

Yellow solid.

Molecular weight: 1478.06 g/mol.

^{1}H-NMR (300 MHz, CD$_2$Cl$_2$, 298 K) δ 0.53 (m, 2H, SiC**H**$_2$), 0.77 (t, $^3J_{H-H}$ = 7.0 Hz, C**H**$_3$(CH$_2$)$_3$Si), 1.14-1.23 (m, 4H, C**H**$_2$), 1.50 (d, $^3J_{H-H}$ = 7.0 Hz, 12H, CH(C**H**$_3$)$_2$), 1.90 (s, 18H, (C**H**$_3$)$_3$), 3.07 (t+d, $^3J_{H-H}$ = 3.8 Hz, $^2J_{Pt-H}$ = 113 Hz, 2H, Si**H**$_2$), 5.65 (sept, $^3J_{H-H}$ = 6.8 Hz, 2H, C**H**(CH$_3$)$_2$), 7.06 (d, $^3J_{H-H}$ = 2.0 Hz, 2H, =C**H**), 7.20 (d, $^3J_{H-H}$ = 2.0 Hz, 2H, =C**H**) ppm.

^{13}C{^{1}H} NMR (100 MHz, CD$_2$Cl$_2$, 298 K) δ 13.7 (CH$_2$**C**H$_3$), 23.5 (CH(**C**H$_3$)$_2$), 25.9 (**C**H$_2$), 28.3 and 30.6 (br, **C**H$_2$), 32.8 (C(**C**H$_3$)$_3$), 54.5 (**C**H(CH$_3$)$_2$), 59.4 (**C**(CH$_3$)$_3$), 116.2 (br, =**C**H), 120.9 (br, =**C**H), 179.5 (Pt-**C**$_{carbene}$) ppm.

^{29}Si{^{1}H} NMR (79 MHz, CD$_2$Cl$_2$, 298 K) δ -28.5 (s+d, $^1J_{Pt-Si}$ ~ 1450 Hz, ^{n}Bu**Si**H$_2$Pt) ppm.

There is *ca*. 20% of the imidazolium salt I^{t}Bu^{i}Pr·HBAr^F present together with the silyl complex. All attempts to remove it by washing with pentane or through crystallization were unsuccessful, precluding its obtention in pure form.

Complex [Pt(SiH$_2$Ph)(I^{t}Bu^{i}Pr)$_2$][BAr$_4$^{F}] (32)
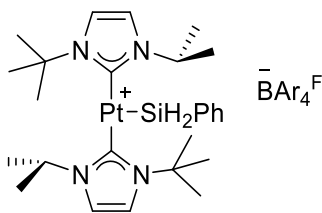
[416]

Spectroscopic and analytical data

Yellow solid.

Molecular weight: 1498.05 g/mol.

^{1}H-NMR (400 MHz, CD$_2$Cl$_2$, 298 K) δ 1.42 (d, $^3J_{\text{H-H}}$ = 6.5 Hz, 12H, CH(C**H**$_3$)$_2$), 1.83 (s, 18H, C(C**H**$_3$)$_3$), 3.77 (s+d, $^2J_{\text{Pt-H}}$ = 115 Hz, 2H, Si**H**$_2$), 5.61 (sept, $^3J_{\text{H-H}}$ = 6.5 Hz, 2H, C**H**(CH$_3$)$_2$), 7.00 (d, $^3J_{\text{H-H}}$ = 7.3 Hz, CH-Ph$_{ortho}$), 7.06 (m, 2H, =C**H**), 7.18 (t, $^3J_{\text{H-H}}$ = 7.3 Hz, 2H, C**H**-Ph$_{meta}$), 7.21 (m, 2H, =C**H**), 7.30 (t, $^3J_{\text{H-H}}$ = 7.3 Hz, 1H, C**H**-Ph$_{para}$) ppm.

^{13}C{^{1}H} NMR (100 MHz, CD$_2$Cl$_2$, 298 K) δ 23.6 (CH(**C**H$_3$)$_2$), 32.8 (C(**C**H$_3$)$_3$), 54.7 (**C**H(CH$_3$)$_2$), 59.6 (**C**(CH$_3$)$_3$), 116.5 (=**C**H), 121.2 (=**C**H), 128.7 (**Ph**$_{meta}$), 130.3 (**Ph**$_{para}$), 134.6 (**Ph**$_{ortho}$), 178.2 (Pt-**C**$_{\text{carbene}}$) ppm. Ph$_{ipso}$ was not observed

^{29}Si{^{1}H} NMR (79 MHz, CD$_2$Cl$_2$, 298 K) δ -38.1 (s+d, $^1J_{\text{Pt-Si}}$ ~ 1560 Hz, Ph**Si**H$_2$Pt) ppm.

There is *ca*. 12% of the imidazolium salt I^{t}Bu^{i}Pr·HBAr^F present together with the silyl complex. All attempts to remove it by washing with pentane or through crystallization were unsuccessful, precluding its obtention in pure form.

[417]

Experimental Part

Complex [Pt(SiH$_2$^{n}Bu)(IMes)$_2$][BAr$_4$^{F}] (35)
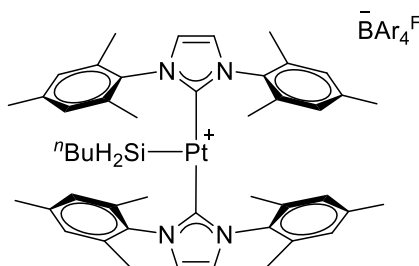
Spectroscopic and analytical data

Yellow solid.

Molecular weight: 1754.39 g/mol

Yield: 69% (70 mg, 0.040 mmol).

^{1}H-NMR (400 MHz, CD$_2$Cl$_2$, 298 K) δ -0.07 (m, 2H, Si-CH_2), 0.76 (t, $^3J_{H-H}$ = 7.3 Hz, 3H, CH_3(CH$_2$)$_3$Si), 0.85 (m, 2H, CH_2), 1.08 (m, 2H, CH_2), 1.83 (s, 24H, CH_3), 2.01 (m+d, $^2J_{Pt-H}$ ~ 100 Hz, 2H, SiH_2), 2.41 (s, 12H, CH_3), 6.99 (s, 8H, CH-Mes), 7.02 (s, 4H, =CH) ppm.

^{13}C{^{1}H} NMR (100 MHz, CD$_2$Cl$_2$, 298 K) δ 13.7 (CH_3), 14.9 (CH$_2$CH_2Si), 18.5 (CH_3), 21.2 (CH_3), 26.0 and 28.1 (CH_2), 124.2 (=CH), 130.0 (CH-Mes), 134.9 (C$_q$-Mes), 135.2 (C$_q$-Mes), 140.3 (C$_q$-Mes), 184.4 (Pt-C$_{carbene}$) ppm.

^{29}Si{^{1}H} NMR (79 MHz, CD$_2$Cl$_2$, 298 K) δ -24.2 (^{n}BuSiH$_2$Pt) ppm.

Elem. Anal. Calcd. for C$_{78}$H$_{71}$BF$_{24}$N$_4$PtSi: C, 53.40; H, 4.08; N, 3.19. **Found**: C, 53.2; H, 4.1; N, 3.1

[418]

Complex [Pt(SiH₂Ph)(IMes)₂][BAr₄ᶠ] (36)
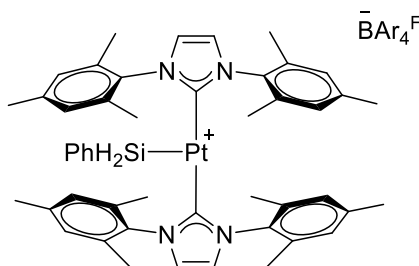
Spectroscopic and analytical data

Yellow solid.

Molecular weight: 1774.38 g/mol.

Yield: 64% (66 mg, 0.037 mmol).

¹H-NMR (400 MHz, CD₂Cl₂, 298 K) δ 1.76 (s, 24H, C$\boldsymbol{H}_3$), 2.42 (s, 12H, C$\boldsymbol{H}_3$), 2.56 (s+d, $^2J_{\text{Pt-H}}$ = 108 Hz, 2H, Si$\boldsymbol{H}_2$), 6.96 (s, 8H, C$\boldsymbol{H}$-Mes), 6.98-7.00 (m, 6H, C$\boldsymbol{H}$-Ph$_{meta}$ and =C$\boldsymbol{H}$), 7.21 (t, $^3J_{\text{H-H}}$ = 7.4 Hz, 1H, C$\boldsymbol{H}$-Ph$_{para}$) ppm.

¹³C{¹H} NMR (100 MHz, CD₂Cl₂, 298 K) δ 18.5 ($\boldsymbol{C}$H₃), 21.3 ($\boldsymbol{C}$H₃), 124.2 (=$\boldsymbol{C}$H), 127.4 ($\boldsymbol{C}$H-Ph$_{meta}$), 129.7 ($\boldsymbol{C}$H-Ph$_{para}$), 130.1 ($\boldsymbol{C}$H-Mes), 132.2 ($\boldsymbol{Ph}_{ipso}$), 134.8 ($\boldsymbol{C}$H-Ph$_{ortho}$), 135.2 ($\boldsymbol{C}_q$-Mes), 135.3 (br, C$_{ortho}$-BAr^F + $\boldsymbol{C}_q$-Mes), 140.5 ($\boldsymbol{C}_q$-Mes), 183.1 (Pt-$\boldsymbol{C}_{\text{carbene}}$) ppm.

²⁹Si{¹H} NMR (79 MHz, CD₂Cl₂, 298 K) δ -34.3 (s+d, $^1J_{\text{Pt-Si}}$ ~ 1400 Hz, Ph$\boldsymbol{Si}$H₂Pt) ppm.

Elem. Anal. Calcd. for C₈₀H₆₇BF₂₄N₄PtSi: C, 54.15; H, 3.81; N, 3.16. **Found**: C, 54.1; H, 3.9; N, 3.2

[419]

Experimental Part

Complex [Pt(SiH₂*ⁿ*Bu)(IMes*)₂][BAr₄*ᶠ*] (37)
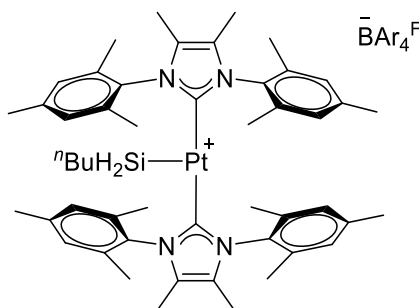
Spectroscopic and analytical data

Yellow solid.

Molecular weight: 1810.50 g/mol.

Yield: 83% (87 mg, 0.048 mmol).

¹H-NMR (400 MHz, CD₂Cl₂, 298 K) δ 0.02 (m, 2H, SiCH_2(CH₂)₂CH₃), 0.78 (t, $^3J_{\text{H-H}}$ = 7.2 Hz, 3H, CH_3(CH₂)₃Si), 0.93 (m, 2H, CH₂CH_2CH₂), 1.13 (sext, $^3J_{\text{H-H}}$ = 7.2 Hz, 2H, CH₃CH_2), 1.72 (s, 24H, CH_3), 1.74 (s, 12H, CH_3), 2.03 (t+d, 2H, $^3J_{\text{H-H}}$ = 4.5 Hz, $^2J_{\text{Pt-H}}$ ~ 100 Hz, SiH_2), 2.42 (s, 12H, CH_3), 6.96 (s, 8H, CH-Mes) ppm.

¹³C{¹H}-NMR (100 MHz, CD₂Cl₂, 298 K) δ 9.3 (=CCH₃), 13.9 (CH₂CH₃), 15.4 (CH₂Si), 18.5 (CH₃), 21.5 (CH₃), 26.3 (CH₂), 28.3 (CH₂), 127.5 (=CCH₃), 130.0 (CH-Mes), 133.6 (C_q-Mes), 135.9 (C_q-Mes), 140.1 (C_q-Mes), 182.5 (Pt-C_{carbene}) ppm.

²⁹Si{¹H} NMR (79 MHz, CD₂Cl₂, 298 K) δ -26.2 (*ⁿ*BuSiH₂Pt) ppm.

Elem. Anal. Calcd. for C₈₂H₇₉BF₂₄N₄PtSi: C, 54.40; H, 4.40; N, 3.09. **Found**: C, 53.94; H, 4.30; N, 2.94

[420]

Complex [Pt(SiH₂Ph)(IMes*)₂][BAr₄^F] (38)
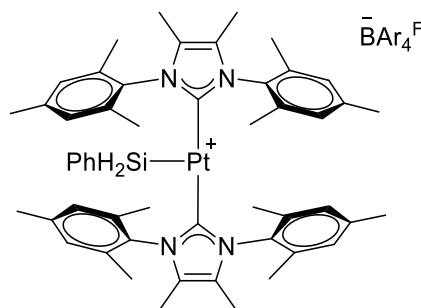
Spectroscopic and analytical data

Yellow solid.

Molecular weight: 1830.49 g/mol.

Yield: 92% (97 mg, 0.053 mmol)

¹H-NMR (400 MHz, CD₂Cl₂, 298 K) δ 1.64 (s, 24H, C**H**₃), 1.70 (s, 12H, C**H**₃), 2.42 (s, 12H, C**H**₃), 2.48 (s+d, $^2J_{Pt-H}$ = 103 Hz, 2H, Si**H**₂), 6.76 (d, $^3J_{H-H}$ = 7.4 Hz, 2H, C**H**-Ph$_{ortho}$), 6.94 (s, 8H, C**H**-Mes), 6.99 (t, $^3J_{H-H}$ = 7.4 Hz, 2H, C**H**-Ph$_{meta}$), 7.21 (t, $^3J_{H-H}$ = 7.4 Hz, 1H, C**H**-Ph$_{para}$) ppm.

¹³C{¹H} NMR (100 MHz, CD₂Cl₂, 298 K) δ 9.1 (=C**C**H₃), 18.3 (**C**H₃), 21.3 (**C**H₃), 127.1 (**C**H-Ph$_{meta}$), 127.5 (=**C**CH₃), 129.4 (**C**H-Ph$_{para}$), 130.0 (**C**H-Mes), 133.3 (**C**$_q$-Mes), 133.5 (**Ph**$_{ipso}$), 135.5 (**C**H-Ph$_{ortho}$), 135.9 (**C**$_q$-Mes), 140.2 (**C**$_q$-Mes), 181.0 (Pt-**C**$_{carbene}$) ppm.

²⁹Si{¹H} NMR (79 MHz, CD₂Cl₂, 298 K) δ -35.7 (s+d, $^1J_{Pt-Si}$ ~ 1430 Hz, Ph**Si**H₂Pt) ppm.

Elem. Anal. Calcd. for C₈₄H₇₅BF₂₄N₄PtSi: C, 55.12; H, 4.13; N, 3.06. **Found**: C, 55.2; H, 4.4; N, 3.1

[421]

Experimental Part

Low temperature NMR studies: Characterization of σ-SiH complexes with primary silanes.

Complex [Pt(I^{t}Bu^{i}Pr')(I^{t}Bu^{i}Pr)(H$_3$SiPh)][BAr$_4^F$] (19·PhSiH$_3$)
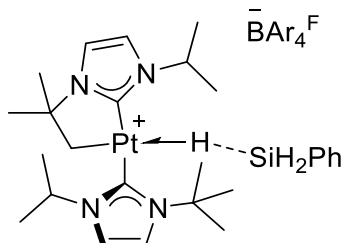
Synthesis

Complex **19** (60 mg, 0.043 mmol) was dissolved in 0.4 mL of CD$_2$Cl$_2$ in a screw-cap NMR tube. The solution was cooled to -80 °C and a solution of PhSiH$_3$ (5.9 μL, 0.047 mol) was injected. The sample was analyzed by NMR in a pre-cooled (-80 °C) NMR apparatus increasing the temperature at intervals of 10 °C.

Spectroscopic and analytical data

Pale-yellow solution.

Molecular weight: 1498.05 g/mol.

^{1}H-NMR (400 MHz, CD$_2$Cl$_2$, 248 K) δ -4.79 (s+d, $^1J_{Pt-H}$ = 435.5 Hz, $^1J_{Si-H}$ = 74 Hz, Pt-***H***-Si), 1.06 (d, $^3J_{H-H}$ = 6.1 Hz, 3H, CH(C***H***$_3$)$_2$), 1.21 (d, $^3J_{H-H}$ = 6.1 Hz, 3H, CH(C***H***$_3$)$_2$), 1.34 (d, $^3J_{H-H}$ = 6.1 Hz, 3H, CH(C***H***$_3$)$_2$), 1.45 (s, 3H, CC***H***$_3$), 1.49 (d, $^3J_{H-H}$ = 6.1 Hz, 3H, CH(C***H***$_3$)$_2$), 1.56 (s, 3H, CC***H***$_3$), 1.65 (s, 9H, (C***H***$_3$)$_3$), 2.08 (d+d, $^2J_{H-H}$= 12.6 Hz, $^2J_{Pt-H}$ = 85.5 Hz, 1H, Pt-C***H***$_a$H$_b$), 2.46 (d+d, $^2J_{H-H}$= 12.6 Hz, $^2J_{Pt-H}$ = 53.5 Hz, 1H, Pt-CH$_a$***H***$_b$), 4.28 (sept, $^3J_{H-H}$ = 6.1 Hz, 1H, C***H***(CH$_3$)$_2$), 5.14 (sept, $^3J_{H-H}$ = 6.1 Hz, 1H, C***H***(CH$_3$)$_2$), 5.35 (m, 2H, Si***H***$_{2(terminal)}$), 6.98 (br, 1H, =C***H***), 7.08 (br, 2H, =C***H***), 7.24-7.34 (br m, 5 H, ***Ph***, =C***H***), 7.37 (br, 1H, C***H***-Ph$_{para}$) ppm.

[422]

^{13}C{^{1}H}-NMR (100 MHz, CD$_2$Cl$_2$, 193 K) δ 20.6, 22.7, 23.7, 24.2 and 28.4 (***C**H$_3$), 30.4 (C(***C**H$_3$)$_3$), 31.5 (***C**H$_3$), 42.9 (Pt-***C**H$_2$), 52.4 and 52.7 (***C**H(CH$_3$)$_2$), 58.2 and 65.4 (***C**(CH$_3$)$_3$), 116.1, 116.4, 117.9 and 120.9 (=***C**H), 127.7, 128.5, 129.5, 130.1, 133.9 and 135.4 (***Ph***), 161.3 and 164.1 (Pt-***C**_{carbene}) ppm.

^{29}Si{^{1}H} NMR (79 MHz, CD$_2$Cl$_2$, 248 K) δ -51.8 (Pt-H-***Si***) ppm.

Complex [Pt(IMes*')(IMes*)(H$_3$Si^{n}Bu)][BAr$_4$^{F}] (25·^{n}BuSiH$_3$)
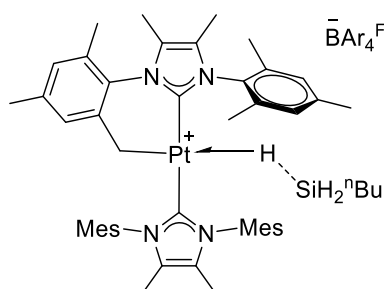
Synthesis

Complex **25** (60 mg, 0.035 mmol) was dissolved in 0.4 mL of CD$_2$Cl$_2$ in a screw-cap NMR tube. The solution was cooled to -78 °C and a solution of ^{n}BuSiH$_3$ (5.0 μL, 0.038 mmol) was injected. The sample was analyzed by NMR in a pre-cooled (-80 °C) NMR apparatus increasing the temperature at intervals of 10 °C.

Spectroscopic and analytical data

Pale-yellow solution.

Molecular weight: 1808.49 g/mol.

^{1}H-NMR (400 MHz, CD$_2$Cl$_2$, 263 K) δ -7.98 (d+d+d, $^2J_{H-H}$ = 3.0 Hz, $^1J_{Si-H}$ = 67 Hz, $^1J_{Pt-H}$ = 500 Hz, Pt-***H***-Si), -0.40 and -0.25 (m, 1H each, Si-C***H***$_2$), 0.58 (m, 1H, C***H***$_2$), 0.66 (t, $^3J_{H-H}$ = 7.2 Hz, C***H***$_3$(CH$_2$)$_3$Si), 0.76 (m, 1H, C***H***$_2$), 0.98 (m, 1H, C***H***$_2$), 1.28 (s, 3H, C***H***$_3$), 1.36 (m, 1H, C***H***$_2$), 1.67 (s, 6H, 2 C***H***$_3$), 1.76 (s, 3H, C***H***$_3$), 1.89 (s, 6H, 2 C***H***$_3$), 1.93 (s, 9H, 3 C***H***$_3$), 2.07, 2.10 and 2.20 (s, 3H each, C***H***$_3$), 2.35-2.45 (m, 10H,

[423]

Experimental Part

3 CH_3+ Pt-CH_aH$_b$), 2.62 (d+d, $^2J_{H-H}$ = 10.3 Hz, $^2J_{Pt-H}$ = 67 Hz, 1H, Pt-CH$_a$$H_b$), 3.18 (m, 1H, Si$H_aH_{b(terminal)}$), 3.95 (t+d, $^3J_{H-H}$ = 7.5 Hz, $^3J_{Pt-H}$ ~40 Hz, 1H, SiH$_a$$H_{b(terminal)}$), 6.38, 6.76, 6.78 and 6.95 (s, 1H each, CH-Mes), 6.98 and 7.02 (s, 2H each, CH-Mes) ppm.

^{29}Si{^{1}H} NMR (79 MHz, CD$_2$Cl$_2$, 263 K) δ -53.5 (Pt-H-Si) ppm.

Complex [Pt(H)(IMes*)$_2$(H$_3$Si^{n}Bu)][BAr$_4^F$] (34·^{n}BuSiH$_3$)
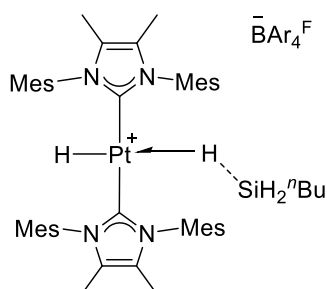
Synthesis

[Pt(IMes*')(IMes*)][BAr^F], **25** (40 mg, 0.023 mmol) was dissolved in 0.4 ml of CD$_2$Cl$_2$ in a J. Young NMR tube with a screw-cap. Then, H$_2$ (3 bar) was charged at r.t. After 30 min, the sample was degassed (freeze-pump-thaw) and was cooled down to -90 °C. A solution of ^{n}BuSiH$_3$ (4.5 μL, 0.035 mmol) in 0.2 mL of CD$_2$Cl$_2$ was added at -90 °C and the sample was analyzed by NMR in a pre-cooled (-90 °C) NMR apparatus increasing the temperature at intervals of 10 °C.

Spectroscopic and analytical data

Colorless solution.

Molecular weight: 1810.50 g/mol.

^{1}H-NMR (400 MHz, CD$_2$Cl$_2$, 183 K) δ -6.08 (d+d, $^2J_{H-H}$ = 17.0 Hz, $^1J_{Pt-H}$ = 1544.4 Hz, Pt-H), -5.55 (d+d, $^2J_{H-H}$ = 17.0 Hz, $^1J_{Pt-H}$ = 423.6 Hz, Pt-H-Si), 0.35 (br, 2H, CH_2), 0.77 (br, 3H, CH_3(CH$_2$)$_3$Si), 1.06 and 1.25 (br, 2H each, CH_2), 1.60 (s, 24H, CH_3),

1.36 and 2.36 (s, 12H each, CH_3), 3.72 (br, 2H, Si$H_{2(terminal)}$), 6.80 (s, 8H, CH-Mes) ppm.

^{29}Si{^{1}H} NMR (79 MHz, CD$_2$Cl$_2$, 183 K) δ -49.8 (Pt-H-**Si**) ppm.

Synthesis of PtIPr complexes (Molecular rotors)

Complex [Pt(D)(D·BD$_3$)(IPr)$_2$][BAr$_4^F$] (41)
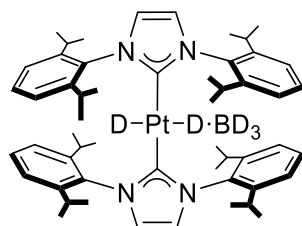
Synthesis

In the glovebox, a Schlenk flask was charged with **39-D** (215 mg, 0.177 mmol) and NaBD$_4$ (11.2 mg, 0.267 mmol, 1.5 eq). In the Schlenk line, THF (4 mL) was added to the mixture of solids, and the resulting suspension was stirred at r.t. After a few seconds, the yellow colour disappeared and the reaction mixture became colourless. It was stirred for 1 h, after which the solvent was removed under reduced pressure. The resulting solid was extracted with pentane (2 x 10 mL), and the resulting yellowish solution was evaporated under vacuum to give **41** as an off-white solid (165 mg, 0.166 mmol, 94% yield). The compound was deprotected without further characterization (see below).

Spectroscopic and analytical data

Off-white solid.

Molecular weight: 993.16 g/mol.

[425]

Experimental Part

¹H-NMR (400 MHz, C₆D₆, 25 ⁰C): δ 1.00 (d, $^3J_{\text{H-H}}$ = 7 Hz, 24H, CH(C**H**₃)₂), 1.15 (d, $^3J_{\text{H-H}}$ = 7 Hz, 24H, CH(C**H**₃)₂), 3.07 (sep, $^3J_{\text{H-H}}$ = 7 Hz, 8H, C**H**(CH₃)₂) 6.43 (s, 4 H, **H**C=), 7.04 (d, $^3J_{\text{H-H}}$ = 7.7 Hz, 8H, Ph-C**H**ₘ), 7.27 (t, $^3J_{\text{H-H}}$ = 7.7 Hz, 4H, Ph-C**H**ₚ) ppm. **¹¹B{¹H}-NMR (128 MHz, C₆D₆, 25 ⁰C):** δ -37.57 (bs, **B**D₃) ppm.

Complex [Pt(D)₂(IPr)₂][BAr₄ᶠ] (40)
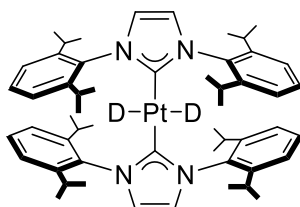
Synthesis (deprotection of 41)

In the glovebox, a Schlenk flask was charged with **41** (150 mg, 0.151 mmol). In the Schlenk line, toluene (3 mL) and Et₃N (1.8 mL, 12.91 mmol, 85 eq) were added. The resulting solution was stirred at 70 °C for 19 h, after which the solvent was removed under vacuum to give an off-white solid that was extracted with pentane at -40 °C (4 x 20 mL). The obtained solution was evaporated under reduced pressure, affording the desired compound as an off-white solid (122 mg, 0.125 mmol, 83% yield). X-Ray quality crystals can be grown by slow diffusion of hexamethyldisiloxane into a concentrated solution of **40-D** in dichloromethane (10:1).

Spectroscopic and analytical data
Off-white solid.
Molecular weight: 976.31 g/mol.

¹H-NMR (400 MHz, C₆D₆, 25 ⁰C): δ 1.09 (d, $^3J_{\text{H-H}}$ = 7 Hz, 24H, CH(C**H**₃)₂), 1.12 (d, $^3J_{\text{H-H}}$ = 7 Hz, 24H, CH(C**H**₃)₂), 2.94 (sep, $^3J_{\text{HH}}$ = 7 Hz, 8H, C**H**(CH₃)₂) 6.36 (s+d, $^4J_{\text{Pt-H}}$

[426]

= 5.8 Hz, 4 H, HC=), 7.06 (d, $^3J_{\text{H-H}}$ = 7.7 Hz, 8H, Ph-CH_{m}), 7.26 (t, $^3J_{\text{H-H}}$ = 7.7 Hz, 4H, Ph-CH_{p}) ppm.

^{13}C{^{1}H}-NMR (100 MHz, C$_6$D$_6$, 25 ^{0}C): δ 24.4 (CH(CH$_3$)$_2$), 24.8 (CH(CH$_3$)$_2$), 28.7 (CH(CH$_3$)$_2$), 122.1 (s+d, $^3J_{\text{Pt-C}}$ = 35 Hz, HC=), 123.7 (Ph-CH$_{\text{m}}$), 128.9 (Ph-CH$_{\text{p}}$), 138.5 (Ph-C_{ipso}), 146.3 (Ph-CH$_{\text{o}}$), 184.5 (s+d, $^1J_{\text{Pt-C}}$ = 1027.3 Hz, C_{carbene}) ppm.

Elem. Anal. Calcd. for C$_{54}$H$_{74}$D$_2$N$_4$Pt: C, 66.30; H, 8.04; N, 5.73. **Found**: C, 66.61; H, 7.80; N, 5.65.

Experimental Part for Chapter 4

CO$_2$ hydrosilation experiments

General procedure for a 0.5 mol % catalyst loading

An HPLC vial was charged with [Pt] (0.776 μmol), to which CD$_2$Cl$_2$ (0.4 mL) was added under argon by means of a microsyringe. The resulting solution was then transferred via cannula to a J. Young NMR tube, after which silane (20 μL, 155.2 μmol) was added. The NMR tube was charged with CO$_2$ (5 bar), and conversion to silyl formate at room temperature was obtained from the integration values in the ^{1}H NMR spectrum, using a relaxation delay (D1) of 10 seconds in the acquisition process. In the case of [PtH(I^{t}Bu)$_2$][BAr$_4$^{F}], **15**, the J. Young NMR tube was initially charged with [Pt(I^{t}Bu')(I^{t}Bu)][BAr$_4$^{F}], **13**, CD$_2$Cl$_2$ and H$_2$ (2 bar). Once the hydride complex was formed, the solution was degassed with 4 freeze-pump-thaw cycles and treated in the same way as in the other cases.

NMR characterization of the silyl formates

HCOOSiHEt$_2$

^{1}H-NMR (300 MHz, CD$_2$Cl$_2$, 298 K): δ 0.80-0.87 (m, 4H, C*H*$_2$CH$_3$), 0.88-1.05 (t, $^3J_{H-H}$ = 7.5 Hz, 6H, CH$_2$C*H*$_3$), 4.64 (quint, 1H, $^3J_{H-H}$ = 2.6 Hz, Si*H*), 8.11 (s, 1H, *H*COO) ppm.

^{13}C{^{1}H}-NMR (75 MHz, CD$_2$Cl$_2$, 298 K): δ 4.9 (*C*H$_3$CH$_2$), 6.5 (CH$_3$*C*H$_2$), 161.4 (H*C*OO) ppm**.**

^{29}Si{^{1}H}-NMR (79 MHz, CD$_2$Cl$_2$, 298 K): δ 13.3 (O-*Si*H-Et$_2$) ppm.

HCOOSiH2*n*Bu

¹H-NMR (300 MHz, CD$_2$Cl$_2$, 298 K): δ 0.88-0.93 (t, 3H, $^3J_{\text{H-H}}$ = 7.1 Hz, C*H*$_3$), 0.93-1.00 (m, 2H, C*H*$_2$) 1.32-1.48 (m, 4H, C*H*$_2$), 4.66 (t, 2H, $^3J_{\text{H-H}}$= 2.7 Hz, Si*H*), 8.10 (s, 1H, *H*COO) ppm.

¹³C{¹H}-NMR (75 MHz, CD$_2$Cl$_2$, 298 K): δ 10.7 (*C*H$_2$) 13.0 (*C*H$_3$), 25.3 (*C*H$_2$), 161.2 (H*C*OO) ppm.

²⁹Si{¹H}-NMR (79 MHz, CD$_2$Cl$_2$, 298 K): δ -10.8 (O-*Si*H$_2$-^{n}Bu) ppm.

Dehydrogenative coupling of silanes and amines
Synthetic procedures

General procedure for a catalytic reaction performed in a Man-on-the-Moon flask leading to either monosilazanes (RSiH$_2$(NR'R'')) or disilazanes (RSiH(NR'R'')$_2$). Example of a catalytic loading of 50 ppm.

In a typical procedure, a stock solution of complex **13** (1.35 mg in 1 mL of CH$_2$Cl$_2$ or CD$_2$Cl$_2$) is prepared immediately before used. Then, 10 µL of this solution (containing 9.5 x 10^{-6} mmol of **13**, 0.005 mol%) is placed, under argon, in a 35 mL round-bottom flask containing the amount of dichloromethane required to reach a total volume of 0.25 mL of solvent. The amine (0.185 mmol or 0.37 mmol) is then added, and the pressure inside the system is allowed to stabilize. Thereafter, 1 equivalent (0.185 mmol) of the corresponding silane is injected and the pressure inside the flask is measured at intervals of 1.38 s until no increase in the internal pressure is observed. Conversion values and characterization of the products were determined by ¹H NMR in reactions carried out in CD$_2$Cl$_2$.

[429]

Experimental Part

General procedure for a catalytic reaction performed in a 1 mmol scale leading to either monosilazanes (RSiH$_2$(NR'R'')) or disilazanes (RSiH(NR'R'')$_2$). Example of a catalytic loading of 50 ppm.

0.75 mg (5.3 x 10^{-4} mmol) of complex **13** are dissolved in 0.5 mL of CH$_2$Cl$_2$ under argon. Then, 47 µL of this solution (containing 5 x 10^{-5} mmol of **13**, 0.005 mol%) are diluted in 1 mL of CH$_2$Cl$_2$ in a J. Young tube, after which the amine (1 or 2 mmol, depending on the desired aminosilane) and the silane (1 mmol) are sequentially added (in this order). The reaction is stirred at r.t. until gas evolution ceases. At this point, several purification methods can be applied depending on the nature (and volatility) of the product:

a) The solvent is evaporated to dryness and the aminosilane is extracted with pentane (4 mL), filtering with a cannula. Evaporation of the solvent led to the corresponding silazane.

b) The solvent and the product are transferred via trap-to-trap distillation to a J. Young tube under high vacuum (*ca.* 5 x 10^{-4} mbar). Removal of the solvent at -25 °C leads to a colorless liquid analytically pure.

Method a) applies for PhSiH$_2$(N^{t}BuH), PhSiH(N^{t}BuH)$_2$, PhSiH$_2$(NEt$_2$), PhSiH(NEt$_2$)$_2$, PhSiH$_2$(N^{i}Pr$_2$), ^{n}BuSiH$_2$(N^{i}Pr$_2$), Ph$_2$SiH(N^{t}BuH), Ph$_2$SiH(NEt$_2$), Ph$_2$SiH[N(CH$_2$)$_4$], PhSiH[N(CH$_2$)$_4$]$_2$, ^{n}BuSiH(N^{t}BuH)$_2$, ^{n}BuSiH(NEt$_2$)$_2$ and ^{n}BuSiH[N(CH$_2$)$_4$]$_2$.

Method b) applies for ^{n}BuSiH$_2$(N^{t}BuH), ^{n}BuSiH$_2$(NEt$_2$), Et$_2$SiH(N^{t}BuH), Et$_2$SiH(NEt$_2$) and Et$_2$SiH[N(CH$_2$)$_4$].

Compounds $PhSiH_2[N(CH_2)_4]$ and $PhSiH_2(NMesH)$ proved too sensitive and have not been isolated. NMR data has been obtained from the crude reaction mixture in CD_2Cl_2.

We have noticed that compound $^nBuSiH_2[N(CH_2)_4]$ is unstable due to a disproportion reaction leading to $^nBuSiH_3$ and $^nBuSiH[N(CH_2)_4]_2$. This process slowly takes place in dichloromethane solutions both in the presence or absence of catalyst. Exposure to vacuum favours the formation of the diaminosilane $^nBuSiH[N(CH_2)_4]_2$ through removal of the volatile $^nBuSiH_3$. Thus, no pure $^nBuSiH_2[N(CH_2)_4]$ could be isolated, although reactions carried out in NMR tubes in CD_2Cl_2 indicated that $nBuSiH_2[N(CH_2)_4]$ is the major product (*ca.* 95%) contaminated with *ca.* 5% of $^nBuSiH[N(CH_2)_4]_2$.

Characterization of the resulting products
-PhSiH₂(NH*t*Bu)

¹H NMR (300 MHz, CD₂Cl₂, 298 K) δ 1.06 (br, 1H, N*H*), 1.22 (s, 9H, *t**Bu**), 4.88 (d, 2H, $^3J_{H-H}$ = 3.0 Hz, Si*H₂*), 7.39-7.42 (m, 3H, ***Ph***), 7.66-7.69 (m, 2H, ***Ph***) ppm.

¹³C{¹H} (125 MHz, CD₂Cl₂, 298 K) δ 33.1 (C(***C***H₃)₃), 49.8 (***C***(CH₃)₃), 128.3, 130.2, 135.0, 136.6 (***Ph***) ppm.

²⁹Si (79 MHz, CD₂Cl₂, 298 K) δ -38.2 (t, $^1J_{Si-H}$ = 205 Hz) ppm.

-PhSiH(NH*t*Bu)₂

¹H NMR (400 MHz, CD₂Cl₂, 298 K) δ 0.98 (br, 2H, N*H*), 1.26 (s, 18H, *t**Bu**), 5.22 (t, 1H, $^3J_{H-H}$ = 2.9 Hz, Si*H*), 7.37-7.39 (m, 3H, ***Ph***), 7.68-7.70 (m, 2H, ***Ph***) ppm.

[431]

^{13}C{^{1}H} (100 MHz, CD$_2$Cl$_2$, 298 K) δ 33.7 ((C(**C**H$_3$)$_3$), 49.7 (**C**(CH$_3$)$_3$), 128.0, 129.5, 134.5 and 140.7 (**Ph**) ppm.

^{29}Si (79 MHz, CD$_2$Cl$_2$, 298 K) δ -37.5 (d, $^1J_{\text{Si-H}}$ = 214 Hz) ppm.

-PhSiH$_2$(NEt$_2$)

^{1}H NMR (300 MHz, CD$_2$Cl$_2$, 298 K) δ 1.08 (t, 6H, $^3J_{\text{H-H}}$ = 7 Hz, NCH$_2$C**H**$_3$), 2.96 (q, 4H, $^3J_{\text{H-H}}$ = 7 Hz, NC**H**$_2$CH$_3$), 4.91 (s, 2H, Si**H**$_2$), 7.41-7.43 (m, 3H, **Ph**), 7.63-7.64 (m, 2H, **Ph**) ppm.

^{13}C{^{1}H} (100 MHz, CD$_2$Cl$_2$, 298 K) δ 15.6 (NCH$_2$**C**H$_3$), 42.9 (N**C**H$_2$CH$_3$), 128.3, 130.2, 135.0 and 136.0 (**Ph**) ppm.

^{29}Si (79 MHz, CD$_2$Cl$_2$, 298 K) δ -25.5 (t, $^1J_{\text{Si-H}}$ = 204 Hz) ppm.

-PhSiH(NEt$_2$)$_2$

^{1}H NMR (400 MHz, CD$_2$Cl$_2$, 298 K) δ 1.10 (t, 12H, $^3J_{\text{H-H}}$ = 7 Hz, NCH$_2$C**H**$_3$), 3.00 (q, 8H, $^3J_{\text{H-H}}$ = 7 Hz, NC**H**$_2$CH$_3$), 4.91 (s, 1H, Si**H**), 7.43-7.44 (m, 3H, **Ph**), 7.66-7.67 (m, 2H, **Ph**) ppm

^{13}C{^{1}H} (100 MHz, CD$_2$Cl$_2$, 298 K) δ 15.4 (NCH$_2$**C**H$_3$), 40.0 (N**C**H$_2$CH$_3$), 128.1, 129.7, 135,0 and 138.1 (**Ph**) ppm.

^{29}Si (79 MHz, CD$_2$Cl$_2$, 298 K) δ -19.5 (d, $^1J_{\text{Si-H}}$ = 214 Hz) ppm.

[432]

-PhSiH$_2$[N(CH$_2$)$_4$]

^{1}H NMR (300 MHz, CD$_2$Cl$_2$, 298 K) δ 1.79 (m, 4H, NCH$_2$C*H*$_2$), 3.06 (m, 4H, NC*H*$_2$CH$_2$), 4.93 (s, 2H, Si*H*$_2$), 7.41-7.43 (m, 3H, *Ph*), 7.61-7.65 (m, 2H, *Ph*) ppm.

^{13}C{^{1}H} (100 MHz, CD$_2$Cl$_2$, 298 K) δ 27.5 (NCH$_2$*C*H$_2$), 49.1 (N*C*H$_2$CH$_2$), 128.4, 130.2 and 135.1 (*Ph*) ppm.

^{29}Si (79 MHz, CD$_2$Cl$_2$, 298 K) δ -29.8 ppm.

-PhSiH[N(CH$_2$)$_4$]$_2$

^{1}H NMR (300 MHz, CD$_2$Cl$_2$, 298 K) δ 1.86 (m, 8H, NCH$_2$C*H*$_2$), 3.18 (m, 8H, NC*H*$_2$CH$_2$), 5.13 (s, 2H, Si*H*), 7.48-7.50 (m, 3H, *Ph*), 7.72-7.75 (m, 2H, *Ph*) ppm.

^{13}C{^{1}H} (100 MHz, CD$_2$Cl$_2$, 298 K) δ 27.2 (NCH$_2$*C*H$_2$), 47.5 (N*C*H$_2$CH$_2$), 128.2, 129.8, 134.8 and 137.4 (*Ph*) ppm.

^{29}Si (79 MHz, CD$_2$Cl$_2$, 298 K) δ -25.8 (d, $^1J_{Si-H}$ = 213 Hz) ppm.

-PhSiH$_2$(N^{i}Pr$_2$)

^{1}H NMR (300 MHz, CD$_2$Cl$_2$, 298 K) δ 1.18 (d, 12H, $^3J_{H-H}$ = 6.8 Hz, NCH(C*H*$_3$)$_2$), 3.25 (sept, 2H, $^3J_{H-H}$ = 6.8 Hz, NC*H*(CH$_3$)$_2$), 4.95 (s, 2H, Si*H*$_2$), 7.39-7.42 (m, 3H, *Ph*), 7.66-7.67 (m, 2H, *Ph*) ppm.

^{13}C{^{1}H} (100 MHz, CD$_2$Cl$_2$, 298 K) δ 24.5 (NCH(*C*H$_3$)$_2$), 47.9 (N*C*H(CH$_3$)$_2$), 128.3, 129.9, 135.0 and 137.2 (*Ph*) ppm.

[433]

^{29}Si (79 MHz, CD$_2$Cl$_2$, 298 K) δ -39.0 ppm.

-PhSiH$_2$(NHMes)

^{1}H NMR (400 MHz, CD$_2$Cl$_2$, 298 K) δ 2.26 (s, 3H, C**H**$_3$-Mes), 2.33 (s, 6H, C**H**$_3$-Mes), 2.94 (br, 1H, N**H**), 5.14 (d, 2 H, $^3J_{H-H}$ = 3.1 Hz, Si**H**$_2$), 6.86 (s, 2H, C**H**-Mes), 7.43-7.50 (m, 3H, **Ph**), 7.71-7.74 (m, 2H, **Ph**) ppm.

^{13}C{^{1}H} (100 MHz, CD$_2$Cl$_2$, 298 K) δ 19.7 and 20.7 (**C**H$_3$-Mes), 128.6, 130.8, 134.3 and 135.1 (**Ph**), 129.6, 130.3, 131.2 and 140.2 (**C**H-Mes) ppm.

^{29}Si (79 MHz, CD$_2$Cl$_2$, 298 K) δ -31.2 ppm.

-Ph$_2$SiH(NH^{t}Bu)

^{1}H NMR (300 MHz, CD$_2$Cl$_2$, 298 K) δ 1.26 (s, 10H, **tBu + NH**), 5.48 (d, 1H, $^3J_{H-H}$ = 3.3 Hz, Si**H**), 7.40-7.42 (m, 6H, **Ph**), 7.66-7.68 (m, 4H, **Ph**) ppm.

^{13}C{^{1}H} (125 MHz, CD$_2$Cl$_2$, 298 K) δ 33.5 (C**Me**$_3$), 50.0 (**C**Me$_3$), 128.3, 130.0, 135.0 and 137.6 (**Ph**) ppm.

^{29}Si (79 MHz, CD$_2$Cl$_2$, 298 K) δ -24.9 (d, $^1J_{Si-H}$ = 205 Hz) ppm.

-Ph$_2$SiH(NEt$_2$)

^{1}H NMR (400 MHz, CD$_2$Cl$_2$, 298 K) δ 1.10 (t, 6H, $^3J_{H-H}$ = 7 Hz, NCH$_2$C**H**$_3$), 3.03 (q, 4H, $^3J_{H-H}$ = 7 Hz, NC**H**$_2$CH$_3$), 5.38 (s, 1H, Si**H**), 7.42-7.47 (m, 6H, **Ph**), 7.67-7.69 (m, 4H, **Ph**) ppm.

¹³C{¹H} (100 MHz, CD₂Cl₂, 298 K) δ 15.6 (NCH₂CH₃), 41.4 (NCH₂CH₃), 128.3, 130.1, 135.5 and 136.3 (**Ph**) ppm.

²⁹Si (79 MHz, CD₂Cl₂, 298 K) δ -14.8 ppm.

-Ph₂SiH[N(CH₂)₄]

¹H NMR (400 MHz, CD₂Cl₂, 298 K) δ 1.82 (m, 4H, NCH₂CH₂), 3.12 (m, 4H, NCH₂CH₂), 5.40 (s, 1H, SiH), 7.44-7.47 (m, 6H, **Ph**), 7.66-7.68 (m, 4H, **Ph**) ppm.

¹³C{¹H} (100 MHz, CD₂Cl₂, 298 K) δ 27.4 (NCH₂CH₂), 48.5 (NCH₂CH₂), 128.4, 130.1, 135.4 and 135.9 (**Ph**) ppm.

²⁹Si (79 MHz, CD₂Cl₂, 298 K) δ -17. 9 (d, $^1J_{\text{Si-H}}$ = 203 Hz) ppm.

-^{n}BuSiH₂(NH^{t}Bu)

¹H NMR (300 MHz, CD₂Cl₂, 298 K) δ 0.62 (br, 1H, NH), 0.69 (m, 2H, CH₂), 0.90 (t, $^3J_{\text{H-H}}$ = 7 Hz, 3H, CH₃), 1.17 (s, 9H, **^tBu**), 1.37 (m, 4H, 2 CH₂), 4.31 (m, 2H, SiH₂) ppm.

¹³C{¹H} (100 MHz, CD₂Cl₂, 298 K) δ 14.2, 14.3, 26.6 and 26.9 (**^nBu**), 33.2 (CMe₃), 49.5 (CMe₃) ppm.

²⁹Si (79 MHz, CD₂Cl₂, 298 K) δ -33.2 ($^1J_{\text{Si-H}}$ = 195 Hz) ppm.

APCI HR-MS (+): [M+H]⁺, *m/z* **theoretical** 160.1516, **found** 160.1515.

[435]

Experimental Part

-*n*BuSiH(NH*t*Bu)$_2$

^{1}H NMR (400 MHz, CD$_2$Cl$_2$, 298 K) δ 0.55 (m, 2H, C*H*$_2$), 0.68 (br, 2H, N*H*), 0.92 (m, 3H, C*H*$_3$), 1.22 (s, 18H, *t*Bu), 1.37 (m, 4H, 2 C*H*$_2$), 4.62 (m, H, Si*H*) ppm.

^{13}C{^{1}H} (100 MHz, CD$_2$Cl$_2$, 298 K) δ 14.4, 18.1, 26.9 and 27.0 (*n*Bu), 34.0 (C*Me*$_3$), 49.7 (*C*Me$_3$) ppm.

^{29}Si (79 MHz, CD$_2$Cl$_2$, 298 K) δ -30.1 (d, $^1J_{Si-H}$ = 205 Hz) ppm.

All attempts to obtain spectroscopic data by APCI, FAB or ESI experiments failed due to decomposition of the sample under the experimental conditions.

-*n*BuSiH$_2$(NEt$_2$)

^{1}H NMR (300 MHz, CD$_2$Cl$_2$, 298 K) δ 0.73 (m, 2H, C*H*$_2$), 0.94 (t, $^3J_{H-H}$ = 6.5 Hz, 3H, C*H*$_3$), 1.05 (t, 6H, $^3J_{H-H}$ = 7 Hz, NCH$_2$C*H*$_3$), 1.41 (m, 4H, C*H*$_2$), 2.87 (q, 4H, $^3J_{H-H}$ = 7 Hz, NC*H*$_2$CH$_3$), 4.36 (m, 2H, Si*H*$_2$) ppm.

^{13}C{^{1}H} (100 MHz, CD$_2$Cl$_2$, 298 K) δ 14.1 and 14.3 (*n*Bu), 15.9 (NCH$_2$*C*H$_3$), 26.7 and 26.9 (*n*Bu), 43.2 (N*C*H$_2$CH$_3$) ppm.

^{29}Si (79 MHz, CD$_2$Cl$_2$, 298 K) δ -20.0 (t, $^1J_{Si-H}$ = 194 Hz) ppm.

APCI HR-MS (+): [M+H]$^+$, *m/z* **theoretical** 160.1516, **found** 160.1516.

[436]

-*n*BuSiH(NEt$_2$)$_2$

^{1}H NMR (300 MHz, CD$_2$Cl$_2$, 298 K) δ 0.67 (m, 2H, C*H*$_2$), 0.93 (t, $^3J_{H-H}$ = 7.0 Hz, 3H, C*H*$_3$), 1.03 (t, 12H, $^3J_{H-H}$ = 7 Hz, NCH$_2$C*H*$_3$), 1.38 (m, 4H, C*H*$_2$), 2.87 (q, 8H, $3J_{H-H}$ = 7 Hz, NC*H*$_2$CH$_3$), 4.33 (t, 1H, $^3J_{H-H}$ = 2.6 Hz, Si*H*) ppm.

^{13}C{^{1}H} (100 MHz, CD$_2$Cl$_2$, 298 K) δ 14.1 and 14.3 (*^{n}Bu*), 15.9 (NCH$_2$*C*H$_3$), 26.6 and 27.0 (*^{n}Bu*), 40.6 (N*C*H$_2$CH$_3$) ppm.

^{29}Si (79 MHz, CD$_2$Cl$_2$, 298 K) δ -11.8 (d, $^1J_{Si-H}$ = 203 Hz) ppm.

All attempts to obtain spectroscopic data by APCI, FAB or ESI experiments failed due to decomposition of the sample under the experimental conditions.

-*n*BuSiH$_2$[N(CH$_2$)$_4$]

^{1}H NMR (300 MHz, CD$_2$Cl$_2$, 298 K) δ 0.75 (m, 2H, C*H*$_2$), 0.90 (m, 3H, C*H*$_3$), 1.39 (m, 4H, CH$_2$), 1.72 (m, 4H, NCH$_2$C*H*$_2$), 2.94 (m, 4H, NC*H*$_2$CH$_2$), 4.32 (t, 1H, $^3J_{H-H}$ = 2.8 Hz, Si*H*$_2$) ppm.

^{13}C{^{1}H} (100 MHz, CD$_2$Cl$_2$, 298 K) δ 12.4, 14.0, 26.4 and 26.8 (*^{n}Bu*), 27.4 (NCH$_2$*C*H$_2$), 49.1 (N*C*H$_2$CH$_2$) ppm.

^{29}Si (79 MHz, CD$_2$Cl$_2$, 298 K) δ -23.1 (t, $^1J_{Si-H}$ = 192 Hz) ppm.

[437]

Experimental Part

$-^{n}BuSiH[N(CH_2)_4]_2$

^{1}H NMR (400 MHz, CD$_2$Cl$_2$, 298 K) δ 0.72 (m, 2H, CH_2), 0.94 (m, 3H, CH_3), 1.39 (m, 4H, CH_2), 1.72 (m, 8H, NCH$_2$CH_2), 3.00 (m, 8H, NCH_2CH$_2$), 4.48 (br, 1H, SiH) ppm.

^{13}C{^{1}H} (100 MHz, CD$_2$Cl$_2$, 298 K) δ 13.8, 14.4, 26.5 and 27.0 (^{n}Bu), 27.5 (NCH$_2$$CH_2$), 47.7 (N$CH_2CH_2$) ppm.

^{29}Si (79 MHz, CD$_2$Cl$_2$, 298 K) δ -17.9 (d, $^1J_{Si-H}$ = 203 Hz) ppm.

All attempts to obtain spectroscopic data by APCI, FAB or ESI experiments failed due to decomposition of the sample under the experimental conditions.

$-nBuSiH_2(N^{i}Pr_2)$

^{1}H NMR (400 MHz, CD$_2$Cl$_2$, 298 K) δ 0.69 (m, 2H, CH_2), 0.93 (t, 3H, $^3J_{H-H}$ = 7.0 Hz, CH_3), 1.13 (d, 12H, $^3J_{H-H}$ = 6.6 Hz, NCH(CH_3)$_2$), 1.39 (m, 4H, CH_2), 3.17 (sept, 2H, $^3J_{H-H}$ = 6.6 Hz, NCH(CH$_3$)$_2$), 4.37 (t, 2H, $^3J_{H-H}$ = 2.5 Hz, SiH_2) ppm.

^{13}C{^{1}H} (100 MHz, CD$_2$Cl$_2$, 298 K) δ 14.3 and 15.4 (^{n}Bu), 24.7 (NCH(CH$_3$)$_2$), 26.6 and 26.8 (^{n}Bu), 27.5 (NCH$_2$$CH_2$), 47.9 (N$C$H(CH$_3$)$_2$) ppm.

^{29}Si (79 MHz, CD$_2$Cl$_2$, 298 K) δ -33.2 (d, $^1J_{Si-H}$ = 196 Hz) ppm.
APCI HR-MS (+): [M+H]$^+$, *m/z* **theoretical** 188.1831, **found** 188.1829.

-Et$_2$SiH(NEt$_2$)

^{1}H NMR (400 MHz, CD$_2$Cl$_2$, 298 K) δ 0.63 (t, 4H, $^3J_{\text{H-H}}$ = 7.2 Hz, SiC**H**$_2$CH$_3$), 1.00 (t, 6H, $^3J_{\text{H-H}}$ = 8.0 Hz, SiCH$_2$C**H**$_3$), 1.03 (t, 6H, $^3J_{\text{H-H}}$ = 7.0 Hz, NCH$_2$C**H**$_3$), 2.87 (q, 4H, $^3J_{\text{H-H}}$ = 7 Hz, NC**H**$_2$CH$_3$), 4.19 (m, 1H, Si**H**) ppm.

^{13}C{^{1}H} (100 MHz, CD$_2$Cl$_2$, 298 K) δ 6.2 (SiCH$_2$**C**H$_3$), 8.0 (Si**C**H$_2$CH$_3$), 16.1 (NCH$_2$**C**H$_3$), 41.9 (N**C**H$_2$CH$_3$) ppm.

^{29}Si (79 MHz, CD$_2$Cl$_2$, 298 K) δ 3.0 (d, $^1J_{\text{Si-H}}$ = 204 Hz) ppm.

APCI HR-MS (+): [M+H]$^+$, *m/z* **theoretical** 160.1516, **found** 160.1517.

-Et$_2$SiH(NH^{t}Bu)

^{1}H NMR (400 MHz, CD$_2$Cl$_2$, 298 K) δ 0.59 (t, 4H, $^3J_{\text{H-H}}$ = 8.1 Hz, SiC**H**$_2$CH$_3$), 0.99 (t, 6H, $^3J_{\text{H-H}}$ = 8.1 Hz, SiCH$_2$C**H**$_3$), 1.19 (s, 9H, **^{t}Bu**), 4.32 (m, 1H, Si**H**) ppm.

^{13}C{^{1}H} (100 MHz, CD$_2$Cl$_2$, 298 K) δ 7.1 (SiCH$_2$**C**H$_3$), 7.8 (Si**C**H$_2$CH$_3$), 33.8 (C**Me**$_3$), 49.5 (**C**Me$_3$) ppm.

^{29}Si (79 MHz, CD$_2$Cl$_2$, 298 K) δ -8.9 (t, $^1J_{\text{Si-H}}$ = 189 Hz) ppm.

APCI HR-MS (+): [M+H]$^+$, *m/z* **theoretical** 160.1516, **found** 160.1517.

[439]

Experimental Part

-Et₂SiH[N(CH₂)₄]

¹H NMR (400 MHz, CD₂Cl₂, 298 K) δ 0.66 (m, 4H, SiCH_2CH₃), 1.00 (t, 6H, $^3J_{\text{H-H}}$ = 8.0 Hz, SiCH₂CH_3), 1.72 (m, 4H, NCH₂CH_2), 2.98 (m, 4H, NCH_2CH₂), 4.24 (quint, 1H, $^3J_{\text{H-H}}$ = 2.5 Hz, SiH) ppm.

¹³C{¹H} (100 MHz, CD₂Cl₂, 298 K) δ 5.2 (SiCH₂CH₃), 7.9 (SiCH₂CH₃), 27.4 (NCH₂CH₂), 48.4 (NCH₂CH₂) ppm.

²⁹Si (79 MHz, CD₂Cl₂, 298 K) δ -1.1 (t, $^1J_{\text{Si-H}}$ = 188 Hz) ppm.

APCI HR-MS (+): [M+H]⁺, *m/z* **theoretical** 158.1360, **found** 158.1361.

*Low Temperature NMR reaction of **13**, NEt₂H and Ph₂SiH₂*

50 mg (0.035 mmol) of complex **13** and 3.7 μL of NEt₂H (0.035 mmol) were dissolved in 0.4 mL of d^8-THF in a screw-capped NMR tube. The solution was cooled to -80 °C and a cooled solution (-80 °C) of Ph₂SiH₂ (7.8 μL, 0.042 mmol) in 0.2 mL of d^8-THF was transferred via cannula to the NMR tube. The solution was shaken and immediately inserted in a pre-cooled (-80 °C) NMR apparatus. ¹H NMR spectra were recorded at several temperatures between -70 to 25 °C, at intervals of 10 °C.

[440]

Synthesis of the ammonium salt [Et$_2$NH$_2$][BAr$_4^F$]
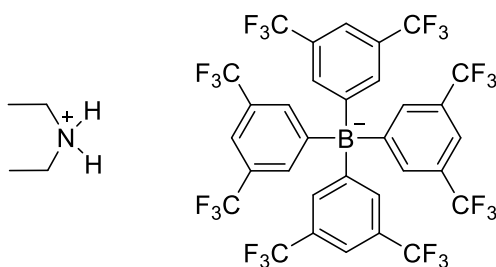
Synthesis

In a glovebox, a solution of Et$_2$NH (2.7 µL, 25.9 µmol) in CD$_2$Cl$_2$ (0.2 mL) was added to a screw-capped NMR tube containing a solution of H(Et$_2$O)$_2$BAr$_4^F$ (25 mg, 24.7 µmol) in CD$_2$Cl$_2$ (0.3 mL). After confirming by ^{1}H NMR the formation of the ammonium species, the solution was transferred via cannula to a J. Young flask. The solvent and the slight excess of amine were removed under vacuum, affording a white solid, which was redissolved in d^8-THF and analyzed by NMR to compare the spectra with those of the low-temperature experiments. The NH$_2$ protons were detected only at low temperatures (see below).

Spectroscopic and analytical data
White solid.
Molecular weight: 937.37 g/mol.

^{1}H-NMR (400 MHz, d^8-THF, 298 K) δ 1.31 (t, $^3J_{\text{H-H}}$ = 7.3 Hz, 6H, C*H*$_3$), 3.14 (m, 4H, C*H*$_2$), 7.59 (s, 4H, Ph-C*H*$_{para}$), 7.79 (s, 8H, Ph-C*H*$_{ortho}$) ppm.

^{13}C{^{1}H}-NMR (100 MHz, CD$_2$Cl$_2$, 298 K) δ 12.2 (*C*H$_3$), 43.0 (*C*H$_2$) ppm.

^{1}H-NMR (400 MHz, d^8-THF, 223 K) δ 7.60 (bs, 2H, N*H*$_2$) ppm.

[441]

Experimental Part

*Procedure for kinetic measurements of the reaction of PhSiH₃ and NEt₂H catalyzed by complex **13**. Determination of partial orders.*

Kinetic measurements were carried out using a Man-on-the-Moon apparatus. In a typical procedure, a stock solution of complex **13** (1.35 mg in 1 mL of CH_2Cl_2 or CD_2Cl_2) prepared immediately before use is placed, under argon, in a 35 mL flask containing the amount of CH_2Cl_2 required to reach a total amount of 0.25 mL of solvent. Catalyst loadings of 100, 150, 200, 250, 300 and 350 ppm were used in each case. NEt₂H (1.48 mmol) is then added and the internal pressure is allow to stabilize. Thereafter, the PhSiH₃ (23 μL, 0.185 mmol) is injected and the pressure inside the flask measured at intervals of 1.38 s. until no increase in the internal pressure is observed.

Rate Law

Equation 1 gives the overall stoichiometry of the chemical reaction that constitutes the objective of our chemical kinetics study.

$$PhSiH_3 + NEt_2H \xrightarrow{[Pt]} PhSiH_2(NEt_2) + H_2 \qquad (1)$$

[Pt] stands for the platinum catalyst **13**. The solvent used was dichloromethane and the reaction was carried out at room temperature. Rate law was assumed to follow the expression in equation 2:

$$v = k[PhSiH_3]^\alpha [NEt_2H]^\beta [Pt]^\gamma \qquad (2)$$

where the rate constant is k, and the exponents α, β, and γ are the partial orders. Expressing the rate law as a function of concentrations implies assuming the ideal behavior of our chemical system. In real systems, the rate law is written in terms of activities and it also depends on a special function based on temperature, pressure and concentrations.

The isolation method has been chosen to determine α because the catalyst concentration remains constant during the process and the amine concentration may be considered nearly constant if it is present in large excess

[442]

over the silane. Under these conditions, the rate constant multiplied by the catalyst and amine concentrations (raised to their corresponding partial orders) generates a new apparent rate constant, k'.

$$k' = k[\text{NEt}_2\text{H}]^\beta [\text{Pt}]^\gamma \tag{3}$$

Accordingly, the rate law is transformed to

$$v = k'[\text{PhSiH}_3]^\alpha \tag{4}$$

An eightfold excess of the amine over the silane has been selected. The initial amount of silane was fixed at $0.184 \cdot 10^{-3}$ mol. 0.25 mL of dichloromethane were used to dissolve the silane. According to the chosen ratio, the initial amount of amine was $1.472 \cdot 10^{-3}$ mol (0.15 mL). There are no restrictions, from the standpoint of the isolation method, to choose the catalyst loading. The decision was taken attending solely to the effectiveness (cost, time, etc.) of the experiment. To begin with, the amount of catalyst was 0.010 % of the initial amount of silane. Once established all conditions, the experiment was run three times. In the experiments, the pressure is measured as a function of time. It is assumed that changes in pressure are due, exclusively, to the production of hydrogen. The calculations will be performed only with the experiment in which the standard deviation of temperature, during the run, is minimal. Plot of $(n/V)/(\text{mol L}^{-1})$, obtained by applying the ideal gas law, versus t/s for the selected experiment is shown (blue dots) in Figure 1. A linear relationship between (n/V) and t is evident. A least-squares linear fit (red straight line) confirms the linear dependence. The sum-of-squares-due-to-error (SSE) is $7.863 \cdot 10^{-6}$ and the square of the correlation coefficient (r^2) is 0.9977. It then follows that $\alpha = 0$.

Experimental Part
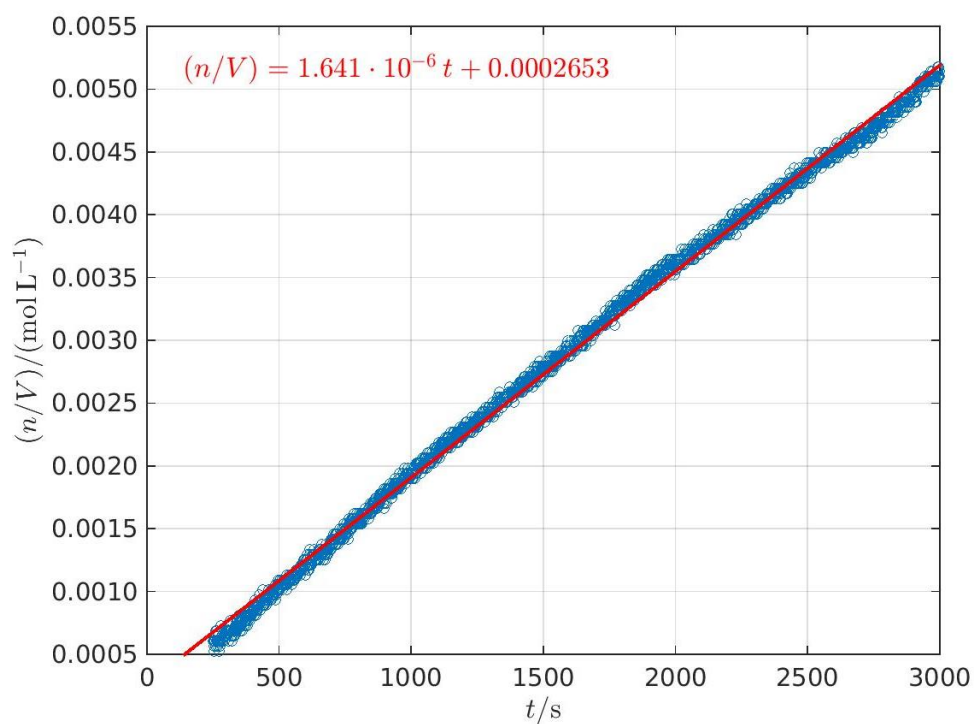
Figure 1. Hydrogen concentration versus time. For this experiment, $\bar{T} = 297.2092$ K and $s(T) = 0.0535$ K. The mathematical equation of the straight red line is written inside the figure.

To confirm that this result is independent of the catalyst loading, a series of experiments has been performed with different catalyst loadings (3 runs in each case). Results are shown in Table 1. In all cases, the pseudo order is unequivocally confirmed.

[444]

Catalyst loading/ mol %	$k'/(\text{mol L}^{-1} \text{ s}^{-1})$	SSE	r^2
0.010	$1.641 \cdot 10^{-6}$	$7.863 \cdot 10^{-6}$	0.9977
0.015	$3.867 \cdot 10^{-6}$	$9.607 \cdot 10^{-7}$	0.9979
0.020	$7.324 \cdot 10^{-6}$	$4.809 \cdot 10^{-7}$	0.9988
0.025	$1.224 \cdot 10^{-5}$	$4.093 \cdot 10^{-7}$	0.9983
0.030	$2.011 \cdot 10^{-5}$	$3.804 \cdot 10^{-7}$	0.9980
0.035	$2.502 \cdot 10^{-5}$	$1.963 \cdot 10^{-7}$	0.9985

Table 1. Results of the isolation method (to determine the partial order in silane) using different catalyst loadings.

The partial order in catalyst, γ, was determined by means of a log-log plot, using previous results from the isolation method applied to obtain α, the partial order in silane. A brief description of the procedure follows. Let us begin writing equations 2 and 4 with a slightly different notation.

$$v = k[\text{PhSiH}_3]^{\alpha}[\text{NEt}_2\text{H}]^{\beta}[\text{Pt}_{\langle 0.010 \rangle}]^{\gamma} = k'_{\langle 0.010 \rangle}[\text{PhSiH}_3]^{\alpha} \qquad (5)$$

Number enclosed in angular brackets represents the catalyst loading. Equation 6 is easily derived from equation 5.

$$k[\text{NEt}_2\text{H}]^{\beta}[\text{Pt}_{\langle 0.010 \rangle}]^{\gamma} = k'_{\langle 0.010 \rangle} \qquad (6)$$

And taking natural logarithms, equation 7 is obtained.

$$\ln k + \beta \ln[\text{NEt}_2\text{H}] + \gamma \ln[\text{Pt}_{\langle 0.010 \rangle}] = \ln k'_{\langle 0.010 \rangle} \qquad (7)$$

Clearly, if the catalyst loading is, for example, 0.015 %, the equation 7 is written like this:

$$\ln k + \beta \ln[\text{NEt}_2\text{H}] + \gamma \ln[\text{Pt}_{\langle 0.015 \rangle}] = \ln k'_{\langle 0.015 \rangle} \qquad (8)$$

Comparing equations 7 and 8 (and all that can be generated in the same way), it is concluded that a plot of the natural logarithm of the apparent constants versus the natural logarithm of the catalyst loadings must exhibit a linear relationship. The slope is γ (our target), and the intercept is $\ln k + \beta \ln[\text{NEt}_2\text{H}]$. Using the first two columns of table 1 (blue dots) and performing a linear fit using the least-squares regression technique (red straight line), $\gamma = 2.203$ (see Figure 2).

[445]
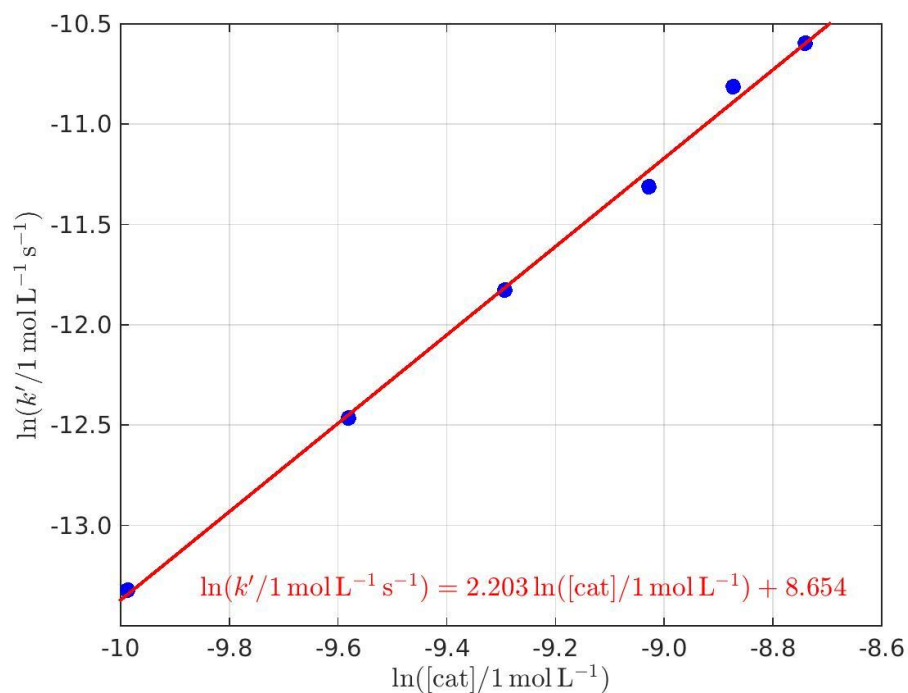
Figure 2. Log-log plot. 1 mol L^{-1} and 1 mol L^{-1} s^{-1} are standard values to turn the arguments of the natural logarithms into dimensionless quantities. The mathematical equation of the straight red line is written inside the figure.

The goodness of the fit is reflected in the parameters $SSE = 0.01308$ and $r^2 = 0.9976$. This result points out that the partial order in the catalyst is 2.

It has not been possible to use the isolation method to calculate β, the partial order in amine, due to inhibition or side reactions of the catalyst in the presence of large excess of the silane. This shortcoming hinders the calculation of the rate constant.

[446]

Computational Details

General considerations

Calculations were carried out at the DFT level with the Gaussian 09 suite of programs.[10] Unless otherwise stated, geometry optimizations were carried out without restrictions. Vibrational analysis was used to characterize the stationary points in the potential energy surface, as well as for calculating the Zero Point, Enthalpy and Gibbs energy corrections at 298 K and 1 atm.

Chapter 1

These calculations were performed in collaboration with Prof. Joaquín López-Serrano, from the University of Seville.

All geometries were optimized in the gas phase with the PBE0 functional, as implemented in the G09 software.[11] Non-metal atoms were described with the 6-31G(d,p) basis set with polarization functions,[12] and the Ni atom was modelled with the Stuttgart/Dresden SDD basis set and its associated effective core

---

[10] Gaussian 09, Revision D.01, M. J. Frisch, G. W. Trucks, H. B. Schlegel, G. E. Scuseria, M. A. Robb, J. R. Cheeseman, G. Scalmani, V. Barone, B. Mennucci, G. A. Petersson, H. Nakatsuji, M. Caricato, X. Li, H. P. Hratchian, A. F. Izmaylov, J. Bloino, G. Zheng, J. L. Sonnenberg, M. Hada, M. Ehara, K. Toyota, R. Fukuda, J. Hasegawa, M. Ishida, T. Nakajima, Y. Honda, O. Kitao, H. Nakai, T. Vreven, J. A. Montgomery, Jr., J. E. Peralta, F. Ogliaro, M. Bearpark, J. J. Heyd, E. Brothers, K. N. Kudin, V. N. Staroverov, R. Kobayashi, J. Normand, K. Raghavachari, A. Rendell, J. C. Burant, S. S. Iyengar, J. Tomasi, M. Cossi, N. Rega, J. M. Millam, M. Klene, J. E. Knox, J. B. Cross, V. Bakken, C. Adamo, J. Jaramillo, R. Gomperts, R. E. Stratmann, O. Yazyev, A. J. Austin, R. Cammi, C. Pomelli, J. W. Ochterski, R. L. Martin, K. Morokuma, V. G. Zakrzewski, G. A. Voth, P. Salvador, J. J. Dannenberg, S. Dapprich, A. D. Daniels, Ö. Farkas, J. B. Foresman, J. V. Ortiz, J. Cioslowski, and D. J. Fox, Gaussian, Inc., Wallingford CT, **2009**.

[11] C. Adamo, V. Barone, *J. Chem. Phys.,* **1999**, *110*, 6158-6170.

[12] a) W. J. Hehre, R. Ditchfield, J.A. Pople. *J. Phys. Chem.* **1972**, 56, 2257-2261; b) P.C. Hariharan, J. A. Pople. *Theor. Chim. Acta.* **1973**, *28*, 213-222; c) M. M. Francl, W.J. Pietro, W.J. Hehre, J.S. Binkley, M.S. Gordon, D.J. DeFrees, J.A. Pople. *Chem. Phys.* **1982**, *77*, 3654-3665.

potential.[13] The nature of the species connected by a given transition state (TS) was established by means of intrinsic reaction coordinate (IRC)[14] calculations or by allowing the TS geometries to vibrate along their imaginary frequency and optimizing the resulting geometries to the nearest minima. Bulk solvent effects (benzene) were modelled by single-point calculations on the gas-phase geometries, using Truhlar's SMD continuum solvent model.[15] Empirical dispersion corrections were shown to have substantial effects on the energy barriers of our systems and also have been introduced with the D3 version of Grimme's dispersion[16] by single-point calculations on the gas-phase geometries (optimizing the molecular geometries with the PBE0-D3 corrected functional yielded very similar results). Exploratory calculations were carried out using a simplified version of the catalyst, in which the ^tBu groups on the P atoms of the PBP ligand were replaced by Me groups. These calculations were used to favour one mechanistic pathway, which was then recalculated with the real catalyst. Also, we have used Me_3SiH instead of larger silanes; however, the use of the real Lewis acid, $B(C_6F_5)_3$, in the calculations (instead of BF_3 or $B(CF_3)_3$) was shown to be critical to account for the experimental results.

Translational entropy, while accurately calculated in the gas phase,[17] is greatly overestimated by standard calculation methods for reactions in solution.[18]

---

[13] For 1st row transition metals, see: M. Dolg, U. Wedig, H. Stoll, H. Preuss, *J. Chem. Phys.,* **1987**, *86*, 866-872. For 2nd and 3rd row transition metals, see: D. Andrae, U. Häussermann, M. Dolg, H. Stoll, H. Preuss, *Theor. Chim. Acta,* **1990**, *77*, 123-141.

[14] K. Fukui, *Acc. Chem. Res.,* **1981**, *14*, 363-368.

[15] A. V. Marenich, C. J. Cramer, D. G. Truhlar, *J. Phys. Chem. B.,* **2009**, *113*, 6378-6396.

[16] a) S. Grimme, J. Anthony, S. Ehrlich, H. Krieg. *J. Chem. Phys*. **2010**, *132*, 154104; b) F. M. Miloserdov, D. McKay, B. K. Muñoz, H. Samouei, S. A. Macgregor, V. V. Grushin. *Angew. Chem. Int. Ed*., **2015**, *54*, 8466-8470; c) F. M. Miloserdov, C. L. McMullin, M. M. n. Belmonte, J. Benet-Buchholz, V. U. Bakhmutov, S. A. Macgregor, V. V. Grushin, *Organometallics*, **2014**, *33*, 736-752.

[17] L. Watson, O. Eisenstein, *J. Chem. Educ.,* **2002**, *79*, 1269-1277.

[18] L-L. Han, S-J. Li, D-C. Fang, *Phys. Chem. Chem. Phys.,* **2016**, *18*, 6182-6190.

Theoretical[188-19] and experimental[20] investigations suggest that a 50% correction[21] to gas-phase entropy yields better agreement between experimental (solution) and calculated (gas-phase) data. Some authors choose to omit entropy data entirely, and only use enthalpy values.[22]

In this mechanistic study, zero-point energies (ZPEs) (with solvent and dispersion corrections) are used to describe the system. 50% corrected-free energy varations (ΔG_{50}) are also given for comparison (values in parentheses).

Chapter 2

These calculations were performed during a short stay (1 month) at the Universitat Autónoma de Barcelona (UAB), under the supervision of Prof. Agustí Lledós.

Exploratory calculations were carried out using the B97-D functional.[23] Optimization of the molecular geometries was performed taking into account solvent effects (toluene) by using the SMD continuum model specified above.[15] Non-metal atoms were described with the 6-31g(d,p) basis set with polarization functions,[12] and the Ni atom was modelled with the SDD basis set and its associated effective core potential.[13]

---

[19] a) M. Mammen, E. I. Shakhnovich, J. M. Deucth, G. M. Whitesides, *J. Org. Chem.,* **1998**, *63*, 3821-3820; b) R. L. Martin, P. J. Hay, L. R. Pratt, *J. Phys. Chem. A.,* **1998**, *102*, 3565-3573.

[20] a) D. H. Wertz, *J. Am. Chem. Soc.,* **1980**, *102*, 5316-5322; b) M. H. Abraham, *J. Am. Chem. Soc.,* **1981**, *103*, 6742-6744.

[21] a) J. K-C. Lau, D. V. Deubel, *J. Chem. Theor. Comput.,* **2006**, *2*, 103-106; b) D. V. Deubel, *J. Am. Chem. Soc.,* **2008**, *130*, 665-675; c) J. Kua, H. E. Krizner, D. O. De Haan, *J. Phys. Chem. A,* **2011**, *115*, 1667-1675.

[22] M-A. Courtemanche, M-A. Légaré, L. Maron, F-G. Fontaine, *J. Am. Chem. Soc.,* **2014**, *136*, 10708-10717.

[23] S. Grimme, *J. Comput. Chem.,* **2006**, *27*, 1787-1799.

Experimental Part

Once the exploratory results discarded some mechanistic possibilities, the *nucleophilic attack* and *ligand cooperativity* pathways were calculated with the PBE0 functional,[11] using 6-311++G(2d,p) and 6-311G for the non-metal atoms and for the Ni atom, respectively.[12] The nature of the species connected by a given transition state (TS) was established by allowing the TS geometries to vibrate along their imaginary frequency and optimizing the resulting geometries to the nearest minima. In all cases, the D3 version of Grimme's dispersion was included.[16] Wiberg bond index analyses was performed with the Multiwfn software.[24] The thermochemical data obtained from Gaussian frequency calculations (at 298 K and 1 atm) were corrected with the GoodVibes program[25] to obtain the data at 298 K and 1 M for Ni-BCat and 343 K and 1 M for Ni-Bpin.

The structure of boryl complex **11** was studied by performing a single-point calculation on the geometry obtained by X-Ray diffraction studies by using the PBE0 functional[11] (with D3 empirical dispersion),[16] and 6-311++G(2d,p) and 6-311G basis sets for non-metal atoms and Ni, respectively. Solvent effects (tetrahydrofuran) were taken into account by using the SMD continuum model.[15] An orbital localization procedure was used to characterize the electronic structure of the Ni(II) complexes. For this purpose, an optimized method developed in Prof. Lledós's group was applied. Orbital localization of canonical Density Functional Theory orbitals was performed with the CP2K code.[26] The PBE exchange-correlation functional was used.[27] The Quickstep algorithm was used to solve the electronic structure problem,[28] employing a double zeta plus polarization (DZVP) basis set to represent the valence orbitals and plane waves

[24] T .Lu, F. Chen, *J. Comput. Chem*., **2012**, *33*, 580–592.
[25] I. Funes-Ardoiz, R. S. Paton, **2016**. GoodVibes: GoodVibes v1.0.1 (Version 1.0.1). Zenodo. http://doi.org/10.5281/zenodo.60811.
[26] www.cp2k.org.
[27] J. P. Perdew, K. Burke, M. Ernzerhof*, Phys. Rev. Lett.,* **1996**, *77*, 3865-3868.
[28] G. Lippert, J. Hutter, M. Parrinello, *Mol. Phys.,* **1997**, *92*, 477-488.

for the electron density (300 Ry cutoff). Goedecker-Teter-Hutter (GTH) type pseudopotentials were used for valence core interactions.[29] Models were treated as isolated in a cubic box of 20 Å edge.

Chapter 3

I^{t}Bu complexes

The interaction of silanes and Pt I^{t}Bu complexes were calculated by using Truhlar's hybrid meta-GGA functional M06.[30] The Pt atom was modelled with the SDD basis set and its associated effective core potential.[13] The rest of the atoms were represented by means of the 6-31g(d,p) basis set.[12] The effects of the bulk solvent (dichloromethane) were accounted for in the final energy by single-point calculations at the above level of theory with the SMD continuum model.[15]

Mechanistic investigations (C-Si and Pt-Si coupling)

Exploratory mechanistic studies on the C–Si and/or Pt–Si bond formation mediated by σ-SiH complexes were calculated by using the M06 functional.[30] Optimization of the molecular geometries was performed taking into account solvent effects (dichloromethane) by using the SMD continuum model specified above.[15] Non-metal atoms were described with the 6-31g(d,p) basis set with polarization functions,[12] and the Pt atom was modelled with the SDD basis set and its associated effective core potential.[13] Then, single point calculations were carried out on the optimized structures by using the same functional, the 6-311++g(d,p) basis set for non-metal atoms and the Pt atom was described with the SDD basis set and its associated effective core potential. The thermochemical data obtained from Gaussian frequency calculations (at 298 K and 1 atm) were corrected with the GoodVibes program[25] to obtain the data at 273 K and 1 M.

---

[29] a) S. Goedecker, M. Teter, J. Hutter, *Phys. Rev. B. Condens. Matter,* **1996**, *54*, 1703-1710; b) M. Krack, *Theor. Chem. Acc.,* **2005**, *114*, 145-152.

[30] Y. Zhao, D. G. Truhlar, *Theor. Chem. Acc.,* **2008**, *120*, 215-241.

Experimental Part

I^{t}Bu^{i}Pr

The Pt(II) σ-SiH complexes stabilized by I^{t}Bu^{i}Pr ligands and their comparison with other reported systems were described using the TPSSh functional.[31] Non-metal atoms were represented by means of the 6-31G(d,p) basis set,[12] whereas the Pt, Ir and Ru atoms were described with the SDD basis set and its associated effective core potential SDD.[13] Bulk solvent (dichloromethane) was taken into account by using the SMD continuum model[15] and empirical dispersion corrections were introduced through the D3 version of Grimme's dispersion.[16] NBO analysis was performed with NBO 6.0 as implemented in Gaussian 09.[32] The interaction between silanes and the organometallic complexes was also studied by means of the quantum theory of atoms in molecules (QTAIM).[33] QTAIM and Wiberg Bond Index analyses were performed with the Multiwfn software[24] on electron densities computed on the optimized geometries, but using def2QZVP[34] as the basis set for the metals and 6-311G++G(2d,p) for the rest of the atoms.

A localized orbital analysis similar to that described for Chapter 2 was performed on the σ-SiH complexes described in Chapter 3.

Chapter 4

Calculations were performed by Prof. Joaquín López-Serrano, from the University of Seville.

[31] V. N. Staroverova, G. E. Scuseria, J. Tao, J. P. Perdew, *J. Chem. Phys.* **2003**, *119*, 12129-12137.

[32] NBO 6.0. E. D. Glendening, J. K. Badenhoop, A. E. Reed, J. E. Carpenter, J. A. Bohmann, C. M. Morales, C. R. Landis, and F. Weinhold, Theoretical Chemistry Institute, University of Wisconsin, Madison (**2013**).

[33] R. F. W. Bader, Atom in Molecules: A Quantum Theory; Oxford University Press: Oxford, U.K., **1995**.

[34] a) F. Weigend, R. Ahlrichs. *Phys. Chem. Chem. Phys.* **2005**, *7*, 3297-3305; b) F. Weigend, *Phys. Chem. Chem. Phys.*, **2006**, *8*, 1057-1065.

The dehydrocoupling of silanes and amines was calculated by using Truhlar's hybrid meta-GGA functional M06.[30] The Pt atom was represented by the SDD basis set and its associated effective core potential as implemented in Gaussian 09.[13] The rest of the atoms were represented by means of the 6-31G(d,p) basis set.[12] The nature of the intermediates connected by a TS was determined by IRC calculations[14] or by perturbing the transition states along the TS coordinate and optimizing to a minimum. The solvent effects (dichloromethane) were modelled with the SMD continuum model by single-point calculations on gas phase optimized geometries and free optimizations in solution.[15]

[453]

References

[1] N. Curado, C. Maya, J. López-Serrano, A. Rodríguez, *Chem. Commun.,* **2014**, *50*, 15718-15721.

[2] O. Rivada-Wheelaghan, B. Donnadieu, C. Maya, S. Conejero, *Chem. Eur. J.,* **2010**, *16*, 10323-10326.

[3] O. Rivada-Wheelaghan, M. A. Ortuño, J. Díez, A. Lledós, S. Conejero, *Angew. Chem. Int. Ed.,* **2012**, *51*, 3936-3939.

[4] O. Rivada-Wheelaghan, M. Roselló-Merino, M. A. Ortuño, P. Vidossich, E. Gutiérrez-Puebla, A. Lledós, S. Conejero, *Inorg. Chem.,* **2014**, *53*, 4257-4268.

[5] R. E. Cowley, R. P. Bontchev, E. N. Duesler, J. M. Smith, *Inorg. Chem.,* **2006**, *45*, 9771-9779.

[6] M. Brookhart, B. Grant, A. F. Volpe. Jr, *Organometallics*, **1992**, *11*, 3920-3922.

[7] N. A. Yakelis, R. G. Bergman, *Organometallics*, **2005**, *24*, 3579-3581.

Given that the BAr$_4^F$ anion is present in several compounds throughout this thesis, its NMR signals are the following: **^{1}H-NMR (400 MHz, CD$_2$Cl$_2$, 298 K): δ** 7.58 (bs, 4 H, CH_{para}), 7.74 (bs, 8 H, CH_{ortho}) ppm. **^{13}C-NMR (100 MHz, CD$_2$Cl$_2$, 298 K): δ** 117.9 (bs, C_{para}), 124.9 (q, $^1J_{C-F}$ = 272 Hz, CF$_3$), 129.2 (br q, $^2J_{C-F}$ = 31 Hz, C_{meta}), 135.2 (bs, C_{ortho}), 162.2 (q, $^1J_{C-B}$ = 50 Hz, C_{ipso}) ppm.

[8] R. Bassan, K. H. Bryars, L. Judd, A. W. G. Platt, P. G. Pringle, *Inorg. Chim. Acta*, **1986**, *121*, L41-L42.

[9] The assignation of the *E*-isomer was made based on the coupling constants and chemical shifts observed by ^{1}H NMR, which match those described in the literature. See: S. Tanaka, Y. Saito, T. Yamamoto, T. Hattori, *Org. Lett.,* **2018**, *20*, 1828-1831 (Supporting information).

[10] Gaussian 09, Revision D.01, M. J. Frisch, G. W. Trucks, H. B. Schlegel, G. E. Scuseria, M. A. Robb, J. R. Cheeseman, G. Scalmani, V. Barone, B. Mennucci, G. A. Petersson, H. Nakatsuji, M. Caricato, X. Li, H. P. Hratchian, A. F. Izmaylov, J. Bloino, G. Zheng, J. L. Sonnenberg, M. Hada, M. Ehara, K. Toyota, R. Fukuda, J. Hasegawa, M. Ishida, T. Nakajima, Y. Honda, O. Kitao, H. Nakai, T. Vreven, J. A. Montgomery,

Jr., J. E. Peralta, F. Ogliaro, M. Bearpark, J. J. Heyd, E. Brothers, K. N. Kudin, V. N. Staroverov, R. Kobayashi, J. Normand, K. Raghavachari, A. Rendell, J. C. Burant, S. S. Iyengar, J. Tomasi, M. Cossi, N. Rega, J. M. Millam, M. Klene, J. E. Knox, J. B. Cross, V. Bakken, C. Adamo, J. Jaramillo, R. Gomperts, R. E. Stratmann, O. Yazyev, A. J. Austin, R. Cammi, C. Pomelli, J. W. Ochterski, R. L. Martin, K. Morokuma, V. G. Zakrzewski, G. A. Voth, P. Salvador, J. J. Dannenberg, S. Dapprich, A. D. Daniels, Ö. Farkas, J. B. Foresman, J. V. Ortiz, J. Cioslowski, and D. J. Fox, Gaussian, Inc., Wallingford CT, **2009**.

[11] C. Adamo, V. Barone, *J. Chem. Phys.,* **1999**, *110*, 6158-6170.

[12] a) W. J. Hehre, R. Ditchfield, J.A. Pople. *J. Phys. Chem.* **1972**, 56, 2257-2261; b) P.C. Hariharan, J. A. Pople. *Theor. Chim. Acta.* **1973**, *28*, 213-222; c) M. M. Francl, W.J. Pietro, W.J. Hehre, J.S. Binkley, M.S. Gordon, D.J. DeFrees, J.A. Pople. *Chem. Phys.* **1982**, *77*, 3654-3665.

[13] For 1st row transition metals, see: M. Dolg, U. Wedig, H. Stoll, H. Preuss, *J. Chem. Phys.,* **1987**, *86*, 866-872. For 2nd and 3rd row transition metals, see: D. Andrae, U. Häussermann, M. Dolg, H. Stoll, H. Preuss, *Theor. Chim. Acta,* **1990**, *77*, 123-141.

[14] K. Fukui, *Acc. Chem. Res.,* **1981**, *14*, 363-368.

[15] A. V. Marenich, C. J. Cramer, D. G. Truhlar, *J. Phys. Chem. B.,* **2009**, *113*, 6378-6396.

[16] a) S. Grimme, J. Anthony, S. Ehrlich, H. Krieg. *J. Chem. Phys.* **2010**, *132*, 154104; b) F. M. Miloserdov, D. McKay, B. K. Muñoz, H. Samouei, S. A. Macgregor, V. V. Grushin. *Angew. Chem. Int. Ed.*, **2015**, *54*, 8466-8470; c) F. M. Miloserdov, C. L. McMullin, M. M. n. Belmonte, J. Benet-Buchholz, V. U. Bakhmutov, S. A. Macgregor, V. V. Grushin, *Organometallics*, **2014**, *33*, 736-752.

[17] L. Watson, O. Eisenstein, *J. Chem. Educ.,* **2002**, *79*, 1269-1277.

[18] L-L. Han, S-J. Li, D-C. Fang, *Phys. Chem. Chem. Phys.,* **2016**, *18*, 6182-6190.

[19] a) M. Mammen, E. I. Shakhnovich, J. M. Deucth, G. M. Whitesides, *J. Org. Chem.,* **1998**, *63*, 3821-3820; b) R. L. Martin, P. J. Hay, L. R. Pratt, *J. Phys. Chem. A.,* **1998**, *102*, 3565-3573.

[455]

[20] a) D. H. Wertz, *J. Am. Chem. Soc.,* **1980**, *102*, 5316-5322; b) M. H. Abraham, *J. Am. Chem. Soc.,* **1981**, *103*, 6742-6744.

[21] a) J. K-C. Lau, D. V. Deubel, *J. Chem. Theor. Comput.,* **2006**, *2*, 103-106; b) D. V. Deubel, *J. Am. Chem. Soc.,* **2008**, *130*, 665-675; c) J. Kua, H. E. Krizner, D. O. De Haan, *J. Phys. Chem. A,* **2011**, *115*, 1667-1675.

[22] M-A. Courtemanche, M-A. Légaré, L. Maron, F-G. Fontaine, *J. Am. Chem. Soc.,* **2014**, *136*, 10708-10717.

[23] S. Grimme, *J. Comput. Chem.,* **2006**, *27*, 1787-1799.

[24] T .Lu, F. Chen, *J. Comput. Chem.*, **2012**, *33*, 580–592.

[25] I. Funes-Ardoiz, R. S. Paton, **2016**. GoodVibes: GoodVibes v1.0.1 (Version 1.0.1). Zenodo. http://doi.org/10.5281/zenodo.60811.

[26] www.cp2k.org.

[27] J. P. Perdew, K. Burke, M. Ernzerhof, *Phys. Rev. Lett.,* **1996**, *77*, 3865-3868.

[28] G. Lippert, J. Hutter, M. Parrinello, *Mol. Phys.,* **1997**, *92*, 477-488.

[29] a) S. Goedecker, M. Teter, J. Hutter, *Phys. Rev. B. Condens. Matter,* **1996**, *54*, 1703-1710; b) M. Krack, *Theor. Chem. Acc.,* **2005**, *114*, 145-152.

[30] Y. Zhao, D. G. Truhlar, *Theor. Chem. Acc.,* **2008**, *120*, 215-241.

[31] V. N. Staroverova, G. E. Scuseria, J. Tao, J. P. Perdew, *J. Chem. Phys.* **2003**, *119*, 12129-12137.

[32] NBO 6.0. E. D. Glendening, J. K. Badenhoop, A. E. Reed, J. E. Carpenter, J. A. Bohmann, C. M. Morales, C. R. Landis, and F. Weinhold, Theoretical Chemistry Institute, University of Wisconsin, Madison (**2013**).

[33] R. F. W. Bader, Atom in Molecules: A Quantum Theory; Oxford University Press: Oxford, U.K., **1995**.

[34] a) F. Weigend, R. Ahlrichs. *Phys. Chem. Chem. Phys.* **2005**, *7*, 3297-3305; b) F. Weigend, *Phys. Chem. Chem. Phys.*, **2006**, *8*, 1057-1065.

[456]

Conclusions

Conclusions

1. The utilization of a bis(phosphino)boryl scaffold as a ligand has given rise to a series of square planar Ni(II) complexes, where the *strong* trans influence exerted by the boryl moiety was explored. The strong σ-donor ability of the boron atom was leveraged in the field of CO_2 activation. In this way, a hydride ligand *trans* to the boryl fragment proved to be nucleophilic enough so as to activate carbon dioxide in a few seconds under mild conditions, giving the corresponding formate complex (^{tBu}PBP)–Ni–OC(O)H. This species, in combination with the Lewis acid tris(pentafluorophenyl)borane turned out to be an effective catalytic system to selectively carry out CO_2 hydrosilation to the bis(silyl)acetal stage when using tertiary silanes like Et_3SiH. Experimental and theoretical studies showed that efficient sequestration of the Lewis acid is crucial in order to achieve selective transformation to the aldehyde level, avoiding over-reduction to methoxide derivatives or methane.

2. The PBP ligand proved to be a successful platform to stabilize elusive compounds, barely described in the literature. As an example, a square planar Ni(II) complex containing two boryl ligands *trans* to each other was synthesized by reaction of the (^{tBu}PBP)–Ni–CH$_3$ complex with bis(catecholato)diboron, releasing MeBCat as a by-product. The corresponding boryl complex was isolated and its structure elucidated by means of X-Ray diffraction studies. The mechanism of its formation was studied by DFT calculations, where nucleophilic attack from the methyl group and cooperativity of the PBP ligand (with participation of the boron atom) were considered as possible mechanistic pathways. The role of nickel boryl complex (^{tBu}PBP)–Ni–BCat as a reactive intermediate in dehydrogenative

[458]

borylation reactions was demonstrated, employing styrene derivatives as substrates.

3. The Lewis acidity of electronically deficient NHC-stabilized Pt(II) compounds was utilized in the formation of σ-silane complexes. Cyclometalated I^{t}Bu species [Pt(I^{t}Bu')(I^{t}Bu)]$^+$ showed broad signals in the ^{1}H NMR spectrum at low temperatures when using hydrosilanes like ^{n}BuSiH$_3$ or Et$_2$SiH$_2$, indicative of a weak contact between one of the hydrogen atoms of the silane and the metal centre. This was corroborated by DFT methods, which pointed out to a η^1-coordination mode of the silane. In the case of Et$_2$SiH$_2$, the corresponding σ-SiH complex evolved at room temperature to yield the cationic silyl derivative [Pt(SiHEt$_2$)(I^{t}Bu)$_2$]$^+$.

4. Removal of one of the methyl groups from the NHC ligand I^{t}Bu led to the formation of the carbene I^{t}Bu^{i}Pr. The resulting less sterically hindered cyclometalated species [Pt(I^{t}Bu^{i}Pr')(I^{t}Bu^{i}Pr)]$^+$ established stronger interactions with hydrosilanes, as evidenced by NMR experiments. The bigger cavity allowed the formation of σ-silane complexes even with tertiary silanes. In fact, two of these compounds (namely [Pt(I^{t}Bu^{i}Pr')(I^{t}Bu^{i}Pr)(HSiEt$_3$)]$^+$ and [Pt(I^{t}Bu^{i}Pr')(I^{t}Bu^{i}Pr)(HSiPh$_3$)]$^+$) were crystallized, and their structure was borne out by X-Ray crystallography, providing experimental evidence of this type of intermediates, widely proposed in the literature. A combination of experimental and theoretical analyses led to the conclusion that these σ-SiH complexes adopt intermediate geometries between η^1 and η^2 coordination modes. DFT studies indicate that such structures are flexible towards the η^1 binding mode, in which the electrophilicity of the silicon atom is increased. These complexes evolve at room temperature towards the formation of [Pt(SiR$_3$)(I^{t}Bu^{i}Pr)$_2$]$^+$ species.

[459]

Conclusions

5. Formation of C–Si and/or Pt–Si bonds was observed when using primary silanes with Pt(II) complexes stabilized by I^{t}Bu^{i}Pr, IMes and IMes* ligands. Starting from [Pt(NHC')(NHC)]$^+$ complexes, C–Si coupling products [Pt(NHCSiHR')(NHC)]$^+$ were obtained, with concomitant release of hydrogen. On the other hand, employing [Pt(H)(NHC)$_2$]$^+$ as a precursor afforded the corresponding silyl derivatives [Pt(SiH$_2$R)(NHC)$_2$]$^+$ instead. The role of σ-SiH complexes as reactive intermediates during these reactions was confirmed by means of low temperature NMR experiments when using cyclometalated and hydride complexes derived from the IMes* carbene. DFT calculations provided additional supporting data to these observations.

6. The increased electrophilicity of the σ-SiH complexes was exploited in catalytic applications. Complex [Pt(I^{t}Bu')(I^{t}Bu)]$^+$ was chosen as a catalyst in CO$_2$ hydrosilation reactions as well as in Si–N dehydrogenative coupling processes. Remarkable results were obtained in both cases in terms of selectivity and activity. In CO$_2$ reduction, selective formation of silyl monoformates was observed when using primary or secondary silanes, in contrast to numerous cases described in the literature. Regarding Si–N coupling, the strong Lewis acidity of the σ-SiH compounds and the robustness of the platinum systems allowed to decrease the catalyst loading down to 10 ppm without catalyst decomposition, obtaining some of the highest TON and TOF values described so far. Additionally, mono- or di-silazanes could be selectively synthesized by modifying the stoichiometry of the reagents. Finally, experimental (low temperature NMR analyses, kinetic measurements) and computational studies suggested that two equivalents of amine are

[460]

necessary in a mechanism where the platinum complex acts as a mere Lewis acid, abstracting the hydrogen atom from the silane.

Conclusiones

1. La utilización de la plataforma bis(fosfino)borilo como ligando ha dado lugar a una serie de complejos de geometría plano-cuadrada de Ni(II), donde se exploró la fuerte influencia *trans* ejercida por el fragmento borilo. El fuerte carácter donador σ del átomo de boro se aprovechó en el ámbito de la activación de CO_2. De esta manera, un ligando hidruro *trans* al grupo borilo demostró ser lo suficientemente nucleófilo como para activar el dióxido de carbono en pocos segundos en condiciones de reacción suaves, dando lugar al correspondiente complejo formiato (tBuPBP)–Ni–OC(O)H. Esta especie, junto con el ácido de Lewis tris(pentafluorofenil)borano resultó ser un sistema catalítico eficiente para llevar a cabo la hidrosililación selectiva de CO_2 a la etapa de bis(silil)acetal utilizando silanos terciarios como el Et_3SiH. Estudios experimentales y teóricos mostraron que el secuestro eficiente del ácido de Lewis es crucial para conseguir la transformación selective al nivel de aldehído, evitando así la sobrerreducción a derivados de metóxido, o metano.

2. El ligando PBP demostró ser una plataforma efectiva para estabilizar compuestos elusivos, apenas descritos en la bibliografía. Como ejemplo, un complejo de geometría plano cuadrada de Ni(II) conteniendo dos ligandos de tipo borilo en una disposición *trans* se sintetizó a partir de la reacción del complejo (tBuPBP)–Ni–CH₃ con bis(catecolato)diboro, liberando MeBCat como subproducto. El complejo borilo correspondiente fue aislado y su estructura se confirmó mediante técnicas de difracción de rayos X. El mecanismo de su formación se estudió mediante cálculos DFT, los cuales evaluaron el ataque nucleofílico por parte del grupo metilo o la cooperatividad del ligando PBP (con participación del átomo de boro) como posibles alternativas. Además, se demostró el papel del complejo borilo de níquel

[462]

(^{tBu}PBP)−Ni−BCat como un intermedio reactivo en reacciones de borilación deshidrogenante, utilizando estirenos como sustratos.

3. La acidez de Lewis de compuestos electrónicamente deficientes de Pt(II) estabilizados por ligandos NHC se utilizó en la formación de complejos σ-silano. La especie ciclometalada [Pt(I^{t}Bu')(I^{t}Bu)]$^{+}$ mostró señales anchas en el espectro de RMN ^{1}H a baja temperatura, utilizando silanos como ^{n}BuSiH$_3$ o Et$_2$SiH$_2$, lo cual es indicativo de un contacto débil entre uno de los átomos de hidrógeno del silano y el centro metálico. Esto se corroboró mediante cálculos DFT, los cuales apuntan a un modo de coordinación η^1 del silano. En el caso de Et$_2$SiH$_2$, el complejo σ-SiH correspondiente evolucionó a temperatura ambiente para dar el sililo catiónico [Pt(SiHEt$_2$)(I^{t}Bu)$_2$]$^{+}$.

4. La eliminación de uno de los grupos metilo del ligando NHC I^{t}Bu dio lugar a la formación del carbeno I^{t}Bu^{i}Pr. La especie ciclometalada resultante [Pt(I^{t}Bu^{i}Pr')(I^{t}Bu^{i}Pr)]$^{+}$, menos impedida estéricamente, estableció interacciones más fuertes con los silanos, tal y como demuestran los experimentos de RMN. La mayor cavidad permitió la formación de complejos σ-silano incluso con silanos terciarios. De hecho, dos de estos compuestos (a saber [Pt(I^{t}Bu^{i}Pr')(I^{t}Bu^{i}Pr)(HSiEt$_3$)]$^{+}$ y [Pt(I^{t}Bu^{i}Pr')(I^{t}Bu^{i}Pr)(HSiPh$_3$)]$^{+}$) fueron cristalizados, y su estructura se confirmó mediante cristalografía de rayos X, proporcionando así pruebas experimentales de este tipo de intermedios ampliamente propuestos en la bibliografía. Una combinación de estudios experimentales y teóricos concluyeron que estos complejos σ-SiH adoptan geometrías intermedias entre modos de coordinación η^1 y η^2, Los estudios DFT indican que dichas estructuras son flexibles hacia el modo de unión η^1, en el cual la electrofilia del átomo de silicio se incrementa. Estos compuestos evolucionan a temperatura ambiente hacia la formación de especies [Pt(SiR$_3$)(I^{t}Bu^{i}Pr)$_2$]$^{+}$.

[463]

Conclusiones

5. Se observó la formación de enlaces C–Si y/o Pt–Si cuando se utilizaron silanos primarios en combinación con complejos de Pt(II) estabilizados por ligandos I^{t}Bu^{i}Pr, IMes e IMes*. Comenzando por los complejos [Pt(NHC')(NHC)]$^+$, se obtuvieron los productos de acoplamiento C–Si [Pt(NHCSiHR')(NHC)]$^+$, junto con la formación de hidrógeno molecular. Por otra parte, utilizando [Pt(H)(NHC)$_2$]$^+$ como precursor se obtuvieron los correspondientes derivados de tipo sililo [Pt(SiH$_2$R)(NHC)$_2$]$^+$ en su lugar. El papel de los complejos σ-SiH como intermedios reactivos durante estas reacciones se confirmó a través de experimentos de RMN a baja temperatura, utilizando los complejos ciclometalado e hidruro derivados del carbeno IMes*. Los cálculos DFT proporcionaron datos de apoyo adicionales a estas observaciones.

6. El aumento de electrofilia observado en los complejos σ-SiH se empleó en aplicaciones catalíticas. El complejo [Pt(I^{t}Bu')(I^{t}Bu)]$^+$ fue elegido como catalizador en reacciones de hidrosililación de CO$_2$, así como en reacciones de acoplamiento deshidrogenante de silanos y aminas. Se obtuvieron resultados destacables en ambos casos, tanto en términos de selectividad como de actividad. En la reducción de CO$_2$, se observó la formación selectiva a silil monoformiatos cuando se utilizaron silanos primarios o secundarios, al contrario de lo descrito en numerosos precedentes en la bibliografía. Con respecto al acoplamiento Si–N, la fuerte acidez de Lewis de los compuestos σ-SiH y la robustez de las especies de platino permitieron reducir la carga catalítica a 10 ppm sin degradación del catalizador, obteniéndose así algunos de los valores de TON y TOF más altos descritos hasta la fecha. Además, modificando la estequiometría de los reactivos se pudo obtener de manera selectiva mono- y disilazanos. Finalmente, estudios experimentales (análisis de RMN a baja temperatura, medidas cinéticas) y teóricos indicaron que se necesitan dos equivalentes de amina en un mecanismo en el que el

complejo de platino actúa como un mero ácido de Lewis, abstrayendo el átomo de hidrógeno del silano.